

Yu-Dong Zhang
Tomonoby Senjyu
Chakchai SO-IN
Amit Joshi *Editors*



Smart Trends in Computing and Communications: Proceedings of SmartCom 2020

Smart Innovation, Systems and Technologies

Volume 182

Series Editors

Robert J. Howlett, Bournemouth University and KES International,
Shoreham-by-sea, UK

Lakhmi C. Jain, Faculty of Engineering and Information Technology,
Centre for Artificial Intelligence, University of Technology Sydney,
Sydney, NSW, Australia

The Smart Innovation, Systems and Technologies book series encompasses the topics of knowledge, intelligence, innovation and sustainability. The aim of the series is to make available a platform for the publication of books on all aspects of single and multi-disciplinary research on these themes in order to make the latest results available in a readily-accessible form. Volumes on interdisciplinary research combining two or more of these areas is particularly sought.

The series covers systems and paradigms that employ knowledge and intelligence in a broad sense. Its scope is systems having embedded knowledge and intelligence, which may be applied to the solution of world problems in industry, the environment and the community. It also focusses on the knowledge-transfer methodologies and innovation strategies employed to make this happen effectively. The combination of intelligent systems tools and a broad range of applications introduces a need for a synergy of disciplines from science, technology, business and the humanities. The series will include conference proceedings, edited collections, monographs, handbooks, reference books, and other relevant types of book in areas of science and technology where smart systems and technologies can offer innovative solutions.

High quality content is an essential feature for all book proposals accepted for the series. It is expected that editors of all accepted volumes will ensure that contributions are subjected to an appropriate level of reviewing process and adhere to KES quality principles.

**** Indexing: The books of this series are submitted to ISI Proceedings, EI-Compendex, SCOPUS, Google Scholar and Springerlink ****

More information about this series at <http://www.springer.com/series/8767>

Yu-Dong Zhang · Tomonoby Senjyu ·
Chakchai SO-IN · Amit Joshi
Editors

Smart Trends in Computing and Communications: Proceedings of SmartCom 2020

 Springer

Editors

Yu-Dong Zhang
School of Informatics
University of Leicester
Leicester, England, UK

Chakchai SO-IN
Khon Kaen University
Khon Kaen, Thailand

Tomonoby Senju
University of the Ryukyus
Nishihara, Japan

Amit Joshi
Global Knowledge Research Foundation
Gujarat, India

ISSN 2190-3018

ISSN 2190-3026 (electronic)

Smart Innovation, Systems and Technologies

ISBN 978-981-15-5223-6

ISBN 978-981-15-5224-3 (eBook)

<https://doi.org/10.1007/978-981-15-5224-3>

© The Editor(s) (if applicable) and The Author(s), under exclusive license to Springer Nature Singapore Pte Ltd. 2021

This work is subject to copyright. All rights are solely and exclusively licensed by the Publisher, whether the whole or part of the material is concerned, specifically the rights of translation, reprinting, reuse of illustrations, recitation, broadcasting, reproduction on microfilms or in any other physical way, and transmission or information storage and retrieval, electronic adaptation, computer software, or by similar or dissimilar methodology now known or hereafter developed.

The use of general descriptive names, registered names, trademarks, service marks, etc. in this publication does not imply, even in the absence of a specific statement, that such names are exempt from the relevant protective laws and regulations and therefore free for general use.

The publisher, the authors and the editors are safe to assume that the advice and information in this book are believed to be true and accurate at the date of publication. Neither the publisher nor the authors or the editors give a warranty, expressed or implied, with respect to the material contained herein or for any errors or omissions that may have been made. The publisher remains neutral with regard to jurisdictional claims in published maps and institutional affiliations.

This Springer imprint is published by the registered company Springer Nature Singapore Pte Ltd. The registered company address is: 152 Beach Road, #21-01/04 Gateway East, Singapore 189721, Singapore

Preface

This SIST volume contains the papers presented at the SmartCom 2020: Fourth International Conference on Smart Trends for Computing and Communications. The conference was held during January 24–25, 2020, at Hotel Novotel, Siam Square, Bangkok, and organized by Global Knowledge Research Foundation with support from Knowledge Chamber of Commerce and Industry and InterYIT IFIP—International Federation for Information Processing.

The books presents the state-of-the-art as well as emerging topics pertaining to information, computer communications and effective strategies for its implementation for engineering and managerial applications.

The conference attracts a large number of high-quality submissions and stimulates the cutting-edge research discussions among many academic pioneering researchers, scientists, industrial engineers, students from all around the world and provides a forum to researchers on proposing new technologies, sharing their experiences and discussing future solutions for design infrastructure for ICT, providing common platform for academic pioneering researchers, scientists, engineers and students to share their views and achievements, enriching technocrats and academicians by presenting their innovative and constructive ideas and focusing on innovative issues at international level by bringing together the experts from different countries.

Research submissions in various advanced technology areas were received, and after a rigorous peer review process with the help of program committee members and 56 external reviewers for 262 papers from 20 different countries including Australia, China, Malaysia, Indonesia, Thailand, Bangladesh, Japan, South Korea and Sri Lanka, etc., out of which 50 were accepted with an acceptance ratio of 0.19.

This event’s success was possible only with the help and support of our team and organizations. With immense pleasure and honor, we would like to express our sincere thanks to the authors for their remarkable contributions, all the Technical Program Committee members for their time and expertise in reviewing the papers within a very tight schedule and the publisher Springer for their professional help. This is the fourth conference of the series SmartCom in which proceedings is published as a CCIS volume by Springer. We are overwhelmed by our two

distinguished scholars and appreciate them for accepting our invitation to deliver keynote speeches to the conference and six technical session chairs for analyzing the research work presented by the researchers. Most importantly, we are also grateful to our local support team for their hard work for the conference. This series has already been made a continuous series which will be hosted at different locations every year.

This event's success was possible only with the help and support of our team and organizations. With immense pleasure and honor, we would like to express our sincere thanks to the authors for their remarkable contributions, all the Technical Program Committee members for their time and expertise in reviewing the papers within a very tight schedule and the publisher Springer for their professional help. This is the fourth conference of the series SmartCom in which proceedings is published as a SIST volume by Springer. We are overwhelmed by our three distinguished scholars and appreciate them for accepting our invitation to deliver keynote speeches including Prof. Mike Hinchey, President IFIP; Prof. Milan Tuba, Singidunum University, Serbia; and Dr. ChakChai So-In, Khon Kaen University, Thailand, in the conference and further six technical session chairs for analyzing the research work presented by the researchers. Most importantly, we are also grateful to our local support team for their hard work for the conference. This series has already been made a continuous series which will be hosted at different locations every year.

Bangkok, Thailand

Yu-Dong Zhang
Tomonoby Senjyu
Chakchai SO-IN
Amit Joshi

Contents

1	Accurate Detection of Facial Landmark Points Using Local Intensity Information for Emotion Detection	1
	Payal Bhattacharjee and M. M. Ramya	
2	Statistical Approach to Detect Alzheimer’s Disease and Autism Spectrum-Related Neurological Disorder Using Machine Learning	17
	Akhilesh Kumar Sharma and Devesh K. Shrivastav	
3	The Development and Gap of Chinese and American Open Access Journals: From the Perspective of Network Influence	25
	Danyang Li, Xinlai Li, and Biying Gao	
4	The Use of Mobile Apps to Facilitate Customers’ Choice-Making When Grocery Shopping	39
	Asle Fagerström, Niklas Eriksson, and Valdimar Sigurdsson	
5	Implementation of Best Hybrid Adaptive and Intelligent MIMO Detector on Reconfigurable Architecture for 5G LTE/IoT Environment	49
	Tipparti Anil Kumar and Lokam Anjaneyulu	
6	Automated Detection of Retinal Hemorrhage Based on Supervised Classifiers and Implementation in Hardware	57
	K. A. Sreeja, S. S. Kumar, and Arun Pradeep	
7	Data Encryption as Security Measure in IoT-Enabled Healthcare	69
	M. Shankar Lingam, G. S. Raghavendra, Arun Kumar, V. Anand, and A. M. Sudhakara	
8	Agents-Based Service Restoration in Electrical Secondary Distribution Network	83
	Rukia J. Mwifunyi, Nerey H. Mvungi, and Mussa M. Kissaka	

9	Packet-Level and Physical-Level Cross-Technology Communications: A Brief Introduction	95
	Liwen Qiu, Qinglin Zhao, Lianbo Zhang, Shumin Yao, Jing Zhao, and Li Feng	
10	Smart Traffic Navigation System (STNS) to Reduce Travel Time by Integrating Signals from Navigation and Traffic Systems	101
	S. Sripranav, Akshay Ravi, K. Gautham, and R. Leela Velusamy	
11	Selective Sensor Control via Cauchy Schwarz Divergence	113
	Nida Ishtiaq, Sabita Panicker, Amirali K. Gostar, Alireza Bab-Hadiashar, and Reza Hoseinnezhad	
12	Step-Factor Resampling Technique for Imbalanced Sequence Data Classification	125
	Iroshan Aberathne, Chamila Walgampaya, and Udara Rathnayake	
13	Rice Disease Detection Based on Image Processing Technique	135
	Md. Asfaqur Rahman, Md. Shahriar Nawal Shoumik, Md. Mahbubur Rahman, and Most. Hasna Hena	
14	Electromagnetic Radiation from Cell Phones Used in Dhaka City	147
	M. Quamruzzaman, Munima Haque, Shahina Haque, and Utpal Chandra Das	
15	Expressing Opinions Application: A Case Study at Rajamangala University of Technology, Isan, Khon Kaen Campus	159
	Ekaphong Tangtrakul, Jatupol Nampromma, and Phoemporn Lakkhanawannakun	
16	Toward Clarifying Human Information Processing by Analyzing Big Data: Comparing Response Time to Questionnaires Included Heteronym Word for Problem Solving Between Visually and Auditory Types	171
	Keiko Tsujioka	
17	Mango Species Detection from Raw Leaves Using Image Processing System	183
	Most. Hasna Hena, Md. Helal Sheikh, Md. Shamim Reza, and Ahmed Al Marouf	
18	Frequency Reconfigurable Planner Antennas for Wireless Applications: A Review	193
	Dinesh Yadav and Vivekanand Tiwari	
19	Room Temperature Pt-Modified WO₃/p-Si Film Gas Sensor for Detection of Methanol	201
	Anup Dey, Komal Kumari, Abir Jana, Bijoy Goswami, Poushali Nandi, and S. K. Sarkar	

20 Graph Degree Linkage Clustering for Identify Student’s Performance on *Kompetisi Sains Madrasah* in Indonesia. 211
 Ahmad Hanif Asyhar, A. Umar, Dian Candra Rini Novitasari, Kusaeri, Ahmad Fauzi, Nurissaidah Ulinnuha, Dwi Rolliawati, Noor Wahyudi, Ahmad Yusuf, Ali Mustofa, and Zakiyatul Ulya

21 Stepwise Iterative Maximum Likelihood Clustering Based on *Kompetisi Sains Madrasah*’ Scores for Identifying Quality of Junior High School Grading Distribution 221
 Kusaeri, Nanik Puji Hastuti, Ali Musthofa, Ahmad Fauzi, Ahmad Hanif Asyhar, Dian Candra Rini Novitasari, Dwi Rolliawati, Zakiyatul Ulya, Ahmad Yusuf, Nurissaidah Ulinnuha, and Noor Wahyudi

22 Detecting the Width of Pap Smear Cytoplasm Image Based on GLCM Feature 231
 Nita Merlina, Edi Noersasongko, Pulung Nurtantio, M. A. Soeleman, Dwiza Riana, and Sri Hadianiti

23 Design of a Novel Wideband Dipole Antenna for mm-Wave Frequencies 241
 Paikhomba Loktongbam, Chaitali Koley, Debashish Pal, and Ayan Kumar Bandhopadhyay

24 Forecasting Sea Surface Temperature in Java Sea Using Generalized Regression Neural Networks 249
 Dian Candra Rini Novitasari, Wahyu Tri Puspitasari, Rahmat Pramulya, Hetty Rohayani, R. R. Diah Nugraheni Setyowati, Dwi Rukma Santi, Muhammad Fahrur Rozi, and Ary Widjajanto

25 Natural Disaster Predictions of Whirlwinds in Cilacap Region of Central Java Using Adaptive Neighborhood Modified Backpropagation (ANMBP) 259
 Dian Candra Rini Novitasari, Fitria Febrianti, Arnita, Rinda Nariswari, R. R. Diah Nugraheni Setyowati, Putri Wulandari, Ahmad Zoebad Foeady, Moh. Hafiyusholeh, and Fajar Setiawan

26 Designing Memristor-Based Timing Circuits and Performance Comparison with CMOS Counterparts. 269
 Abir Jana, Disha Bhattacharjee, Komal Kumari, Anup Dey, Bijoy Goswami, and Subir Kumar Sarkar

27 Identify Elementary Student Distribution Based on *Kompetisi Sains Madrasah* Data Using Probabilistic Distance Clustering 281
 Ahmad Yusuf, Noor Wahyudi, Zakiyatul Ulya, Nurissaidah Ulinnuha, Dwi Rolliawati, Ali Mustofa, Ahmad Fauzi, Ahmad Hanif Asyhar, Kusaeri, Ratna Indriyati, Dian Candra Rini Novitasari, and Maryunah

28	Classification of Tomato Plant Diseases Through Leaf Using Gray-Level Co-occurrence Matrix and Color Moment with Convolutional Neural Network Methods	291
	Anton Anton, Supriadi Rustad, Guruh Fajar Shidik, and Abdul Syukur	
29	Leverage from Blockchain in Commodity Exchange: Asset-Backed Token with Ethereum Blockchain Network and Smart Contract	301
	Richard, Yaya Heryadi, Lukas, and Agung Trisetyarso	
30	A Review of Focused Crawling Schemes for Search Engine	311
	Suresh Kumar and Manisha Gupta	
31	Design and Simulation of Multi-channel V-TDMA for IoT-Based Healthcare Systems	319
	Anita Ramachandran, Malaika Afra Taj, Raghav Maheshwari, and Anupama Karuppiah	
32	Design and Development of Tiny Humanoid Walking and Dancing Robot with Obstacle Detection for Visual Impaired People	331
	Amrita Ganguly, Jasmine Ara, and Bijan Paul	
33	A Survey on DBN for Intrusion Detection in IoT	339
	Harsh Namdev Bhor and Mukesh Kalla	
34	Organ Detection in Surgical Videos Using Neural Networks	345
	Amit Kumar, Anshu Gupta, and Ankita Pramanik	
35	Implementation Aspects of Multi-bit Adders Using UTBSOI Transistors	355
	Rekib Uddin Ahmed and Prabir Saha	
36	Accelerating Latency of Binary Division Through Vedic Methodology	365
	Deepak Kumar and Prabir Saha	
37	Monitoring the torsional vibrations on the main propulsion plant of marine cargo ship installed two-stroke diesel engine: Theoretical case study	379
	Do Duc Luu and Cao Duc Hanh	
38	Analysing Different Full Adder Based on 45 nm Technology	393
	Ankit Kumar, Shyam Akashe, and Seelam VSV Prabhu Deva Kumar	
39	Design of RF Energy Harvesting Circuit at 900 MHz for Low-Powered DC Applications	401
	Anoop Chiluveru, Shyam Akashe, and Shailendra Singh Ojha	

40 Noise Voltage: A New Dependability Concern in Low-Power FinFET-Based Priority Encoder at 45 nm Technology 411
 Vishwas Mishra, Abhishek Kumar, Shobhit Tyagi, Divya Mishra, and Shyam Akashe

41 Assessment of Suitability of Metaheuristics and Machine Learning for Task Scheduling Process: A Review of Aptness in Heavy Task Environments 419
 Shantanu Anandrao Lohi and Nandita Tiwari

42 A Review on Indian UID-Based Automated Electoral Roll Generation Mechanism Shunning Duplication and Redundancy . . . 427
 Harish Vasant Rao Gorewar and Nandita Tiwari

43 A Review of Deep Learning Techniques for Identification and Diagnosis of Plant Leaf Disease 435
 Ravindra Namdeorao Jogekar and Nandita Tiwari

44 Analysis and Prediction of Student Data Using Data Science: A Review 443
 Sandeep S. Ganorkar, Nandita Tiwari, and Varsha Namdeo

45 Efficient Target Detection and Classification of SAR Images Using Z-Buffer Convolutional Neural Networks 449
 P. Vasuki, A. Shakin Banu, S. Mohamed Mansoor Roomi, and G. Maragatham

46 Context-Aware Deep Convolutional Neural Network Application for Fire and Smoke Detection in Virtual Environment for Surveillance Video Analysis 459
 Akm Ashiqzaman, Sung Min Oh, Dongsu Lee, Jihoon Lee, and Jinsul Kim

47 Design and Development of Efficient Cost-Saving Algorithms for Guiding Customer Purchasing Patterns in Modern Consumerism Scenario Using Feed Forward Back Propagation Neural Networks 469
 Sonia Maria D’Souza and K. Satyanarayan Reddy

48 Mild Cognitive Impairment and Technology for Older Adults: A Review 477
 Nita Rosa Damayanti and Nazlena Mohamad Ali

49 Identify Education Quality Based on Islamic Senior High School Data in *Kompetisi Sains Madrasah* Using Fuzzy C-Means Clustering 487
 Dian Candra Rini Novitasari, Abdullah Faqih, Noor Wahyudi, Nurissaidah Ulinnuha, Zakiatul Ulya, Ali Mustofa, Ahmad Fauzi, Ahmad Hanif Asyhar, Kusaeri, Dwi Rolliawati, and Ahmad Yusuf

50 Obstacle Avoidance with Sensors Using Soft Computing Techniques 497
Amit Yadav, Garima Jain, Divya Mishra, and Dharvendra P. Yadav

Author Index 507

About the Editors

Prof. Yu-Dong Zhang received his B.S. and M.S. degrees from Nanjing University of Aeronautics and Astronautics in 2004 and 2007, prior to completing his Ph.D. in Signal and Information Processing at Southeast University in 2010. From 2010 to 2012, he worked at Columbia University as a postdoc. From 2012 to 2013, he worked as a research scientist at Columbia University and New York State Psychiatric Institute. From 2013 to 2017, he worked as a Full Professor and doctoral advisor at the School of Computer Science and Technology, Nanjing Normal University. Since 2018, he has been a Full Professor at the Department of Informatics, University of Leicester, UK.

Prof. Tomonoby Senjyu received his B.S. and M.S. degrees in Electrical Engineering from the University of the Ryukyus, Nishihara, Japan, in 1986 and 1988, respectively, and his Ph.D. in Electrical Engineering from Nagoya University, Japan, in 1994. He is currently a Full Professor at the Department of Electrical and Electronics Engineering, University of the Ryukyus. His research interests include renewable energy, power system optimization and operation, power electronics, and advanced control of electrical machines.

Prof. Chakchai SO-IN has been with the Department of Computer Science at Khon Kaen University since 2010. Dr. SO-IN received his B.E. and M.E. degrees from Kasetsart University (KU), Bangkok, Thailand, in 1999 and 2001, respectively. He also completed M.S. and Ph.D. degrees in Computer Engineering at the Department of Computer Science and Engineering, Washington University, in St. Louis (WUSTL), MO, USA, in 2006 and 2010. He has authored more than 100 publications in prominent journals and proceedings, together with 10 books. His research interests include mobile computing/sensor networks, Internet of Things, computer/wireless/distributed networks, cyber security, intelligent systems and the future Internet. He is a senior member of the IEEE and ACM.

Dr. Amit Joshi is currently Director of the Global Knowledge Research Foundation, and an entrepreneur and researcher. Holding a B.Tech. in Information Technology and M.Tech. in Computer Science and Engineering, he has conducted extensive research in the areas of cloud computing and cryptography in medical imaging, with a focus on analyzing current government strategies and global forums concerning security. Dr. Joshi has more than 10 years of experience in academia and industry, having worked at prestigious organizations. He is an active member of the ACM, IEEE, CSI, AMIE, IACSIT Singapore, IDES, ACEEE, NPA, and many other professional societies. Currently, he is the International Chair of InterYIT at the International Federation of Information Processing (IFIP, Austria). He has presented and published more than 50 papers in national and international journals/conferences of the IEEE and ACM, and has edited more than 20 books for Springer, ACM, and other reputed publishers. He has also organized more than 40 national and international conference and workshops in association with the ACM, Springer, and the IEEE, e.g. in India, the UK, Thailand, and Europe.

Chapter 1

Accurate Detection of Facial Landmark Points Using Local Intensity Information for Emotion Detection



Payal Bhattacharjee and M. M. Ramya

Abstract Face is the gateway to mind. Understanding facial expressions gives the affective state of human mind. Accurate detection of facial expressions is one of the open challenges in machine vision. The fulcrum of facial expression detection and classification depends on extraction of salient points on the face. The accurate detection of these points is a mandatory step for emotion detection as these facial points undergo tremendous change as emotion expressed by human changes. This paper proposes an accurate adaptive algorithm for extraction of the distinct facial points which will make identification of various expressions a feasible task. Viola–Jones face detection algorithm was used for detection of face. The extracted face region was decimated into various regions of interest (ROIs) based on prior knowledge of human face anatomy. Eye centers were located using horizontal and vertical projections of histogram of eye ROI. The ROI for eyebrows was located using the location of eye centers. The eyebrows were detected by taking advantage of the sign of double edges produced by second-order differential used for edge detection. Lip corners were extracted from the bottom half of the face by obtaining the highest contrast points from the contrast image. The algorithm was tested on the UNBC Pain Archive and achieved 100%, 100%, and 99.87% accuracy for eye centers, lip corners, and eyebrow corners, respectively. The algorithm is learning free, computational inexpensive, and can be modeled into embedded platforms.

P. Bhattacharjee · M. M. Ramya (✉)
Center for Automation and Robotics, Hindustan Institute of Technology and Science, Padur,
Chennai, Tamil Nadu, India
e-mail: mmramya@hindustanuniv.ac.in

P. Bhattacharjee
e-mail: payal.bhattacharjee708@gmail.com

© The Editor(s) (if applicable) and The Author(s), under exclusive license
to Springer Nature Singapore Pte Ltd. 2021

Y.-D. Zhang et al. (eds.), *Smart Trends in Computing and Communications: Proceedings of SmartCom 2020*, Smart Innovation, Systems and Technologies 182,
https://doi.org/10.1007/978-981-15-5224-3_1

1.1 Introduction

Facial expression-based research has gained a lot of pace during the last decade. There has been a plethora of research in this field. Face animation, driver drowsiness, shopper's interest, video surveillance, and face tracking are few of the areas where expression analysis plays a pivotal role. The idea of better human-machine interaction can be made feasible with computers understanding expressions and altering their response in accordance with one's state of mind. The problem of facial expression analysis is discriminated into identification of action units (AU). Facial Action Coding System (FACS) [6] categorizes each muscle movement into action units. Combination of action units leads to an expression. Precise detection of action unit depends on identifying and tracking facial points, respective of pose, illumination, facial hair, wrinkles, and spectacles. Landmark points are designated as fiducial and ancillary points. Fiducial points are primary points like eye centers, eyebrow corners, nose tip, and lip corners. Detection of these points will help in identification of ancillary points like chin, cheeks, and forehead [2].

Landmark detection and localization may seem like a simple task at hand. Face variability is in terms of facial hair and race. Imaging conditions and number of landmarks required for a specific application make the development of a generic algorithm for an accurate detection of facial landmark points an acute task. The research on landmark point detection can be broadly classified into two: model-based methods and texture-based methods.

Elucidation of images containing objects of varying shape is a difficult task which can be handled by deformable models like active appearance model (AAM) and active shape models (ASM) [3]. In model-based methods, a model is generated from training images, and this model is made fit to the current shape of face in the test images. ASM searches for points with similar gray-level intensities around the current point which duplicates the texture of model at that given landmark. AAM searches for similar intensities in the convex hull of the point. Both the models require large image samples during each search. In recent years, Belhumeur [1] has calculated SIFT features and trained SVM for each landmark point to get a probability of a point occurring in that region. Bayesian network was used to generate a global model from these individual probabilities [17]. Extracted histogram-of-gradient (HOG) features are given a global shape by establishing quadratic spring between them.

Pioneering texture-based landmark point detection work was done by Vukadinovic and Pantic [15], wherein Gabor features were extracted and AdaBoost templates were built on these Gabor features and gray-level intensities to identify 20 facial landmark points. They considered mouth region to be 0.85 times distance between two eyes, which always does not hold true. They have trained weak classifiers, wherein the algorithm searches for a facial point in a given ROI in a sliding window approach. As the search area increases, the time required also increases linearly; to speed up the detection rates, gradient descent approach was implemented which reportedly failed as learned algorithm generated local extremes [13]. Regression techniques were explored to overcome the sliding window approach, wherein local information

along with support vector regressions was utilized to predict first 22 points. Markov networks were used to sample new locations [14]. Ding and Martinez [5] carried out discriminant analysis to detect fiducial points. Yun and Ling [16] have generated five difference of Gaussian (DoG) images. Each pixel in a given DoG image is compared to its eight neighbors in the same scale and nine neighbors in one scale up image and down image. If this certain point intensity is greater than its neighborhood, it is chosen as a possible point. HOG features are calculated, and AdaBoost classifiers are trained for detection. The methods discussed above have a common trait of fitting a learnt model to the new data that comes. Human faces are very unique from one another; no two faces are similar; hence, detection of landmark points is a very subjective topic, wherein local information which is unique to each face is explored for better detection rates.

Shape and texture of human face are non-rigid, and it fluctuates with expression and is diverse in nature in terms of ethnic background, the way each individual expresses emotions. Dey [4] has used fast corner detection for identification of facial points on images of northeastern Indian people. Fast corners respond well to areas where information is residing but use of a fixed global threshold hits the robustness of the algorithm.

On the understanding of intensity variations around the landmark point, template images were built. These template images when applied on facial images generated blob images which were used for identification and detection [9]. The closely related work of Happy [7] is dependent on Haar classifiers for eye and mouth detection. The Haar-based classifiers are always not dependable and give poor detection rates. Gabor feature-based work of Vukadinovic and Pantic [15] though covers the entire texture information, it generates huge feature vector for processing. Therefore, a learning-free approach for landmark point is investigated and presented in the following sections.

1.2 Materials and Methods

1.2.1 Materials

This research is aimed at automatic pain estimation of patients from facial images. The McMaster University and University of Northern British Columbia have made a part of database UNBC Pain Archive [10] available online which contains images of 25 individuals suffering from shoulder pain. These images are taken from video sequences and annotated by the individual about the level of pain experienced by them. Images are captured in set standard environment. Algorithms are computed with OpenCV 3.1.0 in C++ on Xcode.

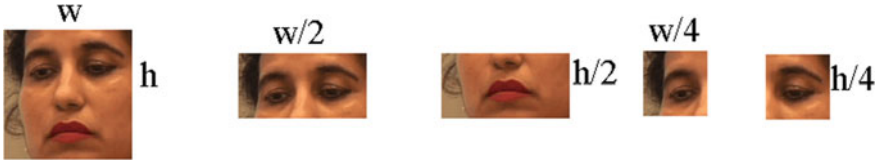


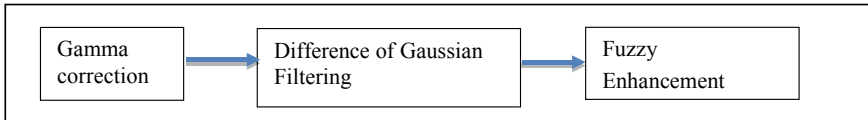
Fig. 1.1 Face detection and selection of ROI

1.2.2 Proposed Methodology

The problem of landmark point detection can be approached by analyzing the histogram projections, generating contrast images, and looking for largest connected component at the center of the related ROI. The proposed algorithm follows the above-mentioned approach.

1.2.2.1 Preprocessing

Images are captured in varied settings with varying illumination; hence, a preprocessing step is mandatory for precise detection of landmark points. The proposed algorithm works on images which have been preprocessed with a chain of image enhancement techniques as shown below.



1.2.2.2 Face Detection

The proposed algorithm is utilized for Viola–Jones face detection [8]. It returns the face region in a rectangular bounded box. By understanding the anatomy of human face, coarse ROIs are selected and the facial image is divided into upper half and bottom half. The upper half of face is further subdivided into right and left as shown in Fig. 1.1.

1.2.2.3 Eye Center Detection

The eye center is one of the first points to be detected. The accurate detection of this point is one of the prominent steps as the success of this detection is responsible for eyebrow corner detection. The eye centers are also used to remove in-plane head

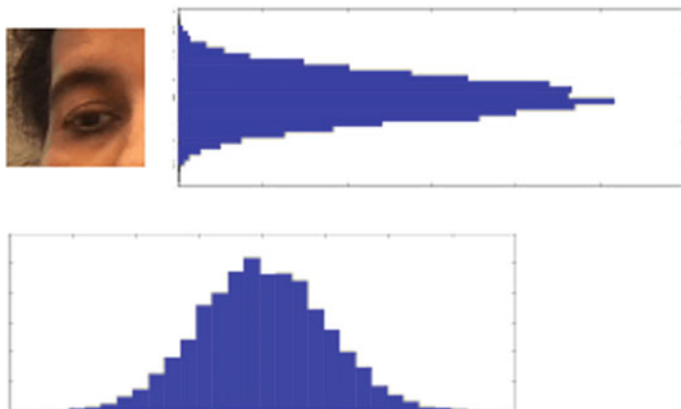


Fig. 1.2 Vertical and horizontal histogram of eye ROI

rotation. The location of eye centers in the coarse ROI is detected by analyzing vertical histogram (pixel-wise difference along the rows and summing each difference) and horizontal histogram (pixel-wise difference along the columns and summing each difference). The peak of vertical histogram gives y coordinate, whereas peak of horizontal histogram gives x coordinate [15] (Fig. 1.2).

1.2.2.4 Eyebrow Detection

The eye centers serve as seed point for eyebrow corner detection; by human knowledge, eyebrows exist in the region above eyes. Coordinates of eye centers enable for selection for eyebrows [11]. Steps for eyebrow corner detection are as follows:

Apply Gaussian blur to the right eyebrow ROI with a kernel of size (3, 3) and standard deviation 1.

Obtain the Sobel edge detected image Grad_y in the y direction on the smoothed image.

Apply Otsu's threshold on the gradient image to get edge map E_y . Second-order differential of intensities in y direction produces double edges with positive sign for transition between dark region and white region and vice versa. Hence, edge map E_y is divided into signed edge map E_{y+} and E_{y-} such that they contain the lower and upper edges of the eyebrow simultaneously.

$$E_{y-}(x, y) = 255 \quad \text{if } \text{Grad}_y(x, y) < 0 \wedge E_y(x, y) = 255 \quad (1.1)$$

$$E_{y+}(x, y) = 255 \quad \text{if } \text{Grad}_y(x, y) > 0 \wedge E_y(x, y) = 255 \quad (1.2)$$

Image E_{y-} is divided into overlapping horizontal bins of bandwidth Δ_T^{\max} * height of the face, which is maximum thickness of eyebrow determined empirically.

Each bin is taken individually, and pixel values are summed up to determine the most distinct edges. Non-maximal suppression function is applied to determine the bin which contains the upper edge of eyebrow as the bins are overlapping. The bins where summation is greater than the threshold as shown in Eq. 1.3 are considered for further processing. $\Delta_l * \text{width of the face}$, which is the average length of eyebrow determined empirically as shown in Eq. 1.3. Δ_l is the in between

$$\sum_{i=0}^n E_{y-}(b_n) \geq 255 * \Delta_l * \text{width of the face}/2 \tag{1.3}$$

The bins satisfying the threshold contain the prominent edges. Let there be B such bins; in each bin, the connected component with highest area is determined. Area of all the highest connected components among all the B bins is calculated. The bin with the highest connected component area is determined as the bin with the upper edge of the eyebrow. The above steps are repeated with E_{y-} to determine lower edge of the eyebrow as shown in Eq. 1.4.

$$\sum_{i=0}^n E_{y+}(b_n) \geq 255 * \Delta_l * \text{width of the face}/2 \tag{1.4}$$

The entire process is repeated for left eyebrow ROI (Figs. 1.3, 1.4, 1.5, and 1.6).

Fig. 1.3 Maximum length and maximum thickness of eyebrow in comparison with w and h

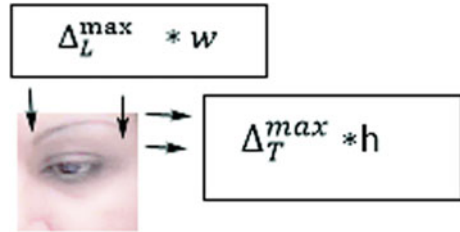
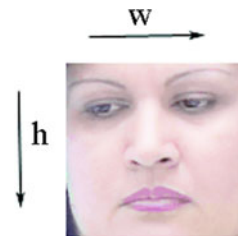


Fig. 1.4 Width w and height h of detected face



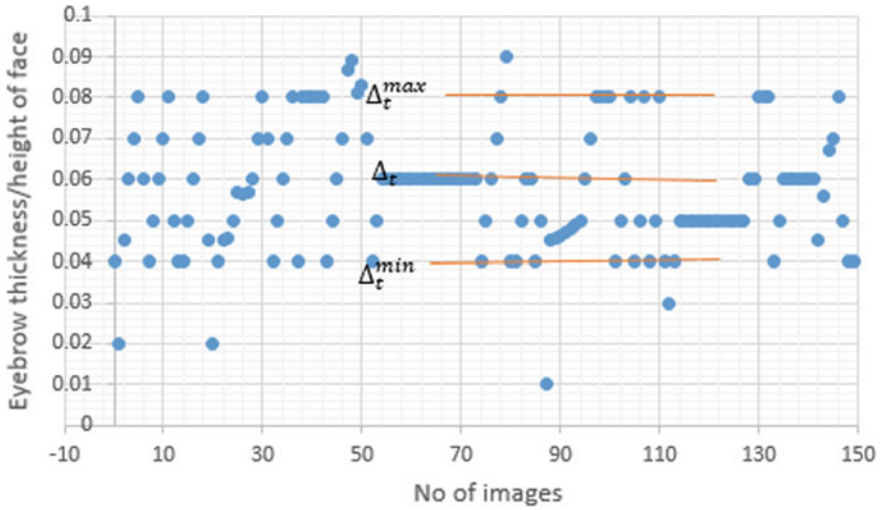


Fig. 1.5 Graph depicting eyebrow thickness to height of detected face over 150 images

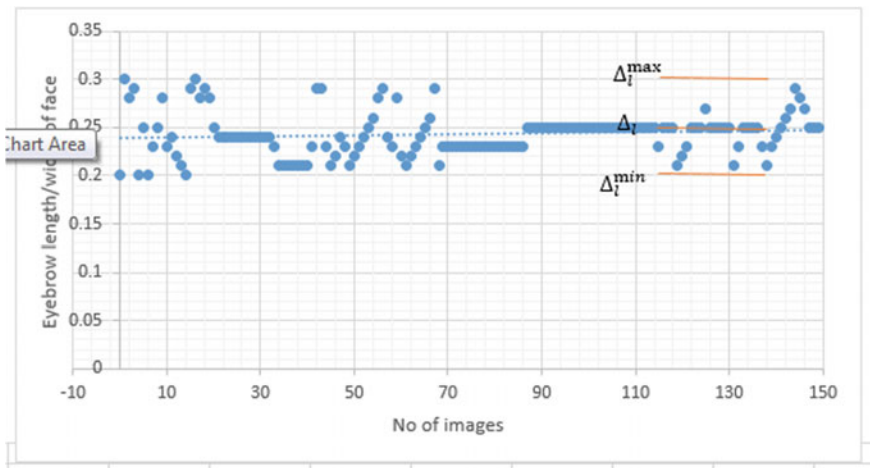


Fig. 1.6 Graph depicting length of eyebrow to width of detected face over 150 images

1.2.2.5 Lip Corner Detection

Lips are located in the lower half of the face, and hence, it is chosen as ROI for the purpose. The algorithm is as follows:

Obtain the contrast image $im_c(i, j)$ from the input $roi_{lips}(i, j)$ image, i.e., average difference between pixels in a $2 * 2$ region.

$$im_c(i, j) = [(roi_{lips}(i, j) - roi_{lips}(i, j + 1)) + (roi_{lips}(i, j) - roi_{lips}(i + 1, j))]$$

$$+(\text{roi}_{\text{lips}}(i, j) - \text{roi}_{\text{lips}}(i+, j))]/3 \quad (1.5)$$

Subtract the contrast image $\text{im}_c(i, j)$ from input image $\text{roi}_{\text{lips}}(i, j)$ to obtain difference image $\text{diff}(i, j)$.

Obtain the compliment image $\text{im}_{\text{comp}}(i, j)$ from $\text{diff}(i, j)$

$$\text{im}_{\text{comp}}(i, j) = 255 - \text{diff}(i, j) \quad (1.6)$$

Lip corners have the highest contrast; to locate the left lip corner, each column from the left of the compliment image to the middle is examined. In each column, we take the highest intensity and compare it to a threshold. If the contrast of any such pixel is greater than threshold, that particular pixel is considered as left lip corner.

Above step is repeated for right lip corner by searching the compliment image from the rightmost column. Threshold is determined by examining the histogram of an image. It is set as the average between highest peak and last peak.

1.3 Performance Metrics

Performance evaluation of the eye centers and lip corners is carried out by computing the Euclidean distance between the points detected by algorithm and points manually marked. The Euclidean distance is the measure of pixel separation between points. To normalize, Euclidean distance is divided by the total number of pixels in an image which gives the error rate.

$$E_d = \text{sqrt}((x_{\text{gt}} - x_d)^2 + (y_{\text{gt}} - y_d)^2) \quad (1.7)$$

$$E_{\text{dn}} = \frac{E_d}{\text{total number of image pixels}} \quad (1.8)$$

where

- E_d Euclidean distance
- $(x_{\text{gt}}, y_{\text{gt}})$ x and y coordinates of ground truth
- (x_d, y_d) x and y coordinates of detected points
- E_{dn} Normalized Euclidean distance

The proposed algorithm for eyebrow detection bounds a rectangle around the region where the eyebrow is detected. A rectangle is manually marked around the eyebrow to generate the ground truth. The number of pixels which overlap with the ground truth is taken as true positive. The number of pixels which overlap in the non-eyebrow region in the ground truth is taken as true negative, and the number of pixels where the ground truth detects an eyebrow pixel and does not detect bounding box is taken as false negative and vice versa for false positive. Accuracy, precision, and recall are computed as shown in Eqs. 1.9–1.11.

$$\text{Accuracy} = \frac{T_p + T_n}{T_p + T_n + F_p + F_n} \quad (1.9)$$

$$\text{Precision} = \frac{T_p}{T_p + F_p} \quad (1.10)$$

$$\text{Recall} = \frac{T_p}{T_p + F_n} \quad (1.11)$$

T_p Number of eyebrow pixels correctly detected

T_n Number of non-eyebrow pixels correctly detected

F_n Number of eyebrow pixels which are not detected

F_p Number of non-eyebrow pixels which are falsely detected as eyebrow.

1.4 Results

Detailed experimentation of the proposed methodology was done on the UNBC Pain Archive. The proposed algorithm was tested on 250 images of twenty-five individuals of varying age, gender, and race suffering from shoulder pain. The images were carefully selected to exhibit variation in pain intensity, head pose, eye state, facial hair, spectacles, and occlusion of eyebrow by hair. The preprocessed images were given to the face detector module, which uses Viola–Jones algorithm for detection and approximates the face bounded by a rectangle. Detected images are divided into top half and bottom half. Top half is further divided into top left half and top right half which are subsequently processed to detect the eyebrow and eye centers.

1.4.1 Eye Centers

Eye centers were localized by calculating the horizontal and vertical projections of the eye ROI; by analyzing the respective histograms, the coordinates for left eye of image a in Fig. 1.7 were found to be (192, 132) and for right eye (254, 134); similarly for image b, the coordinates were (104, 95) and (152, 99). For validating the detected points, eye centers were marked manually. Euclidean distance between the marked points and detected points was calculated. Euclidean distance was normalized by the total number of pixels in the image to decide the error rate, which was found to be 0. Eye center algorithm projected 100% detection rate for both the eyes.

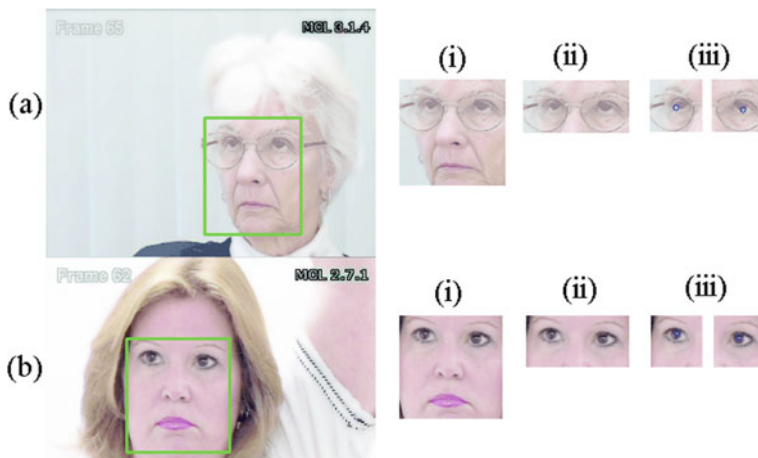


Fig. 1.7 Eye center results

1.4.2 Eyebrows

Eyebrows are located on the upper half of the face; there is a distinct change in intensity in y direction while traversing through the eyebrow. Second-order differential of intensity produces double edges. Otsu thresholding of the edge detected image retains only desired edges, and obstacle by spectacles is avoided. Upper edge of the eyebrow is the intensity transition from high to low which produces negative values for second-order differential; similarly, lower edges produce positive. This approach works efficiently for facial images where the eyebrow intensity is not too similar to skin intensity. Since only y direction edges are considered, partial occlusion by hair is vanquished.

Figure 1.8 (i) is the ROI for eyebrow on which Sobel filter is applied to get image, (ii) which is Otsu thresholded. Image (IV), i.e., E_{y+} contains positive edges, and image (v), i.e., E_{y-} contains negative edges; both the images are divided into overlapping horizontal bins with height equal to average thickness of eyebrow. The bins with summation of pixels greater than one by fourth of width of face are considered.

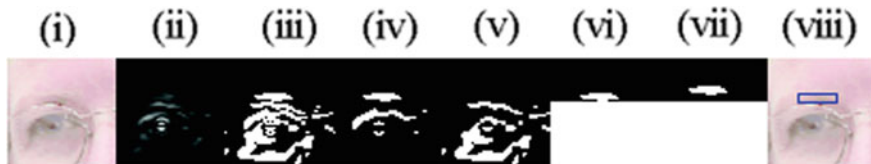


Fig. 1.8 (i) Left eyebrow ROI, (ii) Sobel edge detected image, (iii) Otsu thresholded image, (iv) E_y negative, (v) E_y plus, (vi) upper eyebrow edge bin, (vii) lower eyebrow edge bin, (viii) bounded eyebrow

This helps picking up eyebrows of smaller length. Eighteen such bins were obtained for positive edges, and 30 bins were obtained for negative edges. First five bins are analyzed as eyebrow exists in the upper region of ROI. Bin0 of E_{y+} and Bin0 of E_{y-} contain the largest connected component. A rectangular bounding box is drawn around the region using coordinates of both the connected components which are $[x = 94, y = 93, \text{width} = 18, \text{height} = 3]$. The proposed algorithm yielded 99.89% accuracy, for both the eyebrows for 250 images. Misdetection happens in cases when the intensity of eyebrow and skin is too similar, wrinkles are too strong on the forehead and produce strong edges, and eye edge is stronger than lower eyebrow edge (Fig. 1.9).



Fig. 1.9 Eyebrow detection results

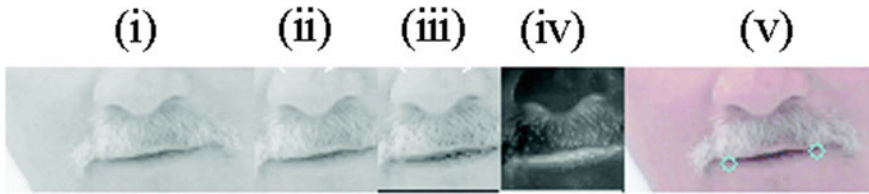


Fig. 1.10 (i) Mouth image, (ii) image ROI, (iii) contrast image, (iv) difference image, (v) compliment image, (vi) lip corners detected image

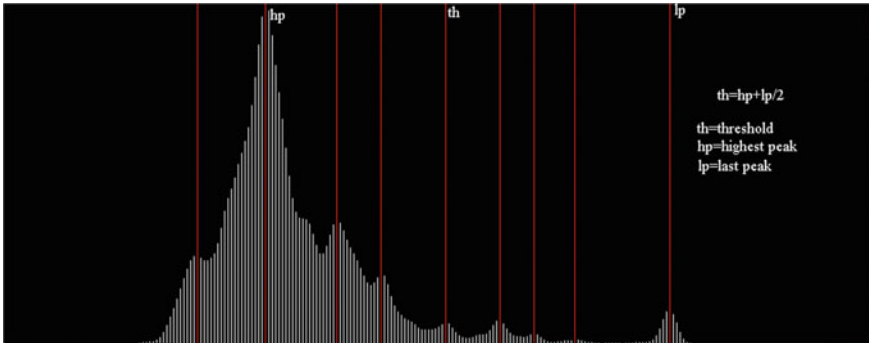


Fig. 1.11 Histogram marked with highest peak and last peak to select the threshold

1.4.3 Lip Corners

Understanding of human facial anatomy, the ROI for mouth was segmented in the lower half of the face. Contrast in the lip corner detection algorithm is the average difference in a $2 * 2$ region.

Figure 1.10 (ii) shows the contrast image of the mouth, (iii) is the image obtained after subtracting contrast image from the ROI, and (iv) shows the compliment of the difference image. It can be seen that the lip corners have highest contrast. The threshold is set as 136 average between highest peak at 77 in the histogram and last peak at 196. The coordinates of the lip corners were found to be (41, 38) and (76, 33). Lip corner detection algorithm projected 100% accuracy for both points (Figs. 1.11 and 1.12).

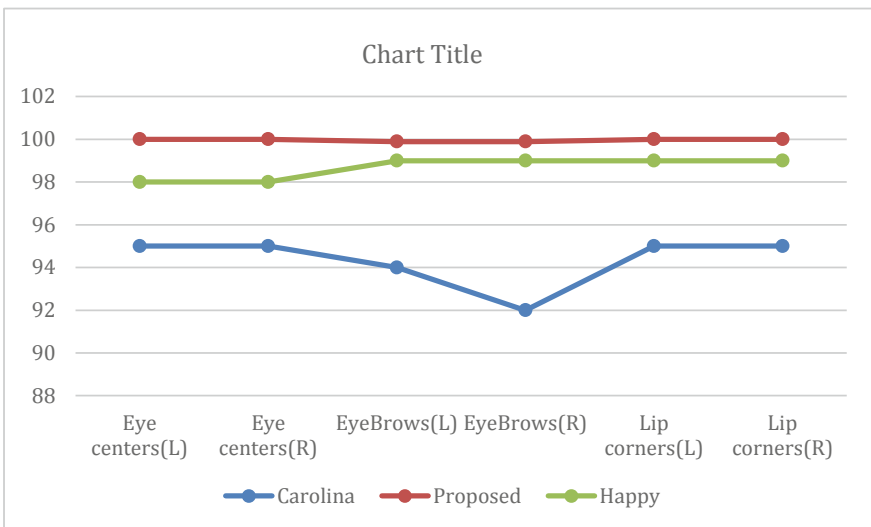
1.5 Discussion

Accurate pain estimation from facial images is significant contribution to patients who are unable to communicate their level of pain. Estimation of vital points on the face is the preliminary work in that direction. The proposed methodology is



Fig. 1.12 Lip corner result

computationally inexpensive, learning free, and not specific to any model. It is based on the idea that intensity variation is consistent in face, irrespective of geometry of the face. In comparison with Silva et al. [12], Happy [7], the proposed algorithm represented better detection rate for UNBC Pain Archive. It particularly performs extremely well for eye detection and eyebrow detection. The proposed algorithm for eyebrow detection uses vertical edge information which represents change in intensity, which will be uniform for human faces.



1.6 Conclusion

A learning-free facial landmark detection algorithm is proposed with state-of-the-art adaptability on frontal faces of varied contrast, gender, and race. The algorithm is robust in detection in spite of partial occlusion by facial hair, wrinkles, and scar. In-plane head rotation can be handled by the algorithm by using the eye coordinates to align the face. Precise detection of iris center, lip, and eyebrow corners has been achieved. Various types of features like gray-level intensity and histogram-of-gradient texture will be explored for deep learning, around the extracted facial points for classification of action units. In addition to this, these points can be tracked over a period of time to check for driver drowsiness, attentiveness of students in class, and interest of shoppers in a store.

References

1. Belhumeur, P.J.: Localizing parts of faces using a consensus of exemplars. *IEEE Trans. Pattern Anal. Mach. Intell.* **35**(12), 2930–2940 (2013)
2. Çeliktutan, O.S.: A comparative study of face landmarking techniques. *EURASIP J. Image Video Process.* **2013**, 1 (2013)
3. Cootes, T.F., Edward, G., Taylor, C.J.: Comparing active shape models with active appearance models. In: *Proceedings of the British Machine Vision Conference* (pp. 173–182). BMVA Press, London (1999)
4. Dey, T. (2013). Detection of facial landmarks of North Eastern Indian People. *Int. J. Inform. Comput. Technol.* 953–962
5. Ding, L., Martinez, A.M.: Features versus context: an approach for precise and detailed detection and delineation of faces and facial features. *IEEE Trans. Pattern Anal. Mach. Intell.* **32**(11), 2022–2038 (2010)
6. Ekman, P., Rosenberg, E.L.: *What the Face Reveals: Basic and Applied Studies of Spontaneous Expression Using the Facial Action Coding System (FACS)*. Oxford University Press, Oxford (1997)
7. Happy, S.L.: Automatic facial expression recognition using features of salient facial patches. *IEEE Trans. Affect. Comput.* **6**(1), 1–12 (2015)
8. Jones, M., Viola, P.: Rapid object detection using a boosted cascade of simple features. In: *Proceedings of the 2001 IEEE Computer Society* (vol. 1, pp. 137–154). Kluwer Academic Publishers, Dordrecht (2001)
9. Lee, T., Park, S.-K., Park, M.: An effective method for detecting facial features and face in human-robot interaction. *Inf. Sci.* 3166–3189 (2006)
10. Lucy, P.C.: Painful data: the UNBC-McMaster shoulder pain expression archive database. In: *IEEE International Conference on Automatic Face and Gesture Recognition* (2011)
11. Sathyanarayana, S., et al.: A compute-efficient algorithm for robust eyebrow detection. In: *The IEEE Conference on Computer Vision and Pattern Recognition (CVPR) Workshops* (2014)
12. Silva, C., Schnitman, L., Luciano, O.: Detection of facial landmarks using local-based information. In: *The 19th edition of the Brazilian Conference on Automation—CBA 201* (2012)
13. Torre, M. H.: Learning image alignment without local minima for face detection and tracking. In: *Proceedings of IEEE International conference on Automatic Face and Gesture Recognition* (pp. 1–7). IEEE (2008)
14. Valstar, M.F.: Facial point detection using boosted regression and graph models. In: *CVPR* (pp. 2729–2736). IEEE Computer Society (2010)

15. Vukadinovic, D., Pantic, M.: Fully automatic facial feature point detection using gabor feature based boosted classifiers. In: IEEE International Conference on Systems, Man and Cybernetics, Waikoloa, HI, USA (vol. 2, pp. 1692–1698). IEEE (2005)
16. Yun, T., Ling, G.: Automatic landmark point detection and tracking for human facial expressions. EURASIP J. Image Video Process. (2013)
17. Zhu, X., Ramanan, D.: Face detection, pose estimation, and landmark localization in the wild. In: 2012 IEEE Conference on Computer Vision and Pattern Recognition (CVPR), Providence, RI, USA (pp. 2879–2886). IEEE (2012)

Chapter 2

Statistical Approach to Detect Alzheimer's Disease and Autism Spectrum-Related Neurological Disorder Using Machine Learning



Akhilesh Kumar Sharma  and Devesh K. Shrivastav

Abstract Cases of mental disorders are not very uncommon to find, especially when the pace of life is rapidly increasing. People neither have time to eat healthy and maintain a properly balanced life cycle nor to give rest to their mind and body. Thus, the occurrences of cases of mental disorders are increasing at an epidemic rate. 5% of persons who are 18 years above may experience mental illness once in year. This is regardless of the fact that they have any kind of lifestyle, its equivalent to 43.8 million people. This fact becomes more alarming and disturbing when well-trained medical experts are less in numbers to treat such a large number of people. The process of diagnosis and detection of the disorders of such a complex organ is also not an easy and straightforward task. It may often take a lot of time, thus delaying the commencement of the patient's treatment. Proposed model predicts and diagnoses the disease effectively and can help practitioners by reducing diagnosis time. The logistic algorithm achieved the highest percentage 99.16% of prediction on the disease datasets obtained from Kaggle. This research work proposes the technique for an early prediction and performance-based technique.

2.1 Introduction

Mental disorders can be thought of as a wide range of conditions caused of wrong brain functions which can affect behavior of a person, their mood, and the ability to think, talk, interpret, and may even impair the person physically. These conditions can be divided into eight major classes of mental diseases, like the depression, neuro anxiety disorders, bipolar disorder, neuro brain dementia, brain attention deficit, neuro hyperactivity disorder, schizophrenia, neuro obsessive–compulsive disorder, autism and posttraumatic stress disorder, etc. [6]. Of all these classes of mental

A. K. Sharma (✉) · D. K. Shrivastav
SCIT, Manipal University Jaipur, Jaipur, India
e-mail: akhileshsham@gmail.com

D. K. Shrivastav
e-mail: devesh988@yahoo.com

© The Editor(s) (if applicable) and The Author(s), under exclusive license to Springer Nature Singapore Pte Ltd. 2021

Y.-D. Zhang et al. (eds.), *Smart Trends in Computing and Communications: Proceedings of SmartCom 2020*, Smart Innovation, Systems and Technologies 182,
https://doi.org/10.1007/978-981-15-5224-3_2

disorders, dementia, autism, and schizophrenia require laboratory tests for diagnosis [1]. Others are determined based on patient history and behavior and may or may not have a pattern. Dementia is a group of symptoms that mainly affect three parts of the brain that are responsible for language, memory, and decision making. Dementia includes Alzheimer's disease (shrinkage of brain tissues), Parkinson's disease (nerve cell damage), Creutzfeldt–Jakob's disease (abnormal forms of normal cellular proteins), Huntington's disease (breakdown of nerve cells prematurely), etc. Schizophrenia impairs a person's thinking, behavior, feelings, etc. Autism is a neuro-developmental disorder. Developing a machine learning model to detect the presence of these diseases will help bridge the gap between diagnosis and treatment. This research aims at finding out the most suitable and accurate machine learning algorithm to detect ASD and Alzheimer's disease.

2.2 Literature Review

Machine learning is a field of exponentially increasing research and use. It is something that can be applied to any field of life to bring about intelligent automation. It is very common to find various artificial intelligence and machine learning algorithms to the field of medical sciences to distribute or reduce the work load, make testing faster, treating more patients more efficiently [2], reducing the chances of error in diagnosis and even in conducting operations. Automation and, more specifically, artificial intelligence are slowly taking over every field one could possibly imagine leading the world to the "HI-TECH FUTURE" we always imagined as children [1].

Detection of various mental disorders [3] using machine learning is one of the most important and sought-after field of research and study in these advancing times. These detection techniques are more accurate for some than the others. Diseases which require some or the other form of laboratory tests (like EEG, MRI, f-MRI) are more easier to detect and predict using machines than the other more symptom-related disorders such as depression and PTSD.

A very common and successful algorithm applied in these researches belongs to machine learning in accurately predicting autism and Alzheimer's disease [4]. Some of them are clustering algorithms [5, 6] (for unsupervised data), SVM, regression algorithms, and artificial neural networks [7, 8]. The logistic regression and the affected accuracy can be measured by logistic regression presented in the study [10–13]. This study intended to determine if regression models [9, 10] can be applied to classification problems and what would be the results of this, as well as how accurately the classification algorithms logistic regression and K -nearest neighbors can predict autism in patients.

2.3 Methodology

This research follows application of algorithms on the different datasets, the dataset of working of the brain, its different parts and what function they are responsible for performing various human tasks, what causes various mental disorders. Various tools that are used to measure the intensity of these disorders and course of action should be taken for each kind of disorder are studied and utilized. The preprocessing of the datasets has been done, and the algorithms have been selected. Finally, compare the results that were inferred while applying these algorithms to determine which model is best for our prediction.

The algorithms were applied on the selected datasets. Datasets were obtained from Kaggle. The datasets have been cleaned and preprocessed to be made fit for applying on various machine learning algorithms. The algorithms were first applied to the dataset for the prediction of Alzheimer's disease. The combination of algorithms like "linear regression" and "multiple linear regression" was applied to the Alzheimer's disease dataset. The multiple attributes to the regression line were exploited, and different results were studied. Then, "polynomial regression" was applied. After the regression models, the data were fitted into classification models. The two classification models applied were "logistic regression" and "*K*-nearest neighbors." At the end, the accuracy of all the five models was compared to determine which model is best for the detection of autism in patients.

The same procedure was followed for the other datasets to predict ASD in patients.

1. Simple linear regression: It is a statistical method that allows learner to summarize and study the relationships between continuous and quantitative variables:

Here, variable x is known as predictor and the other is known as response variable. The data are modeled on a straight line.

The equation for simple linear regression is:

$$Y = b_0 + b_1X$$

where

Y is known as predicted value.

b_0 is known as estimate of the regression intercept value

b_1 is regression slope, and

x is value of observation.

2. Mean Square Error

The MSE shows how close the regression line is to the set of points. The distances from the points to the regression line and squaring them would be calculated in it. The squaring will remove any negative signs in it.

3. Score or R^2 Value

Used to show how close the data points are with fitted regression line. It can be mathematically described using the formula:

$$R * R = \frac{\sum(Y_p - Y')}{\sum(Y - Y')}$$

where

Y_p distance of predicted point from regression line.

Y' is the mean distance

Y distance of actual point from regression line.

4. Multiple Linear Regression

MLR will explain the relationship in one continuous dependent variable and two or more independent variables.

The equation is given by:

$$Y = b_0 + b_1X_1 + b_2X_2 + b_3X_3 + \dots + \text{error}$$

where, $b_0 + b_1X_1 + b_2X_2 + \dots$ are linear parameters.

5. Polynomial Regression

It is based on relationship in independent variable x and dependent variable y , which is modeled as n th degree polynomial in x . It can be observed that polynomial regression fits a nonlinear relationship with value of x , corresponding conditional mean of y .

$$Y = b_0 + b_1X_1 + b_2X_2^2 + b_3X_3^3 + \dots + b_nX_n^n$$

6. Logistic Regression

LR is for classification, when one needs to decide whether something lies in one class of things or another. If one uses linear regression for this problem, then there is a need to set up threshold based on which classification can be done. Linear regression is unbounded; thus, it is not suitable for such kind of predictions. Now emerged logistic regression. Their value strictly ranges from 0 to 1.

$$\text{Logit}(p) = \log\left(\frac{p(y=1)}{1-p(y=1)}\right) = \beta_0 + \beta_1 \cdot x_{i2} + \beta_2 \cdot x_{i2} + \dots + \beta_P \cdot x_m$$

Binary logistic regression, multinomial logistic regression, and ordinal logistic regression: These models are used to predict the output in various modes; it can be used to classify into two classes or categories.

7. *K*-Nearest Neighbors

KNN is used as predictive model in this study. *K* refers to the number of neighbors we are referring to while classifying the data points. With increasing *K*, we get smoother, more defined boundaries across different classifications.

$$y = \frac{1}{K} \sum_{l=1}^K y_l$$

Any distance metric can be used while calculating the nearest neighbors. KNN does not work very well with large number of input points as it takes a lot of time in the training phase.

2.4 Result

Dataset: Alzheimer’s disease dataset: The dataset is downloaded from Kaggle. The select models are used to test the time; accuracy of dataset ranges from 30 to 75%. The key features across these five models were kept the same. These features include years of education, socioeconomic status, results of mini-mental state examination, clinical dementia rating, normalized brain volume, total intracranial volume, and ATLAS scaling factor. In this research work, a total of 373 data entries of numerical results of patients took MRI scans and the mini-mental state examination (Table 2.1).

Model 1: Multiple Linear Regression

The missing values were imputed with mean, median, and mode separately and then fitted into the regression model to compare accuracies of prediction,

MLR: $Y = w_0 + w_1x_1 + w_2x_2$

Accuracy = 68.65%.

Table 2.1 Model with statistical parameter estimates

Algorithm	Mean	Median	Mode (most frequent)
Multiple linear regression	37.475	37.402	37.391
Polynomial regression	63.61	62.95	62.88
Logistic regression	76.16	75.16	75.15

Table 2.2 Model with K value estimates accuracy comparison

K value	Accuracy (in percentage)
3	45.33
5	45.33
7	48
9	45.33

Model 2: Polynomial Regression

Again, upon comparing the dataset with imputed values as mean, median, and mode separately, in terms of accuracy on the model (degree = 2), the following results were obtained: Polynomial regression:

$$y = w_0 + w_1x + w_2x^2 + w_3x^3$$

Mean = 63.61%, median = 62.95%, mode = 62.88%, accuracy 83.06%, 96.26%.

Model 3: Logistic Regression

The results obtained were as follows:

Mean = 76.16%, median = 75.16%, mode = 75.15%, accuracy = 99.16%

Model 4: K -Nearest Neighbors

The dataset was fitted onto the model with different sizes of number of neighbors each time to compare how many neighbors need to be considered to get the most accurate classification. The accuracy calculated through the following class label formulates (Tables 2.2 and 2.3):

All models will be utilized with testing, time, accuracy of the dataset, the accuracies ranging from 68 to 99%. The key features across these four models were kept the same. The features include the feature scores obtained for the patients, gender of the child, ethnicity, family history of ASD, and age (in months).

This research work used a total of 705 data entries of various patients with their respective class as ASD status (autistic or not). All the data entries are kept in csv format and used for this study (Tables 2.4 and 2.5).

The accuracy of the applied models has been studied and compared with each other, and the estimated accuracy comparison is listed in Fig. 2.1. The comparative chart shown in Fig. 2.1 displays the logistic regression-based model that estimated highest accuracy of 99.16%, which is maximum among all.

Table 2.3 Model accuracy formula

		Predicted class	
		C_1	C_2
Actual class	C_1	True positives	False negatives
	C_2	False positives	True negatives

Table 2.4 Comparison of model accuracy

Algorithm	Accuracy (in percentage)
Multiple linear regression	68.65
Polynomial regression	96.25
Logistic regression	99.16
KNN	97.57

Table 2.5 Model accuracy of KNN with varying K values

K value	Accuracy (in percentage)
3	97.57
5	96.10
7	97.27
9	97.10

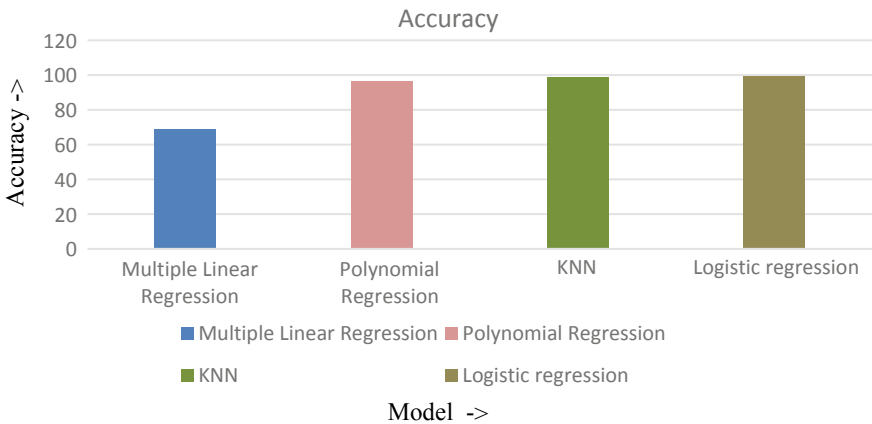


Fig. 2.1 Accuracy for various models

2.5 Conclusion

It was observed that the classification model gave more accurate results than the regression models for both the given datasets. Classification models should be preferred. Also, for our datasets, it was also noticed that filling the missing values with mean values gave the highest accuracy on selected models. Polynomial regression also gave decently accurate predictions; however, polynomial regression is very prone to overfitting; thus, it is not preferred for such kind of classification problems. Therefore, for both the given datasets (detection of Alzheimer’s disease and detection of autism in patients), logistic regression is the best model for classification.

2.6 Future Work

This research work discusses machine learning in the medical domain is helping the world to innovate and help society in many ways. Its contribution to the medical society can continue to save many lives. It can be used to predict many other diseases related to the brain, the heart, etc., which require laboratory tests. Data can be collected directly from research laboratories to improve the consistency of prediction. Pictorial data can also be used to directly predict results from MRI scans, EEG scans, ultrasound scans, as well as ECG scans. The IoT devices can be used to capture the real-time health statistics and can be used to predict and to perform real-time alerts systems as well.

References

1. Tariq, Q., et al.: Mobile detection of autism through machine learning on home video: a development and prospective validation study. *PLoS Med.* 150–110 (2018)
2. Horikawa, H., Suguimoto, S.P., Musumari, P.M., Techarivichienet, T.: Development of a prediction model for child maltreatment recurrence in Japan: a historical cohort study using data from a Child Guidance Center. *Child Abuse Neglect* **59**, 55–65 (2017)
3. Setoh, P., Marschik, P.B., Einspieler, C., et al.: Autism spectrum disorder and early motor abnormalities: connected or coincidental companions? *Res. Dev. Disabil.* **60**, 13–15 (2018)
4. Usta, M.B., Karabekiroglu, K., et.al.: Use of machine learning methods in prediction of short-term outcome in autism spectrum disorders. *Psych. Clin. Psychopharmacol.* (2018)
5. Sharma, A.K., Ramani, P.: Rigorous data analysis and performance evaluation of Indian classical raga using RapidMiner. In: Pant, M., Ray, K., Sharma, T., Rawat, S., Bandyopadhyay, A. (eds.) *Soft Computing: Theories and Applications. Advances in Intelligent Systems and Computing*, vol. 583. Springer, Singapore (2018)
6. Masri, R.Y., Jani, H.M.: Employing artificial intelligence techniques in mental health, diagnostic expert system. In: 2015 International Conference on Computer & Information Science (ICIS), vol. 1, pp. 495–499, 12–14 June 2015
7. Yun, J., Rong, C., Ke, X., Kangkang, C., et.al.: Predictive models of autism spectrum disorder based on brain regional cortical thickness. *NeuroImage* **50**(2), 589–599 (2010)
8. Garg, D., Sharma, A.K.: Prediction and analysis of liver patient data using linear regression technique. In: Reddy Edla, D., Lingra, P., Venkatanareshbabu, K. (eds.) *Advances in Machine Learning and Data Science. Advances in Intelligent Systems and Computing*, vol. 705. Springer, Singapore (2018)
9. Shappot, S.J., Gorgees, H.M.: Use of logistic regression approach to determine the effective factors causing renal failure disease. *Ibn AL-Haitham J. Pure Appl. Sci.* **31**(3), 143–150 (2018)
10. Ramani, P., Pradhan, N., Sharma, A.K.: Classification algorithms to predict heart diseases—a survey. In: Gupta, M., Konar, D., Bhattacharyya, S., Biswas, S. (eds.) *Computer Vision and Machine Intelligence in Medical Image Analysis. Advances in Intelligent Systems and Computing*, vol. 992. Springer, Singapore (2020)
11. Kaye, J.A., Melero-Montes, M., Jick, H.: Mumps, measles and rubella vaccine and the incidence of autism recorded by general practitioners: a time trend analysis. *BMJ* **322**, 460–463 (2001)
12. Mehra, C., Sil, A., Hedderly, T., Kyriakopoulos, M., Lim, M., Turnbull, J., Happe, F., Baird, G., Absoud, M.: Childhood disintegrative disorder and autism spectrum disorder: a systematic review. *Develop. Med. Child Neurol.* **61**(5), 523–534 (2018)
13. Müller, R.-A., Fishman, I.: Brain connectivity and neuroimaging of social networks in autism. *Trends Cogn. Sci.* (2018). <https://doi.org/10.1016/j.tics.2018.09.008>

Chapter 3

The Development and Gap of Chinese and American Open Access Journals: From the Perspective of Network Influence



Danyang Li, Xinlai Li, and Biying Gao

Abstract It is a new perspective and opportunity for evaluation of journal influence based on Altmetrics in the new environment and situation. The emergence of Altmetrics means that the “five metrics” have developed another stage, indicating that the evaluation of academic achievements in the field of metrology has been extended to online media platforms and network communication, which also marks a new platform and tool for measuring the academic influence of journals. The paper conducts the principal component analysis using SPSS, builds monophyletic data model through thorough comparison on network influence of open access journals between China and the USA, and comments on the result of the evaluation, discusses the differences in the aspects based on the results of principal component analysis. In order to enhance the international academic influence of Chinese open access journals, it is of practical significance for China to put forward some corresponding improvement suggestions according to the shortcomings.

3.1 Introduction

Open access journals are a research field that has emerged in recent years. Its prototype is the electronic journal first proposed in 1976, formally proposed by the open society institute of America (OSI) released in December 2001. Since the middle and late 1990s, especially in the new century, the importance of open access journals has been widely concerned. Scholars, scientific research institutes, publishers, and library practitioners are closely following the trend, especially in the countries that initiated the open access movement abroad, in order to improve the degree of open access in their own countries. With the development of open access movement, it has become a worldwide trend. The number of open access journals is increasing, and

D. Li (✉) · X. Li

Research Center for Chinese Science Evaluation, Wuhan University, 430072 Wuhan, China
e-mail: whusimldy@163.com

D. Li · X. Li · B. Gao

School of Information Management, Wuhan University, 430072 Wuhan, China

© The Editor(s) (if applicable) and The Author(s), under exclusive license to Springer Nature Singapore Pte Ltd. 2021

Y.-D. Zhang et al. (eds.), *Smart Trends in Computing and Communications: Proceedings of SmartCom 2020*, Smart Innovation, Systems and Technologies 182,

https://doi.org/10.1007/978-981-15-5224-3_3

the scope of subject coverage is expanding. Open access journals are an inevitable trend of globalization and the future direction of academic communication.

According to statistics, the number of papers published in open access journals in China has exceeded that of the USA since 2015 [1]. The output of SCI papers in China ranks the second in the world, which shows that the quantity and quality of Chinese papers are relatively competitive. However, only 107 open access journals in China are included in DOAJ, while 1,217 open access journals in Brazil are included. In addition, although the output of SCI papers ranks the second in the world, less than 2% of SCI journals are in the world, and a large number of excellent papers are exported [2]. As can be seen from the above data, Chinese academic circles show a trend of “many papers” and “weak journals.” There is a certain gap between the academic influence of China’s open access journals and that of western developed countries. This paper aims to find out the shortcomings of China’s open access journals through a variety of comparisons between Chinese and American academic influence, so as to improve the international academic influence of China’s open access journals.

Periodical evaluation originated from “core journals” that had relatively concentrated published article volume proposed by Bradford’s law in 1934. The traditional methods of periodical evaluation are qualitative peer review and quantitative citation evaluation. With the development of science and technology and the advent of Web2.0 online communication, the disadvantages of traditional evaluation methods become more and more obvious. At this time, Altmetrics—a new metrology combining the characteristics of online social networks—comes into being. Academic influence of journals is a complex phenomenon involving academic influence, social practice influence, readers, social recognition, and so on. It is a comprehensive effect of an academic journal, which is based on the academic level and characteristics and marked by social credibility and reader recognition [3, 4]. As mentioned by Jinping Zhou in her doctoral dissertation, the academic influence on open access journals is mainly studied from the perspectives of citation measurement index, link measurement index, and social attribute factor [5]. There is no doubt that traditional citation indexes can measure and compare the academic influence of journals. However, the evaluation system of academic influence should be integrated into the network influence caused by website influence and online communication in the network environment with the development of The Times. With the development and popularization of science and technology and the Internet, there are similarities between network citation and traditional citation, so the academic influence of journals should be integrated into the relevant index data of network information metrology. In order to better open sharing, the quality of the website of open access journal greatly influences the academic influence of the journal. With the advent of Web2.0 of online communication, academic influence is not limited to traditional citation and website construction. With the development of Altmetrics and the improvement of relevant tools and indicator systems, the academic impact of online dissemination of open access journals should be included.

3.2 Data and Method

This paper uses principal component analysis to construct a single-source journal evaluation model, and measures and compares the network influence of open access journal based on Altmetrics. The approach adopted is the Altmetrics based on online scientific communication [6], and the data from the relevant data at the journal level provided by Altmetric Explorer [7].

3.2.1 Sample Selection Method

Journal Citation Report (JCR) published by ISI based on WOS is a widely spread and influential tool in the field of journal evaluation. JCR publishes the citation and cited data, the impact factor, the annual index, the cited items, the characteristic value score, and other data of some journals every year. The research topic of this paper is a comparative study of open access journals between Chinese and American; therefore, JCR was selected as the journal data source in this paper, the data of 2016 was selected, the open access check box was checked, the country selected “China mainland,” and customize relevant query indexes and submit the retrieval. A total of 29 search results were obtained, and 28 open access journals were selected as the research samples in China after deleting duplicate data.

Using the same search criteria, 142 records were obtained by selecting “USA” for the country, and 133 results were obtained by deleting records with incomplete information. It is decided to select 28 search results as the same open access journal research samples in the USA in order to compare with China. 133 is the product of 19 and 7, so it was decided to conduct stratified sampling, divide 133 into 7 groups, and then randomly select 4 numbers from each group. The final 28 numbers are 1, 5, 12, 18 and 22, 27, 32, 36 and 42, 43, 48, 49 and 60, 64, 65, 72 and 77, 80, 86, 92 and 98, 105, 107, 112 and 116, 118, 120, 122.

To sum up, this paper selects 28 journals of Chinese open access journals and 28 representatives of American open access journals obtained through stratification and random sampling collected by JCR in 2016. A total of 56 open access journals are selected as research objects.

3.2.2 Data Acquisition Platform

At present, there are three measurement institutions or companies with online academic influence: Altmetric.com, ImpactStory, and Plum Analytics, among which Altmetric.com has the most extensive influence. Altmetric.com was founded to track and analyze the online communications of academic resources, extract the number of mentions of individual academic papers on different social networks and

online media, and combine this data to measure the impact of academic papers. Altmetric.com developed four evaluation products for the service users and analysis function: Altmetric API, Altmetric Badges, Altmetric Explorer, and Altmetric bookmarklets. Altmetric Explorer mainly serves non-profit organizations such as libraries, which is also the acquisition platform of network indicator data in this paper [8].

3.2.3 Data Collection Method

Input the journal ISSN number at Altmetric.com for retrieval. Two of the 56 journals were not queried by ISSN number of JCR, but by ISSN number of DOAJ, namely Nano-Micro Letters (NO. 4) and Canadian Journal of Gastroenterology and Hepatology (NO. 42). In addition, it was found in the query that some journals were special—ISSN numbers were the same, but the journal names were different, such as Progress in Natural science-materials International (JCR), Progress in Natural Science: Materials International (DOAJ), Progress in Natural Science (Altmetric). After the search and verification found that is the same journal, do not distinguish treatment.

Based on the retrieval of data from Altmetric.com, the academic influence of open access journals based on Altmetrics was obtained. In other words, the measurement indexes of network influence evaluation were as follows: News, Blog, Policy, Twitter, Patent, Peer review, Weibo, Facebook, Wikipedia, Google+, LinkedIn, Reddit, Pinterest, F1000, Q&A, and Video. Three journals had no search results, and the names were China Foundry (NO. 27), JOURNAL OF INFRARED AND MILLIMETER WAVES (NO. 28), and the ultimate X (NO. 29), so the remaining 53 journals were used for the comparative study of network influence.

3.3 Results and Discussion

Excluding the three journals that did not collect data, the principal component analysis was carried out on the 16 index data of the network influence of the remaining 53 Chinese and American open access journals, and the indexes that contributed more to the network influence were found out. Due to the large gap in many index data retrieved from the Altmetric Explorer, the data was standardized to avoid adverse effects and facilitate later ranking calculation (see appendix for the original data of network influence). The “min-max normalization” method is used to conduct linear transformation of original data and drop the results into the interval [0, 1]. “Max” is the maximum value of sample data, and “Min” is the minimum value of sample data [9].

Transform the sequence x_1, x_2, \dots, x_n :

$$y_i = \frac{x_i - \min_{1 \leq j \leq n} \{x_j\}}{\max_{1 \leq j \leq n} \{x_j\} - \min_{1 \leq j \leq n} \{x_j\}}$$

The new sequence $y_1, y_2, \dots, y_n \in [0, 1]$ is dimensionless, and data can be considered to undertake normalization processing first when needed.

Open the Excel file with SPSS, and take these 16 indicators as variables for principal component analysis. Firstly, correlation test was performed to decide whether it was suitable for principal component analysis.

The results of correlation test can be seen that almost all of the 16 variables are in a significant bilateral correlation state at the level of 0.01, showing a strong linear relationship, which is suitable for principal component analysis.

In Bartlett’s sphericity test, approximate chi-square is 1205.202, df is 120, and Sig is 0.000, which is suitable for factor analysis. The KMO value is 0.766, and it can be seen from the table of KMO and fit factor analysis that it is suitable for factor analysis.

As can be seen from the first extraction value in Table 3.1, the extraction value of both Policy and Video is lower than 0.6, indicating that the original index is extracted with less information in the common factor, and generally less than 50% of the indicators there is no need to exist. Therefore, considering the accuracy and representativeness of the model, it is decided to delete these two indicators and generate the common factor variance of the remaining 14 network influence measurement indicators.

Table 3.1 Common factor variance of network influence index

Indicators	Original value	Extraction value 1	Extraction value 2
News	1.000	0.779	0.819
Blog	1.000	0.830	0.842
Policy	1.000	0.547	
Twitter	1.000	0.954	0.985
Patent	1.000	0.689	0.690
Peer review	1.000	0.861	0.866
Weibo	1.000	0.873	0.878
Facebook	1.000	0.861	0.886
Wikipedia	1.000	0.705	0.712
Google+	1.000	0.940	0.940
LinkedIn	1.000	0.801	0.803
Reddit	1.000	0.927	0.933
Pinterest	1.000	0.819	0.863
F1000	1.000	0.914	0.919
Q&A	1.000	0.701	0.709
Video	1.000	0.289	

By comparing two extracted values of the common factor variances, it can be seen that the extracted information of each index increases slightly after deleting the indexes that have lost a lot of information. Therefore, it is reasonable to delete the “Policy” and “Video” indicators.

As can be seen from Table 3.2, the eigenvalue of the first component is 8.156, accounting for 58.258% ($8.156/14 * 100\%$) of the total variance of the original 14 variables. The eigenvalue of the second component is 2.433, which explains 17.378% ($2.433/14 * 100\%$) of the total variance of the original 14 variables. The eigenvalue of the third component was 1.255, accounting for 8.963% ($1.255/14 * 100\%$) of the total variance of the original 14 variables, and the cumulative variance contribution rate was 84.600.

As can be seen from Fig. 3.1, there are three components with the eigenvalue greater than 1 among the 14 components. The eigenvalue of principal component 1 is greater than 8, which contributes the most to the interpretation of original variables. The third and subsequent component eigenvalues are small and are ignored here.

The component matrix in Table 3.3 is the core of principal component analysis. As can be seen from Table 3.3, the load values of other variables on the first principal component are all greater than 0.5 except for variables “Pinterest” and “Q&A,” indicating that they are highly correlated with the first principal component. The load values of variables “Wikipedia” and “Q&A” were higher, and the correlation was much higher than other variables for principal component 2. The load value of “Pinterest” is 0.830 for principal component 3, and the correlation with the third principal component is the highest compared with other variables.

The scoring formula of the three principal components can be obtained according to Table 3.4:

$$\begin{aligned}
 F1 &= -0.236\text{News} + 0.131\text{Blog} + 0.206\text{Twitter} \\
 &\quad - 0.031\text{Patent} + 0.057\text{Peerreview} + 0.089\text{Weibo} \\
 &\quad + 0.218\text{Facebook} - 0.129\text{Wikipedia} + 0.110\text{Google}+ \\
 &\quad - 0.021\text{LinkedIn} + 0.104\text{Reddit} - 0.176\text{Pinterest} \\
 &\quad + 0.066\text{F1000} - 0.132\text{Q\&A} \\
 F2 &= -0.079\text{News} + 0.032\text{Blog} + 0.005\text{Twitter} \\
 &\quad + 0.201\text{Patent} + 0.132\text{Peerreview} - 0.141\text{Weibo} \\
 &\quad - 0.074\text{Facebook} + 0.258\text{Wikipedia} - 0.064\text{Google}+ \\
 &\quad + 0.225\text{LinkedIn} - 0.067\text{Reddit} + 0.034\text{Pinterest} \\
 &\quad + 0.176\text{F1000} + 0.276\text{Q\&A} \\
 F3 &= -0.191\text{News} - 0.039\text{Blog} - 0.195\text{Twitter} \\
 &\quad + 0.002\text{Patent} - 0.022\text{Peerreview} + 0.332\text{Weibo} \\
 &\quad - 0.114\text{Facebook} + 0.088\text{Wikipedia} + 0.206\text{Google}+ \\
 &\quad - 0.062\text{LinkedIn} + 0.226\text{Reddit} + 0.639\text{Pinterest} \\
 &\quad - 0.154\text{F1000} + 0.026\text{Q\&A}
 \end{aligned}$$

Table 3.2 Total variance of 14 indicators of network influence

Component	Initial eigenvalues			Extract sum of squares load			Rotate sum of squares load		
	Summation	Variance (%)	Cumulation (%)	Summation	Variance (%)	Cumulation (%)	Summation	Variance (%)	Cumulation (%)
1	8.156	58.258	58.258	8.156	58.258	58.258	5.915	42.250	42.250
2	2.433	17.378	75.636	2.433	17.378	75.636	4.141	29.579	71.829
3	1.255	8.963	84.600	1.255	8.963	84.600	1.788	12.771	84.600
4	0.656	4.687	89.286						
5	0.588	4.203	93.490						
6	0.392	2.804	96.293						
7	0.168	1.201	97.494						
8	0.139	0.992	98.486						
9	0.098	0.702	99.188						
10	0.052	0.371	99.558						
11	0.028	0.197	99.756						
12	0.018	0.125	99.881						
13	0.013	0.090	99.971						
14	0.004	0.029	100.000						

Fig. 3.1 Scree plot of network influence factor extraction

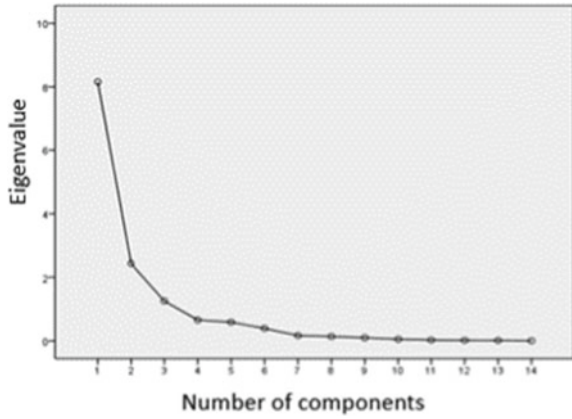


Table 3.3 Component matrix of network influence factor extraction

	Component		
	1	2	3
News	0.754	-0.384	-0.320
Blog	0.908	-0.085	-0.099
Twitter	0.925	-0.174	-0.314
Patent	0.698	0.450	0.012
Peer review	0.906	0.206	-0.051
Weibo	0.680	-0.534	0.362
Facebook	0.831	-0.381	-0.221
Wikipedia	0.511	0.654	0.152
Google+	0.880	-0.353	0.202
LinkedIn	0.734	0.510	-0.068
Reddit	0.867	-0.359	0.229
Pinterest	0.416	0.038	0.830
F1000	0.872	0.337	-0.212
Q&A	0.432	0.719	0.079

Extraction method: principal component

Three ingredients have been extracted

Table 3.4 Coefficient matrix of network influence component score

	Component		
	1	2	3
News	0.236	-0.079	-0.191
Blog	0.131	0.032	-0.039
Twitter	0.206	0.005	-0.195
Patent	-0.031	0.201	0.002
Peer review	0.057	0.132	-0.022
Weibo	0.089	-0.141	0.332
Facebook	0.218	-0.074	-0.114
Wikipedia	-0.129	0.258	0.088
Google+	0.110	-0.064	0.206
LinkedIn	-0.021	0.225	-0.062
Reddit	0.104	-0.067	0.226
Pinterest	-0.176	0.034	0.639
F1000	0.066	0.176	-0.154
Q&A	-0.132	0.276	0.026

Extraction method: principal component
 Rotation method: Kaiser standardized orthogonal rotation method
 Constitute scores

Table 3.5 Covariance matrix of network influence component score

Component	1	2	3
1	1.000	0.000	0.000
2	0.000	1.000	0.000
3	0.000	0.000	1.000

Extraction method: principal component
 Rotation method: Kaiser standardized orthogonal rotation method
 Constitute scores

3.4 Comparison of Network Influence Based on Principal Component Analysis

According to the evaluation model of network influence based on principal component analysis, 56 journals were ranked and compared. Firstly, the weight of the principal components was determined according to Table 3.5. The three principal components reflected most of the information of the original variables, and their cumulative contribution rate was about 84.6%. The comprehensive evaluation score of open access journals network influence was calculated by $F = 0.58258F1 + 0.17378F2 + 0.08963F3$. Due to the problem of incomplete data in the data acquisition stage, the research object of this part is 53 Chinese and American open access journals.

Table 3.6 Rotation component matrix of 14 indicators of network influence

	Component		
	1	2	3
News	0.899	0.094	-0.038
Blog	0.796	0.426	0.165
Twitter	0.923	0.363	-0.021
Patent	0.316	0.758	0.126
Peer review	0.627	0.668	0.162
Weibo	0.703	-0.080	0.614
Facebook	0.928	0.137	0.077
Wikipedia	0.016	0.825	0.175
Google+	0.818	0.183	0.487
LinkedIn	0.337	0.829	0.049
Reddit	0.802	0.171	0.510
Pinterest	0.048	0.250	0.893
F1000	0.583	0.796	-0.022
Q&A	-0.057	0.837	0.073

Extraction method: principal component

Rotation method: Kaiser standardized orthogonal rotation method

The rotation converges after five iterations

It can be roughly divided into the three categories according to the comprehensive score of network influence:

The first category: Open access journal network has great influence ($F \geq 0.3$): 3;

The second category: Open access journal network has a greater influence ($F \geq 0.15$): 0;

The third category: Open access journal network influence is small ($F < 0.15$): 50.

According to the overall evaluation results of network influence of open access journals, the first three influential journals are all from the USA. The second category has greater influence and has a comprehensive score between 0.15 and 0.3 without a journal. A third group of low-impact open access journals has 50, compared with 24 in America and 26 in China. Through the mean processing of the ranking numbers of all Chinese periodicals and American periodicals, it is found that the average ranking number of the USA is 23.78, while the average ranking number of China is 30.35. Therefore, the network influence of Chinese open access periodicals is obviously worse than that of the USA from the comprehensive situation of network influence.

It can be learned from Table 3.4 that the absolute value of principal component load of each variable does not show a polarization trend toward 0 and 1. Since the load of many variables on multiple principal components exceeds 0.2, which is not conducive to the interpretation of factors, factors need to be rotated.

As can be seen from Table 3.6, Facebook and Twitter contribute a lot to principal component 1. For principal component 2, Q&A and LinkedIn contributed a lot to it. For principal component 3, Pinterest contributes a lot to it (Table 3.7).

In terms of principal components $F1$ and $F2$, the number of Chinese journals is only 1 or 2 in the top 10, which is obviously lower than that of the USA. Although China and the USA account for half of the principal component of $F3$, Chinese journals are ranked behind. Therefore, it can be seen that the network influence of American open access journals is obviously higher than that of Chinese open access journals from the evaluation model of journal network influence.

3.5 Conclusion

Quality level of journals and papers. First of all, the sample selection showed that 28 Chinese journals included in JCR could not be compared with the world-renowned journals such as “Nature” and “Cell” in the USA in terms of quality level, and the origin of a lot of research is abroad, on the scientific research level at a disadvantage. Secondly, Chinese open access platform does not attach as much importance to the process of paper review and evaluation as the USA, which will affect the academic level of journal papers. Finally, language difference is also a factor affecting the influence of papers and periodicals.

Website platform construction. Network originated in the USA, the global root server in the USA, so China is fundamentally inferior to the USA in the construction of website network. Secondly, due to the lack of policies and social awareness, people know little about the website platforms of open access, which makes the construction of these platforms have no incentive to progress.

Objective factors of online influence. As it is a comparative analysis of the international academic influence of open access journals, Altmetric online information measurement platform was selected, which to some extent determines the result that Chinese journals are inferior to American journals. It can also be seen from the indicator system that only “Weibo” is accessible to Chinese people, so it is expected that the network influence is worse than that of the USA.

3.6 Limited

The language difference has certain influence on the international academic influence of periodicals. Although this paper selects English international journals published in China and the USA, it seems to avoid the differences in academic influence caused by language. However, it is undeniable that scholars’ preferences, translation problems in both Chinese and English, English expressiveness, and other issues will have a certain impact on the international academic influence of Chinese journals.

Table 3.7 Main components and important indicators of network influence of journals (top 10)

<i>F</i>	<i>F1</i>	Facebook	Twitter	<i>F2</i>	Q&A	LinkedIn	<i>F3</i>	Pinterest
NO. 31	NO. 31	NO. 33	NO. 31	NO. 30	NO. 30	NO. 31	NO. 32	NO. 32
NO. 33	NO. 33	NO. 31	NO. 33	NO. 31	NO. 55	NO. 30	NO. 35	NO. 35
NO. 32	NO. 32	NO. 32	NO. 32	NO. 55	NO. 31	NO. 35	NO. 39	NO. 39
NO. 38	NO. 38	NO. 47	NO. 38	NO. 35	NO. 42	NO. 55	NO. 30	NO. 30
NO. 30	NO. 34	NO. 38	NO. 30	NO. 41	NO. 45	NO. 33	NO. 40	NO. 40
NO. 34	NO. 47	NO. 30	NO. 9	NO. 37	NO. 22	NO. 32	NO. 8	NO. 8
NO. 47	NO. 40	NO. 34	NO. 47	NO. 42	NO. 5	NO. 38	NO. 6	NO. 6
NO. 40	NO. 53	NO. 37	NO. 34	NO. 38	NO. 56	NO. 9	NO. 19	NO. 19
NO. 53	NO. 3	NO. 4	NO. 40	NO. 44	NO. 9	NO. 47	NO. 21	NO. 21
NO. 3	NO. 13	NO. 36	NO. 13	NO. 22	NO. 16	NO. 34	NO. 11	NO. 11

Acknowledgments This paper is supported by National Social Science Foundation in China (Grant No. 18ZDA325 and No. 16BTQ055).

Appendix

China–US comparison table of sample journals

	Full name of Chinese open access journals		Full name of American open access journals
NO. 1	Light-Science & Applications	NO. 29	Physical Review X
NO. 2	Bone Research	NO. 30	Molecular Systems Biology
NO. 3	Protein & Cell	NO. 31	mBio
NO. 4	Nano-Micro Letters	NO. 32	Translational Psychiatry
NO. 5	Geoscience Frontiers	NO. 33	Journal of the American Heart Association
NO. 6	Chinese Journal of Cancer	NO. 34	Annals of Clinical and Translational Neurology
NO. 7	International Journal of Oral Science	NO. 35	Molecular Pain
NO. 8	ASIAN JOURNAL OF ANDROLOGY	NO. 36	IEEE Access
NO. 9	Journal of Sport and Health Science	NO. 37	BIOSCIENCE REPORTS
NO. 10	Current Zoology	NO. 38	G3-Genes Genomes Genetics
NO.11	Journal of Animal Science and Biotechnology	NO. 39	Plant Genome
NO.12	Progress in Natural Science-Materials International	NO. 40	Journal of Diabetes Research
NO. 13	Neural Regeneration Research	NO. 41	IEEE Photonics Journal
NO. 14	Journal of Modern Power Systems and Clean Energy	NO. 42	Canadian Journal of Gastroenterology and Hepatology
NO. 15	Petroleum Science	NO. 43	ARCHAEA
NO. 16	Chinese Journal of Aeronautics	NO. 44	Journal of Nanomaterials
NO. 17	Asian Journal of Surgery	NO. 45	Advances in High Energy Physics
NO. 18	Journal of Advanced Ceramics	NO. 46	Journal of Sensors
NO. 19	International Journal of Ophthalmology	NO. 47	AIP Advances
NO. 20	Engineering Applications of Computational Fluid Mechanics	NO. 48	ANGLE ORTHODONTIST
NO. 21	Thoracic Cancer	NO. 49	Molecular Therapy-Oncolytics
NO. 22	CHINESE MEDICAL JOURNAL	NO. 50	Marine and Coastal Fisheries

(continued)

(continued)

	Full name of Chinese open access journals		Full name of American open access journals
NO. 23	Avian Research	NO. 51	Canadian Respiratory Journal
NO. 24	International Journal of Agricultural and Biological Engineering	NO. 52	INFORMATION TECHNOLOGY AND LIBRARIES
NO. 25	Mycosphere	NO. 53	CTS-Clinical and Translational Science
NO. 26	Journal of Exercise Science & Fitness	NO. 54	Advances in Mechanical Engineering
NO. 27	China Foundry	NO. 55	MATHEMATICAL PROBLEMS IN ENGINEERING
NO. 28	JOURNAL OF INFRARED AND MILLIMETER WAVES	NO. 56	JOURNAL OF INEQUALITIES AND APPLICATIONS

References

- Lewis, D.W.: The inevitability of open access. *Coll. Res. Libraries* **73**(5), 493–506 (2012)
- CNKI: Future of Chinese Academic Journals BBS. Retrieved March 3, 2018 from: <http://hi.cnki.net/refreport2015/dhfbcg01.html#>
- Zhang, J.: Influence of academic journals and its assessing system's construction. *J. Shaanxi Normal Univ. (Philos. Social Sci. Ed.)* **39**(5), 70–76 (2010)
- Yang, C.: Evaluation and analysis on the academic influence of women's research journals. *J. of Shanxi Norm. Univ. (Social Sci. Ed.)* **5**, 136–139 (2014)
- Zhou, J.: The study on academic influence of open access journal. *Jilin Univ.* 39–46 (2013)
- Zhang, Y, Wu, J., Lang, L.: The evaluation of academic journals based on different web data. *Chin. J. Sci. Tech. Period.* **02**, 176–183 (2017)
- He, W.: Correlation research on evaluation of journal influence based on altmetrics and citation analysis. *Nanjing Univ.* 29–45(2015)
- Zhao, R., Wang, S., Chen, Z.: Research on altmetrics and its analysis implements. *Inform. Stud. Theory Appl.* **06**, 29–34(2015)
- Zhang, B.: Three common methods of data standardization. Retrieved March 17, 2018 from: <https://blog.csdn.net/bbbeoy/article/details/70185798>

Chapter 4

The Use of Mobile Apps to Facilitate Customers' Choice-Making When Grocery Shopping



Asle Fagerstrøm, Niklas Eriksson, and Valdimar Sigurdsson

Abstract This paper aims to expand the knowledge of how mobile apps can be used to establish a smart grocery retail setting. By offering real-time, personalized digital information, mobile apps enable bidirectional interaction with customers in the grocery shopping situation. A conjoint experiment ($n = 90$) was used to examine the use of mobile apps in a consumer choice situation where participants were choosing fresh salmon in a grocery store. Findings show that, relative to static information given by the mobile app about expiry date, price, offers, and quality indicator, digital information was the most prominent attribute. Among digital information given by the mobile app, quality indicators by other customers were the most prominent, followed by an offer based on a product in the shopping basket, updated expiry date, and real-time price. The results expand our understanding of how mobile apps can be used to design a setting in the grocery store that creates value for customers. Based on this result, we recommend that managers that plan to invest in mobile app technology to improve the electronic commerce ecosystem should include digital information.

4.1 Introduction

The establishment in 1859 of the Great Atlantic & Pacific Tea Company, with its focus mostly on dry grocery items, marked the birth of the modern grocery store.

A. Fagerstrøm (✉) · N. Eriksson
Kristiania University College, Prinsensgate 7-9, 0107 Oslo, Norway
e-mail: asle.fagerstrom@kristiania.no

N. Eriksson
e-mail: niklas.eriksson@arcada.fi

N. Eriksson
Arcada University of Applied Sciences, Jan-Magnus Janssonin Aukio 1, 00560 Helsinki, Finland

V. Sigurdsson
Reykjavik University, Menntavegur 1, 101 Reykjavik, Iceland
e-mail: valdimars@ru.is

© The Editor(s) (if applicable) and The Author(s), under exclusive license to Springer Nature Singapore Pte Ltd. 2021

Y.-D. Zhang et al. (eds.), *Smart Trends in Computing and Communications: Proceedings of SmartCom 2020*, Smart Innovation, Systems and Technologies 182,
https://doi.org/10.1007/978-981-15-5224-3_4

The Piggly Wiggly stores (established in 1916) created the self-service concept. Suddenly, packaging and brand names were crucial for manufacturers. Since then, four major periods characterize the development of the retail grocery business [1]: the establishing of the grocery chain store, the introduction of the grocery supermarket format, the rise of computerization and the explosion in grocery product variety, and the development of national grocery chains. According to Desai et al. [2], the retail grocery businesses are now in a new major period of digital and omnichannel retailing. Digitalization is driving the future of retailing, and this gives traditional retail stores the possibility to develop “smart store” concepts where information technology can be used to augment customer values [3]. New capabilities in grocery retail are provided by developments in blockchain technologies, Internet of things (IoT), virtual reality (VR), artificial intelligence (AI), augmented reality (AR), and robotics [4]. By leveraging on capabilities offered by these new technologies, retailers are improving the electronic commerce ecosystem by using self-service information technologies such as mobile apps to deliver decision support to their customers [5].

The smartphone has become a personal assistant for many retail consumers. Through the use of mobile apps on their own devices, customers can search for product information, search and compare prices, and ask their friends about their opinion [6]. According to Mehta [7], mobile apps function as a bridge for “forward-thinking organizations trying to create smarter devices that could boost every aspect of people’s lives.” However, Kallweit et al. [5] highlight that the technology itself only barely mediates users’ intention to use self-service technology in retail; rather, what matters to the user is what kind of service quality, such as information quality, the technology can provide. Also, another study by Hyun-Joo [8] highlighted the quality of self-service technology as the main factor for the use of that technology in retail.

Self-service technology, such as mobile apps, can improve the electronic commerce ecosystem by adding value for the retailer as well as for the customers [9]. When it comes to value for the retailer, Inman and Nikolova [10] emphasize that increased revenue and/or decreased costs are most important. According to a study by Dacko [9], the mobile app creates value for the customers through efficiency or better shopping value. However, personal customer attributes also seem to have an impact on the attitude toward self-service technologies in retail [11]. Lee and Lyu [11] found that a need for human interaction and the self-service technology self-efficiency impact the personal attitude toward using self-service technologies.

Investigating how mobile apps can create value contributes to both researchers and practitioners who are interested in refining the grocery electronic commerce ecosystem. Thus, the overall goal of this study is to develop knowledge of how mobile apps can be used to design a smart grocery retail setting that produces value for customers.

4.2 Method

The conjoint experiment is a method that can statistically predict which combinations of attributes the customers will prefer. The participants are asked to make judgments about their preferences for combinations of attributes (e.g., price and brand) that have various levels (e.g., for price: above market price/market price/below market price, and for brand: unknown/known). The objective is to determine the trade-offs that participants make for each of the attributes and to derive the importance they place on each attribute [12, 13]. Conjoint experimentation is often used in scientific research [12, 14], applied research [15], and business studies [16].

Conjoint experimentation is used in the present study to investigate how attributes such as expiry date, price, offer, and quality indicator given by the mobile app fit together to deliver values to customers in a grocery retail shopping situation. All four attributes are measured on two levels: standard information and digital information.

4.2.1 Participants

The participants of the study comprise 90 undergraduate students from Kristiania University College (Norway, Oslo). Five participants were taken out because of no valid cases. There were 30 males and 60 females between the ages of 19 and 38. The average age was 23 years. Twenty-four participants had experience with shopping for groceries online, and 31 participants had used a mobile app as an assistant when shopping for groceries from a physical grocery store. The duration of the study was approximately 20 min. The participants were not offered any incentives for participating.

4.2.2 Apparatus and Setting

To ensure good ecological validity, Holbrook and Moore [17] suggest using visual stimuli when developing stimulus cards for conjoint experiments. Thus, a mobile app user interface was designed in Microsoft PowerPoint™ to make the study as realistic as possible. The conjoint experiment was run using a presentation for the participants in a lecture room together with a questionnaire.

4.2.3 Attributes

Four value-driving attributes were chosen for this study: expiry date, price, offer, and quality indicator. These four attributes were chosen as they are common attributes in the grocery choice situation, they fit well as information sources on the display

Table 4.1 The study was designed with four attributes given by the mobile app with two levels each

Attributes	Levels
Expiry date	1. Standard expiry date 2. Updated expiry date
Price	1. Fixed price 2. Real-time price
Offer	1. Standard offer 2. Personalized offer based on product in the basket
Quality indicator	1. Standard quality statement 2. Aggregated national customer experience index

of a mobile device (a mobile app), and they represent attributes that can be updated, aggregated, or personalized by new digital technology; that is, they can create a smart grocery shopping setting. The four attributes (expiry date, price, offer, and quality indicator) were measured on two levels: standard information and digital information. It was assumed that the participants had different preferences for combinations of attributes and levels. Table 4.1 presents an overview of the study design, attributes, and how the levels were designed.

A fractional factorial design [18] created 12 stimulus cards (integrating four hold-out cards). The dependent variable was defined as the participant's likelihood to buy the product based on information given by the mobile app and was measured on a scale ranging from "Not at all likely to buy" (code 0) to "Certainly would like to buy" (code 7). After finishing the evaluation of the 12 stimuli cards, the participants filled in our questions regarding gender, age, experience with online grocery shopping, and experience with using a mobile app when shopping for groceries in the physical store.

4.2.4 Procedure

The study started by informing the participants about the background and their role (to evaluate choice situations when shopping for groceries) in the study. The task was described as a scenario in which the participants should assume that they were going to buy some groceries for a barbecue party with their friends. The groceries that they had been asked to buy were fresh salmon, dill, charcoal, potatoes, crème fraîche, and barbecue spices. They were told to assume that they were in the grocery store and were using the store's mobile app when purchasing the products. The mobile app shows products that are already purchased. They should assume that they were in the process of selecting fresh salmon, and the mobile app provided the information they needed to make the purchase. The participants were presented with 12 different stimulus cards and were asked to make judgments about their preferences for the

combinations of attributes and levels in relation to buy the salmon based on the given information.

4.2.5 Analysis

IBM SPSS™ version 22 was used to analyze the data. This statistical tool offers only a main-effect model [18], which assumes that there are no interaction effects between the attributes. This means that the study does not account for interactions between attributes (e.g., “price” and “offer” given by the grocery store). In addition, a linear effect was assumed for all attributes (expiry date, price, offer, and quality indicator). A linear effect indicates that the data was expected to have a linear relationship to the levels (e.g., participants show lower preferences for “Standard offer” than “Personalized offer based on product in the basket”).

4.3 Findings

The analysis revealed that the correlations between the observed and estimated preferences were significant (Pearson’s $r = 0.947, p = 0.000$). Table 4.2 shows the impact estimate, standard error, and relative importance values. In relative terms, the quality

Table 4.2 Conjoint impact estimate and relative importance values for each attribute

	Likelihood to buy based on information from the mobile app		
	Impact estimate	Standard error	Importance values (%)
<i>Expiry date</i>			
Standard expiry date	0.056	0.129	25
Updated expiry date	0.111	0.257	
<i>Price</i>			
Fixed price	-0.100	0.129	20
Real-time price	-0.200	0.257	
<i>Offer</i>			
Standard offer	0.489	0.129	26
Personalized offer based on product in the basket	0.978	0.257	
<i>Quality indicator</i>			
Standard quality statement	0.428	0.129	29
Aggregated national customer experience index	0.856	0.257	
Constant	2.581	0.392	

indicator was perceived as the most important attribute by the participants, with an average score of 29%, followed by offer (26%), expiry date (25%), and price (20%).

The constant was calculated to be 2.581, and the attribute values of the levels vary both negatively and positively with this value. Table 4.2 shows that the digital information levels have the highest impact estimate. A personalized offer based on the product in the basket had the highest impact estimate score of 0.978, followed by an aggregated national customer experience index (0.852) and updated expiry date (0.111). Real-time price had the least impact estimate score of -0.200 . In total, standard offer, standard quality statement, standard expiry date, and standard price had higher impact estimate scores than real-time price.

4.4 Discussion

This study aimed to expand knowledge of how mobile apps can be used to design a smart grocery retail setting that produced value for customers. Based on a scenario where participants were asked to buy groceries for a barbecue party with friends, they made choices based on information given on the grocery stores' mobile app. Findings show that compared to standard information, digital information given by the mobile app was the most preferred. Updated expiry date, personalized offer based on products in the basket, and an aggregated national customer experience index were the most salient information given by the mobile app when participants purchased fresh salmon.

Mobile apps have formed the groundwork for the development of digital information that can create smart settings in many aspects of people's lives [7]. The present study demonstrates that mobile app information creates value in a grocery retail choice situation compared to traditional static information given to customers in the choice situation. This supports findings from Dacko [9], which demonstrated that users see mobile apps in retail stores as enablers providing high extrinsic value, for example, efficiency or better shopping value. Also, findings from the present study may demonstrate that the technology only barely mediates users' intention to use self-service technology in retail. What matters is more about what kind of service quality, such as information quality, the mobile app can provide to the user [5].

When adopting mobile app solutions, grocery retailers should evaluate the benefits of the technology compared to the costs of its purchase, implementation, and maintenance. Thus, the economic profit of investments in grocery retail technology must increase revenue, decrease costs, or preferably both. According to Inman and Nikolova [10], revenue can be generated by charging a higher price from customers who are willing to pay more for groceries, increasing the purchase volume per customer, attracting new customers to the grocery store, and increasing the contribution from suppliers. Costs can be decreased by offloading labor in the grocery store (self-scan or digital shelves). To be able to generate an economic profit of mobile app investments in grocery retail, Inman and Nikolova [10] suggest starting by analyzing

how the retail shopper, facing technology, impacts consumer evaluation and reactions. Zeithaml [19] emphasizes that the evaluation of a product is based on what the customer receives and what is given, and thus, consumer evaluation is an important determinant of consumer likelihood to buy the product. To maximize consumer value, the grocery retailer should adopt technologies that either increase the benefit and/or decrease monetary sacrifices, time, and effort involved in making a purchase [10]. The present study demonstrates the advantages of using a conjoint experiment as a method in applied electronic commerce research. It enables us to make statistical predictions on how new technologies can generate value for customers.

4.4.1 Practical Implications

Based on the results of this study, mobile apps can create a smart grocery retail setting that adds value to the customers' shopping experience and thus influences their choices. The four attributes that were investigated in this study should be noted by grocery retailers, suppliers, and brands that are involved in designing mobile app-based in-store solutions. Especially personalized offers and quality indicators for fresh food can have a significant impact on consumers' likelihood to buy a product [20, 21]. This ought to make these types of attributes attractive to include in mobile app solutions for smart grocery settings. From a sustainability perspective, smart quality indicators and updated expiry dates can also help customers make better choices, such as selecting healthier options and reducing waste. On the other hand, real-time price information may not increase the likelihood of buying the product. Instead, real-time price information seemed to have a negative effect relative to the other attributes investigated. A real-time or fluctuating price may indeed increase customer uncertainty of a good price. Hence, designers of mobile app solutions for fresh food should carefully consider how or whether they include real-time or fluctuating price information as an attribute. It should also be noted that standard offer, standard quality statement, and standard expiry date, as presented in the mobile app, had a positive effect on the reported likelihood to buy. Hence, a mix of digital information and standard information in a mobile app can facilitate the customer decision process.

4.4.2 Limitations and Future Research

One of the main limitations of this study is that the interaction effect was overlooked between the different attributes and levels because a main-effect-only model was used in the conjoint experiment. A possible interaction effect could occur between different attributes like quality indicator and price (i.e., different quality indicator levels may have different implications for price levels). Also, order effects occurred during data collection because the 12 situations were presented in the same order

[22]. Future research can address these limitations by using a more advanced conjoint tool like Sawtooth™ software to study interaction effects and to address order effect issues. Also, the dependent variable was an indirect measure of purchasing behavior because the participants indicated their likelihood to buy fresh salmon based on information from the mobile app through a questionnaire. As a solution, we suggest an experiment in a natural setting that uses a prototype mobile app, which will increase both ecological validity and external validity [23]. This could also expand opportunities to follow up and study consumers' actual interaction with mobile in a more natural setting.

References

1. Ellickson, P.B.: The evolution of the supermarket industry: From A&P to Wal-Mart. Simon School Working Paper Series No. FR 11–17 (2011)
2. Desai, P., Potia, A., Salsberg, B.: Retail 4.0: The Future of Retail Grocery in a Digital World. McKinsey & Company. <http://www.mckinseyonmarketingandsales.com/retail-4-0-the-future-of-retail-grocery-in-a-digital-world>
3. Accenture: Customers are shouting, are apparel retailers listening? Accenture Global Research (2016). https://www.accenture.com/t20160526T041237__w__/us-en/_acnmedia/Accenture/Conversion-Assets/NonSecureClients/Documents/PDF/1/Accenture-Retail-Adaptive-Research-Results-Global-Generational-Data-2016-SCROLL.pdf
4. Barile, S., Polese, F.: Grocery retailing in the I4.0 era. SYMPHONYA Emerg. Issues Manage. **2018**(2), 38–51 (2018)
5. Kallweit, K., Spreer, P., Toporowski, W.: Why do customers use self-service information technologies in retail? The mediating effect of perceived service quality. J. Retail. Consum. Serv. **21**(3), 268–276 (2014)
6. Piotrowicz, W., Cuthbertson, R.: Introduction to the special issue information technology in retail: toward Omnichannel retailing. Int. J. Electron. Commerce, **18**(4), 5–16 (2014)
7. Mehta, R.: How will the Internet of Things impact mobile application development (2017). Cited 21 April 2018. Available from: <https://www.itproportal.com/features/how-will-the-internet-of-things-impact-mobile-application-development/>
8. Hyun-Joo, L.: Consumer-to-store employee and consumer-to-self-service technology (SST) interactions in a retail setting. Int. J. Retail Distribut. Manage. **43**(8), 676–692 (2015)
9. Dacko, S.G.: Enabling smart retail settings via mobile augmented reality shopping apps. Technol. Forecast. Soc. Chang. **124**, 243–256 (2017)
10. Inman, J.J., Nikolova, H.: Shopper-facing retail technology: a retailer adoption decision framework incorporating shopper attitudes and privacy concerns. J. Retail. **93**(1), 7–28 (2017)
11. Lee, H.-J., Lyu, J.: Personal values as determinants of intentions to use self-service technology in retailing. Comput. Hum. Behav. **60**, 322–332 (2016)
12. Green, P.E., Srinivasan, V.: Conjoint analysis in consumer research: issues and outlook. J. Consum. Res. **5**(2), 103–123 (1978)
13. Green, P.E., Wind, Y.: New way to measure consumer's judgments. Harvard Bus. Rev. **53**, 107–117 (1975)
14. Green, P.E., Srinivasan, V.: Conjoint analysis in marketing: new developments with implication with implications for research and practice. J. Market. **54**, 3–19 (1990)
15. Vriens, M.: Solving marketing problems with conjoint analysis. J. Market. Manage. **10**, 37–55 (1994)
16. Wittink, D.R., Vriens, M., Burhenne, W.: Commercial use of conjoint analysis in Europe: results and critical reflections. Int. J. Res. Mark. **11**, 41–52 (1994)

17. Holbrook, M.B., Moore, W.L.: Feature interactions in consumer judgments of verbal versus pictorial presentations. *J. Consum. Res.* **8**(1), 103–113 (1981)
18. Hair, J.F., et al.: *Multivariate data analysis*, 7th edn. Pearson Prentice Hall, Upper Saddle River (2014)
19. Zeithaml, V.A.: Consumer perceptions of price, quality, and value: a means-end model and synthesis of evidence. *J. Market.* **52**(3), 2–22 (1988)
20. Grewal, D., et al.: Innovations in retail pricing and promotions. *J. Retail.* **87**(Supplement 1), S43–S52 (2011)
21. Dellarocas, C.: The digitization of word of mouth: promise and challenges of online feedback mechanisms. *Manage. Sci.* **49**(10), 1407–1424 (2003)
22. Chrzan, K.: Three kinds of order effects in choice-based conjoint analysis. *Market. Lett.* **5**(2), 165–172 (1994)
23. Fagerstrøm, A., Sigurdsson, V.: The experimental analysis of consumer choice. In: Foxall, G.R. (Ed.) *The Routledge Companion to Consumer Behavior Analysis*. Routledge: London (2016)

Chapter 5

Implementation of Best Hybrid Adaptive and Intelligent MIMO Detector on Reconfigurable Architecture for 5G LTE/IoT Environment



Tipparti Anil Kumar and Lokam Anjaneyulu

Abstract Internet of things (IoT) in wearable health care is the major area facilitates the usage of numerous transmitters on board, leading to the employment of multiple-input–multiple-output (MIMO) system (with high-performance decoders) for an effective communication. Employing MIMO system suitable for IoT applications with quality of performance (QoP), low power, and minimum computational complexity with reconfigurable architectures is a challenge. This paper presents a new MIMO detector called best hybrid adaptive and intelligent (B-HAI) detector which consists of various combinations of conventional MIMO detectors, such as zero forcing (ZF) with fuzzy K -best and minimum mean squared error (MMSE) with fuzzy K -best. One of these combinations of detectors will be chosen using cognitive selective permutation theory, which is adaptive to the spatially multiplexed (SM) input parameters signal-to-noise (S/N) ratio, to achieve high QoP parameters. In the proposed algorithm, intelligence (fuzzy based) has been incorporated to dynamically upgrade the value of K and to reduce complexity as well as power. Simulations were performed in the reconfigurable programmable architecture, employing a MIMO system suitable for IoT applications. The proposed detector offers better performance compared to other detectors.

5.1 Introduction

Wireless communications have become rapid growing markets worldwide [1]. To support growing number of users, new applications requiring better quality of service (QoS) with high reliability and data rates are in demand. Hence, new transceiver

T. Anil Kumar (✉)
CMR Institute of Technology, Hyderabad, India
e-mail: tvakumar2000@yahoo.co.in

L. Anjaneyulu
National Institute of Technology Warangal, Warangal, India
e-mail: anjan@nitw.ac.in

© The Editor(s) (if applicable) and The Author(s), under exclusive license to Springer Nature Singapore Pte Ltd. 2021

Y.-D. Zhang et al. (eds.), *Smart Trends in Computing and Communications: Proceedings of SmartCom 2020*, Smart Innovation, Systems and Technologies 182,
https://doi.org/10.1007/978-981-15-5224-3_5

algorithms with proper architectures are necessary to take advantage of the available spectrum and to counter the impairments of radio channel efficiently.

The basic idea is the usage of multiple antennas at both transmitter and receiver. The important features of MIMO systems are higher spectral efficiency (SE) and high link reliability [2, 3], which results in data throughput and link range increase, without any additional bandwidth and/or transmit power. Unfortunately, tremendous gains associated with MIMO technology also entail a considerable increase in computational complexity particularly at the receiver, due to the complex algorithms required for the separation of these spatially multiplexed streams [4–7]. The hybrid combinations of the different detectors were designed to reduce the computational complexity without sacrificing the performance. In [3], mixed detectors which consist of the combination of the search first (SF) and depth first (DF) were proposed, which require higher computation. In [6], a hybrid method in the combination of the K -best and sphere decoding has been proposed, which does not need the initial radius estimation, and the authors used the layered ordering of decomposition which in turn increases the complexity. For reducing the computational complexity, combination of K -best and sphere decoding was proposed in [8]. The algorithm proves to be better in terms of complexity reduction but not for all modulations schemes.

Hence, in this paper, a B-HAI MIMO detector on reconfigurable architecture for 5G LTE/IoT environment is proposed and studied.

5.2 Proposed B-HAI MIMO Detector

B-HAI MIMO detector consists of signal-to-noise ratio calculator and scheduler, hybrid adaptive permutation (HAP) engine and performance calculator- post processing. The block diagram of B-HAI MIMO detector is shown in Fig. 5.1.

SNR calculator block calculates the signal-to-noise (S/N) ratio of incoming SM data bits and sends to the scheduler and selector sub-block. Scheduler and selector sub-block compares the S/N levels (supplied from the SNR calculator sub-block) to the threshold SNR level and selects the suitable detector as per the following

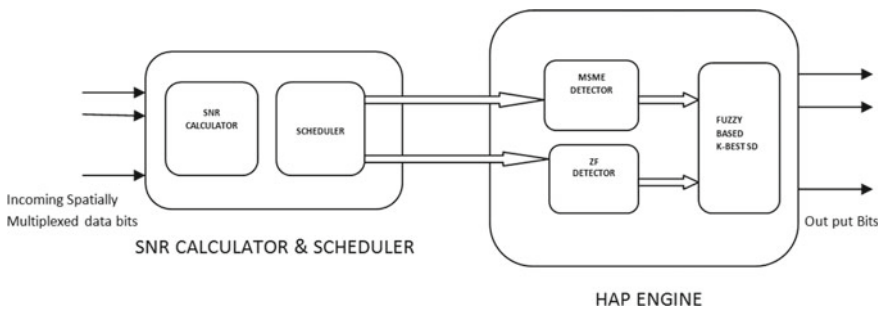


Fig. 5.1 Block diagram of B-HAI detector

condition. If SNR level < SNR_THLD, ZF detector is selected; otherwise, MMSE detector is selected. Accordingly, for each SNR preprocessed value, either one of the linear detectors is selected to get the optimal solutions, which are suitable for the fuzzy K -best sphere decoding stage in order to have the less dimension for the processing.

HAP engine block consists of ZF decoder, MMSE decoder, and fuzzy K -best decoder, and two hybrid engines, namely ZF with fuzzy K -best SD and MMSE with fuzzy K -best SD.

These engines are selected based on the adaptive inputs of preprocessed SNR calculations as per the above condition. Depending on the selected hybrid engine, incoming bits are decoded either by ZF decoder or by MMSE decoder. In the next level, these bits are given to fuzzy K -best SD. Fuzzy rule set is applied, to intelligently select the initial value of L and dynamically upgrade the value of K , which gives high performance with reduced computational complexity.

After SNR/BER calculation, cognitive permutation theory is applied. Accordingly, the incoming bits are decoded to MMSE or zero-forcing algorithms. In order to maintain the K value optimum for maintaining the low complexity and high performance, the fuzzy K -best sphere decoding is adopted for the group of the MMSE/zero-forcing bits which are to be determined first.

In the next level, decoding tree for the sphere decoding has been constructed based on the obtained bits which are close to the maximum likelihood (ML) optimal detection. For the intensified and simplified tree search, fuzzy rule has been incorporated. Fuzzy-based K -best searching phase in B-HAI MIMO detector is shown in Fig. 5.2.

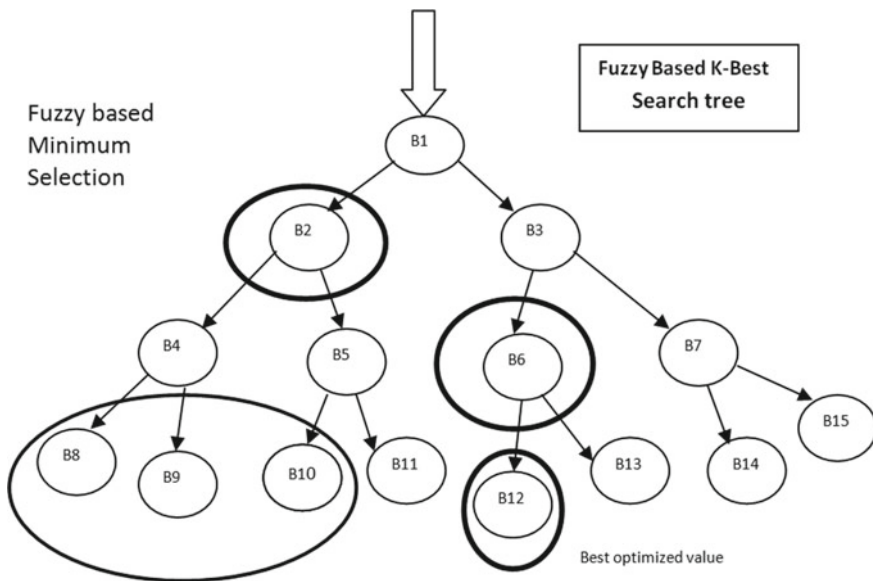


Fig. 5.2 Fuzzy-based K -best searching phase in B-HAI MIMO detector

At this point, nodes of the decoding tree are stored as the information of the partial solution in order to find the optimal solution. For each and every level of tree, partial Euclidean distance (PED) is calculated. Also, the difference between the PED of the optimal and sub-optimal (first-stage bits) is calculated, to find the best one. The HAP engine incorporates the fuzzy rule sets, and the tree grows on as it reaches the optimal values.

5.3 System Model

The MIMO system model with T number of transmit antennas and R number of receiving antennas (with $R > T$) is given as [9, 10]

$$Y = HX + N \quad (5.1)$$

where Y represents complex received bit vector, X represents the complex transmitted received bit vector that contains the infinite entries with the finite modulations S , H is $T \times R$ channel matrix, and N is the additive white Gaussian noise (AWGN) with the 0 mean and σ^2 variance.

5.4 Architecture of HAI Detector

Architecture of proposed detector is presented in Fig. 5.3.

In the Stage 1, SNR is calculated for the SM-based input signals. As the SNR is calculated in the preprocessing stage, two types of the linear detection are chosen in HAP engines.

For each SNR preprocessed values, either one of the first stage of the linear decoder engines is selected to get the optimal solutions which are suitable for the fuzzy K -best sphere decoding stage in order to have the less dimension for the processing. Second stage of the HAP engine consists of the low dimension K -best sphere decoding algorithm in which K values are adaptive based on fuzzy rule sets.

Consider $N_t + 1$ is the number of the levels in the formation of the tree and N_t and N_r be the number of antennas in the transmitter and the receiver, respectively. Partial Euclidean distance (PED) will be calculated for each level which stores the optimal solutions.

The noise of the optimal solution has less bit error rate (BER) than the partial solutions which are obtained from the inputs, and then, PED values can be adjusted in accordance with the adaptive K -values. The fuzzy rule sets are implemented with the different thresholds, as the difference in PED values is large in sense the partial solutions reach the maximum likelihood (ML) solution and K value remains to be

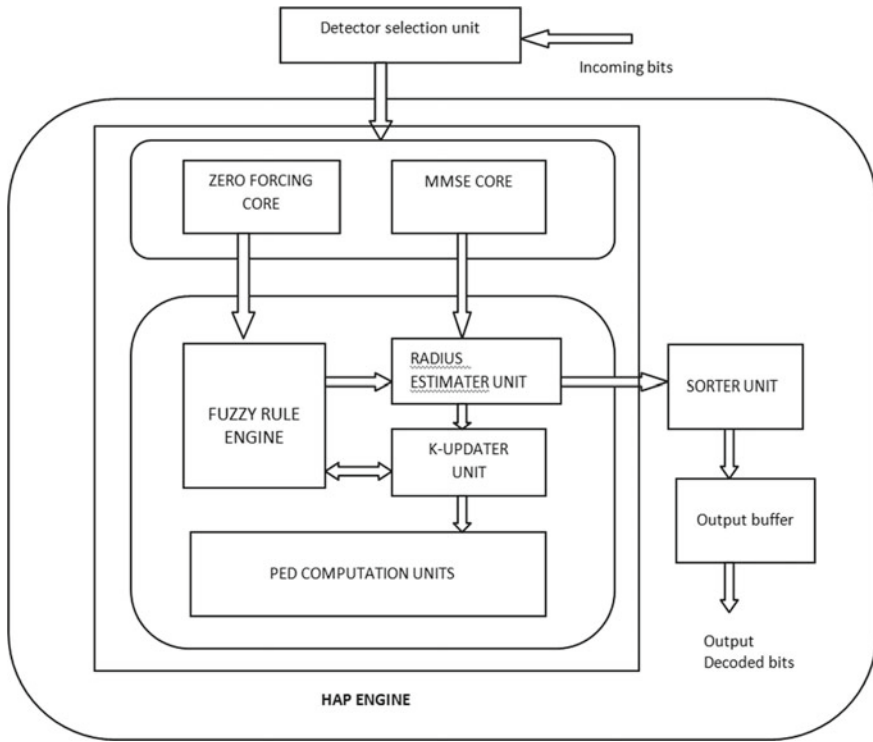


Fig. 5.3 Architecture of proposed B-HAI detector

small and vice versa condition is applied for this mechanism. The mathematical description of implementation is given in Table 5.1.

After finding the smallest value of K with the expanding 'I' leaves of the nodes again check the condition if I is not equal to the one, then implement the fuzzy rule

Table 5.1 Fuzzy rule sets for the adaptive K -best sphere decoding algorithm

S. No.	Conditions/fuzzy rule sets	Outputs
01	Let us consider the five thresholds like A1, A2, A3, A4, and A5	
02	Calculation of PED between the optimal D(opt) and sub-optimal distance D(Sub)	
03	IF(D(opt)-D(Sub)) \leq D1) is LesBER than or Equal to A1	K=Kt1
04	IF(D(opt)-D(Sub)) \leq D2) is LesBER than A2 and greater than A1	K=Kt2
05	IF(D(opt)-D(Sub)) \leq D3) is LesBER than A3 and greater than A2	K=Kt3
06	IF(D(opt)-D(Sub)) \leq D4) is LesBER than A4 and greater than A3	K=Kt4
07	IF(D(opt)-D(Sub)) \leq D5) is LesBER than A5 and greater than A4	K=Kt5

sets which are mentioned in above Table 5.1. Finally, the smallest optimal solutions are determined.

5.5 Computational Complexity Reduction

In the proposed algorithm, first L bits were detected adaptively using SNR values of the incoming data. The value of L is large for low SNR and small for high SNR. First, L value is detected by the detectors (MMSE/ZF) and next $N_t - L$ bits were detected by fuzzy K -best sphere decoding. Besides, the proposed algorithm uses the minimum dynamic K -best values updation methodology using the fuzzy rules sets which can be adopted intelligently to reduce the complexity. This method is suitable for different modulation schemes.

As seen, all mixed or hybrid detectors use the K -best searching algorithm as the primary layer which can reduce the complexity. But the proposed algorithm adopts the K -best for the $N_t - L$ bits to reduce the complexity and adopts the K -best which in terms of the next layer leads to the more computation, in which proposed detector uses the SD for the further computations.

The value of L can be taken from 0 to N_t or N_t to 0 in which the detectors are selected based on the adaptive environment of SNR. Hence, the proposed detector performance is enhanced with the lower complexity.

Above observations clearly illustrate that the number of computations has been reduced to one half of any hybrid detectors. Further, number of additions and multiplications will also reduce which leads to the occupation of the less BER and low power consumption.

5.6 Performance Evaluation

The performance of proposed B-HAI MIMO detector was evaluated using test bench designed with 2×2 MIMO with various modulation techniques assuming AWGN channel. Proposed detector was also evaluated using simulation results with four transmitting antennas and four receiving antennas.

The SNR versus BER has been plotted with the different modulation techniques like 4-QAM, 16-QAM, and 64-QAM, and the simulation results are given in Figs. 5.4, 5.5, and 5.6.

The performance of the proposed B-HAI MIMO detector has been compared with the hybrid detector like MMSE and zero-forcing hard detectors proposed in [2]. Simulation results support the enhanced performance of proposed detector.

Fig. 5.4 BER performance of proposed detector for 2×2 MIMO system with 16 QAM modulation with AWGN channel

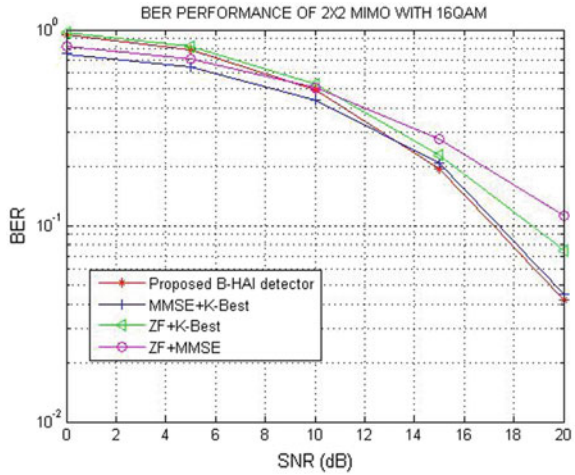
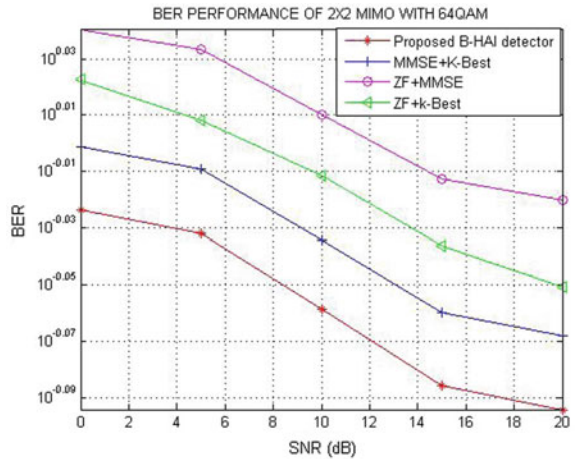


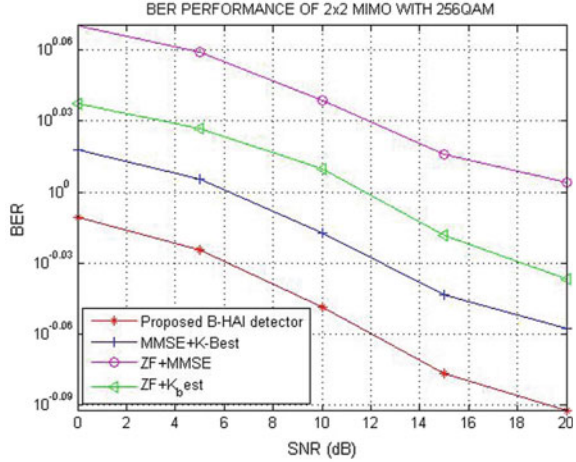
Fig. 5.5 BER performance of proposed detector for 2×2 MIMO system with 64 QAM modulation with AWGN channel



5.7 Conclusions

In this paper, B-HAI MIMO detector was proposed for 5G LTE/IoT environment with various modulation techniques using 2×2 and 4×4 MIMO test benches. From simulation results, it is observed that the proposed detector outperforms other combinations of the hybrid detectors in terms of power, area, and throughput. The proposed detector with the high throughput can be implemented in the Internet of things also. The proposed detector with intelligence may lead to the cognitive MIMO detector which can be used as pervasive and ubiquitous transceivers.

Fig. 5.6 BER performance of proposed detector for 2×2 MIMO system with 256 QAM modulation with AWGN channel



References

1. Tariqul Islam, M., et al.: A low complexity MIMO channel estimation design and FPGA implementation using orthogonal matrix triangularization. *WSEAS Trans. Adv. Eng. Educ.* **7**(12), (2010)
2. Kim, H. S., et al.: An efficient FPGA based MIMO-MMSE detector. In: 15th European signal processing conference (EUSIPCO), Poznan, Poland, 3–7 Sept 2007
3. Yin, B., Cavallaro, J.R.: LTE uplink MIMO receiver with low complexity interference cancellation. *Analog Integr. Circ. Sig Process.* **73**(2) (2012). ISSN 0925-1030
4. Umamaheswar, S., Anil Kumar, T., Srinivasa Rao, K.: K-best sphere decoder algorithm for spatial multiplexing MIMO systems. *Indian J. Sci. Res.* **14**(2), 21–28 (2017)
5. Mahender, K., Kumar, T.A., Ramesh, K.S.: Simple transmit diversity techniques for wireless communication systems. In: *Advances in Intelligent Systems and Computing* (2019)
6. Yousef Abdullah, A.I., et al.: Design and FPGA implementation of reduced complexity MIMO-MLD systems. *IEEE* (2011). ISSN 978-1-4244-9991-5
7. Shirly Edward, A., Malarvizhi, S.: Low complexity breadth first search sphere detector for MIMO systems. *J. Eng. Sci. Technol. Rev.* **8**, 101–104 (2015)
8. Yoon, C., Lee, H.: Implementation of low-complexity MIMO detector and efficient soft-output demapper for MIMO-OFDM-based wireless LAN systems. *EURASIP J. Wirel. Commun. Network.* (2013)
9. Sabella, D., Rost, P., Banchs, A., Savin, V., Consonni, M., Di Girolamo, M., Lalam, M., Maeder, A., Berberana, I.: Benefits and challenges of cloud technologies for 5G architecture. *IEEE* (2015). ISSN 978-14799- 8088-8,2015
10. Cattoni, A.F., Moullec, Y.L., Sacchi, C.: Efficient FPGA implementation of a STBC-OFDM combiner for an IEEE 802.16 software radio receiver. *Telecommun. Syst. J.* (2013)

Chapter 6

Automated Detection of Retinal Hemorrhage Based on Supervised Classifiers and Implementation in Hardware



K. A. Sreeja , S. S. Kumar , and Arun Pradeep 

Abstract Supervised machine learning algorithm based retinal hemorrhage detection and classification is presented. For developing an automated diabetic retinopathy screening system, efficient detection of retinal hemorrhage is important. Splat, which is a high level entity in image segmentation is used to mark out hemorrhage in the pre-processed fundus image. Here, color images of retina are portioned into different segments (splats) covering the whole image. With the help of splat level and GLCM features extracted from the splats, two classifiers are trained and tested using the relevant features. The ground-truth is established with the help of a retinal expert and using dataset and clinical images the validation was done. The trained classifier's output is evaluated and the classifier with the best output is chosen for implementation in hardware.

Keywords Retinal hemorrhage · Diabetic retinopathy · Fundus image · Splat feature classification · GLCM features · Raspberry Pi

6.1 Introduction

The World Health Organization estimated that by 2030, there will be nearly 366 million people with Diabetic Mellitus (DM) [1]. A microvascular complication of DM that is responsible for a major share of cases of blindness in the world is the Diabetic Retinopathy (DR). The severe complications like Microaneurysms, Exudates,

K. A. Sreeja (✉)

SCMS School of Engineering and Technology, Ernakulam, India

e-mail: ka.sreeja@gmail.com

S. S. Kumar · A. Pradeep

Noorul Islam University, Kanyakumari, India

e-mail: kumarss@live.com

A. Pradeep

e-mail: arunpradeep@msn.com

Occlusion, hemorrhages, etc., together known as DR. The early diagnosis can reduce the risk of losing vision. In order to reduce the diagnosing time, human error and increase the accuracy, several methodologies were developed for early diagnosis of DR and most of them use machine learning techniques. In this paper, classification of hemorrhage and non-hemorrhage fundus images, carried out using two different classifiers is presented. The classifier that performs the best, is chosen for realization in a Raspberry Pi computer system. The techniques used to develop the algorithm was chosen based on recent researches. When compared to large hemorrhages, it is seen that hemorrhages of small size are irregular in shape. Several algorithms were developed to find these abnormalities. In our work one of the classifier decisions is based on Neural network (NN) as described in [2]. Kumar et al. [3] presented a radiomics-driven Computer Aided Diagnosis (CAD) based method. In order to overcome the limitations with current CAD approaches such as decision making a CLASS-Enhanced Attentive Response Discovery Radiomics CLEAR-DR is proposed to aid clinical diagnosis of DR. Another important symptom of diabetic retinopathy is exudates, which are similar to hemorrhage pixels. An Early detection of exudates is presented by Wisaeng [4] using Morphology Mean Shift Algorithm (MMSA). Detection of bright and dark lesion which can be hemorrhages or exudates, using a combination of matched filter response (MFR) and Laplacian of Gaussian Response (LoG) [5] produced a 96.10–96.99% accuracy for various publicly available database in hemorrhage detection. Multi-resolution analysis (MRA) is given importance in the work done by Lahmiri [6]. The statistical features obtained after MRA is fed to a support vector machine to grade retinal hemorrhage. Detection of hemorrhage pixels from the bright optical disc is always a constraint. Many methods are already prevailing in order to remove optical disc from the fundus image. Five optic disc detection methods with an algorithms committee having waited voting is presented by Silva et al. [7] where, 6 public benchmark databases with 1566 images are employed. Even though, in our work the optical disc is not removed, this method is useful when pixel based approach is considered. One such method of optic disc removal is used in exudate detection that involves mathematical morphology [8]. After morphological operation, the hard exudates are extracted using adaptive fuzzy logic. The purpose of this research is to develop a supervised classification model using two different classifiers and compare the output based on their sensitivity, specificity and accuracy. Retinal hemorrhages are demarcated with the help of an ophthalmologist who use a high-level representation entity known as splat [9]. Splats are a collection of pixels that have similar fundamental features. A two-step feature selection process is carried out to remove redundant features from the splat and these features are applied to a supervised classification to predict the possibility of hemorrhage splats in the whole image. The hemorrhage is finally detected and shown as bright spots on the dark opponency image. The two classifiers are tested, and their responses are tabulated. Section 6.2 describes the research method. Feature extraction, classification and embedded system realization are portrayed in this section. Section 6.3 gives the result and discussion and Sect. 6.4 summarizes and concludes the work.

6.2 Methodology

After Initial Pre-processing of fundus images by strategies performed in [28, 29] an enhanced image is obtained in which pixels that are assumed to have similar spatial location and share same structural features such as color and intensity are partitioned into non-overlapping splats and spread over the entire image [10]. Splat based method uses several re-sampling strategies. In a fundus image with hemorrhage, the total number of hemorrhage pixels is comparatively less when the entire image is considered [11]. Therefore, a splat-based method is more likely to have better diversity in training the samples. Splats are generated using watershed segmentation algorithm [10]. In order to create meaningful splats, a scale specific over segmentation is performed. This is done in two steps. At first the gradient magnitude of contrast enhanced dark-bright opponent image is taken using different scales. It is done because of the variability in appearance of hemorrhages. All these values are aggregated and the maximum of the gradient value with its scale of interest (SOI) is taken to perform watershed segmentation. Lin et al. [12] The gradient magnitude is computed using Eq.6.1.

$$|\nabla I(x, y; s)| = \sqrt{I_x(x, y; s)^2 + I_y(x, y; s)^2} \quad (6.1)$$

where $I_x(x, y; s)$ is the image. Now establishing a scale-space representation of the image using Gaussian kernels G_s , the gradient magnitude is calculated from its horizontal and vertical derivative. The maximum of the gradient magnitude is given in Eq.6.2

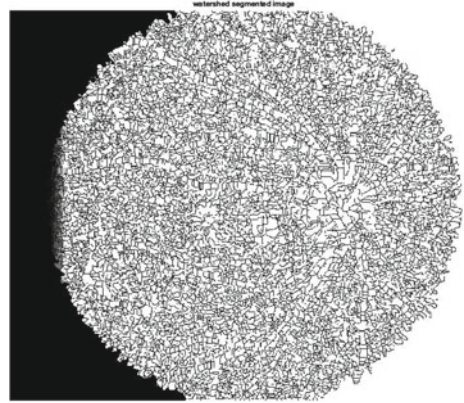
$$|\nabla I(x, y)| = \max_i |\nabla I(x, y; s_i)| \quad (6.2)$$

Splats are created using a modified watershed algorithm. The watershed segmented image is shown in Fig.6.1. All the splats generated throughout the total image area is refrained to a threshold limit. Even though the number of splats increase accuracy, the computation time tends to increase. So a compromise between the efficiency and accuracy has been considered.

6.2.1 Feature Extraction from Splats

After assigning reference labels for splats, a classifier can be trained to detect the target objects. An altogether of 352 potentially relevant features are taken to train the classifiers. They are: *Color*, *Difference Of Gaussian (DoG) Filter*, *Responses from Gaussian Filter Bank*, *Responses from Schmid Filter Bank*, *Responses from Local Texture Filter Banks*. These features are aggregated to obtain a meaningful response image which has low inter splat similarity and high intra splat similarity [13–19].

Fig. 6.1 Watershed segmented image



The features mentioned are pixel- based responses. In addition to these features, we take splat wise features according to Gray-Level Co-occurrence Matrix (GLCM) [16–22] statistics.

6.2.2 Preliminary Feature Selection and Classification

A two-step feature selection method is taken here so as to take only the relevant features and discard the irrelevant and redundant ones [23]. The preliminary feature selection is done using a filter approach in order to eliminate the features that are immaterial in discriminating hemorrhage and non-hemorrhage splats. A quadratic discriminant analysis (QDA) [24] is performed and by inspecting the features' variation with Misclassification Error (MCE) [25]. The preliminary features are chosen when the smallest MCE is reached. After preliminary selection, a wrapper approach is performed in order to get an optimal combination of relevant features with minimum redundancy. It is the peculiarity of the wrapper approach that it assesses different combinations of feature subsets customized for a certain classification algorithm with higher computation time [26]. The combinations are evaluated using a kNN Classifier. All the selected features are now applied to a sequential forward feature selection subset(SFS). After feature selection, two distinct trained classifiers are set up with the set of features and reference label instances.

kNN and ANN Classification: The kNN algorithm assigns soft class labels. The two classes defined or the outputs are hemorrhage splat or non-hemorrhage splat. The classifier decides the class of a particular splat based on the Euclidean distance of the features in an optimized feature space. The feature vector dimension is 19. As the value of k is increased the computation time increases and the splats are more accurately identified. But since all the k nearest neighbors are not near, an optimum value of k is chosen instead of an arbitrary value. In this work, the value of k is chosen

as 100 with a compromise between computational time and accuracy based on the work in [27]. For ANN, the features are selected that are required to train the neural network. These are the 19 features that were selected by wrapper approach. The neural network is initialized and the number of layers are defined. The weights are assigned arbitrarily small value so as to start the computation. The value of output for each layer is computed and error is calculated. The weights are updated for the output and the hidden layers and is repeated till the all the layers are trained. After training all the layers, it is checked whether all the splat features are used in training purpose. If not the process is repeated until the selection of all splat features is performed. The network is trained τ epochs each time irrespective of whether the network is convergent or not. When the difference of error between the current training series and the previous series is smaller than a threshold, then it can be concluded that the network is convergent and the training is stopped. After the training is completed, the classifier is validated for its accuracy using the validation set. The validation set does not change the trained values of the classifier and it is done only to ensure that overfitting has not occurred. To determine the class of splat sigmoid transfer function $S(x) = \frac{1}{1+e^{-x}}$ is used. When $S(x) = 1$ then it comes under a hemorrhage splat and when $S(x) = 0$, it is a non-hemorrhage splat.

6.3 Results and Discussions

Histogram equalization is done using the strategy proposed in [28, 29]. Also each image is normalized according to its prevailing pixel value at the three colour channels. The pixel values that occur frequently are shifted to the beginning of RGB colour space. Among the total of 1500 images obtained from the publically available database DIARETDB1 and the clinical images from Dr. Bhejan Singh's eye hospital, Nagercoil, 1050 were taken for training, 225 images for testing and 225 for validation. 10,500 splats were created among which 300 are hemorrhage splats. Images with at least 6 splats are taken for training. After sequential forward feature selection subset (SFS) only the relevant features were considered whereas the insignificant and redundant ones were removed from the feature set. The final feature set consists of 50 features from the 352 features obtained by filter approach and from this set 19 features were finally obtained by wrapper approach. The details of the final selected features are given in Table 6.1.

6.3.1 Classification of Splats Using kNN and ANN Classifiers

The splats are represented as a 19 dimensional feature vector. The kNN classifier and the ANN Classifier are trained on these features. Different values of k were tested whose values are chosen between 15 and 160 that involves both feature selection as well classification. After repeated iterations, the value of k was fixed at 100 without

Table 6.1 Details of final selected features

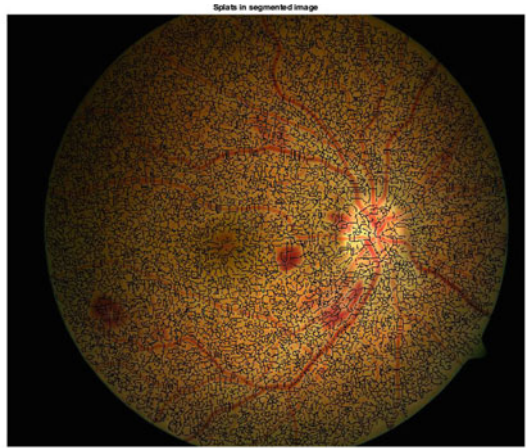
Features	Number	Description
DoG filter bank	s2-s0.5	From Green channel
DoG filter bank	s4-s0.5	From db and rg opponency
DoG filter bank	s8-s0.5	From db opponency
Gaussian filter bank	s = 8 orientation: 2, 3	Mean of second order Gaussian derivative from green channel
Gaussian filter bank	s = 1, 2, 4 orientation: 1, 2, 3	Mean of second order Gaussian derivative from green channel
Schmid filter bank	Response = 11	From db opponency
Mean of Gaussian	s = 8, 16	From Green channel

compromising the computation time and prediction accuracy. The target class for the classifier or the output consists of two classes: Hemorrhage or Non-Hemorrhage. The two classifiers were tested with the equal number of images and the results were compared. The splat centered Region of Convergence (ROC) curve for the fundus image given in Fig. 6.2 using the two classifiers are shown in Figs. 6.3 and 6.4. For a fundus image with 469 splats, the level of accomplishment of these classifiers are represented in the ROC curve. From the ROC curve for various threshold values, it is found that, among the two, ANN outperforms kNN classifiers in terms of sensitivity with an Area Under Curve (AUC) of 0.80 than 0.75 of kNN classifier. The confusion matrix calculated is given in Figs. 6.5 and 6.6 where n denotes the total number of splats for 520 images. A total 22574 splats were identified from the 520 images and they provide different accuracy at a certain threshold. The best classifier that performed in evaluation which is the ANN is now chosen for implementation in hardware.

6.3.2 Implementation in Hardware

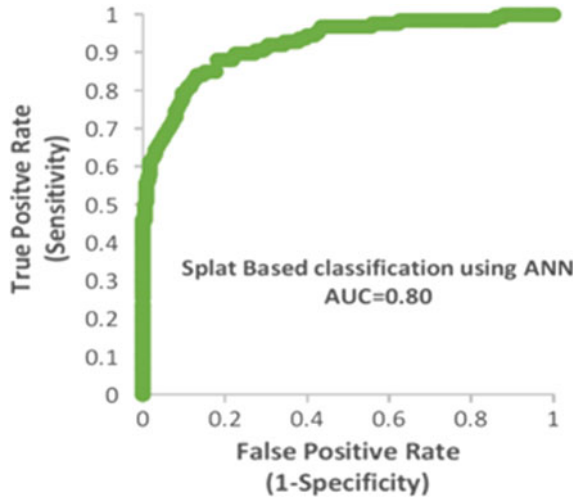
Image preprocessing, processing and classification was done in MATLAB using Intel i5 dual-core processor which has 8 GB RAM memory specification and a clock speed of 1.6 GHz. The motivation behind this work was to develop an aid to assist medical practitioners for an early and accurate diagnosis of DR. An easy diagnosis is accomplished if the whole process of detection was implemented on an integrated hardware. The tested and successfully executed algorithms were then implemented in Raspberry-Pi system as seen in Fig. 6.7. The inclination towards Raspberry-Pi board is the ease of designing a portable convenient handheld device. The Mobile Industry Processor Interface (MIPI) interface is connected to a fundus camera by which the real time images can be directly processed to detect hemorrhages which

Fig. 6.2 Splats identified



Pixel info (X, Y) (R G B)

Fig. 6.3 ROC for ANN



can predict the possibility of DR. This system can also be used with the help of a smart-phone camera and an aspheric lens to capture retinal images. Two Fundus

Fig. 6.4 ROC for kNN

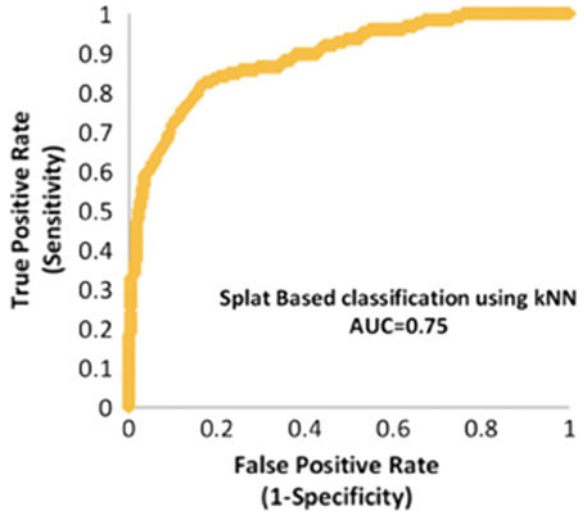


Fig. 6.5 Confusion matrix for ANN

n= 18892	Predicted NO	Predicted YES	
	Actual NO	TN= 9246	FP=202
Actual YES	FN= 669	TP=8775	
	9915	8977	

Fig. 6.6 Confusion matrix for kNN

n=22574	Predicted NO	Predicted YES	
	Actual NO	TN= 11257	FP=139
Actual YES	FN= 720	TP=10458	
	11977	10597	

images 1 and 2 were taken from standard diabetic retinopathy database DIARETDB1 and from clinical database for testing. Figures 6.8 and 6.9 shows the various stages of hemorrhage detection on images obtained from these source.

6.4 Conclusion

The presented work is a novel technique to detect exudates using morphological operation. The new enhancement method IIHE was used to increase the sensitivity of our existing algorithm that originally involved enhancement using CLAHE. A considerable increase in specificity indicates that the algorithm is more accurate while considering low intensity images. Using the same feature set to the classifier, the score of evaluation parameters could be increased by changing the enhancement technique. Further studies can be implicated to increase the PPV and *F*-Score of this algorithm. Thus a splat-based feature classification using Raspberry Pi is presented for the detection of retinal hemorrhage. The proposed classification strategy can model different lesions with different texture size and appearance. The algorithm is



Fig. 6.7 Raspberry Pi implementation

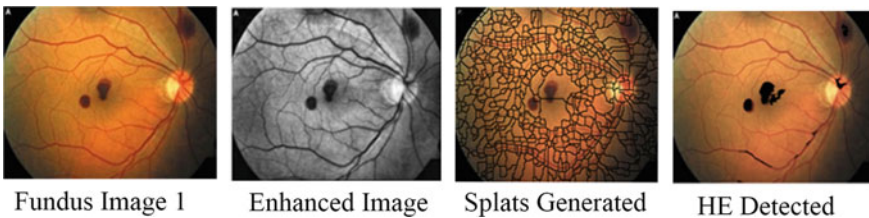


Fig. 6.8 Hemorrhage detection process applied on DIARETDB1 fundus image

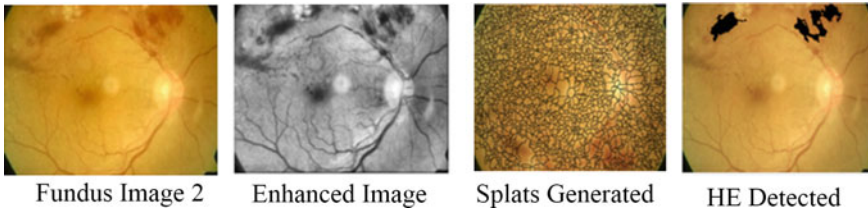


Fig. 6.9 Hemorrhage detection process applied on Clinical fundus image

validated on the publically available database DIARETDB1 and clinical image which was captured using a “Remidio Non-Mydriatic Fundus on Phone (FOP-NM10). The proposed detector can be incorporated into comprehensive DR assisting system for ophthalmologists.

References

1. World Health Organization: Prevent ion of blindness from diabetes mellitus (2006)
2. Zeng, X., Chen, H., Luo, Y., Ye, W.: Automated diabetic retinopathy detection based on binocular siamese-like convolutional neural network. *IEEE Access* **7**, 1 (2019)
3. Kumar, D., Taylor, G.W., Wong, A.: Discovery radiomics with CLEAR-DR: interpretable computer aided diagnosis of diabetic retinopathy. *IEEE Access* **7**, 25891–25896 (2019)
4. Wisaeng, K., Sa-Ngiamvibool, W.: Exudates detection using morphology mean shift algorithm in retinal images. *IEEE Access* **7**, 11946–11958 (2019)
5. Kar, S.S., Maity, S.P.: Automatic detection of retinal lesions for screening of diabetic retinopathy. *IEEE Trans. Biomed. Eng.* **65**(3), 608–618 (2018)
6. Lahmiri, S.: High-frequency-based features for low and high retina haemorrhage classification. *Healthc. Technol. Lett.* **4**(1), 20–24 (2016)
7. Silva, R.R.V.E., De Araújo, F.H.D., Dos Santos, L.M.R., Veras, R.M.S., De Medeiros, F.N.S.: Optic disc detection in retinal images using algorithms committee with weighted voting. *IEEE Lat. Am. Trans.* **14**(5), 2446–2454 (2016)
8. Ranamuka, N.G., Meegama, R.G.N.: Detection of hard exudates from diabetic retinopathy images using fuzzy logic. *IET Image Process.* **7**(2), 121–130 (2013)
9. Tang, L., Niemeijer, M., Reinhardt, J.M., Member, S., Garvin, M.K., Abramoff, M.D.: Splat feature classification with application to retinal hemorrhage detection in fundus images. *IEEE Trans. Med. Imaging* **32**(2), 364–375 (2013)
10. Fairfield, J.: Toboggan contrast enhancement for contrast segmentation. In: 1990 10th International Conference on Pattern Recognition, vol. 1, pp. 712–716 (1990)
11. Chawla, N.V., Japkowicz, N., Ko, A.: Editorial: special issue on learning from imbalanced data sets. *SIGKDD Explor. Newsl.* **6**, 1–6 (2004). <https://doi.org/10.1145/1007730.1007733>
12. Lin, Y.-C., Tsai, Y.-P., Hung, Y.-P., Shih, Z.-C.: Comparison between immersion-based and toboggan-based watershed image segmentation. *IEEE Trans. Image Process.* **15**(3), 632–640 (2006)
13. Abraoff, M.D., et al.: Automated segmentation of the optic disc from stereo color photographs using physiologically plausible features. *Investig. Ophthalmology Vis. Sci.* **48**(4), 1665 (2007)
14. Romeny, B.M.: *Front-End Vision and Multi-scale Image Analysis: Multi-scale Computer Vision Theory and Applications*, 1st edn. Springer, Berlin (2003)

15. Tang, L., Niemeijer, M., Abramoff, M.D.: Splat feature classification: detection of the presence of large retinal hemorrhages. In: 2011 IEEE International Symposium on Biomedical Imaging: From Nano to Macro, pp. 681–684 (2011)
16. Engler, O.: Introduction to Texture Analysis: Macrotecture, Microtexture, and Orientation Mapping, 2nd edn. CRC Press LLC, Boca Raton (2017)
17. Varma, M., Zisserman, A.: A statistical approach to texture classification from single images. *Int. J. Comput. Vis.* **62**(1/2), 61–81 (2005)
18. Alharan, A.F.H., Fatlawi, H.K., Ali, N.S.: A cluster-based feature selection method for image texture classification. *Indonesian J. Electr. Eng. Comput. Sci.* **14**(3), 1433–1442 (2019)
19. Hasan, A.M.: A hybrid approach of using particle swarm optimization and volumetric active contour without edge for segmenting brain tumors in MRI scan. *Indonesian J. Electr. Eng. Inform.* **6**(3), 292–300 (2018)
20. Tamura, H., Mori, S., Yamawaki, T.: Textural features corresponding to visual perception. *IEEE Trans. Syst. Man. Cybern.* **8**(6), 460–473 (1978)
21. Niemeijer, M., Staal, J., van Ginneken, B., Loog, M., Abramoff, M.D.: Comparative study of retinal vessel segmentation methods on a new publicly available database. In: Proceedings of the SPIE 5370, Medical Imaging 2004: Image Processing (12 May 2004). <https://doi.org/10.1117/12.535349>
22. Niemeijer, M., Abramoff, M.D., van Ginneken, B.: Segmentation of the optic disc, macula and vascular arch in fundus photographs. *IEEE Trans. Med. Imaging* **26**(1), 116–127 (2007)
23. Kohavi, R., John, G.H.: Wrappers for feature subset selection. *Artif. Intell.* **97**(1–2), 273–324 (1997)
24. Srivastava, S., Gupta, M.R., Frigiyik, B.A.: Bayesian quadratic discriminant analysis. *J. Mach. Lear. Res.* **8**, 1277–1305 (2007)
25. Duda, R.O., Hart, Peter E., Stork, D.G.: Pattern Classification, 2nd edn. Wiley, Hoboken (2000)
26. Tarassenko, L., Roberts, S.: Supervised and unsupervised learning in radial basis function classifiers. *IEE Proc. Vis. Image Signal Process.* **141**(4), 210–216 (1994). <https://doi.org/10.1049/ip-vis:19941324>
27. Sreeja, K.A., Kumar, S.S.: Comparison of classifier strength for detection of retinal hemorrhages. *Int. J. Innovative Technol. Exploring Eng. (IJITEE.org)* **8**(S63), 688–693 (2019)
28. (9) (2019)
29. Arun, P., Felix, J.X.: Intensity index based histogram equalization technique for retinal image enhancement and classification of hard exudates using supervised learning. *Int. J. Eng. Adv. Technol. (IJEAT.org)* **8**(5) (2019)

Chapter 7

Data Encryption as Security Measure in IoT-Enabled Healthcare



M. Shankar Lingam, G. S. Raghavendra, Arun Kumar, V. Anand,
and A. M. Sudhakara

Abstract Wearable and implantable IoT medical devices like glucose meters, blood pressure cuffs, defibrillators and other sensors and devices are used in today's patients monitoring systems as a part of digital health initiative. This is an important measure taken up by healthcare industries and organizations, and this would go on well as long as trouble creators called medhackers do not meddle with patients' data for disruptive purposes. Information transaction of sensed medical data among patients and healthcare professionals is usually carried out via wire or wireless media or via intranet, Internet and dedicated channels. Most of the regular hackers intercept data transfer in Internet for economic and political gains, whereas medhackers who are psychos intercept and manipulate medical data for vengeance and possibly for sadistic self-gratification. In any case, IoT-enabled healthcare system is not exempted from cyber-attack. A number of people have worked on solving this problem in order to ensure safe and secured medical data transaction in terms of firewall and enhancement of security in communication protocols. Not much work has been done in improving security using robust data encryption and possibly data compression

M. Shankar Lingam (✉)
NIRDPR, Hyderabad, India
e-mail: shankumacharla@gmail.com

University of Mysore, Mysore, India

G. S. Raghavendra
BIMS, University of Mysore, Mysore, India
e-mail: raghavtejeswi@gmail.com

A. Kumar
Department of Computer Science, BITS, Warangal, India
e-mail: arun.arigala@gmail.com

V. Anand
KITS, Warangal, India
e-mail: valupadas2@gmail.com

A. M. Sudhakara
CIST, University of Mysore, Mysore, India
e-mail: sudhakara.mysore@gmail.com

© The Editor(s) (if applicable) and The Author(s), under exclusive license to Springer Nature Singapore Pte Ltd. 2021

Y.-D. Zhang et al. (eds.), *Smart Trends in Computing and Communications: Proceedings of SmartCom 2020*, Smart Innovation, Systems and Technologies 182,
https://doi.org/10.1007/978-981-15-5224-3_7

techniques. In this context, this paper proposes reliable techniques for data encoding and compression in order to have considerable security in healthcare systems, which make use of IoT sensors and devices.

7.1 Introduction

The term ‘Internet of things (IoT)’ refers to networking of physical sensors and devices that are smart and connected. These sensors and devices are essentially embedded systems and are IP-enabled. At present, there is a growing concern about the security aspects of using IoT sensors and devices in healthcare systems. No doubt, IoT-enabled healthcare is a significant step taken towards improving life expectancy of global population. The present world population is 7,713,010,247, and it increases by four every second. (This data was obtained on 24 June 2019 at 1100 h from <https://www.worldometers.info/world-population/>.) The population growth increases by 39,057,124, on an average, every year. For the past one year, till date, the number of births in the global level is 67,314,230 and number of deaths 28,242,900. This means that about 42% of people die of malnutrition, disease, accident or ill health as against the number of people born every year. This calls for immediate attention of the government, healthcare professionals and, of course, people also to consider various steps to be taken so that the death rate may decrease as years pass by. One such step is to increase expenditure towards healthcare support and automation.

With reference to records given in <https://ourworldindata.org/health-meta>, one may observe a global trend in healthcare expenditure, which exposes a great amount of heterogeneity. Figure 7.1 shows how total expenditure on healthcare varies from country to country resulting in appropriate improvement in life expectancies. In spite of the fact that there is awareness and efforts taken by people, professionals and governments to allocate funds for healthcare systems, one cannot rule out the possibility of IoT-enabled healthcare system getting affected by cyber-attacks due to intellectual crooks and psychos. Of course, efforts are on to curb this menace, but most of the

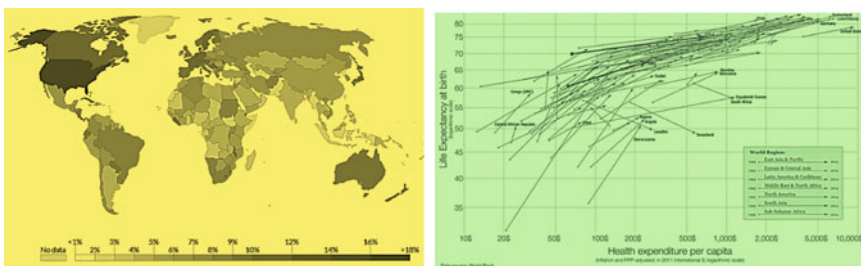


Fig. 7.1 Global expenditure during a year and improvement in life expectancy. Courtesy <https://ourworldindata.org/health-meta>

efforts are made in developing channel coding techniques to increase cryptanalytic time. Hardly few people have worked on source coding techniques meant for securing medical data from intercept and disruption. In this context, this paper proposes certain techniques for sensed medical data encryption and compression for a safe and secured information transaction via any medium, aiming at risk-free improvement of life expectancies.

7.2 IoT Data in Healthcare

Typically, a healthcare system would consist of hospitals, medical colleges, diagnostic centres, drug stores, physicians, radiologists, surgeons, pharmacists, paramedical staff, administrative staff, mobile medical units, data centres and patients. A healthcare support system would consist of medical instruments manufacturers, pharmaceutical companies, call centres, emergency units, medical technologists, insurance companies and governments. IoT-enabled healthcare system and its support system play a significant role in monitoring the health condition of patients by sensing signatures due to various organs mostly in the form of transduced electrical signals and in sending relevant data to potential users, be it a doctor or a patient. Figure 7.2 shows some of the wireless implantable medical devices.

Data collected from such sensors and devices are of two formats (i) linearly ordered sequence of measured data samples and (ii) multi-dimensional array of measured data samples. For example, the data collected by an electrocardiogram device would be of the form shown in Fig. 7.3. This image was obtained using a wearable monitor that provides a standardized method of wireless ECG and mobile ECG measurement (Fig. 7.4).

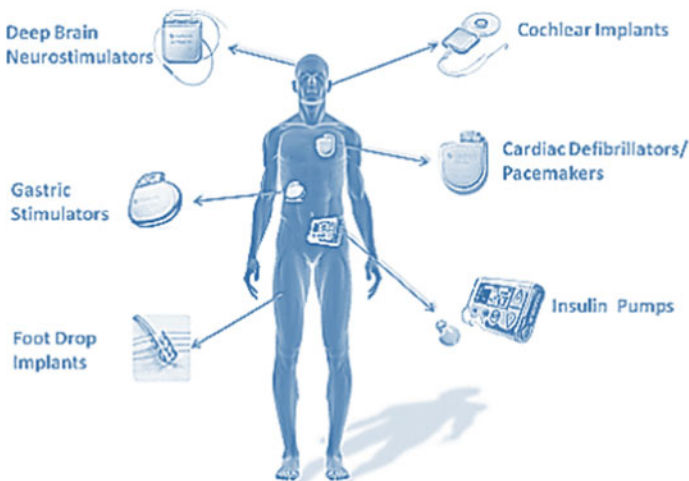


Fig. 7.2 Implantable medical devices

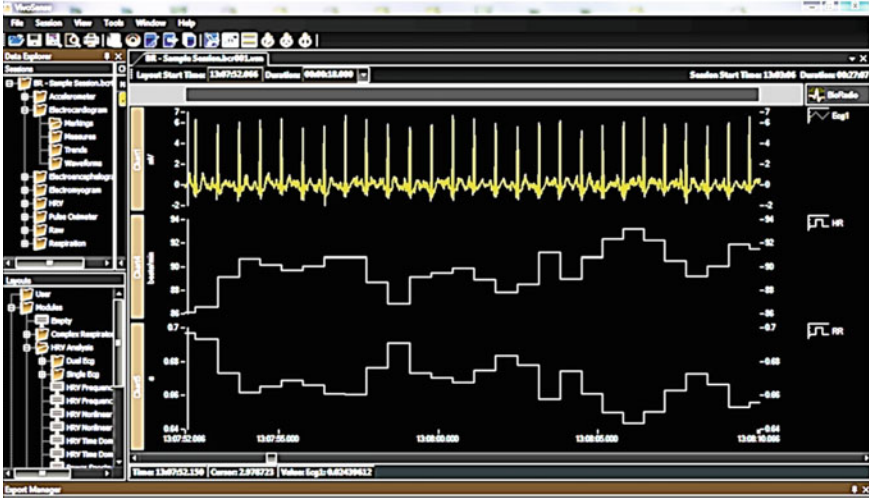


Fig. 7.3 ECG waveform from a mobile ECG monitor. *Courtesy* <https://glnurotech.com/bioradio/physiological-signal-monitoring/wireless-ecg-measurement-analysis-teaching/>

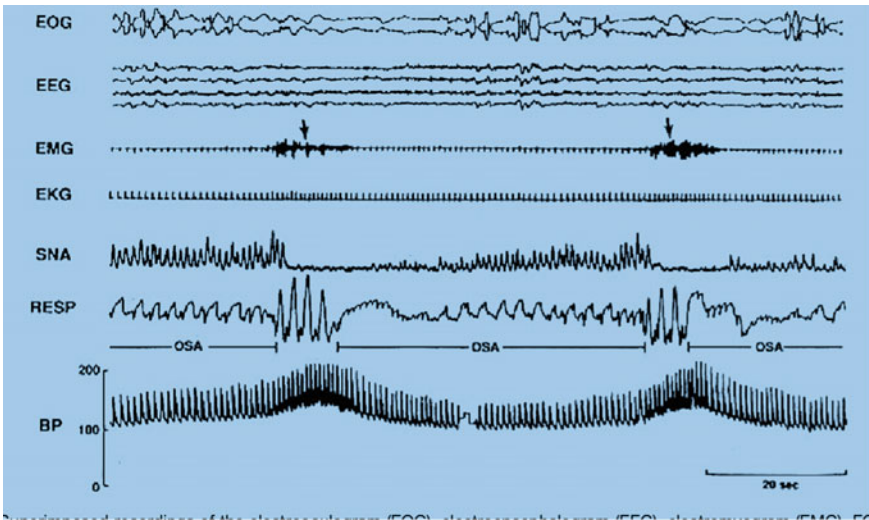


Fig. 7.4 Superimposed recordings of the electrooculogram (EOG), electroencephalogram (EEG), electromyogram (EMG), ECG (EKG), sympathetic nerve activity (SNA), respiration (RESP) and blood pressure (BP) during REM sleep in a patient with OSA. *Courtesy* Somers et al. 14 Copyright © 1995. Journal of Clinical Investigation

7.3 IoT Data Encryption and Compression

7.3.1 Basic Philosophy

IoT-sensed medical data, be it one-dimensional or multi-dimensional, is encrypted, compressed and stored using the following steps:

- Step #1 Apply discrete Rajan transform (DRT) to the medical data.
- Step #2 Sparse the spectral form of the data, compress and store.

IoT-sensed medical data which is encrypted, compressed and stored is uncompressed and decrypted to retrieve original data using the following steps:

- Step #1 The compressed data is uncompressed using morphological methods.
- Step #2 Uncompressed data is decrypted using inverse discrete Rajan transform (IDRT) to retrieve original data.

7.3.2 Basic Details DRT and IDRT

Consider a signal $x(n)$. DRT is applied to $x(n)$ and the spectrum $X(k)$ obtained after n number of stages. At every stage of computation, a unique matrix denoted as \mathbf{R}_k of dimension $(\frac{N}{2^{k-1}} \times \frac{N}{2^{k-1}})$ has to be constructed, and it is defined as: $\mathbf{R}_k = \begin{bmatrix} \mathbf{I}_p & \mathbf{I}_p \\ -e_k^1 \cdot \mathbf{I}_p & e_k^1 \cdot \mathbf{I}_p \end{bmatrix}$ where \mathbf{I} is the p th-order identity matrix. For example, at stage k , the order of the relevant identity matrix is $p_k = N/2^k$; $k \in \{1, 2, \dots, n\}$ and e_k^i is called ‘auxiliary information’, which indicates the intrinsic relationship between every equilibrium segment of the corresponding signal spectrum generated during the i th stage of computation. For instance, let the sequence at a particular stage be $\bar{s} = \{a, b, c, d, e, f, g, h\}$. Then, the ‘auxiliary information’ e_k would have certain intrinsic phasor relationship between the sample points a and e .

$$e_k^i = \begin{cases} -1, & \mathbf{x}_k^i(p_k + 1) < \mathbf{x}_k^i(1) \\ 1, & \text{otherwise} \end{cases}$$

where $i = \{1, 2, \dots, 2^{k-1}\}$. At every stage k , let \mathbf{Y}_k denote the output sequence and it is obtained based on the following equation $\mathbf{Y}_k = \mathbf{R}_k \mathbf{X}_k = [\mathbf{y}_k^1 \ \mathbf{y}_k^2 \ \dots \ \mathbf{y}_k^i]$. Here \mathbf{Y}_k has $2^k p_k$ elements in every stage. When $k = 1$, $\mathbf{X}_1 = \mathbf{x}$ (the original input sequence) and for $k > 1$, 2^{k-1} equilibrium segments are considered at every stage. Now, every segment is associated with relevant ‘auxiliary information’. Vector \mathbf{e}_k corresponds to the ‘auxiliary information’ pertaining to equilibrium segments in k stages. In this context, the following equations are valid: $\mathbf{e}_k = [e_k^1 \ e_k^2 \ \dots \ e_k^i]$ For example, if

$$s_k = [a \ b \ c \ d \ e \ f \ g \ h] \text{ and } s_{k+1} = \begin{bmatrix} a & e \\ b & f \\ c & g \\ d & h \end{bmatrix},$$

then e_k^1 and e_k^2 are the auxiliary phasor information pertaining to a and e and e and g , respectively. Note that auxiliary phasor values in e_k are derived from above equation. The operator matrix \mathbf{R}_k is constructed at a stage k using values of e_k^1 from e_k . In addition, for $k > 1$, the output at a stage is restructured into equilibrium segments, of course, iteratively and it is defined as:

$$\mathbf{X}_{k+1} = [\bar{x}_{k+1}^1 \ \mu_k^1 \cdot \bar{x}_{k+1}^2 \ \dots \ \mu_k^{i-1} \cdot \bar{x}_{k+1}^i] \text{ where } \mu_k = [\mu_k^1 \ \mu_k^2 \ \dots \ \mu_k^{i-1}]$$

and $\mu_k^{i-1} = e_k^1 \times e_k^i$ for $k > 1$

$$\text{Also, } \mathbf{X}_{k+1} = \begin{bmatrix} y_k^i(1) & y_k^i(2) \dots & y_k^i(p_k) \\ y_k^i(p_k + 1) & y_k^i(p_k + 2) & y_k^i(2p_k) \\ \vdots & \vdots & \vdots \\ y_k^i(2^{k-1}p_k + 1) & \dots & y_k^i(2^k p_k) \end{bmatrix}^T \\ = [\bar{x}_{k+1}^1 \ \bar{x}_{k+1}^2 \ \dots \ \bar{x}_{k+1}^i]$$

\mathbf{X}_{k+1} is a general expression that splits signal spectrum into equilibrium segments. This procedure is continued till the final DRT spectrum is obtained after n number of stages. The first value of the final DRT spectrum is known as ‘Cumulative Point Index (CPI)’. In fact, CPI is a quantitative measure of the cumulative energy of the input signal. Consider a discrete signal sequence $x(n) = \{1, 9, 6, 2, 3, 1, 5, 1\}$ of length $N = 8$. Then, one would carry out DRT computation in three iterative stages ($n = 3$) so that $k = \{1, 2, 3\}$. Now, at the initial stage, $k = 1, p = 4$ and $\mathbf{X}_1 = \mathbf{x}$. The operating matrix \mathbf{R}_1 would be of dimension of (8×8) . ‘Auxiliary information’ is obtained, and comparison is made between respective equations. The value of e_1^1 is evaluated as 1. Now, the operating matrix \mathbf{R}_1 takes the form:

$$\mathbf{R}_1 = \begin{bmatrix} I_4 & I_4 \\ -I_4 & I_4 \end{bmatrix}$$

The output of the first stage is computed as

$$\mathbf{Y}_1 = \mathbf{R}_1 \mathbf{X}_1 = [4 \ 10 \ 11 \ 3 \ 2 \ -8 \ -1 \ -1]^T.$$

The next step is to consider $k = 2, p = 2$ and \mathbf{R}_2 of dimension (4×4) . \mathbf{X}_2 is obtained by restructuring \mathbf{Y}_1 . Thus,

$$[\bar{x}_2^1 \bar{x}_2^2] = \begin{bmatrix} 4 & 2 \\ 10 & -8 \\ 11 & -1 \\ 3 & -1 \end{bmatrix}.$$

One can observe two equilibrium segments at this stage, that is, $i = 2$ and so, $e_2 = [e_2^1 e_2^2]$. The values are obtained as $e_2 = [1 -1]$, $\mu_2 = [\mu_2^1]$ and $\mu_2^1 = 1 \times -1 = -1$. Thus, X_2 is obtained as

$$X_2 = \begin{bmatrix} 4 & -2 \\ 10 & 8 \\ 11 & 1 \\ 3 & 1 \end{bmatrix}.$$

To construct operator matrix R_2 , $e_2^1 = 1$ is used so that

$$R_1 = \begin{bmatrix} 1 & 0 & 1 & 0 \\ 0 & 1 & 0 & 1 \\ -1 & 0 & 1 & 0 \\ 0 & -1 & 0 & 1 \end{bmatrix}.$$

The output of the second stage is calculated as

$$Y_2 = R_2 X_2 = \begin{bmatrix} 15 & -1 \\ 13 & 9 \\ 7 & 3 \\ -7 & -7 \end{bmatrix}.$$

Similarly for the last stage, $k = 3$, $p = 1$ and R_3 is of dimension (2×2) . Now,

$$[\bar{x}_3^1 \bar{x}_3^2 \bar{x}_3^3 \bar{x}_3^4] = \begin{bmatrix} 15 & 7 & -1 & 3 \\ 13 & -7 & 9 & -7 \end{bmatrix}.$$

The values of the 'auxiliary information' are obtained for four equilibrium segments (because $i = 4$) as $e_3 = [e_3^1 e_3^2 e_3^3 e_3^4] = [-1 -1 1 -1]$ and $\mu_3 = [\mu_3^1 \mu_3^2 \mu_3^3] = [1 -1 1]$. The value of X_3 is thus calculated as

$$X_3 = \begin{bmatrix} 15 & 7 & 1 & 3 \\ 13 & -7 & -9 & -7 \end{bmatrix}.$$

The final DRT spectrum is:

$$Y_3 = R_3 X_3 = \begin{bmatrix} 28 & 0 & -8 & -4 \\ 2 & 14 & 10 & 10 \end{bmatrix}.$$

The DRT spectrum in the sequence form is $X(k) = [28, 2, 0, 14, -8, 10, -4, 10]$. Note that the CPI of $X(k)$ is 28.

7.3.3 Inverse Discrete Rajan Transform

As explained already, discrete Rajan transform (DRT) is a homomorphic function and it also exhibits the isomorphism property when the auxiliary phasor information is preserved. Since DRT is also viewed as an isomorphic function, one should be able to retry the original signal data from its DRT spectrum by means of its inverse transform. Indeed, the inverse discrete Rajan transform (IDRT) is used to retrieve the input data with the help of e_k^1 and μ_k . Now, the DRT operator R_k is obtained using the values of e_k^1 and μ_k . The general expression used to retrieve intermediate signal data at every stage is:

$$\tilde{X}_m = \frac{1}{2} [R_m Y_m] = [x_m^1 \ x_m^2 \ \dots \ x_m^i]^T$$

where $m = \{k, k-1, \dots, 1\}$. As in the case of forward DRT computation wherein the sequence is split into equilibrium segments, in the case of IDRT computation, the segments are recombined and input sequence retrieved iteratively. When $m = k$, $Y_m = Y_k$ (the final DRT transformed output) and for $m < k$,

$$Y_{m-1} = [\bar{Y}_m(1) \ \mu_k^1 \cdot \bar{Y}_m(2) \ \dots \ \mu_k^{i-1} \cdot \bar{Y}_m(i)]$$

$$\bar{Y}_{m-1} = \begin{bmatrix} x_m^i(1) & x_m^i(2p_k + 1) & \dots & x_m^i(2^{k-1}p_k + 1) \\ x_m^i(2) & \vdots & & \vdots \\ \vdots & \vdots & & \vdots \\ x_m^i(2p_k) & x_m^i(2^2 p_k) & & x_m^i(2^k p_k) \end{bmatrix}$$

The final stage of IDRT computation yields the original input signal.

Example A procedure of obtaining DRT spectrum for a sequence and getting back original sequence from the spectrum by applying IDRT is given below. Consider a sample real-time speech data discrete sequence $x(n)$ of length 64.

$$x(n) = 0.123016357, 0.137512207, 0.163513184, 0.169403076, 0.154754639, \\ 0.151794434, 0.146972656, 0.156585693, 0.148101807, 0.143676758, \\ 0.13269043, 0.125610352, 0.11920166, 0.116485596, 0.11630249, \\ 0.09942627, 0.09197998, 0.091918945, 0.081085205, 0.05847168,$$

0.048126221, 0.035888672, 0.028137207, 0.014251709, 0.006439209,
 - 0.001617432, -0.034362793, -0.049682617, -0.065917969,
 - 0.080383301, -0.110229492, -0.137573242, -0.155883789,
 - 0.176696777, -0.194366455, -0.22088623, -0.228210449,
 - 0.254638672, -0.269989014, -0.274810791, -0.277496338,
 - 0.258209229, -0.270233154, -0.259857178, -0.242462158,
 - 0.221923828, -0.206390381, -0.176635742, -0.140960693,
 - 0.12878418, -0.109222412, -0.099914551, -0.063812256,
 - 0.037109375, -0.00189209, 0.032470703, 0.058349609,
 0.06451416, 0.072418213, 0.092376709, 0.099212646,
 0.116790771, 0.114685059, 0.119567871.

DRT is applied to $x(n)$ in block-wise manner and corresponding spectral blocks obtained as $X(k)$ (Fig. 7.5).

$X(k) = 1.203552, -0.02704, -0.0694, 0.003967, -0.01666, -0.01373, -0.07538,$
 $- 0.02118, 1.001495, 0.031097, 0.053436, -0.01682, 0.098663, -0.00809,$
 $0.013519, 0.011505, 0.44986, 0.048798, 0.085968, -0.0242, 0.197052,$
 $- 0.00345, 0.002716, -0.0209, -0.47333, 0.065186, 0.190369,$
 $- 0.02014, 0.31488, -0.01843, -0.01263, 0.005615, -1.77548,$
 $0.078583, 0.144623, 0.0159, 0.279816, 0.016083, 0.020721,$
 $- 0.02731, -1.91321, -0.07996, -0.08698, 0.000305, -0.21838,$
 $0.02063, 0.075745, -0.01813, -0.54922, -0.08255, -0.19211,$
 $0.004791, -0.40854, 0.039581, 0.070892, -0.01053, 0.737915, -0.04858,$
 $- 0.06018, 0.001099, -0.1626, -0.00366, -0.02368, 0.026489.$

Now, let us carry out sparsification of DRT spectrum and reconstruct sound wave from the sparsified spectrum using IDRT algorithm.

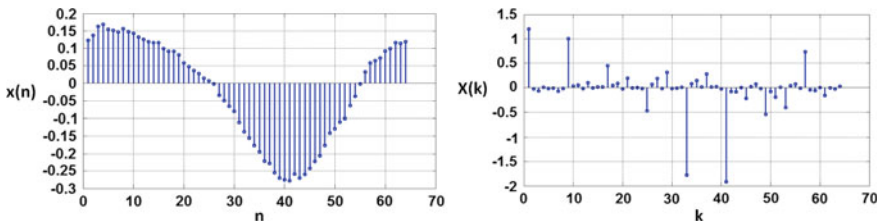


Fig. 7.5 Plot of $x(n)$ and $X(k)$

7.3.4 Sparsing of Data by Retaining CPI Alone

$X(k)$ is sparsed keeping the CPI alone in every block of length 8 and forcing other elements to 0. Then, the sparsed spectral sequence is $X_{s1}(k)$.

$$\begin{aligned} X_{s1}(k) = & 1.203552246, 0, 0, 0, 0, 0, 0, 0, 1.001495361, 0, 0, 0, 0, 0, 0, 0, \\ & 0.449859619, 0, 0, 0, 0, 0, 0, 0, -0.473327637, 0, 0, 0, 0, 0, 0, 0, \\ & -1.775482178, 0, 0, 0, 0, 0, 0, 0, -1.913208008, 0, 0, 0, 0, 0, 0, 0, \\ & -0.549224854, 0, 0, 0, 0, 0, 0, 0, 0.737915039, 0, 0, 0, 0, 0, 0, 0. \end{aligned}$$

The sparsed spectral representation in this case has just 8 nonzero samples. The compressed version of $X_{s1}(k)$ is obtained as $X'_{s1}(k)$.

$$\begin{aligned} X'_{s1}(k) = & 1.203552246, 1.001495361, 0.449859619, -0.473327637, \\ & -1.775482178, -1.913208008, -0.549224854, 0.737915039. \end{aligned}$$

$X'_{s1}(k)$ is stored as a representative biometric vector of a speaker. The degree of sparsity obtained in this case is 12.5%. The compressed sequence is shown in Fig. 7.6. During the testing phase, $X'_{s1}(k)$ is uncompressed and $X_{s1}(k)$ obtained. Now, IDRT is applied to $X_{s1}(k)$ and the reconstructed form of the original signal is obtained as $[\tilde{x}(n)]_1$.

$$\begin{aligned} [\tilde{x}(n)]_1 = & 0.150444031, 0.150444031, 0.150444031, 0.150444031, 0.150444031, \\ & 0.150444031, 0.150444031, 0.150444031, 0.12518692, 0.12518692, \\ & 0.12518692, 0.12518692, 0.12518692, 0.12518692, 0.12518692, \\ & 0.12518692, 0.056232452, 0.056232452, 0.056232452, 0.056232452, \\ & 0.056232452, 0.056232452, 0.056232452, 0.056232452, -0.059165955, \\ & -0.059165955, -0.059165955, -0.059165955, -0.059165955, \\ & -0.059165955, -0.059165955, -0.059165955, -0.221935272, \\ & -0.221935272, -0.221935272, -0.221935272, -0.221935272, \\ & -0.221935272, 0.221935272, -0.221935272, -0.239151001, \end{aligned}$$

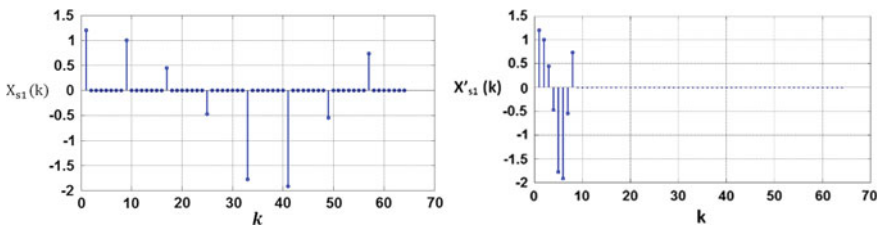


Fig. 7.6 Plot of $X_{s1}(k)$ and its compressed form

$-0.239151001, -0.239151001, -0.239151001, -0.239151001,$
 $-0.239151001, -0.239151001, -0.239151001, -0.068653107,$
 $-0.068653107, -0.068653107, -0.068653107, -0.068653107,$
 $-0.068653107, -0.068653107, -0.068653107, 0.09223938,$
 $0.09223938, 0.09223938, 0.09223938, 0.09223938,$
 $0.09223938, 0.09223938, 0.09223938.$

One can sparse the data by retaining CPI and the mid-frequency components. Then, one can obtain a compression of 25%. Figure 7.7 shows the plots of $x(n)$ and $[\tilde{x}(n)]_1$ in the same plot.

This technique has been tried on various sequential data and results studied. Figure 7.8 shows a real-time voice data. Figure 7.9 shows its 12.5% compressed form with the reconstructed signals. Figure 7.10 shows its 25% compressed form with the reconstructed signal.

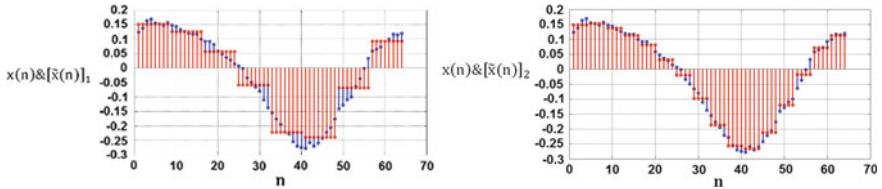


Fig. 7.7 Plots of $x(n)$ and $[\tilde{x}(n)]_1$ and plots of $x(n)$ and $[\tilde{x}(n)]_2$

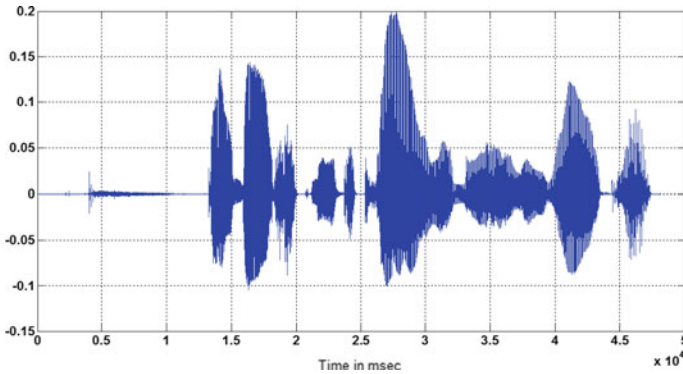


Fig. 7.8 A real-time voice data

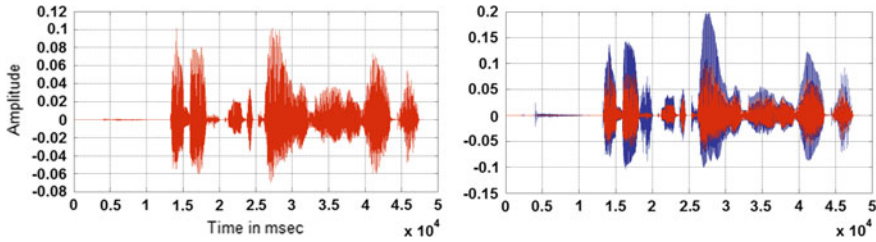


Fig. 7.9 Data compressed to 12.5% with the reconstructed signal

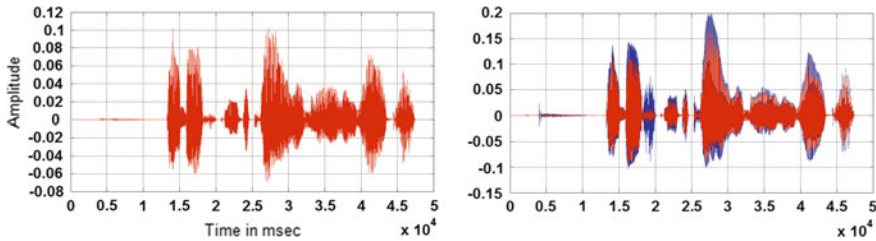


Fig. 7.10 Data compressed to 25% with the reconstructed signal

7.4 Summary

1. Any sensed medical data could be encrypted and compressed to a minimum of 12.4% and decrypted to the original form with minimum error.
2. This technique is applicable to multi-dimensional data also.
3. This robust source coding technique could be applied in all IoT-enabled healthcare system.
4. The application of IoT is growing day by day in each feature of the healthcare industry.

References

1. Harpham, B. (Writer and Editor): How the Internet of Things is changing healthcare and transportation. CIO, 8 Sept 2015. <http://www.cio.com/article/2981481/healthcare/howthe-internet-of-things-is-changing-healthcare-andtransportation.Html>
2. Finkle, J.: J&J warns diabetic patients: insulin pump vulnerable to hacking. Technology News, 4 Oct 2016. <http://www.reuters.com/article/us-johnsonjohnson-cyber-insulin-pumps-e-idUSKCN12411L>
3. Brook, C.: Health and fitness applications poor at protecting privacy, FTC says. Threatpost, 8 May 2014. <http://threatpost.com/health-and-fitness-applicationspoor-at-protecting-privacy-ftc-says>
4. BCC Research: Mobile health (mHealth) technologies and global markets 2014, 14 Mar 2014. <http://www.bccresearch.com/marketresearch/healthcare/mobile-health-hlc162a.html>

5. Privacy Rights Clearinghouse: Fact Sheet 39: mobile health and fitness applications: what are the privacy risks? 1 Dec 2014. <https://www.privacyrights.org/mobile-health-andfitness-applications-what-are-privacy-risks>
6. Michael, K.: Hackers create more IoT botnets with Mirai source code. PC World, 18 Oct 2016. <http://www.pcworld.com/article/3132571/hackerscreate-more-iot-botnets-with-mirai-source-code.html>
7. Lee, K.: Healthcare IoT security issues: risks and what to do about them, Dec 2015. <http://searchhealthit.techtarget.com/feature/Healthcare-IoT-security-issues-Risks-and-what-to-do-about-them>
8. Catalin, C.: Thousands of IoT medical devices found vulnerable to online attacks, 29 Sept 2015. <http://news.softpedia.com/news/thousands-of-iotmedical-devices-found-vulnerable-to-online-attacks-493144.shtml>
9. William, T.: Healthcare's 'Internet of Things' should be the 'security of Things', 19 May 2015. <http://www.healthcareitnews.com/blog/healthcaresinternet-things-should-be-security-things>
10. Mahmood, S.: Medjacking: the newest health care risk? 24 Sept 2015. <http://www.healthcareitnews.com/news/medjackingnewest-healthcare-risk>
11. Harriet, T.: How the 'Internet of Things' could be fatal, 4 Mar 2016. <http://www.cnn.com/2016/03/04/howthe-internet-of-things-could-be-fatal.html>
12. Luis, A.: Cyber security for Hospitals and Healthcare facilities—a guide to detection and prevention, Fredericksburg, VA. www.allite.com

Chapter 8

Agents-Based Service Restoration in Electrical Secondary Distribution Network



Rukia J. Mwifunyi, Nerey H. Mvungi, and Mussa M. Kissaka

Abstract Service restoration (SR) is one of the fundamental functionalities of distribution management system during fault management process. Several approaches have been devised to solve the SR problem on distribution network including centralized and distributed approaches. Most of the existing studies focused on the service restoration in the medium voltage network with very few focusing on the secondary distribution network (SDN). In most countries including Tanzania, the service restoration is accomplished manually through relying on operational experiences, rated capacity of the transformers and peak hour demand for decision making. This study aimed at designing distributed algorithm based on multi-agent system for SR in the SDN. The study has been conducted through intensive literature review together with focus group discussion with key stakeholders from utility company, study visits to the Tanzania SDN in Dar es Salaam region and interviews with the technical people. SDN with three transformers rated at 315, 200 and 100 kVA have been chosen as the pilot site for designing the distributed algorithm. The designed algorithm includes designing of multi-agent system, objective functions to be optimized and design for the equipment specifications and power system network topology to support SR. Four agents, namely control agent, grid agent, load agent and switch agent, have been found to be optimal for the SR process. The designed restoration process mainly focuses on load transfer to the nearby transformer and load shedding. The future work will focus on real implementation of the designed algorithm and consideration of the integration of the renewable distributed generations.

R. J. Mwifunyi (✉) · N. H. Mvungi

Department of Computer Science and Engineering, University of Dar es Salaam, Dar es Salaam, Tanzania

e-mail: rukiahilda@gmail.com

M. M. Kissaka

Department of Electronics and Telecommunications, University of Dar es Salaam, Dar es Salaam, Tanzania

R. J. Mwifunyi

Department of Electronics and Telecommunication, University of Dodoma, Dodoma, Tanzania

© The Editor(s) (if applicable) and The Author(s), under exclusive license to Springer Nature Singapore Pte Ltd. 2021

Y.-D. Zhang et al. (eds.), *Smart Trends in Computing and Communications: Proceedings of SmartCom 2020*, Smart Innovation, Systems and Technologies 182,

https://doi.org/10.1007/978-981-15-5224-3_8

8.1 Introduction

Demand of power continuously increases due to the rise in the industrialization, economic growth, expansion of power network and population growth in most of the developing countries. As a result, the size and complexity of the secondary distribution networks increases significantly. Occurrence of fault and the size of areas affected by fault are also increasing [1]. Due to the rise in the need of power and that industries need stable power supply; power supply should be restored as quickly as possible after occurrence of fault in order to improve safety, reliability and overall customer satisfaction [2]. In most SDN including that in Tanzania, the service restoration is accomplished manually in which the decision making is based on the operational experience through closing and opening wire jumpers to serve customers or waiting repairing process of the fault [3]. As a result, the process can take a number of hours and even days, resulting in losses to both customers and the utility company.

Various smart grid techniques have been proposed including the integration of renewable distribution network and demand side management programs in the SDN to ensure service reliability during normal operation and after occurrence of fault [4]. These efforts will easily be realizable if the overall network topology is changed to support network reconfiguration and service restoration, dedicated equipment for monitoring and controlling and well-planned communication infrastructures. This study focuses on the design of the service restoration algorithm in the SDN.

Significant work has been done to improve service restoration in the medium voltage distribution networks [5–9] and very few studies conducted in the secondary distribution networks [4, 10]. Both centralized and distributed approaches have been devised to solve the service restoration optimization problem. The centralized approaches include heuristic approaches [11, 12], mixed integer linear programming [13], genetic algorithms [14] and particle swarm optimization [15, 16]. Centralized approaches require high performing computing situated at the central control center and high-speed communication which have some disadvantages like the single point of failure. Existing studies in the low voltage focused on the use of centralized approach during network reconfiguration and service restoration. The study conducted by Xu et al. in [10] focused on the use of DGs to support service restoration using heuristic search method, and the study in [4] by Qiao and Yang focused on network reconfiguration considering penetration of electric vehicles using branch exchange method and exhaustive search algorithm.

With ever-increasing demand in computing and communication technology capacity, distributed intelligence applications, as an alternate solution, have been developed based on multi-agent systems (MAS) [5]. In distributed control approaches, there is more than one decision-making unit and data processing can be done in parallel that makes it faster and requires less processing capabilities which have been realized that can work well in complex networks [7, 17]. This study aimed at designing distributed algorithms for the service restoration in the SDN.

The designed distributed algorithm uses multi-agent technology for decision making and for sending actuation commands during service restorations. The designed algorithm includes the designing of multi-agent system, objectives function to be optimized during restoration and design for the equipment specifications and power system network topology to support service restoration. Apart from the adoption of the distributed control approach, the proposed algorithm has also considered the stochastic nature of load demand and load shedding during service restoration for improved capacity and avoiding overloading. Intelligent actuators with inbuilt processing capabilities have been proposed to be used to enable actuation decisions at the distribution substation level without relying on the central control center. Tanzanian secondary distribution network was used as the case study.

The rest of the paper is organized as follows: Sect. 8.2 discusses the study approach, Sect. 8.3 describes the current status for the Tanzanian secondary distribution network, Sect. 8.4 highlights the proposed distributed control model for SR, and Sect. 8.5 concludes the paper.

8.2 Study Approach

The designing process have involved a number of methods including intensive literature review for gaining the overall knowledge on the SR approaches and technologies and research directions, focus group discussions and interviews with Tanzanian utility company personnel to discuss the technical viability of the designed algorithm and lastly, study visits to the real network have also been conducted. Three secondary distribution transformers with the power rating of 315, 200 and 100 kVA have been selected to be used during designing of the agent-based service restoration approach. Selection criteria were based on the network size, network with customers of different priorities, mixed three and single-phase customers, and a network with at least open jumpers for supporting load transfer during restoration. This is an ongoing work, as the designed algorithm will be implemented and tested in simulation and on real network.

8.3 Current Status of the Tanzanian Secondary Distribution Network

The power distribution system is powered through the primary substations and has two main parts; namely primary distribution network having 33 kV or 11 kV and SDN having 0.23 kV/0.4 kV [18]. In Tanzanian power utility system, the automation of the primary distribution networks has partially been done in which fault can be detected, localized, isolated and restored automatically and visualized in the distribution control center. This is due to the availability of voltage and current sensors,

remote terminal units, remote operated switches and communication infrastructures in the network. The SDNs are invisible in the control center as there is only automated meter reading (AMR) for transferring data to central databases for analysis and billing purposes at the distribution transformers, fuses at some parts and wire jumpers as seen in Fig. 8.1. Fuses are installed at the low voltage side for transformer protection caused by overloading. There are no sensors, switches and no communication network at other parts of the network. The Tanzanian, SDN is slightly meshed in nature but operated radially, with at least one wire jumper used to reconnect during failure of the SDN. The existing wire jumpers are operated manually. There is no intelligent controller to decide on the available capacity at a specific time interval rather than relying on the rated capacity of the transformers.

The load demand in the secondary distribution networks changes with time of the day as seen in Fig. 8.2. The load also increases frequently as new customers are installed or new electrical equipment is connected at the customer side. Therefore, relying on the pre-configured information is no longer valid for the growing electrical network during service restoration. With rated capacity values, the service restoration cannot be done in some situation resulting to the loss of important loads like hospitals, schools and others. Thanks to the advancement of renewable energy technologies which have shown promising results in supporting service restoration in many developed countries during power shortage and power failure. Therefore, this study aims at proposing the design for the capacity-based distributed service

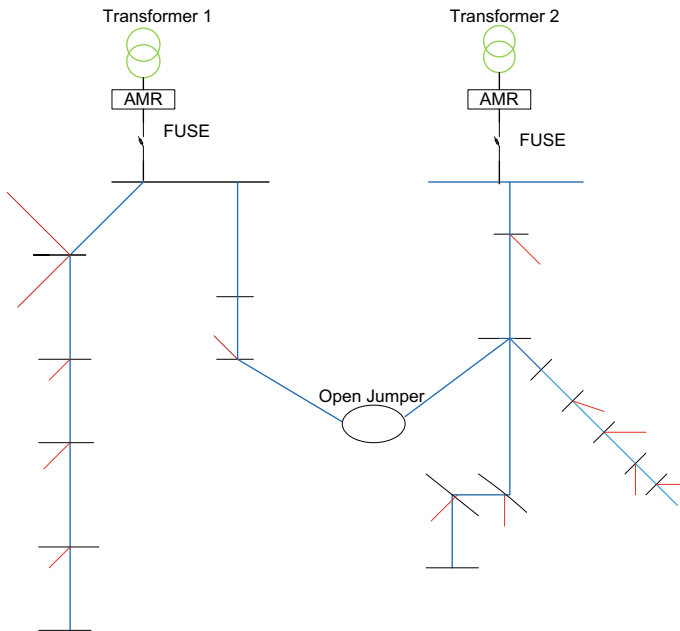


Fig. 8.1 Existing secondary distribution network topology

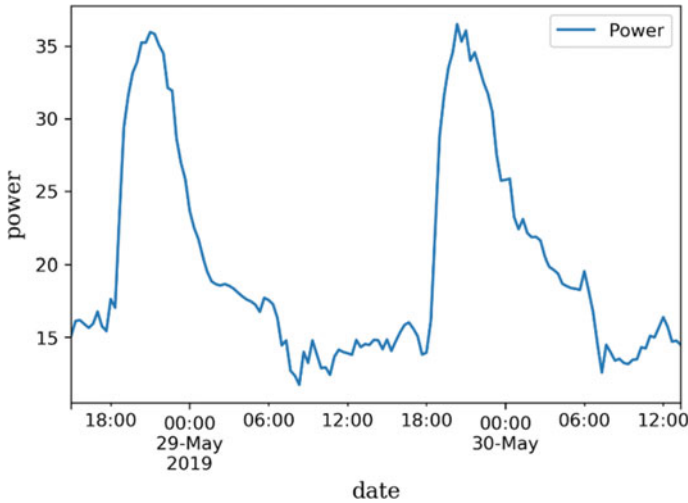


Fig. 8.2 Load profile

restoration algorithm considering the uncertainty nature of load demand which will further take advantage of the renewable generation sources installed at the customer sides for increased capacity.

8.4 Proposed Distributed Control Model for Service Restoration

The SDN is large in size and complex with a number of branches and laterals as seen in Fig. 8.3. Adding intelligence to this part of the network requires robust algorithms and may lead to large amount of data as a result, centralized control approaches may not be appropriate. This is due to the requirements of large processing unit and may suffer from single point of failure. The aim is to take advantage of computer technologies which has inverted distributed control approaches with more than one decision-making units for deploying in complex network. In this study, distributed control based on multi-agent system is used.

The proposed distributed algorithm for service restoration comprises of four agents, namely control agent (CA), grid agent (GA), load agent (LA) and switch agent (SA). The grid agent once resides in the area under fault, becomes the control agent. Table 8.1 describes the input, actions to be performed, conditions to be met and output by different agents. Features and capability of these agents will be implemented in the Raspberry Pi in which all decision making will be done and then send control commands to the actuators. In built processors for the smart meters

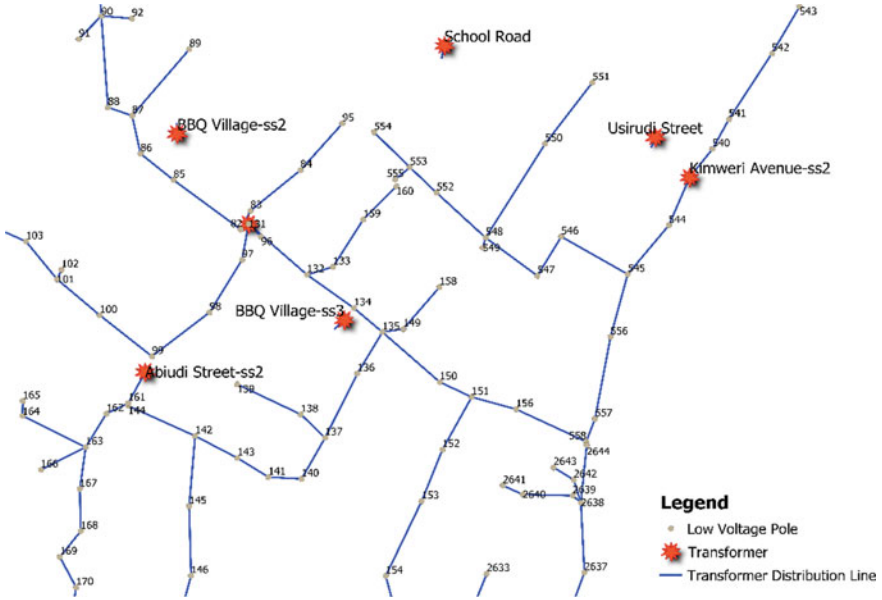


Fig. 8.3 Tanzania secondary distribution network

Table 8.1 Agent operation

	Control agent	Grid agent	Load agent	Switch agent
Input	<ul style="list-style-type: none"> Forecasted load demand Switch status 	<ul style="list-style-type: none"> Load demand Available capacity 	Fault information	Switching request
Actions	<ul style="list-style-type: none"> Receive request for power supply from load agent Send power request to the nearby GA Run optimization problem Sends switching request to the SA 	<ul style="list-style-type: none"> Receive request for power supply from nearby GA Forecast the available capacity based on loading history 	<ul style="list-style-type: none"> Request the power from the CA Forecast load for the estimated fault duration 	Sends control command to the circuit breakers and smart isolators
Condition	$P_{grid} \geq P_{load}$	$P_{available} \geq P_{load}$	$P_{supply} \geq P_{load}$	Pre-fault status
Output	<ul style="list-style-type: none"> Load to be restored Voltage levels Load to shed 	Remaining capacity	<ul style="list-style-type: none"> Forecasted load Shedding load 	Switch status

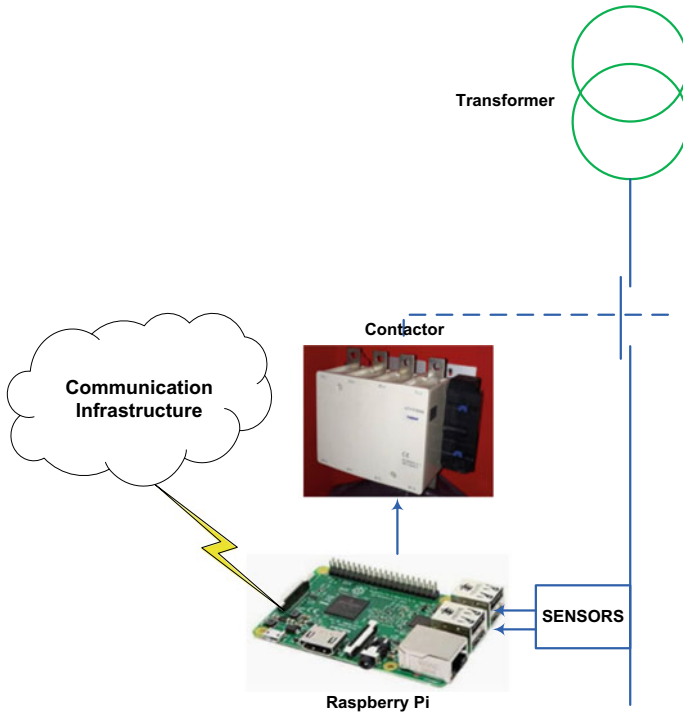


Fig. 8.4 Actuation node

throughout the secondary distribution network will be used as the load agents, and microprocessors connected to intelligent switches as the switch agents. The system design architecture for the actuators to be used in the secondary distribution network is shown in Fig. 8.4 in which sensors sense voltage and current levels and then send information to the Raspberry Pi which processes and sends the control commands to the contactors or relays which performs actuation during service restoration.

8.4.1 Objective Functions

Service restoration problem in power distribution system is a multi-objective, multi-constraint and nonlinear optimization problem. Among others, three objective functions have been found to be key for the service restoration in the secondary distribution network due to the overall physical nature of the network and overall needs for the service reliability. These objectives are maximizing the number of restored

customers [10, 19], minimizing power losses [4] and minimization of the cost associated with load shedding [12] as stated in (8.1–8.3). Together with the mentioned objective functions, voltage limits, line current limits and available capacity limits for the load transfer constraints need to be satisfied. The cost associated with load shedding will merely be attributed by the amount of load demand and/or the priority of load in which high priority customers will have higher cost as compared to lower priority customers.

Maximizing the number of restored loads based on their priorities.

$$\max f(x) = \sum_{i=1}^N w_i \times L_i \times y_i \quad (8.1)$$

where L_i : the load at bus i , y_i : status of the load at the bus i , w_i : priority level of the load at bus i , x : network configuration undergoing service restoration represented by status of switches and N : total number of branches.

Minimization of power loss.

$$P_{\text{loss}} = \sum_{i=1}^N I_i^2 R_i \quad (8.2)$$

where P_{loss} is the total power loss, I_i is the current through branch i and R_i is the resistance of branch i .

Minimizing cost (C) associated with Load Shedding (LS). The cost associated with load shedding is directly related to the amount of load shed and the criticality of the shedding load.

$$\min \sum_{i \in I_{\text{LS}}} C_i^{\text{LS}} \times \text{LS}_i \quad (8.3)$$

where C_i^{LS} is the cost associated with shedding load at bus i and LS_i is the amount of load to be shed at bus i .

8.4.2 Recommendations for the Improvement of the SDN

For realization of the self-healing in the Tanzanian secondary distribution networks, the following issues need to be taken into consideration:

- Motorized air circuit breakers should be installed at the distribution transformers to allow the protection of the transformers as shown in Fig. 8.5. The circuit breakers will comprise of the contactors for making and breaking purposes, as well as microcontrollers with decision-making capabilities.

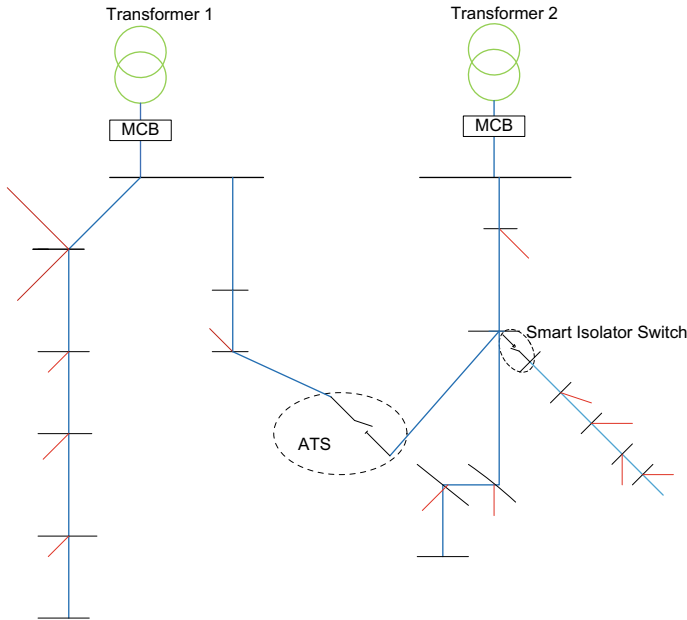


Fig. 8.5 Proposed network topology to support SR

- Smart switches along the branches also need to be installed to facilitate the load shedding in case the power supply is not sufficient enough to supply all loads in the network.
- Making use of the renewable energy sources to allow restoration of more loads apart from high priority loads.
- Open wire jumpers at the point of interconnection between two secondary distribution networks can be replaced with the automatic load transfer switches.

8.4.3 Design for the Equipment Specifications to Be Installed to Support Service Restoration in the Pilot Site

Specifications for the low voltage automation equipment are mainly based on IEC-60947 standard. General specifications for the equipment to be used in Tanzanian electrical SDN are as follows: AC electrical properties, applicable at electrical distribution level, support remote control operation, 400 V rated voltage and operate at 50 Hz frequency. Moreover, other parameters like the rated current in (8.4) and short circuit current in (8.5) vary with transformer capacity. Table 8.2 summarizes the design specifications for three distribution transformers in terms of breaker ratings.

Table 8.2 Circuit breaker specifications

Item	Application	Specifications
Motorized circuit breaker	315 kVA transformer	Rated current: 455 Short circuit current: 12 kA
	200 kVA transformer	Rated current: 289 Short circuit current: 7.2 kA
	100 kVA transformer	Rated current: 144 A Short circuit current: 3.6 kA

$$\text{Rated_Current} = \frac{S}{\sqrt{3} \times V} \tag{8.4}$$

$$I_{sc} = \frac{\text{Rated_Current}}{Z\%} \tag{8.5}$$

where S is the rated transformer capacity, V is the rated voltage and Z is the impedance of the transformer.

8.5 Conclusion

In this paper, we have proposed the design of the distributed algorithm for the service restoration in secondary distribution networks. Four agents have been designed to support the service restoration process, namely control agent, grid agent, load agent and switch agent. Realization of the service restoration process requires the installation of smart meters and smart switches across the secondary distribution network. Proposed changes for the network topology have also been highlighted. Integration of the renewable energy resources to the secondary distribution network is also crucial for increased capacity. The future work will be the implementation of the designed distributed algorithm for service restoration considering the integration of renewable energy sources.

Acknowledgements This material is based on the work supported by iGrid-Project at the University of Dar es salaam (UDSM) under sponsorship of Swedish International Development Agency (SIDA).

References

1. Ferreira, G.D., Gazzana, D.S., Bretas, A.S., Netto, A.S.: A unified impedance-based fault location method for generalized distribution systems. In: 2012 IEEE Power and Energy Society General Meeting. IEEE, San Diego, CA, USA (2012)
2. Kumar, Y., Das, B., Sharma, J.: Service restoration in distribution system using non-dominated sorting genetic algorithm. *Electr. Power Syst. Res.* **76**(9–10), 768–777 (2006)
3. Mnyanghwalo, D., Kawambwa, S., Mwifunyi, R., Gilbert, G.M., Makota, D., Mvungi, N.: Fault detection and monitoring in secondary electric distribution network based on distributed processing. In: MEPCON. IEEE, Cairo, Egypt (2018)
4. Qiao, Z., Yang, J.: Low-voltage distribution network reconfiguration considering high penetration of electric vehicles—a UK case study. In: ICRERA. IEEE, Birmingham, UK (2016)
5. Sekhavatmanesh, H., Cherkaoui, R.: Distribution network restoration in a multi-agent framework using a convex OPF model. *IEEE Trans. Smart Grid* **10**(3), 2618–2628 (2019)
6. Zidan, A., El-saadany, E.F.: A cooperative multiagent framework for self-healing mechanisms in distribution systems. *IEEE Trans. Smart Grid* **3**(3), 1525–1539 (2012)
7. Zidan, A., et al.: Fault detection, isolation, and service restoration in distribution systems: state-of-the-art and future trends. *IEEE Trans. Smart Grid* **8**(5), 2170–2185 (2017)
8. Sharma, A., Trivedi, A., Srinivasan, D.: Multi-stage restoration strategy for service restoration in distribution systems considering outage duration uncertainty. *IET Gener. Transm. Distrib.* **12**(19), 4319–4326 (2018)
9. Kumar, Y., Das, B., Sharma, J.: Genetic algorithm for supply restoration in distribution system with priority customers. In: International Conference on Probabilistic Methods Applied to Power Systems, Stockholm, Sweden (2006)
10. Xu, Y., et al.: DGs for service restoration to critical loads in a secondary network. *IEEE Trans. Smart Grid* **10**(1), 435–447 (2017)
11. Kleinberg, M.R., Miu, K., Chiang, H.D.: Service restoration of power distribution systems incorporating load curtailment. In: IEEE International Symposium on Circuits and Systems, pp. 1709–1712. IEEE, Taipei, Taiwan (2009)
12. Kleinberg, M.R., Miu, K., Chiang, H.D.: Improving service restoration of power distribution systems through load curtailment of in-service customers. *IEEE Trans. Power Syst.* **26**(3), 1110–1117 (2011)
13. Chen, B., Chen, C., Wang, J., Butler-Purry, K.: Sequential service restoration for unbalanced distribution systems and microgrids. *IEEE Trans. Power Syst.* **33**(2), 1507–1520 (2018)
14. Zidan, A., El-Saadany, E.F.: Incorporating customers' reliability requirements and interruption characteristics in service restoration plans for distribution systems. *Energy* **87**, 192–200 (2015)
15. Abdelaziz, A.Y., Mekhamer, S.F., Badr, M.A.L., Mohamed, F.M.: A modified particle swarm algorithm for distribution systems reconfiguration. In: 2009 IEEE Power & Energy Society General Meeting. IEEE, Calgary, AB, Canada (2009)
16. Wu, W.C., Tsai, M.S., Hsu, F.Y.: A new binary coding particle swarm optimization for feeder reconfiguration. In: International Conference on Intelligent Systems Applications to Power Systems. IEEE, Toki Messe, Niigata, Japan (2007)
17. Mwifunyi, R.J., Kissaka, M.M., Mvungi, N.H.: Distributed approach in fault localisation and service restoration: state-of-the-art and future direction. *Cogent Eng.* **6**(1) (2019)
18. Joseph, R., Mvungi, N.: Concept of automation in management of electric power systems. *Int. J. ECECE* **8**(12), 1849–1853 (2014)
19. Ibrahim, M.M.R., Mostafa, H.A., Salama, M.M.A., El-Shatshat, R., Shaban, K.B.: A graph-theoretic service restoration algorithm for power distribution systems. In: ITCE, pp. 338–343. Aswan, Egypt (2018)

Chapter 9

Packet-Level and Physical-Level Cross-Technology Communications: A Brief Introduction



Liwen Qiu, Qinglin Zhao, Lianbo Zhang, Shumin Yao, Jing Zhao,
and Li Feng

Abstract In the Internet of things, cross-technology communication (CTC) enables direct communication between heterogeneous devices without a gateway. CTC is receiving growing attention, because it can significantly reduce the hardware cost and the complexity of network deployment for communication between heterogeneous devices, as well as improve the network performance. At present, there are two types of CTC techniques, namely packet-level CTC and physical-level CTC. In this paper, we first provide an overview of the two types of techniques. Then, we detail the packet-level CTC via two typical protocols: Freebee and ZigFi, and the physical-level CTC via a typical protocol: WeBee. Finally, we compare the two CTC techniques in terms of hardware cost, communication direction, throughput, spectrum efficiency, and parallelism.

9.1 Introduction

In recent years, the extensive application of the Internet of things (IoT) has led to the widespread deployment of dense heterogeneous networks (e.g., Wi-Fi, ZigBee, and Bluetooth). In this scenario, since the devices use the same SIM band, inter-device interference is becoming more and more serious. But it also provides an opportunity for communication between the devices with different protocols. Recent research shows that cross-technology communication (CTC) has many benefits such as reducing hardware overhead, reducing the complexity of network deployment, and improving network performance. Traditionally, we use a gateway to build communication among heterogeneous devices by converting the protocols in high layer. However, this will introduce additional hardware overhead, increase network deployment complexity, and decrease network performance. In addition, if heterogeneous devices want to communicate with each other, we need to deploy gateways in advance. To overcome these drawbacks, some researchers propose packet-level CTC technique

L. Qiu (✉) · Q. Zhao · L. Zhang · S. Yao · J. Zhao · L. Feng
Macau University of Science and Technology, Macau, China
e-mail: 18098535ii20001@student.must.edu.mo

© The Editor(s) (if applicable) and The Author(s), under exclusive license
to Springer Nature Singapore Pte Ltd. 2021

Y.-D. Zhang et al. (eds.), *Smart Trends in Computing and Communications: Proceedings of SmartCom 2020*, Smart Innovation, Systems and Technologies 182,
https://doi.org/10.1007/978-981-15-5224-3_9

which utilizes some features like packet energy, packet interval, and packet duration to transmit information to other heterogeneous devices. For example in [1], a sender transmits a sequence of Wi-Fi packets by shifting the beacon frame position to emulate symbol message. These packets can be decoded by the ZigBee receiver through sensing the energy of emulated signal. In [2], the transmitter encodes CTC bits by mapping them to a unique packet duration which is different from the normal communication packet length. In [3], the sender will encode CTC bits in two different packet energy levels to transmit CTC information. Packet-level CTC only can carry limited bits in one packet and therefore obtain limited system throughput. Because of its low throughput, it is not suitable for deployment in high-speed and dense networks.

In recent years, some researchers proposed physical-level CTC techniques which embed CTC bits in the payload to communicate among heterogeneous devices by emulating the signal of heterogeneous devices. The receiver will consider the emulated signals as a legal signal and demodulate it correctly. For example, in [4], the Wi-Fi sender will emulate ZigBee signals by selecting payload bit pattern carefully. ZigBee receiver cannot identify the difference between the emulated signals and normal ZigBee signals. Since a packet can transmit thousands of bits, the physical-level CTC can achieve high throughput.

In this survey paper, we focus on packet-level CTC and physical-level CTC techniques. And we also consider some common features like cost, communication direction, throughput, data rate, spectrum efficiency, and parallelism.

The rest of the paper is organized as follows. First, we introduce two packet-level CTC techniques named FreeBee and ZigFi, respectively, in Sect. 9.2. Next, we present one representative physical-level CTC WeBee in Sect. 9.3. Finally, we summarize the common features of these two kinds of CTC in Sect. 9.4.

9.2 Packet-Level CTC

In this section, we introduce FreeBee and ZigFi in details. FreeBee realizes communication from Wi-Fi to ZigBee by utilizing the beacon position to encode CTC bits. ZigFi can make ZigBee communicate to Wi-Fi through different CSI in Wi-Fi packet.

9.2.1 FreeBee

FreeBee modulates the messages by shifting beacon position which is different from normal beacon position in wireless standard to encode CTC bits. In Fig. 9.1, we consider a standard beacon position is at t position where the modulating range of beacon interval is t . According to FreeBee, we shift the beacon from its standard position to another position that in the range of $[-T/2, T/2]$ to show the symbol is

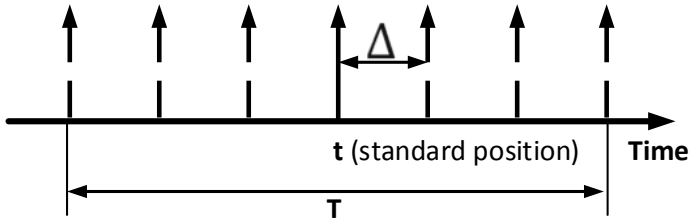


Fig. 9.1 The beacon position

encoded. As we know, the number of bits that can be embedded is determined by the shift unit Δ . According to the 802.11 standard, we can set the shift unit as 1.024 ms. And the range of intervals is equal to 100Δ . So the beacon shift can express 6 bits. If we want to transmit 0 bit and 1 bit, we set $t - 2\Delta$ as 0 bit and $t - \Delta$ as 1 bit. To promise the realizability of communication, FreeBee needs to retransmit the same beacon pattern many times which is depended on the channel noise.

Because of the incompatible physical protocol between Wi-Fi and ZigBee, the ZigBee receiver needs to adopt a folding algorithm to get the beacon position from collected RSSI samples. Next, we need to compare the collected beacon position with the standard beacon position. If it is in front of the standard beacon position, we decode it into 1 bit, otherwise, we decode it as 0 bit.

9.2.2 ZigFi

In [5], ZigFi realizes ZigBee communicates to Wi-Fi by different channel state information (CSI) values to encode CTC bits with 1 or 0. At the receiver, it proposed a receiver-initiated protocol which translates the decoding problem into CSI classification problem with support vector machine (SVM).

As shown in Fig. 9.2, when the Wi-Fi sender is transmitting Wi-Fi packets, we control the ZigBee packet to overlap with the Wi-Fi packet. It will make different CSI value that is overlapped by ZigBee packet from normal CSI value. We set the interfered CSI as 0 bit and the non-interfered CSI as 1 bit. As we can see in Fig. 9.2, the packet length will interfere the CTC communication. If the ZigBee packet is too short, the collision probability of ZigBee and Wi-Fi is low and the variation of CSI value is so small that the receiver cannot identify the overlapped CSI from normal CSI.

$$T_{DZ} > 2T_{DW} + T_{IW} \tag{9.1}$$

Wi-Fi packet length and ZigBee packet length must satisfy Eq. (9.1) to ensure discriminative CSI value. Where T_{DZ} is the transmission time of the ZigBee packet. T_{DW} is the transmission time of the Wi-Fi packet and T_{IW} is the transmission interval between two adjacent Wi-Fi packets.

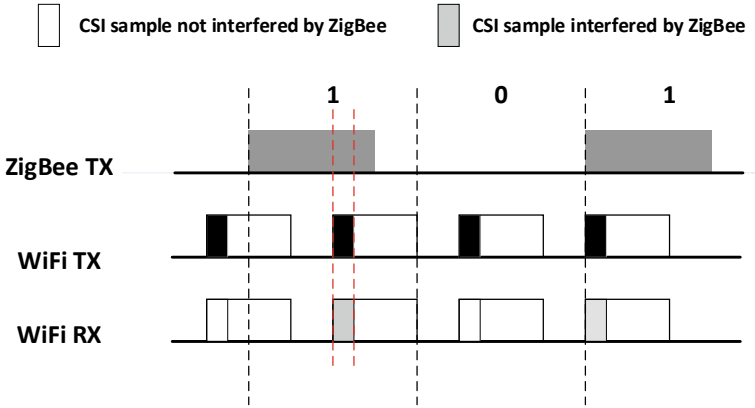


Fig. 9.2 Illustration of ZigFi

The Wi-Fi receiver will receive Wi-Fi packets and collect CSI values in each packet. Then, CSI classifier will classify CSI values by trained SVM classifiers. Next, the receiver demodulates the CSI values into 1 bit or 0 bit according to the decoding rule.

9.3 Physical-Level CTC

In this section, we introduce a representative physical-level CTC named WeBee in details. Because of the low throughput of packet-level CTC, the researcher proposed physical-level CTC to greatly improve throughput. WeBee makes Wi-Fi communicate to ZigBee by emulating ZigBee signals in Wi-Fi device.

As shows in Fig. 9.3, Wi-Fi sender will embed the ZigBee message in the payload portion and send emulated ZigBee signals to the receiver. ZigBee receiver considers

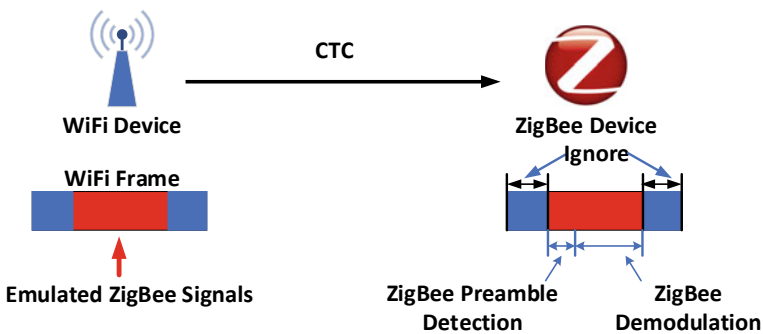


Fig. 9.3 Process of WeBee

the emulated signal as a normal ZigBee signal and ignores the Wi-Fi header and trailer. If the receiver detects the ZigBee preamble, it will demodulate emulated ZigBee signals.

However, we need to modify some Wi-Fi processes to emulate ZigBee signal perfectly. The sender sends an emulated ZigBee signal followed by follow steps. First, get the constellation points of the emulated ZigBee signal by reversing the Wi-Fi transmission procedure. Then, we quantify constellation points of the emulated ZigBee signal into predefined points according to the minimum Euclidean distance. Since the pilot signal affects the emulated ZigBee signal, we need to carefully select the transmitter central frequency to avoid overlapping the pilot frequency position with the emulated ZigBee signal frequency range. Because of the interfered by cyclic prefix (CP) which only exists in Wi-Fi transmission process, the sender will flip the packet header and trailer to reduce error. Finally, Wi-Fi sender sends the emulated signals.

When the ZigBee receiver detects the preamble of emulated ZigBee signal, it first converts the analog signal into the digital signal. Then, the receiver will get the phrase shift according to $\arctan(s(n) * s * (n - 1))$. ZigBee outputs the chip value “1” if the phase shift is bigger than 0 and otherwise outputs the chip value “0”. After collecting 32 chips, the receiver will map these chips into four bits symbol according to the predefined symbol-to-chips table.

9.4 Conclusion

In this section, we compare three CTC techniques in Table 9.1.

From Table 9.1, CTC realizes direct communication among heterogeneous devices without a gateway. So it has a low-cost feature. The physical-level CTC can transmit more bits than the packet-level CTC depending on the number of bits transmitted by a single packet. So the former has the characteristics of high throughput. Because the Wi-Fi band is larger than the ZigBee band, WeBee can embed two different CTC messages at different Wi-Fi frequencies. WeBee has higher spectrum utilization than the other two packet-level CTC techniques and supports parallel

Table 9.1 Comparison of three CTC techniques

		Cost	Communication direction	Throughput	Spectrum efficiency	Data rate	Parallelism
Packet layer CTC	FreeBee	Low	Wi-Fi to ZigBee	Low	Medium	Low	Not support
	ZigFi	Low	ZigBee to Wi-Fi	Low	Low	Low	Not support
Physical layer CTC	WeBee	Low	Wi-Fi to ZigBee	High	High	High	Support

CTC. Compared with ZigFi that can only transmit one bit in one packet, FreeBee can transmit more bits in one packet. In addition, FreeBee has higher spectrum efficiency than ZigFi.

Acknowledgements This work is funded in part by the National Nature Science Foundation of China (File no. 61872451 and 61872452) and in part by the Science and Technology Development Fund, Macau SAR (File no. 0098/2018/A3 and 0076/2019/A2). Li Feng is the corresponding author.

References

1. Kim, S.M., He, T.: FreeBee: cross-technology communication via free side-channel. In: Proceedings of the Annual International Conference on Mobile Computing and Networking, MOBICOM, vol. 2015, pp. 317–330 (2015)
2. Chebrolu, K., Dhekne, A.: Esense: communication through energy sensing. In: Proceedings of the Annual International Conference on Mobile Computing and Networking, MOBICOM, pp. 85–96 (2009)
3. Guo, X., Zheng, X., He, Y.: WiZig: cross-technology energy communication over a noisy channel. In: Proceedings—IEEE INFOCOM, pp. 1–9 (2017)
4. Li, Z., He, T.: Webee: physical-layer cross-technology communication via emulation. In: Proceedings of the 23rd Annual International Conference on Mobile Computing and Networking, pp. 2–14 (2017)
5. Guo, X., He, Y., Zheng, X., Yu, L., Gnawali, O.: Zigfi: harnessing channel state information for cross-technology communication. In: IEEE INFOCOM 2018-IEEE Conference on Computer Communications, pp. 360–368 (2018)

Chapter 10

Smart Traffic Navigation System (STNS) to Reduce Travel Time by Integrating Signals from Navigation and Traffic Systems



S. Sripranav, Akshay Ravi, K. Gautham, and R. Leela Velusamy

Abstract The status quo in navigation systems is to use real-time traffic detection to determine congestion-free paths and routes vehicles accordingly. However, such a service does not communicate with the traffic signals to regulate the traffic flow. As a result, there is a potential for reducing travel time that is not being leveraged. If the navigation system and the traffic system could communicate and were part of the same feedback loop, traffic systems can take decisions based on the destinations of vehicles queued. Furthermore, traffic signals can detect when certain roads are blocked with vehicles, and prioritize clearing of the blocked roads. Yet another benefit of such a system is that ambulances and government vehicles can be given a higher priority. In this paper, such a feedback loop is implemented on a custom-built simulator to analyze if the average travel time of all the vehicles reduces in the system under various traffic conditions.

10.1 Introduction

In the current society, the quick transport is one of the basic needs. With increase in population, the number of automobiles will increase faster than transportation infrastructure due to which traffic congestion will become a pressing issue.

S. Sripranav (✉) · A. Ravi · K. Gautham · R. Leela Velusamy
National Institute of Technology Trichy, Trichy 620015, India
e-mail: pranavsureshkumar@yahoo.co.in

A. Ravi
e-mail: akshaynitt97@gmail.com

K. Gautham
e-mail: heygautham@gmail.com

R. Leela Velusamy
e-mail: leela@nitt.edu

Most of the past studies were based on prediction of traffic flows [1–3]. These models would be effective in handling recurring traffic congestions, but would fail in the case of congestions caused due to unprecedented events. Therefore, compared to solutions based on prediction models, solutions which route traffic dynamically would be better [4–6].

The most advanced solutions use satellite feedback to identify congested roads in the city. This information is then used to control traffic signals in real time. This approach has the potential to be much more effective. If it is possible for the traffic signal to know the vehicle's position and destination, then the traffic management system could ensure that the vehicle reaches its destination in the least possible time as it has both the congestion information and the destination information. Certain vehicles such as ambulances and fire engines could also be given a higher priority so that they can reach their destination quickly. These are the features that have been incorporated in the proposed model.

The proposed model (STNS) aims to decrease the average travel time of the entire grid network. In order to effectively remove congestion at every junction, the lane with the highest idle time at a particular junction would be given a green light. Using concepts from Internet of things, the real-time data from the traffic system is used for decision making.

10.2 Related Work

The existing literature on traffic management is given in Table 10.1. As can be observed from Table 10.1, the solution suggested in “Large-Scale Traffic Congestion Prediction Based on the Symmetric Extreme Learning Machine Cluster Fast Learning Method” [1], “A Hybrid Method for Short-Term Traffic Congestion Forecasting Using Genetic Algorithms and Cross Entropy” [2] and “An Urban Traffic Flow Model integrating Neural Networks” [3] only predict congestion but do not take the necessary steps to avoid it. Moreover, there could be unpredictable congestion scenarios that are not detected.

The solution suggested in “Shortest Processing Time Scheduling to Reduce Traffic Congestion in Dense Urban Areas” [4] does focus on reducing congestion in an area but it does not take an added effort to reduce travel time by considering navigation. Although, the solution proposed in “On a Hopfield Net Arising in the Modeling and Control of Oversaturated Signalized Intersections” [5] which uses Hopfield neural network is highly optimized, it has been implemented only with two light phases and tries to reduce travel time only by reducing parameters like waiting time and not through navigation itself. Lastly, even though the solution proposed in “Deep Learning System for Vehicular Re-Routing and Congestion Avoidance” [6] reduces congestion and focuses on re-routing the vehicles, it requires probe cars at all points of time to get information on congestion.

Table 10.1 Existing solutions

Paper title	Concepts	Problems solved	Advantages	Limitations
Large-Scale Traffic Congestion Prediction Based on the Symmetric Extreme Learning Machine Cluster Fast Learning Method [1] (2019)	S-ELM-cluster fast learning methodology	Large-scale traffic congestion data learning	Accuracy over smaller subsets, high training speed	Predicts congestions but does not help to avoid it
A Hybrid Method for Short-Term Traffic Congestion Forecasting Using Genetic Algorithms and Cross Entropy [2] (2016)	Genetic algorithm (GA) and Cross entropy (CE)	Predicts congestion for specific time horizons	Optimizes the hierarchical rule-based systems further	Predicts congestions but does not help to avoid it
An Urban Traffic Flow Model integrating Neural Networks [3] (1997)	Neural networks	Prediction of traffic flow	Good accuracy	Predicts congestions but does not help to avoid it
Shortest Processing Time Scheduling to Reduce Traffic Congestion in Dense Urban Areas [4] (2017)	MDDF and MADDF	Traffic congestion in dense urban areas	Reduce the traffic congestion at intersections by up to 80%	Reduces congestion but not travel time
On a Hopfield Net Arising in the Modeling and Control of Oversaturated Signalized Intersections [5] (1999)	Hopfield neural network (RNN)	Dynamic control of oversaturated signalized intersections	Highly optimized and fast computation	Considers only two light phases
Deep Learning System for Vehicular Re-Routing and Congestion Avoidance [6] (2019)	Alternate routes are generated using EBkSP algorithm	Detect congested areas and redirect vehicles	Inexpensive, easy to implement and no new infrastructure	Requires vehicles acting as probe cars at all points of time

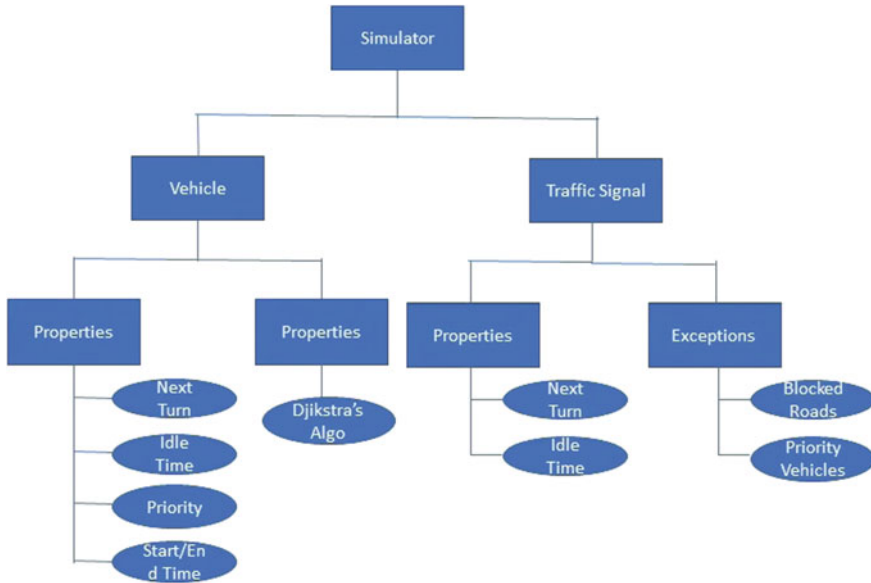


Fig. 10.1 STNS simulator flow diagram

10.3 Design of the Proposed Model

An infrastructure has to be designed to allow the vehicles and traffic signals to interact with each other. The goal of this infrastructure is to minimize the latency in communication between the vehicles and traffic signals. There are two possible architectures when designing such a system. One is a typical **client-server model** and the other is a **decentralized system**, with peer-to-peer communication, processing will be split among all the nodes of this decentralized network.

While the client-server model may seem simpler to implement, and more enticing from a cost perspective, there are plenty of disadvantages in this model such as high latency and the risk of single point of failure. For this reason, the decentralized model, despite its increased cost of implementation, is preferred. Keeping this in mind, each vehicle and each traffic signal will be processing the set of properties mentioned in Fig. 10.1, according to the algorithm of the STNS model. The data can be stored and processed on the cloud so that the traffic signal itself would require minimum infrastructure.

The evaluation metric used to analyze the performance of STNS is the average travel time where

$$\text{Average Travel Time} = \frac{\sum \text{Travel Time } \forall \text{ vehicles}}{\text{Total Number of vehicles}} \tag{10.1}$$

$$\text{Travel Time} = (\text{Vehicle destination reached time}) - (\text{Vehicle start time}) \tag{10.2}$$

10.4 Experimental Setup

The proposed model was tested for various test cases in order to measure the average travel time for all the vehicles in the system using a simulator with a grid layout consisting of six traffic junctions, each with four roads leading to and away from it. The grid layout was chosen to simulate the downtown metropolitan areas, thus widening the scope for which this proposed model can be implemented. For simplicity's sake, each road consists of a single lane.

10.5 Implementation

The two models incorporated in the simulator were the vehicle and the traffic signal.

10.5.1 Vehicle

Each vehicle maintains the following major properties:

1. **nextTurn**: This determines which direction the vehicle should travel to reach its destination as quickly as possible.
2. **idleTime**: Maintains the time the vehicle has spent waiting at traffic signals. This data is used by each traffic signal to assign priorities to its four edges. (Vehicles that have been idle longer are given higher priority)
3. **isPriority**: A simple Boolean that tells the traffic signals if the vehicle is a priority vehicle (like an ambulance/police vehicle) or a regular vehicle.
4. **startTime, endTime**: This is set when the vehicle reaches its destination and is used to determine the average travel time of all vehicles in order to tabulate the results of this proposed model against the existing timed signal model.

The navigation system determines the direction the vehicle should turn at the next traffic signal in order to reach its destination as quickly as possible. This navigation system uses **Dijkstra's algorithm** to do so.

The city's roads are converted into a graph representation, where each road is an edge, and the traffic junctions are nodes. Since Dijkstra's is a relatively expensive algorithm, this functionality is called only when it has to be, i.e., when a vehicle reaches the end of the road must know which direction it should turn.

$$\text{Time Complexity} = O(E \log V) \quad (10.3)$$

E number of edges (roads),

V number of vertices (traffic junctions + endpoints).

Dijkstra's algorithm also requires a weight to be assigned to each edge. In order to find the quickest path to the destination, this weight has to take into account two

factors—the length of the road and the traffic on the road. To account for both of these factors, the weight of an edge is defined as

$$\text{Weight} = a + (b * \text{number Of Vehicles On Road}) \quad (10.4)$$

a constant accounting for the length of the road,

b constant accounting for the number of vehicles on the road.

A collision proof move function that enables the vehicle to move to the end of the road or until it detects a vehicle in front of it as shown in Algorithm 1.

A function that is called when the vehicle's next turn matches the direction the traffic signal indicates. This enables the vehicle to make a collision proof turn to the next road.

Algorithm 1: Vehicle movement

```

while true do
    Calculate next position of vehicle;
    if vehicle can move to next position then
        | Update vehicle model to next position;
    else
        if vehicle reached destination then
            | Calculate travelTime of vehicle;
            | Update Average Travel Time;
        else
            Find the next turn direction of vehicle;
            while Traffic Signal shows red light do
                | Wait;
            end
            vehicle makes turn;
        end
    end
end
end

```

10.5.2 Traffic Signal

Each traffic signal consists of the following major properties:

1. **edges:** An array of the four edges surrounding the signal. Each edge contains a list of all the vehicles on it. This gives the traffic signal a view of the vehicles on all of its sides, where each vehicle needs to go, as well as the **idleTime** of each vehicle (how long each vehicle has been waiting at traffic signals).
2. **priorityOrder:** A property that defines what priority each of the four edges surrounding the traffic signal has with respect to each other. For example, if any of the edges contains a priority vehicle, that edge is automatically assigned the highest priority.

Table 10.2 Traffic states

North	East	South	West
Straight	Stop	Straight	Stop
Straight	Stop	Left	Left
Left	Left	Straight	Stop
Left	Right	Left	Stop
Left	Stop	Left	Right
Left	Straight	Stop	Left
Left	Left	Left	Left
Right	Left	Stop	Left
Stop	Left	Left	Straight
Stop	Left	Right	Left
Stop	Straight	Stop	Straight

Now that the each traffic signal has access to the state of the vehicles on its surrounding edges, it uses this data to determine which side gets a green light.

Each traffic signal assigns a priority order to its four surrounding edges based on each edge’s Total Idle Time:

$$\text{Total Idle Time} = \Sigma \text{ Idle Time } \forall \text{ vehicles on that edge} \tag{10.5}$$

The priorities are assigned in ascending order of total idle time, i.e., an edge with a higher total idle time will have a higher priority.

There are two exceptions to the above explained priority order assignment method, wherein a road is automatically assigned the highest priority:

1. **Blocked Roads:** If any road is entirely filled with vehicles such that no new vehicle will be able to turn onto this road
2. **Priority Vehicles:** If any road consists of a priority vehicle.

Note: Roads with priority vehicles are given preference over blocked roads.

Now that a priority order has been assigned, the traffic signal has to assign lights to each of its four sides. Table 10.2 gives all possible turn directions for vehicles in each edge. These are all the state combinations that are possible such that no collision occurs in the traffic junction. The traffic signal will determine which of these states to use based on the priority order as shown in Algorithm 2.

With the change in the traffic signal’s operation algorithm, a starvation could occur where any single edge does not get a green light for an extended period of time. This problem was eliminated by using idle time as a measure of priority. The longer a vehicle waits at a signal, the more its idle time increases and so does its priority and its chance of getting a green light.

Algorithm 2: Assigning Traffic Lights

```

Input : List of viable traffic states
Output: Optimal Traffic State
while Optimal Traffic State not determined do
    Obtain nextHighestPriorityEdge;
    Obtain turnDirection of nextHighestPriorityEdge's first vehicle;
    foreach trafficState  $\in$  Viable Traffic States do
        if turnDirection matches that of trafficState then
            | Keep trafficState in list of Viable Traffic States;
        else
            | Remove trafficState from list of Viable Traffic States;
        end
    end
end
return Optimal Traffic State;

```

10.6 Experiments and Results

Experiments were run on the simulator that was built. In order to test the potential benefits of the STNS model, the results of the evaluation metric (average travel time) was compared to that of a timed signal model that has a predetermined time assigned to each edge.

10.6.1 Test Cases

The cases mentioned below are tested multiple times and the average time taken for all the tries is considered. The results were plotted against the same situation, with a timed signal model and are shown in Tables 10.3 and 10.4.

- **Shortest Distance:** This is a study of the time required for a vehicle to travel from a source to its closest destination.
- **Longest Distance:** This is a study of the time required for a vehicle to travel from a source to its furthest destination.
- **All sources to all destinations:** This is a test meant to replicate a real life scenario where a multitude of vehicles are on the streets, each heading to its own destination.
- **Congestion Case:** This is a test which concentrates traffic around one signal, to test how the proposed model deals with a situation where there are vehicles waiting on all sides.
- **Priority Analysis:** In this test, preference was given to priority vehicles such as ambulances, to see how much faster they could reach their destinations when the roads were congested. In Fig. 10.2, the blue vehicle is a priority vehicle.

Table 10.3 Test cases results

Test case	Average travel time (s)	
	Timed signal (s)	Proposed model (s)
Shortest distance	9.182	6.709
Longest distance	28.822	22.781
All sources to all destinations	27.502	22.004
Congestion case	25.364	22.921

Table 10.4 Priority vehicle result

Travel time of priority vehicle (s)	
Timed signal (s)	Proposed model (s)
25.697	14.01

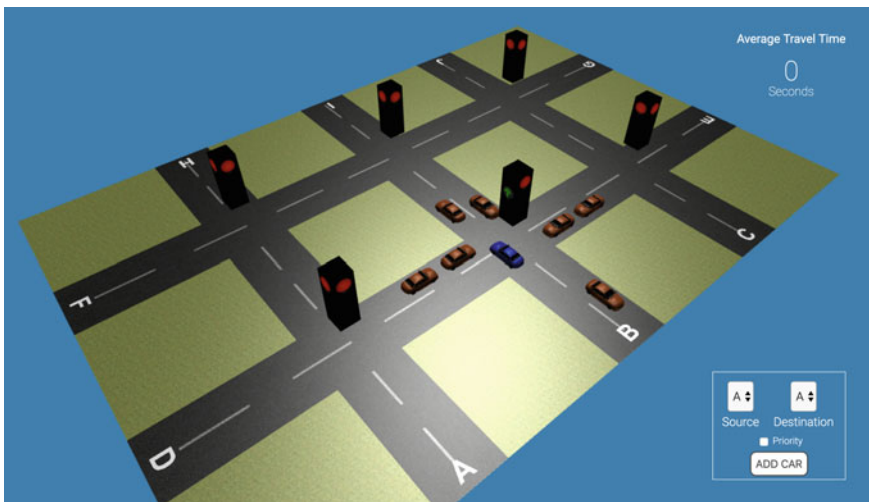


Fig. 10.2 Priority vehicle simulation

10.6.2 Test System Specifications

The experiments are performed on a Lenovo G50, which uses an Intel Core i7 processor with a 2.0GHz clock speed and 8 GB of DDR3 main memory. The graphics card used is a 2 GB AMD Radeon Card.

Table 10.5 Travel time improvement

Test case	Travel time improvement (%)
Shortest distance	26.93
Longest distance	20.95
All sources to all destinations	19.99
Congestion case	9.63
Priority vehicle	45.48

10.6.3 Results

- **Average Travel Time Test Cases:** A comparison of the average travel times for all test cases between the existing timed signal model and the proposed model can be observed in Table 10.3. It can be inferred that the average travel time of vehicles is lesser when using STNS compared to the timed signal model.
- **Priority Vehicle Observation:** The test was run and the average result is tabulated in Table 10.4. In this case, the evaluation metric is the travel time of the priority vehicle. From Table 10.4, it can be seen that the STNS model performs very well in the case of priority vehicles when compared to the conventional timed signal modal.
- **Travel Time Improvement:** Finally, the travel time improvement of all test cases was calculated and tabulated in Table 10.5 using Formula 10.6. From Table 10.5, it can be inferred that in the crucial cases where there is a congestion, the STNS model results in a roughly 10% improvement in the average travel time when compared to the timed signal model, and in the case of clearing the road for a priority vehicle, the average travel time improvement is 45% when compared to the conventional model.

$$\text{Travel Time Improvement} = \frac{\text{Timed Signal Time} - \text{STNS Model Time}}{\text{Timed Signal Time}} * 100 \quad (10.6)$$

10.7 Conclusion

In the STNS model that has been proposed, the traffic signals and navigation systems are a part of the same feedback loop, thus communicating to each other in order to reduce the average travel time of vehicles. The current implementation is limited to grid systems in downtown metropolitan areas and will face issues if it has to be implemented for any other road systems. Also, the fact that the STNS model has been proposed only for single lane roads is another limitation.

Currently, only the average travel time is being measured. An additional data point that can be analyzed in the future is the variance of the travel time, to see how the proposed model distributes travel time among all the cars. Also, while the proposed system proves effective in a small city consisting of six traffic junctions, future work could include increasing the size of the city to get a better understanding of how this system will perform with respect to scalability.

References

1. Xing, Y., Ban, X., Liu, X., Shen, Q.: Large-scale traffic congestion prediction based on the symmetric extreme learning machine cluster fast learning method. *Symmetry* **11**(6), 730–749 (2019)
2. Lopez-Garcia, P., Onieva, E., Osaba, E., Masegosa, A.D., Perallos, A.: A hybrid method for short-term traffic congestion forecasting using genetic algorithms and cross entropy. *IEEE Trans. Intell. Transp. Syst.* **17**(2), 557–569 (2016)
3. Ledoux, C.: An urban traffic flow model integrating neural networks. *Transp. Res. Part C: Emerg. Technol.* **5**(5), 287–300 (1997)
4. Ahmad, F., Mahmud, S.A., Yousaf, F.Z.: Shortest processing time scheduling to reduce traffic congestion in dense urban areas. *IEEE Trans. Syst. Man Cybern.* **47**(5), 838–855 (2017)
5. Maghrebi, F.: On a hopfield net arising in the modelling and control of over-saturated signalized intersections. *Neural Process. Lett. (NPL)* **10**, 401–406 (1999)
6. Perez-Murueta, P., Gomez-Espinosa, A., Cardenas, C., Gonzalez-Mendoza Jr., M.: Deep learning system for vehicular re-routing and congestion avoidance. *Appl. Sci.* **9**(13), 2717–2731 (2019)

Chapter 11

Selective Sensor Control via Cauchy Schwarz Divergence



Nida Ishtiaq, Sabita Panicker, Amirali K. Gostar, Alireza Bab-Hadiashar, and Reza Hoseinnezhad

Abstract A novel information theoretic objective function is introduced for optimal control of sensors in multi-object systems (e.g., multi-target tracking solutions) in which the sensors need to be controlled toward acquiring the most accurate measurements relative to a selected subset of objects (not all of them). This is continuation of our previous works where we tackled the same problem by devising task-driven cost functions to be optimized within the sensor control solution. In this paper, a novel objective function is presented. It is formulated using an information divergence that presents the difference in information contents between prior density and posterior density. Numerical experiments are presented for a multi-target tracking application. The tracking results show the proposed method adequately works in principle, and the tracking MSE error for the targets of interest is similar or better than the state of art in most of the times.

11.1 Introduction

In multi-object multisensor tracking scenarios, sensor control (SC) solutions are commonly used to control sensor(s) with the objective of gaining the *most informative* measurements for the purpose of object state estimation and tracking [1–4]. The common approaches for defining the *most informative* measurement are *information-driven* methods and *task-driven* methods. In the former approach, the difference in the *information content* of the prior and posterior is considered to measure the utility of the received measurement/information. This difference is usually measured by an information *divergence* function such as Cauchy-Schwarz (CSD), Kullback-Leibler (KLD) or Rényi divergence [5–7].

An alternative approach is using task-driven objective functions. Here, the expected state estimation or tracking error is taken as a cost function and minimized

N. Ishtiaq · S. Panicker · A. K. Gostar · A. Bab-Hadiashar · R. Hoseinnezhad (✉)
RMIT University, Melbourne, VIC 3000, Australia
e-mail: reza.hoseinnezhad@rmit.edu.au
URL: <https://reza.hoseinnezhad.com>

© The Editor(s) (if applicable) and The Author(s), under exclusive license to Springer Nature Singapore Pte Ltd. 2021

Y.-D. Zhang et al. (eds.), *Smart Trends in Computing and Communications: Proceedings of SmartCom 2020*, Smart Innovation, Systems and Technologies 182,
https://doi.org/10.1007/978-981-15-5224-3_11

via choosing the right control action for the sensor(s). Examples of task-driven objective functions are: estimated object cardinality variance [7] and “posterior expected error of cardinality and states” (PEECS) [8, 9].

Apart from the above-mentioned approaches, a new family of methods has emerged that depends on the *purpose of tracking* [2]. The common sensor control solutions are designed for improved tracking of all targets regardless of their identity. The aim of the new method, *selective sensor control*, is just better tracking of specific targets. Consequently, the goodness of measurements received by sensors is defined in terms of how accurately the targets of interest (ToIs) are being tracked.

A natural framework for SC implementation is “partially observed Markov decision processes” (POMDPs). POMDP framework for systems with one sensor is described in [10, 11]. These solutions have employed “random finite set” (RFS) theory [12] to find a solution for the SC problem. The idea of RFS theory is to model each object state and each measurement returned by a sensor as an RFS. Using RFS framework, various multi-target tracking solutions have been developed. Some examples of these solutions are included but not limited to “probability hypothesis density (PHD)” [13], “cardinalized probability hypothesis density (CPHD)” [14], “multi-Bernoulli” filters [13, 15], and “labeled RFS filters” [12, 16].

This paper proposes a SC solution via formulating a novel objective function that follows the information-driven methodology to tackle the *selective SC* problem. The proposed objective function is based on Cauchy-Schwarz divergence (CS-Divergence) [17]. We formulate and utilize this objective function in a labeled RFS-based multi-object system (MOS) within an “labeled multi-Bernoulli (Labeled-MB)” filter. In a challenging scenario, the tracking performance of our approach is also evaluated.

11.2 Background and Problem Statement

11.2.1 Sensor Control Framework

In this work, the problem of SC is formulated based on the “partially observed Markov decision process” (POMDP) framework. The POMDP framework is suitable for sensor movement planning which is based on a series of action commands. Within this approach, the action command that maximizes/minimizes a reward/cost function is defined to be the optimal one.

In POMDP framework, the true *states* are not accessible. Thus, measurements are used and they contain clutter and miss-detection. Commonly POMDP formulation is defined by:

$$\omega = \{X_k, \mathbb{U}, f_{k|k-1}(x_k|x_{k-1}), Z_k, g_k(z|x), \vartheta(\pi_+, u, \pi)\}. \quad (11.1)$$

Table 11.1 Variable description in Eq. (11.1)

Variable	Description
X_k	The set of single-object states
\mathbb{U}	The space of all admissible sensor actions
$f_{k k-1}(x_k x_{k-1})$	State transition density for a single-object
Z_k	A set of point measurements
$g_k(z x)$	Likelihood function
$\vartheta(\pi_+, u, \pi)$	Objective (cost or reward) function

The variables in Eq. (11.1) are defined in Table 11.1. For each sensor command $u \in \mathbb{U}$ applied, a reward/cost is returned by the objective function.

The objective of SC solution is to find the sensor action u^* that optimizes $\vartheta(\pi_+, u, \pi)$. An information theoretic objective function is the divergence from time-updated multi-object density to the posterior. Let us denote the time-updated and measurement-updated multi-object densities by π_+ and π , respectively. Also, Ω at time k depends on the measurements at time $k|k+1$ which are the function of the applied sensor command. The sensor command u^* is chosen such that the expectation of the objective function is maximized over all future measurements.

$$u^* = \operatorname{argmax}_{u \in \mathbb{U}} \left\{ \mathbb{E}_{Z_k} [\vartheta(\pi_+, u, \pi)] \right\}. \quad (11.2)$$

11.2.2 Labeled MB Filter

A review of notation and formulation of the “labeled-MB filter” [16] is presented in this section.

11.2.3 Notation

In this paper, the following notation has been used:

Notation	Description	Example
Lower-case	A single-object state	x, \mathbf{x}
Upper-case	A multi-object state	X, \mathbf{X}
Bold	A labeled state	\mathbf{x}, \mathbf{X}
Blackboard bold	A space	$\mathbb{X}, \mathbb{L}, \mathbb{C}$

In addition, $\mathcal{F}(\mathbb{X})$ denotes the ensemble of all finite subsets of \mathbb{X} . The standard “inner product” is denoted by

$$\langle u, v \rangle \triangleq \int u(x)v(x)dx,$$

and “generalized Kronecker delta” is defined as

$$\delta_Y(X) \triangleq \begin{cases} 1, & \text{if } X = Y \\ 0, & \text{otherwise} \end{cases}$$

Finally, the “inclusion function” is shown by

$$1_Y(X) \triangleq \begin{cases} 1, & \text{if } X \subseteq Y \\ 0, & \text{otherwise} \end{cases}.$$

11.2.4 Labeled-MB RFS

A “labeled multi-Bernoulli (Labeled-MB)” RFS is completely described by its components: $\pi = \{(r^{(\mathfrak{S})}, p^{(\mathfrak{S})}) : \mathfrak{S} \in \mathcal{L}\}$. The parameter \mathfrak{S} denotes an object label in the space \mathbb{L} . Each object label \mathfrak{S} exists with a probability of $r^{(\mathfrak{S})}$ and its state is distributed according to the density $p^{(\mathfrak{S})}(\cdot)$. The multi-object density of an Labeled-MB RFS is derived by Reuter et al. [16] as follows:

$$\pi(\mathbf{X}) = \Delta(\mathbf{X})w(\mathcal{L}(\mathbf{X})) [p]^{\mathbf{X}}, \quad (11.3)$$

where

$$p(x, \mathfrak{S}) = p^{(\mathfrak{S})}(x) \quad (11.4)$$

$$w(L) = \prod_{i \in \mathbb{L}} (1 - r^{(i)}) \prod_{\mathfrak{S} \in L} \frac{1_{\mathbb{L}}(\mathfrak{S})r^{(\mathfrak{S})}}{(1 - r^{(\mathfrak{S})})} \quad (11.5)$$

Note that:

$$p^{\mathbf{X}} \triangleq \prod_{x \in X} p(x)$$

$\mathcal{L} : \mathbb{X} \times \mathbb{L} \rightarrow \mathcal{F}(\mathbb{L})$ is the label function that returns all the object labels in a set.

11.2.5 Labeled-MB Filter

The labeled-MB filter is a Bayesian filter with a prediction and an update step. It propagates an Labeled-MB RFS as prior through those steps and returns an Labeled-MB RFS as posterior. Assume that the Labeled-MB prior at time step $k - 1$, is:

$$\pi_-(\mathbf{X}) = \Delta(\mathbf{X})w_-(\mathcal{L}(\mathbf{X})) [p_-]^{\mathbf{X}}. \quad (11.6)$$

where

$$w_-(L) = \prod_{i \in \mathbb{L}_-} \left(1 - r_-^{(i)}\right) \prod_{\mathfrak{S} \in L} \frac{1_{\mathbb{L}_-}(\mathfrak{S}) r_-^{(\mathfrak{S})}}{1 - r_-^{(\mathfrak{S})}}, \quad (11.7)$$

$$p_-(x, \mathfrak{S}) = p_-^{(\mathfrak{S})}(x). \quad (11.8)$$

Note that in above equations, the space of labels at time $k - 1$ is denoted by \mathbb{L}_- . The time-updated multi-object density is:

$$w_+(L) = \prod_{i \in \mathbb{L}_+} \left(1 - r_+^{(i)}\right) \prod_{\mathfrak{S} \in L} \frac{1_{\mathbb{L}_+}(\mathfrak{S}) r_+^{(\mathfrak{S})}}{1 - r_+^{(\mathfrak{S})}}, \quad (11.9)$$

$$p_+(x, \mathfrak{S}) = p_+^{(\mathfrak{S})}(x), \quad (11.10)$$

with the time-updated existence probability $r_+^{(\mathfrak{S})}$ and spatial density $p_+^{(\mathfrak{S})}(\cdot)$. Note that the time-updated Labeled-MB includes a birth process modeled which is a Labeled-MB with following parameters: $\left(r_B^{\mathfrak{S}_B}, p_B^{\mathfrak{S}_B}(\cdot)\right)_{\mathfrak{S}_B \in \mathbb{B}}$. The time-updated space of labels is given by $\mathbb{L}_+ = \mathbb{L}_- \cup \mathbb{B}$. Given the time-updated Labeled-MB multi-object density, the measurement-updated multi-object posterior is given by

$$\pi(\cdot|Z) = \{(r^{(\mathfrak{S})}, p^{(\mathfrak{S})}(\cdot) : \mathfrak{S} \in \mathbb{L}_k\} \quad (11.11)$$

where Z denotes the measurement set acquired by the sensor(s). Note that the space of measurement-updated labels is the same as the space of time-updated labels. The measurement-updated parameters are computed according to equations given in [16].

11.3 Selective Sensor Control via CS-Divergence

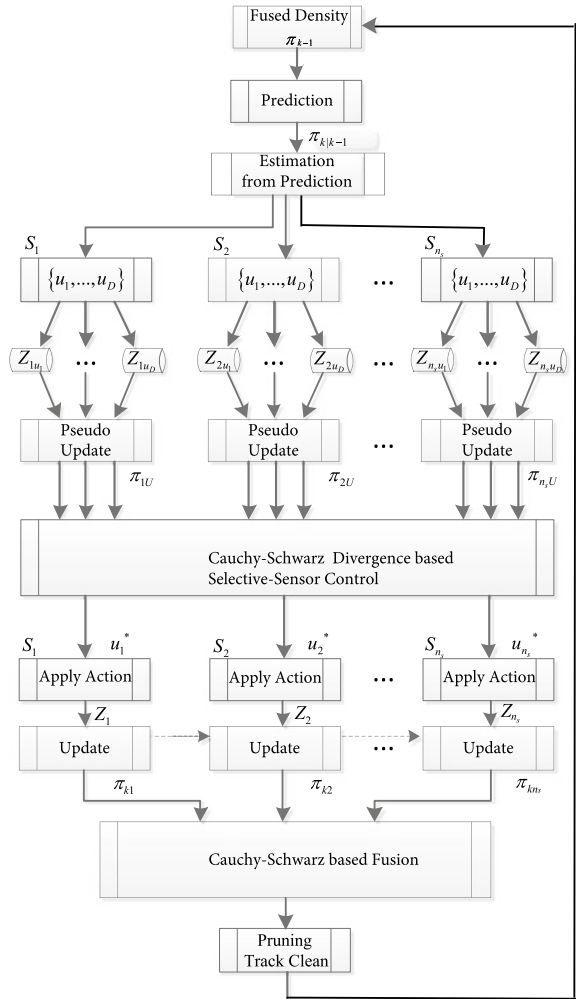
Assume that \mathbb{L}_{ToI} is the space of labels of targets of interest (ToI), then the time-updated labeled-MB density is:

$$\{(r_+^{(\mathfrak{S})}, p_+^{(\mathfrak{S})}(\cdot))\}_{\mathfrak{S} \in \mathbb{L}_+}$$

where the space of all object labels is denoted by \mathbb{L}_+ . Figure 11.1 demonstrates the general operation of SC solution implemented in POMDP framework. The procedure of the solution is as follows:

- Multi-object state is estimated via the time-updated density,
- For each sensor action $u_i \in \mathbb{U}$ a “predicted ideal measurement set (PIMS)” [18] is calculated for only for target of interests,

Fig. 11.1 Generalized block diagram for a multi-SC application



- For each sensor action a pseudo-update is computed. Note that in this step, the PIMS is used as measurement,
- The objective function is computed and optimized, leading to the best sensor action u^* .

In this paper, we employ an analytical form of the CS-divergence for time-updated and measurement-updated Labeled-MB posteriors to compute the objective function. Note that the first moment of a multi-object density determines the intensity function of the “best” Poisson process approximation to that multi-object density, where the “best” approximation means the one that returns the smallest Kullback-Leibler divergence between the original density and the approximate [13].

We approximate the time-updated and measurement-updated posterior of the Labeled-MB density, computed in Labeled-MB filter [16], by their first moments. Using this approximation, the CS-divergence between the time-updated and measurement-updated Labeled-MB posterior could be derived analytically.

11.3.1 CS-Divergence

The CS-divergence for two random vectors with probability densities u and v is given by [19]:

$$D_{\text{CS}}(u, v) = -\ln \frac{\langle u, v \rangle}{\|u\| \|v\|}. \quad (11.12)$$

In general, the computation of the CS-divergence, using Eq. (11.12), for two labeled-MB density does not accept any closed-form and needs expensive numerical approximation. However, for Poisson point processes (PPP) it accepts the closed-form formulation. Hoang et al. [17] showed that the CS-divergence for two PPP is half the squared distance between their intensity functions. Indeed, if $\pi_+(\cdot)$ and $\pi_k(\cdot)$ are densities of two Poisson RFSS with intensity functions $D_+(\cdot)$ and $D_k(\cdot)$, then their CSD is given by

$$D_{\text{CS}}(\pi_+, \pi) = \frac{K}{2} \int_{x \in \mathbb{X}} \|D_+(x) - D(x)\|^2 dx. \quad (11.13)$$

Suppose that in the time-updated Labeled-MB density each $p_+^{(\text{S})}(\cdot)$ is approximated by a set of particles:

$$p_+^{(\text{S})}(x) = \sum_{j=1}^{J^{(\text{S})}} w_{+,j}^{(\text{S})} \delta(x - x_{+,j}^{(\text{S})}).$$

Similarly, the pseudo-measurement-updated Labeled-MB density (derived by running the update step using PIMS measurements for each hypothesized action command $u \in \mathbb{U}$) is also represented by:

$$p^{(\text{S})}(x; u) = \sum_{j=1}^{J^{(\text{S})}} w_j^{(\text{S})}(u) \delta(x - x_{+,j}^{(\text{S})}).$$

Note that through the update step, the particles themselves do not change but their weights are actually measurement-updated and the pseudo-measurement-updated weights $w_j^{(\text{S})}(u)$ depend on the chosen action command, u .

The PHDs of the time-updated and pseudo-measurement-updated Labeled-MB densities are then given by:

$$D_{CS}(\pi_+, \pi) = \sum_{\mathfrak{S} \in \mathbb{L}} \sum_{j=1}^{J^{(\mathfrak{S})}} r_+^{(\mathfrak{S})} w_{+,j}^{(\mathfrak{S})} \delta(x - x_{+,j}^{(\mathfrak{S})}), \quad (11.14)$$

and,

$$D(x) = \sum_{\mathfrak{S} \in \mathbb{L}} \sum_{j=1}^{J^{(\mathfrak{S})}} r^{(\mathfrak{S})}(u) w_j^{(\mathfrak{S})}(u) \delta(x - x_{+,j}^{(\mathfrak{S})}). \quad (11.15)$$

Substituting the above in Eq. (11.13) leads to the following divergence between the prior and pseudo-posterior multi-object densities:

$$D_{CS}(\pi_+(\cdot), \pi(\cdot; u)) = K/2 \times \sum_{\mathfrak{S} \in \mathbb{L}} \sum_{j=1}^{J^{(\mathfrak{S})}} \left[r_+^{(\mathfrak{S})} w_{+,j}^{(\mathfrak{S})} - r^{(\mathfrak{S})}(u) w_j^{(\mathfrak{S})}(u) \right]^2. \quad (11.16)$$

For selective SC, we choose the above divergence as the reward function, but computed only over the labels of the targets of interest, denoted by \mathbb{L}_{ToI} . Thus, the following objective function is used in Eq. (11.2) to find the right sensor action:

$$\mathbb{E}_Z [\vartheta(\pi_+, u, \pi)] \triangleq \sum_{\mathfrak{S} \in \mathbb{L}_{ToI}} \sum_{j=1}^{J^{(\mathfrak{S})}} \left[r_+^{(\mathfrak{S})} w_{+,j}^{(\mathfrak{S})} - r^{(\mathfrak{S})}(u) w_j^{(\mathfrak{S})}(u) \right]^2. \quad (11.17)$$

11.4 Numerical Results

In the simulation conducted for the verification of the proposed method, four targets are considered to maneuver along straight lines. The motion model is based on the nearly constant velocity. The surveillance region is of set to $[-400, 1000]\text{m} \times [0, 1000]\text{m}$. Two targets are selected as targets of interest, the labels of these targets are 2 and 3. Each target state consists of a label and its unlabeled state vector which is comprised of the position and velocity components.

$$x = [p_x \ \dot{p}_x \ p_y \ \dot{p}_y]^\top \quad (11.18)$$

The transition density is:

$$f(x_k | x_{k-1}, \mathfrak{S}) = \mathcal{N}(x_k; Fx_{k-1}, Q) \quad (11.19)$$

where F, Q are:

$$F = \text{diag}(A, A) \quad Q = \text{diag}(B, B) \quad (11.20)$$

in which

$$A = \begin{bmatrix} 1 & T \\ 0 & 1 \end{bmatrix} \quad B = \sigma_{\text{motion}}^2 \begin{bmatrix} T^3/3 & T^2/2 \\ T^2/2 & T \end{bmatrix}. \quad (11.21)$$

T is the sampling interval which is taken as $1s$ and the variance parameter $\sigma_{\text{motion}}^2 = 5 \text{ m}^2/\text{s}^3$. The birth components are considered uniform over the entire region of surveillance and $P_s = 0.99$. P_d is distance dependent and is similar to P_d used in [2, 3, 9, 20] where the probability of detection increases as the distance between the sensor and target decreases. Thus, in a multi-target tracking scenario, a moving sensor always tries to position itself in a way to minimize the distance from all targets. The sensor returns a range and bearing measurement for each target. Measurement noise is modeled by multi-variate Gaussian density in which

$$\mathcal{N}(\cdot; [0 \ 0]^\top, R)$$

where

$$R = \text{diag}(\sigma_\theta^2, \sigma_r^2)$$

The noise scales for bearing and range are set as $\sigma_\theta^2 = \pi/60 \text{ rad}$ and $\sigma_r^2 = 5 \text{ m}^2$. The false alarms have been modeled as Poisson RFS with a constant clutter rate of $\lambda_c = 5$.

Our experimental setup includes nine action commands for sensor movement. Four of these commands are for horizontal and vertical sensor movements, four are for diagonal motions and one for zero movement. The experiment was run with hundred time steps, repeated for fifty times, i.e., fifty Monte Carlo runs of hundred time steps each. Figure 11.2 shows the result of our selective SC method. The sensor trajectory depicts that our proposed algorithm compels the sensor to follow the ToIs, i.e., targets 2 and 3. The sensor always stays as close as possible to these targets ensuring minimum distance from the ToIs and acquiring most accurate measurements for detecting and tracking them.

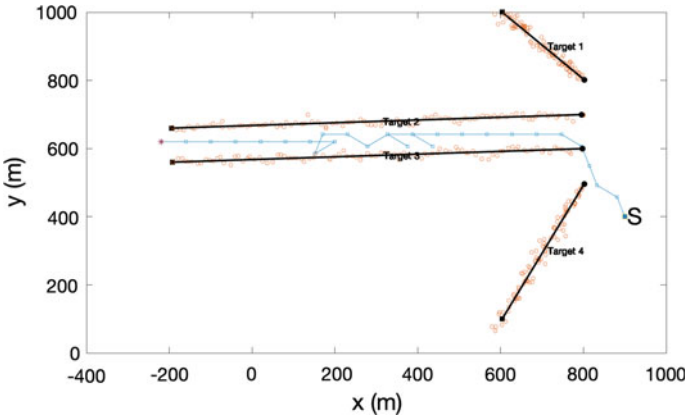


Fig. 11.2 Sensor trajectory for CS-divergence-based SC

The performance of our proposed CS-divergence-based method is evaluated using the mean square error (MSE) of the ToIs' state estimates (of ToIs) averaged over 50 Monte Carlo trials. A comparison of the MSE plots of our new method and the selective-PEECS method proposed in [2] is shown in Fig. 11.3. It can be observed that the MSE of our proposed method is less than the state-of-art method for most of the times.

11.5 Discussion and Conclusion

Selective SC is a relatively new avenue in the MOS-SC field. Earlier works in selective tracking [11, 21] use task-driven approach. This paper proposes a novel information-driven approach using an objective function based on Cauchy-Schwarz divergence, which performs better than the task-driven method for most instances, as seen in Fig. 11.3.

Our information theoretic reward function has the mathematical form of CS-divergence, derived for applications where the core of the MOS is an Labeled-MB filter. This work is an extension of our recent works on selective target tracking in which we devised new cost functions in a task-driven approach. The main difference is that in this work, we follow an information-driven approach.

In a challenging multi-target tracking application context, we ran 50 Monte Carlo repetitions of numerical experiments and visualized the sensor trajectories. In our application, the detection profile improves when sensor is close to targets. Hence, the

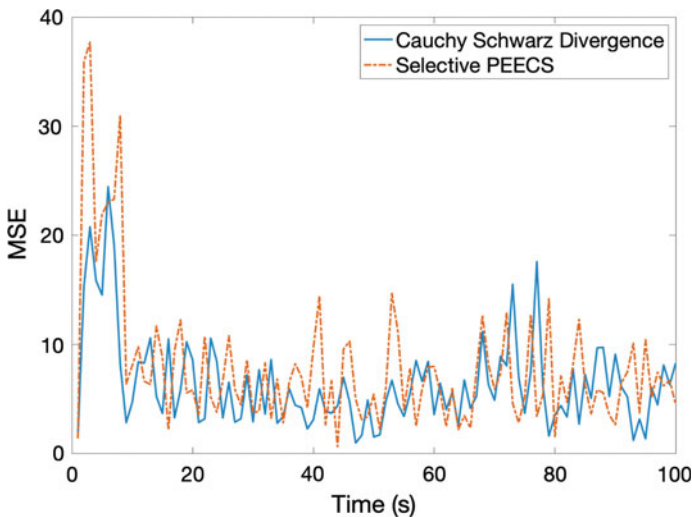


Fig. 11.3 Mean square error (MSE) for Cauchy-Schwarz divergence and selective-PEECS-based SC

SC solution was expected to move the sensor in vicinity of the targets of interest. Our observations confirmed this, and demonstrated that our solution works in principle. Furthermore, we computed the MSE of tracking for ToIs, and compared the results when the sensor is controlled using a recently published solution. The comparative tracking errors show that our method outperforms the state of art in most of the times during the numerical experiment scenario.

This work will be extended to include multi-SC and the objective function will be reformulated to include more challenging scenarios where the sensors have limited fields of view and the targets of interest can intermittently hide from the sensors.

Acknowledgements This research was funded by the Australian Government through the Australian Research Council Discovery Project grant DP160104662. Also, it received support from Australian Government Research Training Program (RTP) scholarship.

References

1. Mahler, R.: Multitarget Sensor Management of Dispersed Mobile Sensors. Series on Computers and Operations Research. World Scientific, Singapore (2004)
2. Panicker, S., Gostar, A.K., Bab-Haidashar, A., Hoseinnezhad, R.: Sensor control for selective object tracking using labeled multi-Bernoulli filter. In: 2018 21st International Conference on Information Fusion (FUSION), pp. 2218–2224 IEEE, New York (2018)
3. Ristic, B., Vo, B.N.: Sensor control for multi-object state-space estimation using random finite sets. *Automatica* **46**(11), 1812–1818 (2010)
4. Beard, M., Vo, B.T., Vo, B.N., Arulampalam, S.: Void probabilities and Cauchy-Schwarz divergence for generalized labeled multi-Bernoulli models. *IEEE Trans. Signal Process.* **2017**, 5047–5061 (2017)
5. Ristic, B., Vo, B.N., Clark, D.: A note on the reward function for PHD filters with sensor control **47** (2011)
6. Gostar, A., Hoseinnezhad, R., Bab-Hadiashar, A.: Information theoretic approach to robust multi-Bernoulli sensor control. In: 2014 IEEE Workshop on Statistical Signal Processing (SSP), pp. 224–227 (June 2014)
7. Hoang, H.G.: Control of a mobile sensor for multi-target tracking using multi-target/object multi-Bernoulli filter. In: 2012 International Conference on Control, Automation and Information Sciences (ICCAIS), pp. 7–12 (2012)
8. Gostar, A., Hoseinnezhad, R., Bab-Hadiashar, A.: Multi-Bernoulli sensor control for multi-target tracking. In: 2013 IEEE Eighth International Conference on Intelligent Sensors, Sensor Networks and Information Processing, pp. 312–317 (2013)
9. Gostar, A.K., Hoseinnezhad, R., Bab-Hadiashar, A.: Multi-Bernoulli sensor control via minimization of expected estimation errors. *IEEE Trans. Aerosp. Electron. Syst.* **51**(3), 1762–1773 (2015)
10. Hoang, H.G., Vo, B.T.: Sensor management for multi-target tracking via multi-Bernoulli filtering. *Automatica* **50**(4), 1135–1142 (2014)
11. Panicker, S., Gostar, A.K., Bab-Hadiashar, A., Hoseinnezhad, R.: Recent advances in stochastic sensor control for multi-object tracking. *Sensors* **19**(17), 3790 (2019)
12. Vo, B.T., Vo, B.N.: Labeled random finite sets and multi-object conjugate priors. *IEEE Trans. Sign. Process.* **61**(13), 3460–3475 (2013)
13. Mahler, R.: Statistical Multisource-Multitarget Information Fusion. Artech House, Norwood, MA (2007)

14. Vo, B.T., Vo, B.N., Cantoni, A.: Analytic implementations of the cardinalized probability hypothesis density filter. *IEEE Trans. Sign. Process.* **55**(7), 3553–3567 (2007)
15. Vo, B.T., Vo, B.N., Cantoni, A.: The cardinality balanced multi-target multi-Bernoulli filter and its implementations. *IEEE Trans. Sign. Process.* **57**(2), 409–423 (2009)
16. Reuter, S., Vo, B.N., Vo, B.T., Dietmayer, K.: The labeled multi-Bernoulli filter. Preprint (2014)
17. Hoang, H.G., Vo, B.N., Vo, B.T., Mahler, R.: The Cauchy-Schwarz divergence for Poisson point processes. *IEEE Trans. Inf. Theory* **2015**, 4475–4485 (2015)
18. Mahler, R.P.S., Grundel, D., Murphey, R., Pardalos, P.M.: Multitarget Sensor Management of Dispersed Mobile Sensors. *Theory and Algorithms for Cooperative Systems*, vol. 2004. World Scientific, Singapore, pp. 239–310 (2004)
19. Kampa, K., Hasanbelliu, E., Principe, J.C.: closed-form Cauchy-Schwarz PDF divergence for mixture of Gaussians. In: *The 2011 International Joint Conference on Neural Networks (IJCNN)*, pp. 2578–2585 (2011)
20. Gostar, A.K., Hoseinnezhad, R., Bab-Hadiashar, A.: Robust multi-Bernoulli sensor selection for multi-target tracking in sensor networks. *IEEE Sign. Process. Lett.* **20**(12), 1167–1170 (2013)
21. Panicker, S., Gostar, A.K., Bab-Hadiashar, A., Hoseinnezhad, R.: Accelerated multi-sensor control for selective multi-object tracking. In: *International Conference on Control, Automation and Information Sciences (ICCAIS)*, pp. 183–188 (2018)

Chapter 12

Step-Factor Resampling Technique for Imbalanced Sequence Data Classification



Iroshan Aberathne, Chamila Walgampaya, and Udara Rathnayake

Abstract The mobile ad fraud detection plays a vital role in research community nowadays since a large sum of money is being circulated in this industry. The fraudsters who generate illegal revenue by executing various types of fraudulent activities are difficult to be detected. Various researches are being conducted by academics and industry experts to find optimum solutions to tackle these fraudulent activities. One of the barriers they face is the class imbalance problem in the datasets. In an imbalance dataset, the frequency of the states of the target class varies significantly. A particular dataset which is suffered with class imbalance problem will mislead the final results of the predictive model. The researchers have proposed a number of methods to address this class imbalance problem. A novel technique which is composed with smoothing and resampling techniques has been proposed in this study to solve the class imbalance problem in the context of sequence data. The proposed technique is evaluated with a hidden Markov scoring model—HMSM. The model shows significant improvement in accuracy, recall, precision and F-score with this novel resampling technique and smoothing approach. Moreover, the model becomes more sensitive towards the specificity which is the key factor of any kind of fraud detection methods.

I. Aberathne (✉) · C. Walgampaya
Faculty of Engineering, University of Peradeniya, Peradeniya, Sri Lanka
e-mail: iroshan.du@gmail.com

C. Walgampaya
e-mail: ckw@pdn.ac.lk

U. Rathnayake
Faculty of Computing and Technology, University of Kelaniya, Kelaniya, Sri Lanka
e-mail: udarak@kln.ac.lk

© The Editor(s) (if applicable) and The Author(s), under exclusive license to Springer Nature Singapore Pte Ltd. 2021

Y.-D. Zhang et al. (eds.), *Smart Trends in Computing and Communications: Proceedings of SmartCom 2020*, Smart Innovation, Systems and Technologies 182,

https://doi.org/10.1007/978-981-15-5224-3_12

12.1 Introduction

Smartphones and tablets become more popular nowadays because they are smaller, affordable and portable compared with desktops or laptops. This popularity and huge usage of smartphones and tablets lead to dramatic increase of the mobile advertising industry all over the world. Since a large amount of money is being circulated in this industry, fraudsters are trying to take advantage of this ecosystem [9].

Various types of techniques and tools have been studied and implemented to address this threat in the context of click fraud detection and prevention [1, 3]. Any kind of dataset that is related to fraud detection including the click fraud suffers with *Class Imbalance* problem [5, 7]. The class imbalance occurs when the dataset carries only a small number of data points representing the minor class compared to the major class in a particular dataset [2]. Generally, a small percentage of the total number of data points is actually fraud and the majority of the data are in the not-fraud class which leads to an imbalance in click fraud datasets. The general machine learning algorithms do not consider the distribution of the data and whether it is balanced or imbalanced. In this situation, class imbalance could produce a prediction bias in favour of the majority class [10].

In their paper, Aberathne et al. have implemented a supervised learning algorithm called hidden Markov scoring model—HMSM to classify fraudulent clicks [1]. The dataset which was used to evaluate the HMSM also suffers from class imbalance problem. Thus, we are addressing this class imbalance problem and proposing a novel solution to overcome the barriers in supervised learning algorithms which can be used in the HMSM as well. The remainder of this paper is organized as follows. In Sect. 12.2, we discuss related work with existing smoothing methods and resampling techniques to address the class imbalance problem. Proposed approach to resolve the class imbalance problem is discussed in detail under Sect. 12.3. The experimental results of the proposed approach are available in Sect. 12.4. Conclusions are given in Sect. 12.5.

12.2 Related Work

There is a high possibility to arise zero probabilities in sequence data for some scenarios due to the unseen emission-state combinations [12]. This does not imply that occurring that event is impossible; hence, smoothing techniques can be introduced to the model which flattening the probability distribution by giving a valid probability without any zero values. There are various types of smoothing techniques such as absolute discounting, Good–Turing estimation, additive smoothing, shrinkage which can be found in the literature [4]. Studies showed that using a smoothing technique as a pre-processing step leads to a significant improvement in the performance of the model [6, 8]. Ojokoh et al. [12] showed the effectiveness of smoothing techniques in hidden Markov models where Nivre [11] proposed that Good–Turing estimation

and the additive smoothing are good techniques to use to avoid zero probabilities by achieving efficient results for his study.

Some of the existing methods to overcome this class imbalance issue are resampling, hybrid sampling, Synthetic Minority Oversampling Technique (SMOTE), boosting, cluster-based resampling, etc. [2, 5]. Brennan [5] has investigated different methods to overcome the class imbalance problem using two fraudulent datasets and found that applying data methods are more successful to attain a balanced dataset than algorithmic methods. Leevy et al. [10] also have done a survey to address class imbalance problem in big data and showed that data sampling methods generally give better results over algorithmic methods. Perera [13] applied different types of methods to remove class imbalance in an online advertising dataset with fraudulent events and proposed a novel method using ensemble learning to have better results on training, validation and test datasets.

12.3 Methodology

The proposed approach of this study has introduced a novel methodology to solve the class imbalance problem in a sequence data via a resampling technique and smoothing approach. A number of parameters are being introduced to the proposed approach as tuning parameters so that the best performing model can be identified.

12.3.1 Smoothing Technique

One of the major smoothing techniques called additive smoothing is used in this study to upturn the zero probabilities for unseen data using ε as a tuning parameter since it provides better estimates compared to the other methods. Here, ε is referred to as the *smoothing factor* in additive smoothing. Estimated probabilities p_ε based on the actual counts can be calculated as follows for each value x of a variable X in a sample of N observations [11].

$$p_\varepsilon = \frac{(x + \varepsilon)}{(N + \varepsilon * N_x)} \quad (12.1)$$

where N_x is the number of possible values contained in the sample space.

12.3.2 Resampling Technique

The proposed resampling technique identifies the major and minor classes from a dataset and then calculates the optimum number of records to be converted so-called

conversion factor-Z from major class in to minor class in order to balance the dataset. The derivation of the proposed resampling technique is illustrated as follows.

C_{major}^i	number of major class instances before resample
C_{minor}^i	number of minor class instances before resample
C_{major}^f	number of major class instances after resample
C_{minor}^f	number of minor class instances after resample
Z	number of instances to be converted from major to minor class

$$R_i = \frac{C_{\text{major}}^i}{C_{\text{minor}}^i} \quad (12.2)$$

$$R_f = \frac{C_{\text{major}}^f}{C_{\text{minor}}^f} \quad (12.3)$$

Since $C_{\text{major}}^f < C_{\text{major}}^i$ and $C_{\text{minor}}^f > C_{\text{minor}}^i$, the relationship among the major and minor classes before and after the resampling can be expressed with Z as shown in Eqs. (12.4) and (12.5).

$$C_{\text{major}}^f = C_{\text{major}}^i - Z \quad (12.4)$$

$$C_{\text{minor}}^f = C_{\text{minor}}^i + Z \quad (12.5)$$

Equation (12.3) is rearranged according to Eqs. (12.4) and (12.5) as shown in Equation (12.6).

$$R_f = \frac{C_{\text{major}}^i - Z}{C_{\text{minor}}^i + Z} \quad (12.6)$$

The formula to calculate conversion factor - Z is derived with Equations (12.2) and (12.6).

$$Z = \left(\frac{R_i - R_f}{R_f + 1} \right) C_{\text{minor}}^i \quad (12.7)$$

The R_f is considered as a tuning parameter to the algorithm where different values from 1 to $R_i - R_f = 1$ are assigned to R_f so that a set of Z values can be calculated.

Once the conversion factors are calculated, the respective number of records should be converted from major to minor class in order to overcome the class imbalance problem. There should be a consistent procedure to perform this conversion. The proposed method calculates the index distance of adjacent minor class instances

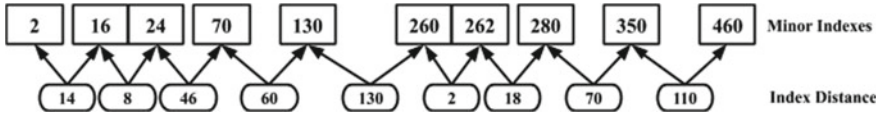


Fig. 12.1 Index distance of minor class instances

and arrange them in three different ways called *ASC*, *DESC* and *MID* to perform the conversion so that the consistency is guaranteed. The term *Step-Factor* is used to refer to these minor class instances arrangement methods.

The target class of the dataset contains two states called *OK* and *Fraud* where *OK* is genuine and *Fraud* means not genuine records [1]. The target class sequence is arranged as a list so that the index distance of adjacent minor class instances can be calculated. The graphical representation of this process is shown in Fig. 12.1.

The implementation of the first two step-factors is straightforward. The index distances are arranged in ascending order in *ASC* and descending order in *DESC* method. The index distances are arranged by the *MID* step-factor following a shuffling mechanism. The *MID* step-factor algorithm first calculates the number of index distances available in the list. If the number of indexes is odd, the last index value of the list is omitted and then index distance list so-called initial index distance list is divided into two sublists named left and right index distance sub-lists. Then the shuffling starts at the last index value of the left index distance sub-list and then first index value of the right index distance sub-list and so on. The shuffling process of the indexes based on the *MID* step-factor is illustrated in Fig. 12.2.

The algorithm performs conversion of major to minor class instance with respect to selected step-factor. The pseudocode of the algorithm can be written as follows.

- T target class sequence as a list, containing *OK* and *Fraud* labels
- R_i initial balance factor, calculated by equation (12.2)

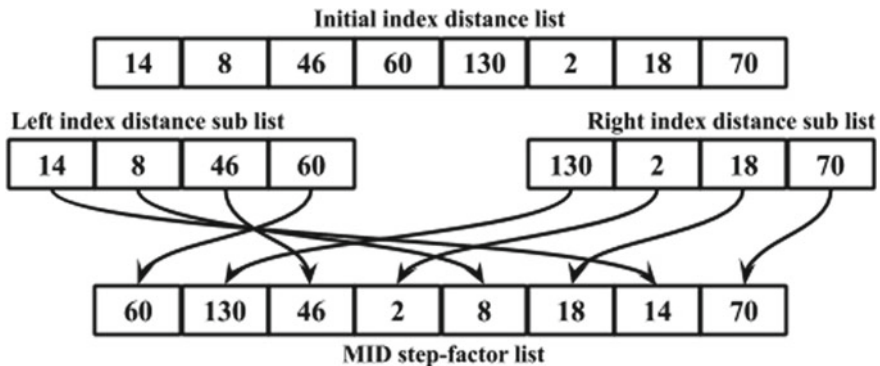


Fig. 12.2 MID step-factor index shuffling process

R_f *final balance factor as a tuning parameter*
 S_f *one of the step-factors out of ASC, DESC and MID*
 S_f^l *list of index distances based on S_f*
 S_f^i *current index of respective S_f^l*
 S_f^v *value of the S_f^i*
 Z_c *current converted count*

```

for  $R_f$  in range(start=1, end= $R_i-1$ , step=1):
    convertedTargetInstances = majorToMinorConversion
( $T, R_i, R_f, S_f$ )

```

```

function majorToMinorConversion( $T, R_i, R_f, S_f$ ):
    fraudList = filterFraudInstancesFrom T
    okList = filterFraudInstancesFrom T
    majorClass = "Fraud", minorClass = "OK"
    if length(okList) > length(fraudList):
        majorClass = "OK"
        minorClass = "Fraud"
    if  $R_i > R_f$ :
         $Z$  = calculated by equation(12.7)
         $Z_c = 0$ 
         $S_f^i = -1$ 
        while  $Z > Z_c$ :
             $S_f^i += 1$ 
             $S_f^v = S_f^l[S_f^i]$ 
            for x in range(start=0, end=length( $T$ ), step= $S_f^v$ ):
                if  $Z == Z_c$ :
                    break
                if  $T[x] == majorClass$ :
                     $T[x] = minorClass$ 
                     $Z_c += 1$ 
    return T

```

12.4 Experimental Results

Proposed performance enhancement techniques called smoothing factor and resampling were applied to 20 different datasets with HMSM algorithm [1]. The experimental results show significant improvement of all the performance measures with respect to both techniques.

Table 12.1 Model performance with smoothing factor

Dataset	Factor	Accuracy		Recall		Precision		Specificity		F-Score	
		μ	σ								
3000	0	0.82	0.06	0.83	0.06	0.96	0.02	0.53	0.40	0.90	0.03
	0.06	0.84	0.05	0.85	0.06	0.98	0.02	0.58	0.39	0.91	0.03
	0.09	0.82	0.08	0.84	0.06	0.98	0.02	0.58	0.39	0.90	0.04
5000	0	0.84	0.05	0.85	0.05	0.99	0.01	0.79	0.23	0.91	0.03
	0.06	0.88	0.04	0.88	0.04	0.99	0.01	0.82	0.26	0.93	0.02
	0.09	0.87	0.04	0.87	0.04	0.99	0.01	0.82	0.26	0.93	0.02
8000	0	0.80	0.08	0.80	0.08	0.96	0.03	0.61	0.50	0.87	0.05
	0.06	0.81	0.07	0.81	0.07	0.98	0.02	0.65	0.40	0.89	0.04
	0.09	0.80	0.07	0.81	0.07	0.98	0.02	0.68	0.41	0.89	0.04
12,000	0	0.73	0.16	0.74	0.15	0.96	0.03	0.53	0.44	0.83	0.01
	0.06	0.75	0.14	0.76	0.14	0.98	0.02	0.55	0.43	0.84	0.01
	0.09	0.74	0.14	0.75	0.14	0.98	0.02	0.55	0.43	0.84	0.01

12.4.1 Model Tuning with Smoothing Factor

The HMSM was enhanced with smoothing factor— ε as a tuning parameter to the model in order to scale the performance of the model. The major advantage of smoothing factor is that, it ensures the first priority objective of HMSM by increasing specificity while keeping almost constant values for all other performance measures. The experimental results in Table 12.1 show that there is a significant effect on the model performance and stability for all training sets with the smoothing factor. Moreover, it is clear that specificity is much more sensitive to the smoothing factor than all the other performance measures where a slight change in the smoothing factor produce significant performance change in specificity.

12.4.2 Model Tuning with Resampling Technique

The resampling technique was applied to all 20 sample training datasets and then evaluated the HMSM model with the smoothing factor as 0.06. The experimental results show that step-factor plays a vital role in classifying test data. Each step-factors equally contribute to enhance the performance of the model where 7 samples with DESC, 8 samples with ASC and 5 samples with MID step-factor to enhance the performance of the model. Moreover, 17 samples show highest performance when the sample size equals or less than 6000 records. The maximum percentage of conversion factor-Z out of the training size is 25% and the rest of the samples are below 20%. The experimental results are visualized in Fig. 12.3.

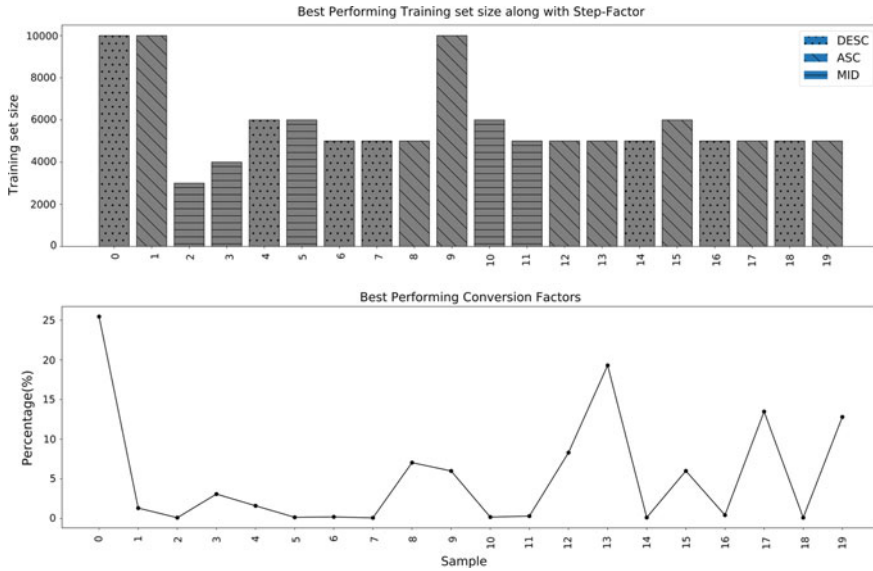


Fig. 12.3 Model performance with resampling

12.4.3 Performance Evaluation of Models

There are three models for HMSM. The first model is identified as the initial model where neither smoothing factor nor resampling technique is applied. The second and third models are incorporated with smoothing factor and resampling technique, respectively. The experimental results in Table 12.2 shows a significant improvement of all performance measures after applying smoothing factor and resampling technique to HMSM. The lower standard deviation of all the models reflects the consistency of each model.

Table 12.2 Performance evaluation of the models

	Initial		Smoothing		Resampling	
	μ	σ	μ	σ	μ	σ
Accuracy	0.84	0.05	0.88	0.04	0.94	0.03
Recall	0.85	0.05	0.88	0.04	0.95	0.03
Precision	0.99	0.01	0.99	0.01	0.99	0.01
Specificity	0.79	0.26	0.82	0.23	0.91	0.17
F-Score	0.91	0.03	0.93	0.02	0.97	0.01

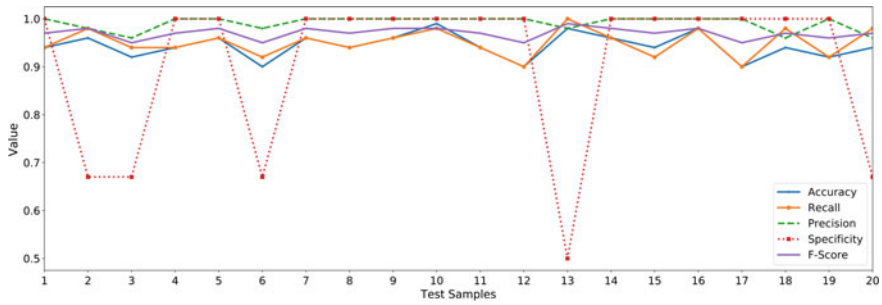


Fig. 12.4 Best performing model

12.4.4 Best Performing Model

Experimental results show that HMSM model performs better after enhancing the model with smoothing factor and resampling technique. Figure 12.4 illustrates the HMSM performance across 20 different samples after applying the resampling and smoothing factor. There are only four instances with specificity less than 70% and the lowest is 50%. All other performance measures are above 90% for all samples.

12.5 Conclusions

In this paper, we proposed a new resampling technique to address the class imbalance problem in sequence data. The proposed resampling approach applies to the HMSM model along with smoothing factor in order to enhance the performance of the model. The model performs with resampling and smoothing factor show dramatic increase of all performance measures. The model has increased the accuracy and recall by 10% , F-Score by 6% and specificity by 12% from the initial model. Moreover, the consistency of the model is also enhanced by reducing the standard deviation of performance measures. The findings of this study proof that proposed resampling and smoothing techniques perform well with HMSM in sequence data.

The smoothing factor can be introduced as a tuning parameter to this algorithm since it shows significant improvement in all performance measures with each training dataset. Furthermore, specificity is much more sensitive to the smoothing factor than all the other performance measures where a slight change in the smoothing factor causes significant performance change in specificity. This is an important finding of the study since specificity is the top priority performance measurement in the context of fraud detection.

The proposed resampling technique performs well with HMSM by showing significant improvement of all the performance measures. There are a number of interesting features in this resampling technique. No synthetic data are introduced to the

dataset instead we have converted existing major class instances that are identified via step-factors to minor. Adjacent index distance of minor class instances and step-factor enables the random but consistent distribution of minor class instances in the target sequence. Since the number of conversions from major to minor instances are very low, the patterns and the characteristics of the initial dataset are narrowly affected. The training dataset size can be reduced while increasing the model performance after applying the resampling technique.

References

1. Aberathne, I., Walgampaya, C., Rathnayake, U.: Novel Hidden Markov Scoring Algorithm for Fraudulent Impression Classification in Mobile Advertising. Accepted for publication in *Advances in Intelligent Systems and Computing*. Springer (2020)
2. Akila, S., Reddy, U.S.: Data imbalance: effects and solutions for classification of large and highly imbalanced data. *Proc. ICRECT* **16**, 28–34 (2016)
3. Berrar, D.: Random forests for the detection of click fraud in online mobile advertising. In: *Proceedings of the 1st International Workshop on Fraud Detection in Mobile Advertising*, pp. 1–10 (2012)
4. Boodidhi, S.: Using smoothing techniques to improve the performance of Hidden Markov's Model. UNLV Theses, Dissertations, Professional Papers, and Capstones, 1007 (2011)
5. Brennan, P.: A comprehensive survey of methods for overcoming the class imbalance problem in fraud detection. Master's Thesis, Institute of Technology Blanchardstown, Dublin (2012)
6. Chen, S.F., Goodman, J.: An empirical study of smoothing techniques for language modeling. *Comput. Speech Lang.* **13**(4), 359–394 (1999)
7. Galar, M., Fernandez, A., Barrenechea, E., Bustince, H. and Herrera, F.: A review on ensembles for the class imbalance problem: bagging-, boosting-, and hybrid-based approaches. *IEEE Trans. Syst. Man Cybern. Part C (Appl. Rev.)* **42**(4), 463–484 (2011)
8. Hazem, A., Morin, E.: A comparison of smoothing techniques for bilingual lexicon extraction from comparable corpora. In: *Proceedings of the Sixth Workshop on Building and Using Comparable Corpora*, pp. 24–33 (2013)
9. Kim, W., Jeong, O.R., Kim, C., So, J.: The dark side of the Internet: attacks, costs and responses. *Inform. Syst.* **36**(3), 675–705 (2011)
10. Leevy, J.L., Khoshgoftaar, T.M., Bauder, R.A., Seliya, N.: A survey on addressing high-class imbalance in big data. *J. Big Data* **5**(1), 42 (2018)
11. Nivre, J.: Sparse data and smoothing in statistical part-of-speech tagging. *J. Quant. Linguistics* **7**(1), 1–17 (2000)
12. Ojokoh, B.A., Adewale, O.S. and Falaki, S.O., 2008. Improving on the smoothing technique for obtaining emission probabilities in hidden Markov models. *Orient. J. Comput. Sci. Technol.* **1**, 12008
13. Perera, B.K.: A class imbalance learning approach to fraud detection in online advertising. Master's Thesis, Masdar Institute of Science and Technology (2013)

Chapter 13

Rice Disease Detection Based on Image Processing Technique



**Md. Asfaqur Rahman, Md. Shahriar Nawal Shoumik,
Md. Mahbubur Rahman, and Most. Hasna Hena**

Abstract Rice plant diseases are major problems in Bangladesh. Detection and monitoring of these rice plant diseases is a critical issue. Rice plants are affected in various kind of disease like hispa, brown spot, and leaf blast and show the syndrome in the leaf of these diseases. If these diseases are detected early and take appropriate action, it will restrain extensive economic loss for the farmer. In this research paper, the proposed model will successfully classify and find out the rice leaf diseases based on image processing techniques. Machine learning algorithm CNN is used to implement this model. Healthy and disease-affected leaves are taken for the proposed method and separated healthy and unhealthy characteristics of rice plant leaves. After that, these images are being processed with the proposed model and classified the leaf as either infected by disease or healthy. This proposed model provided the accuracy of 90%. This model successfully identifies the infected and healthy rice plant.

13.1 Introduction

Bangladesh is mainly known as an agricultural country. Our agriculture depends on rice. About 75% cultivated land is being used for rice cultivation. Rice farming plays a vital role on agricultural economy; it contributes one half of the agricultural GDP. As the population is increasing, demand of rice is also increasing and it is a major

Md. Asfaqur Rahman (✉) · Md. Shahriar Nawal Shoumik · Md. Mahbubur Rahman ·
Most. Hasna Hena
Department of Computer Science and Engineering, Daffodil International University (DIU),
Dhaka, Bangladesh
e-mail: asfaqur15-7086@diu.edu.bd

Md. Shahriar Nawal Shoumik
e-mail: nawal15-7156@diu.edu.bd

Md. Mahbubur Rahman
e-mail: mahbubur15-7012@diu.edu.bd

Most. Hasna Hena
e-mail: hena.cse@diu.edu.bd

© The Editor(s) (if applicable) and The Author(s), under exclusive license
to Springer Nature Singapore Pte Ltd. 2021

Y.-D. Zhang et al. (eds.), *Smart Trends in Computing and Communications: Proceedings of SmartCom 2020*, Smart Innovation, Systems and Technologies 182,
https://doi.org/10.1007/978-981-15-5224-3_13

challenge to producing more crops to encounter the increasing demand. For the past few years, its production level decreases due to some unexpected disease. But in our agriculture, rice plants are often affected with serious disease like hispa, brown spot, and leaf blast, which causes serious damage of rice plant and also decrease the production of rice [1]. When rice plants are affected in disease, some syndromes are seen on their leaves. There emerges some spot on the leaf of the plant. Leaf blast and brown spots are viewed in many shapes on the leaf. From these spots, disease can be identified and can take an appropriate action. This paper proposed a machine learning method to identify these diseases from rice plant leaves. Huge numbers of images of paddy's leaves are needed for this research because the research is based on images. Hispa, healthy, brown spot, and leaf blast these four types of images are collected. Total images divided into two parts for training and testing purpose. Almost 70% of images are in training folder, and the rest will be in the testing folder. The proposed model can identify the healthy and infected rice leaves. In a result of that, farmer can easily identify the infected leaves and will take appropriate action and increase their productivity.

13.2 Literature Review

Mango tree is the national tree of Bangladesh. It also has a great effect on the economy of Bangladesh. Hena et al. [2]. Published RGB (Red, Green Blue), binary, and grayscale image dataset of different mango species leaves consist of about 8000 images from 54 different trees. In their dataset, they had only 1.5% noise and blur images.

Orillo et al. [3] described a model in plant disease identification using back propagation where at first the entire image is transferred to binary image and differentiates spot and then extracting all the spot using back propagation. But the limitation of using back propagation is once a network teaches one sets of weights, any new learning causes catastrophic forgetting.

Orillo et al. [4] described a model on rice plant disease identification using fuzzy neural network. They describe a method of identification of rice disease using sound signal processing system. The classification is done by MATLAB function and fuzzy neural network. But the disadvantages of fuzzy network are if the model is nonlinear with a disturbance term, the testing error is very large.

Arivazhagan et al. [5] used texture features to classify unhealthy plant leaves in their model. Color transformation structure is created for the inputted RGB images. Creating a color transformation structure for input RGB images using support vector machines is very difficult task.

Phadikar and Sil [6] described a method for rice disease using software prototype system based on pattern recognition technique. Their prototype works based on the infected rice leaf's images. Classification of the infected parts is done by neural network. It only identified the infected part from an infected image, but it could not differentiate the leaf into healthy and infected.

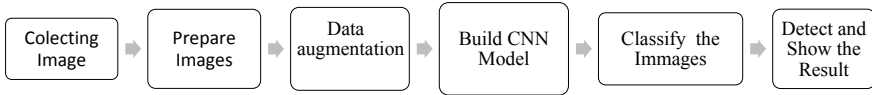


Fig. 13.1 Block diagram

13.3 Methodology

13.3.1 Working Diagram

For detecting rice leaf's disease, there are couple of successful steps that have to finish. Block diagram of the model is given in Fig. 13.1.

13.3.2 Dataset Collection

Data is the main assets of this project. Images are collected from Kaggle and Dataquest, and some images are captured manually. Almost 3000 images are collected, but all these were not useful for us. Some pictures' resolution is very poor; some are hardly classified as healthy and unhealthy. That's why, 300 images are selected for brown spot, healthy, and leaf blight, hispa for the training purposes. Similarly, 110 images are selected per folder for the validation. The dataset which is used for this research is not relatively clean. We have to perform data processing to get ready our data for modeling.

13.3.3 Neural Network

CNN is both supervised and unsupervised learning architecture. They can used for predict something or classification. But mostly CNN is used for supervised method. CNN classify images based on their attributes [7]. By using activation function, CNN computes future maps. The function was

$$y_j^l = f(z_j^l) \quad (13.1)$$

where y_j^l is the future map and $f(z_j^l)$ is the activation function. Datasets are stored in 2-dimensional convolution operation in convolutional neural network (CNN).

$$O = \frac{(W - F + 2P)}{(S + 1)} \quad (13.2)$$

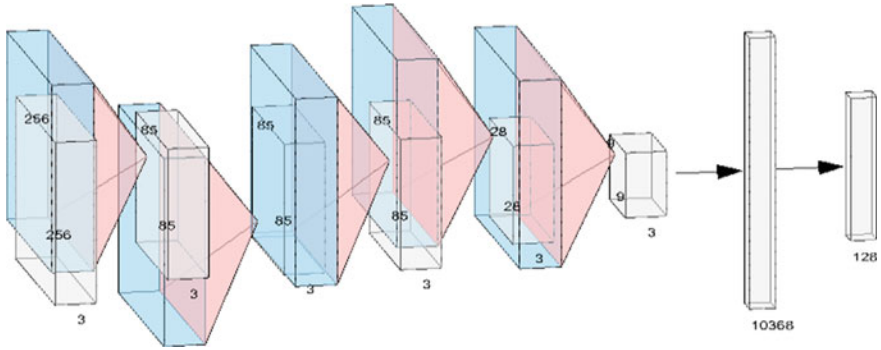


Fig. 13.2 Convolutional neural network (CNN)

where O refers to length of output, W refers to length of input, K refers to filter size, S refers to stride, and P refers to padding.

Figure 13.2 shows the basic structure of CNN of the model using the layer, padding, height, width, and dense that used on the model.

13.3.4 Building Model

The sequential model is built up by using CNN algorithm [8]. Keras helps to build this model as layer by layer [9]. For adding layers, `add()` function is used. Convolutional 2D layer is used for input images as 2-dimensional matrices, and dense layer is used for output images. The kernel size was 3×3 as a filter matrix. ReLU [10] or rectified linear activation was used as an activation function for this model [11]. Images must be inputted in this model. The input size of the images is (256,256). That means height and weight of the images should be 256. Between the convolutional 2D layer and dense layer, there was a flatten layer which serves as a connection between them. For prediction based on the highest probability, SoftMax is added as activation in the model. SoftMax function equation is given below:

$$P(y = j|x) = \frac{e^{X^T W^j}}{\sum_{k=1}^k e^{X^T W^k}} \quad (13.3)$$

Here, $X^T W$ denotes the inner product of X and W .

Pictorial view of the sequential model is given in Fig. 13.3.

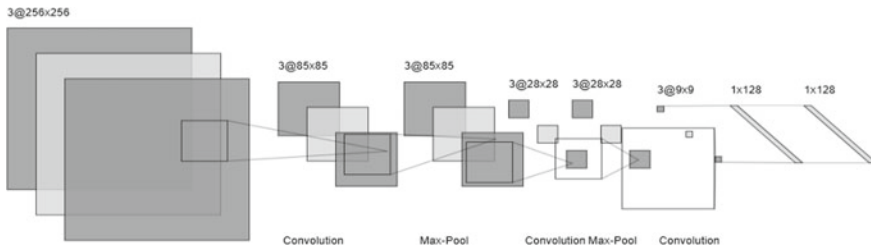


Fig. 13.3 Pictorial view of the sequential model

13.3.5 *Compiling the Model*

Optimizer, loss, and metrics these parameters are used for compiling the model. ‘adam’ was used as an optimizer. It is actually a good optimizer for adjusting the learning rate throughout training. ‘Categorical cross entropy’ is used for the loss function. To make things even easier to interpret, ‘accuracy’ metric is used to see the accuracy score on the validation set during training the model.

13.3.6 *Training and Testing the Model*

To train, ‘fit ()’ function is used on the model. Testing dataset is used as validation data. In the fit function, we set the epochs number which will cycle the model through the data. After finishing the training process, the testing process is processed. It verifies the effectiveness of the trained CNN.

13.4 **Result and Outcome**

13.4.1 *Learning Rate*

With respect to the loss gradient learning rate shows a visual graph of adjusting the weights of our network. Relationship between weight, gradient, and learning is given below:

$$\text{New weight} = \text{existing weight} - \text{learning rate} \times \text{gradient} \quad (13.4)$$

Figure 13.4 displays the accuracy function graph of the model. From the graph, it is seen that at the beginning, training accuracy is very low; however, with increasing

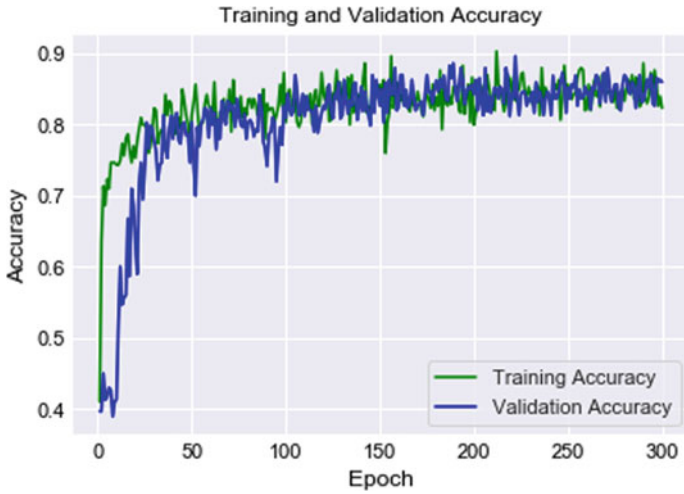


Fig. 13.4 Accuracy graph

the no of epochs, the accuracy is increased. On the other hand, initially the validation loss is very high, but after time being, validation loss is reduced, which is shown in Fig. 13.5.

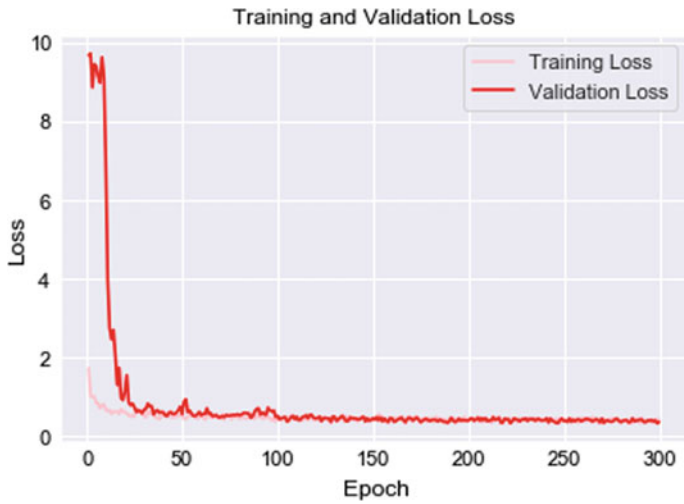


Fig. 13.5 Loss graph

13.4.2 Confusion Matrix

Confusion matrix visually shows the performance of an algorithm. It counts the values of correct and incorrect predictions [12]. Accuracy or classification rate formula and error of the model formula are given below:

$$\text{Accuracy} = \frac{TP + TN}{TP + TN + FN + FP} \tag{13.5}$$

$$\text{Error} = 1 - \text{accuracy} \tag{13.6}$$

Figure 13.6 shows the confusion matrix of the classification model of this research. It shows that the diagonal value in each row is the highest value. These conclude that the proposed algorithm will give a good accuracy.

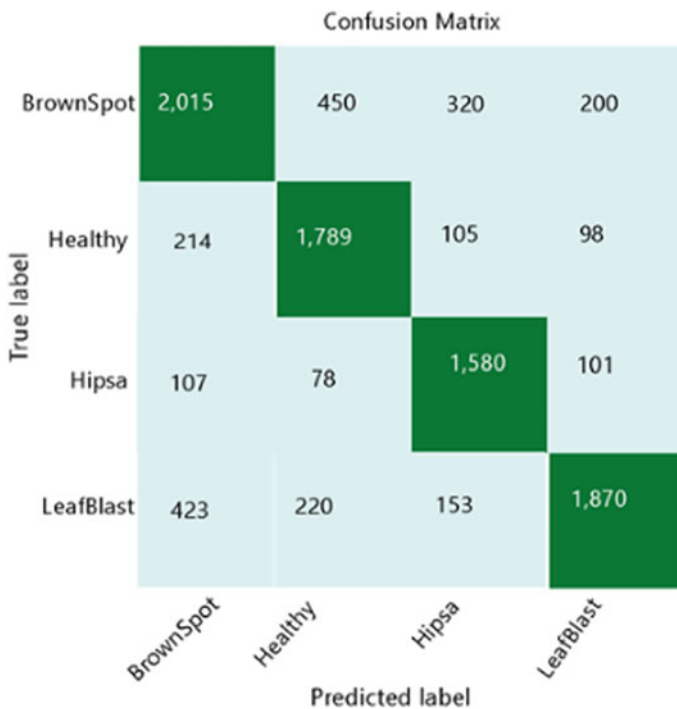


Fig. 13.6 Confusion matrix



```
BrownSpot : 76.52562856674194  
Healthy : 16.32694900035858  
LeafBlast : 5.967319011688232  
Hipsa : 1.180107705295086
```

Fig. 13.7 BrownSpot classified

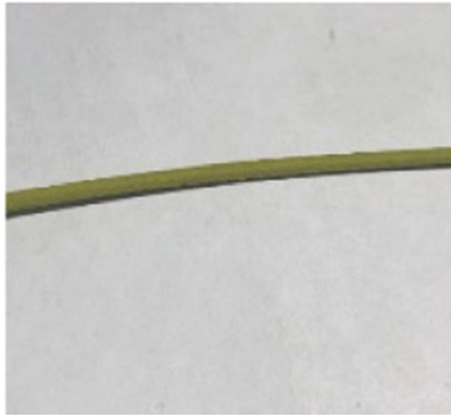
13.4.3 Classification

In Jupyter notebook, the entire process is implemented. In the first phase, different infected rice leaf image was inputted for classify those. The images are selected from the dataset folder. At the end, expected classified outcome is founded.

Figures 13.7, 13.8, 13.9, and 13.10 illustrate the output result of this model. When brown spot image is inputted, it shows 76.6% for brown spot and for other types it shows rest of them. From the result, it easily shows that the leaf is infected by brown spot. Similarly, Figs. 13.8, 13.9, and 13.10 indicate highest percentage for healthy leaf, hispa, and leaf blast-infected leaf, respectively. Thus, we can conclude that this model successfully works and can detect all diseases and healthy images.

13.5 Conclusions

For real-time rice disease detection, we have proposed convolutional neural network (CNN) based on classifier model named as sequential. For achieving desired accuracy, two-stage training has also introduced. Comprehensive studies on various kinds



Healthy : 64.75053429603577
Hispa : 29.152795672416687
LeafBlast : 3.9731431752443314
BrownSpot : 2.1235205233097076

Fig. 13.8 Healthy classified



BrownSpot : 12.45128745236984
Healthy : 10.45217896541235
LeafBlast : 7.425987412365478
Hispa : 69.670546169852332

Fig. 13.9 Hispa classified



Fig. 13.10 LeafBlast classified

of rice disease are conducted. Lots of images of rice plants are collected from the rice field. Different types of algorithm based on the CNN architecture implemented for finding the best result. The model has successfully been able to classify the disease affected plant and healthy plant. This model also helps the farmer in detecting the diseases while farming. It will give more accurate result when the dataset will be larger. Processed dataset is valuable in the prediction, whereas raw data affects in the efficiency of the model. Because of well classification of the training, validation as well as test set, the validation and test accuracy of this model is very high. We plan to work with memory efficient non-sequential CNN models in order to achieve higher accuracy in plant disease classification in future.

References

1. Bangladesh Agricultural Research Institute: en.wikipedia.org (2019). [Online]. Available: https://en.wikipedia.org/wiki/Bangladesh_Agricultural_Research_Institute. Accessed: 10 Dec 2019
2. Hena, H., Marouf, A.A., Sultana, R.: MangoLDB: a dataset of mango leaves RGB, binary and gray-scale image. *Int. J. Innov. Technol. Exploring Eng. (IJITEE)* **8**(7) (2019)
3. Orillo, J.W.F., Cruz, J.D., Valenzuela, I.: Identification of diseases in rice plant back propagation artificial neural network. In: *International Conference on Humanoid, Nanotechnology, Information Technology, Communication and Control, Environment and Management (HNICEM)* (2014)

4. Orillo, J.W.F., Amado, T., Arago, N., Fernandez, E.: Rice plant disease identification and detection technology through classification of microorganisms using fuzzy neural network. *J. Teknol. (Sci. Eng.)* **778**(5–8), 25–31 (2016)
5. Arivazhagan, S., Newlin Shebiah, R., Ananthi, S., Vishnu Varthini, S.: Detection of unhealthy region of plant leaves and classification of plant leaf diseases using texture features. *Agric. Eng. Int. CIGR e-J.* **15**(1), 211–217 (2013)
6. Phadikar, S., Sil, J.: Rice disease identification using pattern recognition techniques. Paper presented at the 11th International Conference on Computer and Information Technology, Khulna, Bangladesh (2008)
7. Wei, Y., Xia, W., Lin, M., Huang, J., Ni, B., Dong, J., Yan, S.: HCP: a flexible CNN framework for multi-label image classification. *IEEE Trans. Pattern Anal. Mach. Intell.* **38**(9), 1901–1907 (2015)
8. Denoyer, L., Gallinari, P.: Deep Sequential Neural Network (2014). arXiv preprint [arXiv:1410.0510](https://arxiv.org/abs/1410.0510)
9. Gulli, A., Pal, S.: *Deep Learning with Keras*. Packt Publishing Ltd. (2017)
10. Kingma, D.P., Ba, J.: Adam: A Method for Stochastic Optimization (2014). [arXiv:1412.6980](https://arxiv.org/abs/1412.6980)
11. Avinash, S.: *Understanding Activation Functions in Neural Networks* (2018)
12. Saito, T., Rehmsmeier, M.: Basic Evaluation Measures from the Confusion Matrix (2016)

Chapter 14

Electromagnetic Radiation from Cell Phones Used in Dhaka City



M. Quamruzzaman, Munima Haque, Shahina Haque,
and Utpal Chandra Das

Abstract Substantial anxieties has been presented regarding probable health effects from exposure to radiofrequency Electromagnetic Fields (EMF) particularly after the speedy ushering in of contemporary amenities like the mobile telecommunication practices. Several epidemiological surveys on the probable unfavorable health consequences linked to environmental contact to extremely low frequency (ELF) (0–300 Hz) non-ionizing radiation (NIR) similar to that produced by electrical substations and power cables associating such contact to brain cancer, leukemia, skin cancer, eye melanoma, etc. Extensive, well conducted epidemiological and laboratory studies need to be performed extensively. Cell phones are being used everywhere on earth due to its success in making one’s life comfortable for all walks of life including academic, office, and business. Millions of cell phones are also being consumed in Bangladesh, EMF is emitted by these phones too. There have not been more studies done in Bangladesh. The study was performed from multiple locations in Dhaka city, Bangladesh. Epidemiological surveys were performed on the users of these cell phones. Also power radiated for normal data (on but not talking), with mobile data, with Wi-fi, and with signals (on and talking) were measured for these phones. These outcomes indicated that in many instances the magnetic field emitted from the various sources are higher than the threshold value and cell phone users underwent different sorts of ailments, e.g., headaches, pain in hands, insomnia, etc., due to extended exposure to EMF. Smoking further added to their usual health difficulties.

M. Quamruzzaman · U. C. Das
Department of Electronics and Telecommunication Engineering, Daffodil International University, Dhaka, Bangladesh

M. Haque (✉)
Relevant Science and Technology Society, Dhaka, Bangladesh
e-mail: munima.haque@gmail.com

S. Haque
General Educational Development, Daffodil International University, Dhaka, Bangladesh

© The Editor(s) (if applicable) and The Author(s), under exclusive license to Springer Nature Singapore Pte Ltd. 2021

Y.-D. Zhang et al. (eds.), *Smart Trends in Computing and Communications: Proceedings of SmartCom 2020*, Smart Innovation, Systems and Technologies 182,

https://doi.org/10.1007/978-981-15-5224-3_14

14.1 Introduction

Energy of NIR is comparatively low (<10 eV) and it simply succeeds in vibrating molecules and causing heating effects. Biological effects result from exposure to ELF magnetic and electrical fields. Nevertheless, excluding for areas that are large enough to stimulate existing densities higher than the edge for stimulating of nerve tissue, there is no agreement if these influences establish a risk to human health. Since the magnetic field is more destructive than the electrical field, a limit of $0.2\text{--}0.3$ μT or 2.5 mG, which is worldwide acknowledged as a benchmark level in several countries, must be defined at both the occupational and residential levels. For electric field 25 V/m is the accepted value. Body radiation level must not surpass the endorsed highest limit (10 mW/cm², 195 V/m in U.S.A. and 0.1 mW/cm², 20 V/m in CIS). Human made electric and magnetic fields (usually 25 V/m and 2.5 mG or 0.25 μT) are significantly higher than natural environmental electric and magnetic fields of 10^{-4} V/m and 10^{-13} T respectively [1]. For high frequency radio waves, the radiated power limit from high frequency sources differs as suggested by International Commission on Non-Ionizing Radiation Protection (ICNIRP): April 1998/IEEE C95.1/Council Recommendation 1995/519/EC. These values vary for different ranges. For example for 950 MHz (42 V/m, 4.75 W/m²) and for 1850 MHz (59 V/m, 9.25 W/m²). There were measurements and software simulations that the basic absorption rate (SAR) decreases by $10\text{--}15\%$ for each millimeter cell phone separation due to rapidly decreasing EM fields in the cell phone antenna near-field area [2].

It is found that lower animals are extremely sensitive to EMFs. Animals such as rats and bees have been found to defend themselves and their young people with NIR/EMF in the prolonged nature. As a result, health physicians and scientists in developed countries are now alert of the outcomes of NIR [3]. Some amazing results were found from these study and inspections associating low dose alternating electromagnetic fields with severe health risks. Further proof has biological effects such as reactive lymphocytes, immune deficiency, cell breakdown, and DNA destruction have been found to be affected by NIR [4].

Much research has been implemented in this area. Of late, epidemiological studies of persons employed in the presence of EMF field subjected to high frequency were explored [5]. Moreover, epidemiological studies on effect of EMF emitted by photocopy machines normally utilized in Dhaka were investigated [5]. Research was performed on EMF released by laboratory appliances in several laboratories of a private University in Bangladesh for probable health risks [6]. There was a case study on the EMF parallel to the high-voltage transmission-line [7]. Further, a review was performed on NIR, detrimental outcomes of NIR from cell or mobile phone and towers [8]. An epidemiological survey was done on CRT monitor switch the users [9]. Investigations showing the magnetic fields produced by different sources laboratory electronic and electrical equipments and appliances (textile and pharmacy laboratories, EEE and CSE laboratory and classrooms) in Southeast University, also Laboratory facilities and electrical equipment in Daffodil International University's

ETE laboratories, Bangladesh were performed [7, 10–14]. EMF health effects due to usage of cell phones by University students were also examined [15].

Many mobile devices are all equipped with Wi-fi, such as cell phones, laptops, audio players, video cameras, and have become an important part of our everyday life. Seven trillion wireless devices were reported to serve 7 billion people in 2017–2022 [16]. Several research have been conducted and published of EMF on television, radio, etc., but not much on cell phones. Since the discovery of contemporary cell phones there has been incredible upsurge in usage of mobile phone globally. Phone calls, texting, video conference, internet, etc., are all various common features of cell phones. The use of mobile phone is increasing every day numbering more than 8 billion according to International Telecommunication Union (ITU, 2018) [17]. Due to increase in use, many health symptoms due to cell phone radiation are observed earlier and pave the way to further severe illnesses. The International Agency for Research on Cancer in 2011 identified electrical radiofrequency fields from cell phones as potentially carcinogenic to humans [18]. These comprise of chronic cold and flu, chronic pain, headache and mind fog, digestive problems, sleep interruption, anxiety or depression, dizziness, memory loss, child behavioral problem, etc. [19–21]. A case-control study on 292 women having an unexplained spontaneous abortion at less than 14 weeks development and 308 female >14 weeks growth show that the usage of cell phones can be linked to the premature unplanned abortions [22]. A study involving 7720 middle school Chinese teenager students shows that reducing cell phone handling to below 60 min per day might assist teenagers to remain attentive [23]. Intensity of radiation Maximum Permissible Dose (MPD) should not exceed: 10 mW/cm², 195 V/m in USA and 0.1 mW/cm², 20 V/m in CIS. WHO recommends: 2.5 mT MF, 0.2–0.3 μT and 25 V/m EF, 200–300 nT [1]. A cell phone base station is planned in such a way that cell phone has range for few kilometers. Such phone towers emit radiation 24×7 , so the full grounded flag will be given to people living near the tower [24]. There were various impact of mobile phone battery charging on electromagnetic wave emissions [25].

Bright screens and smaller texts can strain the eyes of the mobile phone users. Since tablet computers, smartphones, and other hand-held appliances are intended for reading at close scale, eyes of the users need to constantly reposition and refocus to process the graphics and text on screen. With increase of digital usage, potential vision difficulty, also eye strain increase. Various symptoms of digital eye strain involve eye redness or irritation, blurred vision, dry eyes, neck pain, back pain, and headaches. A study conducted discussed about cell phone and cataract [26]. In May 31, 2011, the World Health Organization (WHO) labeled mobile phones as a “carcinogenic hazard” for human health [27].

With the efficiency increase of the cell phones and the appealing reduction in its price, most adult persons in Bangladesh have their own cell phones. The mobile phone subscribers in Bangladesh has reached 162.583 million by August, 2019 [28] and according to the telecoms regulators, The total number of internet subscribers has reached 98.136 million by August, 2019 [29]. The objective of this study is to explore if the EMF emission from these mobile/cell phones are within threshold levels and further whether the users are harmless from these devices.

14.1.1 Motivation

The main object of this survey was to measure whether the radiation from a device was above or below or as per the recommended value from ICNIRP/ITU. Another objective was to motivate people to use the devices with precautions distance, degree and duration (DDD). This will develop awareness among the people of all ages in the society.

14.1.2 Novelty and Contribution

Though the research was conducted in Dhaka city but the findings of the research will be helpful for others as well, especially for younger generation.

14.2 Materials and Methods

A Power density meter named Electrosmog meter, Model no. CORNET®ED-78SPlus was used for measuring Electromagnetic wave field strength, power density level and low frequency Magnetic field (Gauss, Tesla) for living environment [30]. It has RF bandwidth of 100 MHz to 8 GHz with high sensitivity ($0.5 \mu\text{W}/\text{m}^2$ to $1.8 \text{W}/\text{m}^2$) and LF bandwidth of 50 Hz to 10 kHz (for 50 Hz to 1 kHz) with sensitivity of $0.1\text{--}60 \mu\text{T}$ ($1\text{--}600 \text{mG}$). Data logging Function is also included.

14.2.1 Experimental Setup

Readings were taken for normal data (mobile ON but no talking) with mobile data, with Wi-fi, and with signal (mobile on and talking). Epidemiological data taken from the cell phone users were analyzed. The cell phone users ages are given, along with number of years using cell phone, hours per day usage, smoker or non-smoker, cell phone usage symptoms, and any other observations. The data for this epidemiology survey was performed direct contact with the users (field data collection). Measurement of radiation was done in three steps: (1) device on but not in use, (2) during conversation, (3) with Wi-fi connected, (4) while internet using through mobile data. The measurement was taken around the device and the maximum value was recorded. The date, time and location, user age, any symptoms, model no., operator and duration of use recorded.

14.3 Results

All the epidemiological survey and meter readings were taken from various locations of Dhaka city. Readings were taken from various cell phones owned by students, general public of different ages.

14.3.1 Epidemiological Data from Cell Phones

Epidemiological data were taken from the users of the cell phones under investigation. The cell phone users' ages are given, along with number of years using cell phone, hours per day usage, smoker or non-smoker, cell phones usage symptoms, and any other observations. Figure 14.1 gives the symptoms of the users of the cell phones are: can feel ear pain (13%), feel ear heated (17%), headache (34%), eye blear (7%), listening left ear comparatively low (2%), sweating (1%), and irritation (1%). Age ranges for cell phone users are distributed from 15 years to 65 years old (Fig. 14.2).

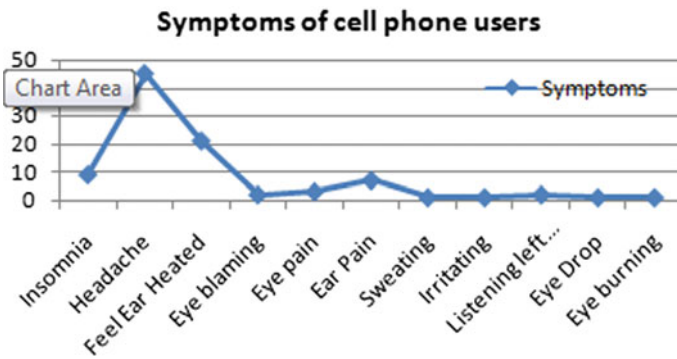


Fig. 14.1 Symptoms for cell phone users

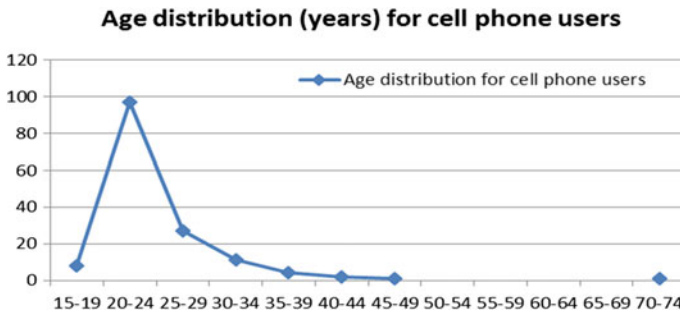


Fig. 14.2 Age ranges for cell phone users

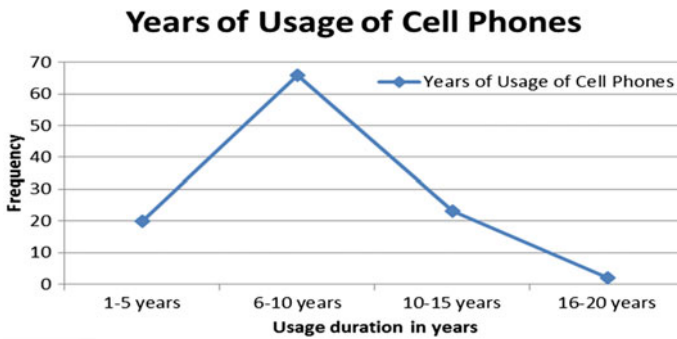


Fig. 14.3 Year of usages of cell phones by the users

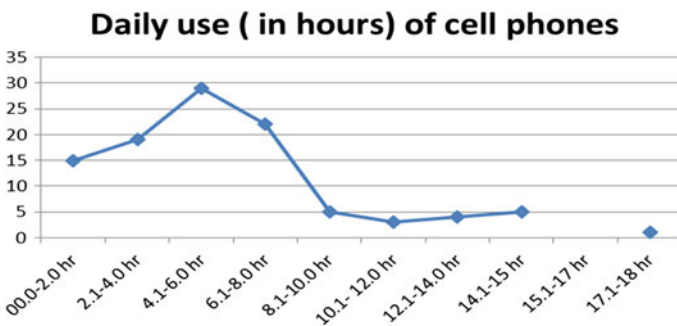


Fig. 14.4 Daily hourly usage of cell phones

Most of the users here under investigation resides in 20–24 year range. Number of years of usage include 1–5 years (20%), 6–10 years (56%), 11–15 years (23%), and 16–20 years (1%) duration (Fig. 14.3). Figure 14.4 shows the daily hours of usage of cell phone which falls in the ranges from 0–2.0 h (15%), 2.1–4.0 h (18%), 4.1–6.0 h (29%), 6.1–8.0 h (21%), 8.1–10.0 h (5%), 10.1–12.0 h (2%), 12.1–14.0 h (4%), 14.1–16.0 h (5%), 16.1–18.0 h (1%). Figure 14.5 gives number of users of various cell phone brands. The brands are Samsung (28%), Xiaomi (18%), Huawei (15%), I-phone 6s (12%), Symphony V85 (8%), Walton H4 (3%), Nokia (1%), Lava (2%), Motorola (1%), and other brands (12%).

Among the users, 64% of cell phone users have smoking habits. Internet data was available for 95% of cell phone users.

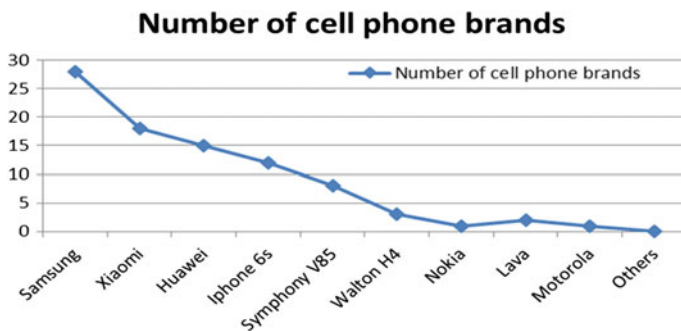


Fig. 14.5 Number of users of various cell phone brands

14.3.2 Radiated Power Measurement from Cell Phones

The cell phones described in Table 14.1 were also checked for Radiated power readings. Radiated power value (in mW/cm²) were measured for each cell phones for normal data, with mobile data, with Wi-fi, and with signal.

Table 14.1 gives radiated power (mW/cm²) for normal data, with mobile data, with Wi-fi, and with signal. Normal data (ON but no signal/no Talking) given as 0.01–0.09 mW/cm² to be 28%, 0.1–0.99 mW/cm² of 48%, 1.0–9.99 mW/cm² of 19%, 10–19 mW/cm² of 2%, while 20–29 mW/cm², 40–49 mW/cm² and 60–69 mW/cm² each of these ranges to be 1%. With mobile data: 1–500 is 47%, 501–1000 range is 10%, 1001–1500 to be 4%, 1501–2000 is 27%, while no data was available from 12% of cell phones. With Wi-fi 1–500 radiated power (mW/cm²) is emitted from 66% of cell phones used, 501–1000 mW/cm² range is 5%, 1001–1500 to be 3%, 1501–2000 is 4%, while no data was available from 12% of cell phones. With signal (while talking): 1–500 radiated power (mW/cm²) is found in 38% of cell phones under study, 501–1000 range is 3%, 1001–1500 to be 11%, while 1501–2000 was available from 48% of cell phones. One mW/cm² equals 10 W/m² or 1 W/m² equals 0.1 mW/cm².

14.4 Discussions

The obtained results of radiated power/magnetic field show that these are higher in some cases than the threshold value. Nearly all of the cell phones studied were manufactured recently (starting from 2014 to 2019), i.e., the users used it for a short duration of time, also there were not many cell phones involved in this research of several brands. Most of the users were in the age ranges from 19 to 26 years. It is also in mind to include more cell phones of various brands, phones with long time usage by the same user, user with higher age range, and cell phones manufactured

Table 14.1 Radiated power from the cell phones in mW/cm^2

Ranges	(n)
<i>Normal data (ON but no signal/no talking)</i>	
0.01–0.09	28
0.1–0.99	48
1.0–9.99	19
10–19	2
20–29	1
30–39	
40–49	1
50–59	
60–69	1
<i>With mobile data (internet browsing)</i>	
1–500	47
501–1000	10
1001–1500	4
1501–2000	27
No data	12
<i>With Wi-fi</i>	
1–500	66
501–1000	5
1001–1500	3
1501–2000	4
No data	12
<i>With signal (while talking)</i>	
1–500	38
501–1000	3
1001–1500	11
1501–2000	48
No data	

and used for a long duration of time period, and also other regions of Bangladesh for the continuation of the study.

Recently the usage of mobile phones in Bangladesh has risen both in urban and rural areas to elevate the working productivity of the people. People of all age ranges and economic backgrounds are using cell phones without knowing the adverse side effects due to EMF.

The European Society delivered universal strategies in its Council Recommendation of July 1999. ICNIRP issued analogous rules in April 1998. A selection of the international and national field strength limits for the overall community and continuous exposure are given below.

- (a) Internationally, both Council (recommendation 1999/519/EC), ICNIRP (Guidelines April 1998) and Germany (26 Deutsche Verordnung) for 950 MHz as 4.75 W/m^2 and for 1850 MHz as 9.25 W/m^2 ,
- (b) United states, IEEE C95.1 for 950 MHz as 6.33 W/m^2 and for 1850 MHz as 12 W/m^2 ,
- (c) China (Draft: National Quality Technology Monitoring Bureau), Japan (Radio-Radiation Protection Guidelines, 1990) and Austria (ONORM S1120) recommend for 950 MHz as 6.33 W/m^2 and for 1850 MHz as 10 W/m^2 ,
- (d) Switzerland (Verordnung 1999) recommends for 950 MHz as 0.04 W/m^2 and for 1850 MHz as 0.1 W/m^2 .

ICNIRP guideline 1998, is mostly used around the world. In our neighbor country India has adopted 1998 guideline, but they have modified the value to 1/10 of ICNIRP limits [31]. In Bangladesh, the ICNIRP 1998 guidelines has been fully implemented without any modifications. Unfortunately although the proper guidelines are there, the cell phone provider are not following the rules properly. Cell phones available in local market are imported illegally and without consent, none of these are checked for ICNIRP guidelines compliance. Using the recommended ICNIRP guidelines limits for radiated power (for 950 MHz as 4.75 W/m^2 and for 1850 MHz as 9.25 W/m^2) in Bangladesh it is 0.475 mW/cm^2 and 0.925 mW/cm^2 . Except for Normal data (ON but no signal/no talking) for 0.01–0.09 mW/cm^2 (28%) and 0.1–0.99 mW/cm^2 (48%), all other cases are above the threshold limit. This shows that in Bangladesh, cell phones are not being marketed checking the ICNIRP guidelines for safe using.

14.5 Conclusion

It was obtained from the cell phone data that in some instances the radiated power has gone over the edge value. In some of the cases, the threshold of both electric field and magnetic field was higher in appliances. Cell phone categories had different power density/magnetic field/electric field values and also their date of manufacturing was not the same ranging from few months to few years.

The safe distance for use of cell phone is “1” or 2.54 cm. Users are advised to use a hand free device which places more space involving the phone and the head of the user. People should try to use their cell phones a bit far from their heads (ear) beyond the threshold values, it is preferable to use hand free device, decrease the duration of talking, as well as using a well coverage area by towers. Also, texting can be done wherever necessary instead of talking. If someone follow the 3D’s (Distance, Degree and Duration), he/she may be free from risk of the EMR from mobile/cell phone. It is expected that this survey would be beneficial as a precautionary health measure for people using cell phones in Dhaka city which may be applicable for other parts of Bangladesh.

14.5.1 Limitations

During data collection many users did not show interest, some could not give exact answer, device manufacturing date was not available, regarding symptoms most of the user could not say (point out) what was his or her real problem/sufferings. Due to shortage of time many users could not reply properly.

References

1. Wertheimer, N., Leeper, E.D.: Electrical wiring configurations and childhood cancer. *Am. J. Epidemiol.* **109**, 273–284 (1979)
2. Gandhi, O.P.: Microwave emissions from cell phones exceed safety limits in Europe and the US when touching the body. *IEEE Access* **7**, 47050–47052 (2019)
3. Repacholi, H.: An overview of WHO's EMF project and the health effects of EMF exposure. In: *Proceedings of the International Conference on Non-ionizing Radiation at UNITEN (ICNIR 2003), Electromagnetic Fields and Our Health*, pp. 1–13 (2003)
4. Nordenson, I., Mild, K.H., Andersson, G., Sandström, M.: Chromosomal aberrations in human amniotic cells after intermittent exposure to fifty hertz magnetic fields. *Bioelectromagnetics* **15**, 293–301 (1994)
5. Haque, M., Quamruzzaman, M.: Epidemiological survey on effect of EMF emitted by photocopy machines generally used in Dhaka city Bangladesh. *IJRET Int. J. Res. Eng. Technol.* **4**(4), 92–100 (2015)
6. Haque, M., Quamruzzaman, M.: Survey of EMF emitted by lab equipments in various labs of Southeast University in Bangladesh for possible preventive health hazards. *IFRSA Int. J. Electron. Circ. Syst.* **4**(1), 26–32 (2015)
7. Quamruzzaman, M., Haque, M., Ahmed, F., Zaman, M.S.: Effects of electromagnetic fields (EMF) near high voltage transmission line: a case study. *Bangladesh J. Med. Phys.* **7**(1), 66–68 (2014)
8. Quamruzzaman, M., Haque, M.: Non ionizing radiation (NIR), its harmful effects especially from mobile/cell phone and towers. *Southeast Univ. J. Sci. Eng.* **8**(1:2), 34–39 (2014)
9. Haque, M., Quamruzzaman, M.: Survey on effect of EMF emitted by CRT computer monitors in Bangladesh. *Univ. J. Electr. Electron. Eng.* **3**(5), 149–158 (2015)
10. Haque, M., Quamruzzaman, M.: Survey of EMF emitted from lab equipments and air conditioners in textile engineering labs of Southeast University in Bangladesh. *Int. J. Innov. Res. Electr. Electron. Instrum. Control Eng.* **4**(3), 218–222 (2016)
11. Haque, M., Quamruzzaman, M.: Survey of EMF emitted by lab equipments in pharmacy labs of Southeast University in Bangladesh. *Int. J. Res. Eng. Technol. (IJRET)* **4**(9), 13–17 (2015)
12. Haque, M., Quamruzzaman, M.: Measurement of magnetic field from electrical appliances in EEE classrooms of Southeast University Bangladesh. *Univ. J. Electr. Electron. Eng.* **4**(2), 51–56 (2016)
13. Haque, M., Quamruzzaman, M.: Measurement of magnetic field from lab equipment in computer science and engineering labs of Southeast University Bangladesh. *Int. J. Electr. Electron. Commun. Eng.* **1**(1), 1–11 (2016)
14. Md. Quamruzzaman, M., Haque, S., Haque, M.: Measurement of magnetic field emitted from lab equipments and electrical appliances in ETE labs of Daffodil International University, Bangladesh. *Int. J. Adv. Res. Rev.* **1**(9), 47–56 (2016)
15. Haque, M., Quamruzzaman, M.: Health effects of EMF emitted from cell phones used by students of Southeast University in Bangladesh. *Southeast Univ. (SEU) J. Sci. Eng.* **10**(1), 28–38 (2016)

16. Melnick, R.L.: Commentary on the utility of the National Toxicology Program Study on cell phone radiofrequency radiation data for assessing human health risks despite unfounded criticisms aimed at minimizing the findings of adverse health effects. *Environ. Res.* **168**, 1–6 (2019)
17. The State of Broadband 2015: Broadband as a foundation for sustainable development. Broadband Commission for Digital Development (2015). <http://www.broadbandcommission.org/documents/reports/bb-annualreport2015.pdf>. Last accessed 11 Nov 2019
18. Wall, S., Wang, Z.M., Kendig, T., Dobraca, D., Lipsett, M.: Real-world cell phone radiofrequency electromagnetic field exposures. *Environ. Res.* **171**, 581–592 (2019)
19. Ahuja, Y.R., Sharma, S., Bahadur, B.: Autism: an epigenomic side-effect of excessive exposure to electromagnetic fields. *Int. J. Med. Med. Sci.* **5**(4), 171–177 (2013)
20. Pall, M.L.: Review. Microwave frequency electromagnetic fields (EMFs) produce widespread neuropsychiatric effects including depression. *J. Chem. Neuroanat.* **75**, 43–51 (2016)
21. Birks, L., Guxens, M., Papadopoulou, E., Alexander, J., Ballester, F., Estarlich, M., Gallastegi, M., Hai, M., Haugen, M., Huss, A., Kheifets, L., Lim, H., Olsen, J., Santa-Marina, L., Sudan, M., Vermeulen, R., Vrijkotte, T., Cardis, E., Vrijheid, M.: Maternal cell phone use during pregnancy and child behavioral problems in five birth cohorts. *Environ. Int.* **104**, 122–131 (2017)
22. Mahmoudabadi, F.S., Ziaei, S., Firoozabadi, M., Kazemnejad, A.: Use of mobile phone during pregnancy and the risk of spontaneous abortion. *J. Environ. Health Sci. Eng.* **13**, 34 (2015)
23. Zheng, F., Gao, P., He, M., Li, M., Wang, C., Zeng, Q., Zhou, Z., Yu, Z., Zhang, L.: Association between mobile phone use and inattention in 7102 Chinese adolescents: a population-based cross-sectional study. *BMC Public Health* **14**(1022), 1–7 (2014)
24. Sharma, P., Yadav, S., Kumar, J.: Hexagon based approach for detection of electromagnetic radiation. In: 2019 6th International Conference on Signal Processing and Integrated Networks (SPIN), pp. 120–122. IEEE (2019)
25. Sajedifar, J., Nassiri, P., Monazzam, M.R., Shamsipour, M., Ramezani, R.: The effect of battery charge levels of mobile phone on the amount of electromagnetic waves emission. *J. Environ. Health Sci. Eng.* **17**(1), 151–159 (2019)
26. Lin, J.: Cataracts and cell-phone radiation. *IEEE Antennas Propag.* **45**(1) (2003). (Illinois University, Chicago, IL, USA)
27. Radiation: do cell phones present a cancer risk? *Antenna Theory*. Retrieved from <http://www.antenna-theory.com/tutorial/cancer/cellphone.php>. Last accessed 11 Nov 2019
28. Bangladesh Telecommunication Regulatory Commission. Retrieved from <http://www.btrc.gov.bd/content/mobile-phone-subscribers-bangladesh-august-2019>. Last accessed 11 Nov 2019
29. Bangladesh Telecommunication Regulatory Commission. Retrieved from <http://www.btrc.gov.bd/content/internet-subscribers-bangladesh-august-2019>. Last accessed 11 Nov 2019
30. Electrosmog Meter. Model no. CORNET®ED-78SPlus. Cornet. Retrieved from <http://electrosmog.org/>. Last accessed 11 Nov 2019
31. Pillai, R.R.: Radiation norms: clean cheat for mobile towers in state. The Hindu Website. <http://www.thehindu.com/news/national/Kerala/radiation-norms-clean-cheat-for-mobile-towers-in-state/article/5987030.ece>. Last accessed 11 Sept 2019

Chapter 15

Expressing Opinions Application: A Case Study at Rajamangala University of Technology, Isan, Khon Kaen Campus



Ekaphong Tangtrakul , Jatupol Nampromma ,
and Phoemporn Lakkhanawannakun 

Abstract This research study presents an application for expressing opinions by addressing the problems and expressing opinions. To find the solutions to these problems that usually occur quickly, by using the application, the document format makes it convenient to follow up and check. This research has been presented through the application system to listen to the problems and make comments. The application system is developed with Dart, Flutter, and database management, and with MySQL. The test results show that the system can work correctly.

15.1 Introduction

Because within the Rajamangala University of Technology Isan, Khon Kaen Campus, there are many staff and students, and there is a spacious area within the university, when people cause problems or need improvement, they have to wait for a long time to proceed the problems in overlapping areas, and this may cause danger to surrounding people. Therefore, this research has been prepared to listen to problems and express opinions. This system is like a database that opens the topic of the problem to people of all levels to express their opinions and solutions as a way to facilitate the concerned parties to view and solve the problem quickly and precisely in order to prevent the danger that may occur.

E. Tangtrakul · J. Nampromma · P. Lakkhanawannakun (✉)
Department of Computer Engineering, Faculty of Engineering, Rajamangala University of
Technology Isan, Khon Kaen Campus, Khon Kaen 40000, Thailand
e-mail: phoemporn@hotmail.com

E. Tangtrakul
e-mail: ekaphong.ta@gmail.com

J. Nampromma
e-mail: jatupol.nampromma@hotmail.com

© The Editor(s) (if applicable) and The Author(s), under exclusive license
to Springer Nature Singapore Pte Ltd. 2021

Y.-D. Zhang et al. (eds.), *Smart Trends in Computing and Communications: Proceedings of SmartCom 2020*, Smart Innovation, Systems and Technologies 182,
https://doi.org/10.1007/978-981-15-5224-3_15

15.2 Tools and Theories

15.2.1 Flutter

Flutter [1] is a framework for creating UI for mobile application. It can work across platforms for both iOS and Android at the same time. The language used in Flutter is Dart, which was developed by Google, and, most importantly, it is an open source that can be used for free. The highlight of Flutter is the hot reload system. When testing, creating, or editing, the system shows the changes in the UI immediately and helps the development easier. The more beautiful UI design such as Material Design and Cupertino (iOS-flavor), and compatible with both Android Studio and VS Code IDE, can be used with existing programming languages such as Java, Swift, or Objective-C.

The disadvantage of Flutter is that it was launched in May 2017, so it is not familiar with the syntax that uses Dart writing [2] as in Fig. 15.1, and compared to other frameworks like React Native, the library selection is available for use less.

Flutter has two types of widgets: StatelessWidget and StatefulWidget. StatelessWidget is used to create widgets that do not handle any working state, such as displaying text, icons, or images without animation involved, etc. StatefulWidget is used to create widgets that manage various status operations such as creating an icon with animation to be able to move and buttons on the UI.

Fig. 15.1 Dart language syntax

```

1 import 'package:flutter/cupertino.dart';
2 import 'package:flutter/material.dart';
3
4 void main() {
5   runApp(MaterialApp(
6     debugShowCheckedModeBanner: false,
7     home: Login(),
8   ));
9 }
10
11 class Login extends StatefulWidget {
12   @override
13   State<StatefulWidget> createState() {
14     // TODO: implement createState
15     return _Login();
16   }
17 }
18
19 class _Login extends State {
20   @override
21   Widget build(BuildContext context) {
22     // TODO: implement build
23     return Scaffold(
24       body: ListView(
25         children: <Widget>[
26           ],
27       ),
28     );
29 }
30 }

```

15.2.2 Spring Framework

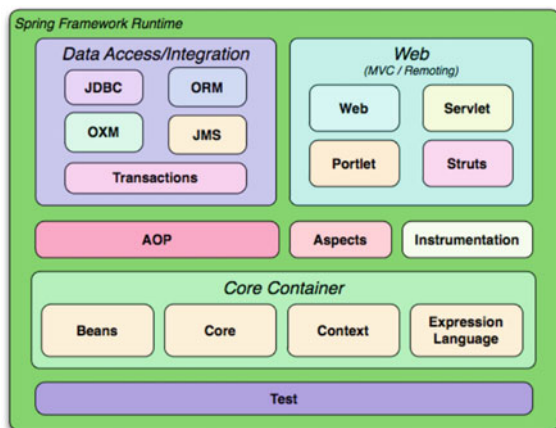
Spring Framework [3] is a tool that is used to create APIs for communication between applications and servers. It is a framework suitable for use with Java Enterprise Application because it helps to manage objects automatically. It consists of many modules which have separate names such as Spring MVC and Spring AOT, and currently, there are Spring Boots which help to develop and write programs more easily than Spring. The structure is shown in Fig. 15.2. The most important module is the Spring Core Container that consists of Core, Beans, Context, and Expression Language modules (SpEL). It is a part of preparation for Spring containers such as BeanFactory and ApplicationContext. Next, the Data Access/Integration comprises of five parts: JDBC, Data access, OXM, JMS, and Transactions modules. **Web layer is the providing service in terms of Web development, whether connecting or uploading files consisting of Web modules, Web-MVC, Web-Socket, and Web-Portlet modules.**

Spring Boot [4] allows for fast application development with Auto-Configuration. This eliminates the need to waste time configuring, including the ability to create a stand-alone application that is exported as .jar or .war and can be deployed at the application server as well. Spring Boot has the following features:

- It is built as a stand-alone Spring application with main methods.
- It has an embed Web Server, usually a tomcat, but can be chosen as another option.
- There is a POM “starter” that is prepared for use. No need to worry about dependency.
- It provides features for monitoring to see memory, thread, and metrics.
- It does not require XML configuration anymore because everything is written as Java-based configuration.

Researches in application have been developed in many ways. The most related research uses the Spring Framework [5–7]. Gajewski et al. [5] have analyzed and

Fig. 15.2 Structure of the Spring Framework [3]



compared the performance of the Spring framework and the Play framework. Both application frameworks let the creation of efficient servers that supported in the large platform and popular website. The Spring framework was adapted on the cross-platform application to support the front end [6].

15.2.3 *Java Script Object Notation (JSON)*

JSON [8] is a data format used for exchanging small data. It makes the user understand easily and can be created and read. The JSON tool is actually a standard format that is text and can be read with the naked eye. It is used to create objects, to send data between applications or as application program interface (API). The format is in the form of Key-Value pairs or Arrays and can be used instead of the XML format's two types:

Object. That is a set of data which will begin with a "{" and end with a "}". Each value will have a symbol ":" between the data name and the value of the data. And each data is separated by a symbol "," such as {"phone": 0868594516}.

Array. That is the sequence of data that begins with the symbol "[" and ends with the symbol "]". Each value of the data is separated by a symbol "," such as {"phone": [0868594516, 0868668505]}.

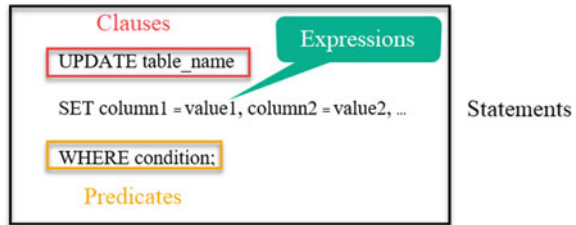
15.2.4 *SQL*

Structured Query Language (SQL) [9] is the standard language for accessing the database. We can use the SQL language from various programs to do with the database system, such as using SQL to retrieve data (Retrieve Data) from the database, and it is the standard used in the system. Various databases are an American National Standard Institute (ANSI) standard designed to manage data in the relational database management system (RDBMS) for searching, changing, adding, and reducing data or to create new tables (create) and delete (drop) and alter (alter) the table that is stored in the database in a tabular format.

SQL Syntax. The SQL language is divided into the following components, as shown in Fig. 15.3:

- Clauses are components of statements and query.
- Expressions are the creation of results in the form of a table consisting of columns and rows from the data.
- Predicates are conditional forms in which results are true/false/or Boolean.
- Queries are important clauses in SQL.
- Statements are things that affect data structures, manage data, transactions, program flow, and sessions, or even analyze problems. It is necessary to end with semicolon (;) which is a must every time for SQL.

Fig. 15.3 Structure of SQL



- Insignificant whitespace or spaces for SQL statements and query are ignored.

15.3 Procedure

Analyze the requirement of user needs at each level where users can set topics for listening to their opinions including comments to solve problems, and in order to be clear of the place and problems that occur, it can be necessary to add pictures.

System usage is shown in Fig. 15.4.

1. Users who encounter a problem or want to ask a question add the desired topic.
2. Users who want to comment on each topic should make their own comments.
3. The department is responsible for planning and solving problems according to comments by users.

15.3.1 The Operation of the System

The system design operation is divided into two parts: (1) mobile, users will use the application on the smartphone, and (2) server will have an API to communicate to manage the data in the database. When users use the system via mobile applications, the application sends information over the Internet to the API to store topics, comments, and users in the database, and then the API will send results to the application on mobile phone as shown in Fig. 15.5.

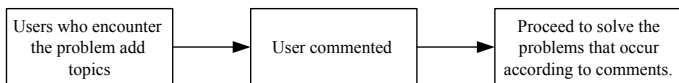


Fig. 15.4 Procedure of system

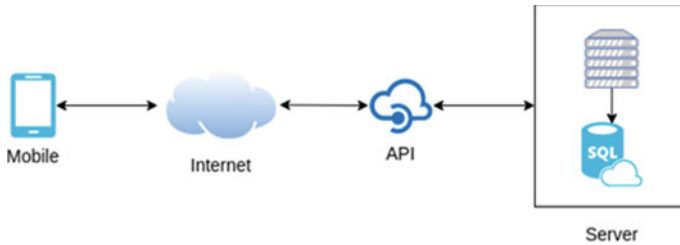


Fig. 15.5 An overview of system operations

15.3.2 System Design and Development

The researchers have analyzed, designed, and developed the system with Dart, Flutter, and MySQL in order to operate correctly and achieve the target set. We have designed and presented it as an application on a smartphone in order to make the application easily accessible and responsive to users conveniently and quickly considering that mobile phones are more involved in human daily life, allowing easy access to applications. The details are as follows:

15.4 Login Page

When accessing the login page, users must log in. If there is no username, they must first register by pressing the “Register” button and complete the information. Then, the system returns to the login page again to use the registered code to log in as in Fig. 15.6.

If the login is correct, the system will enter the category page, as shown in Fig. 15.7. If data is not correct, the user will have to correct the information and click the “Login” button again to access.

Figure 15.7 shows the main page once users are logged successfully. The page will show each category, such as building, Internet, and electricity. In each category, there will be related topics, as posted in Fig. 15.8, showing each topic posted, including the username of the person who posted it and the date of posting the topic.

15.4.1 Adding Topics and Comments

When entering the topic page shown in Fig. 15.7, users can add topics by clicking the “+” button and then go to the topic page to fill out additional topics and details, as shown in Fig. 15.9. To add an image, they click on the camera image to take a picture.

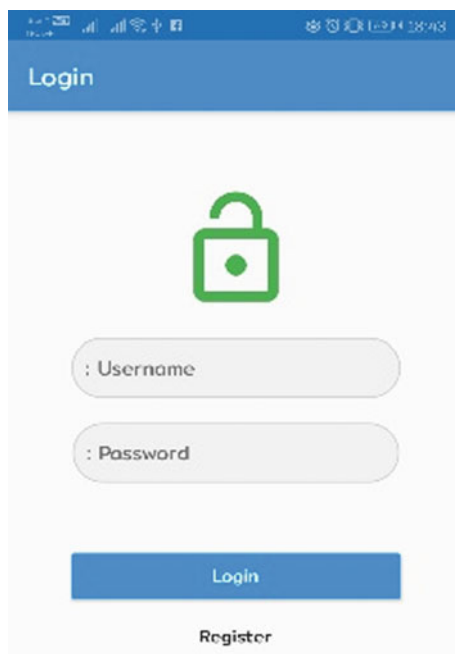
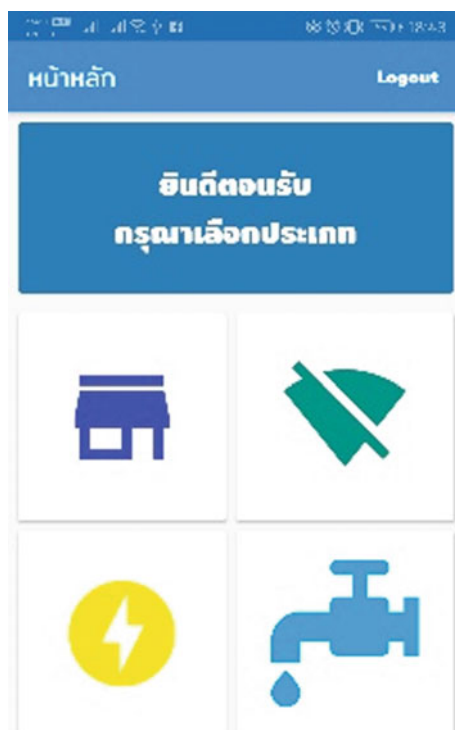
Fig. 15.6 Login page**Fig. 15.7** Main application

Fig. 15.8 Topics in application



When finished, click “OK” and the system will save the image to the database. Then, it will return to the topic display page again.

When entering the topic display page, as in Fig. 15.9, users will click to see the topic and then enter the comment page as shown in Fig. 15.10, where Number 1 is information about the selected topic, and Number 2 is a comment from users. In this section, the relevant staff accounts in each section look at user comments on this page, analyze and lead to the best edits. When users want to post a comment, they press the “+” sign, which will display the add comment page as in Fig. 15.11, and fill in the text. To add a picture, press the camera image to take a picture and then press OK to add a comment.

15.4.2 Tools for System Development

In developing this application for listening to problems and comments, the developer has used the Hybrid-Native Flutter Framework tool. The one-time development will

Fig. 15.9 Inserting the topic

work on both iOS and Android, including Flutter. There are basic components to be used successfully, without having to manually build it all, resulting in increased speed in development. To connect to the database, the developer uses the Spring Framework, one of the basic frameworks based on the highly popular Java language.

15.5 Experimental Results

To evaluate the use of the application, whether it works correctly and is objective or not, we have prepared an online satisfaction evaluation form by collecting data from a total of ten real users and having the scoring criteria as shown in Table 15.1 and then perform satisfaction testing in various aspects as follows:

1. Evaluation of design satisfaction.
2. Evaluation of processing satisfaction.

Fig. 15.10 Expressing opinion



After collecting evaluation results from users, the developers have analyzed the data as shown in Table 15.2.

Table 15.2 shows the results of satisfaction evaluation. It can be seen that the assessors have given the design evaluation an average of 4.1 and a standard deviation of 0.69. For the processing side, the assessors gave an average of 3.9 and a standard deviation of 0.81, which is considered to be in a good level. The application listens and comments, also meets the needs of users by helping them to enhance the repair and maintenance work as well.

15.6 Conclusion

This is an application on a smartphone that listens to problems and comments in order to help the staff in solving problems quickly. And, the solution to the problem is fast and appropriate. Problems arising from system development, since Flutter is a Hybrid Native whose operating speed may not be equal to Native, include a new

Fig. 15.11 Inserting new opinions



Table 15.1 Evaluation criteria scores

Score	Meaning
4.51–5.00	Very good
3.51–4.50	Good
2.51–3.50	Medium
1.51–2.50	Low
1.00–1.50	Very low

Table 15.2 Overall satisfaction assessment results

List	Satisfaction level		
	X	SD	Result
Design	4.1	0.69	Good
Processing	3.9	0.81	Good
Overall result	4.0	0.75	Good

framework and limited library support. Flutter is the Google's UI toolkit that built the beautiful and the single codebase was naively compiled for mobile (both iOS and Android). The Spring Boot application is connected to the MySQL database including the data transmission in the JSON format, which reduced the confusion of developers. Therefore, the data exchange is correct because the JSON data format is clear.

Further development in the operational status tracking is a section that will help the application to better respond to users. Also, it will make it more convenient to manage the problem due to the process of reporting the problem. Finally, GPS point assignments may be added to accurately tell the problem location.

Acknowledgements This research was supported by Department of Computer Engineering, Faculty of Engineering, Rajamangala University of Technology Isan, Khon Kaen Campus, Thailand.

References

1. Flutter Documentation. <https://flutter.dev/docs>. Last accessed 10 Apr 2019
2. Dart Tutorials. <https://dart.dev/tutorials>. Last accessed 10 Apr 2019
3. Introduction to Spring Framework Part I. Overview of Spring Framework. <https://docs.spring.io/spring/docs/3.0.x/spring-framework-reference/html/overview.html>. Last accessed 10 Apr 2019
4. Spring Boot. <https://spring.io/projects/spring-boot>. Last accessed 10 Apr 2019
5. Gajewski, M., Zabierowski, W.: Analysis and comparison of the Spring framework and play framework performance, used to create web applications in Java. In: 2019 IEEE XVth International Conference on the Perspective Technologies and Methods in MEMS Design (MEMSTECH), Polyana, Ukraine, pp. 170–173. <https://doi.org/10.1109/memstech.2019.8817390> (2019)
6. Nik Ahmad, N. A., Syed Zamri, S.A.: The cross platform application development adapted Spring framework to support front-end tendering services. In: 2014 International Conference on Computer, Communications, and Control Technology (I4CT), Langkawi, pp. 58–62. <https://doi.org/10.1109/i4ct.2014.6914145> (2014)
7. Guntupally, K., Devarakonda, R., Kehoe K.: Spring Boot based REST API to improve data quality report generation for big scientific data: ARM data center example. In: 2018 IEEE International Conference on Big Data (Big Data), Seattle, WA, USA, pp. 5328–5329. <https://doi.org/10.1109/bigdata.2018.862192> (2018)
8. Introducing JSON. <http://www.json.org/>. Last accessed 10 Apr 2019
9. SQL Tutorial. www.tutorialspoint.com/sql/index.htm. Last accessed 10 Apr 2019

Chapter 16

Toward Clarifying Human Information Processing by Analyzing Big Data: Comparing Response Time to Questionnaires Included Heteronym Word for Problem Solving Between Visually and Auditory Types



Keiko Tsujioka

Abstract I have developed the system which measures response time to 120 questionnaires of psychological testing (YGPI) by presenting two ways (letters or sound voice) in order to clarify human information processing and have standardized the method of the measurement and criteria of individual differences. From the results of analyzing Big Data which have been gathered with this measuring system, I have found two types of cognitive traits, Visually and Auditory types. It has been presumed that they might have processed information by different means. There are some heteronym words in those questionnaires, and it was supposed to make their different ways or patterns of information processing between two types more clear. Then, I have compared response time to questionnaires including heteronym of 「は」/ha/or/wa/ in Japanese (21/120), like lead or minute in English. This word (/wa/) has grammatically important meaning in the sentences. The result has been shown that the average of response time to those sentences was significantly longer than those of non-heteronym /wa/ (over 12 letters; 42/120) for both types, however, t -value of Auditory type ($t = -9.7$) was larger than those of Visually type ($t = -6.6$). On the other hand, the dispersion in a scatter diagram of the latter ones which was shown in the correlations of response time between presented by letters and sound voice has been shown larger than the former ones. Those results might be able to find the different patterns of information processing depending on types and suggest making the rules or criteria for interactive communication between human and computers. The abstract should summarize the contents of the paper in short terms, i.e., 150–250 words.

K. Tsujioka (✉)
Institute for Psychological Testing, Osaka, Japan
e-mail: keiko_tsujioka@sinri.co.jp

© The Editor(s) (if applicable) and The Author(s), under exclusive license to Springer Nature Singapore Pte Ltd. 2021

Y.-D. Zhang et al. (eds.), *Smart Trends in Computing and Communications: Proceedings of SmartCom 2020*, Smart Innovation, Systems and Technologies 182,
https://doi.org/10.1007/978-981-15-5224-3_16

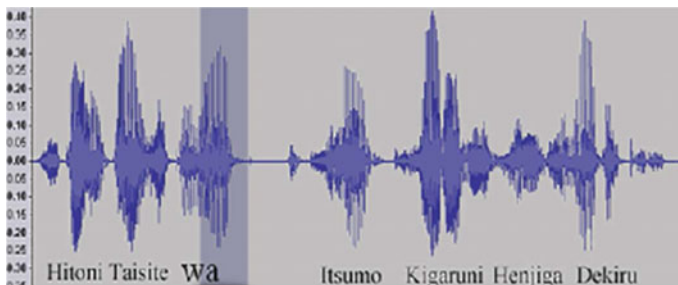
16.1 Introduction

When I seek for interactive communication, it would be needed to clarify language information processing. From this reason, I have developed the measuring system of response time to find cognitive traits and clarify its processing, comparing them between sound voice and letters. Almost of all people can speak and read their language easily, however, it must be difficult for computers or robots now, because each language has not only regular rules but also irregular one, such as homonym, homophone and heteronym; in sequences, run or change, wright and write, lead or minute and so on.

In this paper, I have marked Japanese heteronym 「は」, which is a very important word grammatically, 「は」 is pronounced */ha/* or */wa/*, however, both have also other meanings. In the case of nouns, for instance, the meaning of */ha/* is teeth (tooth) or leave(s), and */wa/*「わ」 is link or sum and so on. Grammatically in the sentences, the role of 「は」*/wa/* is an adverbial particle, whose meanings are a topic or a theme (focus marker or contrastive), a condition (case marker or emphasis) and so on.

Figure 16.1 shows the example of an adverbial particle 「は」*/wa/* in a sentence. When I speak Japanese, I pronounce a sentence with mora timing which is a single prosodic system, comparing with a syllable language such as English. For instance, the Japanese formant structure is shown in Fig. 16.1, “*Hito ni itaishite wa litsu mo ikigaru ni thenji ga idekiru*” (I can always response casually to anyone), 「に」*/ni/*, 「も」*/mo/*, 「が」*/ga/* are the similar particle to *wa*.

They are written by “Kana” letters which are phonogram and have their own grammatical meanings, comparing with ideographic letters of Kanji which have their meanings with shapes. In the case of the example, *wa* is not only indicated as the word which has a grammatical meaning of a condition or topics in a sentence, but also has a meaning of pronunciation, the short pause, in order to emphasize (sound voice) or highlight (letters) points. This rule of Japanese grammar or writing system,



I can always response casually to anyone.
 人に対してはいつも気軽に返事ができる

Fig. 16.1 Japanese formant structure

in which an adverbial particle *wa* is not written with 「わ」, but 「は」 has been decided by Agency for Cultural Affairs, Government of Japan in 1946 [1].

From those of reasons, I have formulated a hypothesis that there might be another pattern of information processing for sentences which are included heteronyms 「は」/*wal*, comparing with them which are not included ones.

I will show the results of experiments in order to verify of these hypotheses visually to find out the patterns depending on cognitive traits.

16.2 Problems

It is considered that the Japanese language writing system has been established by borrowing Kanji (Chinese characters) and Kana (modified a part of Kanji) during Heian Period (around tenth century). The former one has meanings called ideograph and multiple reading (Japanese pronunciation), and the latter one is the Japanese syllabaries. Usually, I write sentences with utilizing a mixture of those Chinese characters (Kanji) and Japanese phonetic characters (Kana). Kanji has been modified by transforming from Chinese into ideograms; both pronouncing and writing ways are adjusting Japanese culture and language.

There are two ways of this mixture writing system: the literary style and the colloquial style. Former one had been used when people had written sentences, but they were not the same way or style as sound voice or speaking. The usage of this literary style was compiled for a handbook as a model in 1889 (Meiji era) which had been gathered by the examples of archaism in all districts in Japan from ninth to eleventh century [2].

On the other hand, the colloquial style is spelled speaking or sound voice. It has begun to be established in Meiji era after increasing the number of people who had been educated and then the requirements of establishing the rule of usage, which would be unified and consisted between speaking and writing, had been launched. Tokieda [3] has proposed “The principle of Japanese Language,” which was explained about his idea or model of language system so that people can keep their culture and know how to educate Japanese language to children. It was the controversial issue of the writing system at that time, and provisional examination committee for Kana was launched in 1921 [4]. After that, the Japanese language committee of regulation for governmental organization has been set up from 1935, and then the criteria of Japanese writing system, “the contemporary usage of Kana,” was established in 1946 [5].

Moreover, Kindaichi [6] and other researchers have been investigating and examining closely for the reform of the writing system from various aspects. For instance, in the case of the *ha* 「は」 column of the Kana syllabary, it has been found that pronounced */fa, if, fu, fe, fo/* for word-initial have been remained, but differentiated into */wa, wi, u, we, wo/* for the medial or ending of word in histrionic literature [7]. From those facts, at first, “I”, 「わたしわ」/*watashi wal*、 “Good afternoon”, 「こんにちは」/*konnichi wal*, were allowed as the right writing. After established writing

system, pronounced /*wa*/ for adverbial particles as the ending of word has been decided the exception of 「は」 as a written letter (「わたしは」 「こんにちは」) [8].

Those has been ruled by referring the usage of adults and children would be able to acquire the language usage by imitating them aurally [9, 10]. Hatano [11] has proposed the problems concerning with the usage of the particle /*wa*/ from the aspect of child developments regarding speaking or listening. She has planned the comparative experiments of case marker between /*wa*/ and /*ga*/. Those particles are important grammatical concepts of hierarchical relations, for instance they are an attached nominal phrase and related to a predictive verb. She has reported that the timing of the acquisition for particle *wa* had late comparing with particle *ga*. They are able to use particle *wa* after entering school.

In addition to this, Ishi has reported about the importance of Kana role from grammatical aspects by investigating the ratio of appearances in the popular newspaper (Asahi) in Japan for one year in 2000 [12]. The ranking of emergency ratio of 「は」 was seventh, but the rate of particle in Kana 「は」 was 95.9%. In addition to this, the ranking of *ga* was tenth, and the rate of particle in Kana 「が」 was 90.1%. Form those results, it was proved how the usage of *wa* during child developments is important grammatically comparing with *ga*.

Along with gathering those literature reviews, it is getting predictable that there might be caused individual differences in human language information processing with particle *wa*, comparing with other written Kana letters. In this research, it might find the cues so that I can clarify human information processing by finding patterns or features, regarding particle *wa*.

16.3 Design

I have conducted experiments presented 120 questionnaires of psychological testing (Yatabe-Guilford Personality Inventory) [13], which consisted of short one sentence each (Fig. 16.2). Participants are required to decide the answer from “Yes,” “No,” “either” for each item. Questionnaires are presented by sound voice or letters. Their response time from starting to present a sentence to the timing of selecting the bottom of answer on the display will be measured. The same 120 questionnaires are presented by sound voice (listening) or letters (silent reading) for each participant.

Our study done thus far is the standardization which is the method of measuring response time (or decision time) and proposal of criteria of cognitive traits, Auditory or Visually types, depending on the strength of correlation coefficient between response time of letters and the period of presenting sound voice (standardization) [Auditory type; $r > 0.5$ [AT], Visually type; $r < 0.3$ [VT] [14].

After calibrating the measurement system, I have examined its reproducibility by implementing experiments twice (January and March in 2015) as far as under the same quality and conclusion, for instance, participants (twenty-eight participants), procedures, environments and so on [15]. The results of comparative analysis between AT and VT for the first and the second time were not significantly difficult, concerning

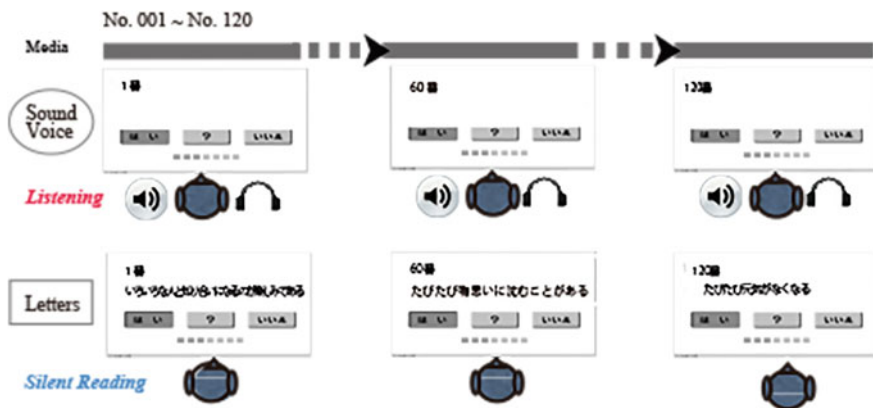


Fig. 16.2 Methods of comparative experiment between sound voice and letters

Table 16.1 Results of representative experiment regarding correlation coefficient between response time (Silent Reading) and sound voice (Duration of Reading)

	R	
	Visually	Auditory
First	2.15	2.82
Second	2.04	2.63

Table 16.2 Significant differences of response time between Auditory and Visually type

	n		\bar{X} (sec)		S.D.		Test	
	Visually	Auditory	Visually	Auditory	Visually	Auditory	t level	
First	720	720	2.15	2.82	0.91	1.02	-13.2	***
Second	720	720	2.04	2.63	0.84	0.84	-13.4	***

*** $p < 0.01$

with correlation coefficient (Table 16.1) and differences of response time between AT and VT (Table 16.2; Fig. 16.3).

Next, I have planned the practical experiments from April in 2015 to March in 2016. Participants were 98 students at the same university as previous verification experiments. Measurement procedures of YGPI have been preserved below:

1. Obtaining acceptance from the ethics boards both the university and authors' affiliation (Osaka University).
2. Preparing for environments of experiments.
3. Getting consensuses from the participants after explanation about practical experiments (Fig. 16.4).
4. Instructing how to take a test (Fig. 16.5).

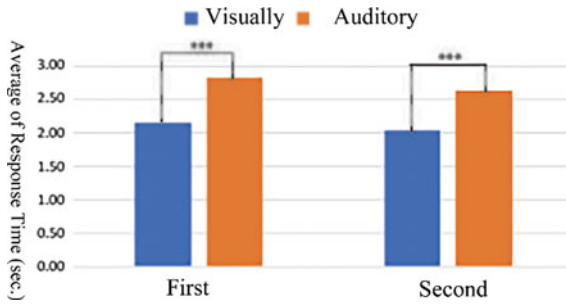


Fig. 16.3 Comparisons of response time between Auditory and Visually type



Fig. 16.4 Scenery of informed consent

5. Conducting tests and measuring each response time presented each sentence of 120 items by sound voice or letters (listing or silent reading); (counter balanced order) (Fig. 16.2).
6. Gathering students' various data, for instance, response time, decision making (chosen repayments), performances in class, results of learning, tracking record, attendance rate and so on.
7. Analyzing and examining those data.

In this paper, I will examine the hypothesis, concerning with information processing patterns of heteronyms *wa*.

Data of their response time are gathered for each subject, totally 240 data per set of experiments. Adverbial particle *wa*, which is heteronym, included twenty-one questionnaires in 120 [c]. The length of sentence included *wa* is over twelve letters (about three words). From this reason, when I compare the response time with those of non-*wa* which are not included *wa*, sentences of under twelve letters will be



Fig. 16.5 Scenery of measuring response time

Table 16.3 Comparisons of response time between non-*wa* and *wa* of each cognitive type; Auditory and Visually depending on presentation of media: sound voice and letters

		Second voice [S]			Letters		
		Under 12 letters		Over 12 letters	Under 12 letters		Over 12 letters
		Non- <i>wa</i> [は]		<i>wa</i> [は]	Non- <i>wa</i> [は]		<i>wa</i> [は]
		[a]	[b]	[c]	[a]	[b]	[c]
Visually type (VT)	df.	377	911	272	377	910	273
	\bar{X}	1.92	2.82	3.15	1.83	2.03	2.46
	S.D.	0.60	0.71	0.76	0.81	0.89	1.06
	<i>t</i> -value		6.6	***		-6.6	***
Auditory type (AT)	df.	899	2169	651	897	2169	651
	\bar{X}	1.94	2.79	3.12	1.94	2.78	3.18
	S.D.	0.67	0.81	0.87	0.73	0.90	1.00
	<i>t</i> -value		-9.0	***		-9.7	***

eliminated (29/120) [a]. The number of sentences with over twelve letters without *wa* (Non-*wa*) is seventy per one hundred and twenty (70/120) [b] [categorization; a, b, c] (Table 16.3).

The method of analysis is based on the comparison between AT and VT of response time for sentences included heteronym *wa* or non-*wa*. After testing for the hypothesis, I will make scattering graphs which compared response time between sound voice and letters. From comparisons between two graphs, I will check whether different patterns existed or not by visualizing Big Data [16].

16.4 Results

Ninety-eight students participated in 2015. The results of comparisons of response time between categories of *wa* [c] and non-*wa* over 12 letters [b] in both types and media those of *wa* were significantly longer than those of Non-*wa* (Table 16.1). In the case of presented by sound voice, there is no difference between types among all categories [a, b, c] (Fig. 16.6, downward). On the other hand, in the case of presented by letters [L], at all the categories they are significantly different between two types; the response time of Auditory type [AT] ([b] = 2.78, [c] = 3.18) is significantly longer than those of Visually type [VT], ([b] = 2.02, [c] = 2.46), especially regarding the category of over 12 letters [b, c] (Fig. 16.6, upward).

Both types of correlation coefficient between response time presented by sound voice and the duration of presented by it were strong ($0.40 < r$). Comparing plots between two types of scatter grams (Fig. 16.7), however, their patterns of points, which are represented by response time of correlations between media, are observed different from each other.

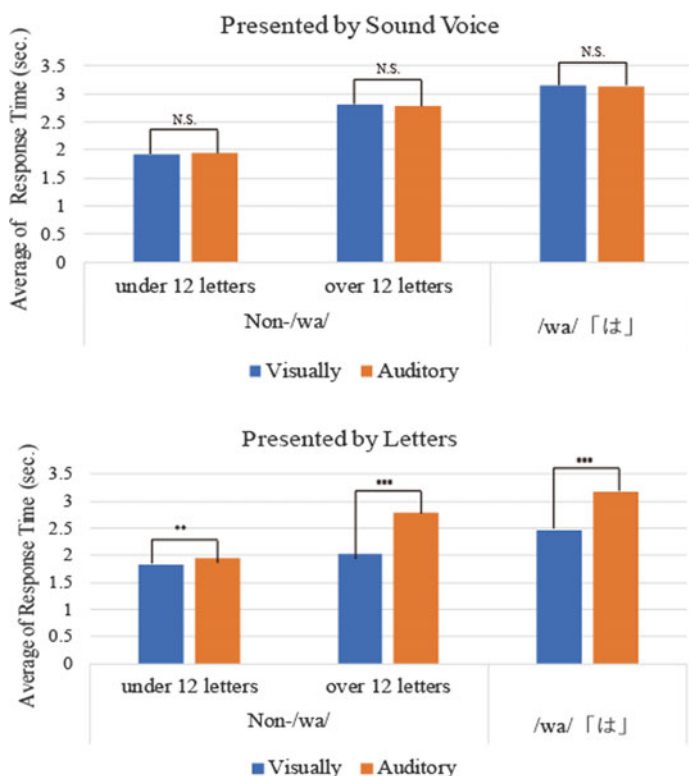


Fig. 16.6 Comparisons of response time between Auditory and Visually types (upward: presented by sound voice, downward: presented by letters)

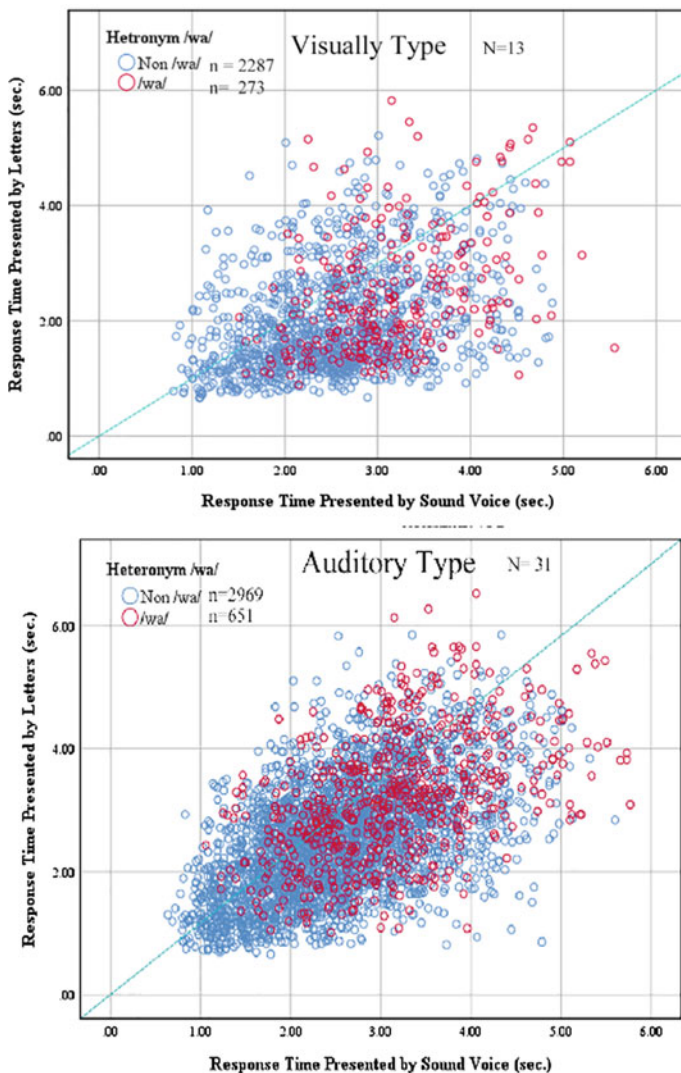


Fig. 16.7 Scatter diagrams of response time which are pointed to show the degree of correlation between two media (sound voice and letters) depending on cognitive types (upward: Visually type, downward: Auditory type)

The average of correlation coefficient between them in category non-*/wa/* [b] for Auditory type [AT] ($r = 0.43$) (Fig. 16.7, downward) is higher than those of Visually type [VT] ($r = 0.14$) (Fig. 16.3, upward). On the other hand, the average of correlation coefficient between them in category */wa/* [c] for Auditory type [AT] ($r = 0.48$) (Fig. 16.3, downward) is the higher than those of Visually type [VT] ($r = 0.20$) (Fig. 16.3, upward). Both types of correlation coefficient of *wa* are higher than

non-*wa*. However, those of five subjects, in thirteen Visually types, are more than $R = 0.30$ ($0.30 < r < 0.65$) regarding questionnaire including *wa* [c]. On the other hand, those of four subjects in thirty-one Auditory types are under $R = 0.25$ ($0.08 < r < 0.25$) concerning with *wa* [c].

16.5 Discussion

In the case of sound voice, there is a pose after *wa* which is shown as the formant structure in Fig. 16.1. This prosodic feature might make listeners wake up that *wa* is not 「わ」 but 「は」 which has grammatical meaning of adverbial particles, topics of focus marker (contrastive) [17] or condition of case marker (emphasis) which has the concept of relationship between nominal phrase and predictive verb.

In contrast, written Japanese language system has two types of letters, Kanji and Kana, and they are mostly written continuously with no space. Obviously, it is controversial issues why letters are not written separately by each one word and how Japanese written language would be comprehended or understood by people, in spite of such an ambiguous appearance. As Ishii [12] has examined about Kana how important grammatically by investigating the rate of emergence in one popular newspaper for one year (Sect. 2), Kana has an obvious role, especially an adverbial particle *wa* which was appeared with the high ratio. From this viewpoint, written Japanese language Kana might be read silently and understood cognitively as grammatical markers by sets of Kanji and Kana.

Therefore, Japanese Government might have decided the system of writing of 「は」 by way of exception [8]. Though it might be convenient to distinguish the word is noun or particle, the results of experiments have shown that it takes significantly longer to respond to sentences included *wa* comparing non-*wa* (not included *wa* in a sentence) (Table 16.3). This means that it is so complicated to process the word “*wa*” that the interactive communication might be interrupted between human and computers. From this viewpoint, it might be made criteria for the writing system regarding carriage control, for instance non-breaking space before *wa*.

16.6 Conclusion

The result of *t*-test which varies the difference of average response time between *wa* and non-*wa* for Auditory type (AT) was larger than Visually type (VT). In contrast, the scatter diagram which described the correlations of response time between sound voice and letters for VT shows larger dispersion than AT. In addition to this, the average of response time to sound voice for AT was similar to those of letters. This means that AT might process characters or written words by phonologization. On the other hand, VT might process them directly without changing sound. Those

phenomena have been shown by visualizing Big Data which are various data, for instance response time, types, different media and so on.

Acknowledgements The author is grateful to Dr. Kiyoko Tokunaga and participants for collaboration on practical research.

References

1. Agency for Cultural Affairs, Government of Japan Homepage: Japanese Language Policy. http://www.bunka.go.jp/english/policy/japanese_language/index.html. Last accessed 17 Nov 2019. http://www.bunka.go.jp/kokugo_nihongo/sisaku/joho/joho/index.html
2. Otsuki, H.: Language Usage Handbook, 「語法指南」 in Japanese, National Diet Library Digital Collections. http://dl.ndl.go.jp/info:ndljp/pid/992861?itemId=info%3AndJp%2Fpid%2F992861&__lang=en (1897). Last accessed 10 Dec 2019
3. Tokieda, M.: Principle of Japanese Language, in Japanese, Iwanami Bunko (2007)
4. Mori, O.: View of Kana Usage (仮名遣意見), in Japanese, in Chikuma Collection, Chikuma Shobo (1971). Aozora Bunko H.P. (<http://www.aozora.gr.jp>). https://www.aozora.gr.jp/cards/000129/files/677_22837.html. Last accessed 10 Dec 2019
5. Agency for Cultural Affairs, Government of Japan Homepage: Japanese Language Policy. 3000 Data Collection of Kana Usage, Cabinet Notification No.33. http://www.bunka.go.jp/kokugo_nihongo/sisaku/joho/joho/sisaku/enkaku/enkaku1.html (1946). Last accessed 04 Dec 2019
6. Kindaichi, K.: Discussing Japanese Language. Sanseido, Tokyo (1962)
7. Keichu: Waji Syouran (倭字正監) in Japanese, National Diet Library Digital Collections. <http://repository.aichi-edu.ac.jp/dspace/bitstream/10424/1037/1/kokugokokubun552940.pdf>. Last accessed 04 Dec 2019
8. Kieda, M.: Usage Manual for Contemporary Writing System of Kana and Chinese Characters for Daily use. In Japanese, 「解説現代かなづかいと当用漢字」, Anomaly Respect wa, e, wo, 「例外事項はへを」, Dekijima Shoten, pp. 15–16 (1947). <https://doi.org/10.11501/1126384>. HP: National Diet Library Digital Collections. <https://www.dl.ndl.go.jp/api/iif/1126384/manifest.json>. Last accessed 2019/12/1
9. Paula, M.: Syntactic Structures in the Language of Children, Wiley on behalf of the Society for Research in Child Development, vol. 34, no. 2, pp. 407–422. <http://doi.org/10.2307/1126736> (1963)
10. Ervin-Tripp, S.: Imitation and structural change in children's language. In: Lenneberg, E. (ed.) *New Directions in the Study of Language*. Cambridge, Mass., M.I.T. (1964)
11. Hatano, E.: A study of children's acquisition of particles wa and ga in Japanese. *J. Educ. Psychol.* **27**(3), 10–18 (1979). https://doi.org/10.5926/jjep1953.27.3_160
12. Ishii, H.: Grammatical and lexical features of hiragana Bulletin of Center for Japanese Language Doshisha University Bulletin of Center for Japanese Language Doshisha University (1), pp. 3–16. <http://doi.org/10.14988/pa.2017.0000013880> (2001)
13. Tsujioka, B., Yatabe T., Shinohara, T.: A factorial study of the temperament of Japanese college male students by the Yatabe-Guilford personality inventory. *Psychologia*, 110–119 (1957)
14. Tsujioka, K.: Toward clarifying human information processing by analyzing big data: making criteria for individual traits in digital societ. In: Orlando, B. (ed.) *Strategy and Behaviors in the Digital Economy*, IntechOpen, pp.125–140. <https://doi.org/10.5772/intechopen.86037> (2020)
15. Tsujioka, K.: Toward clarifying human information processing: a case study of big data analysis in education. In: Karwowski, W., Ahram, T. (eds.) *Intelligent Human Systems Integration, IHSI 2019, AISC 903*, pp. 378–383. https://doi.org/10.1007/978-3-030-11051-2_58 (2019). Last accessed 10 Dec 2019

16. Tsujioka, K.: A case study of ICT used by big data processing in education: discuss on visualization of RE research paper. ICIET, Association for Computing Machinery, pp. 160–164 (2018). ISBN: 978-1-4503-4791-4
17. Nakanishi K.: Prosody and scope interpretations of the topic marker ‘Wa’ in Japanese. In: Lee, C., Gordon, M., Buring, D. (eds) *Topic and focus. Studies in Linguistics and Philosophy*, vol. 82. Springer, Dordrecht, pp. 177–193. https://doi.org/10.1007/978-1-4020-4796-1_10 (2008)

Chapter 17

Mango Species Detection from Raw Leaves Using Image Processing System



Most. Hasna Hena, Md. Helal Sheikh, Md. Shamim Reza,
and Ahmed Al Marouf

Abstract Mango is the national tree of Bangladesh which is one of the most popular fruits here during the hot summer enriching the highest quality of nutrition. Various species of mango cover the fruit market making the summer festivities. In recent times, different species of mango are also being exported to different countries of the world. So more and more people are entering into the commercial mango cultivation nowadays as new farmers. It is necessary for them to know which mango species they are cultivating and what is the market demand of that species. It is hard for the new farmers to find out the species just by asking and trusting the sapling seller. So, we plan to establish a system that can accurately ensure the species of the mango sapling. This research used convolutional neural network (CNN) and deep learning for training the dataset. This method can showcase the species of the mango sapling only by observing the image of a leaf holding an accuracy of 78.65%.

17.1 Introduction

Bangladesh is greatly known through the world for her diversity among various sectors. Having six seasons and their own specialities is one of them. Summer is considered the most disparate season when it comes to fruits [1]. It is the season of more than twelve different fruits. But mango is the most demanding one among all. In Bangladesh, mango is known as the king of fruits. Green mangoes are sour wherein

Most. Hasna Hena (✉) · Md. Helal Sheikh · Md. Shamim Reza · A. A. Marouf
Department of Computer Science and Engineering, Daffodil International University (DIU),
Dhaka, Bangladesh
e-mail: hena.cse@diu.edu.bd

Md. Helal Sheikh
e-mail: helal15-6771@diu.edu.bd

Md. Shamim Reza
e-mail: shamim15-7607@diu.edu.bd

A. A. Marouf
e-mail: marouf.cse@diu.edu.bd

© The Editor(s) (if applicable) and The Author(s), under exclusive license
to Springer Nature Singapore Pte Ltd. 2021

Y.-D. Zhang et al. (eds.), *Smart Trends in Computing and Communications: Proceedings of SmartCom 2020*, Smart Innovation, Systems and Technologies 182,
https://doi.org/10.1007/978-981-15-5224-3_17

ripe mangoes are sweet as well as sour in taste. So the mango species which are sweet in taste have the highest demand among the customers such as Fazli, Langra, Gopalvog, and Amrapali.

Mango has been declared as the national tree of Bangladesh by considering its demand and availability in 2010. Mangoes do not only taste good but also are rich in vitamins. Lashings vitamins A, C, and E are found in a mango and considered as one of the most low-calorie fruits. A maximum number of mangoes are cultivated in south Asian countries, and about 50 species of mango are found in Bangladesh only. They can be differentiated by structure and texture of leaves [2], shape of the tree, sizes of the fruit, color, unique fragrance and taste of the fruits, etc. Weather, geographical balance, soil quality, and texture vary to grow different mango species.

Every species of mango has its own species name, though they all share the same scientific or genetic name ruled by International Code of Botanical Nomenclature (ICBN). Since every species has its own distinctive fragrance, taste, and admirers, it becomes more confusing for the people having less knowledge in this sector and often suffer for the correct species when the tree is only a sapling. So, the mango cultivators who cultivate commercially and also personally emphasize upon those particular species of mango seeds or sapling. So, it is much needed to find out the exact species.

Image processing is becoming the most trustable method for image researching in recent times. It is becoming more and more popular among the researchers for higher accuracy and easy to expose model. For this research work, we are using convolutional neural network (CNN) [3] deep learning algorithm where we can input an image for further calculation and assign that image into filters for an accurate output. Here, about six species of mango are being detected with the help of deep learning algorithms and image processing methods. They are Ashina, Fazli, Gopalvog, Khirsa, Langra, and Lokhna.

17.2 Literature Review

The background studies for this research work are presented in this portion. The previous research work was with fruits, but species detection of mango from the image leaves with the help of CNN is done in this research work. We have taken all kind of necessary ideas, inspiration, and knowledge from this explained work to create an outstanding and unique system. Hena et al. [4] have published an image dataset of six different species of mango leaves concluding about 7900 images from 54 different trees. They have kept the minimal noises and blur in the dataset about 1.5% considering all three versions of images such as red, green, and blue (RGB), binary, and grayscale.

Sutrodhor et al. [5] have presented a neural network ensemble (NNE) for detecting the mango leaf ailment named as mango leaf ailment detection using neural network ensemble and support vector. They have achieved an average accuracy of 80% for the

ailment detection of mango leaves. Arivazhagan et al. [6] have detected the leaf diseases of mangoes using CNN and image processing features on 1200 image dataset. Their proposed model has achieved 96.67% accuracy considering five disease classes of mango. Their work was presented as Mango Leaf Diseases Identification Using Convolutional Neural Network. Sahu and Potdar [7] have found out the defected mango fruits as well as their maturity considering human recognition level and presented their work as Defect Identification and Maturity Detection of Mango Fruits Using Image. MATLAB programming tool and image processing toolbox have been used thoroughly for the project.

Abbas et al. [8] have classified mango fruits depending on their texture and shape features in Pakistan. MaZda and B11 image classification, MRI and MATLAB methods have been used to differentiate various mango classes ensuring 70% accuracy. Sriram et al. [9] have used convolutional neural network (CNN) to classify the mango species from the mango fruit images achieving 99% system accuracy and presented the work of Mango Classification using Convolutional Neural Networks. Even though classification of mango fruits is done by using various methods and processes, CNN as the latest technology ensures the highest accuracy among all. Since detection of mango species has not been applied on leaf images mangoes, we are confident that our research will open more doors for further opportunities in this sector.

17.3 Proposed Methodology

We have used convolutional neural network (CNN) and image processing techniques to train the system with the collected mango dataset as an input. After inputting an image to the system, it processes the image and provides an expected accurate outcome. Since the rural farmers of our country have little knowledge on detection of taxonomy of any kind of plant species and most of them are unaware of the latest technology, we have decided to mobilize that in this research so that they can also use it without facing any complexity.

17.3.1 Primary Steps for Mango Species Detection

The primary steps for mango species detection are shown in Fig. 17.1.



Fig. 17.1 Primary steps for mango species detection



Fig. 17.2 Collected samples of images in dataset

17.3.2 Image Acquisition

Dataset plays a vital role in any research to find the highest accuracy and better outcome. In this research, we have collected more than 4000 images. We collected all images ourselves by capturing them with the help of a camera. These images are red, green, and blue (RGB) standards. The system can get hold of the images like .jpg, .gif, .NEF, .bmp as input.

17.3.3 Image Pre-processing and Classification

In this research, we have assembled 3500 images from the total collected dataset where all the images are 256×256 pixels. We have divided the pre-trained dataset for the train and test folders with the ratio of 80 and 20%. Percentage of sample classes of each breed of mango is as follows: Gopalvog—24%, Fazli—19%, Ashina—17%, Khirsha—15%, Langra—13%, and Lakkha—12%. Some types of collected dataset samples are shown in Fig. 17.2.

17.3.4 Architecture Model

This proposed model has multiple layers of CNN. The first CNN layer of this proposed model is input layer which has used input shaped (256, 256, 3), filters 64, kernel size (8×8), padding “same,” strides (1×1). Convolutional layer two used filters 64, kernel size (8×8), padding “same,” strides (1×1). And the last layer used filters 8, kernel size (3×3), padding “same,” strides (1×1). Every layer has followed the activation ReLU “(1)” and batch normalization.

$$\text{ReLU}(X) = \text{MAX}(0, X) \quad (17.1)$$

This model used dense layers 512 for 50% dropout and 6 units with activation softmax “(2)” and sigmoid “(3)”.

$$\sigma = \frac{e^{z_j}}{\sum_{k=1}^k e^{z_k}} \text{ for } j = 1, \dots, k \tag{17.2}$$

$$\varphi(z) = \frac{1}{1 + e^{-z}} \tag{17.3}$$

The proposed model of this research is given in Table 17.1.

Table 17.1 Proposed layers and output

Layer (type)	Output	Param #	Layer (type)	Output	Param #
conv2d_9 (Conv2D)	(None, 256, 256, 64)	12,352	conv2d_15 (Conv2D)	(None, 64, 64, 8)	1160
conv2d_10 (Conv2D)	(None, 256, 256, 64)	262,208	conv2d_16 (Conv2D)	(None, 64, 64, 8)	584
max_pooling2d_4 (MaxPooling2)	(None, 128, 128, 64)	0	max_pooling2d_6 (MaxPooling2)	(None, 32, 32, 8)	0
conv2d_11 (Conv2D)	(None, 128, 128, 32)	51,232	batch_normalization_4 (Batch)	(None, 32, 32, 8)	32
conv2d_12 (Conv2D)	(None, 128, 128, 32)	25,632	flatten_2 (Flatten)	(None, 819 2)	0
batch_normalization_3 (Batch)	(None, 128, 128, 32)	128	dense_3 (Dense)	(None, 512)	4,194,816
conv2d_13 (Conv2D)	(None, 128, 128, 16)	12,816	dropout_2 (Dropout)	(None, 512)	0
conv2d_14 (Conv2D)	(None, 128, 128, 16)	6416	dense_4 (Dense)	(None, 6)	3078
max_pooling2d_5 (MaxPooling2)	(None, 64, 64, 16)	0			

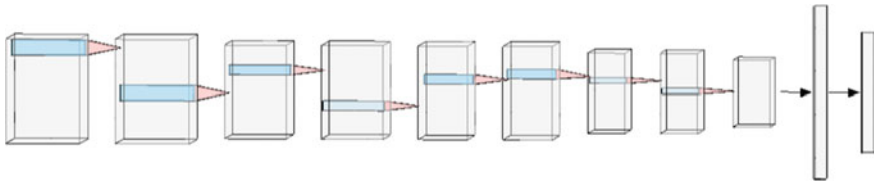


Fig. 17.3 Architecture of this proposed model

The Adam algorithm has been used for reducing the learning rate and value loss after completing every successful epoch. This model has used Adam value (0.0001). The proposed model is shown in Fig. 17.3.

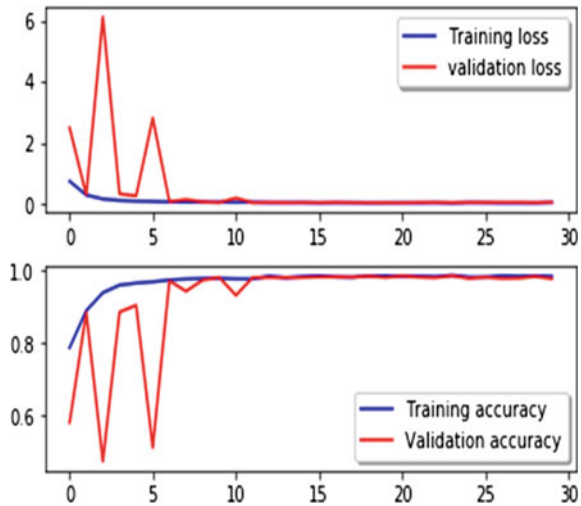
17.4 Result

Basically, result section of any research is the report of the outcome of the proposed method used in the research work. The result of this research states every findings related to this research study without any interpretation or biasness. The brief explanations of the gathered findings and information of this study are going to offer here for further evaluation.

17.4.1 Statistical Analysis

Statistical analysis gives meaning to lifeless numeric values. In this research, how the proposed model worked is briefly explained using numeric values. After every successful run of the model, an accuracy and an error rate have popped out which numerically exhibit how well the proposed model is working and where to alter to achieve the highest accuracy.

In this research, 0.1% training accuracy has been obtained wherein the learning rate found is 0.011 succeeding first epoch. Tailing the first epoch 30.34% training accuracy has been achieved after fifth successful run, and an error rate of 0.0011 has been found. Maintaining the corresponding process the training and testing accuracy after ten epoch 75.08% and 77.79%. After thirty successful runs epoch it has been achieved 78.65% training and 78.02% testing accuracy and 0.001 learning rate have been obtained succeeding the concluding epoch.

Fig. 17.4 Accuracy graph

17.4.2 Accuracy Graph

In this research, the representation of graphical outcome of the proposed model by using CNN and image processing techniques is shown below in Fig. 17.4 and explained briefly. From the following figure, the performance of the model can be measured. Whether a model is overfitted or underfitted can be ensured through accuracy graph of a research study. Our proposed model is working well since the accuracy graph is justifying the statistical outcome of the model, and we obtained an accuracy of 78.65% at the end. Even if the first accuracy graph retains a matter of contention of underfitting, then that has been found fitting in the tailing graph having no issues of overfitting or underfitting.

17.4.3 Confusion Matrix

In this research, a two-dimensional matrix summarizes the classification performance reciprocal to deep learning classifier of the collected mango image test dataset. All the true positive, true negative, false positive, and false negative outcomes can be obtained from this confusion matrix. Confusion matrix interprets the precision of any research study and illustrates how satisfying the proposed model is. In this matrix ($6 * 6$), all the diagonal values are larger than others and much more darker in color which illustrates our research study provides an exceptionally favorable outcome. The confusion matrix of this research is shown in Fig. 17.5.

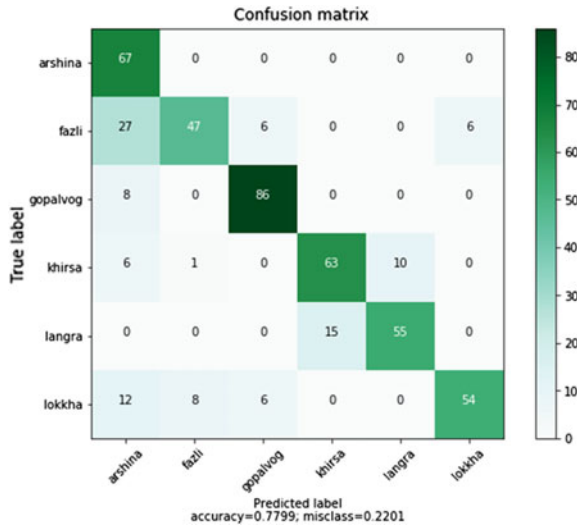


Fig. 17.5 Confusion matrix

17.4.4 Layer Visualization

Impressive classification outcome of the CNN and image processing techniques of this research are shown in Fig. 17.6 by segregating an image in numerous portions through matrixes. Layer visualization satisfies the accuracy of this research study by delving into the input image and helps the system to arrive at a decision.

The layer visualization output of the first four layers of this model is shown in Fig. 6(a), (b), (c), (d) where as the matrix size (2 × 2).

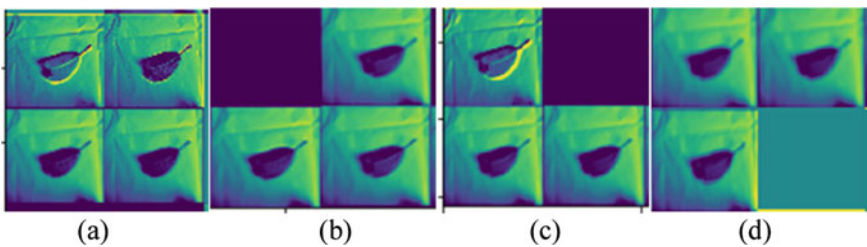


Fig. 17.6 Layer visualization

```

: [[0. 1. 0. 0. 0. 0.]]
{'arsina': 0, 'fazli': 1, 'gopalvog': 2, 'khirsa': 3, 'langra': 4, 'lokkha': 5}
প্রজাতি নামঃ ফজলি
ফজলি বা ফর্কিরভোগ মৌসুমি ফল আমের একটি প্রকারভেদ।
এই ফল দক্ষিণ এশিয়ার সুদিকে বিশেষ করে বাংলাদেশ ও ভারতের পশ্চিম বঙ্গ ও বিহারে পাওয়া যায়।
আমের অন্যান্য প্রজাতির থেকে দেরিতে ফলে এই ফসল।

```

Fig. 17.7 Repercussion

17.4.5 Species Detection

Some fruit class has its own taxonomy species, and mango is one of them. It has one of the largest varieties among the fruit classes. So detecting the species of mango following the manual process can be bothersome, time consuming, and inaccurate at times. In this research, we have used the latest technology of image processing and CNN algorithm to detect the mango species from the image of mango leaf only. If a similar random image is inputted to the pre-trained system, it will disclose the species name and its immediate parent class along with some other knowledge that might be needed to have a glimpse of this species without any help of the expert personnel. Since most of the rural farmers of our country are mostly uneducated, the repercussion is provided in Bengali and English language for their better understanding in Fig. 17.7.

17.5 Conclusion

In this research, we have established a model that can detect the species of a mango tree or sapling from the leaf images only along with a detail of that species as an output. Since every species has own arguments and specialities, they all need different nourishment. So this research can really be helpful for the cultivators if the species is known to them before the blossoms. The new farmers as well as all the mango growers can have potential assistance from our work and fulfill their necessary need according to the detected species. This method can be applied for the disease detection, and we plan to do that later on.

References

1. Karim, M.R., Alam, M.S: Profitability of Summer BARI Hybrid Tomato Cultivation in Jessore District of Bangladesh (2009)
2. Samshunnahar, Mst., Khanum, R., Serajul Islam, M.: Profitability of Small-Scale Tomato (*Lycopersicon esculentum*) Production in Some Selected Areas in Bangladesh. Department of Agricultural Economics, Bangladesh Agricultural University, Mymensingh, Bangladesh (2016)
3. CS23In Convolutional Neural Networks for Visual Recognition. cs231n.github.io. Retrieved 2017-04-25
4. Hena, H., Marouf, A.A., Sultana, R.: Mango LDB: a dataset of mango leaves RGB, binary and gray-scale image. Int. J. Innovative Technol. Explor. Eng. (IJITEE) 8(7) (2019)

5. Sutrodhor, N., Hussein, M.R., Mridha, M.F., Karmokar, P., Nur, T.: Mango leaf ailment detection using neural network ensemble and support vector machine. *Int. J. Comput. Appl.* **181**(13) (2018)
6. Arivazhagan, S., Ligi, S.V.: Mango leaf diseases identification using convolutional neural network. *Int. J. Pure Appl. Math.* **120**(6) (2018)
7. Sahu D., Potdar R.M.: Defect identification and maturity detection of mango fruits using image analysis. *Am. J. Artif. Intell.* **1**(1), 5–14 (2017)
8. Abbas, Q., Iqbal, M.M., Niazi, S., Noureen, M., Ahmad, M.S., Nisa, M., Malik, M.K.: Mango classification using texture & shape features. *Int. J. Comput. Sci. Netw. Secur.* **18**(8) (2018)
9. Sriram, R., Tejas, A.M, Girija, J.: Mango classification using convolutional neural networks. *Int. Res. J. Eng. Technol. (IRJET)*

Chapter 18

Frequency Reconfigurable Planner Antennas for Wireless Applications: A Review



Dinesh Yadav  and Vivekanand Tiwari 

Abstract Reconfigurable antennas are gaining greater attention in this scenario because of its diverse features in different fields. Reconfigurable antennas have an upper hand on the conventional antennas because of its versatility. They can be utilized in much wider domains than smart antennas. The reconfigurable antennas are capable to utilize available spectrum without varying physical structure of the antenna by using switches, RF-chock inductors and biasing networks. Different multi-band and ultra-wide band-notched antennas with frequency reconfigurable characteristic are analyzed, compared and summarized in this paper.

18.1 Introduction

18.1.1 Reconfigurable Antennas

Reconfigurable antennas are those which can adjust their different characteristics such as frequency, polarization, radiation pattern and gain according to user's need. These antennas work on the principle of the positioning of RF switch which affects the distribution of current in the antennas. For switching, fundamental components such as varactor diodes, pin diodes and MEMs switches are used. These reconfigurable antennas can be divided into subcategories based on their rehabilitation features. Antennas which can work on multiple frequencies are called frequency reconfigurable antennas. Those antennas whose radiating structures can change its polarization such as horizontal, vertical, right hand and left hand polarization are called polarization reconfigurable antennas. If the radiating structure is able to tune

D. Yadav (✉) · V. Tiwari
Department of ECE, Manipal University Jaipur, Jaipur, Rajasthan, India
e-mail: dinesh.yadav@jaipur.manipal.edu

V. Tiwari
e-mail: drvntiwari17@gmail.com

© The Editor(s) (if applicable) and The Author(s), under exclusive license to Springer Nature Singapore Pte Ltd. 2021

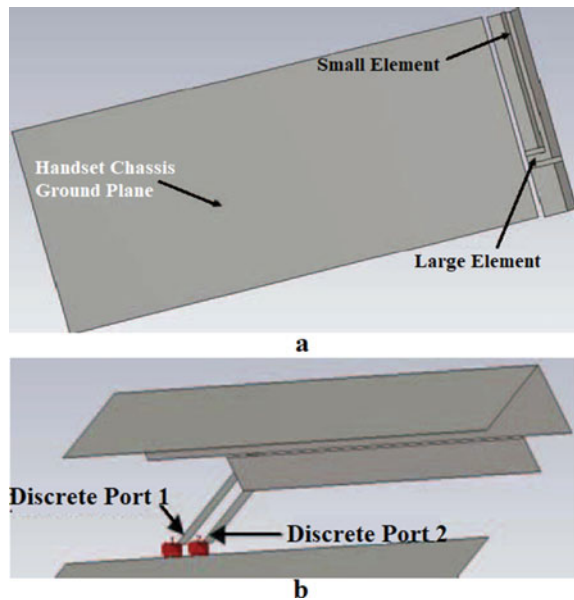
Y.-D. Zhang et al. (eds.), *Smart Trends in Computing and Communications: Proceedings of SmartCom 2020*, Smart Innovation, Systems and Technologies 182,
https://doi.org/10.1007/978-981-15-5224-3_18

the radiating pattern, then those antennas are called radiation reconfigurable antennas. Lastly, if the radiation structures are able to intensify the gain, they are called gain reconfigurable antennas. Pin diodes have low levels of capacitance. They also have switching and variable resistances which make them efficient for switching in RF devices. Their main drawback is that they have high DC bias current. In varactor diodes, capacitance can be varied by changing voltage in the circuit which makes them coherent for tuning circuits like radio frequency oscillators and filters. Their main drawback is that they are non-uniform and have a low dynamic range.

18.1.2 Multiple Frequency Reconfigurable Antennas

Antennas chassis Fig. 18.1 containing four different circuits were designed and fabricated to bespeak frequency swiftness and potential of the system. The authors tested this system to be utilized as a penta-band antenna for cellular phones. It prolongs input return loss aloft 6 db throughout a tuning range of 800–2900 MHz. It has dual-band characteristics and is able to envelope services like GSM900, GPS1575, PCS1900, GSM1800 bands [1]. In 2010, a square slot reconfigurable antennas was proposed by researchers, in which re-configurability between single band UWB including band notch function and multi-resonance characteristic have been investigated. In Fig. 18.2, it is clearly visible that H-shaped slots are cut on the ground plane to lower the coupling and make it switch between frequencies. Pin diodes are also inserted between the slots to make it switchable between multi-resonance and single

Fig. 18.1 Wide tunable dual-band reconfigurable antenna for future wireless devices [1]



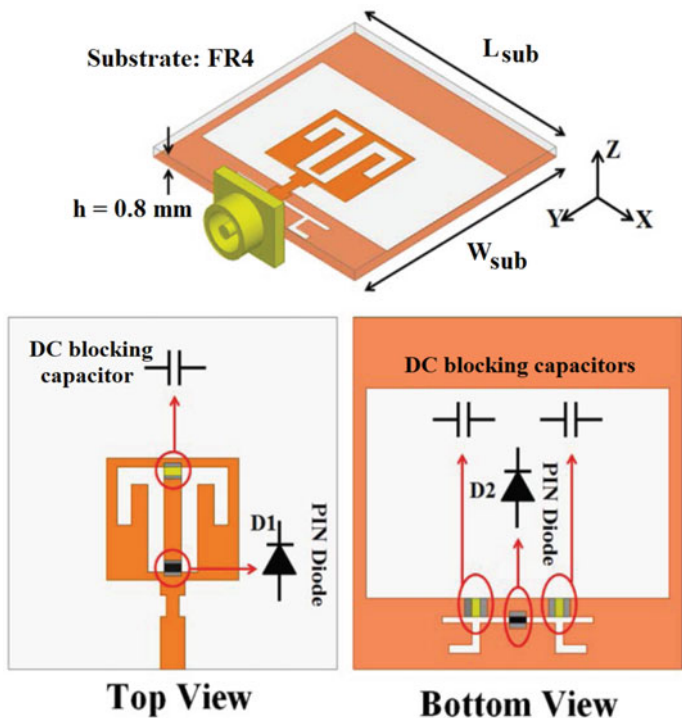


Fig. 18.2 Reconfigurable square slot antenna with switchable single band, UWB and UWB with band notch function performances [2]

band UWB characteristics. By cutting gamma-shaped slots in the radiating stub, it makes the antenna generate an additional resonance at 9.25 GHz. Two notches on the feed line let the antenna to generate additional resonance at 10.2 GHz. When the current flows in the pie-shaped structure, the antenna works on 4.8 GHz frequency [2] (Fig. 18.3).

18.2 Ultra-Wide Band Reconfigurable Antennas

In 2015, the researchers proposed a monopole micro strip antenna with reconfigurable frequency characteristics for WLAN/Wi-Max applications. In this antenna, three pin diodes were used, and the antenna was proficient to operate at four different frequencies depending on the status of the diodes (ON or OFF). The center resonant frequencies are 2.4, 3.3, 5.1 and 5.6 GHz [3]. In 2017, the authors proposed a monopole UWB antenna which has reconfigurable notched characteristics. It is capable of switching its resonance from 5 to 8.2 GHz center frequency bands by two

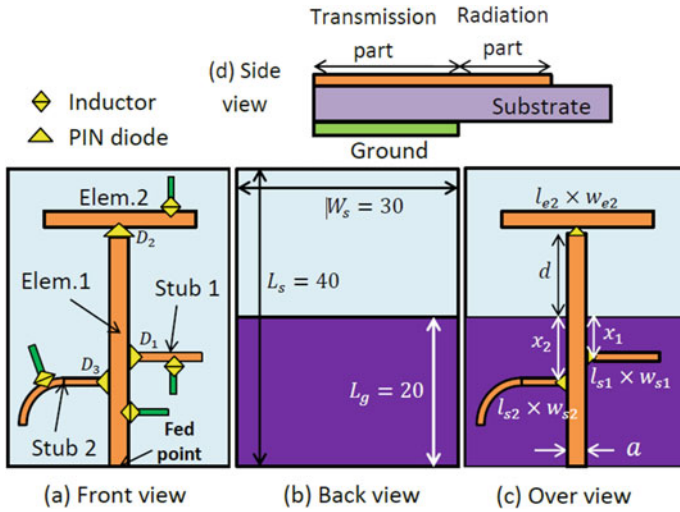


Fig. 18.3 Novel frequency reconfigurable monopole antenna using pin diode for WLAN/Wi-Max applications [3]

Pin diodes. This antenna has a H-shaped parasitic resonator to make it capable for switchable notch characteristics, and a rectangular slot is pushed at metallic ground plate to maximize impedance bandwidth [4]. Figure 18.4 clearly states the shape of the antenna.

In [5], researchers have reported a frequency reconfigurable monopole antenna which is proficient in switching between band-notched ultra-wide band and WLAN applications. The structure shown in Fig. 18.5 consists of five pin diodes and bias-

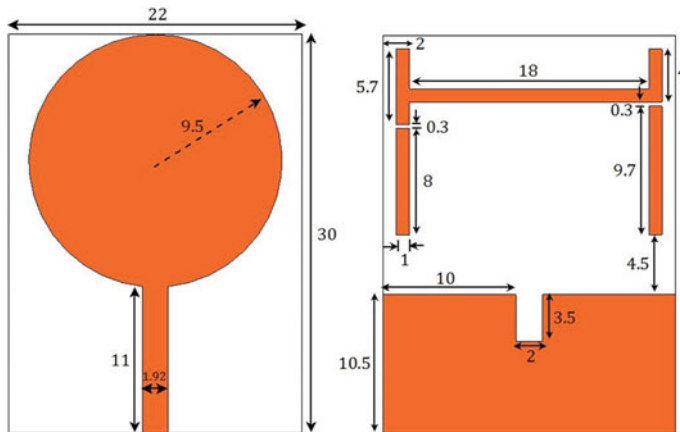


Fig. 18.4 Monopole antenna with reconfigurable notched characteristics from WLAN band-notched UWB to ITU band-notched UWB [4]

done on RT/Duroid 5880 substrate. The switching between the operating frequencies is done using the pin diode. When the diode is in ON state, the antenna operates in full UWB. The notched band is achieved when the diode is in OFF state [6]. The comparison of multiple reconfigurable antenna is shown in Table 18.1. It can be observed that the proposed design in [2] is more efficient since it is able to switch between three operating frequency bands with only two pin diodes, whereas in [3], three pin diodes are used to switch between four operating frequencies (Figs. 18.7 and 18.8).

The comparison of different band-notched antennas is shown in Table 18.2. It is found that antenna reported in [4] is capable to resonate between 3.2–13 GHz and is switchable to two band notches, i.e., between 5–5.35 GHz and 8–8.45 GHz with

Table 18.1 Comparison of multi-band reconfigurable antennas

References	Operating frequency bands (GHz)	Components used for re-configurability	Substrate used	Remarks
Badamchi et al. [2]	9.25, 10.2 and 4.8	Two pin diodes and three capacitors	FR4	Only two diodes are used to switch between three frequencies
Thao et al. [3]	2.4, 3.3, 5.1 and 5.6	Three pin diodes and 4 inductors	FR4	Three diodes are used to switch between 4 frequencies

Fig. 18.7 Frequency reconfigurable monopole antenna with switchable band reconfigurable characteristics from UWB to band-notched UWB to dual-band radiator [7]

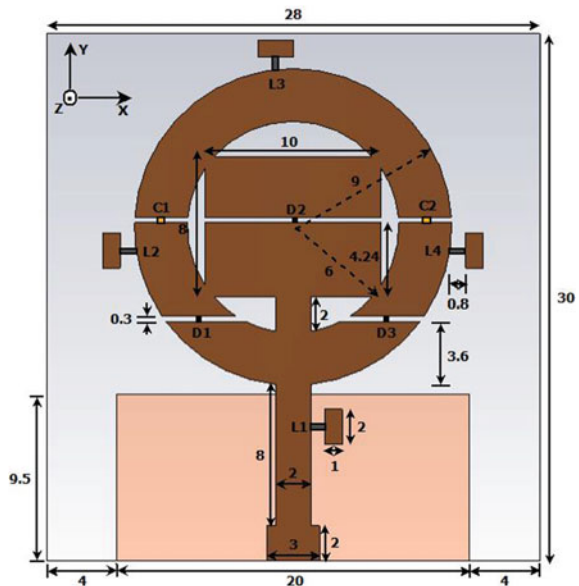


Fig. 18.8 Novel frequency and radiation pattern antenna portable device applications [8]

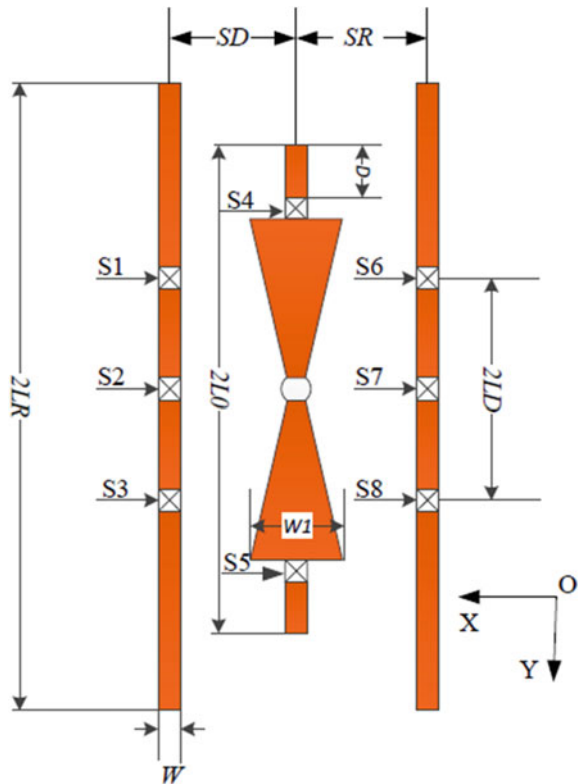


Table 18.2 Comparison of reconfigurable UWB band-notched antennas

References	Operating frequency bands (GHz)	Components used for re-configurability	Substrate used	Band notch frequency	Remarks
Yadav et al. [4]	3.2–13	Two pin diodes and three inductors	RO3003	Between (5–5.35 GHz and 8–8.45 GHz)	Two notch bands are obtained using two pin diodes
Yadav et al. [6]	3.2–13	One pin diode and two inductors	RT/DUROID 5880	Between (4.6 and 6.4 GHz)	One band notch is obtained using one pin diode

the help of two pin diodes, whereas the antenna in [6] is capable to resonate between 3.2–13 GHz and is switchable to only one band notch of 1.8 GHz, i.e., between 4.6 and 6.4 GHz with the help of one pin diode.

18.3 Conclusion

This paper gives a succinct review of some of the most prominent works published in the field of reconfigurable antennas in the past few years. It is purely based on frequency reconfigurable antennas. There can be more reconfigurations such as polarization, radiation pattern and gain which are also under research. These antennas are used in various wireless applications like cognitive radio, satellite communication, medical applications and mobile radio. They are cost effective, have fewer complexities and provide efficient communication.

References

1. Song, C.T.P., Hu, Z.H., Kelly, J., Hall, P.S., Gardner, P.: Wide tunable dual band reconfigurable antenna for future wireless devices. In: Antennas and Propagation Conference. Loughborough, UK. <https://doi.org/10.1109/lapc.2009.5352451> (2009)
2. Badamchi, B., Valizade, A., Rezaei, P., Badamchi, Z.: A reconfigurable square slot antenna with switchable single band, UWB and UWB with band notch function performances. *ACES J.* **29**(5), 383–390 (2014)
3. Thao, H.T.P., Son, T.V., Doai, N.V., Duc, N.T., Yem, V.V.: A novel frequency reconfigurable monopole antenna using PIN diode for WLAN/WiMax applications. In: 2015 International Conference on Communications, Management and Telecommunications. <https://doi.org/10.1109/commantel.2015.7394281> (2015)
4. Yadav, D., Abegaonkar, M.P., Koul, S.K., Tiwari, V., Bhatnagar, D.: A monopole antenna with reconfigurable notched characteristics from WLAN-band notched UWB to ITU-band notched UWB antenna. In: Springer Optical and Wireless Technologies, pp. 647–654. https://doi.org/10.1007/978-981-10-7395-3_72 (2018)
5. Yadav, D., Abegaonkar, M.P., Koul, S.K., Tiwari, V., Bhatnagar, D.: A novel frequency reconfigurable monopole antenna with switchable characteristics between band-notched UWB and WLAN applications. *Prog. Electromagn. Res. C.* **77**, 145–153. <https://doi.org/10.2528/pierc17062203>
6. Yadav, D., Abegaonkar, M.P., Koul, S.K., Tiwari, V., Bhatnagar, D.: Hexagonal monopole antenna with Re-configurability between UWB and band-notched UWB. In: IEEE International Symposium on Antennas and Propagation (2017). <https://doi.org/10.1109/ISANP.2017.8229028>
7. Yadav, D., Abegaonkar, M.P., Koul, S.K., Tiwari, V., Bhatnagar, D.: Frequency reconfigurable monopole antenna with switchable band characteristics from UWB to band-notched UWB to dual-band radiator. In: IEEE Asia-Pacific Microwave Conference. <https://doi.org/10.1109/APMC.2016.7931315> (2016)
8. Li, W., Lei, B., Li, Y.: A novel frequency and radiation pattern reconfigurable antenna for portable device applications. *ACES J.* **30**(12), 1276–1285 (2015)

Chapter 19

Room Temperature Pt-Modified WO₃/p-Si Film Gas Sensor for Detection of Methanol



Anup Dey , Komal Kumari, Abir Jana, Bijoy Goswami, Poushali Nandi, and S. K. Sarkar

Abstract In this proposed work, room temperature fast response and recovery Pt-modified WO₃/p-Si and WO₃ device sensors were fabricated using sol-gel method for the influence of methanol gas concentrations. Two different types of sensors have been fabricated for sensing of methanol concentration in the temperature range of 25–45 °C. TEM, XRD, and FESEM are useful for exploring the structural property and the surface property of Pt-WO₃ and WO₃ thin film. Gas-sensing response is observed at the room temperature range. It was observed that Pt-modified WO₃/p-Si thin film with Al presents higher response as compared to unmodified WO₃/p-Si thin film.

19.1 Introduction

WO₃-based methanol sensor plays an important role in industrial and domestic applications. Therefore, development of methanol sensor is required to detect the concentration of methanol vapor. CH₃OH is a beneficial volatile organic compound (VOC) toxic solution having extensive application in various areas like perfumes,

A. Dey (✉) · K. Kumari · A. Jana · B. Goswami · P. Nandi · S. K. Sarkar
Jadavpur University, E.T.C.E, Kolkata 700032, India
e-mail: anupdey.etce.rs@jadavpuruniversity.in

K. Kumari
e-mail: komalkumari.etce.rs@jadavpuruniversity.in

A. Jana
e-mail: abirjana.etce.rs@jadavpuruniversity.in

B. Goswami
e-mail: bijoy.ete@aec.ac.in

P. Nandi
e-mail: poushalinandi95@gmail.com

S. K. Sarkar
e-mail: sksarkar.etce@jadavpuruniversity.in

© The Editor(s) (if applicable) and The Author(s), under exclusive license to Springer Nature Singapore Pte Ltd. 2021

Y.-D. Zhang et al. (eds.), *Smart Trends in Computing and Communications: Proceedings of SmartCom 2020*, Smart Innovation, Systems and Technologies 182,
https://doi.org/10.1007/978-981-15-5224-3_19

wine industry, detection of colors, etc. Gas sensor is mainly used to detect the various toxic, flammable, and VOC gases like acetone, ethanol, butanol, methanol, etc.

Among several metal oxide semiconductors (TiO_2 , SnO_2 , CuO , ZnO , etc.), WO_3 is highly recommended as a gas-sensing materials because of its high selectivity and sensitivity toward the volatile organic compound gases [1]. It is also observed that WO_3 films have likely optical and electrical properties toward different gases [2]. Various methods were used to synthesis WO_3 film [3]. In recent years, metal oxide thin film has been used as the suitable materials for enhancing gases like CH_4 , NO_x , CO_2 , and H_2S [4, 5]. The sensing properties of tin oxide were produced by sol-gel techniques toward alcohol vapor have proposed by Mishra et al. [4] and the electrical response of mixed metal-based thin film sensor to CH_4 gas has been depicted by Dey et al. [5]. Roy et al. [6] have described $\text{C}_2\text{H}_5\text{OH}$ and CH_3OH properties of WO_3 and ZnO films deposited via spin coating method. The response features of SnO_2 films are placed by thermal process toward different vapors ($\text{C}_2\text{H}_5\text{OH}$, $\text{C}_3\text{H}_6\text{O}$, CH_3OH , $\text{C}_3\text{H}_8\text{O}$, and CH_3COOH) have proposed by Gong et al. [7]. WO_3 thin film-based methanol sensor is not much reported earlier. Main intention of our present work is to fabricate Pt-WO_3 and WO_3 device sensor for exposure of methanol vapors. Sensing features of metal oxide-based film are influenced by noble metal. Many noble metals depositions like Pt, Pd, Al, and Au are used for not only increasing the response magnitude but also decreasing the operating temperature of WO_3 thin films [8–10].

In this paper, two different sensors have been fabricated on P-Si substrate using dip-coating method to detect methanol vapor at room temperature range from 25 to 45 °C. The sensing characteristics of different sensors are investigated at the different concentrations of methanol vapor. It has been observed, Pt-WO_3 sensor with Al contact ensures better response compare to the unmodified tungsten thin film sensor.

19.2 Preparation of Thin Film

WO_3 films were fabricated by choosing of sol-gel process using WCl_6 chemical compound [10]. Initially, isopropanol is mixed with WCl_6 at a ratio of 100 ml/5 g. The solutions are kept in dry for 48 h. Dip-coating method is obtained for dropping the prepared sol on the substrate. Then, the sample is kept in the oven for next 10 min at 120 °C and next the sample was calcined at 500 °C for 2 h to obtain crystalline film less than 100 nm. The detailed structures of sensors are depicted on Fig. 19.1. The surface structure (FESEM) image (WO_3) films are depicted in Fig. 19.2.

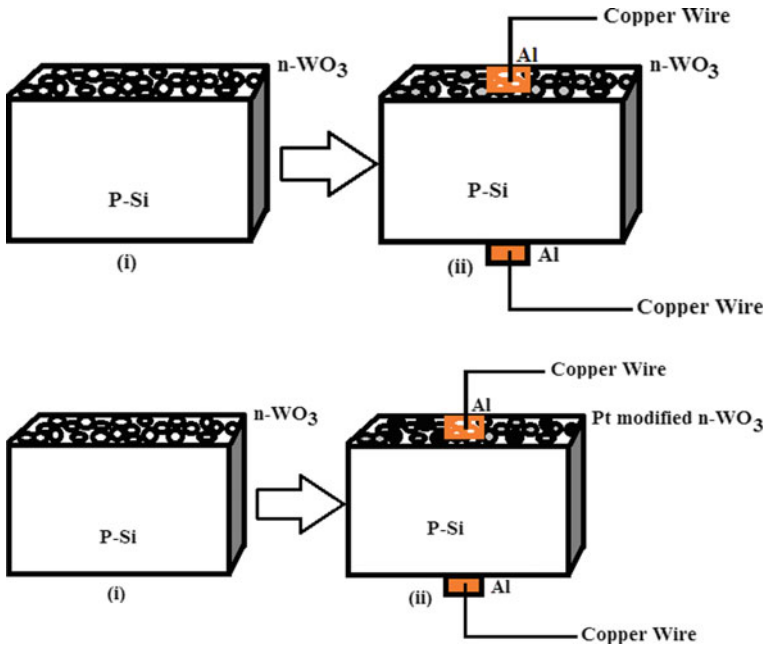
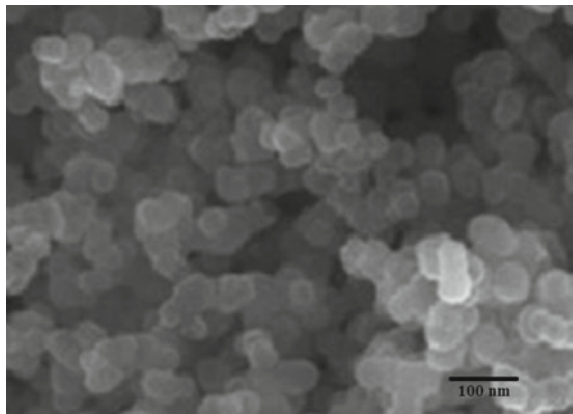


Fig. 19.1 a Structures of unmodified WO₃ thin film sensors with Al contacts, b Structures of Pt-modified WO₃ thin film sensors with Al contacts

Fig. 19.2 FESEM image of Pt-WO₃ sensor



19.3 Results and Discussions

Figure 19.2 FESEM (Model:S-4800) investigation showed that Pt-WO₃ thin film is dropped on the surface of the substrate. Average grain sizes are small whose dimension around 42–68 nm. For analysis of TEM image (model:JSM-6360) Pt-WO₃ based film by consuming copper grid. Figure 19.3 shows low-magnification TEM image which consists of large number of crystalline particles having distribution size between 45 and 70 nm.

Response of the sensor is calculated by,

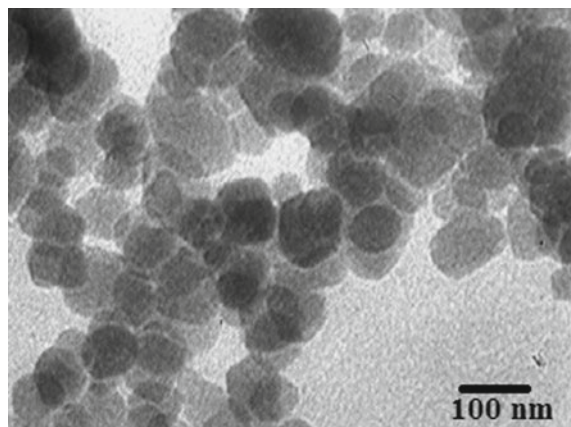
I_a and I_g represent current for gas concentration in air and current for sample sensor at a given concentration of methanol vapor. The whole measurement details are shown in Fig. 19.4

XRD peaks of WO₃ sensor are depicted in Fig. 19.5. The peaks observed at 2-theta: 26.8°, 31.1°, 43.8°, 58.1°, 59.3°, 80.4°, 94.2°, and 97.2° correspond to (020), (101), (210), (022), (202), (221), (401), and (302) plane of WO₃, respectively, and which checking the monoclinic phase (JCPDS no. 83-0961).

For gas sensing measurement of the prepared sensors, CH₃OH is taken as a primary gas and N₂ gas is taken as a carrier gas. Developed sensor is placed in sensing chamber under normal air-free condition. Gas mixture chamber is monitored via MFM and MFC meter, respectively. Multimeter connection is taken for determining the current and resistance of the device. The whole system is presented in Fig. 19.4.

Figure 19.6 showed the response versus operating temperature plot of Pt-WO₃ and WO₃ thin film device. The sensing characteristic of different devices has considered at their room temperatures. The response of Pt-WO₃ with Al contacts reaches the highest value at the working temperature of 35 °C and after that, enhancing the temperature, sensor response decreases. Pt-noble metal is used for enhancing the response characteristics of the prepared sensors.

Fig. 19.3 TEM image of Pt-WO₃ sensor



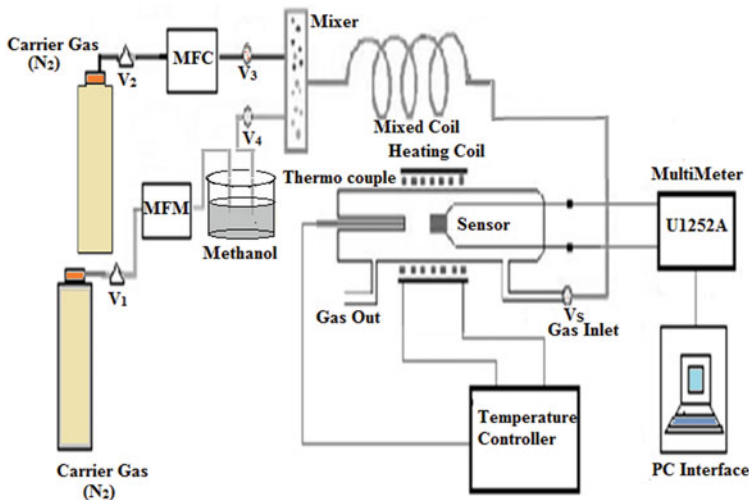


Fig. 19.4 Gas sensing chamber set up diagram

Fig. 19.5 XRD peaks of WO₃ and Pt-WO₃ device

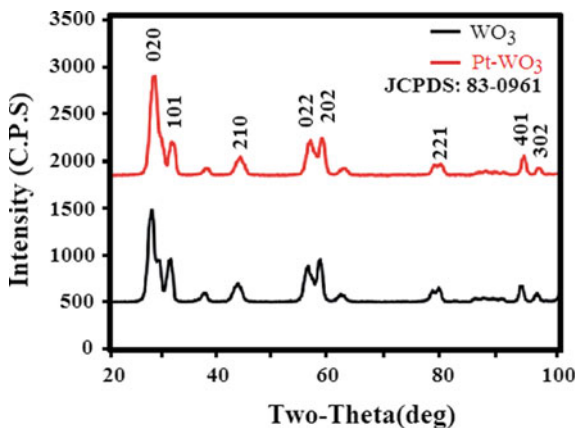


Figure 19.7 shows the two different sensors response magnitude versus different concentrations of methanol vapors curve. The sensitivity of Pt-WO₃ proposed device with Al is significantly higher compared to unmodified thin film WO₃/p-Si sensors.

Sensor response versus time plot of Pt-modified WO₃/p-Si and unmodified WO₃/p-Si sensors is depicted in Fig. 19.8. From curve, it is shown that both response and recovery time have improved because of the modification of noble metal Pt as compared to the modification of sensing material by the WO₃/p-Si thin film sensors. The T_{res} and T_{rec} of thin film proposed devices purely depend on deposition of the metals and the interactions between chemisorbed oxygen species of target gas molecules.

Fig. 19.6 Sensitivity versus temperature plot (0.01% methanol)

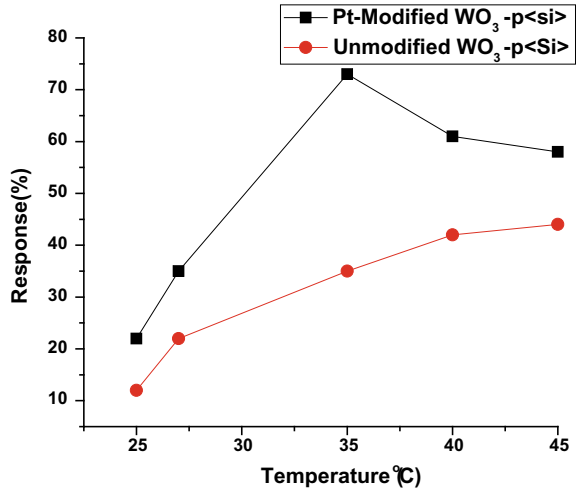
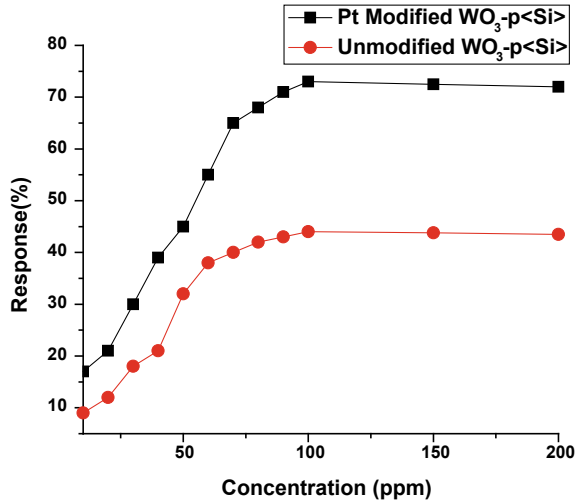


Fig. 19.7 Sensitivity versus different concentrations of methanol vapors



Stability plot of Pt-modified $WO_3/p-Si$ and unmodified $WO_3/p-Si$ heterojunction thin film gas sensors is depicted in Fig. 19.9. It is shown that prepared Pt-modified $WO_3/p-Si$ thin film device produced much better stable current compared to the unmodified $WO_3/p-Si$ thin film sensors for detection of room temperature methanol concentration. The stability is measured up to 15 days at room temperature 35 °C in presence of methanol gas concentrations.

Fig. 19.8 Sensor response versus time plot of Pt-/WO₃/p-Si and WO₃/p-Si sensors with various target gases (room temperature of 35 °C)

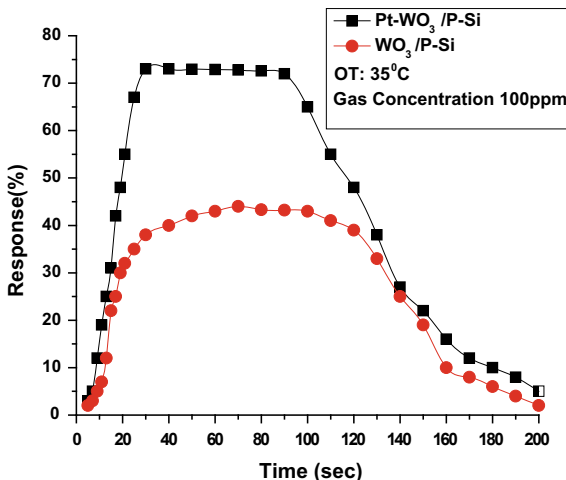
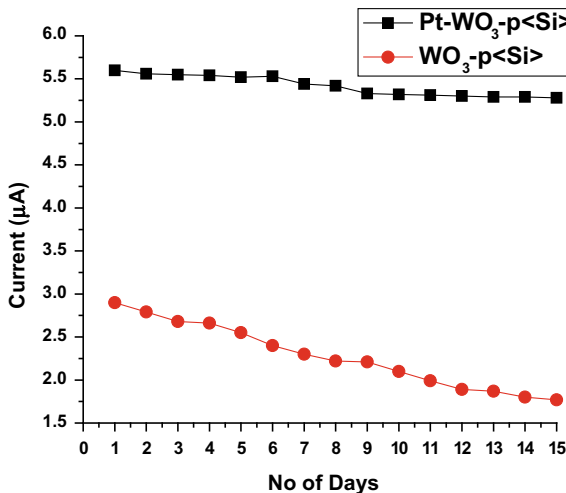
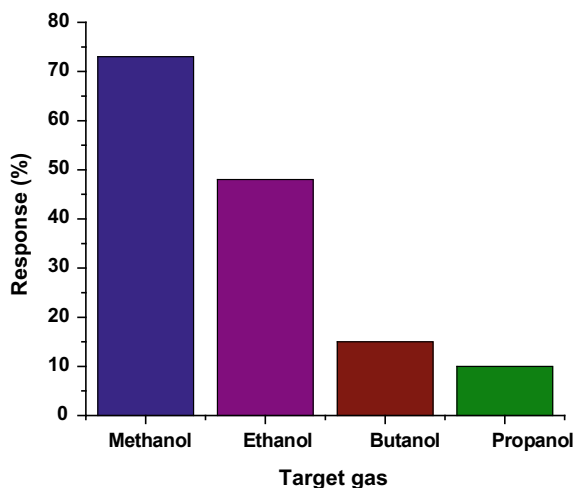


Fig. 19.9 Stability plot of Pt/WO₃/p-Si thin film sensors at room temperature 35 °C



Selectivity analysis is important parameter which needs to be detected under various gases under same operating and same gas concentrations. Figure 19.10 represents the selectivity plot which tested four different gases like methanol, ethanol, butanol, and propanol. It is observed that prepared Pt/WO₃/p-Si sensor takes maximum selectivity associated with others gases.

Fig. 19.10 Selectivity plot of Pt/WO₃/p-Si sensors with different target gases (room temperature of 35 °C)



19.4 Conclusions

In the present work, two different types of sensors Pt-WO₃ and unmodified WO₃ have been developed and fabricated for detecting methanol concentrations. WCl₆ has utilized for the preparation of tungsten thin film. The gas sensing behaviors of tungsten film have been observed in the room temperature ranges from 25 to 45 °C. It is observed that Pt-modified WO₃ thin film with Al contact has better response than the unmodified thin film sensor. In addition, Pt-modified WO₃/p-Si thin film sensor has better response and recovery time as compare to the unmodified WO₃/p-Si thin film sensor. Therefore, Pt-modified WO₃ film-modified Al contact is highly appropriate for the detection of room temperature CH₃OH concentration. The limitation of the proposed sensor is to investigate an indoor air quality under low gas concentration flow.

Acknowledgements The fabrication part is done in ‘IC Design and Fabrication Centre,’ whereas testing is performed at Nanotechnology laboratory, Jadavpur University. A. Dey thankfully acknowledge by CSIR (Ack.No.-143170/2K15/1, fileno: 09/096(0883)/2017-EMR-I) for financial support.

References

1. Khadayate, R.S., Waghulde, R.B., Wankhede, M.G., Salt, J.V., Patil, P.P.: Ethanol vapors sensing properties of screen printed WO₃ thick films. *Bull. Mater. Sci.* **30**(2), 129–133 (2007)
2. Ippolito, S.J., Kandasamy, S., Kalantar-Zadeh, K., Wlodarski, W.: Layered SAW hydrogen sensor with modified tungsten trioxide selective layer. *Sens. Actuators B* **108**(1), 553–557 (2005)

3. Ippolito, S.J., Kandasamy, S., Kalantarzadeh, K., Wlodarski, W.: Hydrogen sensing characteristics of WO₃ thin film conductometric activated by Pt and Au catalysts. *Sens. Actuator B* **108**(4), 154–158 (2005)
4. Mishra, S., Ghanshyam, C., Ram, N., Singh, S.: Alcohol sensing of tin oxide thin film prepared by Sol-Gel process. *Bull. Mater. Sci.* **25**(3), 231–234 (2002)
5. Anup, D., Bikram B., Subir Kumar, S.: Fabrication of Au-modified mixed metal oxide methane gas sensor and experimentation for better performance. *Sens. Lett.* **17**(2), 250–255 (2019)
6. Subhashis, R., Anup, D., Bikram, B., Subir Kumar, S.: Investigation of Pt and Pd modified WO₃ and ZnO based thin film sensors for ethanol sensing. *J. Mater. Eng. Perform.* **27**(6), 2635–2642 (2018)
7. Gong, H., Wang, Y.J., Teo, S.C., Huang, L.: Interaction between thin-film Tin oxide gas sensor and five organic vapors. *Sens. Actuators B* **54**(3), 232–235 (1999)
8. Anup, D., Subhashis, R., Subir Kumar, S.: Synthesis, fabrication and characterization of ZnO based thin films prepared by Sol-Gel process and H₂ gas sensing performance. *J. Mater. Eng. Perform.* **27**(6), 2701–2707 (2018)
9. Higuchi, T., Nakagomi, S., Kokubun, Y.: Field effect hydrogen sensor device with simple structure based on GaN. *Sens. Actuators B* **140**(1), 79–85 (2009)
10. Anup, D., Bijoy, K., Subir Kumar, S.: Sol-gel grown Pd modified WO₃ thin film based methanol sensor and the effect of annealing temperatures. *Microsyst. Technol.* **23**(9), 4195–4201 (2017)

Chapter 20

Graph Degree Linkage Clustering for Identify Student's Performance on *Kompetisi Sains Madrasah* in Indonesia



Ahmad Hanif Asyhar , A. Umar , Dian Candra Rini Novitasari ,
Kusaeri , Ahmad Fauzi , Nurissaidah Ulinuha , Dwi Rolliawati ,
Noor Wahyudi , Ahmad Yusuf , Ali Mustofa , and Zakiyatul Ulya

Abstract Graph degree linkage (GDL) algorithm is a development of agglomerative clustering and graph. The clustering algorithm can be applied to various problems, such as student performance. *Kompetisi Sains Madrasah* (KSM) is one of the competitions by integrating science and Islam held in Indonesia. The final score of the competition will be used in this study to identify the students' performance who participate in the competition. The main goal of the study is obtaining the results of the participant's performance clusters based on the final score of KSM and obtain the information about the quality of students in schools that are participating in the competition. Based on the research, we obtain the best K -neighborhood value of three clusters is equal to 25. The research obtains the silhouette coefficient value for clustering evaluation. They are 0.5104, 0.4838, 0.6853, 0.5943, 0.6605, 0.8037, 0.6455, 0.6723, 0.6996, 0.5767, and 0.6695 in mathematics, natural science, mathematics, natural science, social science, mathematics, biology, physic, chemistry, economics, and geography subjects. The identification of school student performance in each subject tested shows that State Islamic School student performance in KSM has the best performance in elementary and middle-high grade. In senior grade, the best students' performance in KSM is from Private Islamic School.

A. H. Asyhar (✉) · D. C. R. Novitasari · Kusaeri · A. Fauzi · N. Ulinuha · D. Rolliawati ·
N. Wahyudi · A. Yusuf · A. Mustofa · Z. Ulya
UIN Sunan Ampel Surabaya, Ahmad Yani 117, Surabaya, Indonesia
e-mail: hanif@uinsby.ac.id

A. Umar
Kementerian Agama RI, Lapangan Banteng 3-4, Jakarta, Indonesia

© The Editor(s) (if applicable) and The Author(s), under exclusive license
to Springer Nature Singapore Pte Ltd. 2021

Y.-D. Zhang et al. (eds.), *Smart Trends in Computing and Communications: Proceedings
of SmartCom 2020*, Smart Innovation, Systems and Technologies 182,
https://doi.org/10.1007/978-981-15-5224-3_20

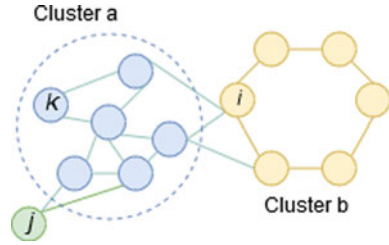
20.1 Introduction

Clustering is one of the analysis methods in data mining to grouping data sets based on similar characteristics of data. Two common techniques used in clustering algorithms are agglomerative hierarchical and partial clusters [1]. Agglomerative clustering also known as linkage method has several types, they are complete linkage, average linkage, etc. [2]. Agglomerative clustering algorithm has some disadvantages to solving high-dimensional space clustering problem because the neighborhood of the characteristics of the data is calculated based on pairwise distances between the data [3]. Therefore, Zhang et al. [4] proposes an agglomerative clustering algorithm based on the graph and it is called as graph degree linkage (GDL) algorithm. The algorithm proposed based on several studies on graph data representations that have been developed widely in various machine learning topics [5–9], but it rarely applied in agglomerative clustering. Furthermore, Zhang et al. [4] made improvements from [10–12] who did research before and tried to use agglomerative clustering on graph data representations. The algorithm has three main advantages. First, the algorithm has good performance even though it was applied to noisy and multiscale data. Second, the algorithm is a simple algorithm to implement. Then, last, the calculation time of the algorithm is very fast. In the algorithm, pairwise distances between sample data are used to construct K -nearest neighbors (K -NN) graphs, where indegree and outdegree become the similar characteristic of two clusters [4].

Clustering can be applied to solve various types of problems, such as data analysis, pattern recognition, image processing, market research, and student performance [13, 14]. The application of clustering algorithms to student performance problems is used to monitor the quality of education in a country [15]. The results of the monitoring can be used as evaluations to further improve the learning process [16], especially for schools and educational institutions. Student performance evaluations between schools are not the same as others, so the wide evaluation is needed. One of the methods to determine students' performance is school competition. One of the competitions held in Indonesia to appraise student performance is *Kompetisi Sains Madrasah* (KSM). The competition measures students' knowledge at various grades by integrating science and Islam. The final score of the competition will be used in this study to identify the students' performance who participate in the competition.

The main goal of the study is to obtain the results of the participant's performance clusters based on the final score of KSM and obtain the information about the quality of students in schools that are participating in the competition. In addition, the result of clustering the students' performance can be used as an evaluation of the committee and it can be used to plan for future activities for the better.

Fig. 20.1 Illustration of indegree and outdegree of graph degree linkage [4]



20.2 Graph Degree Linkage

20.2.1 Algorithm Overview

Graph degree linkage (GDL) algorithm is part of the agglomerative clustering, and the algorithm starts by initializing several small clusters. Then, in every two clusters which have the similarity, they are chosen to be merged. To determine the neighborhood among data, it was calculated based on the indegree and outdegree of the vertex using K -NN graphs. The small clusters initialization are simply constructed as a weakly connected component of the K^0 -NN graph, where the neighborhood size of K^0 is small [4] (Fig. 20.1).

20.2.2 Neighborhood Graph

In graph theory, a vertex called adjacent to the vertex v in a graph if the vertex is connected to v with an edge. The neighborhood of vertex v in graph G is subgraphs of G consist of vertices adjacent to v with each edge connected to v [17].

Given a set of data $X = \{x_1, x_2, x_3, \dots, x_n\}$ and directed graph $G = (V, E)$, where V is a set of vertices that correspond to the sample in X , and E is a set of vertices that connecting vertices. In the algorithm, the graph is connected with adjacency weight matrix $W = [w_{ij}]$, where w_{ij} is the weight of the edge at the vertex i to vertex j . In the problem of high-dimensional space, K -NN graphs are used to determine the neighborhood, where the weight of the edge is defined as follows [4].

$$w_{ij} = \begin{cases} \exp\left(\frac{-\text{distance}(i,j)^2}{\frac{a}{nk} \left[\sum_i^n \sum_{j \in N_i^K} \text{distance}(i,j)^2 \right]}\right) & \text{if } x_j \in N_i^K \\ 0 & \text{otherwise} \end{cases} \quad (20.1)$$

where K and a are the parameters that free to be set, with $\text{distance}(i, j)$ are distances between x_i and x_j , and N_i^K is a set of K -NN from x_i .

20.2.3 Adjacency Measure

The important element of the agglomerative clustering algorithm is the adjacency measure between two clusters. In [4], the adjacency measure is calculated based on indegree and outdegree of the graph. Indegree measures the density near the sample i and outdegree characterizes similarity of K -NN from vertex i to cluster C . Average indegree is defined in Eq. (20.2) and average outdegree is defined in Eq. (20.3), where $|C|$ is the cardinality of the set C .

$$\text{deg}_i^-(C) = \frac{1}{|C|} \sum_{j \in C} w_{ij} \quad (20.2)$$

$$\text{deg}_i^+(C) = \frac{1}{|C|} \sum_{j \in C} w_{ij} \quad (20.3)$$

Furthermore, adjacency is defined as the product of the average indegree and average outdegree in Eq. (20.4). So, the adjacency of cluster C_b to cluster C_a by summing all vertices in C_b .

$$\mathcal{A}_{i \rightarrow C} = \text{deg}_i^-(C) \text{deg}_i^+(C) \quad (20.4)$$

$$\mathcal{A}_{C_b \rightarrow C_a} = \sum_{i \in C_b} \mathcal{A}_{i \rightarrow C_a} = \sum_{i \in C_b} \text{deg}_i^-(C_a) \text{deg}_i^+(C_a) \quad (20.5)$$

$$\mathcal{A}_{C_a, C_b} = \mathcal{A}_{C_b \rightarrow C_a} + \mathcal{A}_{C_a \rightarrow C_b} \quad (20.6)$$

The following is an algorithm of Graph Degree Linkage (GDL).

1. Initialize a set of n small cluster data $X = \{x_1, x_2, x_3, \dots, x_n\}$ with n_T as the target number of clusters
2. Build the K -NN graph by initializing the number of clusters and K -neighborhood value, and get the weighted adjacency matrix W . A set of initial clusters define as $V^c = \{C_1, \dots, C_n\}$, where n_c is the number of clusters
3. Search two clusters C_a and C_b to be merged if has a similar character such $\{C_a, C_b\} = \text{argmax}_{C_a, C_b \in V^c} \mathcal{A}_{C_a, C_b}$. Then, update V^c and n_c
4. Do step 3 repeatedly until $n_c \leq n_T$.

20.3 Clustering Evaluation: Silhouette

Silhouette is one method to evaluate the system of clustering. The value of the silhouette coefficient (sc) can show the quality of a cluster system based on how the algorithm placed the objects on a cluster. The method is used to validate data, a single cluster, and the whole cluster [18]. In [19], the calculation of sc value starts

by calculating the average distance of an object i with each object in one cluster and calculates the average distance from object i with all objects in other clusters to obtain the smallest value. Then, calculate $s(i)$ value of each data, and the average of the result $s(i)$ value is the value of sc . The results of the calculation of sc value are in the range -1 to 1 . Cluster results are called as good if the value of sc is positive. If $s(i) = 1$ means that the object i is already in the right cluster. If $s(i) = 0$ means that the object i is between two clusters. However, If the value of $s(i) = -1$ means that the result of the cluster structure is overlapping. The criteria of sc value by Kaufman table [20].

20.4 Result and Discussion

The dataset processed in this study is the final score of KSM. The competition participated by students of public schools, Islamic schools, private schools, and state schools in various grade, they are Madrasah Ibtidaiyah (MI) or Islamic Elementary School, Madrasah Tsanawiyah (MTs) or Islamic Junior High School, and Madrasah Aliyah (MA) or Islamic Senior High School. Based on 540 data, it consists of scoring on multiple-choice questions and exploration of 11 subjects tested.

Based on the proposed algorithm, the first step in clustering is to determine the number of clusters and the value of K -neighborhood to build the K -NN Graph. In this study, the number of clusters used was three clusters, where each cluster represented the knowledge of the students who participated in the KSM. Clusters are identified as excellent, good, and fair clusters. Then, we used various K -neighborhood values of 10, 15, 20, and 25. It aims to find the best cluster that can represent the data. The results of each clustering experiment are evaluated using the silhouette shown in Table 20.1.

Based on the results of the evaluation of the clustering experiment, the best clustering system is using the value of K -neighborhood equal to 25. Illustration of the distribution of clustering results is shown in Fig. 20.2.

Besides obtaining the results of KSM participant's performance clustering, we identified the schools of each participant. Based on the information from the school and the results of the clustering, we identify the school students' performance is an excellent, good, and fair cluster in each subject tested in the competition.

Based on the graphs of elementary school student performance in Fig. 20.3, in natural science subjects, State Islamic Elementary School has the best student performance in the excellent cluster, then followed by private Islamic Elementary School and Private Elementary School. In mathematics subjects, private Islamic Elementary School is superior in student's performance. However, the number of students from private Islamic Elementary School is not few in the fair cluster.

Based on Fig. 20.4, it represents student performance at the middle grade, and the average number of State Islamic Junior High School student at Mathematics and Social Sciences is in the "Good" cluster, but in natural science subjects, they are in "Excellent" cluster. In participant's performance of State Islamic Junior High

Table 20.1 Results of clustering evaluation using Silhouette

Education grade	Subjects	Number of clusters = 3											
		K = 10			K = 15			K = 20			K = 25		
		Mean	Varian	Mean	Varian	Mean	Varian	Mean	Varian	Mean	Varian		
MI	Mathematic	0.4257	0.2343	0.2396	0.2980	0.5104	0.2702	0.5104	0.2702	0.5104	0.2702		
	Natural Science	0.5957	0.0617	0.4838	0.0571	0.4838	0.0571	0.4838	0.0571	0.4838	0.0571		
	Mathematic	0.2972	0.2836	0.5926	0.1010	0.5926	0.1010	0.6853	0.1010	0.6853	0.0735		
MTs	Natural Science	0.4366	0.1514	0.4366	0.1514	0.6057	0.1034	0.5943	0.1071	0.5943	0.1071		
	Social Science	0.6402	0.0721	0.6402	0.0721	0.6402	0.0721	0.6605	0.0445	0.6605	0.0445		
	Mathematic	0.6502	0.0503	0.5308	0.1936	0.8037	0.0359	0.8037	0.0359	0.8037	0.0359		
MA	Biology	0.4386	0.2668	0.6400	0.0679	0.5414	0.1574	0.6455	0.1476	0.6455	0.1476		
	Physic	0.5667	0.1373	0.6595	0.0569	0.6595	0.0569	0.6723	0.1084	0.6723	0.1084		
	Chemistry	0.5899	0.1811	0.6144	0.1914	0.6313	0.0719	0.6996	0.0639	0.6996	0.0639		
	Economic	0.6203	0.1299	0.6419	0.0934	0.5767	0.1026	0.5767	0.1026	0.5767	0.1026		
	Geography	0.5769	0.1443	0.6146	0.0914	0.6146	0.0914	0.6695	0.0722	0.6695	0.0722		

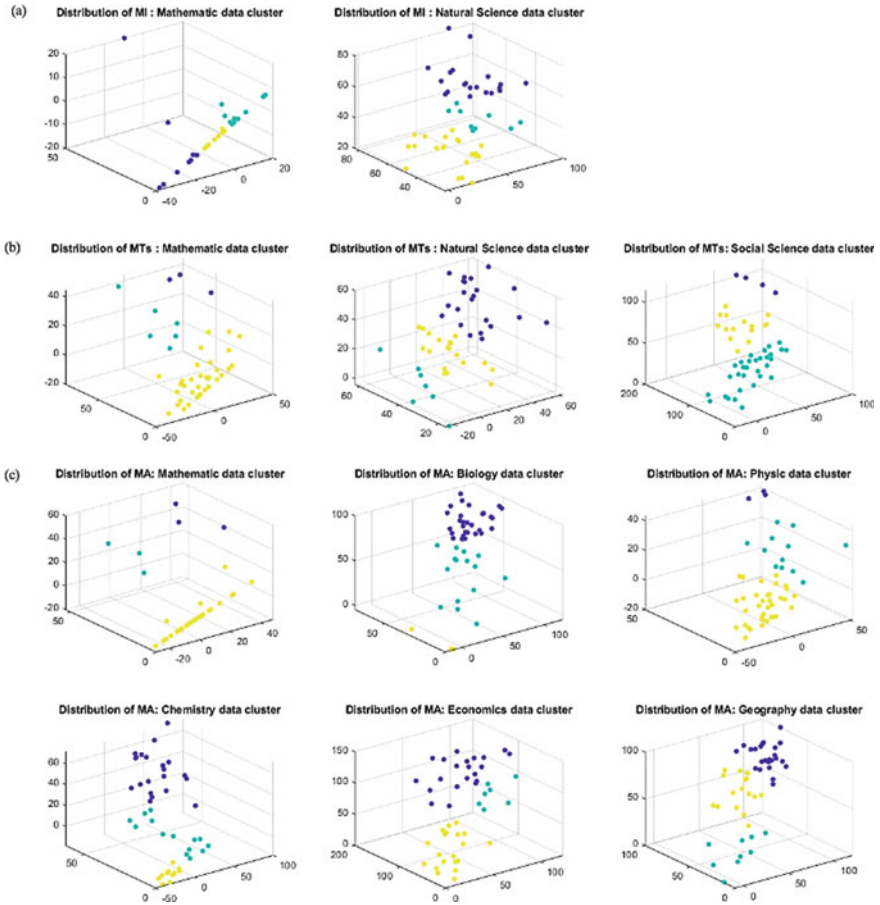


Fig. 20.2 a Illustration of the distribution of KSM participant performance in Madrasah Ibtidaiyah; b illustration of the distribution of KSM participant performance in Madrasah Tsanawiyah; and c illustration of the distribution of KSM participant performance in Madrasah Aliyah

School, the most participants are clustered in “Good” cluster at Mathematics and Social Science subjects, the Natural Science subjects are clustered in the “Fair” cluster (Fig. 20.5).

In the identification of Senior High School student’s performance, based on all subjects tested in KSM (except mathematics), State Islamic Senior High School student performance is superior to the other schools. At mathematics subject, the best student performance is Private Senior High School students. Private Islamic Senior High School student’s performance is clustered in “Good” cluster at all subjects tested. Meanwhile, State Senior High School student performance cannot be identified as well because there are not many students who netted in the national competition.

Elementary Student's Performance

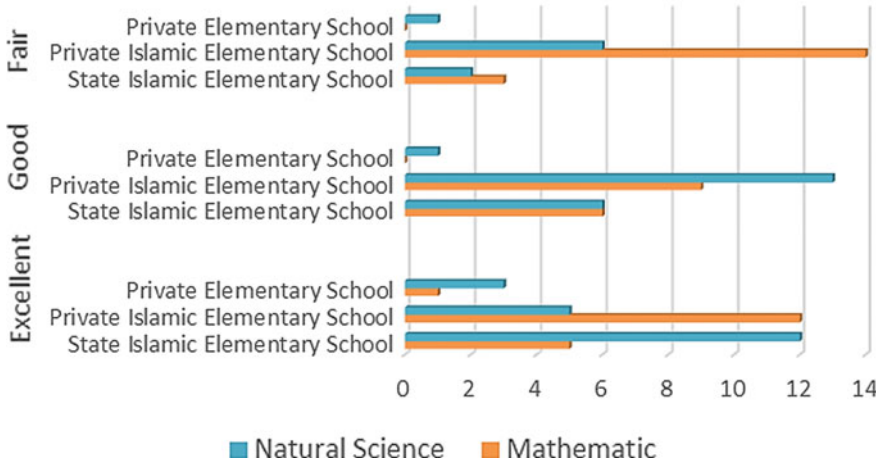


Fig. 20.3 Elementary School student's performance graph

Junior High School Student's Performance

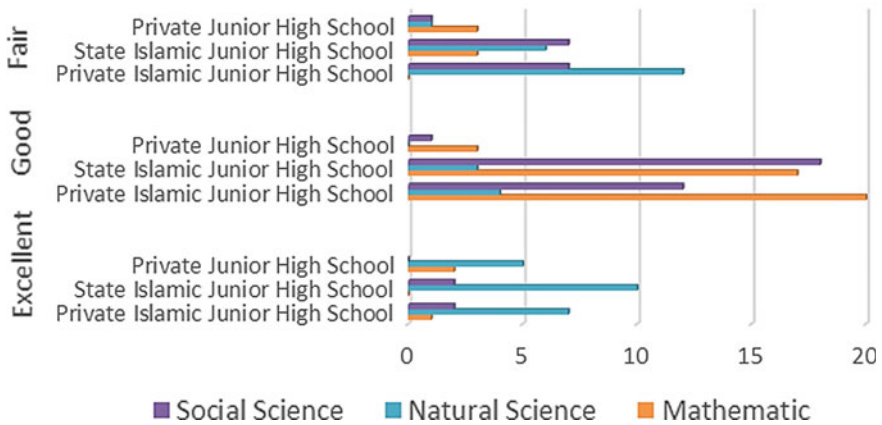


Fig. 20.4 Junior High School student's performance graph

20.5 Conclusion

The identification of students' performance who participates in KSM at the national stage can be used to monitor and evaluate the quality of education in Indonesia. The result of study obtained the best *K*-neighborhood value of three clusters which is equal to 25 with silhouette coefficient values that are 0.5104, 0.4838, 0.6853, 0.5943,

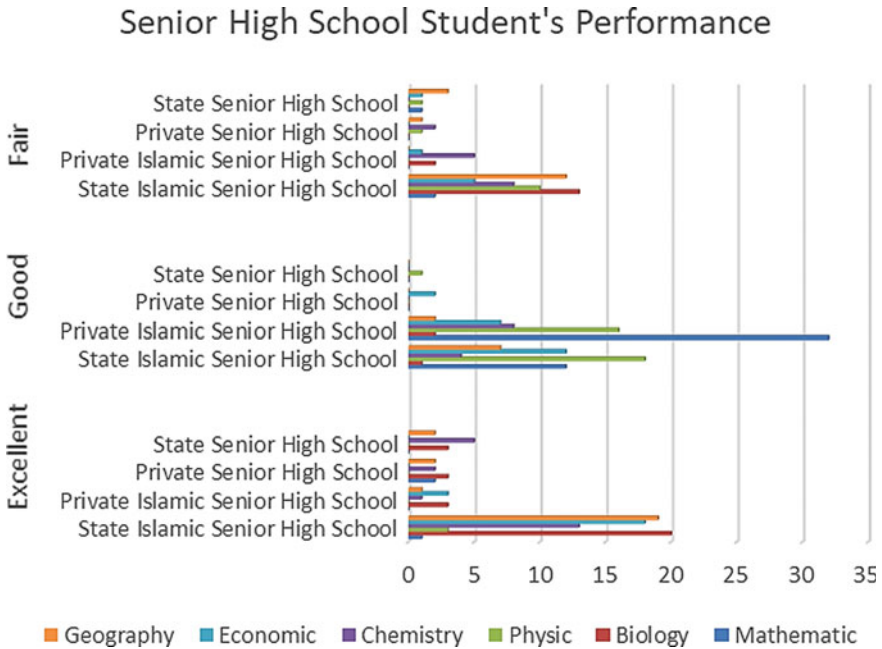


Fig. 20.5 Senior High School student’s performance graph

0.6605, 0.8037, 0.6455, 0.6723, 0.6996, 0.5767, and 0.6695 in all subjects. Based on the clustering result, the student performance generally clustered in excellent cluster in elementary and middle grade is from State Islamic School. In senior high school grades, the student’s performance that clustered in “excellent” cluster generally is from Private Islamic School.

References

1. Omran, M.G.H., Engelbrecht, A.P., Salman, A.: An overview of clustering methods. *Intell. Data Anal.* **11**(6), 583–605 (2007)
2. Alfiani, A.P., Wulandari, F.A.: Mapping student’s performance based on data mining approach (a case study). *Agric. Agric. Sci. Procedia.* **3**, 173–177 (2015)
3. Hastie, T., Tibshirani, R., Friedman, J., Franklin, J.: The elements of statistical learning: data mining, inference and prediction. *Math. Intell.* **27**(2), 83–85 (2005)
4. Zhang, W., Wang, X., Zhao, D., Tang, X.: Graph degree linkage: agglomerative clustering on a directed graph. In: *European Conference on Computer Vision*, pp. 428–441. Springer (2012)
5. Shi, J., Malik, J.: Normalized cuts and image segmentation. *Dep. Pap.* 107 (2000)
6. Ng, A.Y., Jordan, M.I., Weiss, Y.: On spectral clustering: analysis and an algorithm. In: *Advances in Neural Information Processing Systems*, pp. 849–856 (2002)
7. Belkin, M., Niyogi, P.: Laplacian eigenmaps for dimensionality reduction and data representation. *Neural Comput.* **15**(6), 1373–1396 (2003)

8. Grady, L., Schwartz, E.L.: Isoperimetric graph partitioning for image segmentation. *IEEE Trans. Pattern Anal. Mach. Intell.* **28**(3), 469–475 (2006)
9. Zhang, W., Lin, Z., Tang, X.: Learning semi-Riemannian metrics for semisupervised feature extraction. *IEEE Trans. Knowl. Data Eng.* **23**(4), 600–611 (2010)
10. Karypis, G., Han, E.-H.S., Kumar, V.: Chameleon: hierarchical clustering using dynamic modeling. *Computer (Long. Beach. Calif)* **8**, 68–75 (1999)
11. Zhao, D., Tang, X.: Cyclizing clusters via zeta function of a graph. In: *Advances in Neural Information Processing Systems*, pp. 1953–1960 (2009)
12. Felzenszwalb, P.F., Huttenlocher, D.P.: Efficient graph-based image segmentation. *Int. J. Comput. Vis.* **59**(2), 167–181 (2004)
13. Nagesh, A.S., Satyamurty, C.V.S.: Application of clustering algorithm for analysis of student academic performance. *Int. J. Comput. Sci. Eng.* **6**(January), 381–384 (2018)
14. Nagesh, A.S., Satyamurty, C.V.S., Akhila, K.: Predicting student performance using KNN classification in bigdata environment. *CVR J. Sci. Technol.* **13**, 83–87 (2017)
15. Shahiri, A.M., Husain, W.: A review on predicting student's performance using data mining techniques. *Procedia Comput. Sci.* **72**, 414–422 (2015)
16. Jayabal, Y., Ramanathan, C.: Clustering students based on student's performance-a partial least squares path modeling (PLS-PM) study. In: *International Workshop on Machine Learning and Data Mining in Pattern Recognition*, pp. 393–407. Springer (2014)
17. Fronček, D.: Locally linear graphs. *Math. Slovaca.* **39**(1), 3–6 (1989)
18. Prasetyo, E.: *Data Mining Mengolah Data Menjadi Informasi Menggunakan MATLAB*. Andi, Yogyakarta
19. Anggara, M., Sujaini, H., Nasution, H.: Pemilihan distance measure Pada K-Means clustering Untuk Pengelompokkan member di Alvaro fitness. *J. Sist. dan Teknol. Inf.* **4**(1), 186–191 (2016)
20. Swindiarito, V.T.P., Sarno, R., Novitasari, D.C.R.: Integration of Fuzzy C-means clustering and TOPSIS (FCM-TOPSIS) with Silhouette analysis for multicriteria parameter data. In: *2018 International Seminar on Application for Technology of Information and Communication*, pp. 463–468. IEEE (2018)

Chapter 21

Stepwise Iterative Maximum Likelihood Clustering Based on *Kompetisi Sains Madrasah*' Scores for Identifying Quality of Junior High School Grading Distribution



Kusaeri , Nanik Puji Hastuti , Ali Musthofa , Ahmad Fauzi ,
Ahmad Hanif Asyhar , Dian Candra Rini Novitasari , Dwi Rolliawati ,
Zakiyatul Ulya , Ahmad Yusuf , Nurissaidah Ulinnuha ,
and Noor Wahyudi 

Abstract Kompetisi Sains Madrasah (KSM) is a science competition organized by the Ministry of Religious Affairs Indonesia. KSM scores can help to determine the quality distribution of students based on KSM data. Clustering is a method that can group data based on the similarity of data. One method of student clustering that has never been done is Stepwise Iterative Maximum Likelihood. SIML does clustering based on the average value and standard deviation of each cluster. SIML grouping is done several times by creating several different clusters. The best grouping experimental results are in the number of clusters 3. Cluster data is divided into 3 groups consisting of very good, good, and fair students. Silhouette values indicate the best grouping using 3 clusters. The silhouette value is 0.423745 for natural sciences subject data. Social sciences data has a silhouette value of 0.415654, and a silhouette value of 0.487071 for mathematics subjects. Three silhouette values are the best silhouette values when compared to other experiments.

21.1 Introduction

Education has a role in the progress of a nation. A country experiences underdevelopment in various aspects if a country does not pay attention to the development of education. Some developed countries make education as an investment to avoid reducing the quality of society. As a country in the process of becoming a developed

Kusaeri (✉) · A. Musthofa · A. Fauzi · A. H. Asyhar · D. C. R. Novitasari · D. Rolliawati · Z. Ulya · A. Yusuf · N. Ulinnuha · N. Wahyudi
UIN Sunan Ampel Surabaya, Ahmad Yani 117, Surabaya, Indonesia
e-mail: kusaeri@uinsby.ac.id

N. P. Hastuti
Kementerian Agama RI, Lapangan Banteng 3-4, Jakarta, Indonesia

© The Editor(s) (if applicable) and The Author(s), under exclusive license to Springer Nature Singapore Pte Ltd. 2021

Y.-D. Zhang et al. (eds.), *Smart Trends in Computing and Communications: Proceedings of SmartCom 2020*, Smart Innovation, Systems and Technologies 182,
https://doi.org/10.1007/978-981-15-5224-3_21

country, Indonesia has carried out various educational developments. The progress of Indonesian education can affect the progress of the Indonesian state [1]. Increasing the quality of education is one of the efforts aimed at obtaining quality, advanced, and independent communities. One of Indonesia's efforts in developing education is to increase the quantity and quality of education. Enhancing the quality of education is realized by evaluating and developing educational strategies, while one of the quantitative efforts is to provide formal school facilities from urban to rural areas [2].

Formal schools established in Indonesia have various types including public schools and private schools. State schools are schools operated by the government. The government handles all school needs. While private schools are schools that are operated by private parties [3]. In its development, various schools were established to help to advance Indonesian education. The number of schools increases every year. The number of schools from elementary school to senior high school (SLTA), special school in Indonesia, reaches 307,655 schools. This amount is based on the basic education data of the Ministry of Education and Culture. When viewed from the type of school, there are 169,378 public schools and 138,277 private schools [4]. Several educational problems follow the growth of schools in Indonesia. One issue that arises is the school at the junior high school level.

One form of treatment in junior high school problems is holding a competition between students. *Kompetisi Sains Madrasah* (KSM) is a competition held by the Ministry of Religion of the Republic of Indonesia. KSM is followed starting from elementary school, junior high school, and senior high school. Madrasah Science Competition is a science competition that began in 2016. Students participate in KSM from elementary, junior high, and high schools under the auspices of the Ministry of Education and Culture [5]. KSM competition results are a sample of the quality scores of students from various provinces. The distribution of student grades in each region has a different score. A grouping system of score data is needed to see the diversity of student quality in Indonesia.

Clustering is a process of grouping data into a data class with high similarity and having data differences with other clusters. Previous research has conducted clustering of the quality of elementary school students using the k-means algorithm [6]. The clustering aims to identify the quality of elementary school students. In this research, clustering is done using the Stepwise Iterative Maximum Likelihood (SIML) algorithm. Maximum likelihood classifies data by looking at the average and standard deviation values. A random value is raised to be the center point of the cluster. The optimal value of the center cluster is obtained if it has an average and standard deviation [7]. Previous research stated that a maximum likelihood method can distinguish overlapping data. In addition, the maximum likelihood can group the number of samples that are lower than the data dimension [8]. Other studies use maximum likelihood clustering as a method for classifying people with leukemia. Maximum likelihood clustering groups data as 2, 3, 4, and 5 dimensions with excellent success. The success rate of clustering using the maximum likelihood can reach 90% more, as in previous research studies [8].

The previous clustering of education was carried out using the k -means method. Clustering is intended to help to reduce the number of students dropping out of school, and increase the quality of student learning [9]. The use of the k -means method is also provided to classify the quality of students using online learning data [10]. Another method used in the clustering process is the fuzzy c -means method. The clustering of students is aimed at providing evaluations of students needed by a teacher in improving the quality of learning [11]. Some student quality analysis that has been done has not used the SIML method. This study proposes the SIML method for classifying junior high school students based on the score of KSM.

The results of clustering using maximum likelihood require an evaluation system to see the level of success. One form of clustering evaluation is calculating data distance. The calculated distance is the distance of data in one cluster, as well as with other clusters. In addition, evaluation can also be seen from the distance of data to the cluster center point. The silhouette method can calculate all distances [12]. The results of the silhouette evaluation on the SIML clustering are used as a reference for analyzing the results of clustering. KSM data that has been clustered is analyzed for each cluster. Analysis of the results of clustering is intended to determine the quality of students. In addition, the results of the clustering of data can be used as a reference to provide action in improving the quality of education in Indonesia.

21.2 Stepwise Iterative Maximum Likelihood (SIML)

Maximum Likelihood Clustering (MLC) is a method that classify data by looking the average values and standard deviations from the center of the cluster [13–15]. Stepwise Iterative Maximum Likelihood (SIML) is a clustering method developed from MLC. SIML finds the best cluster center by finding the optimal partition repeatedly. Partition search is made by shifting the partition from the initial data to another partition. Partition optimization is given by looking at the log-likelihood value. If the partition shift results in a high log-likelihood value, the partition is directed toward the latest partition point [7]. Suppose the data is grouped into 2 groups, each cluster is marked with a red and orange circle. Each cluster has a midpoint as the center of the initial cluster. Cluster center points have coordinates in the form of a mean (μ) and standard deviation (σ). The log-likelihood value is obtained by adding up the possibilities in the first cluster (L_1), and the likelihood in the second cluster (L_2). If the new log-likelihood (L_{new}) value is greater than the old log-likelihood (L_{old}), the cluster point is changed to the new position. The mean and standard deviation values were obtained using Eqs. (21.1) and (21.2). While the likelihood value in cluster i is calculated using Eq. (21.3) [16].

$$\mu_i = \frac{1}{n_i} \sum_{x \in X_i} x \quad (21.1)$$

$$\sigma_i = \frac{1}{n_i} \sum_{x \in X_i} x(x - \mu_i)(x - \mu_i)^T \tag{21.2}$$

$$L_i = -\frac{1}{2}n_i d - \frac{n_i d}{2} \log 2\pi - \frac{n_i}{2} \log |\sigma_i| + n_i \log \frac{n_i}{n} \tag{21.3}$$

Shifting the cluster center point requires calculations to find a better point. Calculation of new likelihood (L^*) is obtained by adding up the value of the old likelihood (L) with changes in likelihood (ΔL), and constants (C), and mathematically can be written as in Eq. (21.4) [17]. The value of the change in likelihood itself is obtained using Eq. (21.5), and constants (C) are obtained using Eq. (21.6).

$$L_j^* = L_j + (\Delta L_j + C) \tag{21.4}$$

$$\begin{aligned} \Delta L_j = & -\frac{1}{2} \log |\sigma_j| - \frac{n_j + 1}{2} \log \left(1 + \frac{1}{n_j + 1} (x - \mu_j)^T \sigma_j^{-1} (x - \mu_j) \right) \\ & + \log \frac{n_j}{n} + (n_j + 1) \left(\frac{d}{2} + 1 \right) \log \frac{(n_j + 1)}{n_j} \end{aligned} \tag{21.5}$$

$$C = -\frac{d}{2} - \frac{d}{2} \log 2\pi \tag{21.6}$$

21.3 Silhouette

Silhouette is one method of system evaluation. Silhouette is used to evaluate the results of data clustering. Silhouette evaluation is obtained by calculating the distance of each data to the center of the cluster. Each data has calculated the distance at each cluster center. The distance of the two points can be calculated using the Euclidean distance function [18].

The evaluation value of the silhouette aims to see how close the data is to the center of the cluster itself and the center of the other clusters. The results of the silhouette have intervals of -1 to 1 . A value of -1 indicates poor clustering results and a value of 1 indicates clustering has the right results. To get the silhouette value, each cluster is calculated using Eqs. (21.7) and (21.8). The value of $a(i)$ indicates the distance of data $i(X_i)$ to other data (X_p) that are in one cluster (C_h). The value of $b(i)$ is the distance of data $i(X_i)$ to other data (X_p) in the other cluster [19].

$$\text{sil}(i) = \frac{b(i) - a(i)}{\max\{a(i), b(i)\}} \tag{21.7}$$

$$\text{Sil} = \frac{1}{n} \sum_{i=1}^n \text{sil}(i) \tag{21.8}$$

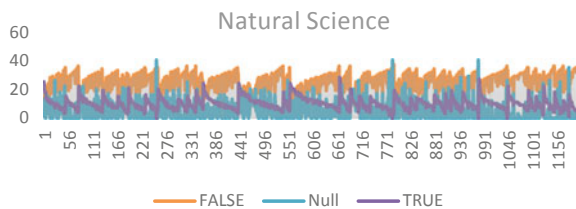
21.4 Results and Discussion

This research is quantitative research. This research is quantitative because it uses numerical data. The intended statistical data is KSM score data as material for analyzing research results using KSM participant data in 2019. The level of competition used is the junior high-level equivalent. The junior high school level has three types of competition. The first competition is the natural sciences subject. This competition has a total data of 1192 participants. Data on science competitions are shown in Fig. 21.1. The second competition is a competition in social sciences subjects. The SMP-level competition in social studies subjects has a total number of 1183 participants. In the third competition, there were 1254 participants with mathematics subjects. The participant data used is the provincial-level participants from the district/city-level selection results. Each data has three parameters. The parameters used include the number of questions answered correctly, answered incorrectly, and not answered. These parameters are used as input values to determine the quality of Indonesian students. The amount of data used comes from 34 provinces. Figure 21.1 presents natural science subjects data for number of questions answered correctly (TRUE), number of questions answered incorrectly (FALSE), and number of not answered (NULL) questions.

Looking at the data shown in Fig. 21.1, participants in science competitions have a higher tendency to answer false questions, followed by the number of questions answered correctly, and questions that were not answered. As with science participants, IPS participants have the same tendency. The difference between science participants is the number of questions answered incorrectly and the number of correct and blank questions. All three parameters have a high enough difference in value. In the mathematical participant data, the score parameters are not answered and the questions answered incorrectly have an almost equal number, while the number of questions answered correctly is relatively small. Data from the three competitions in clustering uses the SIML method which the number of questions answered correctly, the number of questions answered incorrectly, and the number of questions not answered as input data.

SIML clustering requires the determination of some initial parameters before clustering data. The parameters required are the determination of maximum iteration, determination of many classes, and determination of the initial cluster center. This study uses a maximum iteration of 1000 iterations, while many classes in this study were given several experiments. The trial amount is given starting from 3 classes, 4

Fig. 21.1 Natural science participant



classes, 5 classes, and 6 classes. Experiments for the number of classes are intended to see the optimal number of classes in KSM data clustering. The update value is also applied to the cluster center point. The clustering process stops if the L value does not change.

Clustering results are then evaluated using the silhouette method. The output value in Eq. (21.7) is the silhouette for each cluster. To see the overall silhouette value can be obtained using Eq. (21.8). As a reference to see the optimal number of classes, see the overall silhouette (S) silhouette value, and silhouette standard deviation. S value is used to examine the average success of the system in clustering data. While the silhouette standard deviation is to see how high the distribution of the silhouette is. The higher the S value the stronger the clustering results. If you have a large standard deviation silhouette value, it indicates that there are high-value or low-value data far from the average of other data.

The results of clustering experiments using several classes are shown in Table 21.1. Looking at the results of the experiments, it can be seen that clustering using 3 clusters has the highest silhouette value compared to silhouettes in the number of other clusters. In addition, clustering with 3 clusters has a relatively small silhouette value distribution. The distribution of silhouette values is indicated by the standard

Table 21.1 Silhouette values in several experiments

Number of clusters	Subjects	Silhouette	Silhouette standard deviation
3 cluster	Natural sciences	0.423745	0.231354
	Social sciences	0.415654	0.188862
	Mathematics	0.487071	0.202107
4 cluster	Natural sciences	0.450291	0.205557
	Social sciences	0.429888	0.195371
	Mathematics	0.401584	0.226638
5 cluster	Natural sciences	0.409574	0.193355
	Social sciences	0.419559	0.196411
	Mathematics	0.375758	0.200149
6 cluster	Natural sciences	0.427796	0.201309
	Social sciences	0.386807	0.239797
	Mathematics	0.365801	0.215890

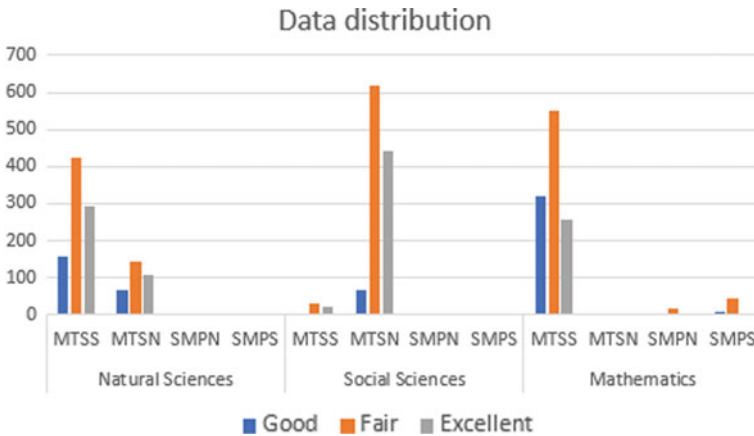


Fig. 21.2 Data distribution from clustering result

deviation of the silhouette values. The standard deviation value in the experiment 3 cluster has a small value.

The results of silhouette calculations in the 3 cluster experiment show that a lot of data has been classified well. Positive silhouette values show a good clustering. The number of data that has a value of less than 0 is 48 data from 1192 data. Overlapping data is 34 data from the 3rd cluster, 2 data from the 2nd cluster, and 12 data from the 1st cluster. In the social studies, subjects have 7 data with a value of less than 0 (overlapping) consisting of 3 data in cluster 1, 3 data from cluster 2, and 1 data from cluster 3. In the data competition, mathematics has overlapping data only 19 data. The overlapping data comes from 19 data in cluster 1, and 1 data from cluster 3. The results of clustering are obtained cluster groups based on the similarity of the data. Clustering results obtained as cluster 1 shows the cluster moderately, while cluster 2 is a cluster that shows data with minimal value. The last cluster is cluster 3 which states a group of data with high values. The distribution of student quality can be seen using the results of clustering. The distribution of clustering results is presented in Fig. 21.2. The distribution of students is divided into 3 categories, namely excellent, good, and fair. In the natural sciences comparison, the number of fair groups is the highest in private MTS, while in social science, the data is in public MTS. In mathematics competitions, the fair group on private MTS data is more dominant.

21.5 Conclusion

Clustering using the SIML method in KSM data has a maximum number of clusters of 3. The first cluster is good student data, followed by the second cluster of fair students, and the final cluster which shows excellent student data. The results of clustering using 3 clusters have the highest silhouette value compared to the silhouette values

in the number of other clusters. Judging from the Kaufman table, the clustering value shows that the cluster structure formed is still weak. The silhouette value with cluster number 3 is 0.423745 for natural science, 0.415654 for social science, and 0.487071 for mathematics subjects.

References

1. Sudarsana, I.K.: Pemikiran tokoh pendidikan dalam buku lifelong learning: policies, practices, and programs (Perspektif Peningkatan Mutu Pendidikan di Indonesia). *J. Penjaminan Mutu*. **2**(2), 44–53 (2016)
2. Raharjo, S.B.: Evaluasi trend kualitas pendidikan di indonesia. *J. Penelit. dan Eval. Pendidik*. **16**(2), 511–532 (2012)
3. Dapodikbud, T.: Temukan Informasi Sekolah di seluruh Indonesia [Internet]. (2019). Available from: <http://sekolah.data.kemdikbud.go.id/>
4. Kemendikbud. Jumlah Sekolah Menurut Jenjang Tahun Ajaran 2017/2018 [Internet]. Data-books (2018). Available from: <https://databoks.katadata.co.id/datapublish/2019/06/23/berapa-jumlah-sekolah-di-indonesia>
5. Zakwandi, R.: Analisis Konsep Pesawat Sederhana Pada Pembelajaran Ilmu Pengetahuan Alam Berbasis Tradisi Sains Islam Di Madrasah Tsanawiyah. *BELAJEA J. Pendidik. Islam*. **2**(1), 21–34 (2017)
6. Luthfi, E.T.: Fuzzy C-Means untuk Clustering Data (studi kasus: data performance mengajar dosen). In: *Seminar Nasional Teknologi*, pp. 1–7 (2007)
7. Sharma, A., Shigemizu, D., Boroevich, K.A., et al.: Stepwise iterative maximum likelihood clustering approach. *BMC Bioinform*. **17**(1), 319 (2016)
8. Sharma, A., Lopez, Y., Tsunoda, T.: Divisive hierarchical maximum likelihood clustering. *BMC Bioinform*. **18**(16), 546 (2017)
9. Shovon, M.H.I., Haque, M.: Prediction of student academic performance by an application of k-means clustering algorithm. *Int. J. Adv. Res. Comput. Sci. Softw. Eng*. **2**(7) (2012)
10. Khalil, M., Ebner, M.: Clustering patterns of engagement in Massive Open Online Courses (MOOCs): the use of learning analytics to reveal student categories. *J. Comput. High. Educ*. **29**(1), 114–132 (2017)
11. Varela, N., Montero, E.S., Vasquez, C., et al.: Student performance assessment using clustering techniques. In: *International Conference on Data Mining and Big Data*, pp. 179–188. Springer, Berlin (2019)
12. Luna-Romera, J.M., del Mar Martinez-Ballesteros, M., Garcia-Gutierrez, J., Riquelme-Santos, J.C.: An approach to silhouette and dunn clustering indices applied to big data in spark. In: *Conference of the Spanish Association for Artificial Intelligence*, pp. 160–169. Springer, Berlin (2016)
13. Ding, M., Hu, K.: Susceptibility mapping of landslides in Beichuan County using cluster and MLC methods. *Nat. Hazards* **70**(1), 755–766 (2014)
14. Shivakumar, B.R., Rajashekararadhya, S.V.: Investigation on land cover mapping capability of maximum likelihood classifier: a case study on North Canara, India. *Procedia Comput. Sci*. **143**, 579–586 (2018)
15. Wang, Y., Jamshidi, M., Neville, P., Bales, C., Morain, S.: Multispectral Landsat image classification using a data clustering algorithm. In: *Proceedings of 2004 International Conference on Machine Learning and Cybernetics (IEEE Cat. No. 04EX826)*, pp. 4380–4384. IEEE (2004)
16. Xu, J., Gangnon, R.E.: Stepwise and stagewise approaches for spatial cluster detection. *Spat. Spatiotemporal. Epidemiol*. **17**, 59–74 (2016)
17. Lozano, S., Calzada-Infante, L.: Computing gradient-based stepwise benchmarking paths. *Omega* **81**, 195–207 (2018)

18. Sharma, D., Thulasiraman, K., Wu, D., Jiang, J.N.: Power network equivalents: a network science based K-means clustering method integrated with silhouette analysis. In: International Conference on Complex Networks and their Applications, pp. 78–89. Springer, Berlin (2017)
19. Swindiaro, V.T.P., Sarno, R., Novitasari, D.C.R.: Integration of fuzzy C-means clustering and TOPSIS (FCM-TOPSIS) with silhouette analysis for multi criteria parameter data. In: 2018 International Seminar on Application for Technology of Information and Communication, pp. 463–468. IEEE (2018)

Chapter 22

Detecting the Width of Pap Smear Cytoplasm Image Based on GLCM Feature



Nita Merlina, Edi Noersasongko, Pulung Nurtantio, M. A. Soeleman,
Dwiza Riana, and Sri Hadianti

Abstract Color image segmentation on cytoplasm Pap smear single cell image identified as normal condition is an interesting subject to study. It is caused by the image limitation and morphological transformation complexity of the cell structural part. Feature analysis on cytoplasm area is an important thing in the process of biomedical image analysis because of the noise and complex background and the bad cytoplasm contrast as well. Thus, an analysis on the feature area on cytoplasm automatically is an urge thing to do to identify Pap smear normal cell image based on feature analysis on cytoplasm area in single cell image identified as normal condition. The purpose of this research is to analyze how far the process color image segmentation on cytoplasm by using normal single cell image is able to produce features of texture and form analysis. To analyze the form of cytoplasm, this research used RGB color to HSV color conversion method which produces metric and eccentricity value. It is then continued to the process of threshold image and counting the wide area by changing threshold into binary image. On the other side, to analyze the texture, this research applied an analysis using gray-level co-occurrence matrix (GLCM) using K -means method to produce contrast, correlation, energy, and homogeneity parameters. The result of the research is the segmentation outcome to Pap smear normal single cell image sample to get metric, eccentricity, contrast, correlation, and energy features.

22.1 Introduction

Women are generally susceptible to cervical cancer, which ranks fourth as a very deadly disease [1]. Papanicolaou test also called Pap smear or Pap test is a health test method that can help prevent cervical cancer. The main purpose of a Pap smear

N. Merlina (✉) · E. Noersasongko · P. Nurtantio · M. A. Soeleman
Universitas Dian Nuswantoro, Semarang, Indonesia
e-mail: nita@mhs.dinus.ac.id

N. Merlina · D. Riana · S. Hadianti
STMIK Nusa Mandiri, Jakarta, Indonesia

© The Editor(s) (if applicable) and The Author(s), under exclusive license
to Springer Nature Singapore Pte Ltd. 2021

Y.-D. Zhang et al. (eds.), *Smart Trends in Computing and Communications: Proceedings of SmartCom 2020*, Smart Innovation, Systems and Technologies 182,
https://doi.org/10.1007/978-981-15-5224-3_22

is to detect cell abnormalities that may occur or before the cancer develops. Correct interpretation of microscopic examination of cells and tissues is very important for the final diagnosis judgment of the disease [2]. However, the Pap smear testing process has weaknesses, especially in many developing countries where the number of pathologists who can examine slides is inadequate. In Indonesia, with a population of productive age women spread across 32 provinces with limited facilities and limited human resources, it is estimated that 80% of the coverage of examinations will be completed in five years with 7,992,486 Pap smear tests per year [3].

The classification of cervical cells in Pap smear images is an interesting thing because of image limitations and the complexity of morphological alterations in the structural parts of cells [4]. Pap smear image processing has been performed for single cell types and non-overlapping. Image segmentation process is expected to identify cytoplasm and nucleus images [5–7]. Segmentation is needed to define the area of interest (ROI) in a normal single cell image and is the basis of an automatic cervical cancer screening system. Efficient image segmentation enables extraction of significant information and streamlines image data for further analysis. Weak segmentation results in weak results during image analysis [8]. Analysis of features in the cytoplasm area in normal Pap smear cell images is interesting. That is due to image limitations and the complexity of morphological changes in the structural parts of cells. Analysis of features in the cytoplasm area is important in the process of analyzing biomedical images, and it is caused by background noise and complex and weak cytoplasm contrast. So, it is necessary to do an analysis of the features of the area in the cytoplasm by automation to identify the normal Pap smear cell image based on the analysis of the features of the cytoplasm area in a single cell image that is detected normally. The purpose of this research is to see the extent of the process of analyzing feature areas in the cytoplasm by using a normal single cell image so that features of texture and shape analysis can be produced. The results of this study are expected to facilitate the identification of cytoplasm images from Pap smear images.

This paper is divided into several sections. Section 22.2, related work, discusses about the methods used in the research. Section 22.3 describes the results and discussion, which will be enclosed with conclusions and further research plans.

22.2 Related Work

There are many methods used to identify the area of cytoplasm image, and this study attempts to do different things, which is to propose a segmentation method for cytoplasm area in a single Pap smear image that utilizes the GLCM feature. This GLCM feature has not been widely used in previous research. In the initial detection of a Pap smear image, a single cell image is easy to observe [9]. In the previous research, cytoplasm detection process has been successfully carried out by

color classification using K -means and joint shape matching. However, this research is limited only to determine the presence of cytoplasm and not to determine the extent of cytoplasm in detail [10, 11]. The gray-level co-occurrence matrix (GLCM) previous studies have been used, but they use a dataset from a nearby hospital and only discuss cervical cancer related without the Pap smear cell being used [12].

22.3 Method

Data processing techniques use the MATLAB application program on color and binary image matrices as well as analyzing textures. In order to determine the area in cytoplasm image, the initial step of this research is to convert RGB color to HSV color (hue, saturation, value). The HSV color model was formulated by searching the RGB color cube along the gray axis of the color wheel, where this model is more widely used than RGB in depicting color sensations. After the HSV color conversion is generated, the next step is to determine the threshold image and calculate the area of the area by changing the threshold image into a binary image that aims to calculate objects in a digital image in a simple way from the original image. In this process, we need a boundary value called the threshold value. Image intensity values that are more than or equal to the threshold value will be changed to white (1), while image intensity values less than the threshold value will be changed to black (0) [13]. Furthermore, to analyze the texture of the image of the area value that has been segmented by the K -means method and the researcher uses the Gray-Level Co-Occurrence Matrix (GLCM) so that the parameters obtained are contrast, correlation, energy, and homogeneity. The results of this research are the results of segmentation of a single Pap smear normal cell image sample so that it can be done well and is able to get the features of metric, eccentricity, contrast, correlation, and energy [14], where the texture has characteristics that can be extracted to distinguish an image with another image. Figure 22.1 shows the image of a single cell used in this study.

In this study, a research flow diagram is shown in Fig. 22.2 on the digital image of papers.

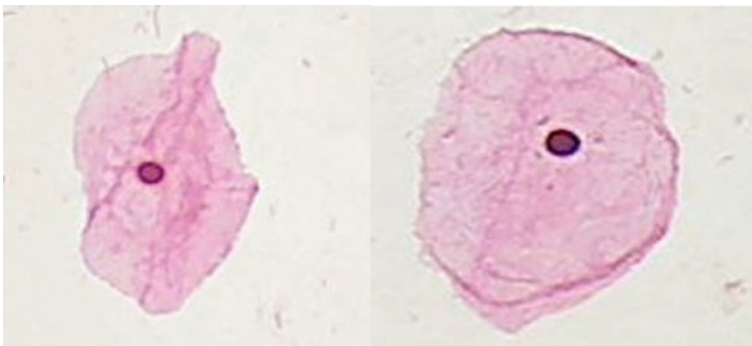


Fig. 22.1 Example of a single cell image

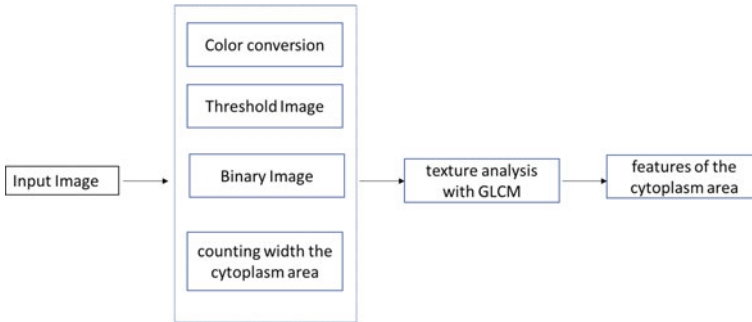


Fig. 22.2 Research stages

22.4 Results and Discussion

22.4.1 Result

The stages of the research consisting of five stages of the process are evaluated on traditional Pap smear images. All of these images were obtained through a Logitech camera (Logitech HD C525 Webcam) adjusted to an optical microscope (Olympus CH20). 40× amplification is used, and the results are saved in JPEG format. The following are the results of the process of segmentation methods in each.

22.4.1.1 Convert RGB Color to HSV Color

The result of the conversion of RGB color into HSV color aims to detect the cytoplasm so as to produce an image as shown in Fig. 22.3, where the cytoplasm has a color that is more dominant than the nucleus.

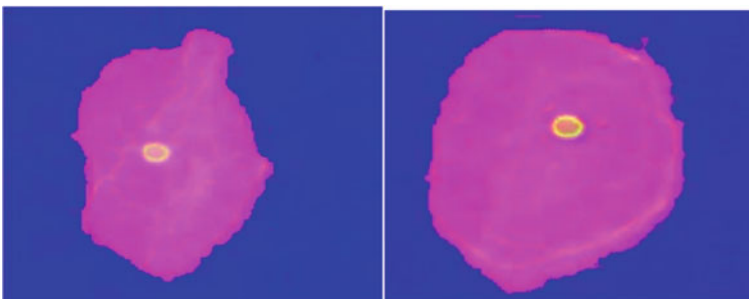


Fig. 22.3 Image results from color conversion

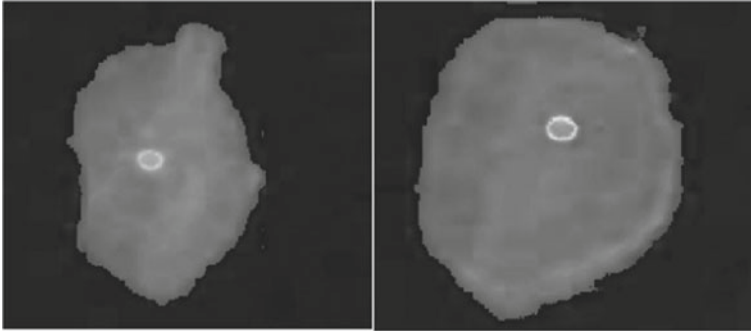


Fig. 22.4 Image from threshold

22.4.1.2 Threshold Image

When analyzing an area in the cytoplasm, the initial process is to determine the edge of the object from a single normal cell. The results of edge detection in normal single cell images are taken from images that have been converted to HSV color, and Fig. 22.4 shows images of edge detection.

22.4.1.3 Binary Imagery

The calculation process of the attributes that exist in a single normal Pap smear cell can be simply done by the process of conversion to binary images; after the conversion process is carried out, the area calculation process can be carried out, along with pictures that present the results of binary images (Figs. 22.5, 22.6, and 22.7).



Fig. 22.5 Binary image

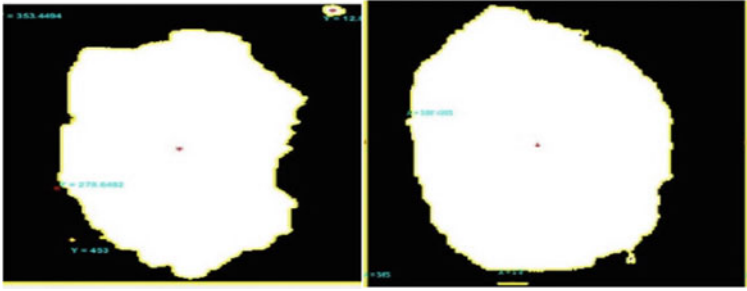


Fig. 22.6 Width binary image

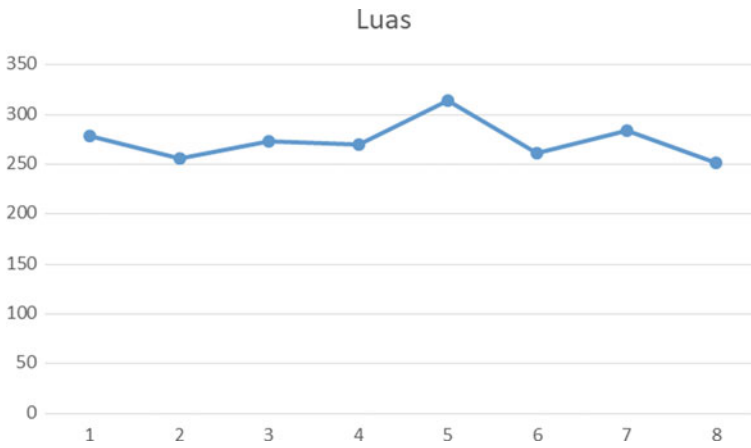


Fig. 22.7 Chart width of binary image

22.4.1.4 Gray-Level Co-occurrence Matrix (GLCM)

The process of this GLCM is to analyze the texture of the cytoplasm area, so that this research results in segmentation of a single Pap smear normal cell image sample by producing metric, eccentricity, contrast, correlation, and energy features. The following are the formulas for calculating the metric feature, eccentricity, contrast, correlation, and energy:

$$\text{Contrast} = \sum_{i_1} \sum_{i_2} (i_1 - i_2)^2 p(i_1, i_2) \tag{22.1}$$

$$\text{Homogeneity} = \sum_{i_1} \sum_{i_2} \frac{p(i_1, i_2)}{1 + |i_1 - i_2|} \tag{22.2}$$

$$\text{Energy} = \sum_{i_1} \sum_{i_2} p^2(i_1, i_2) \tag{22.3}$$

Table 22.1 Texture of the cytoplasm area

Metric	Eccentricity	Contrast	Correlation	Energy	Homogeneity
0.01	1	0.01	0.99	0.57	1
0.01	0.46	0.01	0.98	0.49	0.99
0.01	1	0.01	0.99	0.49	1
0.02	1	0.01	0.99	0.51	1
0.95	0.7	0.01	0.99	0.53	1
0.78	0.7	0.01	0.88	0.95	1
0.01	0.73	0.01	0.98	0.52	0.99
0.67	0.53	0.01	0.99	0.5	1

$$\text{Entropy} = - \sum_{i_1} \sum_{i_2} p(i_1, i_2) \log p(i_1, i_2) \tag{22.4}$$

$$\text{Eccentricity} = e = \sqrt{1 - \frac{b^2}{a^2}} \tag{22.5}$$

$$\text{Metric} = M = \frac{4\pi \times A}{C^2} \tag{22.6}$$

Table 22.1 gives the results of the GLCM calculations that have been carried out.

22.4.2 Discussion

In this study, we segmented Pap smear images by taking ten image from a single normal goal, but there are two images that are not segmented perfectly; this is because there is noise in the image, so the segmentation is done using the method taken less than perfect.

22.5 Conclusion

The results of this study are to see the extent of the cytoplasm color image segmentation process using normal single cell images so that features of texture and shape analysis can be produced. To analyze the shape of the cytoplasm, this study uses the method of converting RGB color conversion into HSV color conversion that produces metric and eccentricity values and then proceeds with the process to determine the threshold image and calculate the area of the area by changing the threshold image which becomes a binary image. For texture analysis, the analysis is done using the gray-level co-occurrence matrix (GLCM) method which uses the *K*-means method

to obtain contrast, correlation, energy, and homogeneity parameters. The results of this research are the results of segmentation of normal Pap smear single cell image samples so that they can be done well and are able to get the features of metric, eccentricity, contrast, correlation, and energy. The limitation of this study is that the number of samples used needs to be increased so that it will produce more feature data to get more extensive information. This research is a preliminary study for cytoplasm recognition. Further research will focus on segmentation of the cytoplasm in single Pap smear cells by adding new features besides GLCM. Another thing to do is research for group Pap smears.

References

1. Irawan, F.: Statistik penderita kanker di Indonesia (2018)
2. Riana, D., Widyantoro, D.H., Mengko, T.L.: Extraction and classification texture of inflammatory cells and nuclei in normal pap smear images. In: 2015 4th International Conference on Instrumentation, Communications, Information Technology, and Biomedical Engineering (2015)
3. Kusuma, F.: Tes Pap Dan Cara Deteksi Dini Kanker Serviks Lainnya, Departemen Obstetri dan Ginekologi Fakultas Kedokteran Universitas Indonesia RSUPN Dr. Cipto Mangunkusumo, Prevention and Early Detection of Cervical Cancer (PEACE), Jakarta (2012)
4. Plissiti, S.E., Dimitrakopoulos, P., Sfikas, G., Nikou, C., Krikoni, O., Charchanti, A.: Dataset for feature and image based classification of normal and pathological cervical cells in pap smear images. In: 25th IEEE International Conference on Image Processing (2018)
5. Lu, Z., Carneiro, G., Bradley, A.P.: Automated nucleus and cytoplasm segmentation of overlapping cervical cells. In: International Conference on Medical Image Computing and Computer-Assisted Intervention, vol 8149. Lecture Notes in Computer Science, pp. 452–460 (2013)
6. Zhao, L., Li, K. Wang, M., Yin, J., Zhu, E., Wu, C., Wang, S., Zhu, C.: Automatic cytoplasm and nuclei segmentation for color cervical smear image using an efficient gap-search MRF 46. *Comput. Biol. Med.* **71**, 46 (2016). ISSN 00104825
7. Riana, D., Hidayanto, A.N., Widyantoro, D.H., Mengko, T.L.R., Kalsoem, O.: Segmentation of overlapping cytoplasm and overlapped areas in Pap smear images. In: Information, Intelligence, Systems & Applications (IISA), pp. 1–5 (2017)
8. Sun, G., Li, S., Cao, Y., Lang, F.: Cervical cancer diagnosis based on random forest. *Int. J. Performability Eng.* (2017)
9. Riana, D., Ramdhani, Y., Prasetyo, R.T., Hidayanto, A.N.: Improving hierarchical decision approach for single image classification of pap smear. *Int. J. Electr. Comput. Eng.* **8**, 5415–5424 (2018)
10. Riana, D., Tohir, H., Hidayanto, A.N.: Segmentation of Overlapping Areas on Pap Smear Images with Color Features Using K-Means and Otsu Methods (2018). <https://ieeexplore.ieee.org/xpl/conhome/8767368/proceeding>
11. Song, Y., Qin, J., Lei, B., He, S., Choi, K.-S.: Joint shape matching for overlapping cytoplasm segmentation in cervical smear images. In: 2019 IEEE 16th International Symposium on Biomedical Imaging (ISBI 2019) Venice, Italy, pp. 191–194 (2019)
12. Nehra, S., Raheja, J.L., Butte, K., Zope, A.: Detection of cervical cancer using GLCM and support vector machines, pp. 49–53. <https://ieeexplore.ieee.org/xpl/conhome/8768798/proceeding>

13. Pamungkas, A.: Pemrograman Matlab (2019). [Online]. Available: <https://pemrogramanmatlab.com/pengolahan-citra-digital/segmentasi-citra>
14. Bhan, S., Vyas, A., Mishra, G.: Supervised segmentation of overlapping cervical pap smear images. In: 2016 International Conference on Signal Processing and Communications (2016)

Chapter 23

Design of a Novel Wideband Dipole Antenna for mm-Wave Frequencies



**Paikhomba Loktongbam, Chaitali Koley, Debashish Pal,
and Ayan Kumar Bandhopadhyay**

Abstract Here, a novel dipole antenna operating in mm-wave frequency is reported. This antenna uses silicon as its substrate. The planar dipole is printed on top of the silicon substrate having pit of optimized dimensions embedded in it. To minimize the surface wave loss, metallic vias are implanted along the sides of the substrate. The proposed antenna structure has a simulated -10 dB bandwidth of ~ 80 GHz (120–200 GHz). The simulated antenna has a radiation efficiency of 98.7% and gain of 4.81 dBi.

23.1 Introduction

Terahertz (THz) band with frequency range from 100 GHz to 10 THz (0.1–10 mm [1]) and its non-ionizing nature [2] have proved it to be a potential candidate for various applications. The utilization of flexible electronics in millimeter-wave and THz systems has also grown tremendously in the past decade. Some of the recent applications include inter- and intra-chip communication [3], electromagnetic energy harvesting [4], biomedical implant devices [5], detection and imaging in the THz region [6], measurement of mm-wave ICs and devices [7], power combining [8], and beam steering [9]. In any communication system, an antenna is a critical passive component [10], as it determines the system size and transmitting power. Silicon-based antenna suffers from two major drawbacks. They are backside power radiation

P. Loktongbam · C. Koley (✉)
National Institute of Technology Mizoram, Aizawl, India
e-mail: chaitali.ece@nitmz.ac.in

P. Loktongbam
e-mail: pailee.li81@gmail.com

D. Pal · A. K. Bandhopadhyay
Central Scientific Industrial Research-CEERI, Pilani, India
e-mail: debasish.pal1975@gmail.com

A. K. Bandhopadhyay
e-mail: akb.ceeri@res.in

© The Editor(s) (if applicable) and The Author(s), under exclusive license to Springer Nature Singapore Pte Ltd. 2021

241

Y.-D. Zhang et al. (eds.), *Smart Trends in Computing and Communications: Proceedings of SmartCom 2020*, Smart Innovation, Systems and Technologies 182,
https://doi.org/10.1007/978-981-15-5224-3_23

when the antenna is excited [11] and surface wave losses. In [12], a hemispherical lens was attached to the substrate to minimize backside radiation and to increase the antenna gain. Other techniques to enhance the performance of lossy silicon substrate are micro-machined horns [13], superstrate focusing scheme [14], substrate thinning [15], artificial magnetic conductor concepts [16], etc. The proposed antenna attempts to decrease the surface waves by implanting metallic vias of copper on the edges of the silicon substrate. This paper is organized as follows: Sect. 23.2 discusses antenna structure and design methodology. Section 23.3 discusses the results obtained in the simulation, and finally, Sect. 23.4 is the conclusion.

23.2 Antenna Geometry and Design Formulae

The proposed antenna is basically a center-fed dipole. The ground plane is made of copper [17]. A pit of optimized dimension is drilled in the silicon substrate. Dipole is printed in it. The top view and front view are shown in Figs. 23.1 and 23.2, respectively. The dimensions of the antenna are given in Table 23.1.

For any half-wave dipole, the length can be calculated by the formula [18] multiplied by a factor “A”.

Fig. 23.1 Top view of the proposed antenna

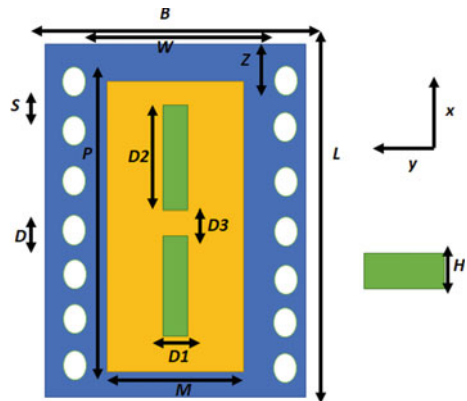


Fig. 23.2 Side view of the proposed antenna

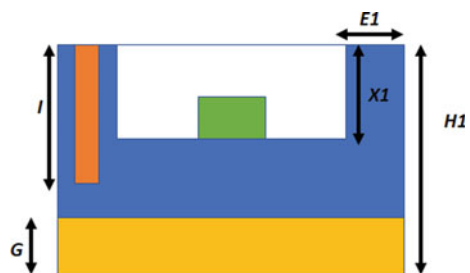


Table 23.1 Dimensions of the antenna

Name of parameter	Dimensions (μm)
L	800
B	540
H1	200
G	3
D1	20
D2	176.595
D3	10
D	20
H	20
S	100
X1	40
E1	50
P	650
M	400
I	50
Z	25
W	450

$$L_d = \frac{c}{2\epsilon_r} A \tag{23.1}$$

The value of A ranges from 0.96 to 0.98. c is the velocity of light in free space, and ϵ_r is the dielectric constant.

Dipole antennas are preferred for on-chip antenna designs because they can be connected to differential circuits and can suppress substrate coupling effects [19]. With reference to Fig. 23.3, uniformly spaced vias are implanted in the substrate.

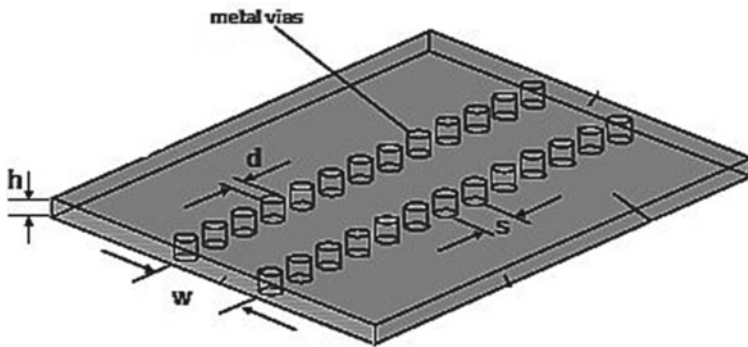
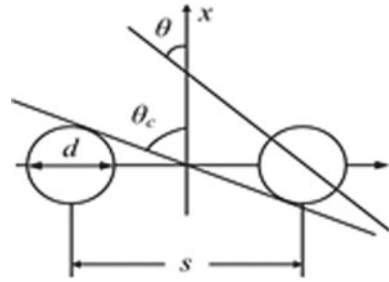


Fig. 23.3 Geometry of the proposed substrate

Fig. 23.4 Schematic of vias



The vias minimize the surface wave loss by acting as electric shielding. As depicted in Fig. 23.4, at critical angle θ_c , some of the surface waves are assumed to leak from the via wall. For $\theta < \theta_c$, the leakage ratio R_{leak} is expressed by Eq. (23.2) and (23.3), where d is via diameter, S is the lateral spacing, and θ is the angle of incidence [20].

$$\cos \theta = \frac{n\lambda}{2w} \tag{23.2}$$

where n = mode order, w = length of the broadside wall of the substrate, and λ = free space wavelength

$$R_{leak} = 1 - \frac{d}{s \cos \theta} \tag{23.3}$$

The inter-distance between the vias, “ S ”, along the z -axis plane of the substrate also must satisfy Eq. 23.5 [21].

$$f_c = \frac{c}{2\sqrt{\epsilon_r}} \times \frac{1}{w - \frac{d^2}{0.95s}} \tag{23.4}$$

where

- f_c cutoff frequency
- c speed of light
- d diameter of vias
- w transverse spacing
- s longitudinal spacing

$$s < \frac{\lambda_0}{2\sqrt{\epsilon_r}} \tag{23.5}$$

where

- λ_0 free space wavelength
- ϵ_r 11.9 for silicon

$$w_{\text{eff}} = w - \frac{d^2}{0.95s} \tag{23.6}$$

where

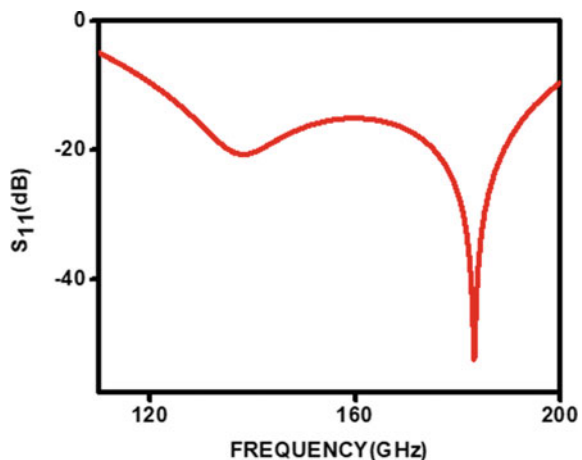
W_{eff} effective width.

Equation (23.6) is non-trivial as w_{eff} is always smaller than w . The field in the substrate between the vias is limited to a region where breadth is narrower than width (w) [20, 21]. Longitudinal spacing denoted by “ S ” between the vias controls the amount of field leakage. It has been established from Eq. (23.6) that the electric field in the substrate between the vias is confined to a region less than w (i.e., w_{eff} which is the transverse gap between the vias). So the radiation intensity will be maximum in the “ w_{eff} ” zone. $M \times P \times XI$ is the dimension of the pit excavated from the silicon substrate. The depth XI is exactly the quarter of the wavelength (with reference to operating frequency). The planar dipole antenna is printed in the pit.

23.3 Result and Analysis

CST Microwave Studio was used to simulate the proposed antenna. The simulated return loss of the antenna is shown in Fig. 23.5. The antenna recorded first resonance at 120 GHz with s_{11} matching of -22 dB. A second-order resonance is recorded at 185 GHz with s_{11} matching of -52 dB. This can be attributed due to the edges in the top of the substrate due to the cut out from the substrate. The -10 dB bandwidth antenna is almost 80 GHz (from 120 to 200 GHz). The surface current plot of the

Fig. 23.5 Return loss of the antenna



antenna is shown in Fig. 23.6. The simulated radiation pattern of the antenna is shown in Fig. 23.7.

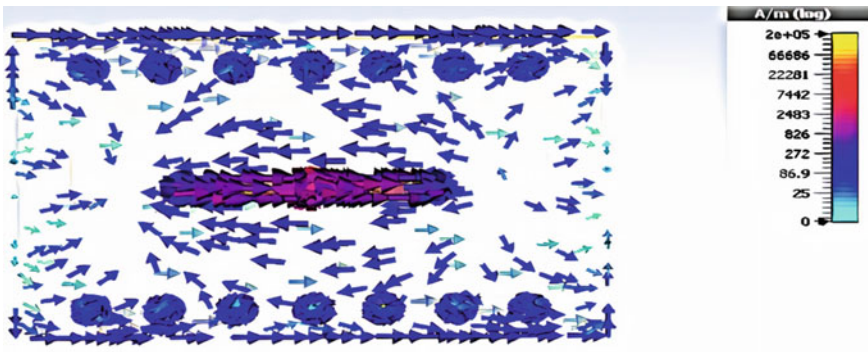


Fig. 23.6 Surface current plot of the antenna

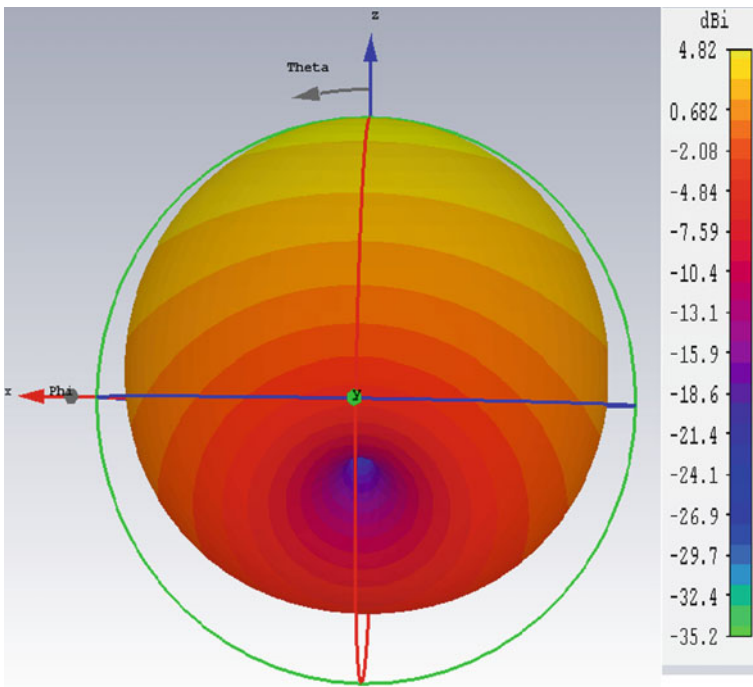


Fig. 23.7 3D radiation pattern of the antenna

23.4 Conclusion

This paper presents a new high-efficiency broadband antenna design based on the silicon substrate. The proposed antenna is a planar dipole antenna. The antenna is comparatively easy to fabricate and quite easy structure-wise. This printed dipole antenna operates in mm-wave frequency range and is suitable for on-chip applications.

References

1. Ian, B., Akyildiz, F., Jornet, J.M., Hana, C.: Terahertz band: next frontier for wireless communications. *Phys. Commun.* **12**, 16–32 (2014)
2. Pigeon, M., Sushko, O., Donnan, R.S., Kreouzis, T., Parini, C.G., Wang, H., Alderman, B., Huggard, P.G., Dubrovka, R.: From simulations to measurements: prototyping an antenna for non-linear applications at sub-THz frequencies. *IET Microwaves Antennas Propag.* **11**, 304–309 (2017)
3. Yi, D., Chong, L., Xiao-Wei, H., Hong-Zhou, T.: 12 GHz wireless clock delivery using on-chip antennas: a case for future intra/inter-chip wireless interconnect. In: *Proceedings of International Conference on Computer Science and Automation Engineering*, pp. 212–215 (2012)
4. Yuxiang, S., Babakhani, A.: A wirelessly powered injection locked oscillator with on chip antennas in 180 nm SOI CMOS. In: *Proceedings of International Microwave Symposium*, p. 3 (2016)
5. Liu, C., Guo, Y.X., Liu, X., Xiao, S.: An integrated on chip implantable antenna in 0.18 um CMOS technology for biomedical applications. *IEEE Trans. Antenna Propag.* **64**, 1167–1172 (2016)
6. Rodrigues, F., Gomes, S., Anacleto, P., Fernandes, J., Mendes, P.M.: RF-CMOS wireless implantable microsystem for sacral roots stimulation with on chip antenna and far field wireless powering. In: *Proceedings of European Microwave Conference*, pp. 76–79 (2015)
7. Lei-jun, X., Fu-cheng, T., Xue, B., Han-ping, M.: The design and matching of THz on chip antennas in CMOS. In *Proceedings of International Conference on Microwave, Millimetre, Wave Technology*, 958–960 (2016)
8. Lischer, S., Heiss, M., Landwehr, M., Fischer, W.J.: A 24 GHz RFID system on a chip with on chip antennas, compatible to ISO 18000-6C/EPC C1G2. In: *Proceedings of International Conference on Microwaves, Communications, Antennas and Electronic Systems*, pp 1–4 (2015)
9. Chen, P., Babakhani, A.: A 30 GHz impulse radiator with on chip Antennas for high resolution 3D imaging. In: *Proceedings of Radio and Wireless Symposium (RWS)*, pp. 32–34 (2015)
10. Chen, Z., Wang, C.-C., Yao, H.-C., Heydari, P.: A BiCMOS W-Band 2×2 focal-plane array with on-chip antenna. *IEEE J. Solid-State Circ.* **47**, 2355–2371 (2012)
11. Han, R., et al.: A 280 GHz Schottky diode detector in 130 nm digital CMOS. *IEEE J. Solid State Circ.* **46**, 564–580 (2011)
12. Grzyb, J., Zhao, Y., Pfeiffer, U.R.: A 288 GHz lens integrated balanced triple-push source in a 65 nm CMOS technology. *IEEE J. Solid State Circ.* **48**, 1751–1761 (2013)
13. Ou, Y.C., Rebeiz, G.M.: On chip slot ring and high gain horn antennas for millimeter wave wafer scale silicon systems. *IEEE Trans. Micro Wave Theory and Tech.* **59**, 1963–1972 (2011)
14. Park, J., Kang, S., Niknejad, A.M.: A 0.38 THz fully integrated utilizing a Quadrature push-push harmonic circuitry in SiGe BiCMOS. *IEEE J. Solid State Circ.* **47**, 2344–2354 (2012)
15. Han, R., et.al: A 280 GHz Schottky diode detector in 130 nm digital CMOS. *IEEE J. Solid State Circ.* **46**, 564–580 (2011)

16. Ojefoires, E., Kratz, H., Gremer, K., Phana, R., Rydberg, A.: Micromachined loop antennas on low resistivity, silicon substrates. *IEEE Trans. Antennas Propag.* **54**, 3593–3601 (2006)
17. Zhu, H., Li, N., Zeng, J., Li, X., Ai, B.: A novel 0.22 THz on chip antenna based AMCs. In: *Proceedings of the Asia Pacific Microwave Conference* (2014)
18. Eriksson, O., Lindh, C.: Designing a GSM dipole antenna. TNE062—RF System Design, 14 May 2008
19. Zhang, Y.P., Liu, D.: Antenna on chip and antenna in package solutions to highly integrated millimeter wave devices for wireless device for wireless communications. *IEEE Trans. Antennas Propag.* **57**, 2830–2841 (2009)
20. Feng, X., Ke, W.: Guided-wave and leakage characteristics of substrate integrated waveguide. *IEEE Trans. Microw. Theory Tech.* **53**, 66–73 (2005)
21. Bozzi, M., Xu, F., Deslandes, D., Wu, K.: Modeling and design considerations for substrate integrated waveguide circuits and components. In: *TELSIKS 2007, Serbia*, 26–28 Sept 2007

Chapter 24

Forecasting Sea Surface Temperature in Java Sea Using Generalized Regression Neural Networks



Dian Candra Rini Novitasari , Wahyu Tri Puspitasari ,
Rahmat Pramulya , Hetty Rohayani , R. R. Diah Nugraheni Setyowati ,
Dwi Rukma Santi , Muhammad Fahrur Rozi , and Ary Widjajanto 

Abstract Sea surface temperature is an important factor that influences climate change and productivity in the sea. Sea surface temperature is measured manually every day. The method of observation is considered to be less efficient because the process is not easy and requires relatively expensive costs. In addition, consideration is taken when extreme weather can hinder the observation process and be able to endanger the observer. In this case, a prediction system is needed that can predict the current conditions and the next few days from sea surface temperature. Before predicting sea surface temperature, the first thing to do is to forecast each parameter of sea surface temperature. Parameters of sea surface temperature consist of air temperature, air humidity, rainfall, duration of solar radiation, and wind speed. Forecasting parameters of sea surface temperature are carried out using TS-GRNN. The best GRNN models for forecasting air temperature, air humidity, rainfall, duration of solar radiation, and wind speed were obtained by RMSE of 0.1421.

24.1 Introduction

Temperature is one of the important variables related to its role in the physical, chemical, and biological processes of the ocean [1]. Sea surface temperature (SST) is used to determine changes in momentum, heat, gas, and humidity throughout the air and

D. C. R. Novitasari (✉) · W. T. Puspitasari · R. R. Diah Nugraheni Setyowati · D. R. Santi · M. F. Rozi
UIN Sunan Ampel Surabaya, Ahmad Yani 117, Surabaya, Indonesia
e-mail: diancrini@uinsby.ac.id

R. Pramulya
University of Teuku Umar, Aceh, Indonesia

H. Rohayani
Adiwangsa Jambi University, Jambi, Indonesia

A. Widjajanto
Perak Maritime Meteorology, Station II Surabaya, Jl. Kalimas Baru No.97B, Surabaya, Indonesia

© The Editor(s) (if applicable) and The Author(s), under exclusive license to Springer Nature Singapore Pte Ltd. 2021

249

Y.-D. Zhang et al. (eds.), *Smart Trends in Computing and Communications: Proceedings of SmartCom 2020*, Smart Innovation, Systems and Technologies 182,
https://doi.org/10.1007/978-981-15-5224-3_24

sea interface. SST is one of the factors that influence marine productivity and climate change including summer and El Nino events [2, 3]. Indonesian water temperatures range from 28 to 38 °C, and Indonesian sea surface temperatures generally range from 19 to 26 °C, as a result of seasonal changes [1]. Changes in sea surface temperature are influenced by several factors including evaporation, air humidity, wind speed, duration of sun exposure, and air temperature [4].

Sea surface temperature can be measured using specialized tools. Observations are made manually by measuring at sea every day. This observation method is considered inefficient because the process is not easy and requires relatively expensive costs. Considerations are taken in the event of extreme weather that can hinder the observation process and be able to endanger the observer. In this case, a prediction system is needed that can predict current conditions and the next few days from sea surface temperature. Before predicting sea surface temperature, the first thing to do is to predict each of the sea surface temperature parameters.

To forecasting cases, a method is needed that is suitable for the problem and the data required. Some methods used for forecasting include autoregression integrated moving average (ARIMA) [5], Fourier regression, fractal analysis, neural networks [6], and adaptive neuro-fuzzy inference system (ANFIS) [7]. Elisa Farcua-Gorritz and Joan Garcia Sanchez have predicted sea surface temperatures in the Western Mediterranean Sea from satellite observations using a neural network. These observations show that neural networks can predict well [7], whereas other researchers predict sea surface temperature using nonlinear autoregression neural networks to obtain MSE results of less than 0.230 with a correlation coefficient of 0.9 [2]. S. B. Mahongo uses artificial neural networks for monthly predictions of sea surface temperature obtained by the correlation coefficient of 0.88 [8].

Based on several researches, some of the most frequently used methods in prediction are neural networks which are one of the models of artificial neural networks (ANNs) [9]. Besides neural networks, ANN has another model for time series data prediction, such as generated regression neural networks (GRNNs) [10]. The GRNN model consists of four layers, namely the input layer, the pattern layer, the sum layer, and the output layer [11]. In the input layer, a parameter of SST is used as input. Then, the activation function on the pattern layer is used. The results of activation are summarized in the summation layer through the process of arithmetic summation and weight summation [10]. The summary results are calculated until the final results obtained are predicted. GRNN has been used in predicting the level of air pollution in the city of Surabaya with good accuracy.

24.2 Sea Surface Temperature

Sea surface temperature (SST) is a factor that needs to be studied. Data from sea surface temperatures is used to predict the weather in the oceans related to their natural underwater life. Sea surface temperature has a relationship with the state of the seawater layer below, so that sea surface temperature data can be used as an

indicator to detect phenomena that occur at seas such as the front (the meeting of two water masses), currents, upwelling mass removal, and activity biological organism [4].

Sea temperature distribution occurs horizontally, which is influenced by geographic location (latitude) and vertically which is affected by depth. The temperature range in the ocean is quite outside starting from $-2\text{ }^{\circ}\text{C}$ for areas that are not affected by sunlight to $38\text{ }^{\circ}\text{C}$ in the surface area in the tropics [12].

24.3 GRNN

Generalized regression neural network (GRNN) is a model of ANN with supervised learning where the activation function uses the radial basis function (RBF). This method is generally used for forecasting/prediction cases where the output variable is modeled based on at least one input variable. GRNN is based on nonlinear regression theory formulated as in Eq. (24.1) [10].

$$E[y|X] = \frac{\int_{-\infty}^{\infty} yf(X, y)dy}{\int_{-\infty}^{\infty} f(X, y)dy} \quad (24.1)$$

where y is the output predicted by GRNN, while X is an input vector (x_1, x_2, \dots, x_p) consisting of p variables. $E[y|X]$ is the expected value of the output Y if given input vectors X , and $f(X, y)$ is a function of the joint probability density of X and Y . The final method in the output analysis of GRNN is calculating the accuracy of predictions by calculating the percent variance on the output variable explained by the input variable by calculating root mean square error (RMSE) [13].

In the GRNN optimization process, only one smoothing parameter must be adjusted once through the data, so that no iteration procedures are performed on GRNN. The estimation of these parameters is limited by the minimum and maximum values of the data. Furthermore, GRNN approaches the arbitrary function between input vectors and target vectors which can be divided into three, namely calculation of each smoothing factor variable, finding the best model, and visual analysis. Visual analysis is to calculate the accuracy of the model by calculating the variance on the output variable explained by the input variable by calculating MSE. The advantages of GRNN are the learning process and the rapid convergence to optimal regression surface even though the training data is very large in number [13]. Therefore, GRNN is a suitable method for making predictions.

GRNN consists of four layers of processing units, where each layer of processing units has a particular computational function when nonlinear regression is formed. The first layer consists of input neurons whose purpose is to retrieve information. These input neurons are unique for each predictor variable in the input vector X . No data processing occurs in these input neurons [14]. The input neurons then forward the data to the second layer, called the pattern neuron. A pattern neuron functions to combine and process data systematically with an activation function. The number

of pattern neurons is equal to the number of cases in the training set. The pattern I neurons contain data from input neurons and calculate the output θ_i by using the activation function in Eq. (24.2) [15].

$$\theta_i = e^{-(X-U_i)'(X-U_i)/2\sigma^2} \quad (24.2)$$

where X is the input vector of the predictor variable for GRNN, U is the training vector represented by the pattern I , and σ is the refinement parameter. The output of the neuron pattern is then sent to the third layer called the neuron summation [16]. Technically, there are two types of summation, namely simple arithmetic summation (sum of simple arithmetic) and weighted summation (weighted sum). In the GRNN topology, the training units separate to complete simple arithmetic summation and weighted summation.

The formulas for simple arithmetic summation and weighted summation are written in Eqs. (24.3) and 24.4 [17].

$$S_S = \sum_i \theta_i \quad (24.3)$$

$$S_W = \sum_i W_i \theta_i \quad (24.4)$$

where S_S is the simple arithmetic summation and S_W is weighted summation. The sum of the neuration summation is then sent to the fourth layer called the output neuron [18].

The output neuron then makes the following division to obtain the GRNN output y with Eq. (24.5) [19].

$$y = \frac{S_W}{S_S} \quad (24.5)$$

The GRNN architecture for one unit of output (univariate), which is used for forecasting time series data, is presented in Fig. 24.1.

24.4 Results and Discussion

The data used is daily data of sea surface temperature parameters from January 2009 to December 2017. The data includes average temperature, relative humidity, and duration of sun exposure/solar radiation. Data analysis was performed based on several tests to see the stationarity of the data. Table 24.1 presents a sample of the maritime weather data of Surabaya waters for nine years.

Furthermore, to analyze the pattern of time series data they have, plotting data and autocorrelation analysis on each data parameter is needed as shown in Figs. 24.2 and

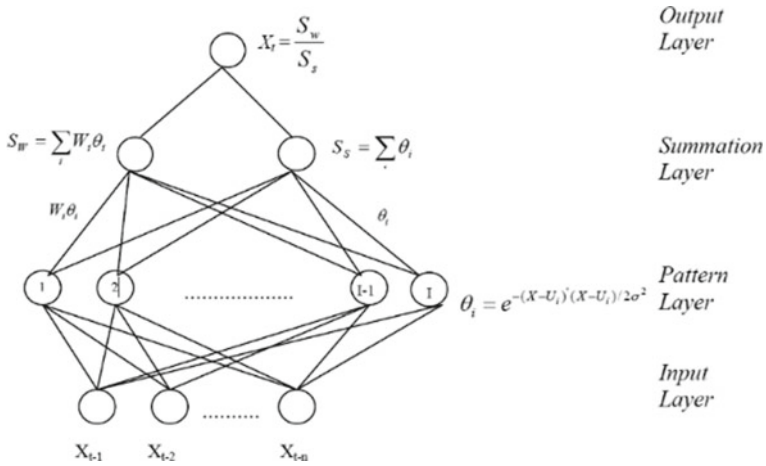


Fig. 24.1 GRNN architecture for one unit of output (univariate) used for forecasting time series data

Table 24.1 Daily data Surabaya sea surface temperature parameters

Date	Temperature	Humidity	Solar radiation
01/01/2017	29.2	79	3.5
02/01/2017	29.1	78	6.2
03/01/2017	27	89	4.9

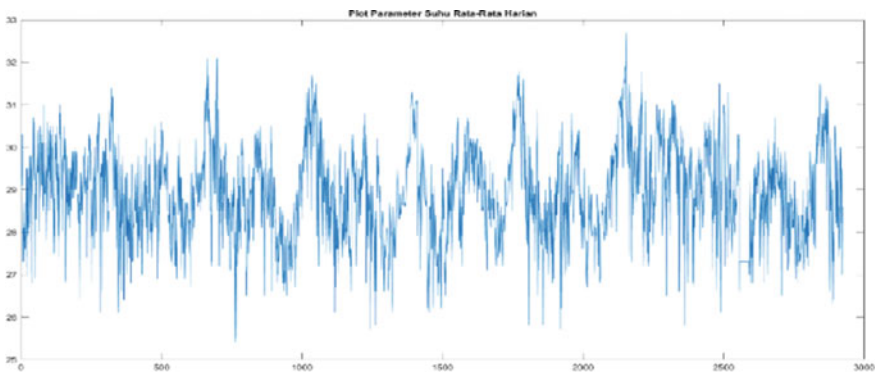


Fig. 24.2 Plot time series mean temperature data

24.3. Based on Fig. 24.2, it shows that the average temperature data in the Surabaya area has a seasonal pattern which is characterized by a pattern of changes that recurs automatically from day to another day. To find out whether the data is stationary can be seen from the autocorrelation function (ACF) plot in Fig. 24.3b.

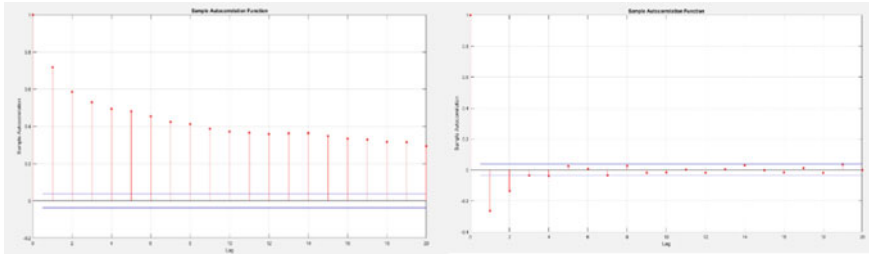


Fig. 24.3 **a** Plot autocorrelation function average temperature in Surabaya. **b** Autocorrelation function after one-time differencing

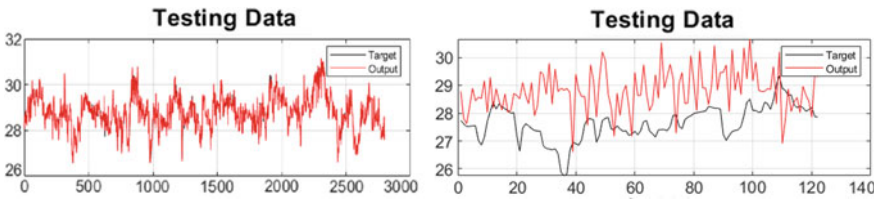


Fig. 24.4 **a** Plot of training result for forecasting sea surface temperature. **b** Plot of testing result for forecasting sea surface temperature

Figure 24.3 shows that the coefficient of autocorrelation from the first lag to the next lag decreases close to zero slowly so that it can be said that the daily temperature data is not stationary, and the results of the unit root test or the Dickey–Fuller test show that it does not have to reject the hypothesis $H_0 = 0$ which means the data has a root unit, so the data is not stationary. To convert the data into stable, differencing processes are needed.

After the differencing process is continued, the autocorrelation function test is continued. For this temperature data, differencing is performed once and then the autocorrelation function test is continued. The autocorrelation function plot is shown in Fig. 24.3b. The same process is applied to other surface temperature parameters. Then, proceed the forecasting stage.

Before construction of GRNN models to predict sea surface temperature parameter, parameter maritime weather data needs to be normalized first. Sample data for each normalized sea surface temperature parameter is given in Table 24.2.

The normalized data is divided into two processes; there are training data and testing data with a ratio of 80%: 20%.

Table 24.2 Samples daily data Surabaya sea surface temperature parameters

Date	Temperature	Humidity	Solar radiation
01/12/2017	0.51	0.57	0.37
02/12/2017	0.50	0.55	0.58
03/12/2017	0.28	0.78	0.48

Table 24.3 Pattern from average temperature data

Data $t - n$	X_1	X_2
1	0.6369	0.50548
2	0.5712	0.6370
3	0.4616	0.5055
4	0.5164	0.4616

Table 24.4 Result prediction SST using GRNN

Date	Actual	Result of forecasting
31/8/2017	27.7	27.7
1/9/2017	27.8	27.8
2/9/2017	27.74	28.79

The time series is built from training data as training input and SPL forecasting targets for the next 3 h. Table 24.3 shows the pattern of input training on average temperature data. The same process is applied to humidity and sun exposure time data.

Based on Table 24.3, time series data on average temperature, average humidity, and irradiation time are data at time $t - 3$, $t - 2$, and $t - 1$ with the target t predicted time. Next, the training data input pattern is predicted using GRNN. In the training process, the training data input patterns are used as input. Then, the weight is calculated using Eq. (24.2), so that we get the optimal weight.

Next, the optimal weights are entered in Eqs. (24.3) and (24.4). Then, the forecast output is calculated using Eq. (24.5). The forecast results are normalized so that the range of forecast values is the same as the actual value. The results of testing sea surface temperature data forecasting are shown in Table 24.4 and Fig. 24.4.

In the training process, test the spread value to get the best results. Based on training process, the best model with speed 0, 0.001 has an RMSE of 0.1421. Spread values of more than 0.001 have a greater RMSE. As well as smaller spreads also have larger RMSE. If the forecasting model has a large RMSE, then there are some errors in the experiment; the smaller the RMSE value, the better the model. So, the estimated spread value cannot be determined precisely but through several experiments. The best model represents that the model is able to predict sea surface temperature well, where the forecast results approach the actual data; spread test results are shown in Table 24.5.

Table 24.5 RMSE value from the spread experiment

Spread	RMSE
1	0.7327
0.1	0.6194
0.05	0.6525
0.001	0.1421
0.0009	0.14216

24.5 Conclusion

The GRNN model includes a neural network model with fast solutions because no large iteration is needed in the weight estimation process. This model also has a standard network architecture, where the number of pattern layer units is the same as the input layer unit.

In this research, the best GRNN model for forecasting sea surface temperature was obtained with an RMSE of 0.1421. Based on experimental results, it shows that forecasting sea surface temperature using GRNN produces a good model. For further research, it is necessary to optimize the weights between the input layer and the hidden layer, because on the GRNN network, weights are taken randomly. With weight optimization, it might get better results beforehand.

References

1. Kantun, W.: *Pengolahan Perikanan Tuna*. UGM Press, Yogyakarta
2. Patil, K., Deo, M.C., Ghosh, S., Ravichandran, M.: Predicting sea surface temperatures in the North Indian Ocean with nonlinear autoregressive neural networks. *Int. J. Oceanogr.* **2013**, 1–11 (2013)
3. Prarikeslan, W.: *Oseanografi*. Kencana, Jakarta
4. Hutabarat, S.: Pengaruh Kondisi Oseanografi terhadap Perubahan Iklim, Produktivitas dan Distribusi Biota Laut. Fakultas Perikanan dan Ilmu Kelautan Universitas Diponegoro, Semarang
5. Sutikno, B.R.D., Susanti, P.: Istriana. Prakiraan Cuaca Dengan Metode Autoregressive Integrated Moving Average, Neural Network, Dan Adaptive Splines Threshold Autoregression Di Stasiun Juanda Surabaya. *J. Sains Dirgant.* **8**(1), 43–61 (2010)
6. Garcia-Gorritz, E., Garcia-Sanchez, J.: Prediction of sea surface temperatures in the western Mediterranean Sea by neural networks using satellite observations. *Geophys. Res. Lett.* **34**(11), 1–6 (2007)
7. Adyanti, D.A., Asyhar, A.H., Novitasari, D.C.R., Lubab, A., Hafiyusholeh, M.: Forecasts marine weather on java sea using hybrid methods: Ts-anfis. *Int. Conf. Electr. Eng. Comput. Sci. Informatics* **4**, 492–497 (2017)
8. Mahongo, S.B., Deo, M.C.: Using artificial neural networks to forecast monthly and seasonal sea surface temperature anomalies in the Western Indian Ocean. *Int. J. Ocean Clim. Syst.* **4**(2), 133–150 (2013)
9. Faye, S., Lazar, A., Sow, B.A., Gaye, A.T.: A model study of the seasonality of sea surface temperature and circulation in the Atlantic North-eastern tropical upwelling system. *Front. Phys.* **3**(September), 1–20 (2015)

10. Warsito, B., Rusgiyanto, A., Amirallah, M.A.: Pemodelan general regression neural network. *Med. Stat.* **1**(1), 43–51 (2008)
11. Tai, K.S., Socher, R., Manning, C.D.: Improved semantic representations from tree-structured long short-term memory networks. In: Proceedings of the 53rd Annual Meeting of the Association for Computational Linguistics and the 7th International Joint Conference on Natural Language Processing, vol. 1 Long Paper, pp. 1556–1566 (2015)
12. Yona D. Fundamental Oseanografi. Pertama. UB Press, Malang
13. Specht, D.F.: A general regression neural network. *IEEE Trans. Neural Networks* **2**(6), 568–576 (1991)
14. Kannan, E., Saravanan, M.S.: Generalized regression neural network **10**(4), 563–569 (2014)
15. Alkaff, M., Sari, Y.: Penerapan Generalized Regression Neural Networks untuk Memprediksi Produksi Padi Terhadap Perubahan Iklim. **2**(2), 117–124 (2017)
16. Sun, X., Liu, J., Zhu, K., Hu, J.: Generalized regression neural network association with terahertz spectroscopy for quantitative analysis of benzoic acid additive in wheat flour (2019)
17. Ghritlahre, H.K., Prasad, R.K.: Exergetic performance prediction of solar air heater using MLP, GRNN and RBF models of artificial neural network technique. *J. Environ. Manage.* **223**, 566–575 (2018). <https://doi.org/10.1016/j.jenvman.2018.06.033>
18. Caraka, R.E.: Modeling Crude Oil Prices (CPO) using General Regression Neural Network (GRNN) (1) (2017)
19. Yadav, V., Nath, S.: Daily prediction of PM 10 using radial basis function and generalized regression neural network. In: 2018 Recent Advanced Engineering Technology and Computer Science, pp. 1–5 (2018)

Chapter 25

Natural Disaster Predictions of Whirlwinds in Cilacap Region of Central Java Using Adaptive Neighborhood Modified Backpropagation (ANMBP)



Dian Candra Rini Novitasari , Fitria Febrianti , Arnita ,
Rinda Nariswari , R. R. Diah Nugraheni Setyowati , Putri Wulandari ,
Ahmad Zoebad Foeady , Moh. Hafiyusholeh , and Fajar Setiawan 

Abstract BNPB's data shows that in the last 10 years, the province of Central Java was the most whirlwind region if compared with other provinces in Indonesia which amounted to 1281 incidents and whirlwinds most often in Cilacap which amounted to 202 incidents. The purpose of this research was to predict whirlwind in Cilacap region of Central Java using meteorological parameters as predictive parameters and adaptive neighborhood modified backpropagation (ANMBP) parameters as a prediction method. In the preprocessing process, the input data variable was reduced from seven input variables to five input variables by using the principal component analysis (PCA) method. The prediction process using ANMBP, and trial and error processes are carried out repeatedly by changing the hidden layer values, learning rate, and the amount of training and testing data. The best performance is obtained from the distribution of training and testing data at 60–40%, it produced an MSE value of 0.0004, and accuracy is 85.59% using two hidden layers with values of 110 and 95 and learning rate of 0.1.

D. C. R. Novitasari (✉) · F. Febrianti · R. R. Diah Nugraheni Setyowati · P. Wulandari ·
A. Z. Foeady · Moh. Hafiyusholeh
UIN Sunan Ampel Surabaya, Jl Ahmad Yani No. 117, Surabaya, Indonesia
e-mail: diancrini@uinsby.ac.id

Arnita
Universitas Negeri Medan, Jl. Willem Iskandar Ps. V, Medan, Indonesia

R. Nariswari
Bina Nusantara University, 11480, Jakarta, Indonesia

F. Setiawan
Perak Maritime Meteorology Station II, Jl. Kalimas Baru No. 97B, Surabaya, Indonesia

© The Editor(s) (if applicable) and The Author(s), under exclusive license
to Springer Nature Singapore Pte Ltd. 2021

Y.-D. Zhang et al. (eds.), *Smart Trends in Computing and Communications: Proceedings
of SmartCom 2020*, Smart Innovation, Systems and Technologies 182,

https://doi.org/10.1007/978-981-15-5224-3_25

25.1 Introduction

Whirlwinds are one of the natural disasters that have a big impact on environmental damage, loss of property, and the emergence of casualties [1]. Whirlwinds are defined as strong winds that come suddenly, have a center, a circular motion resembling a spiral with a speed of 40–50 km/h to touch the surface of the earth, and will disappear in a short time (3–5 min) [2, 3]. Whirlwinds are disasters caused by meteorological parameters. The meteorological parameters obtained from radiosonde observations are carried out by BMKG. The radiosonde is a type of upper-air observation based on technology to determine meteorological conditions in the atmosphere [4, 5]. Some parameters that can be obtained from radiosonde and used to predict whirlwinds are Lifted Index (LI), Severe Weather Threat Index (SWEAT), Convective Available Potential Energy (CAPE), K Index (KI), Convective Inhibition (CIN), Total Totals (TT), and Showalter Index (SI). Each of these parameters has criteria and forecast guidelines that can be used to predict a whirlwind.

The loss caused by whirlwinds can be minimized by predicting the arrival of a whirlwind. To predict the arrival of a whirlwind, the classification is carried out on the parameters obtained from the upper-air observations [6]. Several methods that can be used for classification are K-nearest neighbors (KNN), support vector machine (SVM) [7], naïve Bayes classifier [8], backpropagation [9], adaptive neighborhood modified backpropagation (ANMBP) [10], and other classification methods.

Adaptive neighborhood modified backpropagation (ANMBP) is the development of the backpropagation classification method [10]. In the backpropagation algorithm, there are desired input and output patterns, when the network is patterned, the weight value will be changed so that it can minimize the differences in the output pattern of the network and the desired output pattern. ANMBP combines linear error values and nonlinear error values, neighborhood and adaptive learning rate on backpropagation [11]. Some researches that use ANMBP as a classification method are classifying EEG signals based on normal conditions and epilepsy using fuzzy c-means method, and the accuracy value obtained is 74.37% [11], classifying mammogram data using wavelet transformation and ANMBP to detect breast cancer, and the error value obtained is 0.00096204 [10], classifying brain MRI using ANMBP based on wavelet data which is reduced by NCMF that produces an accuracy value of 91.25% [12].

The main goal of the study is to predict the whirlwind based on meteorological parameters in Cilacap region of Central Java. The preprocessing was applied by principal component analysis (PCA) method to reduce the dimensions of input parameters. The prediction process was carried out with various experiments (changing the hidden layer values, learning rate, and the amount of training and testing data) using ANMBP method to find the best model for predicting the whirlwind.

25.2 Principal Component Analysis (PCA)

Principal component analysis (PCA) is a method that can be used to simplify observed variables (observation variables) by reducing their dimensions [13]. The PCA method solves the problem by looking at eigenvalues which are more than one [14]. Before doing a simplification of variables by reducing, the thing to do is KMO test and Bartlett’s test to see the provisions using PCA as a reduction method using the following Eq. (25.1),

$$KMO = \frac{\sum_{i=1}^p \sum_{j=1}^p r_{ij}^2}{\sum_{i=1}^p \sum_{j=1}^p r_{ij}^2 + \sum_{i=1}^p \sum_{j=1}^p a_{ij}^2} \tag{25.1}$$

where r_{ij} is the correlation coefficient between variables i and j , a_{ij} is the partial correlation coefficient between variables i and j , and the variable will be said to be appropriate using the PCA method if the KMO value is smaller than 0.5 [15, 16].

25.3 Adaptive Neighborhood Modified Backpropagation (ANMBP)

Adaptive neighborhood modified backpropagation (ANMBP) is a development of the backpropagation algorithm. In ANMBP, there is a combination of the number of linear errors and nonlinear errors using adaptive parameter learning and there are neighborhood structures in hidden layers [17]. The ANMBP algorithm can accelerate convergence by reducing iterations, avoiding minimum locality, and reducing memory [11, 18]. In the ANMBP algorithm, linear errors and nonlinear errors in each unit are obtained from this equation,

$$u_j^s = \sum_{i=1}^n w_{ji}^s y_i^{s-1} \tag{25.2}$$

$$f(u_j^s) = \frac{1}{(1 + e^{-u_j^s})} = y_j^s \tag{25.3}$$

where n is the number of units and w_{ji}^s is the weight of the i unit from the layer ($s - 1$) to the j unit from the layer s (output layer) and y is the output generated by the network [10, 19]. Equation E_p is used to calculate the error value obtained from the sum of the squares of linear errors and nonlinear errors obtained from the output which is as follows [20]

$$E_p = \sum_{j=1}^n \frac{1}{2} (e_{1j}^s)^2 + \sum_{j=1}^n \frac{1}{2} \lambda (e_{2j}^s)^2 \tag{25.4}$$

where η is a learning rate, e_1 is a nonlinear error, and e_2 is a linear error obtained from the following equation,

$$e_{1j}^s = d_j^s - y_j^s \tag{25.5}$$

$$e_{2j}^s = ld_j^s - u_j^s \tag{25.6}$$

$$ld_j^s = f^{-1}(d_j^s) \tag{25.7}$$

where d is the desired output and y is the output generated by the network. So that the weight changes in the output layer use the following equation

$$\Delta w_{ji}^s = -\mu \frac{\partial E}{\partial W_{ji}} \tag{25.8}$$

$$\Delta w_{ji}^s = \mu e_{1j}^s f'(u_j^s) y_i^{s-1} + \mu \lambda_{2j}^s y_i^{s-1} \tag{25.9}$$

The equation used to obtain linear error values and nonlinear errors is as follows,

$$e_{1j}^L = \sum_{r=1}^{n_{L+1}} f(u_r^{L+1}) e_{ir}^{L+1} w_{rj}^{L+1} \tag{25.10}$$

$$e_{2j}^L = f^1(u_j^L) \sum_{r=1}^{n_{L+1}} e_{2r}^{L+1} w_{rj}^{L+1} \tag{25.11}$$

So to get the weight change value in the hidden layer use the following equation,

$$\Delta w_{ji}^L = \mu e_{1j}^L y_i^{L-1} f'(u_j^L) + \mu \lambda_{2j}^L y_i^{L-1} \tag{25.12}$$

Learning parameters and are replaced with the following adaptive parameters

$$\eta' = \frac{\mu \|y^2\|}{J \|p y^2\| + \varepsilon} \tag{25.13}$$

$$\mu' = \frac{\lambda \|y^2\|}{J \|p y^2\| + \varepsilon} \tag{25.14}$$

where $e_{1j}^s = d_j^s - y_j^s$ and $J_p^T = \frac{\partial y_p}{\partial w_{ji}}$, so the adaptive learning parameter becomes this equation,

$$\eta' = \frac{\mu \|e_{1j}^2\|}{\|f'(u_j) y_j^{s-1} e_{1j}^2\| + \varepsilon} \tag{25.15}$$

$$\mu' = \frac{\lambda \|e_{1j}^2\|}{\|f'(u_j)y_j^{s-1}e_{1j}^2\| + \varepsilon} \tag{25.16}$$

where λ and ε are constants with small positive values and μ' is a constant with a small positive value used to guarantee instability when the error value becomes 0 [21]. So the weight change in the output layer and the hidden layer becomes the following equation

$$\Delta w_{ji}^S = \eta' e_{1j}^S f'(u_j^S) y_j^{S-1} + \mu' e_{2j}^S y_j^{S-1} \tag{25.17}$$

With this weight change, so the new weights are calculated using the following equation,

$$w(t + 1) = w(t) + \Delta w(t) \tag{25.18}$$

with t shows the iterations.

25.4 Results and Discussion

25.4.1 Preprocessing Data

The data used in this research is upper-air observation data and whirlwinds data in Cilacap region of Central Java for 2 years, from March 2016 to February 2018. The upper-air observation data consists of 7 variables, namely Lifted Index (LI), Severe Weather Threat Index (SWEAT), Convective Available Potential Energy (CAPE), K Index (KI), Convective Inhibition (CIN), Total Totals (TT), and Showalter Index (SI) as given in Table 25.1.

In the next step, a variable reduction will be carried out on the data using the PCA method. The first thing to do is doing the KMO test on the data and getting the accuracy of the data using PCA. The KMO test results are given in Table 25.2.

Then, to find out which variables will be reduced, the transformation will be carried out using the varimax factor rotation methodology. So that the following results obtained are given in Table 25.3.

25.4.2 Whirlwind Predictions Using ANMBP

In this research, the tornado prediction process using ANMBP was not calculated manually but the prediction process was assisted by using the MATLAB application to support the calculation process. To optimize the prediction results using ANMBP

Table 25.1 Sample of upper-air observation data

Date on March 2019	Time (hour)	Upper-air observation variable						
		SI	LI	SWEAT	KI	TT	CAPE	CIN
02	0	-1.14	-2.02	223.2	39.1	46.3	256.77	-82.55
	12	1.62	-0.76	199.4	29.2	41.7	322.23	-30.81
03	0	-0.37	-0.98	209.8	33.6	43.9	152.47	-63.75
	12	-2.7	-1.55	245.8	40.9	47	107.46	-33.98
04	0	-0.99	-2.46	223.38	37.3	44.8	391.55	-11.78
	12	0.72	-1.78	212.81	36.9	41.7	476.55	-18.96
05	0	0.42	-1.07	223.38	37.6	42.5	226.8	-19.92
	12	0.34	-1.76	210.2	34.8	42.8	379.63	-26.69

Table 25.2 KMO test

Kaiser–Meyer–Olkin test of sampling adequacy		0.761
Bartlett’s test of sphericity	Approx. chi-square	5134.720
	<i>Df</i>	21
	Sig.	0.000

Table 25.3 Factor rotation using the varimax method

	Component	
	1	2
SI	-0.930	0.241
LI	-0.857	-0.354
SWEAT	0.695	-0.277
KI	0.826	-0.135
TT	0.890	-0.250
CAPE	0.630	0.606
CIN	0.082	0.802

in the training process, researchers used two hidden layers with different values, the learning rate values ranged from 0.1 to 0.5, and divided the training data and tested the data into three different patterns, there are 60% training data and 40% test data, 70% training data and 30% testing data, and 80% training data and 20% testing data.

25.5 Discussion

Based on KMO test of upper-air observation data (LI, SWEAT, CAPE, K Index (KI), CIN, TT, and SI), the significance value that was obtained at KMO test is 0.761, and it indicates that the input data meets the requirements for variable reduction because the value is more than 0.5.

Table 25.4 shows the relationship between the original variable and the main component variable formed by PCA and is called the loading value. The selected loading value is more than 0.5, where this value is considered to be able to explain the variables that affect the occurrence of whirlwinds, while variables that have a loading value of less than 0.5 are considered to be unable or less influential on the appearance of whirlwinds. So, from Table 25.4, it can be seen that the SI and LI variables which have a loading value of less than 0.5 are -0.93 and -0.857 which are less influential in predicting the occurrence of whirlwinds. Then, the SI and LI variables will be reduced so that the upper-air observation data that will be used as the input variable to predict whirlwinds has 5 variables, namely SWEAT with a loading value of 0.695, KI with a loading value of 0.826, TT with a value of 0.89, CAPE with a loading value of 0.63, and CIN with a loading value of 0.802.

Then, the selected parameters are entered into the ANMBP algorithm where in this study several experiments were conducted. Based on the results of the study, the computational time to predict the whirlwind is influenced by the number of epochs and nodes in the hidden layer. The more the number of nodes and epoch, the longer the calculation time on the model prediction. Determination of hidden layer composition affects the error value obtained; from the results of experiments carried out, the more the number of nodes, the smaller the MSE value obtained, which indicates that the better the prediction model formed. In addition, according to [12] explained that the greater the learning rate, the range for determining weight changes is greater so that it is often trapped in minimum local conditions.

Table 25.4 shows the best prediction results for each pattern formed. The training data and testing data as much as 60% (874 data) and 40% (583 data), 30 and 50 hidden layers, 0.3 learning rate resulted in an accuracy of 85.42% and 0.0003 with 3000 iterations and required 4383 s. By using the same analysis, the best predictive results for training and testing data were obtained 60% and 40% using 110 and 95 hidden layers, 0.5 learning rate. On training and testing data, as much as 70% and 30% produce the best predictions using hidden layers 110 and 95, and 0.5 learning rate. 80% of training data and 20% of data testing produced the best predictions using 90 and 75 hidden layers, and 0.4 learning rate [15].

Table 25.4 ANMBP prediction results

ANMBP parameter		Prediction result							
Training data (%)	Testing data (%)	HL 1	HL 2	Epoch	LR	Time (second)	MSE	Accuracy	Prediction correctly
60	40	30	15	3000	0.3	4383	0.0003	85.42	498
		50	35	3000	0.1	9134	0.0007	85.59	499
		70	55	3000	0.1	12.541	0.0005	85.42	498
		90	75	361	0.5	2299	0.00009	85.07	496
		110	95	369	0.5	3059	0.00004	85.59	499
70	30	30	15	1545	0.3	2548	0.00009	82.37	360
		50	35	270	0.4	943	0.00009	82.37	360
		70	55	909	0.5	8089	0.00009	82.37	360
		90	75	3000	0.5	25433	0.014	82.15	359
		110	95	2293	0.5	26725	0.00005	82.60	361
80	20	30	15	369	0.5	718	0.00009	76.20	222
		50	35	157	0.3	618	0.00009	76.60	223
		70	55	15	0.5	85	0.00008	76.20	222
		90	75	76	0.4	628	0.00003	76.60	223
		110	95	297	0.4	2392	0.00003	76.20	222

25.6 Conclusion

Based on the results and discussion of whirlwind prediction research using adaptive neighborhood modified backpropagation in the Cilacap region of Central Java, it can be concluded that of the seven input variables, five variables have a strong influence on the occurrence of whirlwinds, namely SWEAT, KI, TT, CAPE, and CIN. The optimal parameters used in the training data are 60% (874 data) and testing data are 40% (583 data) using 110 layer 1 hidden, 95 layer 2 hidden, and 0.5 learning rate. Training data is 70% (data 1020) and testing data is 30% (437 data) using 110 layer 1 hidden, 95 layer 2 hidden, and 0.5 learning rate. Training data is 80% (data 1166) and testing data is 20% (291 data) using 90 layer 1 hidden, 75 layer 2 hidden, and 0.4 learning rate. Prediction using testing data is 40% (583 data), resulting in accuracy and MSE of 82.6% and 0.00004 with 499 event data that can be predicted correctly. Prediction using test data is 30% (437 data), resulting in 82.6% accuracy and MSE of 0.00005 with 361 event data being predicted correctly. Prediction using data testing is 20% (291 data), resulting in accuracy and MSE of 76.6% and 0.00003 with 223 data events that can be predicted correctly. In this study, the amount of data in each class processed is not the same. So it causes imbalanced data in training and testing.

References

1. Ginzburg, E.: *Journey into the Whirlwind*. Houghton Mifflin Harcourt, Boston
2. Suryantoro, A.: Siklon Tropis di Selatan dan Barat Daya Indonesia dari Pemantauan Satelit TRMM dan Kemungkinan Kaitannya dengan Gelombang Tinggi dan Puting Beliung. *Maj. Sains dan Teknol. Dirgant.* **3**(1) (2010)
3. Harsa, H., Linarka, U.A., Kurniawan, R., Noviati, S.: Pemanfaatan Sataid Untuk Analisa Banjir dan Angin Puting Beliung: Studi Kasus Jakarta dan Yogyakarta. *J. Meteorol. dan Geofis.* **12**(2) (2011)
4. Doswell, C.A., Weiss, S.J., Johns, R.H.: Tornado forecasting: a review 557–571 (2011)
5. BNPB. *Risiko Bencana Indonesia*. Jakarta
6. Doswell, C.A.: Tornado Forecasting : a review (2015)
7. Foeady, A.Z., Novitasari, D.C.R., Asyhar, A.H., Firmansjah, M.: Automated diagnosis system of diabetic retinopathy using GLCM method and SVM classifier. In: 2018 5th International Conference on Electrical Engineering, Computer Science and Informatics, pp. 154–160 (2019)
8. Rini, D.C., Farida, Y., Puspitasari, D.: Klasifikasi Menggunakan Metode Hybrid Bayessian-Neural Network (Studi Kasus: Identifikasi Virus Komputer). *J. Mat. "MANTIK."* **1**(2), 38 (2016)
9. Soediono, B.: Backpropagation. *J. Chem. Inf. Model.* **53**, 160 (1989)
10. Werdingingsih, I.: Transformasi Wavelet dan Adaptive Neighborhood Based Modified back-propagation (ANMBP) untuk Klasifikasi Data Mammogram. *SCAN.* **IX**, 15–21 (2014)
11. Novitasari, D.C.R.: Klasifikasi Sinyal EEG Menggunakan Metode Fuzzy C-Means Clustering (FCM) Dan Adaptive Neighborhood Modified Backpropagation (ANMBP). *J. Mat. MANTIK.* **1**(1), 31–36 (2015)
12. Astuti, L.W., Handayani, T.: Klasifikasi MRI Otak Menggunakan Jaringan Syaraf Tiruan Berdasarkan Data Wavelet Yang Direduksi Dengan NCMF. In: *Seminar Nasional Informatika, Yogyakarta* (2012)

13. Herrera, L.J., Rojas, I., Pomares, H., Guillen, A., Valenzuela, O., Banos, O.: Classification of MRI images for Alzheimer's disease detection. In: 2013 International Conference on Social Computing
14. Abdi, H., Williams, L.J.: Principal component analysis. *Wiley Interdiscip. Rev. Comput. Stat.* **2**(4), 433–459 (2010)
15. dan Azizah, E.I., Lathif, M.F.A.: Prinsip Fisis Atmosfer Observasi Permukaan Dan Udara Atas. STMKG, Jakarta
16. Wold, S., Esbensen, K., Geladi, P.: Principal component analysis. *Chemom. Intell. Lab. Syst.* **2**(1–3), 37–52 (1987)
17. Singh, E.M., Sharma, A.K.: Diabetes mellitus with ANMBP method on human body part. *OAIJSE* (2017)
18. Werdiningsih, I., Zaman, B., Nuqoba, B.: Application of wavelet transformation and adaptive neighborhood based modified backpropagation (ANMBP) for classification of brain cancer. In: AIP Conference Proceedings, AIP Publishing, 20004 (2017)
19. Supriyati, E., Iqbal, M.: Recognition system of Indonesia sign language based on sensor and artificial neural network. *Makara J. Technol.* **17**(1), 25–31 (2013)
20. Lesmana, I.P.D., Widiawan, B.: Evolving neighborhood based adaptive neural network for breast cancer detection
21. Kathirvalavakumar, T., Subavathi, S.J.: Neighborhood based modified backpropagation algorithm using adaptive learning parameters for training feedforward neural networks. *Neurocomputing* **72**(16–18), 3915–3921 (2009)

Chapter 26

Designing Memristor-Based Timing Circuits and Performance Comparison with CMOS Counterparts



Abir Jana, Disha Bhattacharjee, Komal Kumari, Anup Dey, Bijoy Goswami, and Subir Kumar Sarkar

Abstract The implementation of Memristor will have a wider range of applications in various fields. Digital switching systems depend on reliable and high-quality synchronization from timing circuits and they are the fundamental units of ICs. So we designed timing circuits using hybrid integration of Memristor using the TEAM model, which is simplified yet captures all main characteristics and CMOS (90 nm technology). Timing circuits like astable multivibrator, voltage-controlled oscillators (VCO) are designed and we analyzed all the important parameters like frequency stability, delay, power, phase noise, noise factor, no of devices used and compare them with the timing circuits designed by conventional CMOS. All the circuits are designed and simulated in Virtuoso Cadence.

26.1 Introduction

Memristor (memory resistor) is inferred as the fourth fundamental, passive device with bi-terminal component relating magnetic flux linkage Φ and electric charge q [1–3]. The memristor modeling is detailed in Sect. 26.2.

A. Jana (✉) · D. Bhattacharjee · K. Kumari · A. Dey · B. Goswami · S. K. Sarkar
Department of E.T.C.E, Jadavpur University, Kolkata 700032, India
e-mail: abir93j@gmail.com

D. Bhattacharjee
e-mail: dishabhattach.v@gmail.com

K. Kumari
e-mail: komalkumari.etce.rs@jadavpuruniversity.in

A. Dey
e-mail: anupetce@gmail.com

B. Goswami
e-mail: bijoy.ete@aec.ac.in

S. K. Sarkar
e-mail: su_sircir@yahoo.co.in

© The Editor(s) (if applicable) and The Author(s), under exclusive license to Springer Nature Singapore Pte Ltd. 2021

Y.-D. Zhang et al. (eds.), *Smart Trends in Computing and Communications: Proceedings of SmartCom 2020*, Smart Innovation, Systems and Technologies 182,
https://doi.org/10.1007/978-981-15-5224-3_26

The new approach to hybrid technologies of memristor and CMOS is to achieve the consequential solution from dissolution of Moore's law. Since Memristor is passive so it cannot provide energy to the circuits so they can be more efficient if they are composite with transistors like CMOS where CMOS can provide the functional flexibility and memristor can contribute the high density, low power and non-volatile attributes to system. Moreover hybrid structure can extend CMOS life without further shrinking. Here all the circuits are realized by hybrid integration of Memristor and CMOS technology. This hybrid technology can be used to consummate any analog [4] as well as digital circuits like Logic Gates; NAND Gate is detailed in Sect. 26.3. And using the logic gates like NAND gate we can simulate all sequential and combinational circuits. In this paper we have realized timing circuits like astable multivibrator and voltage-controlled oscillators (VCO) at dc operating voltage of 1.8 V. These circuits are simulated in Virtuoso Cadence and the output waveforms are simulated in Spectre, the schematics and outcome of all the circuits are presented in Sects. 26.4 and 26.5. Analyzing the outcomes of Memristor CMOS hybrid structure we found significance reduction of power, higher endurance and more desirable performance than just conventional CMOS. Section 26.6 discuss conclusion the future prospects of memristor.

26.2 Memristive Device Modeling

Memristor is basically a 2-terminal nanoscale device which provides a relation between magnetic flux and electric charge q developing strong electric field causing several phenomena. Resistance change is always electrically induced by current or voltage and the present resistance is non-volatile and can maintain its state even if the input power supply is removed, and thus it remembers its most recent resistance until it is turned on again [5–7].

A memristor can be used as a building block which can store an input value, an output value, perform logic operation [8] and Boolean function, act as a state register such as latch or flip flop, also act as a configurable switch, perform signal routing. Memristive devices has attracted considerable interest in many areas including neuromorphic and reconfigurable computing architectures [3], memory cells where a single memristor can be configured to two or more discrete states [2]. Other applications like crossbar latches, pattern recognition, analog softcomputing, programmable logic, signal processing, radio frequency identification etc. Formally, a voltage-controlled time-invariant memristive device is represented by Eqs. (26.1) and (26.2):

$$i(t) = M(w, v)v(t) \quad (26.1)$$

$$\frac{dw}{dt} = f(w, v) \quad (26.2)$$

where $M(w, v)$ is the memristance of the device, where f and w are the explicit functions of time and a set of state variables, respectively. Voltage and current with respect to time are represented as $V(t)$ And $i(t)$.

The memristive model that we used to analyze our circuits is TEAM (Threshold Adaptive Memristor) that has the derivative of the state variable given by Eqs. (26.3, 26.4, 26.5), (26.3, 26.4, 26.5) and (26.3, 26.4, 26.5).

$$\frac{dw}{dt} = \begin{cases} k_{\text{off}} \left(\frac{i(t)}{i_{\text{off}}} \right)^{\alpha_{\text{off}}} \cdot f_{\text{off}}(w), & 0 < i_{\text{off}} < i \\ 0, & i_{\text{on}} < i < i_{\text{off}} \\ k_{\text{on}} \left(\frac{i(t)}{i_{\text{on}}} - 1 \right)^{\alpha_{\text{on}}} \cdot f_{\text{on}}(w), & i < i_{\text{on}} < 0 \end{cases} \quad (26.3, 26.4, 26.5)$$

where i_{on} and i_{off} are current threshold parameters, w is the set of state variables, which represents the effective electric tunnel width, α_{on} and α_{off} parameters define the adaptive nonlinearity of device, k_{on} and k_{off} are the constant fitting parameters of memristor, k_{off} is a positive number, while k_{on} is a negative number, and $f_{\text{on}}(w)$ and $f_{\text{off}}(w)$ are the window functions, represent the dependence on the state variable. Current-Voltage Relationship while memristance change linearly in TEAM Model is given by Eq. (26.6):

$$v(t) = \left[R_{\text{ON}} + \frac{R_{\text{OFF}} - R_{\text{ON}}}{w_{\text{off}} - w_{\text{on}}} (w - w_{\text{on}}) \right] i(t) \quad (26.6)$$

Several window functions are implemented such as: Jogelkar, Biolek, Prodromakis. We need TEAM (named Kvatinsky in the Verilog-A model) in this analysis which is not necessary symmetric but resolve boundary conditions and impose non-linear drift. The window function of the TeAM model for state variable $x_{\text{on}} \leq x \leq x_{\text{off}}$ in the undoped region can be defined by Eqs. (26.7) and (26.8):

$$f_{\text{off}}(w) = \exp \left[- \exp \left(\frac{w - a_{\text{off}}}{x_c} \right) \right] \quad (26.7)$$

$$f_{\text{on}}(w) = \exp \left[- \exp \left(\frac{w - a_{\text{on}}}{x_c} \right) \right] \quad (26.8)$$

Some basic concepts of memristor are shown in Fig. 26.1 for two different polarities. We specify increased resistance as R_{ON} which implies logic 0 and decreased resistance as R_{OFF} which implies logic 1. Hence for a memristor, $R_{\text{ON}} \gg R_{\text{OFF}}$.

The primary characteristics of a memristor are (i) The transient response of voltage and current waveform of a memristor having identical Zero-crossing points as shown in Fig. 26.2a (ii) The memristor, response to a sinusoidal excitation of a.c. measurements give rise to a distinctive pinched hysteresis loop shown in Fig. 26.2b, the memory is encoded in the hysteresis, memristance is bounded between minimum R_{ON} and maximum R_{OFF} and limited to 1st and 3rd quadrant (iii) Pinched Hysteresis Loop is Frequency-Dependent: as frequency increases it ascends to become a linear resistance which is shown in Fig. 26.2c [9].

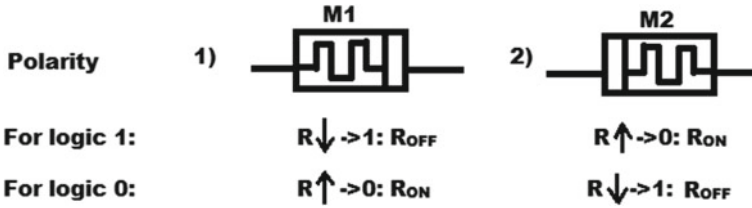


Fig. 26.1 Basic concept for resistance of memristor

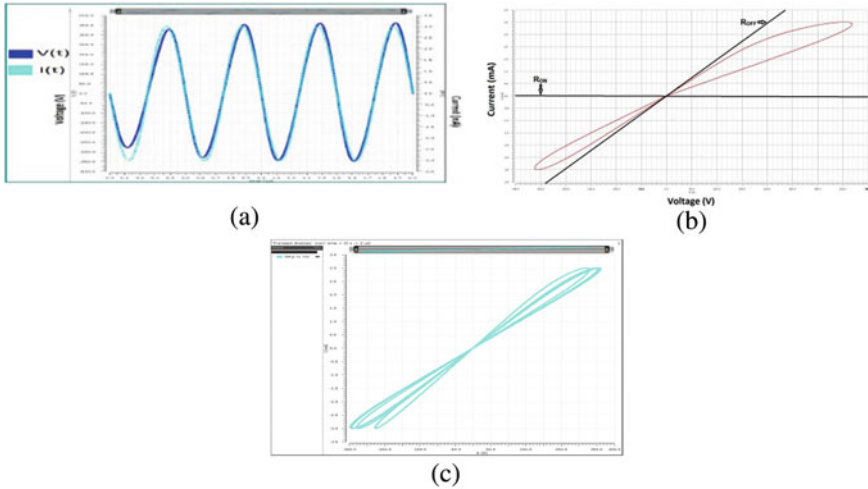


Fig. 26.2 **a** The transient response of voltage $v(t)$ and current $i(t)$ waveform of a memristor have identical Zero-crossing points; **b** VI characteristics response showing pinched hysteresis loop; **c** VI characteristics response showing pinched hysteresis loop in different frequencies

26.3 Logic Gates

In our circuits, we considered memristor ratioed logic (MRL) implementation, MRL which are faster, smaller and consumes less power.

26.3.1 AND and NAND Gate

Here the NAND gates are constructed using MRL, a hybrid integration of Memristor and CMOS as shown in Fig. 26.3. The AND logic is computed and analyzed using only Memristors and the NOT Logic is realized using CMOS 90 nm technology.

The AND operation using memristors has been analyzed below. Case I: when $A = 0$ and $B = 0$, no current flow in the circuit so output out will be equal to input so

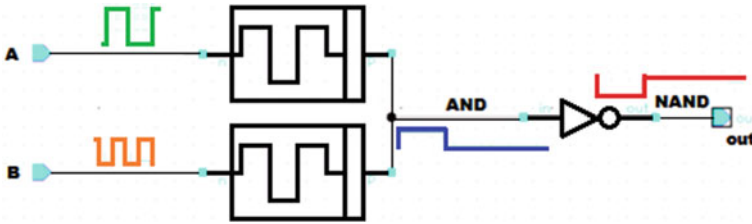


Fig. 26.3 Schematic of NAND Gate with input, output and intermediate waveform AND

out = 0 as shown in Fig. 26.4a. Case II: when $A = 0$ and $B = 1$, the current flows from Vdd to GND. When current passes from memristor M1, the resistance of that memristor decreases to R_{OFF} , the resistance of memristor M2 increases to R_{ON} as shown in Fig. 26.4b. Thus, as per the voltage divider rule given in Eq. (26.9), we get output out = 0 assuming $R_{ON} \gg R_{OFF}$. Case III: when $A = 1$ and $B = 0$, the current flows from Vdd to GND. The memristor resistance switching for M1 and M2 are shown in Fig. 26.4c. Thus, as per the voltage divider rule given in Eq. (26.10), we get output out = 0. Case IV: when $A = 1$ and $B = 1$, no current flow in the circuit so output out will be equal to input so out = 1 as shown in Fig. 26.4d. Similarly reversing the polarity of the memristors we get OR logic. For inputs $A = 0, B = 0$ and $A = 1, B = 1$ the output Y get the value 0 and 1 as no current flow through the circuit like the case I and IV of AND gate. For inputs $A = 0, B = 1$ and $A = 1, B = 0$ the output Y is determined by voltage divider rule given in Eqs. (26.11) and (26.12), respectively (similar to the case II and III of AND gate).

$$V_{out} = \frac{R_{OFF}}{R_{ON} + R_{OFF}} V_B \approx 0 \tag{26.9}$$

$$V_{out} = \frac{R_{OFF}}{R_{ON} + R_{OFF}} V_A \approx 0 \tag{26.10}$$

$$V_{out} = \frac{R_{ON}}{R_{ON} + R_{OFF}} V_B \approx 0 \tag{26.11}$$

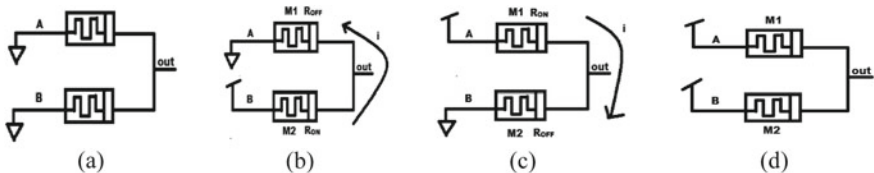


Fig. 26.4 Cases of AND operation: a i/p AB = 00, b i/p AB = 01, c i/p AB = 01, d i/p AB = 01

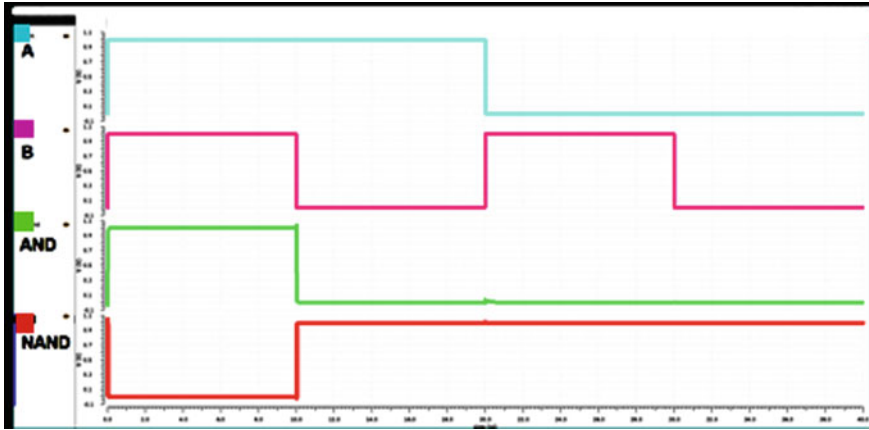


Fig. 26.5 Output response of a NAND and AND Gate

$$V_{out} = \frac{R_{ON}}{R_{ON} + R_{OFF}} V_A \approx 0 \tag{26.12}$$

The schematic of an MRL NAND is depicted in Fig. 26.3, and the output is depicted in Fig. 26.5. NOT Gate is not realized using memristor because it needs an additional voltage trigger to the output memristor to operate NOT logic. Thus, it is not convenient to use memristor for NOT gate and we go for conventional CMOS instead. The NAND gate has higher input impedance enabling easy interfacing with a wide range of on-chip and off-chip circuits and thus used as the fundamental unit in designing all the timing diagrams in this paper.

26.3.2 OR and NOR Gate

Similarly reversing the polarity of the memristors we get OR logic. For inputs $A = 0, B = 0$ and $A = 1, B = 1$ the output Y get the value 0 and 1 like the case I and IV of AND gate. For inputs $A = 0, B = 1$ and $A = 1, B = 0$ the output Y is determined by voltage divider rule given in Eqs. (26.11) and (26.12), respectively (similar to the case II and III of AND gate). NOR is constructed using two memristor and one CMOS as Inverter. Figure 26.6a shows the MRL, OR and NOR gate and the output response is and depicted in Fig. 26.6b.

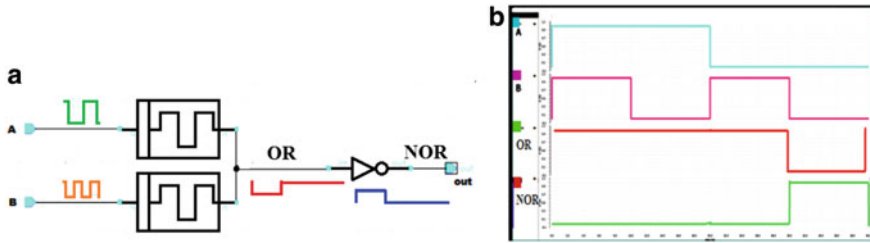


Fig. 26.6 a NOR Gate with input, output and intermediate waveform of OR Gate, b Output response of a NOR and OR Gate

26.4 Multivibrators

In this section, the prevalent Astable multivibrator is designed by memristor CMOS Hybrid structures. The memristors-based astable multivibrator is constructed using inverter of shorted NAND Gate as shown in Fig. 26.7a and CMOS-based astable multivibrator is in Fig. 26.7b.

Assuming output out of the NAND gate designed by M3, M4 and i2 is at logic level “1”, O3 should be at logic “0” which is also the output of NAND gate designed by M1, M2 and i1. So the capacitor C charges at the rate determined by the time constant of resistor R2 and C as it is connected between O3 with the timing resistor, R2 and its output. This junction is also connected to O2 via R1, where the value decreases until the lower threshold value of NAND gate (M1, M2 and i1) is reached and changes its state, so O3 becomes “1” which in turn changes out to logic “0”. Capacitor C is now discharged through NAND gate (M1, M2 and i1). Capacitor is

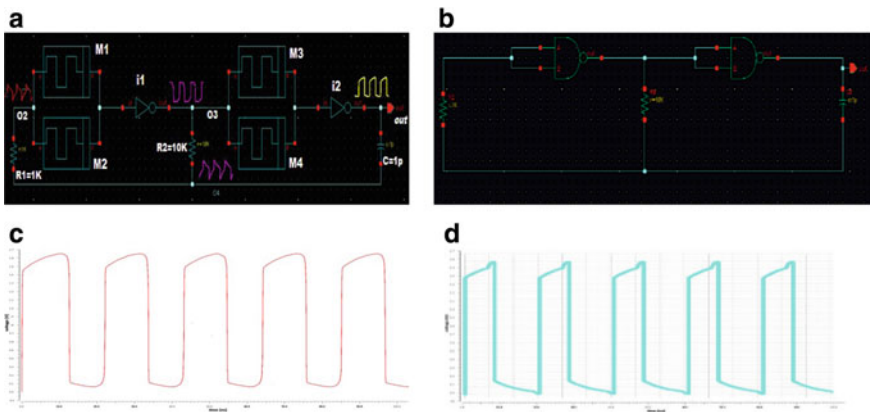


Fig. 26.7 a Memristor-based astable multivibrator with intermediate waveform, b CMOS-based astable multivibrator with intermediate waveform, c Output square wave response of memristor-based astable multivibrator, d Output square wave response of CMOS astable multivibrator

again charged up in reverse direction until upper threshold of NAND gate (M1, M2 and i1) is reached thus changing state to “0” and this cycle repeats again.

Here $R1 = 1 \text{ K}\Omega$, $R2 = 10 \text{ K}\Omega$, $C = 1 \text{ pF}$. The time constant for a NAND gate Astable Multivibrator are $T = 2.2R2C$ in seconds and the output frequency $f = 1/T$, respectively.

$$T = 2.2 \times 10 \times 10^3 \times 1 \times 10^{-12} = 22 \times 10^{-9} = 22 \text{ ns}$$

$$f \approx 45 \text{ cycles per } \mu\text{s}$$

The waveform as per the calculation is shown in Fig. 26.7c where a square wave output of around 22 ns time period is generated from the memristor astable multivibrator, and with none external triggering pulse, only with initial conditional noise. The output response of memristor Astable Multivibrators also contribute perfect and retained square shape waveform as compared to CMOS Astable Multivibrators shown in Fig. 26.7d which also signifies less total conditional noise, total harmonic distortion and noise in Memristor Multivibrators.

26.5 Voltage-Controlled Oscillator (VCO)

We designed a VCO as a supply-controlled ring oscillator, employing NAND gates using memristors and 90 nm CMOS technology as shown in Fig. 26.8. It is composed of an odd number of cascaded NAND gates of active delay stages where the output of each CMOS inverter i1 is used as input for the memristor M3, output of i2 used as input for M5 and the last output of i3 is fed back to the memristor M1. V_{control} is controlled input voltage applied to M2, M4 and M6. Under the standard voltage of 1.8 V the CMOS-based VCO circuit shows obverse operation than to this memristive VCO. In CMOS-based VCO the tuning range is between 0.95 and 1.8 V where the

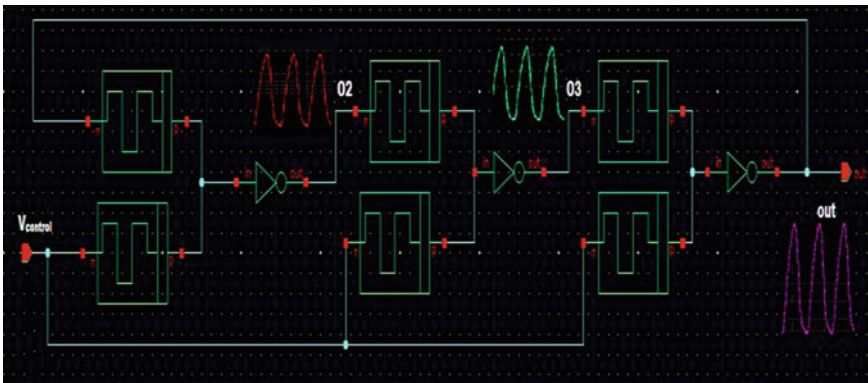


Fig. 26.8 Memristor-based ring oscillator as VCO with intermediate waveforms from NAND gates

oscillation starts, and the oscillation frequency sharply increases with the control voltage. But full voltage swing is observed from 1 to 1.5 V as shown in Fig. 26.9a other than this range a transient voltage swing is found, increasing with $V_{control}$, as shown in Fig. 26.9b. Whereas in case of our designed memristive VCO, the tuning range is from 0.1 to 0.99 V where the oscillation starts and the oscillation frequency sharply decrease with the control voltage, and the full voltage swing is from 0.1 to 0.9 V as depicted in Fig. 26.10a and transient voltage swing is found, decreasing with $V_{control}$, as depicted in Fig. 26.10b The output of the memristor oscillator provides precise and retained sinusoidal shape as compared to CMOS ring oscillator, which signifies less total harmonic distortion and noise, also lower control voltage signifies lower power dissipation in Memristive oscillator (Table 26.1).

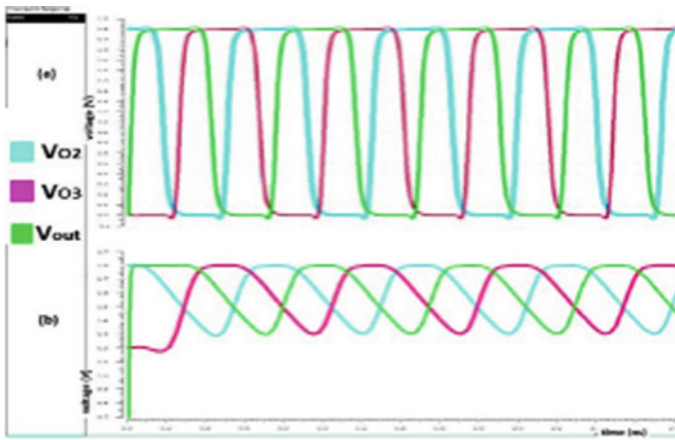


Fig. 26.9 Three output waveforms from each NAND gates of CMOS-based ring oscillator as VCO **a** full voltage swing for $V_{control} = 1.5$ V **b** transient voltage swing for $V_{control} = 1.1$ V

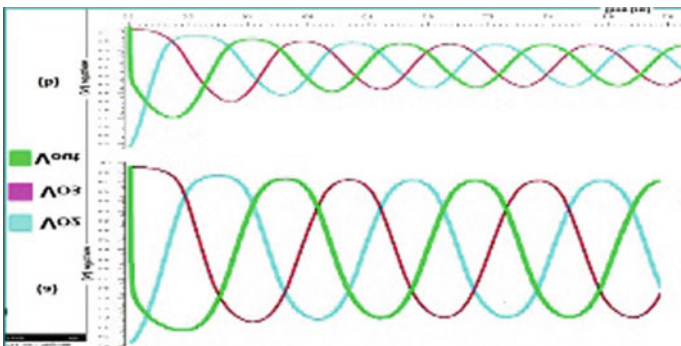


Fig. 26.10 Three output waveforms from each NAND gates of memristive ring oscillator as VCO **a** full voltage swing for $V_{control} = 0.3$ V **b** transient voltage swing for $V_{control} = 0.92$ V

Table 26.1 Simulated values of astable multivibrator and VCO

Circuits	Astable multivibrator		VCO	
	Memristor	CMOS	Memristor	CMOS
Frequency	47.7 MHz	32.7 MHz	2.13 GHz	2.9 GHz
Long term instability (ppm)	$\pm 1.65E03$	$\pm 1.67E03$	$3.87E-04$	± 163
F_{fund}	18 MHz	7 MHz	283.7 MHz	451.2 Mz
Delay	$3.00E-09$	$3.16E-09$	$1.64E-10$	$2.08E-10$
Power consumption	$2.44E-04$	$5.01E-04$	$2.95E-04$	$7.33E-04$
Phase noise	$-1.12E + 02$	$-1.07E + 02$	-90.157	-81
No. of devices	4 Memristor, 4 CMOS	8CMOS	6 Memristor, 6 CMOS	12CMOS

26.6 Conclusions

In From all the analysis we found that merely an abstract model of memristor can provide desirable outcome to considerable usage. For all the parameters frequency stability, delay, power, phase noise, noise factor and no of CMOS. The timing circuits we have designed are nonlinear relaxation oscillator, which are generally used in low frequency and poorer frequency stability than linear oscillator. But we realized all these circuits using memristor and found better frequency stability and endurance, low delay, noise and power consumption. Overall memristor is a robust, dense, and efficient device and can be used to construct and analog and digital circuits with a better circuit performance and will open new areas of applications.

Acknowledgements Abir Jana and Komal Kumari gratefully acknowledge by RUSA2.0, Jadavpur University (Ref. Number- R-11/370/19) and CSIR, Govt. of India (File Number-09/096(0964)/2019-EMR-I; Acknowledgment Number- 143705/2K18/1) for financial support.

References

1. Chua, L.: Memristor-the missing circuit element. *IEEE Trans. Circuit Theory* **18**(5), 507–519 (1971)
2. Ho, Y., Huang, G.M., Li, P.: Nonvolatile memristor memory: device characteristics and design implications. In: *Proceedings of the IEEE International Conference on Computer-Aided Design*, November, pp. 485–490 (2009)
3. Afifi, A., Ayatollahi, A., Raissi, F.: Implementation of biologically plausible spiking neural network models on the memristor crossbarbased CMOS/Nano circuits. In: *Proceedings of the European Conference on Circuit Theory Design*, pp. 563–566 (2009)
4. Pershin, Y.V., Di Ventra, M.: Practical approach to programmable analog circuits with memristors. *IEEE Trans. Circuits Syst. I, Reg. Papers* **57**(8), 1857–1864 (2010)

5. Ho, Y., Ho, G., Huang, M., Li, P.: Nonvolatile memristor memory: device characteristics and design implications. In: *IEEE/ACM International Conference on Computer-Aided Design-Digest of Technical Papers, 2009. ICCAD 2009*, pp. 485–490. IEEE, New York (2009)
6. Hu, B., Zhang, Y., Chen, W., Xu, C., Wang, Z.L.: Self-heating and external strain coupling induced phase transition of VO₂ nanobeam as single domain switch. *Adv. Mater.* **23**(31), 3536–3541 (2011)
7. Iu, H.H.C., Yu, D.S., Fitch, A.L., Sreeram, V., Chen, H.: Controlling chaos in a memristor based circuit using a twin-T notch filter. *IEEE Trans. Circuits Syst. I: Reg. Papers* **58**(6), 1337–1344 (2011)
8. Snider, G.: Computing with hysteretic resistor crossbars. *Appl. Phys. A* **80**(6), 1165–1172 (2005)
9. Chua, L.O., Mo, K.S.: Memristive devices and systems. *Proc. IEEE* **64**, 209–223 (1976)

Chapter 27

Identify Elementary Student Distribution Based on *Kompetisi Sains Madrasah* Data Using Probabilistic Distance Clustering



Ahmad Yusuf , Noor Wahyudi , Zakiyatul Ulya , Nurissaidah Ulinuha , Dwi Rolliawati , Ali Mustofa , Ahmad Fauzi , Ahmad Hanif Asyhar , Kusaeri , Ratna Indriyati, Dian Candra Rini Novitasari , and Maryunah

Abstract Indonesia is a developing country. The quality of human resources also influences the development of a country. The quality of education is one of the benchmarks for the quality of human resources. The quality of human resources can be seen from the quality of education. Improving the quality of education can be done in various ways. One effort designed to improve the quality of education in Indonesia is the provision of educational competitions in each region in Indonesia, and *Kompetisi Sains Madrasah* (KSM) is one of the pre-eminent competitions that have been designed. From the KSM Competition, a set of student scores is obtained which is a sample of the quality of education in each province. The number of students in educational institutions, especially elementary schools, is increasing which causes the data of students in the system to improve. The data can be grouped based on ability. Grouping is done using PD clustering. This method is one of the hierarchical grouping methods that have good performance. The cluster of students' abilities is very helpful in finding out educational information in the regions making it easier for parties to do special handling. The results of clustering using PD clustering show that three clusters represent the distribution of student's abilities with a silhouette coefficient of 0.5384 and a standard deviation of 0.3506 for mathematics subjects. Silhouette coefficient is 0.4351 and standard deviation is 0.4688 for science subjects.

A. Yusuf (✉) · N. Wahyudi · Z. Ulya · N. Ulinuha · D. Rolliawati · A. Mustofa · A. Fauzi · A. H. Asyhar · Kusaeri · R. Indriyati · D. C. R. Novitasari
UIN Sunan Ampel Surabaya, Ahmad Yani 117, Surabaya, Indonesia
e-mail: ahmadyusuf@uinsby.ac.id

Maryunah
Kementerian Agama RI, Lapangan Banteng 3-4, Jakarta, Indonesia

© The Editor(s) (if applicable) and The Author(s), under exclusive license to Springer Nature Singapore Pte Ltd. 2021

Y.-D. Zhang et al. (eds.), *Smart Trends in Computing and Communications: Proceedings of SmartCom 2020*, Smart Innovation, Systems and Technologies 182,

https://doi.org/10.1007/978-981-15-5224-3_27

27.1 Introduction

The country of Indonesia is one of the countries that is experiencing technological and economic development, or it can be called a developing country [1]. The development of a country is also influenced by the quality of human resources [2]. In the last few years, improvement in the quality of human resources is intensively carried out in all regions in Indonesia, especially in the field of education [3]. The quality of education can be seen from the achievement of national examination scores of all students in Indonesia, which can be seen from the statistics of the average test scores written by the Ministry of Education and Culture in 2019 reaching 51.76% [4]. This number shows that the quality of Indonesian education is still low [5]. From all regions in Indonesia, 95% of regions have education quality below 60% of the specified standard. Including large regions such as West Java (51.19%), Central Java (55.88%), and East Java (54.33%) have a low quality of education [4]. So, it is needed to improve the quality of education to support Indonesia for the better.

Improving the quality of education can be done in various ways [2]. One aim intended to improve the quality of education in Indonesia is to hold educational competitions in every region in Indonesia [6]. Competition can trigger a student's interest in learning and a place for students to compete to improve the quality of education. This competition is in the form of academic and non-academic competitions [7]. One of the academic competitions held is the Madrasah Science Competition (KSM) [8].

KSM is a national-level competition for elementary schools to senior high schools [9]. From the KSM Competition, a set of student scores is obtained which is a sample of the quality of education in each province. The students' abilities can be grouped based on students' scores data. The grouping of students' abilities is beneficial in finding out educational information in the regions making it easier for parties to do special handling. This can be called clustering [10].

Clustering is one of the methods in data mining [11]. Data mining is a process of processing money to obtain, explore, and discover hidden knowledge from a dataset or a huge set of data [12]. Clustering in data mining aims to group data based on the characteristics contained in the data into several clusters [13].

Several experts have done some research on clustering. In a study conducted by Harwati, Ardita, and Febriana in 2014 regarding clustering, student performance using the k-mean method showed quite good results with a standard deviation of 1.79 and a mean of 2.64 [14]. In other research concerning the analysis of students' abilities using clustering techniques conducted by Govindasamy and Velmurugan, the study compared several clustering methods, namely K-means, K-medoids, fuzzy c-means (FCM), and expectation-maximization (EM). FCM and EM have good performance compared to k-means and K-medoids [15]. Other research has been carried out by Tortora for solving clustering problems. In 2013, Tortora applied the PDC to the urban wastewater treatment dataset and showed good results. Tortora also compares PDC with other methods such as K-means, and factorial K-means. The results obtained show that using the k-mean method produces two minima, i.e., 39 and 54% [10]. In

the same case, the application of the PD-clustering method shows that it can achieve a convergent minimum JDF so that it can cluster better than other methods [16]. Therefore, FPDC will be used to group students based on their abilities.

27.2 Probabilistic Distance Clustering (PD-Clustering)

Probabilistic distance clustering (PD clustering) is a non-hierarchical algorithm that defines cluster units based on their chances of belonging to a given cluster [17]. PD clustering was first introduced by Ben-Israel and Lyigun in 2008 [15]. Define with $X = x_{i,j}$ a generic matrix with n units and J variables. K represents the number of clusters that are assumed to be non-empty. The center of the cluster is defined as c_k [18]. PD clustering is based on the principle or model of the relationship between $d(x_i, c_k)$ the distance between x_i data from cluster K and $p(x_i, c_k)$ probability for each point held by a cluster with $k = 1, \dots, K$, $i = 1, \dots, n$ and $j = 1, \dots, J$. The relationship between them is the basic assumption of this method, and the probability is inversely proportional to the distance from the center of the cluster; the product between distance and probability is considered constant depending on $F(x_i)$ [18]. The basic assumptions of PD clustering are expressed by the following equation [16].

$$p_{i,k}d_k(x_i) = F(x_i) \quad (27.1)$$

The number of $F(x_i)$ above is called the joint distance function (JDF). A clustering solution is obtained by identifying centers that minimize JDF.

$$\text{JDF} = \sum_{i=1}^n \sum_{k=1}^K d_k(x_i) p_{ik}^2, \quad (27.2)$$

where $d_k(x_i)$ and $p_{i,k}$ depend on the center of the cluster. The higher the JDF value, the higher the probability for that point to be one cluster. The details regarding PD clustering are explained in detail by Ben-Israel and Lyigun who suggest the use of p^2 in Eq. (27.2), to refine the problem and confirmed convergence [15]. Other papers also show that the center of the cluster is calculated by

$$c_k = \sum_{i=1, \dots, n} \left(\frac{u_k(x_i)}{\sum_{j=1, \dots, n} u_k(x_j)} \right) x_i \quad (27.3)$$

where

$$u_k(x_i) = \frac{p_{ik}^2}{d_k(x_i)} \quad (27.4)$$

Minimizing the JDF value and maximizing the probabilistic of each point belonging to only one cluster means that the JDF value at all k centers is zero and always positive elsewhere [15]. Thus, the center can be said to be the global minimum of JDF. There may be other stationary points because these functions are not convex or quasi-convex, but they are saddle points.

In this study, we consider the form [16]

$$d_k(x_i) = \sum_{j=1}^1 |x_{i,j} - c_{kj}|, \tag{27.5}$$

where $k = 1, \dots, K, i = 1, \dots, n$, Until Eq. (27.4) becomes:

$$\text{JDF} = \sum_{i=1}^n \sum_{j=1}^J \sum_{k=1}^K |x_{i,j} - c_{kj}| p_{ik}^2 \tag{27.6}$$

From Eq. (27.7), the final solution $\widehat{\text{JDF}}$ is obtained by minimizing the quantity JDF to be

$$\widehat{\text{JDF}} = \min_C \sum_{i=1}^n \sum_{j=1}^J \sum_{k=1}^K |x_{i,j} - c_{kj}| p_{ik}^2 \tag{27.7}$$

On the condition that $\sum_{i=1}^n \sum_{k=1}^K p_{ik}^2 \leq n$ corresponds to Ben-Israel and Lyigun, where c_k are the center of the generic cluster and $0 \leq p_{ik} \leq 1$.

The problem of PD clustering can be solved using an iterative algorithm whose convergence is shown in Lyigun (2007) [18]. Each unit is assigned to cluster k based on the highest probability calculated posterior using the following formula [19]

$$p_{ik} = \frac{\prod_{m \neq k}^K d_m(x_i)}{\sum_{l=1}^K \prod_{m \neq l}^K d_m(x_i)}, \tag{27.8}$$

where $k = 1, \dots, K$. Keep in mind that p_{ik} understands every necessary condition as a probability. Besides, no assumptions were made concerning the distribution of this function. This shows that p_{ik} can only be calculated if given x_i and for $\forall c_k$ [20].

27.3 Silhouette Coefficient

The silhouette coefficient is an evaluation method to test the accuracy of a cluster that has been formed from the clustering process. The silhouette coefficient value is defined as in Eq. (27.9)

$$s(i) = \frac{(b(i) - a(i))}{\max a(i), b(i)} \tag{27.9}$$

The results of the silhouette coefficients are interpreted using the Kaufmann and Rousseeuw guidelines for silhouette coefficients.

27.4 Result and Discussion

In this study, identification of the distribution of elementary school students from the data of students who joined KSM to identify the quality of education in an area is based on the value obtained from KSM 2019. In 2019, KSM will split the competition into two subjects, such as mathematics and science. This study uses three parameters obtained from each competition. These parameters are the score of the correct answer, a score of the wrong answer, and the score of the blank answer. The data used in this study were the values of participants who participated in the KSM 2019 competition in each district, totaling 2385 students from 34 provinces with 1189 data in mathematics and 1197 data in science subjects. The data will be clustered to find out the quality of education from each region. This study uses data of students who participated in the KSM primary school level or equivalent. The data consists of the score of correct answers, the score of wrong answers, and the score of blank answers. The data is processed to find a cluster of students. The data is illustrated in Fig. 27.1.

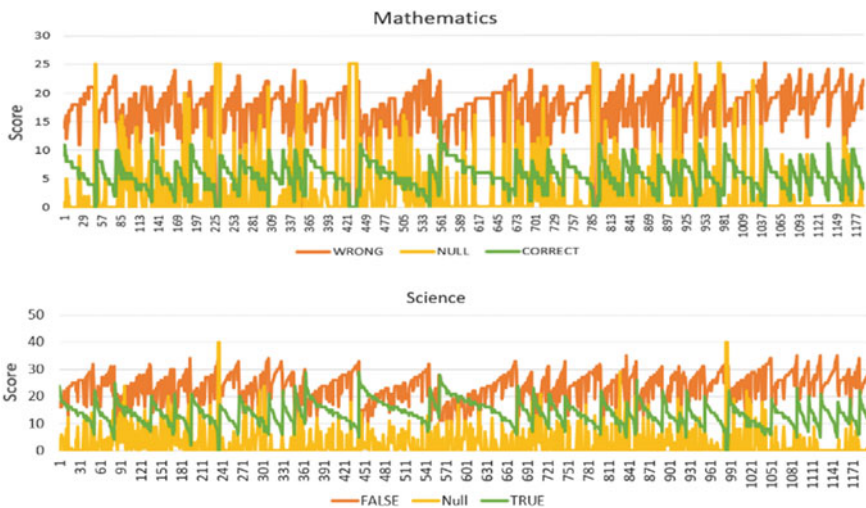


Fig. 27.1 Graph values KSM involving students for science

Figure 27.1 shows that the score chart of students participating in KSM. The orange line represents the score of the wrong answer from the student, yellow represents the blank score of the answer from the student, and the green represents the score of the correct answer from the student. The number of students who answered blanks in mathematics is more numerous than science. The average student answers more wrong than right. This data is used for clustering students who participate in KSM using PD clustering. Initialize some variables needed in PD clustering, such as determining the number of clusters. In this study, the determination of the number of clusters was carried out by trial. The cluster number experiment is intended to see the optimal number of clusters in KSM data grouping. Tests performed four times on each subject. The trial results are evaluated using the silhouette coefficient (Si) and standard deviation (Std) to see the data distribution shown in Table 27.1.

Based on Table 27.1, it can be seen that the optimal number of clusters is three clusters because in the trial of three clusters the largest silhouette value is obtained and the smallest standard deviation compared to the other clusters. A large silhouette coefficient or close to one indicates that each data can be adequately grouped based on its cluster and a small standard deviation means a small data deviation. Figure 27.2 shows the silhouette results of each subject with three clusters.

Figure 27.2 shows the overlapping of the silhouette results, which blends some data that is not in the appropriate cluster. The results of the silhouette of the mathematics subjects were seen overlapping in cluster 1 by 75 data from 1188 data and in

Table 27.1 Clustering results using PD clustering

Number of clusters	Mathematic		Science	
	Si	Std	Si	Std
3	0.5384	0.3506	0.4351	0.4688
4	0.5158	0.4283	0.362	0.4872
5	0.493	0.4333	0.3726	0.529
6	0.3126	0.6402	0.256	0.5348

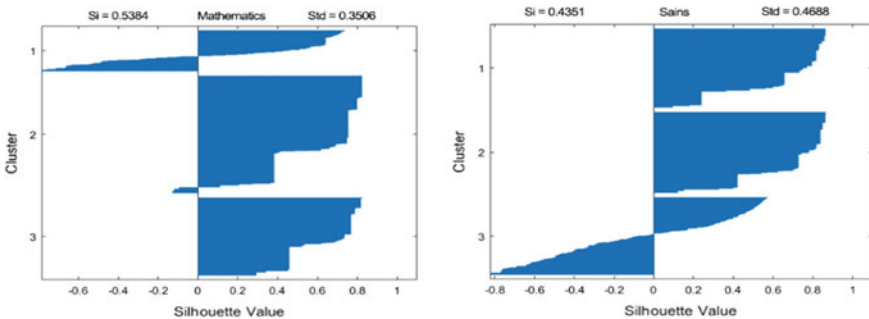


Fig. 27.2 Silhouette results in 3 clusters

cluster 2 by 29 data from 1188 data. In the graphs of science, subjects have 205 overlapping data in cluster 3 and no overlapping in other clusters. Although the results of clustering using PD-clustering are still experiencing overlapping, the results of this study can already be said to be good with silhouette values close to 1. In this research, students are clustered into three clusters of excellent, good, and fair.

In some cases, as shown in Fig. 27.3, some local minimums are obtained. Figure 27.3 shows that the convergence of JDF scores in mathematics subjects starts from the third iteration onwards, whereas in science subjects starting from the second iteration onwards. The JDF value obtained indicates that the cluster center k is said to be the global minimum of JDF. Based on the results obtained using the three clusters in Table 27.2, the cluster center obtained from each cluster, such as cluster 1, cluster 2, and cluster 3 is shown in Table 27.2. The results of identifying the quality of each school in Indonesia are shown in Fig. 27.4.

Figure 27.4 shows that Madrasah Ibtida'iyah (MI) is superior to Elementary Schools (SD) and Madrasah Ibtida'iyah Negeri (MIN) with a percentage of 52% including students with good quality. In science, the average distribution of MI and MIN students has the same quality between excellent, good, and fair while for elementary students 60% of the 9 students participating in KSM. The number of elementary school students participating in KSM is only 2 students, and all of them are clustered into the fair. Based on the results that have been shown, it can be concluded that MI is

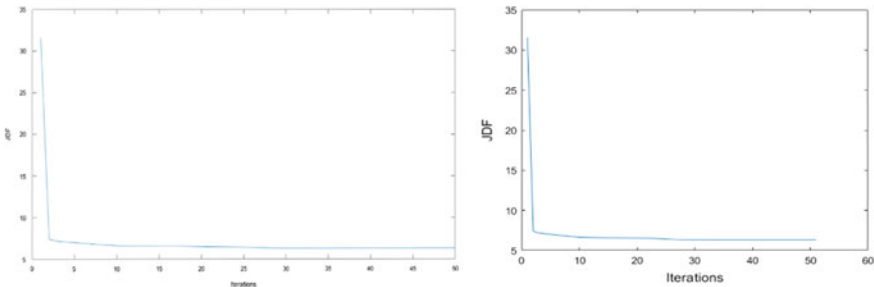


Fig. 27.3 JDF value for each iteration of the PD clustering algorithm

Table 27.2 Cluster center

Subjects	Number of clusters	Data		
		Wrong	Null	Correct
Mathematic	1	4.1594	11.025	9.8153
	2	6	19	2.6985
	3	8	17	4.8282
Science	1	15.99767	23.99824	0.004086
	2	12	28	1.860064
	3	15	19	6.000000009

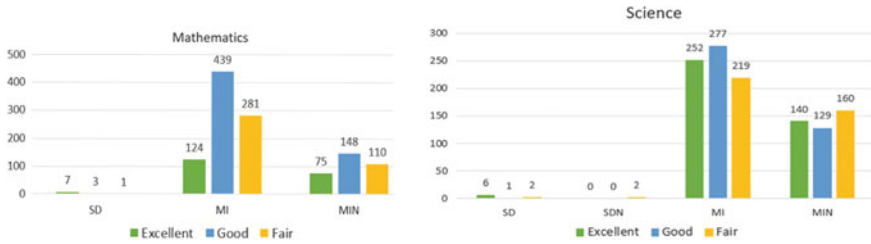


Fig. 27.4 Education quality identification results for each school

an elementary school that has good quality compared to other primary schools. Based on this description, the schools that need evaluation and care regarding improving education are SD and SDN.

27.5 Conclusion

Clustering using the PD clustering method in KSM obtains a maximum number of clusters of 3 clusters because it has the best silhouette coefficient compared to the number of other clusters. These 3 clusters are the first cluster representing fair students, the second cluster represents good students, and the last cluster represents excellent students. Based on Table 27.2, the silhouette coefficient of mathematical subjects produced in this research is intermediate, which means that the cluster structure formed is good while the science subjects have a good cluster structure with a silhouette value of less than 0.5. Based on Fig. 27.4, it can be concluded that MI is an elementary school that has good quality compared to other primary schools. Based on this description, the schools that need evaluation and care regarding improving education are SD and SDN.

References

1. Sutrisno, N.: Pemajuan Kepentingan Negara-Negara Berkembang Dalam Sistem WTO. The Institute for Migrant Rights Press, Indonesia
2. Achola, P.P.: Challenges of primary education in developing countries, 1st edn. Ashgate, New York, NY 10017, USA
3. Kemendikbud. Perbaikan Kualitas Manusia Melalui Pendidikan Dasar dan Menengah. Jakarta
4. Kemendikbud. Laporan Nilai Ujian Nasional Indonesia- Pusat Penilaian Pendidikan [Internet]. Kementerian Pendidik. dan Kebud. (2019). <https://puspendik.kemdikbud.go.id/hasil-un/>
5. Montoya, S.: Quality data to ensure a quality education for every child (2017)
6. Purba, E.: Menuju Indonesia Baru. Pertama. Guepedia, Jakarta
7. Muhaimin, Manajemen Pendidikan: Aplikasi Dalam Penyusunan Rencana Pengembangan Sekolah/Madrasah. Kelima. Kencana Publisher, Jakarta
8. Basori, R., Arif, Gagasan, F.M.: Ucapan, dan Tindakan dalam Mencerahkan Pendidikan Islam dan Kerukunan Umat. LKis, Yogyakarta

9. Nofrion, Komunikasi Pendidikan: Penerapan Teori dan Konsep Komunikasi dalam Pembelajaran. Pertama. Kencana Perdana Media Group, Jakarta
10. Prasetyo, E.: Data Mining, Mengelola Data Menjadi Informasi Menggunakan Matlab. ANDI Yogyakarta, Yogyakarta
11. Swindiarito, V.T.P.: Integration of fuzzy C-means clustering and TOPSIS (FCM-TOPSIS) with Silhouette analysis for multi criteria parameter data. In: 2018 International Seminar on Application for Technology of Information and Communication, pp. 463–468 (2018)
12. Prasetya, E.: Data mining Mengolah Data Menjadi Informasi Menggunakan MATLAB. Andi, Yogyakarta
13. Sindhu, R., Nandal, R., Dhamija, P., Sehrawat, H.A.: Review on K-means algorithm and its' different distance matrices. *Int. J. Eng. Technol. [Internet]* **9**, 1423–1430 (2017). <https://doi.org/10.21817/ijet/2017/v9i2/170902227>
14. Permata, A., Ayu, F.: Mapping student' s performance based on data mining approach (A case study). *Ital. Oral Surg. [Internet]* **3**, 173–177 (2015). <http://dx.doi.org/10.1016/j.aaspro.2015.01.034>
15. Govindasamy, K.: Analysis of student academic performance using clustering techniques **119**(15), 309–323 (2018)
16. Tortora, C., Gettler, M., Marino, M., Palumbo, F.: Factor probabilistic distance clustering (FPDC): a new clustering method. *Adv. Data Anal. Classif.* (2015)
17. Iyigun, C., Ben-israel, A., Iyigun, C.: *Sciences I. Sciences : probabilistic distance clustering adjusted for cluster size* (September 2008), 603–621 (2015)
18. Lyigun, C.: *Probabilistic distance clustering* (2007)
19. Van Den, P.D.: *Algorithms from and for nature and life classification and data analysis*
20. Rachev, S., Klebanov, L., Stoyanov, S., Fabozzi, F.: A new dimension reduction method: factor discriminant k-means. *J. Classif.* **2**(28), 210–226 (2013)

Chapter 28

Classification of Tomato Plant Diseases Through Leaf Using Gray-Level Co-occurrence Matrix and Color Moment with Convolutional Neural Network Methods



Anton Anton, Supriadi Rustad, Guruh Fajar Shidik, and Abdul Syukur

Abstract Tomato is a fruit vegetable source of vitamins and minerals; in addition to being consumed as fresh fruit, it can also be processed into food industry raw materials such as fruit juices and sauces. However, due to various causes such as diseases, pest attacks, and unstable weather conditions, there is a decrease in the quality and quantity of production. In order to contribute to maintaining the productivity of tomato plants, the use of technology can be an alternative to be applied to the cultivation of tomato plants. This study applies image processing techniques to detect the texture of affected leaf using gray-level co-occurrence matrix (GLCM) extraction and color moment using convolutional neural network (CNN) method. Among the diseases that often occur in tomato leaf are late blight, Septoria spot, bacterial spot, target spot, early blight, leaf curl, spider mites, two spotted spider mites, and leaf mold. In this study, a combination of GLCM-color moment and CNN method was chosen because of its reliability in identifying and classifying plant diseases compared to only using CNN. In this study, we used a combination of GLCM color moments and CNN methods.

28.1 Introduction

Tomato is a fruit vegetable that is very potential to be cultivated because the fruit is a source of vitamins and minerals. Besides being consumed as fresh fruit and for cooking spices, it can also be further processed as raw materials for food industries such as fruit juices and sauces [1]. Tomatoes become one of the horticultural commodities that have high economic value and still require serious handling, especially in terms

A. Anton (✉) · S. Rustad · G. F. Shidik · A. Syukur
Universitas Dian Nuswantoro, Semarang, Indonesia
e-mail: anton@mhs.dinus.ac.id

A. Anton
STMIK Nusa Mandiri, Jakarta, Indonesia

© The Editor(s) (if applicable) and The Author(s), under exclusive license to Springer Nature Singapore Pte Ltd. 2021

Y.-D. Zhang et al. (eds.), *Smart Trends in Computing and Communications: Proceedings of SmartCom 2020*, Smart Innovation, Systems and Technologies 182,
https://doi.org/10.1007/978-981-15-5224-3_28

of increasing yields and fruit quality [2]. Plant diseases, pest attacks, and unstable weather conditions can cause a decrease in the quality and quantity of production.

Diseases that attack tomato plants can be caused by fungi, bacteria, and viruses. The symptoms can be seen from changes in the shape and color of leaves. Most farmers do not recognize the symptoms with the naked eye and take immediate action without knowing how to overcome them. Therefore, we need the help of image processing technology that can recognize diseases in tomato plants. Some types of diseases found in tomatoes include yellow leaf curl, potato virus Y, tomato mosaic virus, and leaf spot [3].

Developing research on the identification of tomato plant diseases before [4], the number of classes used was six classes, including mushrooms: 2, bacteria: 2, viruses: 1, and healthy (normal) 1. Therefore, this research class discusses the right features, so it is expected to be suitable for disease identification in tomato leaf. Research on the identification of plant diseases in terms of leaf digital images [5] suggests the use of shape, texture, and color features. This study did not use the shape features because the form of rust disease is not patterned, other than that the shape features are more suitable for classifying of plant species with different leaf patterns [6] and identification of plant diseases with symptoms of hollow or deformed leaves at the edge of the leaf, for example in disease mosaic on cassava leaves [7]. In addition to leaf disease, rain and temperature factors also affect the quality and quantity of production. Therefore, the management of image pattern recognition to detect disease in leaves is a major problem in agriculture [8].

28.2 Related Work

Deep learning has made remarkable progress in identifying images in large numbers. Several previous studies used one of the deep learning architectures namely convolutional neural network (CNN) [9, 10, 11, 13, 18]. Deep learning uses an approach that can learn many layers of features and automatically makes representations of input data. Other studies have modified CNN using feature extraction to improve the performance of CNN [12] (Tables 28.1).

28.3 Method

There are texture differences between normal, diseased, and mosaic leaves [9]. This study chose the gray-level co-occurrence matrix to extract textures because GLCM as an excellent method is used to determine the texture of the leaves and detect plant types and have high accuracy [5], the complexity of image textures is difficult to define and quantify, but GLCM can be used to quantify and compare various aspects of image texture [10, 16, 19]. The use of color moments for extracting color because there are differences in color on healthy and disease leaf [5, 9]. Color moment

Table 28.1 Comparison between all classifications

Classification problem	Method	Accuracy (%)
Leaf recognition for plant	GLCM & PCA	GLCM (78%); PCA (98.46%)
Classification of maize leaf disease	CNN (GoogLeNet)	97.89%
Recognition of maize leaf diseases	CNN	92.85%
Identification of corn leaf disease	CNN (GoogLeNet & Cifar10)	GoogLeNet (98.9%) Cifar10 (98.8%)
Cow race classification	GLCM-CNN	93.763%
Classification of a variety of plant species	CNN	97.47%
Tomato plant leaf disease detection	CNN	91.67%

is an effective image extraction method for analyzing images with color due to the presence of vector dimensions with the lowest computational features and complexity compared to other methods such as color correlation, histogram, and color structure descriptors [8]. An innovative solution is made to maintain the quality of tomato production by utilizing automatic motor technology with a camera that can capture the four sides of the plant to detect and recognize leaf disease. Using 4,923 images of diseased and healthy plant leaves, these image data are trained with in a convolutional neural network, a deep F-RCNN anomaly detection model to identify whether or not the disease exists. This research is expected to facilitate the identification of tomato plant diseases quickly [11, 15, 17]. Research on the analysis of plant diseases through leaf images using SVM for classifying of features including linear, quadratic, Gaussian, and cubic kernels produces an accuracy of 98.3% [12, 14] (Fig. 28.1).

28.4 Result and Discussion

28.4.1 Result

This research uses computer specifications with Intel (R) Core (TM) i5-8250U @ 1.60 GHz 1.80 GHz Processor, 8.00 GB Memory, 256 GB SSD and HDD for 1 TB data and MATLAB. The dataset used for this study was sourced from plant village (<https://plantvillage.org>), divided into training data and test data used to solve small sample size problems in modeling. Training data from ten classes of tomato leaf is 70%, and test data is 30%. Vector features a combined GLCM texture feature called

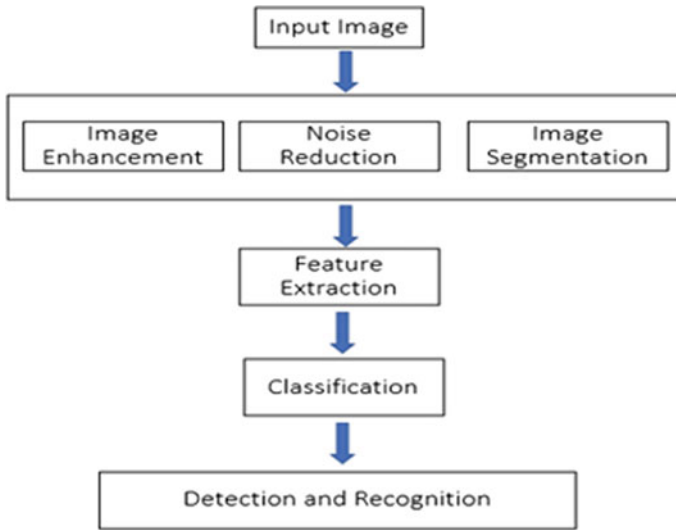


Fig. 28.1 Proposed framework for the detection and classification of plant leaf diseases

Table 28.2 Data on tomato plant leaf

Leaf type	Total leaf
T. Spot	1.404
Mosaic	373
YLCV	3.209
B. Spot	2.127
Early B	1.000
Late B	1.909
Leaf Mold	952
SL. Spot	1.771
SMT. Spotted	1.676
Healthy	1.591
Total all leaf	16.012

contrast, correlation, energy, and homogeneity. The amount of training data is 11.208 images and 4.804 images of test data (Tables 28.2).

28.4.1.1 Gray-Level Co-occurrence Matrix (GLCM)

The improvement of the proposed GLCM-color moment-CNN method uses three approaches, namely comparing GLCM-color moment-CNN with previous studies; second, use ten classes to show increased accuracy; third, reduce the background of

the image to be imported and speed up the process of extracting the texture features of the image in computing. Feature extraction used, namely:

$$\text{Contrast} = \sum |i - j|p(i, j)^2 \tag{28.1}$$

$$\text{Correlation} = \sum \frac{(i - \mu_i)(j - \mu_j)p(i, j)}{\sigma_i \sigma_j} \tag{28.2}$$

$$\text{Energy} = \sum p(i, j)^2 \tag{28.3}$$

$$\text{Homogeneity} = \sum \frac{p(i, j)}{1 + |i - j|} \tag{28.4}$$

Some GLCM extracted textural features are illustrated in Tables 28.3 and 28.4 for two different leaf images (Fig. 28.2).

At degrees 0° and 90°, the GLCM method provides the same accuracy and results. Poor results are obtained at 45° because any change in neighboring degrees will change the value of the extracted leaf features. For any changes to the image using the GLCM method is very sensitive such as changes in rotation and scale. This can be seen in Tables 28.3 and 28.4, differences in features extracted. The introduction of the GLCM method is very fast, and the computing time for the GLCM method is less.

Table 28.3 Some image textures extracted from leaf images (a)

Angle	Contrast	Correlation	Energy	Homogeneity
0°	0.10669	0.95639	0.24762	0.94733
45°	0.14825	0.93958	0.23102	0.92801
90°	0.11157	0.95441	0.24484	0.94491
135°	0.14885	0.93931	0.23178	0.92824
Average	0.12884	0.94742	0.23882	0.93712

Table 28.4 Some image textures extracted from leaf images (b)

Angle	Contrast	Correlation	Energy	Homogeneity
0°	0.23151	0.82838	0.24639	0.8987
45°	0.29727	0.78	0.23092	0.87992
90°	0.23148	0.82861	0.24946	0.90208
135°	0.30544	0.77393	0.22816	0.87725
Average	0.26642	0.80273	0.23873	0.88949

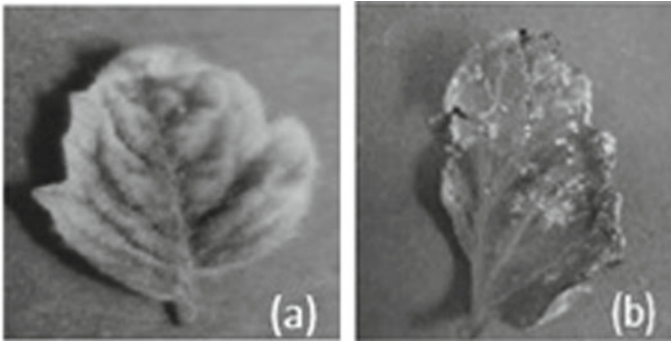


Fig. 28.2 Images textures extracted from leaf images (a) (b)

Table 28.5 Testing accuracy per color moments feature

Color moments (Cm)	Accuracy (%)
Cm 1	52.33
Cm 2	93.67
Cm 3	67.33

28.4.1.2 Color Moment

Color moment is used to distinguish images based on color features and measure the similarity of colors between images. The color distribution of an image is defined as the probability distribution based on the color moment assumption. The color moment feature selection is based on the accuracy results per color moment feature in Table 28.5.

28.4.1.3 Convolutional Neural Networks (CNN)

Convolutional neural network (CNN) is a type of neural network commonly used to analyze visual images and detect and recognize objects in images. Input data performed by CNN uses raw images (RGB images), but in the GLCM-color moment-CNN method, the input data is extracted from the image texture using GLCM-color moment (Fig. 28.3).

Grayscale on the training data image and test data performed on MATLAB, using the function: $I = \text{rgb2gray}(\text{"image_variable"})$ (Figs. 28.4 and 28.5).

The results of this experiment can also be applied in other crops (mangoes, potatoes, rice, or sugarcane) with different dataset sizes. Factor similarity in texture and type of disease from each leaf will be a challenge. Modifying the parameters of the model being trained depends on the size of the dataset used.

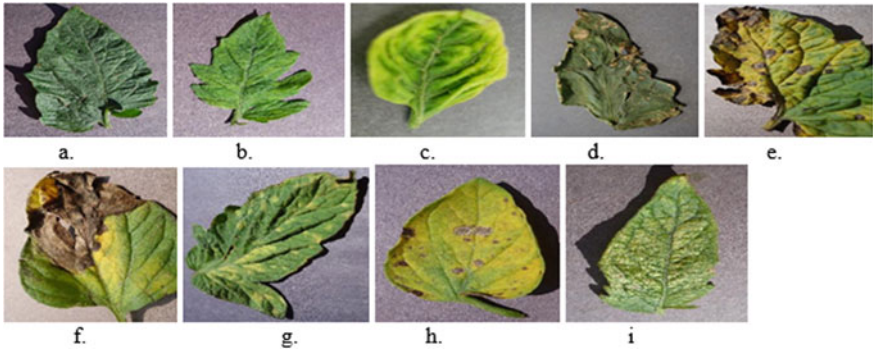


Fig. 28.3 Example of the data used in this research; **a** target Spot, **b** mosaic virus, **c** yellow leaf curl virus, **d** bacterial spot, **e** early blight, **f** late blight, **g** leaf mold, **h** Septoria leaf spot, **i** spider mites. Two spotted spider mites

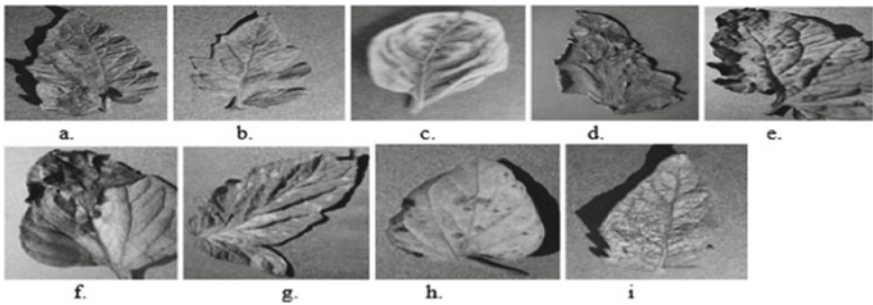


Fig. 28.4 Grayscale image of tomato leaf

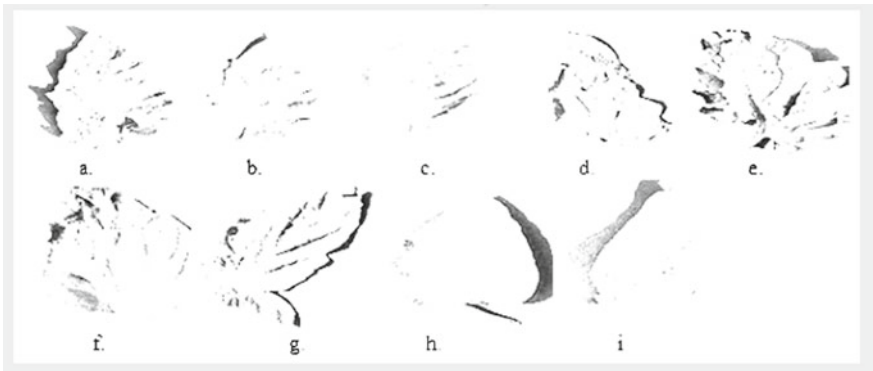


Fig. 28.5 Tomato leaf color segmentation

28.5 Discussion

Based on the strengths and weaknesses of previous studies, there is a research room related to the use of GLCM, color moment, and CNN that can maximize the value of classification accuracy in leaf texture in tomato plant diseases. Three stages of our research were carried out to evaluate the effectiveness of the proposed method. The first stage compares previous research, and in the second stage, we used ten classes of tomato leaf disease, because previous studies were used below. In the third stage, we do image enhancement, image reduction, and Image segmentation so that the extraction process on the GLCM feature does not require a long time.

28.6 Conclusion

The conclusion that can be obtained from this research is the image identification system of diseases of tomato leaf based on the extraction of color moment features and texture features of GLCM with angular orientations of 0° , 45° , 90° and 135° and pixel spacing ranging from 1 to 10 pixels with CNN classification succeeded in identifying the types of diseases found in tomato leaf. The results of the identification are 1.404 images of target spot diseased images, 373 images of mosaic virus and 3.209 images of yellow leaf curl virus, 2.127 bacterial spot images, 1.000 early blight images, 1.909 late blight images, 952 leaf mold images, 1.771 Septoria images leaf spot, 1.676 SMT spot images, and 1.591 healthy images. The GLCM-color moment-CNN method can be implemented to detect diseases in tomato leaf plants with 99% accuracy in detecting tomato leaf plant diseases.

References

1. Wasonowati, C.: Meningkatkan Pertumbuhan Tanaman Tomat (*Lycopersicon esculentum*) Dengan Sistem Budidaya Hidroponik. *Agrovigor* **4**(1), 21–28 (2011)
2. Homepage, D.: Tingkatkan konsumsi sayur dan buah nusantara menuju masyarakat hidup sehat. Accessed 10 December 2019, 2017
3. Alviansyah, F., Ruslianto, I., Diponegoro, M.: Identifikasi Penyakit Pada Tanaman Tomat Berdasarkan Warna Dan Bentuk Daun Dengan Metode Naive Bayes Classifier Berbasis Web. *J. Coding Sist. Komput. Untan* **05**(1), 23–32 (2017)
4. Sabrol, H., Satish, K.: Tomato plant disease classification in digital images using classification tree. pp. 1242–1246 (2016)
5. Camargo, A., Smith, J.S.: Image pattern classification for the identification of disease causing agents in plants. *Comput. Electron. Agric.* **66**(2), 121–125 (2009)
6. Shabanzade, M., Zahedi, M., Amin Aghvami, S.: Combination of local descriptors and global features for leaf recognition. *Signal Image Process. An Int. J.* **2**(3), 23–31 (2011)
7. Aduwo, J.R., Mwebaze, E., Quinn, J.A.: Automated vision-based diagnosis of cassava mosaic disease. *Proc. ICDM Work. Data Min. Agric.* 114–122 (2010)
8. Patil, J.K.: Color feature extraction of tomato leaf diseases. *Int. J. Eng. Trends Technol.* **2**(2), 72–74 (2011)

9. Santoni, M.M., Sensuse, D.I., Arymurthy, A.M., Fanany, M.I.: Cattle race classification using gray level co-occurrence matrix convolutional neural networks. In: *Procedia Computer Science*, vol. 59. ICCSCI 2015, pp. 493–502 (2015)
10. Yalcin, H., Razavi, S.: Plant classification using convolutional neural networks Hulya. *Adv. Intell. Syst. Comput.* **898**, 357–365 (2019)
11. Priyadharshini, R.A.: Maize leaf disease classification using deep convolutional neural networks. *Neural Comput. Appl.* **3** (2019)
12. Zhang, X., Qiao, Y., Meng, F., Fan, C., Zhang, M.: Identification of maize leaf diseases using improved deep convolutional neural networks. *IEEE Access* **6**, 30370–30377 (2018)
13. De Luna, R.G., Dadios, E.P., Bandala, A.A.: Automated image capturing system for deep learning-based tomato plant leaf disease detection and recognition. In: *IEEE Reg. 10 Annual International Conference Proceedings/TENCON*, vol. 2018, pp. 1414–1419 (2018)
14. Zaka-ud-din, W., Aziz, M., Rashid, S., Ismail, J.: Classification of disease in tomato plants' leaf using image segmentation and SVM. *Tech. Journal Univ. Eng. Technol.* **23**(2), 81–88 (2018)
15. Patil, M.A.N., Pawar, M.V.: Detection and classification of plant leaf disease. *Iarjset* **4**(4), 72–75 (2017)
16. Sharath Kumar, Y.: Leaf recognition for plant classification using GLCM and PCA methods. *Orient. J. Comput. Sci. Technol.* **3**(1), 31–36 (2010)
17. Harini, D.N.D., Lalitha Bhaskari, D.: Identification of leaf diseases in tomato plant based on wavelets and PCA. In: *2011 world congress on information and communication technologies*, pp. 1398–1403 (2011)
18. Sibiya, M., Sumbwanyambe, M.: A computational procedure for the recognition and classification of maize leaf diseases out of healthy leaves using convolutional neural networks. *AgriEngineering* **1**(1), 119–131 (2019)
19. Honeycutt, C.E., Plotnick, R.: Image analysis techniques and gray-level co-occurrence matrices (GLCM) for calculating bioturbation indices and characterizing biogenic sedimentary structures. *Comput. Geosci.* **34**(11), 1461–1472 (2008)

Chapter 29

Leverage from Blockchain in Commodity Exchange: Asset-Backed Token with Ethereum Blockchain Network and Smart Contract



Richard, Yaya Heryadi, Lukas, and Agung Trisetiyarso

Abstract Ethereum is one of the most popular blockchain platforms with a high number of adoption in the blockchain world today. Ethereum token (ERC-20) can tokenize any real-world object while it is also possible to exchange the token across the network participants. This utility from the token drives many blockchain enthusiasts to create decentralized applications. ERC-20 token could be used to collect project funds, decision voting, or even can be used to provide investment platforms for people that want to hedge the volatility of the currency with buying an asset that is back to back with the crypto-token. This research shows the main characteristics of asset-backed token and its implementation on a complete end-to-end “*digitalization assets system*” (assets buy and assets redemption). The result shows that asset-backed token needs support from government and other legalizing parties to verify the legitimacy of the asset that backing the token itself.

Richard (✉)

Information Systems Department, School of Information Systems, Bina Nusantara University, Jakarta 11840, Indonesia

e-mail: richard-slc@binus.edu

Richard · Lukas · A. Trisetiyarso

Computer Science Department, BINUS Graduate Program, Doctor of Computer Science, Bina Nusantara University, Jakarta 11840, Indonesia

e-mail: lukas@atmajaya.ac.id

A. Trisetiyarso

e-mail: atrisetiyarso@binus.edu

Y. Heryadi

Cognitive Engineering Research Group (CERG), Faculty of Engineering, Universitas Katolik Indonesia Atma Jaya, Jakarta 12930, Indonesia

e-mail: YayaHeryadi@binus.edu

© The Editor(s) (if applicable) and The Author(s), under exclusive license to Springer Nature Singapore Pte Ltd. 2021

Y.-D. Zhang et al. (eds.), *Smart Trends in Computing and Communications: Proceedings of SmartCom 2020*, Smart Innovation, Systems and Technologies 182,

https://doi.org/10.1007/978-981-15-5224-3_29

29.1 Introduction

Blockchain becomes an exciting technology to be followed by an academic researcher and IT practitioners in recent years. These phenomena are derived from the popularity of bitcoin since the launch in 2008 by a man/group called “Satoshi Nakamoto” [1]. The concept of blockchain technology first recognized as the “extraction” from the bitcoin platform, which becomes a phenomenon of technology with trustless, decentralized, and transparent virtual currency. Blockchain technology described as digitalized records is stored in a distributed ledger within a network that created, maintained, and created by each of its ledger owner [2]. Blockchain can be categorized as public (permissionless) and private blockchain, which related to a different concept of data access property [3].

Fueled with the popularity growth of blockchain technology, people become more interested in applying the blockchain concept in many cases. Several blockchain platforms allow people to participate directly inside the network and even provide a programming platform and learning center to encourage and gain interest from blockchain enthusiasts (Ethereum, IOTA, etc.). Ethereum [4] is a cryptocurrency that runs on the public blockchain network. This cryptocurrency is designed from the ground-up to provide developers with tools to build decentralized applications on its blockchain.

Ethereum offers a utility called ERC-20 token, which people could exchange or buy the token with Ether currency. Ethereum blockchain developers could use this token as a fund-raising medium or any sophisticated implementations. One of the most notable Ethereum token applications are asset-backed tokens or known as *stablecoins*. Stablecoins are blockchain-based digital currencies that have been created to hedge the volatility of cryptocurrencies. The price stability can be achieved through various methods such as a peg against a fiat currency or a commodity, collateralization against other cryptocurrencies, or algorithmic coin supply management [5]. These stablecoins become very popular recently as it eliminates uncertainty for customers. This research will discuss further stablecoins implementation with collateralization against a commodity.

29.2 Background

29.2.1 *The Nature of Blockchain*

Blockchain, with the popular definition, is a linked list of blocks (nodes) that contains a set of information. This linked list forms a chain of the network owned by each participant (miners). The mechanism that decides which miners will be authorized to validate a new block is called the blockchain consensus mechanism (proof-of-work, proof-of-stake, etc.) [6]. Blockchain characterized as an immutable, transparent, and traceable platform could answer the maximum trust, which standard centralized

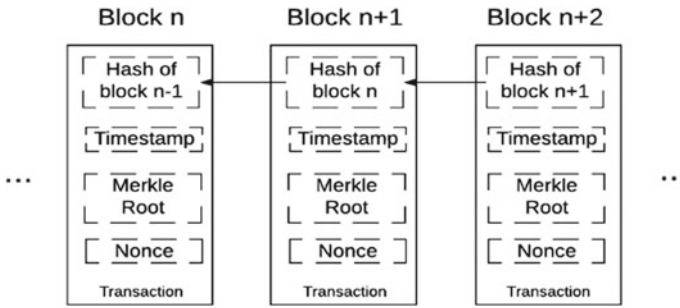


Fig. 29.1 Chain-structured blockchain. Every hash inside a block is a result of calculation from the previous block and used as the starting point for the next block. To achieve consensus, the network participants will validate the hash resulted from the calculation and starts to work on “discovering” the new block [7]. Ethereum and Bitcoin are examples of a blockchain network that uses this chain-structured blockchain

architecture system does not have. Figure 29.1 shows the chain-structured blockchain which becomes the “gold standard” used by many blockchain networks and projects.

29.2.2 Ethereum Network and Smart Contracts

This section will explain the smart contract and its uses in the Ethereum network [4, 8]. The leverage from blockchain technology implementation becomes a hot topic right now as the growth of blockchain is gone beyond cryptocurrency. There is another technological innovation related to the blockchain called “smart contract.” A public blockchain contains a smart contract, which is an agreement between mutually distrusting nodes or participants, which enforced automatically by a set of consensus mechanisms. Figure 29.2 shows the illustration of communication between the Ethereum network and smart contracts.

Ethereum [4] currently, the second-largest cryptocurrency by market-cap, offers extensive uses of blockchain networks beyond the cryptocurrency. The Ethereum coin is called “Ether.” Ethereum blockchain network allows the developer to build a smart contract executed on Ethereum Virtual Machine (EVM) [9]. A smart contract is a self-executing contract that is deployed in a blockchain network that contains a set of attributes and functions that coded to run the program functionality. The smart contract is developed using solidity language, which later could be connected with front-end Web applications through the uses of web3.js API [10]. Following are the facts related to Ethereum and smart contracts:

- A vast number of blockchain developers and contributors use Ethereum blockchain for development. This fact increases the confidant for the future development of Ethereum.

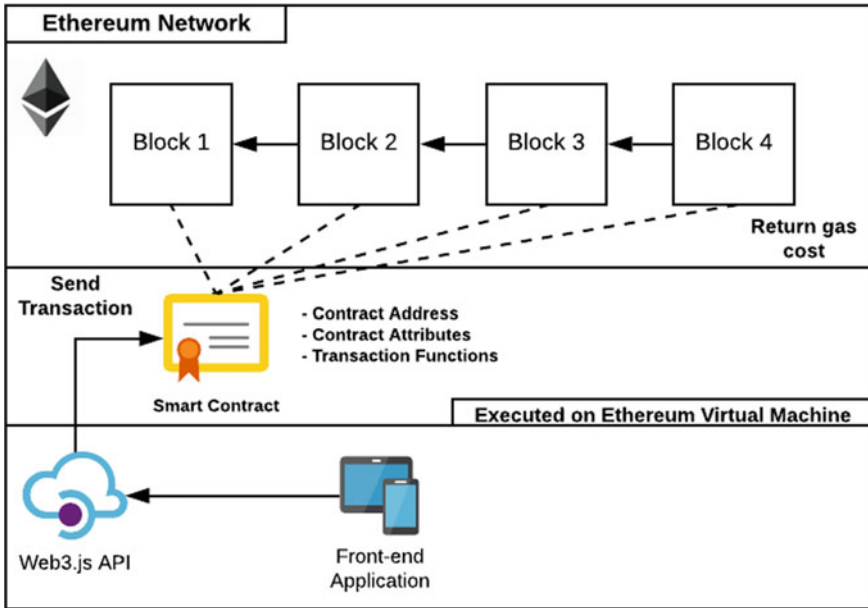


Fig. 29.2 Ethereum Network and Smart Contract: Bottom Section (Web3.js API and Front-end Application) called off-chain application as the program is running outside the Ethereum network. The two top sections are called on-chain applications while the application running inside the blockchain network and require to comply with the blockchain protocol (gas cost, queue, etc.)

- Ethereum system proves to endure severe attacks since its launch. This attack confirms the durability of system security [11].
- Once a smart contract is deployed in the network, it cannot be removed and forever will be existed.
- Every transaction executed by the smart contract will be processed by Ethereum Nodes and require gas.
- The gas is a metric that standardizes the executing cost of the code in the smart contract [12].

These facts drive the blockchain developers to write the smart contract carefully as the smart contract is susceptible to code efficiency and integrity. The availability of web3.js API also stimulates many developers to converge mobile/Web-based applications to the smart contract and Ethereum network to form a decentralized application.

```

function name() public view returns (string)
function symbol() public view returns (string)
function decimals() public view returns (uint8)
function totalSupply() public view returns (uint256)
function balanceOf(address _owner) public view returns (uint256 balance)
function transfer(address _to, uint256 _value) public returns (bool success)
function transferFrom(address _from, address _to, uint256 _value) public returns (bool success)
function approve(address _spender, uint256 _value) public returns (bool success)
function allowance(address _owner, address _spender) public view returns (uint256 remaining)

event Transfer(address indexed _from, address indexed _to, uint256 _value)
event Approval(address indexed _owner, address indexed _spender, uint256 _value)

```

Fig. 29.3 List of functions and events that should be coded to comply with the ERC-20 standard. These standards are mandatory requirements to enable a token to become tradeable in various wallets and crypto exchanges

29.3 Discussion

29.3.1 *Ethereum ERC-20 Token*

Ethereum offers token as a utility that could be used in project development. This utility token was included in the “*Ethereum Improvement Proposal*” (EIP) in 2017. A token is the part of the coin itself. You can create a token and then set the exchange value to the coin (Ether). This token can represent a project or can be backed with real-world assets such as gold or any other commodities. This condition is called the “Tokenized” asset [13]. The “*Energy Efficiency Coin (EECoin)*” [14] is one of the examples of asset tokenization in the energy market.

Ethereum has a standard tokenization procedure. ERC-20 is the most widely used token contract standard in Ethereum, as in November 2019, there are 224.637 Token Contracts found in Etherscan (etherscan.io) [15]. Figure 29.3 shows the standard functions that should be coded during ERC-20 implementations.

With adopting ERC-20 token, the project owner could raise funds for the project by issuing token and publish on the Web site to ask people that interested in the project to buy the token with some amount of Ether—later will be called “Initial Coin Offering” (ICO) [16]. With the growth of ICO popularity, people start to create innovation with the utilization of ERC-20 token by creating an asset-backed token, a token that backed by some commodities to preserve the value by the token itself.

29.3.2 *Asset-Backed Token Using Ethereum Blockchain Network*

In stablecoins with asset collateralization (further called asset-backed tokens), there are 3 involving parties that should have been provided with interfaces to the system.

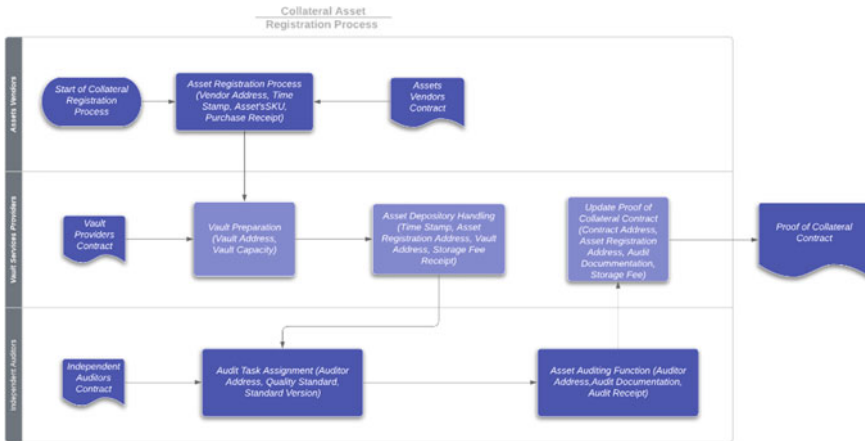


Fig. 29.4 Asset collateral registration process. There are three involved parties (Assets Vendors, Vault Services Provider, and Independent Auditor) in this process and using four smart contracts (Asset Vendors Contracts, Vault Providers Contract, Independent Auditors Contract, and Proof of Collateral Contracts) in the proof of collateral process

These parties include assets vendor, vault service provider, and auditors. Following are the roles of every involving parties.

- **Assets Vendor:** trusted and legitimated vendors for commodity product is important. Only selected vendors who have a certificate to comply with product standard is allowed to supply commodity reserves as collateral reserves.
- **Vault Services Provider:** independent, secure, and certified vault services provider is needed to custody the collateral reserves.
- **Independent Auditors:** independent auditors legitimate the commodity reserves. The auditors have a role in conveying the quality and legitimation of the reserves.

Those three essential parties are interconnected and collaborate with using smart contracts. Every party interacts with the smart contract through application interfaces that developed using web3.js and html5 application. Figure 29.4 shows the legitimations process of the collateral reserves in this asset-backed token.

29.3.3 Building a DApps in Ethereum Blockchain

There are two sections in a decentralized application that using blockchain networks, on-chain, and off-chain applications. As shown in Fig. 29.2, the on-chain application represents a smart contract coded with solidity language and deployed in Ethereum Virtual Machine. Moreover, an off-chain application includes the front-end application that could be coded with HTML5, Java, Swift, or any front-end development

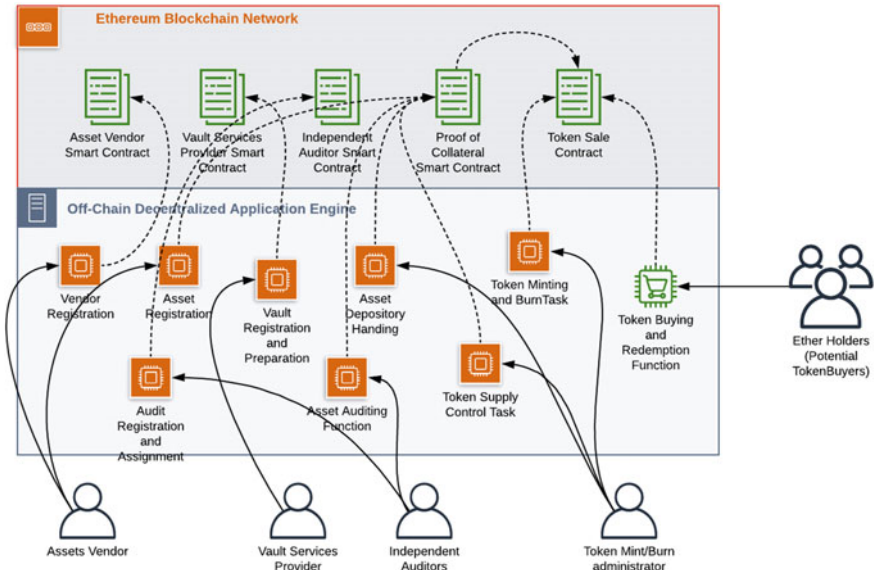


Fig. 29.5 On-chain applications deployed in the Ethereum blockchain network. This figure shows how involved parties interact with the smart contract through the off-chain decentralized application using web3.js API and HTML5

language or framework. In writing the code in on-chain applications (smart contracts), developers have to be very careful and pay attention to code efficiency and algorithm complexity because of the immutability of the smart contract. We use *truffle* and *ganache* as the development environment suite to ensure the function of the smart contract code. The two environments allow the developers to conduct unit tests and console simulation of a smart contract during the development process. Figure 29.5 shows the architecture of asset digitalization and token offering process through decentralized applications developed in this research.

29.3.4 Proof of Collateral

From the figure above, there is a contract called Proof of Collateral smart contract. The contract contains asset collateral legitimation data. Once asset collateral registration is completed, the contract will execute and update the parameter value of the contract. The parameter structure is shown below.

- **CollateralCode** works as the unique key for this contract.
- **TimeStamp** stores the timestamp in the format of an integer.
- **CollateralSignature** stores the chain of custody signature (vendor, vault, auditor).
- **PaymentReceipt** stores the asset value baseline.

- **DepositoryReceipt** stores the deposit time and fee with integer format.
- **CustodyFee** stores the custody fee for legitimation.

The **CollateralCode** is a unique key and generated by a hash function H of multiple variables, such as **VendorHash**, **AssetHash**, **AuditHash**, and **VaultHash**, and following are the combination of the document submitted:

$$\text{Collateral Code} = H(\text{Asset Hash}||\text{Vendor Hash}||\text{Vault Hash}||\text{Audit Hash})$$

Where the symbol (||) means concatenation operation. The **CollateralSignature** stores the signature from the chain of custody from the collateral asset, as shown below:

$$\text{Collateral Signature} = \text{SIGN}(\text{Asset Key}, \text{Asset Hash})$$

29.4 Conclusion

Stablecoins (asset-backed token) become an innovation in blockchain implementation in the financial and commodity market. This coin is a new type of cryptocurrency that has their value pegged to the real-world asset. Since the token is collateralized by real asset value, they designed to tackle the inherent volatility seen in cryptocurrency prices. This research shows that asset-backed token could be implemented by involving some regulating parties to provide custody of the collateralization process. An asset-backed token becomes disruptive innovation in blockchain with the development of decentralized applications using the Ethereum blockchain platform.

This research also shows the collateralization process of the real-world asset in backing the Ethereum ERC-20 token value. The architecture and communication diagram also designed in this research to illustrate the decentralized application architecture for selling an asset-backed token. For future research, the evaluation of cost efficiencies from these applications becomes an essential topic to be discussed. The following are the cost profile of a decentralized application that developed on the top of the Ethereum platform.

References

1. Nakamoto, S.: Bitcoin: A Peer-to-Peer Electronic Cash System (2008)
2. Konstantinidis, I., Siaminos, G., Timplalexis C., et al.: Blockchain for business applications: a systematic literature review. In: Lecture Notes in Business Information Processing. Springer International Publishing, pp. 384–399 (2018)
3. Rosati, P., Čuk, T.: Blockchain beyond cryptocurrencies. *Disrupting Finance*, pp. 149–170. Springer International Publishing, Cham (2019)

4. Buterin, V.: A Next Generation Smart Contract & Decentralized Application Platform, pp. 1–36 (2009)
5. Stablecoins explained—Lukas Schor—medium. <https://medium.com/@schor/stablecoins-explained-206466da5e61>. Accessed 15 Nov 2019
6. Hadi, S., Dmitry, A., Azamat, D.: Uberisation Business Model Based on Blockchain for Implementation Decentralized Application for Lease/Rent Lodging. Springer International Publishing, pp. 225–232 (2019)
7. Florea, B.C.: Blockchain and internet of things data provider for smart applications. In: 2018 7th Mediterranean Conference on Embedded Computing (MECO). IEEE, pp. 1–4 (2018)
8. Wood, G.: Ethereum: A Secure Decentralised Generalised Transaction Ledger. Ethereum Proj Yellow Pap, pp. 1–32 (2014). <https://doi.org/10.1017/CBO9781107415324.004>
9. Hirai, Y.: Defining the ethereum virtual machine for interactive theorem provers. In: Lecture Notes in Computer Science (including subseries Lecture notes in artificial intelligence and lecture notes in bioinformatics), pp. 520–535 (2017)
10. Lee, W.-M.: Beginning Ethereum Smart Contracts Programming. Apress, Berkeley, CA (2019)
11. N. Atzei, M. Bartoletti, T. Cimoli, A survey of attacks on ethereum smart contracts (SoK). In: Maffei M., Ryan M. (eds.) Springer, Berlin, Heidelberg, pp 164–186 (2017)
12. McCorry, P., Shahandashti, S.F., Hao, F.: A smart contract for boardroom voting with maximum voter privacy. In: Financial Cryptography and Data Security. FC 2017. Lecture notes in computer science, pp 357–375 (2017)
13. Adams, B., Tomko, M.: A critical look at cryptogovernance of the real world: challenges for spatial representation and uncertainty on the blockchain. Leibniz Int. Proc. Inform. LIPIcs **114**, 1–6 (2018). <https://doi.org/10.4230/LIPIcs.GIScience.2018.18>
14. Dispenza, J., Garcia, C., Molecke, R.: Energy efficiency coin (EECoin) a blockchain asset class pegged to renewable energy markets, pp. 1–4 (2017)
15. Etherscan Token Tracker. <https://etherscan.io/tokens>. Accessed 14 Nov 2019
16. Fenu, G., Marchesi, L., Marchesi, M., Tonelli, R.: The ICO phenomenon and its relationships with ethereum smart contract environment. In: 2018 IEEE 1st International Work Blockchain Oriented Software Engineering IWBOSE 2018—Proc 2018-January 1–7 (2018). <https://doi.org/10.1109/IWBOSE.2018.8327568>

Chapter 30

A Review of Focused Crawling Schemes for Search Engine



Suresh Kumar and Manisha Gupta

Abstract Nowadays, web is growing rapidly and retrieving information from it is very tedious. But search engines are trying their best to provide relevant results to users. Crawler is a very important component of search engine that works day and night and creates its repository. There are various categories of web crawler like focused crawler, adaptive crawler, breadth-first crawler, incremental web crawler, distributed web crawler, and parallel crawler. A focused crawler crawls web pages related to an area/topic only. In the literature, we have found various schemes of focused crawling and their comparison also. In this paper, we have reviewed all those schemes based on some important parameters such as principle, speed, network consumption, scalability, and strength. So, a review of focused crawling scheme has been presented in this paper.

30.1 Introduction

As we know World Wide Web (WWW) is growing rapidly in terms of web pages, therefore, search engines (SE) are required to manage/index these web pages to provide better and relevant results to users. There are many web search engines like Google, Yahoo, Bing, Baidu, and DuckDuckGo. Various alternatives have been projected and executed to discover information in the WWW such as specially designed meta-hyper documents, robot-based searchable indexes, and client-based search tools [1].

Crawlers are playing a very important role in SE to retrieve the most updated web pages from WWW and create repository of SE. They browse and index the WWW [2]. The basic crawling strategies of crawlers are depth first and breadth

S. Kumar (✉) · M. Gupta
Ambedkar Institute of Advanced Communication Technologies & Research Government of NCT,
Delhi, India
e-mail: sureshpoonia@aiactr.ac.in

M. Gupta
e-mail: 21mgupta@gmail.com

© The Editor(s) (if applicable) and The Author(s), under exclusive license
to Springer Nature Singapore Pte Ltd. 2021

Y.-D. Zhang et al. (eds.), *Smart Trends in Computing and Communications: Proceedings of SmartCom 2020*, Smart Innovation, Systems and Technologies 182,
https://doi.org/10.1007/978-981-15-5224-3_30

first. These techniques were used to crawl the web and then index the web pages. Unfortunately, these schemes retrieved huge amount of information, irrespective of particular topic. So, more effective algorithms like focused crawling have used [3] to retrieve information related to a focused topic. The World Wide Web has much information in its database. The information may be related to given topic, or it may also be unrelated. Finding such information related to specific topic is done by focused crawler. Focused crawler tries to fetch as many web pages related to a particular topic as it can but very less non-related web pages. Moreover, focused crawlers are designed to satisfy the requirements of users to maintain topic-specific collection of web documents [4].

Other than focused crawling, there are also other types of web crawling schemes like incremental crawling, adaptive crawling, distributed crawling, and parallel crawling. Incremental crawling revives step by step the current collection of web documents. It swaps the less significant pages with the more significant pages. Thus, it solves the problem of freshness of web pages. It provides only the valuable information to the user. Adaptive crawling makes use of data from earlier round to make a decision which pages should be examined for updates. It can be created to crawl the web dynamically [5, 6]. Distributed crawling uses many crawlers to distribute in the process of web crawling. A central server synchronizes the various crawlers. It is strong against system crashes. Parallel crawling consists of many crawlers that run in parallel on network of workstations [6].

The basic idea of parallel crawling, distributed crawling, and incremental crawling is to bring efficiently web pages into the repository of SE [7]. They are downloading web pages from web at high rate. Basically, these crawlers are working on efficiency of downloading web pages from web. But focused crawling works on the context, theme, and semantic of the web pages. It provides a great help to indexer component of SE to index web pages [3, 8]. Therefore, in this paper, we have made a comparative analysis of focused crawling schemes based on various parameters such as principle, speed, network consumption, scalability, and strength. There are many schemes of focused crawling. We have done comparative analysis of best focused crawling schemes, namely Fish Search, Shark Search, Info Spiders, N-Best First, and intelligent crawling. Info Spiders is the most scalable and most recent focused crawling scheme.

The description of this paper is as follows: The second section is about different focused crawling schemes. The third section shows the comparative analysis of focused crawling schemes based on various parameters.

30.2 Focused Crawling Schemes

Various focused crawling schemes have been found in the literature, but we have reviewed most prominent schemes such as Fish Search, Shark Search, Info Spiders, N-Best First, and intelligent crawling in the following sub-sections.

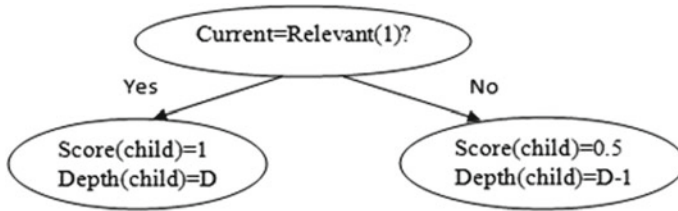


Fig. 30.1 Fish Search approach [3]

30.2.1 Fish Search

This approach fetches web documents according to the relevancy of document. If the document is relevant, then it is given the score as 1, and if it is not relevant, then it is given the score 0. Thus, this approach works on keyword matching. And if document score is 1, then its child score is automatically 1; i.e., if parent document is relevant, then child document is automatically relevant. And if document score is 0, then its child score is 0.5; i.e., if parent document is irrelevant, then child document is less relevant and so on [9, 10]. Actually, this approach imitates a school of fish [1]. The main logic of this approach is shown in Fig. 30.1.

30.2.2 Shark Search

This approach is the extension and improvisation of Fish Search approach. It uses the same technique of giving scores to relevant document, but in this approach, scores are between 0 and 1 instead of binary as scores are calculated using similarity concept of vector space model (VSM) [9, 11].

The child document has the inherited score, i.e., score of its parent document. The second enhancement is that scores are calculated not only on the basis of parent document's score but also on the basis of meta data. This makes this approach more effective than the Fish Search approach [3]. The main logic of this approach is shown in Fig. 30.2.

30.2.3 Info Spiders

This approach uses neural net and back propagation. Info Spiders is the multi-agent system for web mining of the information [3]. Each agent of the system adjusts to its local surroundings by learning to approximate the value of anchor links. An agent interconnects with the information environment that composes of the web and the data placed on local data structures. An agent can alter its neural net-based manner

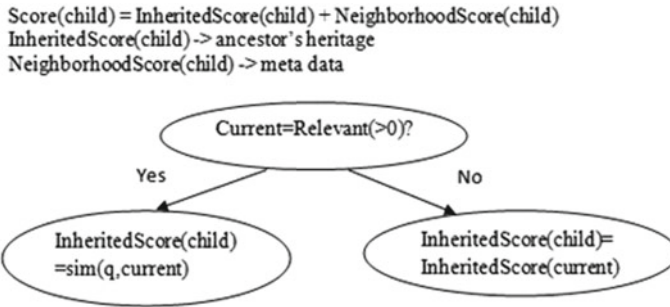


Fig. 30.2 Shark Search approach [3]

during its existence. This is done by reinforcement learning. This approach crawls only the current surroundings and thus does not provide old data [12, 13]. Agents crawl the web dynamically and apply artificial intelligence approaches to adjust to the features of its information domain. It is the most scalable approach.

30.2.4 *N-Best First*

This approach is a generalization of Best First approach. At each move, N web documents are picked for crawling instead of one page [9]. Using some algorithms, it predicts the similarity between seed URLs and target web document and chooses the best one to crawl. The best document is found by calculating score or rank. Naïve Bayes, cosine similarity, and support vector machine (SVM) are applied to calculate score [14, 15].

To improve performance, it uses heuristic methods. The job of heuristics is to assess the web link in view of the provided information before getting its data. Since Best First alludes to the technique for investigating the link with the best score first, an assessment function is utilized to dole out a score to each link. There are various methods for assessing the link before getting the entire data, for example, assessing the words in the link and assessing the clickable text of the link [14].

30.2.5 *Intelligent Crawling*

This approach gives priorities to seed web documents on the basis of particular characteristics in a web document. These characteristics may be page content, URL data, sibling pages, or information about related or non-related pages. This approach is a non-exclusive system in that it enables the client to determine the relevance standard. Thus, this approach is highly effective with the potential of self-learning; i.e., it gathers all data and normalizes the weight of these characteristics to represent

the superior factor at that time [9, 13]. It is an algorithm that figures out how to crawl without direct client preparing [9].

30.3 Review of Focused Crawling Schemes

The key principle of Fish Search is based on keyword matching. As we know, there is a problem of synonymous and polysemy in keyword matching [9]. For example, Java is a polysemous word. Java has multiple senses as Java is a programming language, motorbike, island and coffee and many more. So keyword matching principle is not a good idea to retrieve web pages by SE. For example, our context for Java is programming language, but if SE retrieves web pages of coffee, then they are irrelevant for us. Therefore, various schemes have been found in the literature to resolve this issue.

For example, Shark Search scheme works on VSM principle. VSM is a mathematical model which works in context of word also. Thus, it provides better results to SE as comparative to Fish Search scheme [9].

Fish Search scheme is hampered by lack of adaptability and scalability. Info Spiders scheme is the major solution to the adaptability problem and scalability problem. In this scheme, agents utilize neural nets to choose which web link to track. It is the earliest crawling algorithm to apply reinforcement learning. Reinforcement learning helps in adaptability and scalability [3, 12, 13].

Another scheme N-Best First works on document similarity principle. In this scheme, similarity is computed based on lexical term matching. Documents are similar if they share common terms. But absence of common terms does not indicate that they are distinct. They can be semantically similar. They can also be thematically similar. For example, mouse is a keyword with multiple meanings as computer equipment, animal, etc. So, one page might have content of mouse as computer equipment. Second page might have content of mouse as animal. So both pages are semantically different but they share same keyword mouse. So document similarity in N-Best First scheme is computed by VSM or by semantic similarity retrieval model. It has better performance than Info Spiders and Shark Search approaches. It is the most victorious scheme as a consequence of its simplicity and efficiency [9].

There is also one more scheme, i.e., intelligent crawling. This scheme has the skill of self-learning. It is the highly effective approach that learns to crawl without user training [9, 13].

A detailed review of focused crawling schemes based on five parameters is given in Table 30.1 [16]. Briefing of five parameters is as follows:

Principle—It tells about the basic models/algorithms applied in particular scheme.

Speed—It tells about the efficiency of retrieved results corresponding to users query.

Network consumption—It tells about maximum rate of data/information transfer across a particular network.

Table 30.1 A review of focused crawling schemes

Schemes	Principle	Speed	Network consumption	Scalability	Strength
Fish Search	Keyword matching	Slow	High	Less scalable	<ul style="list-style-type: none"> ● Follow optimized strategy
Shark Search	Vector space model	Fast	Less	Less scalable	<ul style="list-style-type: none"> ● Improvement over Fish Search ● Uses better relevance technique
Info Spiders	Neural network, back propagation	Fast	Less	More scalable	<ul style="list-style-type: none"> ● Complement traditional index-based search engines ● Achieves good coverage of relevant documents
N-Best First	Vector space model	Fast	Less	Less scalable	<ul style="list-style-type: none"> ● Better performance than Shark Search and Info Spiders
Intelligent crawling	Ability of self-learning	Fast	Less	Less scalable	<ul style="list-style-type: none"> ● Highly effective algorithm that learns to crawl without user training

Scalability—It is the property of a scheme/system to handle huge amount of data by adding more resources to system.

Strength—It is the quality of particular scheme with respect to produce relevant results.

30.4 Conclusion

A detailed review of focused crawling schemes based on various parameters has been described in this article. Since focused crawler fetches pages related to particular area, so it is better than other crawlers. In this paper, we have concluded that Shark Search is extension of Fish Search and is more effective than it. N-Best First has better performance than Info Spiders and Shark Search. But Info Spiders is the most scalable of all schemes. Another scheme is an intelligent crawling which has the advantage of self-learning. Thus, different schemes have different advantages over other schemes. Nowadays, we are working on the novel mathematical focused crawling scheme based on ontology to improve the performance of SE in terms of precision and recall.

References

1. De Bra, P.M.E., Post, R.D.J.: Information retrieval in the world wide web: making client-based searching feasible. *Comput. Netw. ISDN Syst.* **27**(2), 183–192 (1994)
2. Diligenti, M., Coetzee, F., Lawrence, S., Giles, C.L., Gori, M.: Focused crawling using context graphs. In: *Proceedings of 26th International Conference on Very Large Databases*, pp. 527–534 (2000)
3. Amrin, A., Xia, C., Dai, S.: Focused web crawling algorithms. *J. Comput.* **10**(4) (2015)
4. Kumar, A., Kumar, A.: A study of focused crawler approaches. *Int. J. Innovative Res. Comput. Commun. Eng.* **3**(12) (2015)
5. Amudha, S.: Web crawler for mining web data. *Int. Res. J. Eng. Technol. (IRJET)* **4**(2) (2017)
6. Udupure, T.V., Kale, R.D., Dharmik, R.C.: Study of web crawler and its different types. *IOSR J. Comput. Eng. (IOSR-JCE)* **16**(1) (2014)
7. Elyasir, A.M.H., Anbananthen, K.S.M.: Focused web crawler. In: *International Conference on Information and Knowledge Management (ICKM 2012)*. IACSIT Press, Singapore (2012)
8. Dorado, I.G.: *Focused Crawling: Algorithm Survey and New Approaches with a Manual Analysis*. Sweden E-huset, Lund, April 7 (2008)
9. Batsakis, S., Petrakis, E.G.M., Milios, E.: *Improving the performance of focused web crawlers*. *Data Knowl. Eng. (Elsevier)* (2009)
10. Pranav, A., Chauhan, S.: Efficient focused web crawling approach for search engine. *IJCSMC* **4**(5) (2015)
11. Hersovici, M., Jacovi, M., Maarek, Y., Pelleg, D., Shtalhaim, M., Ur, S.: The shark-search algorithm—an application: tailored web site mapping. In: *Proceedings of the Seventh International World Wide Web Conference*, Brisbane, Australia (1998)
12. Menczer, F.: Complementing search engines with online web mining agents. *Decis. Support Syst.* **35**(2), 195–212 (2003)
13. Ganguly, B., Sheikh, R.: A review of focused web crawling strategies. *Int. J. Adv. Comput. Res.* **2** 4(6) (2012)
14. Yu, Y.-B., Huang, S.-L., Tashi, N., Zhang, H., Lei, F., Wu, L.-Y.: A survey about algorithms utilized by focused web crawler. *J. Electron. Sci. Technol.* **16**(2) (2018)
15. Shah, V., Patni, R., Patani, V., Shah, R.: Understanding focused crawler. (*IJCSIT*) *Int. J. Comput. Sci. Inf. Technol.* **5**(5), 6849–6852 (2014)
16. Ziya, F., Kumar, S.: Comparative analysis of focused web crawling schemes. *JETIR* **6**(3) (2019)

Chapter 31

Design and Simulation of Multi-channel V-TDMA for IoT-Based Healthcare Systems



Anita Ramachandran, Malaika Afra Taj, Raghav Maheshwari,
and Anupama Karuppiah

Abstract Internet of things (IoT)-based geriatric healthcare monitoring system monitors physiological and biological parameters of members in an elderly care home. This system consists of multiple network elements—wearable nodes for monitoring parameters, master nodes to process the collected information and raise alarms on observing any anomalies and intermediate nodes to relay information between the sensor nodes and master nodes. Maximum reliability, energy efficiency, and minimal latency during the data communication are the major requirements of such a system. Media access control (MAC) layer plays a significant role in achieving the above-mentioned requirements. In this paper, we propose a multi-channel variable time division multiple access (multi-channel V-TDMA) MAC protocol which includes the strengths of both standard time division multiple access (TDMA) and frequency division multiple access (FDMA) protocols. The proposed protocol efficiently provides a solution to the problem of continuous and reliable data transmission by the wearable nodes, along with the freedom of mobility.

31.1 Introduction

IoT systems have gained considerable attention in the area of healthcare monitoring in recent years. IoT-based healthcare monitoring systems for an elderly care home monitor various kinematic and biophysical parameters of the elderly people, detect

A. Ramachandran
BITS Pilani, Bangalore, India
e-mail: anita.ramachandran@pilani.bits-pilani.ac.in

M. A. Taj (✉) · R. Maheshwari · A. Karuppiah
BITS Pilani, KK Birla Goa Campus, Goa, India
e-mail: h20180118@goa.bits-pilani.ac.in

R. Maheshwari
e-mail: f20150763@goa.bits-pilani.ac.in

A. Karuppiah
e-mail: anupkr@goa.bits-pilani.ac.in

© The Editor(s) (if applicable) and The Author(s), under exclusive license
to Springer Nature Singapore Pte Ltd. 2021

Y.-D. Zhang et al. (eds.), *Smart Trends in Computing and Communications: Proceedings of SmartCom 2020*, Smart Innovation, Systems and Technologies 182,
https://doi.org/10.1007/978-981-15-5224-3_31

abnormalities, and raise appropriate alerts to healthcare personnel so that adequate care can be made available in a timely manner. Each person is equipped with a wearable device which has inertial motion unit (IMU) sensors and vital signs sensors embedded in it. IMU sensors measure a person's mobility in terms of acceleration, magnetometer, and gyroscope. Vital signs sensors measure various biophysical parameters such as heart rate, blood pressure, pulse oximetry (SPO2), and galvanic skin response (GSR) values. A brief overview of such a healthcare system is explained in one of our previous works [1]. Such an IoT network consists of a set of nodes with data collection and routing capabilities. The MAC protocols that support communication between the nodes in an IoT system can be TDMA-based or contention-based, and both have their advantages and disadvantages. In this paper, we propose a MAC protocol which suits the requirements of the above-mentioned IoT network. The proposed MAC algorithm performs periodic collection of data as well as support dynamic timeslot allocation scheme to accommodate mobility of nodes in a contextual manner, while being energy-aware. The multi-channel variable time division multiple access (Multi-channel V-TDMA) MAC protocol proposed here includes the strengths of both TDMA and FDMA protocols. The rest of the paper is organized as follows: We briefly discuss several other key MAC protocols in Sect. 31.2. Section 31.3 describes the network topology. The detailed description of the proposed algorithm is mentioned in Sect. 31.4. Section 31.5 presents the comparative performance with standard TDMA and FTDMA. Section 31.6 concludes the paper with the summary of our findings.

31.2 Related Work

The two well-established MAC schemes are reservation-based and contention-based. While each has its own advantages, they also have their shortcomings, and the well-known issues of these traditional schemes apply in the context of healthcare systems also. Many protocols have been developed which address the shortcomings of the traditional time division multiple access (TDMA) and carrier sense multiple access (CSMA) schemes, along with optimizing the energy consumption. Some of these protocols include B-MAC [2], S-MAC [3], WiseMAC [4], T-MAC [5], E-MACS [6], and L-MAC [7]. Flexible TDMA (FTDMA) [8] is developed for mobile sensor networks. In this, the leader broadcasts the number of available slots and fixed slots to the mobile nodes. The mobile nodes send a request message in any one of the free slots. The leader acknowledges the request, allocates slot to the mobile node, and broadcasts the updated schedule in the next cycle. However, the mobile nodes in the communication range of two or more leaders will suffer interferences and collisions. FlexiTP [9] is a TDMA-based protocol in which nodes only transmit and receive packets at their own timeslot(s) and sleep until their slots turn up again. However, it is designed for a static ad hoc network, in which nodes may suffer temporary or permanent failure, and new nodes may be added to the network at any time, but nodes otherwise remain in (nearly) the same location. Aminian [10] explains a deployment

scenario for a hospital healthcare monitoring system, consisting of sensor nodes and coordinator nodes. This design uses the TDMA scheme for timeslot allocation. Jung et al. [11] proposes an 802.15.4-based WSN for healthcare monitoring. Yan and Liu [12] explain the design of a context-aware MAC protocol for WBANs, for a star-topology network consisting of several sensor nodes for collecting data, and a master node which processes the data. The data rate and duty cycle of the sensor nodes are controlled by the master node, which are increased from the normal condition, if an emergency is detected. A system architecture for smart health care for continuous monitoring of assisted-living residents is proposed in [13]. The system comprises of sensors for biophysical and environmental monitoring, backend databases and end devices for visualization, and all components are connected by a backbone network wirelessly or overlaid on to an existing wired infrastructure. Other architectures for remote healthcare monitoring include [14] and [15]. Benhaddou et al. [16] propose a MAC scheme for healthcare sensor networks, MACH, which prioritizes emergency traffic and adapts channel provisioning based on information criticality.

31.3 Network Topology

The various types of nodes that form the overall network are stated as follows:

1. *Mobile Node (MN)*: The wearable device worn by each elderly person.
2. *Room Coordinator (RC)*: Each room in the healthcare home shall be equipped with an RC. The RC is responsible for collecting data from all MNs under its purview.
3. *Central Coordinator (CC)*: Each floor within the healthcare home shall have a CC. This is where all data from MNs gets collated via RCs.

A tree-based network is formed where CC is the root of the tree. Several RCs are connected to CC directly or through a multi-hop path formed via intermediate RCs and multiple MNs are connected to individual RCs. Figure 31.1 represents the network topology of the healthcare system.

31.4 Design of Multi-channel V-TDMA MAC Protocol

31.4.1 Protocol Overview

In the proposed multi-channel V-TDMA protocol, there are two levels of hierarchy in the network: one level between RC and MN and the second level between RC and CC. Data collected by the MNs include physiological and biological parameters of the elderly person wearing the device. This data is relayed by the MNs to the RC via a single-hop communication path. The RCs collect data transmitted from all the

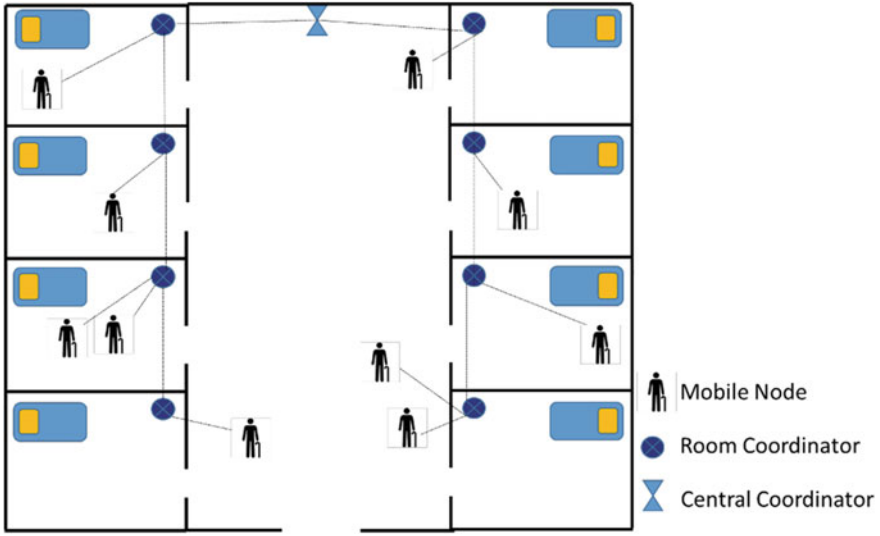


Fig. 31.1 Network topology diagram

CC-RC Broadcast	RC-MN Broadcast	MN-RC Data Transmission	RC-CC Data Transmission
-----------------	-----------------	-------------------------	-------------------------

Fig. 31.2 Overall frame structure

MNs within its range and relays the same to the CC, where the data is analyzed. This is enabled by a multi-hop path between RCs and CC. Figure 31.2 represents the overall frame structure of the protocol.

The maximum number of slots in a frame is determined by Eq. (31.1):

$$T = t/s \tag{31.1}$$

where T = maximum number of slots, t = maximum delay that is allowed before the data reaches CC, and s = size of each slot in the frame.

Based on the variations in the data collected by the wearable bands in an elderly care home, the ideal sampling rate obtained is 1000 ms. This ideal sampling rate is determined using the results of various machine learning algorithms on collected data. The detailed analysis of collected data is mentioned in our previous paper [1]. Therefore, the ideal frame size determined is 1000 ms which is divided into various subframes as follows:

- 100 ms for CC-RC broadcast
- 100 ms for RC-MN broadcast
- 300 ms for MN-RC data communication out of which initial 50 ms is for frequency switching. The remaining 250 ms is divided into slots each of size 10 ms.

- 500 ms for RC-CC data communication out of which initial 50 ms is for switching back to default frequency. The remaining 450 ms is divided into slots with each of size 30 ms.
- The size of the slots is calculated by Eq. (32.2):

$$s = 1.5 * (rx - tx) + td \tag{32.2}$$

where rx = time at which the packet was received, tx = time at which the packet was transmitted, and td = transmission delay of packet.

31.4.2 Multi-channel V-TDMA Algorithm

This section describes the working of the multi-channel V-TDMA protocol, with respect to network discovery, timeslot allocation map advertisement, data transmission and forwarding, and frequency switching.

- (1) **Network discovery:** This protocol begins with the network discovery between CC and RCs.
 - CC sends CC_BCAST_MSG (Fig. 31.3), with its node ID and location coordinates.
 - All RCs in Level-i receives the CC_BCAST_MSG.
 - Each RC in Level-i rebroadcasts the CC_BCAST_MSG, after updating the RC ID, RCx, and RCy field with its own ID and coordinates.
 - The rebroadcast CC_BCAST_MSG is received by RCs at Level-(i + 1).
 - If an RC receives CC_BCAST_MSGs from more than one neighboring RC, it chooses the one which is closer to itself.
 - Network formation completes once all RCs receive the CC_BCAST_MSG.
- (2) **Timeslot allocation map advertisement:** After receiving the CC_BCAST_MSG, each RC waits for a certain time delay which is the function of its geographical coordinates to ensure that the entire network between CC and all RCs is formed.
 - RC sends an RC_BCAST_MSG (Fig. 31.4) containing the timeslot allocation map, with total number of slots (N) and occupied number of slots (O), and the frequency of communication (Channel) for MN-RC data transmission and IDs of MNs to which the slots are allotted (MN1–MNm).

Msg Type	CC ID	RC ID	CCx	CCy	RCx	RCy
----------	-------	-------	-----	-----	-----	-----

Fig. 31.3 CC_BCAST_MSG

Msg Type	RC ID	Channel	N	O	MN1 to MNm
----------	-------	---------	---	---	------------

Fig. 31.4 RC_BCAST_MSG

- This message will be received by all MNs which are present in the communication radius of the RC.

(3) **Data transmission:** The procedure of data transmission between MNs and RC is described as follows:

- Each MN scans through the list of fixed slots in the RC_BCAST_MSG.
- If the MN finds its ID in the list of occupied slots, it sends data in that slot; else it picks up random slot from the list of free slots and sends a timeslot request message to RC. The slot selection by the MN is given by Eq. (31.3):

$$\text{Slot} = (\text{Rssi} \% (N - O + 1)) + O \tag{31.3}$$

where Rssi = receive signal strength of RC_BCAST_MSG, N = Total number of slots, O = Number of occupied slots.

- RC upon receiving the timeslot request message updates the timeslot allocation map before broadcasting the same in the subsequent cycle.
- If the RC does not receive data from a particular MN for subsequent k cycles, then it de-allocates that MNs timeslot in the following cycle (Eq. 31.4).

$$k = f(\mu) \tag{31.4}$$

where μ = mobility rate of mobile nodes.

(4) **Data forwarding:** The process of data forwarding from RC to CC, via the multi-hop path between RC and CC is given below:

- RC at Level $(i + 1)$ transmits data collected from its MNs to its neighboring RC at Level- (i) , during its RC-CC data transmission slot.
- After the RC to CC communication, the cycle repeats all over again from timeslot allocation map advertisement.
- The entire process from network takes place every y cycles (Eq. 31.5) in order to ensure minimum control overhead in the network:

$$y = f(a) \tag{31.5}$$

where a = rate at which the RCs are added or deleted.

31.4.3 Frequency Switching in Multi-channel V-TDMA

In order to ensure minimal packet loss in the network, the data communication between RC and MNs is designed to occur at different frequencies. Each individual RC broadcasts a different frequency according to Eq. (31.6):

$$\text{Frequency}(f) = \text{Default Frequency} + \text{Id of RC} \quad (31.6)$$

where $f \leq$ no. of frequency levels supported by hardware, and default frequency = initial frequency of all the nodes in the network.

The value of f is specified in channel field (see Fig. 31.4). After RC to MN data communication, all the nodes shall switch back to default frequency.

31.4.4 Energy Conservation in Multi-channel V-TDMA

Mobile nodes: Mobile nodes remain awake only during the advertisement of timeslot allocation map and during data communication with RC. The MNs turn their radio off for the remaining duration to conserve energy. The percentage of energy conserved (E) in MNs is 60% calculated by Eq. (31.7):

$$\begin{aligned} \% \text{ of } E = 100 - \{ & (\text{Activetimeofnodes} / (\text{Activetimeofnodes} \\ & + \text{sleeptimeofnodes})) * 100 \} \end{aligned} \quad (31.7)$$

The active time and sleep time for MN are calculated using Eqs. (31.8) and (31.9):

$$\begin{aligned} \text{Active time of MN} = & \text{RC-MN Broadcast time} + \text{MN-RC data} \\ & \text{communication time} \quad (100 \text{ ms} + 300 \text{ ms} = 400 \text{ ms}) \end{aligned} \quad (31.8)$$

$$\begin{aligned} \text{Sleep time of MN} = & \text{Overall frame size} \\ & - \text{Active time of MN} \quad (1000 \text{ ms} - 400 \text{ ms} = 600 \text{ ms}) \end{aligned} \quad (31.9)$$

Room coordinators: The sleep-wake pattern of RCs is shown in Fig. 31.5. The slots which the RCs are active depend on the position in the network architecture. The % of energy conserved in RCs is 39%. The active and sleep time for RC is calculated using Eqs. (31.10) and (31.11):

$$\begin{aligned} \text{Active time of RC} = & \text{CC-RC Broadcast time} + \text{RC-MN Broadcast time} \\ & + \text{MN-RC data communication time} \\ & + \text{Default Frequency switching time} \\ & + \text{Transmit time of RC-CC data} \end{aligned}$$

RC-CC communication

Network discovery	RC - MN broadcast	MN-RC data communication	Sleep	RX from RC i+1	TX to RC i-1	Sleep
-------------------	-------------------	--------------------------	-------	----------------	--------------	-------

RC-Level i

RC-CC communication

Network discovery	RC - MN broadcast	MN-RC data communication	RX from RC i+2	TX to RC i	Sleep
-------------------	-------------------	--------------------------	----------------	------------	-------

RC-Level i+1

Fig. 31.5 Sleep—wake pattern of RC

$$\begin{aligned}
 &+ \text{Receive time of RC-CC data} \\
 &(100 \text{ ms} + 100 \text{ ms} + 300 \text{ ms} + 50 \text{ ms} + 30 \text{ ms} + 30 \text{ ms}) \quad (31.10)
 \end{aligned}$$

$$\begin{aligned}
 \text{Sleep time of RC} &= \text{Overall frame size} \\
 &- \text{Active time of RC} \quad (1000 \text{ ms} - 610 \text{ ms} = 390 \text{ ms}) \quad (31.11)
 \end{aligned}$$

31.5 Simulation and Results

Figures 31.6 and 31.7 show the screenshot of the simulated network with multi-channel V-TDMA, with the MN-RC and RC-CC and communication paths. Because of frequency switching, it is observed that there is no interference between MN-RC (Fig. 31.6) and RC-CC (Fig. 31.7) communication. The simulation was done on Cooja for a network containing 1 CC (Node 1), 6 RCs (Nodes 2–7) and 20 MNs

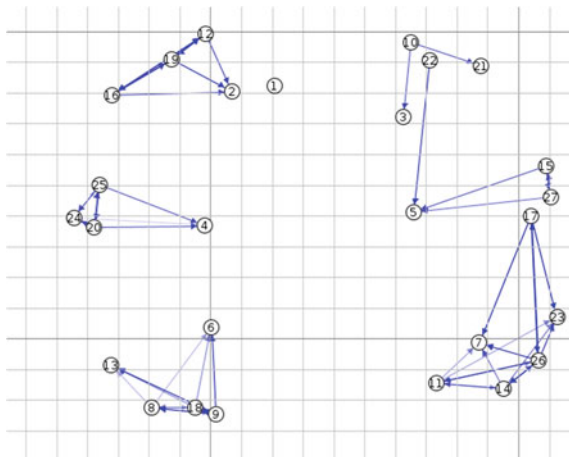


Fig. 31.6 MN-RC communication

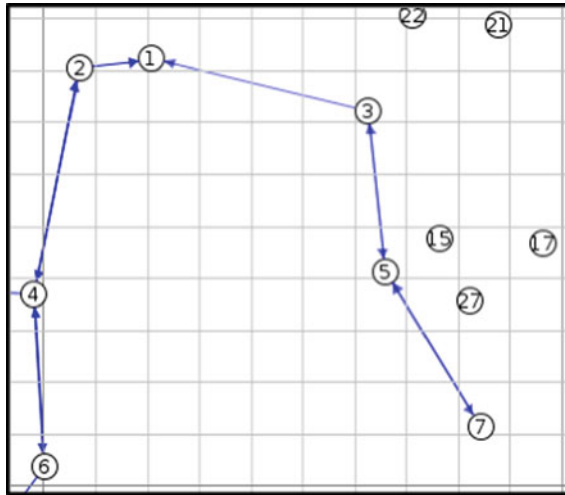


Fig. 31.7 RC-CC communication

(Nodes 8–27). The network was also simulated for MN densities of 5, 10, 15, and 20. The overall frame size considered was 1000 ms. The simulation time was 15 min, and the results are averaged across 5 runs of the simulation. Mobility of MNs was induced every one minute to simulate changes in the network topology.

The performance parameters that were collected were average delay, maximum delay (where delay is the time taken for a data packet originated by an MN, to reach the CC), and packet loss ratio. The performance was then compared with the standard TDMA and FTDMA [8]. The results are shown in Figs. 31.8, 31.9, and 31.10.

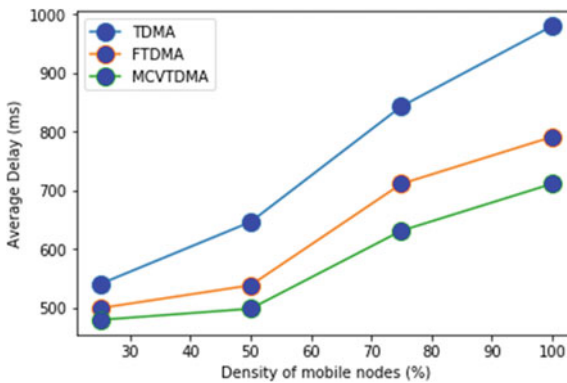


Fig. 31.8 Average delays

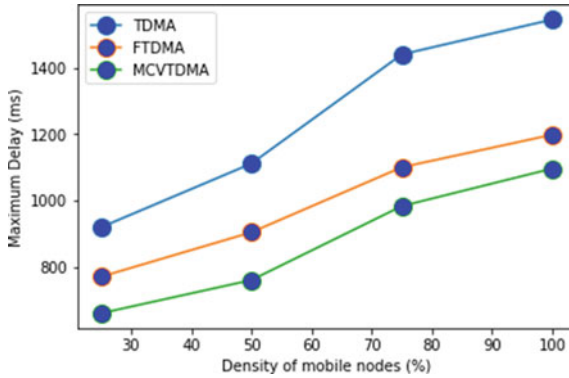


Fig. 31.9 Maximum delay

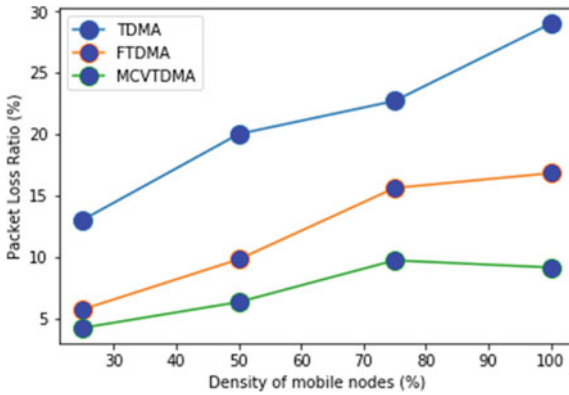


Fig. 31.10 Packet loss ratio

31.6 Conclusions

In this paper, we proposed an energy-aware multi-channel V-TDMA MAC protocol which combines the strengths of both standard FDMA and TDMA schemes. The developed MAC protocol takes advantage of multiple frequencies provided in wireless sensor network (WSN) hardware platforms like MICAZ, Telosb, and CMU FireFly. The step-by-step working of the protocol along with the frame structures was explained. We simulated this protocol on Cooja and compared the performance of multi-channel V-TDMA with basic TDMA and FTDMA. Based on the results, multi-channel V-TDMA performs better than basic TDMA and FTDMA with respect to average delay, maximum delay, and packet loss ratio. As a part of future work, multi-channel V-TDMA will be implemented in real-time test bed for further analysis.

References

1. Anupama, K.R., Adarsh, R., Pahwa, P., Ramachandran, A.: Machine learning-based techniques for fall detection in geriatric healthcare systems. In: 9th International Conference on Information Technology in Medicine and Education (ITME), pp. 232–237. Hangzhou (2018)
2. Polastre, J., Hill, J., Culler, D.: Versatile low power media access for wireless sensor networks. In: Proceedings of the 2nd International Conference on Embedded Networked Sensor Systems, November 2004. Baltimore, MD, USA. <https://doi.org/10.1145/1031495.1031508>
3. Ye, W., Heidemann, J., Estrin, D.: An energy-efficient MAC protocol for wireless sensor networks. In: Proceedings of Twenty-First Annual Joint Conference of the IEEE Computer and Communications Societies, vol. 3, pp. 1567–1576. New York, NY, USA. <https://doi.org/10.1109/infcom.2002.1019408> (2002)
4. El-Hoiydi, A., Jean-Dominique, D.: WiseMAC: An ultra low power MAC protocol for multi-hop wireless sensor networks. In: Algorithmic Aspects of Wireless Sensor Networks, ALGOSENSORS, vol. 3121, pp. 18–31. Turku, Finland. https://doi.org/10.1007/978-3-540-27820-7_4 (2004)
5. van Dam, T., oen Langendoen, K.: An adaptive energy-efficient MAC protocol for wireless sensor networks. In: Proceedings of the First International Conference on Embedded Networked Sensor Systems, vol. 1, pp. 171–180. <https://doi.org/10.1145/958491.958512>
6. Nieberg, T., Dulman, S., Havinga, P., van Hoesel, L., Wu, J.: Collaborative algorithms for communication in wireless sensor networks. In: Basten, T., Geilen, M., de Groot, H. (eds.) Ambient Intelligence: Impact on Embedded System Design. Springer, Boston, MA. https://doi.org/10.1007/0-306-48706-3_14 (2003)
7. van Hoesel, L.F.W., Havinga, P.J.M.: A lightweight medium access protocol (LMAC) for wireless sensor networks: reducing preamble transmissions and transceiver state switches. In: 1st International Workshop on Networked Sensing Systems, INSS 2004, pp. 205–208. Tokio, Japan (2004)
8. Abdullah-Al-Wadud, M.: A TDMA scheme for mobile sensor networks. *Int. J. Distrib. Sens. Netw.* <https://doi.org/10.1155/2013/907583> (2013)
9. Lee, W.L., Datta, A., Cardell-Oliver, R.: FlexiTP: a flexible-schedule-based TDMA protocol for fault-tolerant and energy-efficient wireless sensor networks. *IEEE Trans. Parallel Distrib. Syst.* **19**(6), 851–864 (2008). <https://doi.org/10.1109/TPDS.2007.70774>
10. Aminian, M.: A hospital healthcare monitoring system using wireless sensor networks. *J. Health Med. Inf.* **4**. <https://doi.org/10.4172/2157-7420.1000121> (2013)
11. Jung, S., Kwon, T., Chung, W.: A new approach to design ambient sensor network for real time healthcare monitoring system. In: Sensors, pp. 576–580. Christchurch. <https://doi.org/10.1109/icsens.2009.5398310> (2009)
12. Yan, Z., Liu, B.: A context aware MAC protocol for medical Wireless Body Area Network. In: 7th International Wireless Communications and Mobile Computing Conference, pp. 2133–2138. Istanbul. <https://doi.org/10.1109/iwcmc.2011.5982864> (2011)
13. Virone, G., Wood, A., Selavo, L., Cao, Q., Fang, L., Doan, T., et al.: An advanced wireless sensor network for health monitoring. In: Proceedings of Transdisciplinary Conference on Distributed Diagnosis and Home Healthcare, pp. 95–100 (2006)
14. Shen, X., Zeng, J., Liu, T., Hu, C.: Remote healthcare monitor system. In: 3rd International Conference on Biomedical Engineering and Informatics, pp. 1901–1905. Yantai. <https://doi.org/10.1109/bmei.2010.5639530> (2010)
15. Chauhan, J., Bojewar, S.: Sensor networks based healthcare monitoring system. In: International Conference on Inventive Computation Technologies (ICICT), pp. 1–6. Coimbatore <https://doi.org/10.1109/inventive.2016.7824814> (2016)
16. Benhaddou, D., Balakrishnan, M., Yuan, X.: Remote healthcare monitoring system architecture using sensor networks. In: IEEE Region 5 Conference, pp. 1–6. Kansas City, MO. <https://doi.org/10.1109/tpsd.2008.4562760> (2008)

Chapter 32

Design and Development of Tiny Humanoid Walking and Dancing Robot with Obstacle Detection for Visual Impaired People



Amrita Ganguly, Jasmine Ara, and Bijan Paul

Abstract Over the most recent couple of years, people are indicating more enthusiasm for robotics and planning to rely upon robots for many reasons. One can easily expect that in the twenty-first century, the use of robots will expand in our society. We believe that robots will achieve a wide assortment of undertakings in homes, war zones, atomic plants, government establishments, production line floors, and even space stations. In this paper, we are throwing some light on robotics with a robot that is utilizing the human structure to make movements like walking and dancing. This biped robot is also able to detect an object in front of it. This has been accomplished using Arduino Nano (ATmega328P), servomotors SG90 operating on the principle of servomechanism, and ultrasonic sensor to detect objects near it and prevent the robot from proceeding forward. The robot has ultimate use in entertainment, in marketing, and in assisting visually impaired to navigate.

32.1 Introduction

Humanoid robots have dependably been enchanting and fascinating to the people. It is just our little initiative toward assembling of a humanoid robot to create the replica of ourselves later on.

This Arduino-based bipedal robot (Fig. 32.1) incorporates four servomotors that enable it to walk by rotating servo horns following an algorithm [1] and an ultrasonic sensor above it that can detect any object front of it [2]. Whenever the robot detects any object in front of it, it stops walking and lights the LED on the top of its head as a notifier. This notifier can be replaced by any kind of notifier like a buzzer [3].

A. Ganguly · J. Ara · B. Paul (✉)
University of Liberal Arts Bangladesh, Dhaka 1209, Bangladesh
e-mail: bijan.paul@ulab.edu.bd

A. Ganguly
e-mail: amrita.ganguly.cse@ulab.edu.bd

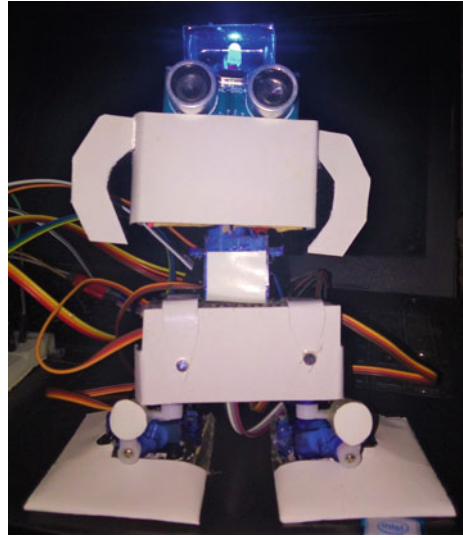
J. Ara
e-mail: jasmine.ara.cse@ulab.edu.bd

© The Editor(s) (if applicable) and The Author(s), under exclusive license to Springer Nature Singapore Pte Ltd. 2021

Y.-D. Zhang et al. (eds.), *Smart Trends in Computing and Communications: Proceedings of SmartCom 2020*, Smart Innovation, Systems and Technologies 182,

https://doi.org/10.1007/978-981-15-5224-3_32

Fig. 32.1 Tiny humanoid walking and dancing robot



A microcontroller ATmega328P goes about as the handling and memory unit of the robot. By using its legs, the robot can also dance in several steps.

Areas engaged with accomplishing this objective that is discussed in this paper are testing the servomotors, understanding its rotation impacts, support system setup calibration, make moving and dancing algorithm, choosing the scope of the ultrasonic sensor and its impact on the servo horns alongside the LED, and programming. The robot (Fig. 32.1) is around 16 cm long and is of very less weight.

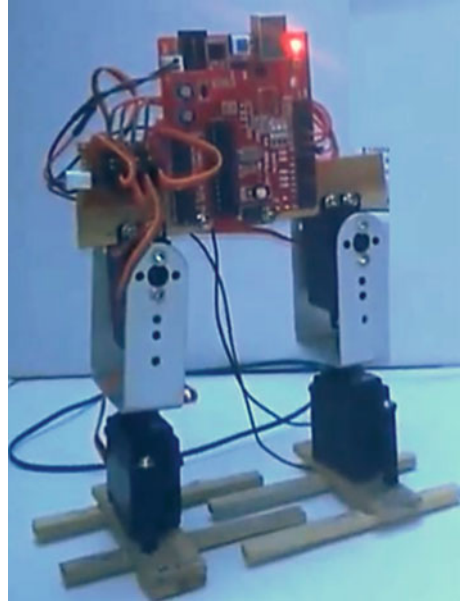
The enduring sections of this paper are prepared as follows: Part 2 describes related works; Part 3 illustrates application. Section 32.4 elicits working mechanism, Sect. 32.5 shows programming mechanism, and Sect. 32.6 describes hardware and financial requirement analysis and user feedback. We conclude in Sect. 32.7, and at the end, references are added.

32.2 Related Work

The most critical piece of humanoid robots is biped robots, where strolling movement investigation is prioritized. Also, the robot association with people and the advancement of the cooperative task are vital aspects that the robots are facing. In this specific situation, in the most recent years, human–robot interaction (HRI) turned into an imperative field of research.

Prakash Chandran, Mohit Jaswal, Dr. T. V. U Kiran Kumar, and Mrs. Raji Pandurangan have presented an autonomous biped robot (Fig. 32.2) using Arduino in their paper published on International Journal of Science, Engineering and Technology Research (IJSETR) where the biped robot is able to range distance and detect

Fig. 32.2 Autonomous biped robot using Arduino



sound. In the paper, they have mentioned two ways of making biped robot. One is the commonplace strategy where the robot moves in an arrangement in which the center of mass of robot continues moving to settle the stance of the structure. Another method for implementing the adjustment is utilizing an accelerometer and gyro sensors. They adopted the first procedure to balance out the structure [4].

Self-guided humanoid robot—Adhvik—developed by Aditya Mishra, Ashutosh Shrivastav, Neha Maurya, and S. Vamshi Krishna—can recognize any red-colored object in front of it along with walking and other functionalities. This has been accomplished using a wireless camera. The red-colored object is split into frames using the camera. The image processing is done by the supplementary MATLAB software. It needs the involvement of the wireless module [5].

To provide independent navigation facility to the blinds, many researchers are working with and invented blind-assistive devices and robots. For example, an intelligent path guidance robot to assist visually impaired described in the paper of M. F. Razali, S. F. Toha, and Z. Z. Abidin published on IEEE International Symposium on Robotics and Intelligent Sensors (IRIS 2015) uses fuzzy logic controller. The fuzzy logic approach offers a manageable, swift, and dependable solution which is an advantage over the conventional controller [6].

Another humanoid robot which is remotely controlled via Bluetooth is illustrated on the paper of Ahmet Aksoz, Salim Engin, and Mahir Dursun on the Journal of Automation and Control Engineering Vol. 4, No. 3, June 2016. The robot uses the wireless communication technology that enables the robot to be controlled by an Android interface. In a remote location, the robot can move independently [7].

There are many types of research capable of accommodating and implementing complex algorithms and theories for dynamic walking, artificial intelligence, navigation, human interaction, human behavior simulation, visual and image recognition using digital image processing [8]. Humanoid biped robots using these theories and algorithms are more advanced and efficient and hence more expensive and complicated. Our work also aims to implement such controlling systems and complex algorithms in our robot in the upcoming future.

32.3 Application

The development of propelled humanoid robots is utilized in applications in a huge scope of fields; our tiny humanoid biped robot has functionalities such as it can detect any object in front of it and stop walking motion lighting the LED as a notifier at its head. The robot can also dance using several steps. These functionalities can be of great use in the following scenario.

This robot can contribute to the bio-engineering by helping the visually impaired patient. It is known that visually impaired person faces difficulties in navigating from one place to another avoiding object. This robot can work as a blind-assistive robot in that case. It can detect object in front of it using the ultrasonic sensor and stop walking by setting the rotating values of the servos to its initial value concerning the blind person that there is an object nearby.

This robot also has applications that can accelerate marketing. Individuals nowadays demonstrate more interest toward humanoid robots. They are more inquisitive to see a robot instead of some other innovation. As this robot can dance in several steps, it can be utilized before restaurants and amusement parks to welcome people with dancing and intriguing movements.

Children are becoming the smartphone centered day by day, but it is harmful to their vision to always play with a smartphone. For children, this robot will be a great tool to play with.

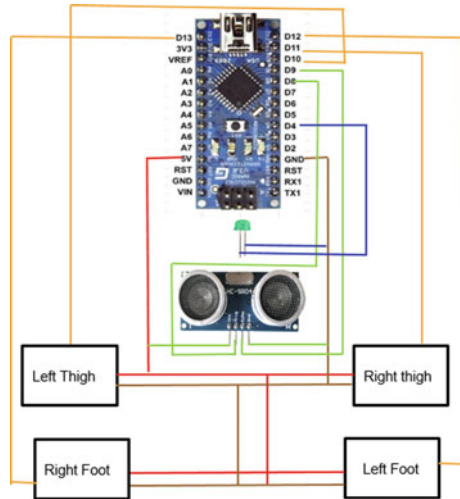
Its object detection capability can be used to ensure the security of a particular place or object so that not even a single object comes near to it.

However, there are many more purposes and applications of this kind of bipedal robots. This robot can be updated with various features such as talking, avoiding objects, and listening to voice command that will undoubtedly enhance its application.

32.4 Working Mechanism

From Fig. 32.3, we can easily understand the connection structure of the robot and how the servos [1], ultrasonic sensor, and the LED are connected to the Arduino Nano board (ATmega328P). We have used two servos per leg. The servos are attached in

Fig. 32.3 Connection diagram of tiny humanoid walking and dancing robot



a way that the thigh servo’s motion will affect the motion of the foot servo but the thigh servos are fixed to the body and are not affected by the foot servo’s motion. The LED works by cooperating with the ultrasonic sensor via code so that when the sensor detects an obstacle, the LED lights.

As a little movement of the robot depends on the rotating values of the servo horns, one has to be careful while attaching the servos knowing the initial rotating values. So, a proper understanding of which servo will turn in which side by getting which degree value is also important.

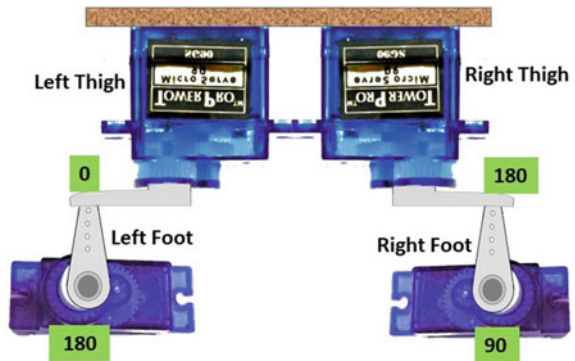
Biped’s walking and objects detecting mechanism:

- Right foot servo rises up, and right thigh servo rotates making the foot servo to come forward.
- At the same time, left thigh servo will rotate to the opposite side a bit to support the right leg go forward.
- After the right leg is placed forward, the left foot raises and left thigh rotates greater than the right servo and moves a step forward.
- In that time, right thigh servo does the same as the left thigh servo did.
- In this forward motion, if an object is detected by the sensor, the LED lights and the robot sets the servo horns to the initial position.
- This process is repeated, while the Arduino is powered.

32.5 Programming Mechanism

Our approach toward the programming started with checking which degree value effects how much to the servo’s horn (Fig. 32.4).

Fig. 32.4 Rotate values of servomotors



Algorithm:

Step 1: Define servo objects.

```
#include <Servo.h>
Servo rightfoot;
Servo rightthigh;
Servo leftfoot;
Servo leftthigh;
```

Step 2: Set ports to the objects.

Step 3: Set the initial position of the servo horns.

```
rightfoot.attach(10);
rightthigh.attach(7);
leftfoot.attach(5);
leftthigh.attach(11);

leftfoot.write(0);
leftthigh.write(90);
rightthigh.write(90);
rightfoot.write(180);
```

Step 4: Walk by rotating the horns in various angles.

```
rightfoot.write(170);
rightfoot.write(160);
```

Step 5: Check if there is an object detected within distance ≤ 30 .

Step 6: If true, set servo horns to its initial position and make the LED high.

Step 7: If false, keep the LED low and repeat Step 4.

The programs are written on the Arduino integrated development environment (IDE) which is a cross-platform application written in Java programming language [9].

32.6 Hardware and Financial Requirement Analysis and User Feedback

Here though we did not use AA cells, it is necessary to use AA cells to power the Arduino instead of powering it with USB so that the robot can walk independently.

Table 32.1 shows the necessary equipment and their corresponding price. Other important stuff includes glue gun, cutter knife, and pieces of cardboard to make the structure of the robot.

As the robot is developed especially for visually impaired people, we have visited to Bangladesh Visually Impaired People’s Society (BVIPS) [10] and Green Disabled Foundation (GDF) [11] for getting user feedback. In Bangladesh, BVIPS is a voluntary organization of blind people. The valuable opinion for this robot is collected from different organization people mentioned in Table 32.2.

Table 32.3 shows the feedback of the robot that we have received from visually impaired people based on robot-assistant behavior, entertainment, and obstacle detection feature.

Table 32.1 Hardware equipment with quantity and corresponding price

Equipment	Quantity	Price (TK)
Arduino Nano V (3.0)	1	300
Micro servo (SG90)	4	130 * 4
Ultrasonic sonar sensor (HC-SR04)	1	90
LED	1	1
Bread board	1	80
AA cells (optional)	1	~70
Jumper wires	Three sets	20 * 3
		Total: 1121

Table 32.2 Number of reviewers from different organizations

Organization	Attendances
IER Dept, Dhaka University	20
BVIPS	30
GDF	20

Table 32.3 Visual impaired people review

Criteria	Satisfaction level (%)
Walking assistant	60
Entertainment with music	40
Obstacle detection	70

32.7 Conclusion

In this paper, we portrayed the mechanism to build up an ease bipedal robot to change over it to an instrument for future research and alteration. Here, however, we have effectively met all the details in our range and there are substantially more to enhance in this task. For example, giving the robot hands and makes it work utilizing voice directions, execute human–robot association framework, and so on.

References

1. Servo Motors Control & Arduino. Future Electronics Egypt Ltd. (Arduino Egypt) (2019) [Online] inmoov.fr. Available at <http://www.inmoov.fr/wp-content/uploads/2015/02/Introduction-to-Servo-Motors-Arduino.pdf>. Accessed 24 Jan 2019
2. What is an Ultrasonic Sensor? Sensor Basics: Introductory Guide to Sensors. KEYENCE. Keyence.com (2019) [Online]. Available <https://www.keyence.com/ss/products/sensor/sensorbasics/ultrasonic/info>. Accessed 24 Jan 2019
3. Ardumotive Arduino Greek Playground: How to Use a Buzzer with Arduino (2019) [Online]. Available at <https://www.ardumotive.com/how-to-use-a-buzzer-en.html>. Accessed 20 Dec 2019
4. Chandran P., Jaswal M., Kumar K., Pandurangan R. : Autonomous biped robot using Arduino. *Int. J. Sci. Eng. Technol. Res. (IJSETR)* 4(4) 2015
5. Mishra A., Shrivastav A., Maurya N., Vamshi Krishna S.: Self Guided Adhvik Humanoid Robot [Online] ijstr.org (2019). Available at <http://www.ijstr.org/final-print/june2014/Self-Guided-Adhvik-Humanoid-Robot.pdf>. Accessed 6 Jan 2019
6. Razali M., Toha S., Abidin Z. : Intelligent Path Guidance Robot for Visually Impaired Assistance [Online] sciencedirect.com (2019). Available at <https://www.sciencedirect.com/science/article/pii/S1877050915038041>. Accessed 24 Jan 2019
7. Aksoz A., Engin S., Dursun M. : The Implementation of Controlled Humanoid Robot with Android [Online] joace.org (2019). Available at <http://www.joace.org/uploadfile/2015/1015/20151015022816477.pdf>. Accessed 24 Jan 2019
8. Hashemi S., Moradinasab Mahdi Najmabadi, M. and Abdoshshah S. [Online]. Available at http://www.ais.uni-bonn.de/humanoidsoccer/qualification/Iran_Fanavaran_TDP.pdf. Accessed 24 Jan 2019
9. Aduino IDE, Wikipedia, 07-Feb-2019 [Online]. Available https://en.wikipedia.org/wiki/Arduino_IDE. Accessed 15 Feb 2019
10. mroberts: Sightsavers Homepage [Online]. Sightsavers. Available at <https://www.sightsavers.org/> (2017)
11. Racoocode.com: Green Disabled Foundation. Racoocode [Online] (2010). Available at <http://racoocode.com/community-development/web-development/gdf-bangladesh>. Accessed 20 Dec 2019

Chapter 33

A Survey on DBN for Intrusion Detection in IoT



Harsh Namdev Bhor and Mukesh Kalla

Abstract In computer networks, intrusion detection systems play the major role to disturb the whole networks. Many latest researches have been done on IDS. Imperfection of intrusion detection systems (IDS) has given a chance for data processing to make many vital contributions to the sphere of intrusion detection. In recent years, several researchers are mistreating data processing techniques for building IDS. In this paper, various data processing techniques like deep belief neural network for IDS in IoT for serving to IDS to achieve higher detection rate are discussed. The term Internet of things (IoT), generally called Internet of objects, proposes the engineered interconnection of basic things, which is regularly observed as a self-managing remote procedure of sensors whose reason is to interconnect all things.

33.1 Introduction

33.1.1 Subsection Sample

An intrusion detection system, or IDS for brief, makes an attempt to sight an unwelcome person breaking into your system or a legitimate user misusing system resources. The IDS can run perpetually on your system, operating away within the background, and solely notifying you once it detects one thing it considers suspicious or hot. Whether or not you appreciate that notification depends on however well you've designed your intrusion detection system.

Note that there are two kinds of potential intruders: Outside intruders are the general public understands the skin world to be the most important threat to their security.

H. N. Bhor (✉)

K.J. Somaiya Institute of Engineering and Information Technology, Sion, Mumbai, India
e-mail: harsh.bhor@spsu.ac.in

M. Kalla

Sir Padarnat Singhania University, Bhatewar, Udaipur, Rajasthan, India

© The Editor(s) (if applicable) and The Author(s), under exclusive license to Springer Nature Singapore Pte Ltd. 2021

Y.-D. Zhang et al. (eds.), *Smart Trends in Computing and Communications: Proceedings of SmartCom 2020*, Smart Innovation, Systems and Technologies 182,

https://doi.org/10.1007/978-981-15-5224-3_33

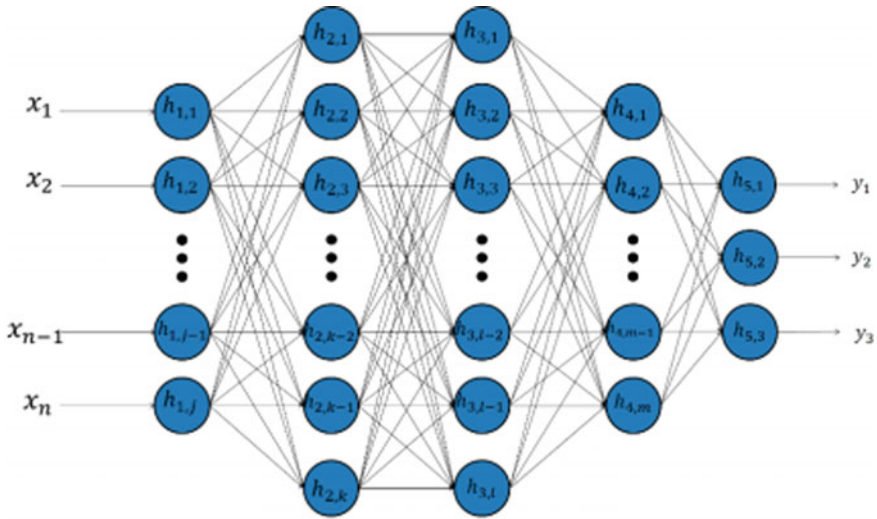


Fig. 33.1 Deep neural network sample

The media scare over “hackers” returning in over the net has solely heightened this perception.

Inside intruders, FBI studies have discovered that eightieth of intrusions and attacks return from at intervals organizations. Consider it—associate in nursing business executive is aware of the layout of your system, wherever the precious knowledge is and what security precautions are in situations.

So despite the very fact that almost all security measures are placed in situ to guard the within from a malevolent outside world, most intrusion tries really occur from at intervals a company. A mechanism is required to sight each kind of intrusions—a burglary try from the skin, or a knowledgeable business executive attack. An efficient intrusion identification system detects each kind of attacks (Fig. 33.1).

33.2 Literature Review

- (a) Anomaly Detection based on Machine Learning: Dimensionality Reduction using PCA and Classification using SVM [1]

AUTHORS: Annie George

Peculiarity discovery has risen as an imperative procedure in a few application territories principally for system security. Inconsistency identification bolstered AI calculations contemplated on the grounds that the characterization downside on the system information has been introduced here. Spatiality decrease and grouping calculations are investigated and assessed abuse KDD99 dataset for system IDS. Main

segment investigation for spatiality decrease and bolster vector machine for characterization are pondered for applying on system information, and hence, the outcomes are broken down [1]. The outcome demonstrates the lessening in execution time for the grouping as we will in general scale back the element of the info document and also the accuracy and review parameter estimations of the characterization algorithmic program demonstrates that the SVM with PCA procedure is extra right on the grounds that the scope of misclassification diminishes.

(b) A Data Mining Framework for Building Intrusion Detection Model [2]

AUTHORS: W. K. Lee, S. J. Stolfo

There is normally the need to refresh a put in invasion ID framework (IDS) because of new assault methodologies or overhauled registering situations. Since a few current IDSs are made by manual coding of expert information, changes to IDSs are exorbitant and moderate. We will in general depict a learning digging structure for adaptively assembling attack discovery (ID) models. The focal arrangement is to use inspecting projects to extricate an inside and out arrangement of choices that depict each system association or host session, and apply information handling projects to be told decides that precisely catch the conduct of interruptions and customary exercises. These guidelines will at that point be utilized for abuse discovery and inconsistency location [2]. New identification models are joined into a current IDS through a meta-learning (or co-usable learning) strategy that creates a meta-location display that blends verification from numerous models. We will in general talk about the qualities of our information handling programs, in particular, order, meta-learning, affiliation leads, and continuous scenes. We report on the aftereffects of applying these projects to the widely accumulated system review learning for the 1998 office Attack Recognition Investigation Program.

(c) A Review of Anomaly Based Intrusion Detection Systems [3]

AUTHORS: V. Jyothsna, V. V. Rama Prasad, K. Munivara Prasad

With the presence of abnormality-based invasion recognition frameworks, a few methodologies and strategies are created to follow novel assaults on the frameworks. High location rate of ninety-eight at an espresso alert rate of one hundred and forty-five is regularly accomplished by misusing these methods. Albeit abnormality-based methodologies are prudent, signature-based location is most well-enjoyed for thought usage of attack recognition frameworks [3]. As a scope of inconsistency identification procedures were guided, it is hard to check the qualities and shortcomings of those systems. The clarification why ventures do not support the inconsistency-based attack discovery techniques is frequently surely known by affirming the efficiencies of the every one of the procedures. To dissect this issue, the current situation with the trial pursue inside the field of inconsistency-based attack identification is assessed and study ongoing investigations amid this. This paper contains account study and ID of the downsides of once studied works.

(d) Research of Intrusion Detection Based on Principal Components Analysis [4]

AUTHORS: CHEN Bo, Ma Wu

The viable methods for raising the power of invasion location are proportional back the genuine learning technique work. Amid this paper, the spatial property decrease utilization of innovation inside the exemplary spatial property decrease rule chief component to examination huge scale learning supply for diminished influenced choices of the main information to be held and improved the intensity of invasion identification. What's more, use BP neural system instructing the information when spatial property decrease will be compelling in typical and anomalous learning refinement, and accomplished reasonable outcomes [4].

(5) Solving Multiclass Learning Problems via Error-Correcting Output Codes [5]

AUTHORS: T. G. Dietterich, G. Bakiri

Multiclass learning issues include finding a definition for AN obscure work $f(x)$ whose fluctuation might be a particular set containing k & gt, two qualities (i.e., k "classes"). The definition is nonheritable by learning accumulations of training tests of the shape $(xi, f(xi))$. Existing ways to deal with multiclass learning issues grasp direct utilization of multiclass calculations like the choice tree calculations C4.5 and Truck, use of twofold origination learning calculations to discover singular parallel capacities for everything about k classifications, and use of double origination learning calculations with dispersed yield illustrations [5]. This paper thinks about these three ways to deal with a spic and span procedure inside which blunder remedying codes are used as a conveyed yield portrayal. We will in general demonstrate that these yield portrayals improve the speculation execution of each C4.5 and back proliferation on a wide scope of multiclass learning assignments. We will in general conjointly show that this methodology is vigorous with reference to changes inside the extent of the training test, the task of circulated portrayals to express classes, and furthermore the utilization of overfitting evasion systems like choice tree pruning [5]. At last, we will in general demonstrate that—like different strategies—the blunder remedying code system will give solid class likelihood gauges. Brought, these outcomes exhibit that blunder remedying yield codes give a universally handy system for the execution of inductive learning programs on multiclass issues.

33.3 Issues in Deep Belief Networks

Nodes that cannot convey straightforwardly depend upon their neighbors to advance their messages to the appropriate goal. Uses of versatile impromptu systems have expanded needs in order to affirm top nature of administration for the given administrations. Security in such framework less systems has been well-attempted to be a troublesome errand. A few security dangers emerge against versatile specially appointed systems, as they're inalienably helpless gratitude to the methodology they construct and save property attributes. The open medium gives the system the first and most genuine helplessness. Rather than wired systems wherever partner attacker so as to dispatch partner assault must access a wired framework, firewalls, and portals, in unintended systems there is no reasonable line of barrier. Every hub is powerless,

Table 33.1 Existing methods used by the various authors with datasets

DBN	Author	Application	Dataset used
Autoencoder	Hardy et al.	Malware detection	Comodo Cloud Security Center
Autoencoder	Wang and Yiu	Malware classification	Public malware API call sequence dataset
Autoencoder RBM	Alom and Taha	Intrusion detection	KDD 1999
CNN	Gibert	Malware classification	Microsoft malware classification challenge
CNN	Zeng, Chang, and Wan	DGA	Synthetic dataset

and hence, the reasonable execution of the system relies upon every hub or if nothing else on every hub working together in an exceedingly way from the supply to a given goal.

DISADVANTAGES of various Deep Belief Networks:

1. The insecure open medium combined with poor physical protection presents another disadvantage.
2. Every node is in a position to stray severally running the danger to be simply compromised by a malicious wrongdoer.
3. Moreover, once additional subtle attacks happen nodes are simply exploited.
4. Additionally, wireless unintended networks lack a centralized watching and management purpose.

Some of the datasets used by the various algorithms are given in Table 33.1

KDDCUP99 [6] and NSL-KDD are the most commonly used datasets in the intrusion detection research. We used NSL-KDD intrusion dataset which is available in CSV format for model validation and evaluations.

Sherasiya and Upadhyay [7] pointed out that IoT objects are also exposed to such types of attacks, and the data that IoT objects exchange are of the same value and importance, or occasionally more important than a non-IoT counterpart.

33.4 Conclusion

In this paper, various surveys are done on IDS detection with IoT. IoT is one of the unavoidable thoughts of mechanical progression in the field of frameworks which will help in the forefront improvement in like way as in the standard proximity of an individual; from this time forward nowadays, IoT is being examined that includes point for the specialists and for the endeavors. Utilizing this will improve the performance of the IDS.

References

1. George, A.: Anomaly detection based on machine learning: dimensionality reduction using PCA and classification using SVM. *Int. J. Comput. Appl.* **47**(21) (2012)
2. Lee, W.K., Stolfo, S.J.: A data mining framework for building intrusion detection model. In: Gong, L., Reiter, M.K. (eds.) *Proceedings of the IEEE Symposium on Security and Privacy*, pp. 120–132. IEEE Computer Society Press, Oakland, CA (1999)
3. Jyothsna, V., Rama Prasad, V.V., Munivara Prasad, K.: A review of anomaly based intrusion detection systems. *Int. J. Comput. Appl.* **28**(7) (2011)
4. Bo, C., Wu, M.: Research of intrusion detection based on principal components analysis. In: *Second International Conference on Information and Computing Science*. Information Engineering Institute, Dalian University, China (2009)
5. Dietterich, T.G., Bakiri, G.: Solving multiclass learning problems via error-correcting output codes. *J. Artif. Intell. Res.* **2**, 263–286 (1995)
6. Tavallae, M., Bagheri, E., Lu, W., Ghorbani, A.: A detailed analysis of the KDD CUP 99 data set. In: *Proceedings of the 2nd IEEE Symposium on Computational Intelligence for Security and Defense Applications (CISDA)*, Ottawa, ON, Canada, July, pp. 1–6 (2009)
7. Alghuried, A.: A model for anomalies detection in Internet of Things (IoT) using inverse weight clustering and decision tree. M.S. thesis, School Comput., Dublin Inst. Technol., Dublin, Republic of Ireland (2017)
8. Neethu, B.: Classification of intrusion detection dataset using machine learning approaches. *Int. J. Electron. Comput. Sci. Eng.* 1044–1051 (2012)
9. Smith, L.I.: *A Tutorial on Principal Components Analysis*
10. Hastie, T.J., Tibshirani, R.J., Friedman, J.H.: *The Elements of Statistical Learning: Data Mining, Inference, and Prediction*. Springer-Verlag (2001)
11. Rifkin, R., Klautau, A.: In defense of one-vs-all classification. *J. Mach. Learn. Res.* **5**, 143–151 (2004)

Chapter 34

Organ Detection in Surgical Videos Using Neural Networks



Amit Kumar, Anshu Gupta, and Ankita Pramanik

Abstract The automatic surgical video processing for anomaly detection is becoming important nowadays since manual feedback from surgeons is subject to errors and time-consuming. It is necessary to have more precise and detailed detection and recognition of organs and tissues as we move into more complete understanding of the surgical videos. Thus, automatic localization and detection of organs have now become a prerequisite in surgical video analysis. In this paper, a convolutional neural network (CNN) is designed to evaluate laparoscopic and endoscopic surgical videos. The neural network will detect and localize the organs for the given videos which lay the path for automatic post-surgical processing.

34.1 Introduction

Surgical data science has undergone much technological advancements in recent years [1]. These advancements in technology are translated into innovative surgical tools and medical facilities, which led to improvement in healthcare quality and treatment of incurable diseases.

In endoscopic surgeries, surgeons are required to examine short video segments for analysis, but analysing such videos manually is inefficient and time-consuming. Due to advancements in image acquisition devices, handling such large complex data for image analysis has become challenging, which requires extensive efforts by medical experts. Thus, it is important to pre-process surgical videos for fast retrieval

A. Kumar · A. Gupta · A. Pramanik (✉)
Indian Institute of Engineering Science and Technology, Shibpur, India
e-mail: ankita@telecom.iiests.ac.in

A. Kumar
e-mail: kramit1510@gmail.com

A. Gupta
e-mail: guptaansu26@gmail.com

of relevant details which will be very helpful for surgeons. For this purpose, an approach towards machine learning techniques proved very efficient to deal with complex data [2].

34.1.1 Machine Learning Approaches

The field of machine learning has progressed rapidly over the last few decades and played an important role in the advancement of medical image processing [3]. Machine learning algorithms map input signals which can be represented as intensity of pixels of an image to output values giving the results based on the mapping of input data.

Using machine learning techniques, doctors can predict and cure diseases accurately and in very less time. But some of these techniques are based on conventional algorithms which may not suit the current requirement due to limited processing speed. Although automatic detection of ailments based on such conventional methods has been proved to be quite accurate for past few years, but with new advancements in medical field, there was always a need for more efficient approach for better results, and thus, deep learning came into existence.

34.1.2 Deep Learning over Machine Learning

With the technological improvement of medical facilities and extensively varied patients' data, reliability of conventional methods became low. For medical image analysis, the field of computer vision using deep learning techniques has made significant advancement in recent years [4]. This approach uses neural network models which approximates human brain to some extent using complex mechanisms. One such neural network models which is being extensively used nowadays are convolutional neural network (CNN). Here, we use deep neural network having multiple layers which models learning method of a human brain, hence the term deep learning. The basic structural and functional unit in a neural network are called a neuron, which works similar to the neuron of a human brain. It takes one or more input signals, does its weighted combination, and then passes through nonlinear functions to generate output signals.

In classical machine learning, experts try to choose such imaging features which can represent the visual data in the best possible way. Deep learning, which is nothing but a subdivision of machine learning, is a type of representation learning in which the algorithm learns and finds out the best feature on its own without any manual selection [5].

This paper aims to

- use a dataset containing surgical video frames to train predefined neural network architectures to classify them into different anatomical structures
- look into the use of deep learning networks for organ detection in endoscopic surgical videos.

34.1.3 Organization of Paper

The remaining paper is structured as follows. The next section consists of background and preliminaries. Section 34.3 presents our proposed work on organ selection using CNN. Experimental results are explored in Sect. 34.4. Finally, the paper is concluded in Sect. 34.5. The scope for future work is also discussed in the conclusion section.

34.2 Background and Preliminaries

34.2.1 Artificial Neural Network

Artificial neural network (ANN) lays the foundation of most deep learning models. ANNs are inspired by biological neurons and functions like a human brain to some extent. Figure 34.1 shows the structure of a single neuron where it takes the input x_i , and the output z is computed as follows:

$$z = f \left(\sum_{i=1}^{\infty} n_i w_i + b \right) \quad (34.1)$$

The parameters w_i , b , $f(\cdot)$ in the figure are the weights, bias, and nonlinear activation function, respectively. Here, weighted combination of inputs x_i is added with the bias and then the nonlinear function, $f(\cdot)$, is applied for final output, z . Nonlinear mappings between input and the output are found in the nonlinear function. The commonly used nonlinear activation functions are the *tangent* function or logistic *sigmoid* function or *ReLU* function.

A neural network comprises a number of neurons arranged in multiple layers, where each neuron's output in a certain layer will act as input to other neurons in the upcoming layer. This working model is known as *multi-layer perceptron* or feed-forward neural network. Here, each layer and its neurons are fully connected with the subsequent layer with no loops or feedbacks. The layer having x_i 's is referred to as input layer, z as output layer, and the intermediate layers as hidden layers. The output, z , depends upon input, x_i , bias, b , and weights w_i .

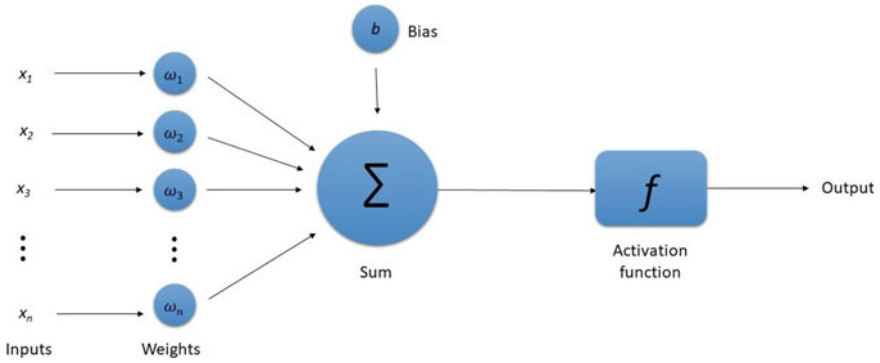


Fig. 34.1 Illustration of a single neuron

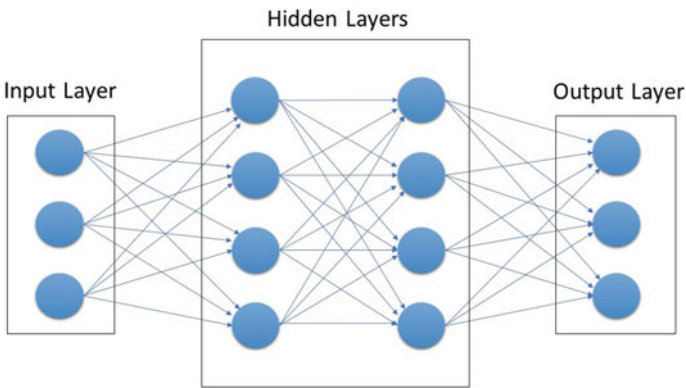


Fig. 34.2 Fully connected ANN

The output computing process of this network is called *forward propagation*. Generally, deep neural network architectures are formed by the addition of multiple hidden layers with differing number of neurons in each layer. Deepening the network increases the number of parameters of network. During network training, these parameters are initialized in a random manner which needs to be updated in each iteration. The two most common training algorithms are *Gradient Descent* and *Back-propagation*. Repeated iterations of such algorithms ultimately lead to an optimized network (Fig. 34.2).

34.2.2 Convolutional Neural Network

Convolutional neural networks (CNN) are a subtype of ANN which consists of convolutional layers followed by the fully connected layers (or standard multi-layer perceptron network). CNN architecture is designed for computation with two-dimensional

input data (or images) received by processing the input data with small-sized kernels (filters). The output which comes after filtering is then followed by pooling operators resulting in invariant features which helps to detect distinct features in the data. Applying such convolutional and pooling operations multiple times, produces new representation which is nonlinear and smaller in size compared to input data which can be passed by normal fully connected neural network layers and trained with lesser parameters.

For example, CNN architecture input is an image with $d \times c \times b$ dimension where d and c are the width and the height of the image, respectively, and b is the number of image channels as applicable (R, G, B for colour image). Applying k filters of size $m \times m$ in first convolutional layer gives k number of feature maps, each one being generated by performing the convolution of input image with each filter. Each feature map sizes $(d - m + 1) \times (c - m + 1)$. Weights w_1, w_2, \dots , of the k feature maps are the parameters which get optimized at each subsequent convolutional layers. The output of the first layer is passed through a layer of pooling. Pooling is performed over $r \times r$ patches in the feature maps at the output where maximum (max pooling layer) or average (average pooling layer) of patch is retained in the output images. We can subsequently add as many numbers of convolutional and pooling layers depending on our need. These layers comprise convolutional layers, pooling layers, normalization or rectified nonlinear units (ReLU) layers.

Usually, computation time is proportional to the number of convolutional layers added and number of parameters used in the network [6]. As the size of feature maps is reduced considerably after a certain number of convolution and pooling layers, they are no more passed by further convolutional layers and then finally processed and computed by fully connected layers. At last, it is fed into nonlinear activation function which then classifies the final output data to one of the categories.

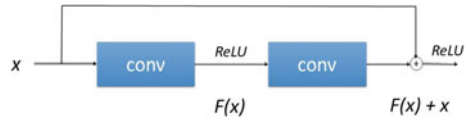
34.3 Proposed Work

CNN is the most widely used deep learning network architecture. It takes the image as input, finds out the detectable features, and maps it into feature vector (or feature maps) that represents the edges and corners contained in small regions of image. On top of this, in higher level, it transforms the edges and corners into structures, then into objects and its associated activities [7].

34.3.1 ResNet Model

ResNet [8], short-form for residual networks, is a classic convolutional neural network used in many computer vision tasks. The main advantage of ResNet is that it can successfully train very deep neural networks with more than hundreds of layers, which was initially very difficult due to vanishing gradient problem. Main issue with

Fig. 34.3 ResNet residual block



deep neural network is that the accuracy saturates and deteriorates rapidly when it starts to converge. To overcome this, ResNet is introduced to realize neural networks with feed-forward and smaller connections as shown in Fig. 34.3. In our study, we used the ResNet-based CNN from ImageAI library [9] for both training and testing.

34.3.2 Dataset

We have used the database which includes 40,000 pairs of rectified stereo images, taken from Hamlyn Centre of Endoscopic/Laparoscopic Video Datasets [10]. Hamlyn Centre contains datasets of images collected from different kinds of surgeries of various patients which are used for the purpose of biomedical and computer vision research (Fig. 34.4).

34.3.3 Training the Dataset

For this work, the training set of 10,000 frames is divided into two sets—*training set* and *validation set* containing 9000 and 1000 images, respectively. Both the sets are divided into ten groups of frames, each belonging to different classes(organs) [11]. The CNN architecture was trained with 20 epochs on the training dataset. One epoch is a loop while passing datasets through the network forward and backward, with the aim to optimize the learning process iteratively and updating the weights accordingly. But one epoch is not enough to optimize the whole network. So, we tried and tested our model with multiple epoch values(greater than one) and finally set it to 20 for best accuracy. Also, it is not possible to give the entire dataset to the neural network at once, so we need to divide it into smaller number of batches and update the weights of the neural networks at the end of each iteration to fit it to the data given. Here, the batch size was set to 32. The total training time was approximately



Fig. 34.4 Samples taken from the dataset of endoscopic video frames

72h. The training process was terminated after observing the maximum accuracy on the validation set. All the training processes were performed using an NVIDIA GeForce GTX Graphics (8GB on-board RAM).

To train a deep neural network model for image representation, thousands of images and high-end computational solving power, same as GPU is for optimizing of weights in each iteration, are required. To get the required model using above strategy is quite a costly process. This problem has alternate solution, transform learning, where a pretrained model is employed for other purposes. Therefore, in our method, we have employed the ResNet model's parameters as our pretrained CNN architecture for feature extraction [12]. The CNNs that were fully trained were initialized with random weights which were sampled from Gaussian distributions.

The model at first takes input images of dimension 300×300 and maps it into feature maps of size 13×13 using two pairs of convolutional and pooling layers. This is then followed by a sequence of three convolutional layers which implements convolution with filters of size 9×9 . After that, there is a pooling layer and finally three fully connected layers. The first fully connected layer can be viewed as a convolution layer with 6×6 kernels and the other two fully connected layers as convolutional layers with 1×1 kernels. The next step is to adjust the learning rate, with the knowledge that a smaller learning rate slows down convergence, but larger learning rate can cause failed convergence. During faster convergence, after a few epochs, the learning rate can be decreased safely that permits the usage of small scheduling rate. But, when the converging rate is slow, larger scheduling rate is employed to keep the learning rate [13] faster.

34.3.4 Testing the Dataset

After training the complete CNN model, we took the video to be tested and then divided the video into frames. Each frame then acted as the image of a particular moment of the surgery. The organ present in that frame was then detected using the algorithms for object detection from that image [14, 15].

34.4 Results

After testing the dataset using designed CNN model and fixing the values of the network parameters, we get the accuracy of 92% approximately. We kept the learning rate as 0.01, as increasing the learning date can increase the accuracy, but inherently slows down the process very much. We have used about 128 layers in our training architecture. The following table clearly shows the parameter values with the accuracy (Table 34.1).

Table 34.1 Values of network parameters

Properties	CNN
Learning rate	0.01
Batch size	32
Epoch	20
Number of layers used	128
Time taken (in h)	22
Accuracy	92%

34.5 Conclusion

In this paper, an organ detection framework is proposed by utilizing CNN architecture's deep features, and we found out the best possible accuracy by optimizing network parameters values, which helps in identifying complex hidden inter-frame sequential patterns in the input features. Here, the video is analysed in K chunks, K depending upon the time interval " T " required for action. Above features give the capability to the proposed method, for learning long complex sequences in videos.

34.5.1 Future Scope

Using CNN, we can only exploit the spatial behaviour of input patterns and features provided, but one can also exploit the temporal behaviour of the image sequence (or video frames) for even better results. Such architecture can be explored using hybrid neural network models. Hybrid model is nothing but a combination of some deep neural network models. One possible hybrid model is the combination of CNN and RNN, which can give better results than using only CNN. This is due to the fact that CNN captures the spatial relationship, whereas RNN works using the temporal relationship. A combination of CNN and RNN will give improved results for recognizing various activities in the input dataset that have different time span and distribution of signals.

References

1. Maier-Hein, L., Vedula, S.S., Speidel, S., Navab, N., Kikinis, R., Park, A., Eisenmann, M., Feussner, H., Forestier, G., Giannarou, S., Hashizume, M., Katic, D., Kenngott, H., Kranzfelder, M., Malpani, A., März, K., Neumuth, T., Padoy, N., Pugh, C.M., Schoch, N., Stoyanov, D., Taylor, R.H., Wagner, M., Hager, G.D., Jannin, P.: Surgical data science: enabling next-generation surgery. CoRR abs/1701.06482 (2017), <http://arxiv.org/abs/1701.06482>
2. Loukas, C.: Video content analysis of surgical procedures. Surg. Endoscopy **32**(02) (2018)

3. Shen, D., Wu, G., Suk, H.I.: Deep learning in medical image analysis. *Ann. Rev. Biomed. Eng.* **19**, 221–248, 28301734 [pmid] (2017). <https://www.ncbi.nlm.nih.gov/pubmed/28301734>
4. Litjens, G., Kooi, T., Bejnordi, B.E., Setio, A.A.A., Ciompi, F., Ghafoorian, M., van der Laak, J.A., van Ginneken, B., Sánchez, C.I.: A survey on deep learning in medical image analysis. *Med. Image Anal.* **42**, 60–88 (2017). <http://www.sciencedirect.com/science/article/pii/S1361841517301135>
5. Linder, T., Jigin, O.: Organ detection and localization in radiological image volumes. Master's thesis, Linköping University, Artificial Intelligence and Integrated Computer Systems (2017)
6. Szegedy, C., Liu, W., Jia, Y., Sermanet, P., Reed, S., Anguelov, D., Erhan, D., Vanhoucke, V., Rabinovich, A.: Going deeper with convolutions. In: 2015 IEEE Conference on Computer Vision and Pattern Recognition (CVPR), June 2015, pp. 1–9
7. Ronneberger, O., Fischer, P., Brox, T.: U-net: convolutional networks for biomedical image segmentation. *ArXiv abs/1505.04597* (2015)
8. Torch residual networks. <https://github.com/gcr/torch-residual-networks> (2015)
9. Moses Olafenwa, J.O.: Image ai. <http://imageai.org/>
10. Ye, M., Johns, E., Handa, A., Zhang, L., Pratt, P., Yang, G.Z.: Self-supervised siamese learning on stereo image pairs for depth estimation in robotic surgery. *ArXiv abs/1705.08260* (2017)
11. Yuan, Z., Izadyazdanabadi, M., Mokkaḡpati, D., Panvalkar, R., Shin, J., Tajbakhsh, N., Gurudu, S., Liang, J.: Automatic polyp detection in colonoscopy videos. In: *Medical Imaging 2017*, vol. 10133. SPIE (2017)
12. Shin, H., Roth, H.R., Gao, M., Lu, L., Xu, Z., Nogues, I., Yao, J., Mollura, D., Summers, R.M.: Deep convolutional neural networks for computer-aided detection: CNN architectures, dataset characteristics and transfer learning. *IEEE Trans. Med. Imag.* **35**(5), 1285–1298 (2016). May
13. Krizhevsky, A., Sutskever, I., Hinton, G.E.: Imagenet classification with deep convolutional neural networks. In: *Advances in Neural Information Processing Systems* (2012)
14. Fan, S., Xu, L., Fan, Y., Wei, K., Li, L.: Computer-aided detection of small intestinal ulcer and erosion in wireless capsule endoscopy images. *Phys. Med. Biol.* **63**(16), 165001 (2018). <https://doi.org/10.1088/1361-6560/aad51c>
15. Yuan, Y., Meng, M.Q.H.: Deep learning for polyp recognition in wireless capsule endoscopy images. *Med. Phys.* **44**(4), 1379–1389 (2017)

Chapter 35

Implementation Aspects of Multi-bit Adders Using UTBSOI Transistors



Rekib Uddin Ahmed and Prabir Saha

Abstract This paper presents implementation aspects of popular multi-bit adders (e.g. ripple carry adder (RCA) and carry look ahead adder (CLA)) through UTBSOI transistors. Performance parameters comparison in terms of power consumption, delay, power-delay product (PDP), and energy-delay product (EDP) have been analysed for the application of the intelligent systems. The 4-bit adders are simulated at 45-nm regime in Cadence-spectre using the BSIM-IMG model for the UTBSOI technology. From the simulation results, it is observed that the power consumption in UTBSOI-based RCA (UTB-RCA) is four times lesser than that of in UTBSOI-based CLA (UTB-CLA). The delay exhibited by the UTB-RCA and UTB-CLA at 20 MHz operating frequency is 0.1085 ns and 0.3151, respectively. Based on the simulation results, the application of UTBSOI in the RCA has resulted in 84.3% and 3.67 times improvements over that of existing design architecture in the literature in terms of power consumption and delay, whereas the use of UTBSOI in CLA does not seem to enhance the power consumption and delay over the conventional designs.

35.1 Introduction

At the present phenomena, a trend has arrived where mobility and the miniaturization of the battery-operated devices are achieved through downscaling of technology node. Due to the downscaling, the dimensions of the MOSFETs inside the chip have entered in nanoscale regime. In nanoscale technology, the shorter channel length of the MOSFETs is prone to various physical effects known as short-channel effects (SCEs) [1, 2]. To overcome the limitations imposed by the SCEs, different advanced architectures of MOSFET were proposed [3, 4]. Out of those architectures,

R. U. Ahmed · P. Saha (✉)
Department of Electronics and Communication Engineering, National Institute of Technology
Meghalaya, Shillong 793003, India
e-mail: sahaprabir1@gmail.com

R. U. Ahmed
e-mail: rekib@nitm.ac.in

© The Editor(s) (if applicable) and The Author(s), under exclusive license
to Springer Nature Singapore Pte Ltd. 2021

Y.-D. Zhang et al. (eds.), *Smart Trends in Computing and Communications: Proceedings of SmartCom 2020*, Smart Innovation, Systems and Technologies 182,
https://doi.org/10.1007/978-981-15-5224-3_35

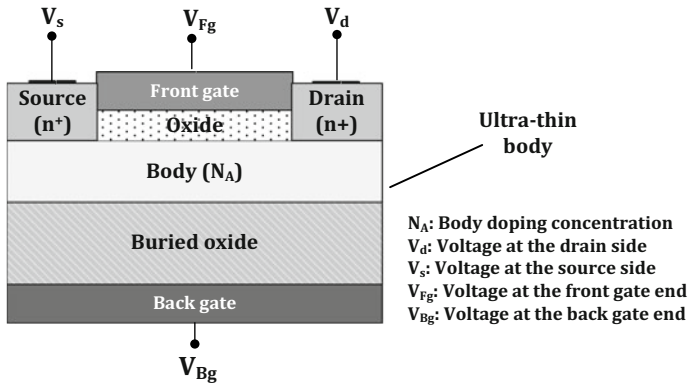


Fig. 35.1 Schematics showing the cross-sectional view of UTBSOI transistor

the ultra-thin-body silicon-on-insulator (UTBSOI) transistor as shown in Fig. 35.1 is the promising one. The UTBSOI is a dual-gated transistor and has better scalability and superior controllability of gates over the shorter channel length. Moreover, the device is now at the production level used by leading semiconductor industries [5]. To utilize the benefits of UTBSOI in the circuit simulators, a model depicting the characteristics of the device is required. BSIM-IMG [6] is the industry standard model for the UTBSOI which can be adopted in the simulators to design any circuits.

Generally, the microprocessors and digital signal processors rely on efficient arithmetic operations for which full adders (FA) cells are highly desirable. Since the small chip area, high speed, and low power consumption are the primary concern in modern electronic systems, so different logic topologies have been used to design the FA cells in CMOS technology [7–17] such as static complementary-CMOS (C-CMOS) [7–9], complementary pass-transistor logic (CPL) [9, 10], transmission gate FA (TGA) [11–13], and transmission function FA (TFA) [14–17]. Apart from this, researchers are considering new technologies like quantum dot cellular automata (QCA) [18–20], single electron transistors (SET) [21, 22], carbon nanotube field effect transistor (CNTFET) [23–27], and FinFET [28, 29] to implement such FA cells. One recent paper [30] has presented design of FA cells using the UTBSOI technology, where it is found that the TFA has the better promising performance in terms of PDP and EDP than the other FA topologies (C-CMOS, CPL, and TGA). The ripple carry adder (RCA) [31–33] is a parallel binary adder that can be constructed with the FA cells connected in cascade as shown in Fig. 35.2. The delay of a RCA is the propagation delay through a typical gate multiplied by the number of gate levels in the circuit. For a 16-bit RCA, the delay is equal to 34 gate delays which tend to be one of the largest delays in a typical computer design. Carry look ahead (CLA) [31–33] as shown in Fig. 35.3 is an alternative design to the RCA with the reduced delay at the price of more complex circuitry.

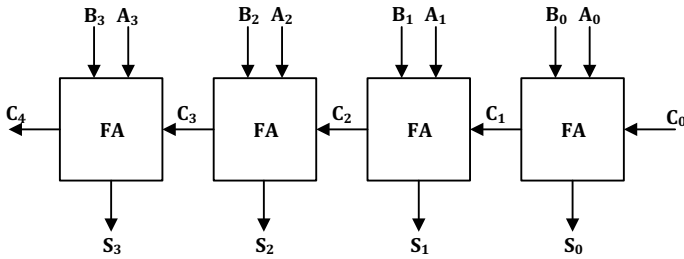


Fig. 35.2 4-bit ripple carry adder

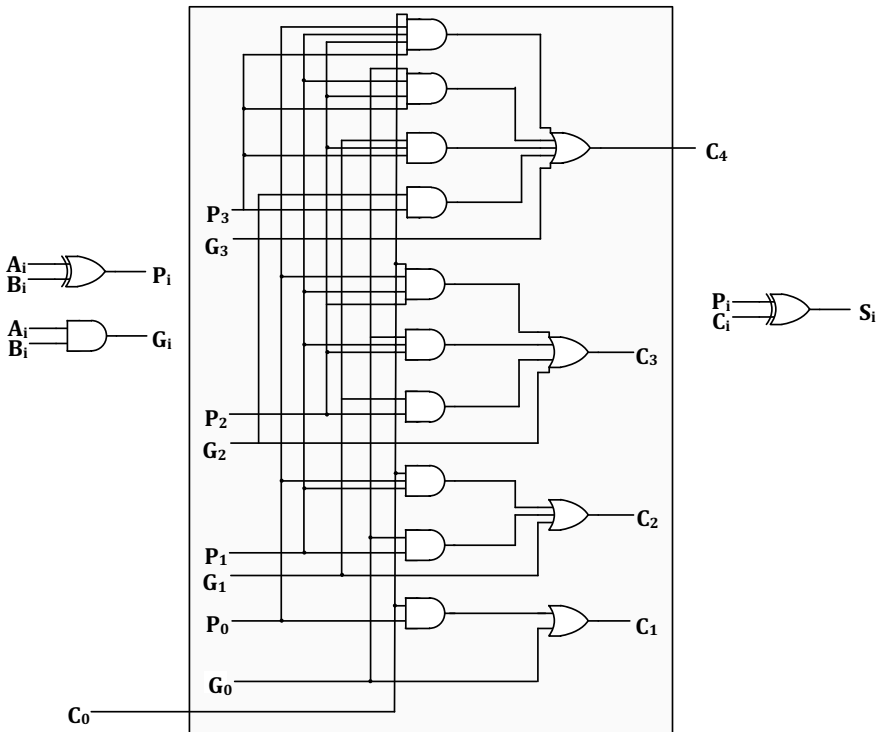


Fig. 35.3 4-bit carry look ahead adder

In this paper, comparison of performance parameters like power consumption, delay, PDP, and EDP achieved by the UTBSOI-based 4-bit adders like RCA (UTB-RCA) and CLA (UTB-CLA) is presented. The UTB-RCA is designed by cascading four 1-bit TFA cells. The simulation is carried out in Cadence-spectre through utilizing the model BSIM-IMG for the UTBSOI-based adders. Table 35.1 shows the optimized values of the device parameters considered while doing the comparison.

Table 35.1 Device parameters used in the UTBSOI transistor

Parameters	UTBSOI (BSIM-IMG)	
	<i>n</i> -channel	<i>p</i> -channel
Channel length (<i>L</i>) [6]	55 nm	55 nm
Channel width (<i>W</i>)	165 nm	330 nm
Threshold voltage (V_{th})	0.272	-0.398 V

The rest of the device parameters are kept default as in [6]

This paper is organized as follows: Sect. 2 presents the results and discussion about the comparisons performed. Finally, Sect. 3 concludes the paper.

35.2 Results and Discussion

Given the three 1-bit inputs, namely A_i , B_i , and C_i , the FA's Boolean expressions to calculate the two 1-bit outputs S_i and C_{i+1} can be described as follows:

$$S_i = (A_i \oplus B_i) \oplus C_i \quad (35.1)$$

$$C_{i+1} = A_i B_i + C_i (A_i \oplus B_i) \quad (35.2)$$

The XOR operation in the Boolean expressions is performed using the transmission gate (TG)-based XOR gates [34]. A summary of the simulation environment used in the comparison is given in Table 35.2.

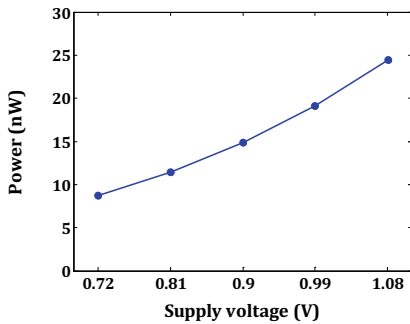
At first, the TFA cell design using the UTBSOI (UTB-TFA) is simulated at different supply voltages [Table 35.2] to find out the nominal supply voltage to carry out the rest part of the simulation. A summary of the performance parameters of the UTB-TFA cell is given in Table 35.3. Figure 35.4 shows the variation of performance parameters with respect to (w.r.t.) V_{dd} , where it is observed that the PDP and EDP

Table 35.2 Simulation environment

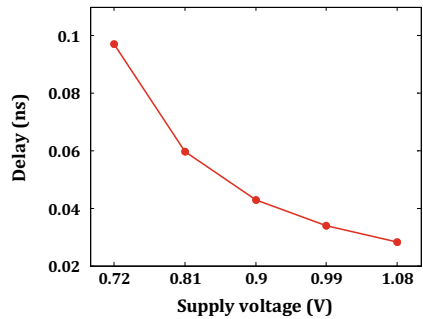
Parameters	Value
Simulator	Cadence-spectre
Technology	UTBSOI [6]
Device model	BSIM-IMG [4, 5]
Supply voltage (V_{dd})	0.72–1.08 V [35]
Amplitude of input pulses	0.72–1.08 V [35]
Operating frequency (f)	20 MHz [10]
Rise and fall time of input pulses (t_{rf})	10 ps
Temperature	27 °C

Table 35.3 Performance parameters of UTB-TFA cell at different supply voltages

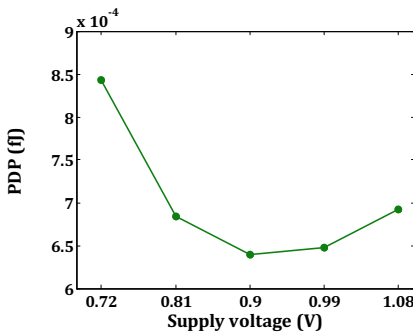
Performance parameters	$V_{dd}=0.72$ V	$V_{dd}=0.81$ V	$V_{dd}=0.90$ V	$V_{dd}=0.99$ V	$V_{dd}=1.08$ V
Power consumption (nW)	8.687	11.45	14.89	19.14	24.46
Delay (ns)	0.09709	0.05974	0.04293	0.03385	0.0283
PDP (fJ)	8.4342×10^{-4}	6.840×10^{-4}	6.3922×10^{-4}	6.478×10^{-4}	6.922×10^{-4}
EDP (fJ \times ns)	0.3373	0.2736	0.2556	0.2591	0.2769



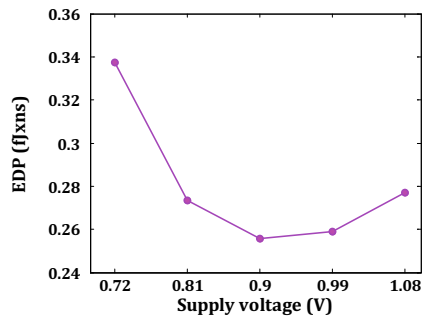
(a)



(b)



(c)



(d)

Fig. 35.4 Variation of **a** power, **b** delay, **c** PDP, and **d** EDP of the UTBSOI-based TFA cell with respect to different supply voltages

attain its least value at $V_{dd} = 0.9$ V. As it has been reported in [35] that the nominal value of V_{dd} for the 45 nm regime is 0.9 V hence gets proven from Fig. 35.4.

The UTB-RCA and UTB-CLA are simulated considering $V_{dd} = 0.9$ V and amplitude of input pulse = 0.9 V under three test conditions: (1) all bits of A_n are 0 and

Table 35.4 Summary of simulation results of UTBSOI-based RCA and CLA

Performance parameters	RCA			CLA		
	$A_n=0$, increment B_n from 0 to 15	Increment A_n from 0 to 15, $B_n=0$	A_n and B_n incremented from 0 to 15	$A_n=0$, increment B_n from 0 to 15	Increment A_n from 0 to 15, $B_n=0$	A_n and B_n incremented from 0 to 15
Power consumption (nW)	59.77	56.76	57.09	226.3	148.3	322.9
Delay (ns)	0.1231	0.1123	0.0901	0.3296	0.1566	0.4593
PDP (fJ)	7.357×10^{-3}	6.374×10^{-3}	5.144×10^{-3}	74.59×10^{-3}	23.22×10^{-3}	148.3×10^{-3}
EDP (fJ \times ns)	5.887	5.099	4.111	59.658	18.572	118.499

B_n is incremented from 0 to 15, (2) A_n is incremented from 0 to 15 and all bits of B_n are 0, (3) A_n and B_n are incremented from 0 to 15. Table 35.4 shows the simulation results of UTB-RCA and UTB-CLA at a glance. The average power consumption, delay, PDP, and EDP of the RCA are calculated as 57.87 nW, 0.1085 ns, 6.291×10^{-3} fJ, and 5.032 fJ \times ns, respectively. The same for the CLA are found to be 232.5 nW, 0.3151 ns, 82.036×10^{-3} fJ, and 65.576 fJ \times ns, respectively. Figure 35.5 shows the comparison of performance parameters given in Table 35.4, where it is observed that the performance achieved by the UTB-RCA is better as compared to the UTB-CLA. The decrease in the performance parameters of the UTB-CLA is due to its considerably large amount of transistor counts. A summary of the performance parameters of UTB-RCA and UTB-CLA in comparison with the prior reported works [36–38] is given in Table 35.5. The pictorial comparison of performance parameters with the existing designs in Fig. 35.6 makes it clear that the UTB-RCA has better performance over the existing design in [36], whereas Fig. 35.6b depicts that the

Fig. 35.5 Comparison of performance parameters achieved by the UTBSOI-RCA and UTB-CLA

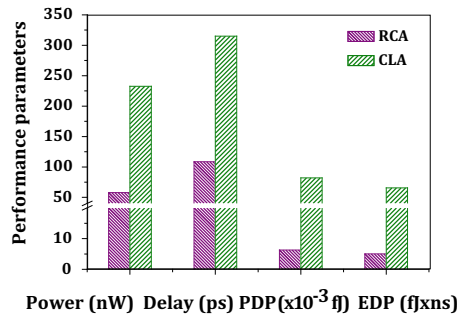


Table 35.5 Performance parameters comparison of UTBSOI-based RCA and CLA with prior reported works

Specifications	RCA			CLA			
	Sher and Arab [36]	Uma et al. [37]	This work	Sher and Arab [36]	Uma et al. [37]	Archana et al. [38]	This work
Technology (nm)	45	120	45	45	120	180	45
Supply voltage (V)	0.9	1.2	0.9	0.9	1.2	1	0.9
Bit size	4-bit	8-bit	4-bit	4-bit	8-bit	4-bit	4-bit
Operating frequency (MHz)	0.0625	500	20	0.0625	500	—	20
Power consumption (nW)	106.7	0.206×10^6	57.87	178.1	0.312×10^6	45.105	232.5
Delay (ns)	0.399	4.208	0.1085	0.178	3.1	25.63	0.3151
PDP (fJ)	42.573×10^{-3}	0.866×10^6	6.291×10^{-3}	31.701×10^{-3}	0.967×10^6	1156.0×10^{-3}	82.036×10^{-3}

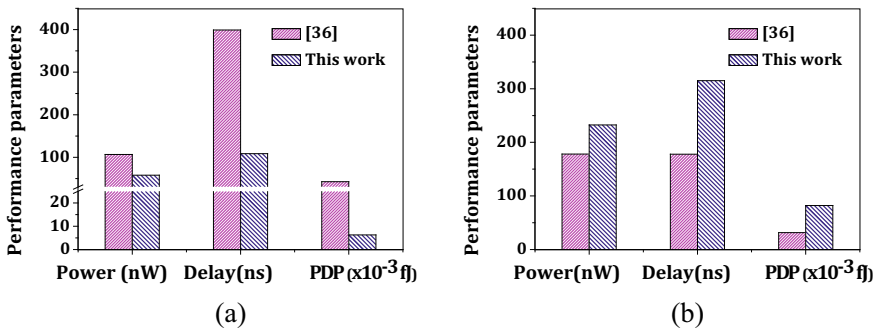


Fig. 35.6 Comparison of performance parameters achieved by the **a** UTB-RCA with the RCA in [36], **b** UTB-CLA with the CLA in [36]

UTB-CLA fails to compete with the existing method [36]. The simulation performed in this presented work clarifies that the RCA using UTBSOI has better performance than the conventional one but the CLA fails to show better performance in UTBSOI technology.

35.3 Conclusion

Transistor-level implementation followed by performance parameter measurement of multi-bit adders (viz. RCA and CLA) through UTBSOI transistors is presented in this paper. The RCA is designed by cascading four UTBSOI-based TFA cells. The XOR operation in the CLA is performed using the TG-based XOR gates. The simulations are carried out at supply voltage of 0.9 V, and amplitude of input pulses is 0.9 V at operating frequency of 20 MHz. The power consumption, delay, PDP, and EDP exhibited by the UTB-RCA are better than that of UTB-CLA by ≈ 6.65 times. The power consumption and delay in UTB-RCA are 84.3% and ≈ 3.67 times lesser than that of existing design in the literature. The use of UTBSOI in the CLA does not seem to enhance the performance so far.

Acknowledgements This work was supported by the Ministry of Electronics and Information Technology, Government of India, under Visvesvaraya Ph.D. Scheme.

References

1. Razavi, B.: Design of Analog CMOS Integrated Circuits, 2nd edn. McGraw-Hill, New York (2001)
2. Vora, P.H., Lad, R.: A review paper on CMOS, SOI and FinFET technology. In: Design and Reuse Industry Articles, pp. 1–10 (2017). <https://www.design-reuse.com/articles/41330/cmos-soi-finfet-technology-review-paper.html>. Last accessed 9 Dec 2019
3. Ferain, I., Colinge, C.A., Colinge, J.-P.: Multigate transistors as the future of classical metal-oxide-semiconductor field-effect-transistor. *Nature* **479**(7373), 310–316 (2011)
4. Paydavosi, N., Venugopalan, S., Chauhan, Y.S., Duarte, J.B., Jandhyala, S., Niknejad, A.M., Hu, C.C.: BSIM-SPICE models enable FinFET and UTB IC. *IEEE Access* **1**, 201–215 (2013)
5. Khandelwal, S., Chauhan, Y.S., Lu, D.D., Venugopalan, S., Karim, M.A.U., Sachid, A.B., Nguyen, B.-Y., Rozeau, O., Fanyot, O., Niknejad, A.M., Hu, C.C.: BSIM-IMG: a compact model for ultrathin-body SOI MOSFETs with back-gate control. *IEEE Trans. Electron Dev.* **59**(8), 2019–2026 (2012)
6. BSIM-IMG. <http://bsim.berkeley.edu/models/bsimimg>. Last accessed 10 Aug 2017
7. Shams, A.M., Darwish, T.K., Bayoumi, M.A.: Performance analysis of low-power 1-bit CMOS full adder cells. *IEEE Trans. VLSI Syst.* **10**(1), 20–29 (2002)
8. Kumar, P., Sharma, R.K.: Low voltage high performance hybrid full adder. *Eng. Sci. Technol. Int. J.* **19**(1), 559–565 (2016)
9. Aguirre-Hernandez, M., Linares-Aranda, M.: CMOS full-adders for energy-efficient arithmetic applications. *IEEE Trans. VLSI Syst.* **19**(4), 718–721 (2011)
10. Zimmermann, R., Fichter, W.: Low-power logic styles: CMOS versus pass-transistor logic. *IEEE J. Solid-State Circ.* **32**(2), 1079–1090 (1997)
11. Weste, N., Eshraghian, K.: Principles of CMOS VLSI Design, A Systems Perspective, 2nd edn. Addison Wesley, Reading, Massachusetts (1993)
12. Alioto, M., Palumbo, G.: Analysis and comparison on full adder block in submicron technology. *IEEE Trans. VLSI Syst.* **10**(6), 806–823 (2002)
13. Zhuang, N., Wu, H.: A new design of the CMOS full adder. *IEEE J. Solid-State Circ.* **27**(5), 840–844 (1992)
14. Wu, X., Prosser, F.: Design of ternary CMOS circuits based on transmission function theory. *Int. J. Electron.* **65**(5), 891–905 (1988)

15. Theja, M.N., Balakumaran, T.: Energy efficient low power high speed full adder design using hybrid logic. In: International Conference on Circuit, Power and Computing Technologies, pp. 1–8. IEEE, Nagercoil, India (2016)
16. Bhattacharyya, P., Kundu, B., Ghosh, S., Kumar, V., Dandapat, A.: Performance analysis of a low-power high-speed hybrid 1-bit full adder circuit. *IEEE Trans. VLSI Syst.* **23**(10), 2001–2008 (2015)
17. Navi, K., Maenen, M., Foroutan, V., Timarchi, S., Kavehei, O.: A novel low-power full-adder cell for low voltage. *Integr. VLSI J.* **42**(4), 457–467 (2009)
18. Cho, H., Swartzlander, E.E.: Adder designs and analyses for quantum-dot cellular automata. *IEEE Trans. Nanoelectron.* **6**(3), 374–383 (2007)
19. Cho, H., Swartzlander, E.E.: Adder and multiplier design in quantum-dot cellular automata. *IEEE Trans. Comput.* **58**(6), 721–727 (2009)
20. Navi, K., Farazkish, R., Sayedsalehi, S., Azghadi, M.R.: A new quantum-dot cellular automata full-adder. *Microelectron. J.* **41**(12), 820–826 (2010)
21. Lee, J., Lee, J.H., Chung, I.-Y., Kim, C.-J., Park, B.-G., Dong, M.K., Dae, H.K.: Comparative study on energy-efficiencies of single-electron transistor-based binary full adders including nonideal effects. *IEEE Trans. Nanotechnol.* **10**(5), 1180–1190 (2011)
22. Griveau, D., Ecoffey, S., Parekh, R.M., Bounouar, M.A., Calmon, F., Beauvais, J., Drouin, D.: Single electron CMOS-like one bit full adder. In: International Conference on Ultimate Integration on Silicon, pp. 77–80. IEEE, Grenoble, France (2012)
23. Moaiyeri, M.H., Mirzaee, R.F., Navi, K., Momeni, A.: Design and analysis of a high-performance CNTFET-based full adder. *Int. J. Electron.* **99**(1), 113–130 (2011)
24. Moaiyeri, M.H., Mirzaee, R.F., Navi, K., Hashemipour, O.: Efficient CNTFET-based ternary full adder cells for nanoelectronics. *Nano-Micro Lett.* **3**(1), 43–50 (2011)
25. Keshavarzian, P., Sarikhani, R.: A novel CNTFET-based ternary full adder. *Circ. Syst. Signal Process.* **33**(3), 665–679 (2014)
26. Mahani, A.T., Keshavarzian, P.: A novel energy-efficient and high speed full adder using CNTFET. *Microelectron. J.* **61**, 79–88 (2017)
27. Hatefinasab, S.: Carbon nanotube field effect transistor-based hybrid full adders using gate-diffusion input structure. *J. Nanoelectron. Optoelectron.* **14**(11), 1512–1522 (2019)
28. Saraswat, R., Akashe, S., Babu, S.: Designing and simulation of full adder cell using FinFET technique. In: International Conference on Intelligent Systems and Control, pp. 261–264. IEEE, Coimbatore, India (2013)
29. Kohlon, J., Kumar, P., Garg, A., Gupta, A.: Low power and temperature compatible FinFET based full adder circuit with optimized area. In: International Conference on Advances in Computing, Communications and Informatics, pp. 2121–2125. IEEE, Jaipur, India (2016)
30. Ahmed, R.U., Saha, P.: Implementation topology of fulladder cells. *Procedia Comput. Sci.* **165**, 676–683 (2019)
31. Mano, M.M., Ciletti, M.D.: Digital Design, 4th edn. Pearson Education, New Jersey (2007)
32. Mewada, M., Zaveri, M., Thakker, R.: Improving the performance of transmission gate and hybrid CMOS full adders in chain and tree structure architectures. *Integr. VLSI J.* **69**, 381–392 (2019)
33. Jhamb, M., Garima, Lohani, H.: Design, implementation and performance comparison of multiplier topologies in power-delay space. *Eng. Sci. Technol. Int. J.* **19**(1), 355–363 (2016)
34. Uyemura, J.P.: CMOS Logic Circuit Design, 1st edn. Kluwer Academic, Dordrecht (2001)
35. Sharma, V.K., Pattanaik, M.: VLSI scaling methods and low power CMOS buffer circuit. *J. Semicond.* **34**(9), 095001-(1–8) (2013)
36. Sher, T.-H., Arab, S.: Comparisons between ripple-carry adder and carry-look-ahead adder. Technical Report, University of Southern California (2015)
37. Uma, R., Vijayan, V., Mohanapriya, M., Paul, S.: Area, delay and power comparison of adder topologies. *Int. J. VLSI Des. Commun. Syst.* **3**(1), 153–168 (2012)
38. Archana, T., Arunkumar, K., Malini, A.H.: Delay depreciation and power efficient carry look ahead adder using CMOS. *J. Chem. Pharm. Sci.* **9**, 101–105 (2017)

Chapter 36

Accelerating Latency of Binary Division Through Vedic Methodology



Deepak Kumar and Prabir Saha

Abstract An improved binary division computation technique for accelerating the latency based on Vedic methodology is introduced in this paper. Substantial modifications of Vedas formula ‘Paravartya-Yojayet (transpose and apply)’ have been constructed through multiplication and addition to accelerate the latency of the divider circuitry. Figure of merits in terms of latency and area (number of Slices, LUTs) of the proposed division circuitry and other popular algorithms were synthesized and compared in same environment using Xilinx. Based on synthesized result, it has been observed that latency is improved substantially from its counterparts.

36.1 Introduction

The computation of division always plays a pivotal role for the design of arithmetic processor [1–7]. Generally, computation of division is sequential in nature; thereby, computational complexity and latency is much higher when compared with other primitive operations such as addition and multiplication [4, 5].

A standard division operation computes $A = QB + R$, where A , Q , B , and R represent dividend, quotient, divisor, and remainder, respectively. Generally, two principal methodologies have been introduced in the literature so far for the computation of such operation [3–21], viz. digit recurrence (restoring [10, 16, 21], non-restoring [14–16]), and iterative (Newton–Raphson method [12, 17]), Goldschmidt algorithm [4, 5, 8, 9, 13]) methods. Digit recurrence algorithm is based on shift-and-subtractions [21]; thereby, architecture is simple, and propagation delay (latency)

D. Kumar (✉)

Department of Computer Science and Engineering, National Institute of Technology Meghalaya, Shillong, India

e-mail: deepak.kumar@nitm.ac.in

P. Saha

Department of Electronics and Communication Engineering, National Institute of Technology Meghalaya, Shillong, India

e-mail: prabir.saha@nitm.ac.in

© The Editor(s) (if applicable) and The Author(s), under exclusive license to Springer Nature Singapore Pte Ltd. 2021

Y.-D. Zhang et al. (eds.), *Smart Trends in Computing and Communications: Proceedings of SmartCom 2020*, Smart Innovation, Systems and Technologies 182,

https://doi.org/10.1007/978-981-15-5224-3_36

is high. Hence, to compute division ‘ n ’ subtraction is required, where ‘ n ’ denotes the bit-width of dividend and divisor. To speed up the operation, high radix [11] constructed methodologies have been investigated. Schemes suffice the problems like hardware complexity and accuracy. Alternatively, iterative methods have been investigated [14, 17], where higher accuracy has been achieved at the cost of latency. However, such iterative schemes require fast multiplication techniques (along with the inverse of the divisor). Moreover, the iterative techniques cannot produce the remainder directly.

Vedic mathematics originates from the age-old Indian scriptures, and its computation techniques are analogous to human’s mental calculations to produce fast result of arithmetic operations [19, 22]. Substantial amount of research has so far been investigated based on such ancient mathematics for VLSI (very large-scale integration) implementation of arithmetic operations. Observation from the reported work summarizes the symmetry property, reduction of the clock cycle, and hence reduction of latency (high speed) [10, 14, 16].

This paper reports implementation of a new binary division circuitry through the improved Vedic formulae. Sanskrit term Paravartya-Yojayet (PY) indicates ‘transpose and apply’, have been re-structured for binary numbers followed the circuit level implementation. From the constructed formula, it has been observed that division operation can be implemented through multiplication followed by addition and ease hardware realization is possible owing to achieve the present VLSI goals. Substantial reduction in dynamic power consumption, and propagation delay is achieved by the reduction of the number of cycles for division computation. Vedic formula for binary numbers followed by the hardware realization of division circuitry was implemented in Verilog hardware description language and synthesized through Xilinx ISE tools for device xc7v2000t of family Virtex7 with package flg1925. Performance evaluators as functions of latency and area have been calculated from the synthesized results. Moreover, comparison of proposed methodology with the existing ones like digit recurrence [10] and non-restoring [14, 16]-based implementation was also carried out.

Organization of the paper in rest sections is as follows: Paravartya formula which illustrates the division procedure is discussed and derived in Sect. 36.2. A numerical example has been considered for better understanding the working procedure of the formula. Algorithms have been described in Sect. 36.3. Section 36.3 also describes hardware-level architecture for the implementation of division. Simulation results are discussed in Sect. 36.4 which is followed by conclusions in Sect. 36.5.

36.2 Paravartya-Yojayet Formula for Division

The inherent capability of ancient Vedic mathematics, particularly for divisions, was recounted by Sri B. K. T. Maharaja, as Vedic sutras (formulae) [22]. Paravartya-Yojayet (PY) formula has been investigated to carry out the proposed division methodology.

36.2.2 Mathematical Description of PY for Binary Number System

Mathematically, sutra can be formulated as: the number $A = \sum_{i=0}^{m-1} a_i 2^i$ to be divided by $B = \sum_{i=0}^{n-1} b_i 2^i$, (where $m > n$ and a_i, b_i are binary digits). To implement the division using PY sutra, the number A and B has been decomposed with respect to 2^{n-1} , i.e.,

$$B = \sum_{i=0}^{n-1} b_i 2^i = b_{n-1} 2^{n-1} - p = x - p \quad (36.1)$$

where $p = \sum_{i=0}^{n-2} (-b)_i 2^i$ and $x = b_{n-1} 2^{n-1}$

$$A = \sum_{i=n}^{m-1} a_i 2^i + \sum_{i=0}^{n-1} a_i 2^i \quad (36.2)$$

$$\begin{aligned} &= 2^n \sum_{i=0}^{m-n-1} a_{i+n} 2^i + \sum_{i=0}^{n-1} a_i 2^i \\ &= 2^n \frac{b_{n-1}}{b_{n-1}} \sum_{i=0}^{m-n-1} a_{i+n} 2^i + \sum_{i=0}^{n-1} a_i 2^i \\ &= 2 \cdot b_{n-1} \cdot 2^{n-1} \frac{1}{b_{n-1}} \sum_{i=0}^{m-n-1} a_{i+n} 2^i + \sum_{i=0}^{n-1} a_i 2^i \end{aligned} \quad (36.3)$$

If $q_1 = \frac{1}{b_{n-1}} \sum_{i=0}^{m-n-1} a_{i+n} 2^i$ and $q_2 = \sum_{i=0}^{n-1} a_i 2^i$ Eq. (3) can be reformulated as

$$\begin{aligned} &= 2 \times q_1 + q_2 \\ &= 2 \times q_1 + q_2 + 2q_1 p - 2q_1 p \\ &= 2q_1(x - p) + q_2 + 2q_1 p \\ &= 2q_1 B + (q_2 + 2q_1 p) \end{aligned} \quad (36.4)$$

where quotient $Q = 2q_1$ and remainder $R = (q_2 + 2q_1 p)$. Now if R is greater than B , then again this process must be performed repeatedly until $R < B$ by using $A = R$.

of the bit and next one represents magnitude of the bit. Transpose unit has been implemented through buffer, assuming that negligible propagation delay. The partial product generation requires only AND and XOR gate; thereby, propagation delay of the AND gate XOR is approximated to one XOR gate. Each row of the partial product array performs in parallel such that the effective latency is measured as one 'XOR' gate delay per iteration. Assuming that the propagation delay of the partial product generation for the entire algorithm takes at most ' n ' XOR gate delay. Propagation delay of one bit of signed digit binary number addition stage takes delay of 8 XOR () gate. Thus, the overall propagation delay produced by adder/subtractor is equal to $\text{totADD} = 8n.t_{\text{XOR}}$. Thus, delay is incorporated at the time of addition of the partial products. There are ' n ' partial product array which are to be added. Since there are $(n-1)$ addition stages, the delay caused by addition can be calculated as $8n^2t_{\text{XOR}}$. Thus, the overall propagation delay ' t_{pd} ' can be stated from Eq. (5) as,

$$t_{\text{pd}} = [n + 8n^2]t_{\text{XOR}} \quad (36.6)$$

36.3 Architecture Implementation

In this section, the proposed division algorithm and its VLSI implementation procedure have been described. The complete architecture for the division of binary numbers is shown in Fig. 36.3. The architecture consists of 4-major stage, viz. preprocessing unit, binary-to-signed binary conversion unit, divider unit for signed binary numbers, and signed binary number-to-binary number conversion unit (Fig. 36.4).

Preprocessing unit is required to count the number of iteration, s and to align the bits of the divisor to left end. Binary-to-signed binary number conversion unit is required to implement the corresponding transpose of the bits, which would be the multiplicand of the subsequent stages. Divider unit operates on the signed binary number, and finally, result is generated in binary with the help of signed binary-to-binary converter.

36.3.1 Preprocessing Unit

The proposed divider algorithm requires that all the divisor bits after removing most significant bit (msb), must be aligned to the left end in the register instead of natural right end alignment. The preprocessing unit converts the divisor in required form. It also decides the number (in unary format) of steps based on divider value by detecting leading bit '1' from left end [24].

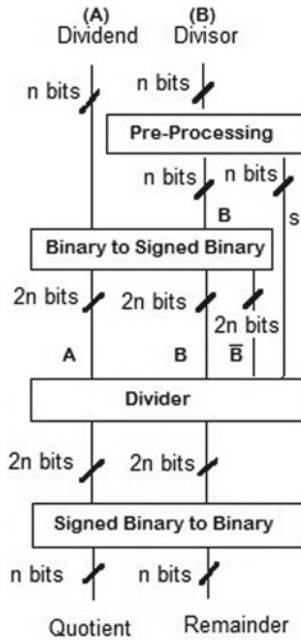


Fig. 36.3 Overall architecture of the division procedure

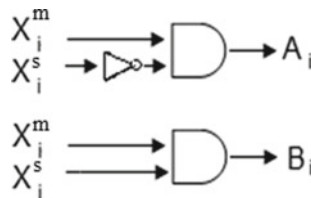


Fig. 36.4 Extraction of binary bits from signed digits

```

Algorithm: Pre-processing
Input: x[n]
Outputs: y[n], steps[n]

```

```

y ← x
steps[n-1] ← x[n-1]
if(steps[n-1] = 0) then y ← y << 1
for i ← n-2 to 0 do
  steps[i] = x[i] OR steps [i+1]
  if(steps[i] = 0) y ← y << 1
  steps ← steps >> 1
  steps ← ~steps // ~ : bitwise complement
y ← y << 1
return y and steps

```

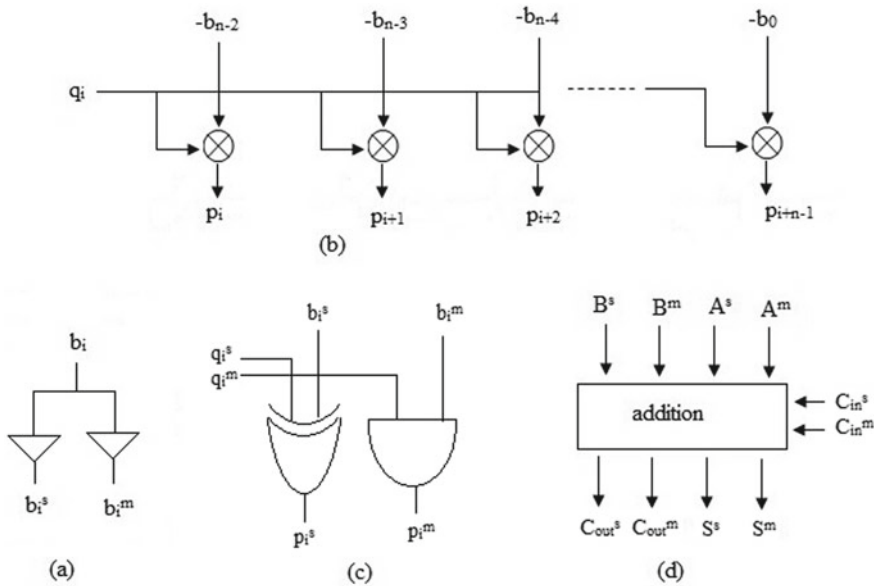


Fig. 36.5 Internal circuit modules of the divider architecture. **a** Circuit of the transposition unit. **b** Multiplication unit. **c** Enlarge view of the single point multiplication unit. **d** Addition unit of the signed number

36.3.2 Binary-to-Signed Binary

The signed digit $t_i \in \{-1, 0, 1\}$ has been encoded by two binary bits t_i^s, t_i^m and assign ‘11’, ‘00’, ‘01’ to t_i^s, t_i^m according as ‘-1’, ‘0’ and ‘1’, respectively. Binary-to-signed binary unit converts an n -bit binary representation to $2n$ -bit signed binary representation by simply using 00/01 for each bit 0/1. It also generates bitwise transpose of the divisor, \overline{dvr} using circuit shown in Fig. 36.5a.

36.3.3 Divider for Signed Binary Number

Division algorithm for $n \div n$ signed digits (SD), i.e., for $2n \div 2n$ binary numbers is given below. Inputs dvd, dvr, \overline{dvr} and steps denote dividend, divisor, bitwise transposed divisor, and required number of steps, respectively. For simplicity ripple carry adder ($+_{SD}$) for signed digits have been used to add the partial products without exploiting the constant time addition property of such adders. After required number of steps, if final remainder value, R is negative then divisor would be needed to add with remainder and quotient, Q would be decremented by one. Finally, bits of remainder register needed to be right aligned.

Algorithm: Division of signed digit (SD) numbers

Inputs: dvd[n], dvr[n], $\overline{\text{dvr}}$ [n], steps[n]

Outputs: Q[n], R[n]

```

R= dvd
for i ← 0 to (steps-1) do
  Q ← Q << 1
  Q[0] ← R[n-1]
  R ← R << 1
  if Q[0] = 1 do
    sum = R +sd  $\overline{\text{dvr}}$ 
  else if Q[0] = -1 do
    sum = R +sd dvr

  if carry then Q[0] = 0
  else R = sum

if R[n-1] = 1 then
  Q ← Q +sb -1
  R ← R >> steps
  R ← R +sb divisor
else
  R ← R >> steps
return Q and R

```

36.3.4 Signed Binary to Binary

Any radix-2 signed digit (SD) binary number with digits $\{-1, 0, 1\}$ can be converted into corresponding radix-2 binary number with digits $\{0, 1\}$ as given in [23]. Let a SD binary number be $X = (1, 0, -1, 1)_{\text{SD}} = 7_{10}$, then extract two numbers $A =$ non-negative digits of X , i.e., 1, 0, 0, 1 and $B =$ negative digits of X , i.e., 0, 0, 1, 0, and $A-B$ would give corresponding binary representation. Circuit for the bits extraction of such two numbers A and B from our signed digit binary number X is shown in Fig. 36.4.

Internal circuit diagram of the division circuitry is given in Fig. 36.5. The circuit diagram Fig. 36.5d has been implemented through Eqs. (7–10). Negative number has been generated via canonical sign digit representation [23, 25–27]. Each signed digit $\{-1, 0, 1\}$ has been represented as both sign and the corresponding magnitude. So each signed digit t_i has been encoded by two binary bits t_i^s, t_i^m and assign ‘11’, ‘00’, ‘01’ to ‘-1’, ‘0’ and ‘1’, respectively, and so b_i as $b_i^s b_i^m$, q_i as $q_i^s q_i^m$ and p_i as $p_i^s p_i^m$.

The sum ($S^s S^m$) and carry ($C_{\text{out}}^s C_{\text{out}}^m$) of the adder have been computed through Eqs. (7–10).

$$\begin{aligned}
 S^s &= \overline{A^m B^m} C_{\text{in}}^s C_{\text{in}}^m + \overline{A^m B^s} B^m \overline{C_{\text{in}}^m} + A^s A^m \overline{B^m} C_{\text{in}}^m \\
 &+ A^m B^s B^m C_{\text{in}}^s C_{\text{in}}^m + A^s A^m B^m C_{\text{in}}^s C_{\text{in}}^m + A^s A^m B^s B^m C_{\text{in}}^m
 \end{aligned} \quad (36.7)$$

$$S^m = \overline{A^m B^m C_{in}^m} + A^m \overline{B^m C_{in}^m} + A^m B^m \overline{C_{in}^m} + \overline{A^m B^m C_{in}^s C_{in}^m} + \overline{A^m B^s B^m C_{in}^m} + A^s \overline{A^m B^m C_{in}^m} \quad (36.8)$$

$$C_{out}^s = \overline{A^m B^s B^m C_{in}^s C_{in}^m} + A^s B^s B^m C_{in}^s C_{in}^m + A^s A^m \overline{B^m C_{in}^s C_{in}^m} + A^s A^m B^s B^m \overline{C_{in}^m} \quad (36.9)$$

$$C_{out}^m = \overline{A^s B^s B^m C_{in}^s C_{in}^m} + \overline{A^m B^s B^m C_{in}^s C_{in}^m} + \overline{A^m B^s B^m C_{in}^s C_{in}^m} + \overline{A^s A^m \overline{B^m C_{in}^s C_{in}^m}} + \overline{A^s A^m B^s B^m \overline{C_{in}^m}} + A^s A^m \overline{B^m C_{in}^s C_{in}^m} + A^s A^m B^s B^m \overline{C_{in}^m} \quad (36.10)$$

36.4 Results and Discussions

Functionality of the reported algorithm in this paper was simulated and synthesized by Xilinx ISE tools for device xc7v2000t of family Virtex7 with package flg1925. The Vedic division methodology application reduces the redundancy of iterations, resulting less amount of overall latency. Latency of the divider can be described as the product of cycle time and average number of cycles.

The synthesized performance analysis in terms of average latency (Average number of cycles \times Clock period), slices register and slice LUTs (look-up tables) are shown in Fig. 36.6. Data for input are selected as a regular fashion for testing purpose. Instead of fixed number of cycles for the W-bits implementation, the proposed algorithm uses actual no. of bits (by detecting leading '1') in divisor to decide the required no. of cycles for division, i.e., if actual no. of bits i then required no. of cycles will be $(W + 1 - i)$. Calculation of average no. of cycles for W-bits implementation is shown below.

Numbers with bit-size 1 = {1} and total such numbers are $1 = 2^{1-1}$

Numbers with bit-size 2 = {10, 11} and total such numbers are $2 = 2^{2-1}$

Numbers with bit-size 3 = {100, 101, 110, 111} and total such numbers are $4 = 2^{3-1}$ and so on. Finally, total count of numbers having bit-size 1 to $W = 1 + 2 + 2^2 + \dots + 2^i + \dots + 2^{W-1}$ and

$$\begin{aligned} \text{Avg. number of cycles} &= \frac{\sum_{i=1}^W (\text{numbers with bit-size } i) \times (W + 1 - i)}{\sum_{i=1}^W (\text{numbers with bit-size } i)} \\ &= \frac{\sum_{i=1}^W 2^{i-1} \times W + 1 - i}{\sum_{i=1}^W 2^{i-1}} \\ &= \frac{1 \times W + 2 \times (W - 1) + \dots + 2^{W-1} \times 1}{1 + 2 + \dots + 2^{W-1}} = \frac{2^{W+1} - W - 2}{2^W - 1} \end{aligned} \quad (36.11)$$

For the comparison purpose, other architectures those are similar in nature have been implemented in the same environment without any effort for optimization. While in general implementation of other architectures, the number of cycles per division operation is usually fixed for input width, our proposed architecture takes into consideration of minimum number of bits required to represent the input to decide the number of cycles necessary. From Fig. 36.6a, it has been observed that latency of the proposed method has been improved by ~68 and ~61% compared to digit recurrence and non-restoring algorithms. This improved latency came at cost of little bit area (Registers and LUTs) as evident from Fig. 36.6b,c.

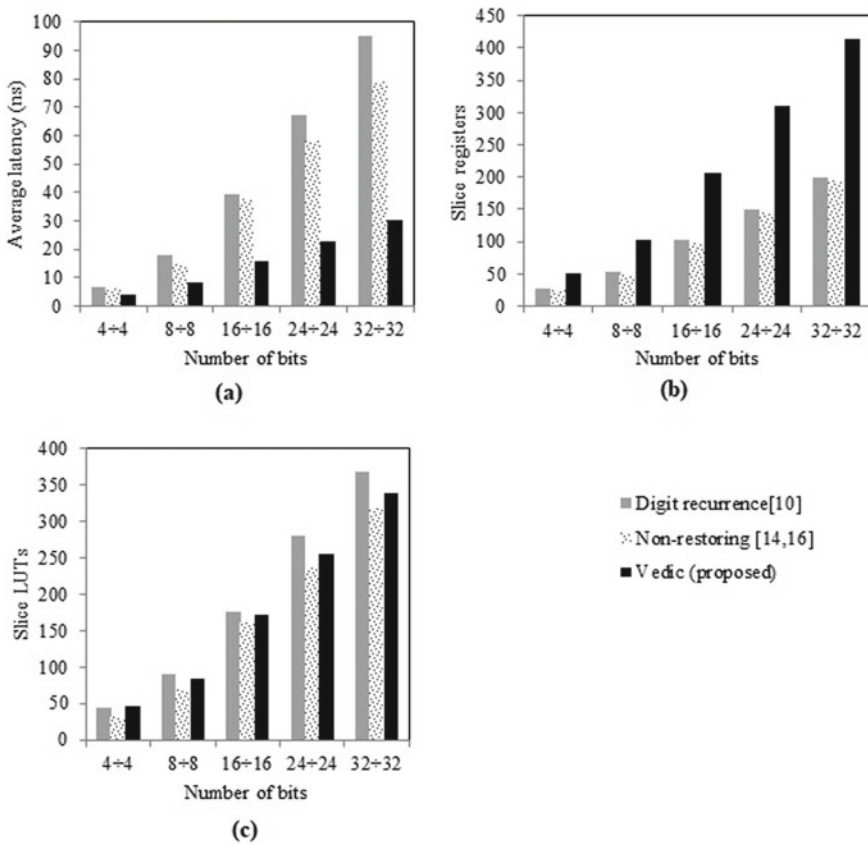


Fig. 36.6 Synthesized performance parameters: **a** Latency. **b** Slice registers. **c** Slice LUTs for different bit lengths

36.5 Conclusions

In this work, a new division algorithm and its architecture have been described based on Vedic mathematics. The architecture has been synthesized through Xilinx ISE tools for device xc7v2000t of family Virtex7 with package flg1925. The synthesized result offered ~68 and ~61% improvements in latency in comparison with widely known algorithms like digit recurrence and non-restoring, respectively. The latency has been improved at the cost of area due to the application of binary signed digit numbers. Efficient architecture implementation of signed digit number may lead to the reduction of area.

References

1. Matula, D.W., Panu, M.T., Zhang, J.Y.: Multiplicative division employing independent factors. *IEEE Trans. Comput.* **64**(7), 2012–2019 (2015)
2. Stanion, T., Sechen, C.: Boolean division and factorization using binary decision diagrams. *IEEE Trans. Comput. Aided Des. Integr. Circ. Syst.* **13**(9), 1179–1184 (1994)
3. Hagglund, R., Lowenborg, P., Vesterbacka, M.: A polynomial-based division algorithm. In: *IEEE Proceedings of the International Symposium on Circuits and Systems*, Phoenix-Scottsdale, AZ, USA, pp. 571–574 (2002)
4. Kong, I., Swartzlander Jr., E.E.: A rounding method to reduce the required multiplier precision for goldschmidt division. *IEEE Trans. Comput.* **59**(12), 1703–1708 (2010)
5. Kong, I., Swartzlander Jr., E.E.: A goldschmidt division method with faster than quadratic convergence. *IEEE Trans VLSI Syst.* **19**(4), 696–700 (2011)
6. Jovanovic, B., Jevtic, R., Carreras, C.: Binary division power models for high-level power estimation of FPGA-based DSP circuits. *IEEE Trans. Ind. Informat.* **10**(1), 393–398 (2014)
7. Ebergen, J., Jamadagni, N.: Radix-2 division algorithms with an over-redundant digit set. *IEEE Trans. Comput.* **64**, 2652–2663 (2015)
8. Piso, D., Bruguera, J.D.: Variable latency goldschmidt algorithm based on a new rounding method and a remainder estimate. *IEEE Trans. Comput.* **60**, 1535–1546 (2011)
9. Bhojar, R., Palsodkar, P., Kakde, S.: Design and implementation of goldschmidts algorithm for floating point division and square root. In: *International Conference on Communications and Signal Processing*, Melmaruvathur, India, pp. 1588–1592 (2015)
10. Liu, W., Nannarelli, A.: Power efficient division and square root unit. *IEEE Trans. Comput.* **61**(8), 1059–1070 (2012)
11. Amaricai, A., Boncalo, O.: Implementation of very high radix division in FPGAs. *Electron. Lett.* **48**, 1107–1109 (2012)
12. Oberman, S.F., Flynn, M.J.: Division algorithms and implementations. *IEEE Trans. Comput.* **46**(8), 833–854 (1997)
13. Ercegovac, M.D., Imbert, L., Matula, D.W., Muller, J.M., Wei, G.: Improving goldschmidt division, square root, and square root reciprocal. *IEEE Trans. Comput.* **49**(7), 759–763 (2000)
14. Deschamps, J.P., Bioul, G.J.A., Sutter, G.D.: *Synthesis of Arithmetic Circuits, FPGA, ASIC and Embedded System*. John Wiley & Sons, USE (2006)
15. Cui, H., Cai, L., Yang, X., Feng, C., Qin, T.: Design of non-restoring binary array divider in quantum-dot cellular automata. *Micro Nano Lett.* **9**(7), 464–467 (2014)
16. Parhami, B.: *Computer Arithmetic: Algorithms and Hardware Designs*. Oxford University Press, London, UK (2000)
17. Gallagher, W.L., Swartzlander Jr., E.E.: Fault-tolerant Newton-Raphson and goldschmidt dividers using time shared TMR. *IEEE Trans. Comput.* **49**(6), 588–595 (2000)

18. Saha, P., Banerjee, A., Dandapat, A.: ASIC design of a high speed low power circuit for calculation of factorial of 4-bit numbers based on ancient vedic mathematics. *Microelectron. J.* **42**(12), 1343–1352 (2011)
19. Saha, P., Banerjee, A., Bhattacharyya, P., Dandapat, A.: Vedic divider: novel architecture (ASIC) for high speed VLSI applications. In: *IEEE International Symposium on System Design*, Kochi, Kerala, India, pp. 67–71 (2011)
20. Aggarwal, N., Asooja, K., Verma, S.S.: An improvement in the restoring division algorithm (needy restoring division algorithm). In: *IEEE International Conference on Computer Science and Information Technology*, Beijing, China, pp. 246–249 (2009)
21. Deschamps, J.P., Sutter, G.: Decimal division: algorithm and FPGA implementations. In: *IEEE Southern Programmable Logic Conference (SPL)*, Ipojuca, Brazil, pp. 67–72
22. Maharaja, J.S.S.B.K.T.: *Vedic Mathematics*. Motilal Banarsidas Publishers, Delhi, India (2001)
23. Koren, I.: *Computer Arithmetic Algorithms*, 2nd edn. Natick, MA, USA, AK Peters (2002)
24. Schmookler, M.S., Nowka, K.J.: Leading zero anticipation and detection—a comparison of methods. In: *IEEE 15th Symposium on Computer Arithmetic*, Vail, USA, pp. 7–12 (2001)
25. Han, L., Zhang, H., Ko, S.B.: Decimal floating-point fused multiply-add with redundant internal encodings. *IET Comput. Digit. Tech.* **10**(4), 147–156 (2016)
26. Kornerup, P.: Reviewing high-radix signed-digit adders. *IEEE Trans. Comput.* **64**(5), 1502–1505 (2015)
27. Saha, P., Banerjee, A., Dandapat, A.: ASIC implementation of high speed processor for calculating discrete fourier transformation using circular convolution technique. *WSEAS Trans. Circ. Syst.* **10**(8), 278–288 (2011)

Chapter 37

Monitoring the torsional vibrations on the main propulsion plant of marine cargo ship installed two-stroke diesel engine: Theoretical case study



Do Duc Luu and Cao Duc Hanh

Abstract The paper presents theoretical monitoring torsional vibrations (TMTVs) on the main propulsion plant (MPP), using two-stroke diesel engine (2DE)-driven propeller of the marine cargo ship. The study was carried out on the base of mathematical modeling of the torsional vibrations on the MPP and realized numerical solution in computer with the simulated software for monitoring TVs (SMTVs) that made by author in LabView in accordance with rules for classification and construction of the sea-going ships, given by one of the register organizations, members of the IACS in the world, such as Russian Maritime Register of shipping (RMR). The TMTVs on the MPP was automatically carried out by the SMTVs in the every numeric experiment in accordance with the designed experimental plan, such as experiment in Normal working of every cylinder, in the Misfire.Cases1–Misfiring in one of the cylinders, and in the Misfire.Case2—Misfiring together of the two of the cylinders. In every experiment was calculated and monitored the torsional vibrations (TVs) in interval $\lambda = [0.4, 1.2]$, $\lambda = n/n_{MCR}$, n and n_{MCR} —current and normal revolutions, rpm (MCR—maximum continuous rate). The MTVs was probated for MV.HR.34000 DWT, which designed and built in PhaRung Shipyard, Viet Nam, in 2007 year.

37.1 Introduction

Monitoring torsional vibrations (TV) on the MPP is certain important to ensure the system working without any damage of torsional pressures in every working from minimum to maximum continuous revolution and with the normal and misfire inside of only one combustion cylinder chamber [1]. Therefore, for the new building marine steel vessel, the received data from the calculated and measured TV shall

D. D. Luu (✉)

Maritime Research Institute of Vietnam Maritime University, Hai Phong, Viet Nam
e-mail: luudd@vimaru.edu.com

C. D. Hanh

Faculty of IT, Vietnam Maritime University, Hai Phong, Viet Nam

© The Editor(s) (if applicable) and The Author(s), under exclusive license to Springer Nature Singapore Pte Ltd. 2021

379

Y.-D. Zhang et al. (eds.), *Smart Trends in Computing and Communications: Proceedings of SmartCom 2020*, Smart Innovation, Systems and Technologies 182,
https://doi.org/10.1007/978-981-15-5224-3_37

be confirmed in the all variants and operation states of the installations (except emergency operation conditions only for TV calculations).

Misfiring of one cylinder is able lead to serious resonance or near resonance by excited moments of different harmonics in the working revolution interval of the MPP [2–4]. In the misfire state of one cylinder, the compression process in the misfired cylinder is normal to ensure balance the inertial moments of the dynamic system. In otherwise, the free torsional vibrations (FTV) of the abnormal MPP will be changed and the free frequencies able to fall in the working revolution interval that means the abnormal MPP able to be damaged with some shaft breakdown [5].

In the technical operation of the main diesel engine (MDE), there is the main goal to keep the normal state (in the state, every cylinder works normally and output moments and powers of the cylinders are equal, respectively). Therefore, except the monitoring (calculation and measurement) TV of the new building marine ships in the design and build stages in the shipyard, the misfire of cylinder could be diagnosed by ones of the directed or in-directed method and technique [5–7].

In practice at the sea-trail tests of new built ships in Vietnam (in period from 2004 to 2019), normally the technical test committees require plan for measuring TV in the cases with misfiring in one of cylinders, such as for the MV.VinashinSky, MV.HR.34000 DWT, at el. (the MDE of the MV. are two-stroke). However, for the some marine ships using four-stroke diesel engine, the technical test committees do not conduct any TV measurement with misfire state of cylinder, such as for MV. “BinhAnValliant”, MV.KN.168 and MV.KN375 (the MDE are four-stroke).

Considering the deferent concepts of the experiments of TV at the sea-trail tests, we carefully verify their TV calculations, respectively, and remark, that the received TV in the MPP with two-stroke DME are very serious high and are established the “barred zone” of working revolution in the “Normal” and “Misfire” states of cylinders [3, 4]. However, the received TV in the MPP with four-stroke DME are very small and lower then permitted TV, respectively [8].

The mathematical modeling TVs of the MMPP, which is used not only in theoretical study, but also in practice, calculation of the TV according to the, respectively, maritime register normally is written in the linear differential equations with second degree for the lumped inertial moments of respective dynamic model [1, 2, 5, 9], in the matrix form:

$$\mathbf{J}\ddot{\varphi} + \mathbf{B}\dot{\varphi} + \mathbf{C}\varphi = \mathbf{M}(t) \quad (37.1)$$

where \mathbf{J} , \mathbf{B} , \mathbf{C} —matrix of TV coefficients of: inertial moments, stiffness, and damping, respectively, have engineering unit [kg.m²], [N.m/rad], and [N.m.s/rad].

M —excited torsional moments (ETM, Nm).

The equations of the every lumped mass i , $i = 1, 2 \dots n$ are received in accordance with Dalambert principle or Lagrange equation of second type. According to the Dalambert principle, in i -th mass the sum moment of the all component moments has to be equal zero. Therefore, the ETM of the cylinder $M_i(t)$ contains gas moment and equivalent moment of the rotary and translational movement of connection—rod—crosshead—piston set [5, 9]. The note is described clearly for the wrong knowledge

of the authors of the article [10] (Daniel P. G. et al.: consider that the moment $M_i(t)$ in the right side of Eq. (37.2) contains also damping parts, like second part of the left side of the equations, that means, the damping effect or not considering, or twice times counting).

The mathematic models of the conventional dynamic model with a limited degree of freedom (LDOF) of the lumped masses are linear and approximated Eq. (37.2), written in the harmonic type of the ETM (right side of Eq. (37.1)) [2]:

$$\mathbf{J}\ddot{\boldsymbol{\varphi}} + \mathbf{B}\dot{\boldsymbol{\varphi}} + \mathbf{C}\boldsymbol{\varphi} = \sum_{k=1}^{Mh} M_{k0} \sin(k\omega t + \gamma_k) \quad (37.2)$$

$$\mathbf{J}\ddot{\boldsymbol{\varphi}} + \mathbf{B}\dot{\boldsymbol{\varphi}} + \mathbf{C}\boldsymbol{\varphi} = \sum_{k=-Mh}^{Mh} \mathbf{ZM}_k e^{ik\omega t} = \sum_{k=0}^{Mh} \mathbf{ZM}_{\pm k} e^{\pm ik\omega t} \quad (37.3)$$

The solution method of FTV with Eqs. (37.1–37.3) when the right components ETM = 0, is numeric matrix to define the eigenvalues and eigenvectors of the matrix $(\mathbf{J}^{-1} \cdot \mathbf{C})$. The method is very easy and simple to realize in MATLAB (m.file) and in LabView [2], for example, using the commands $p = \mathbf{poly}()$ and $\mathbf{roots}(p)$.

The method for solving Eq. (37.3) is integration of the following methods: matrix analysis, complex number, harmonic balance, main axes (independent variables), and superposition. The method shortly is called main-axes method (MAM), that is general to solve damping, linear vibration system, like Eq. (37.3) not only in the resonance, near-resonance regimes, but also in the far-resonance events [2, 5, 9]. Realizing this method to build the software to calculate TV (STVC) is very convenient in the LabView with the sound and vibration toolkit (www.ni.com).

The first stand out point in the proposed paper would be realized TV calculation with the simulated software for monitoring TVs (SMTVs) that made by authors [11].

In accordance with the MAM, we use the substitution:

$$\begin{aligned} \varphi_k &\approx \mathbf{y}_0 + \mathbf{y}_1 \alpha_1 + \mathbf{y}_2 \alpha_2; \quad \varphi_k = [\varphi_{1k}, \varphi_{2k}, \dots, \varphi_{nk}]^T; \\ \alpha_j &= [1, \alpha_{2j}, \dots, \alpha_{jk}]^T; \quad j = 0, 1, 2 \end{aligned} \quad (37.4)$$

The model (37.1) is written in the form of the main axes (y_0 , y_1 , and y_2):

$$\begin{cases} J_{e0} \ddot{y}_0 + d_{e00} \dot{y}_0 + d_{e01} \dot{y}_1 + d_{e02} \dot{y}_2 = M_{e0} \\ J_{e1} (\ddot{y}_1 + \omega_1^2) + d_{e10} \dot{y}_0 + d_{e11} \dot{y}_1 + d_{e12} \dot{y}_2 = M_{e1} \\ J_{e2} (\ddot{y}_2 + \omega_2^2) + d_{e20} \dot{y}_0 + d_{e21} \dot{y}_1 + d_{e22} \dot{y}_2 = M_{e2} \end{cases} \quad (37.5)$$

where

$$J_{e0} = \sum_{i=1}^n J_i; \quad J_{ej} = \sum_{i=1}^n J_i \alpha_{ij}^2; \quad j = 1, 2;$$

$$d_{epq} = \sum_{i=1}^n b_i \alpha_{ip} \alpha_{iq}; \alpha_{i0} = 1; p, q = 0, 1, 2; \tag{37.6}$$

$$M_{ep} = \sum_{i=1}^n \overrightarrow{M_i \alpha_{ip}}; p = 0, 1, 2 \tag{37.7}$$

The second high-light point in proposed paper is described in the realization of the mathematic model and algorithm to calculate the executed TV in accordance with the register requirement, such as requirement of RMR, Edit 2014 [1]. The bold point is formed initially with the given input control vector of firing state in every cylinder:

$$\mathbf{Cf}_k = [Cf_k(1), Cf_k(2) \dots Cf_k(z)] \tag{37.8}$$

where k —an order of simulation realization (numeric experiment);

z —number of cylinder;

In the designed experiment plant, when MDE in “Normal” state, the vector of fire-coefficient (FCV) has: $Cf_1(m) = 1$ with $\forall m = 1, 2, \dots, z$.

In the Misfire.Case1. m : $Cf_k(m) = 0; \forall m = 1, 2, \dots, z; k = m+1; Cf_k(p) = 1; \forall p \neq m$;

In the Misfire.Case2. p : $[Cf_p(m) = 0 \text{ and } Cf_p(k) = 0] \forall (m \neq k; k, m = 1, 2, \dots, z)$;

$$Cf_p(s) = 1; \forall s \notin (m; k)$$

The simulation experiment realization could be carried out on the base of the SMTVs written in LabView [11].

Permitted torsional pressures (PTP, MN/mm², MPa) of shaft pieces, such as of the intermediate shaft (IMS), propeller, and crankshaft of the MDE, ... of the MMPP are calculated in accordance with the guide in given rules of maritime register [1].

The realization the mathematical models given by the rules to make software for automatic calculating the PTP in every revolution $\lambda = n/n_{MCR}$, and showing the PTP (λ) characteristic, $\lambda \in [0.4, 1.2]$, and the end to service for indicating the result of the monitoring process.

The main proposed bold points would be probate in the modern motor vessel, newly built in Viet Nam shipyard.

For realizing the specific idea of the normal and misfire states of cylinder, D. D. Luu proposes the model of the indication diagram $p(\varphi)$ (ID) of current state cylinder pressure p , (MPa, Bar) via crankshaft angle φ which is described of the firing coefficient Cf and two pressures, respectively, the compression curve $p_{comp}(\varphi)$ and firing one $p_{fire}(\varphi)$ in the following form [5]:

$$p(\varphi) = p_{comp}(\varphi) + Cf \cdot p_{fire}(\varphi) \tag{37.9}$$

Using calculating the ID the gas moment of the cylinder is calculated [2, 5, 11]:

$$\begin{aligned}
 M(\varphi) &= p(\varphi) \cdot TF(\varphi); \\
 TF(\varphi) &= \frac{\pi D^2}{4} (\sin \varphi + \frac{\lambda}{2} \sin 2\varphi)
 \end{aligned}
 \tag{37.10}$$

where $\lambda = 0.5S/L$ and D —parameters of the diesel (L —connection rod; m and D —diameter of the cylinder, m ; S —length stroke, m), that are given in the MDE technical document.

The combustion and firing pressures are calculated according to the mathematic models of the working processes that are studied in the theory of the MDE. The ID is improved by integration study of the theoretic and experimental calculations (Luu and Vinh [12]).

The SMTVs are built in the base of mathematic models and realized by writing codes in LabView [11]. The simulation object such as a demonstrated is MPP of the MV.HR.34000 DWT.

37.2 Research Method

37.2.1 Automatic Monitoring TVs on MPP Using the Simulation Software

In Table 37.1, there are 22 experiments which shall be carried out in the SMTVs. In the every experiment, we need to input only technical state by clicking the mouse in the control item “Diesel mode” on the Pront Panel of the SMTVs. After selecting the experimental regime, we only operate the simulation software with some simple acts to display on the PC screen necessary results of the TV calculation (TVC) [11].

The every experiment TVC is automatically conducted via following algorithm, as shown in Fig. 37.1. In this figure, there are blocks, described in Table 37.2.

The numeric experiments for MTV are designed in the plan, as shown in Table 37.1 above mentioned, for example, the MDE with six cylinders.

Table 37.1 Numeric experiment plan for MTVs for MDE with $z = 6$ (MV.HR.34000 DWT)

Number of exp.	Technical state of MDE	FCV: Cf = [.....]
1	Normal, every cylinder work normally	Cf=[1 1 1 1 1 1]
2	Misfire.Case1.1	Cf=[0 1 1 1 1 1]
...
7	Misfire.Case1.6	Cf=[1 1 1 1 1 0]
8	Misfire.Case1.12	Cf=[0 0 1 1 1 1]
...
22	Misfire.Case1.56	Cf=[1 1 1 1 0 0]

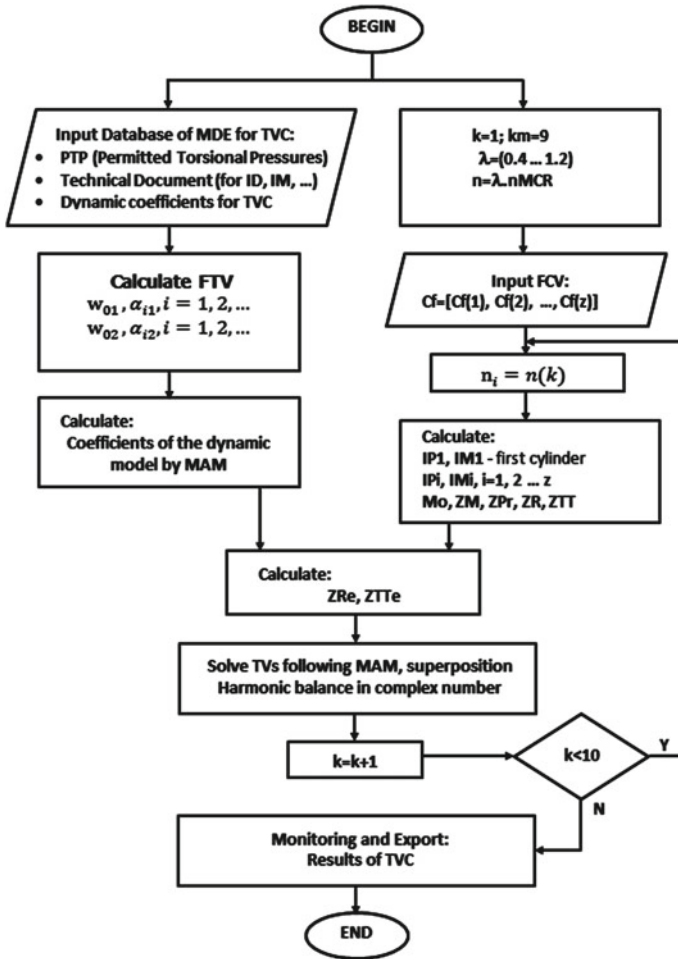


Fig. 37.1 Algorithm for automatic calculating the torsional vibrations on the MPP, using two-stroke marine diesel engine

The reason of using main-axes method (MAM) is that this method is appropriate for calculating TVs at not only the resonance and near-resonance regimes but also the far-resonance regimes of working revolution interval $\lambda = [0.4 \dots 1.2]$. Meanwhile, the traditional method could only be used to calculate TVs at resonance and near-resonance regimes [2, 5, 9]. The equivalent model in accordance with the method is shown in Eq. (37.5).

According to the MAM, the TV of the every lumped mass of the model (37.1) φ_k , $k = 1 \div n$ approximately is substituted via the orthogonal vibrations of the frequencies ω_{0j} , $j = 0, 1, 2, \dots (n-1)$: $y_0, y_1, y_2 \dots y_{n-1}$. Where, $\omega_{00} = 0$ indicates that the TV y_0

Table 37.2 Functional blocks in the algorithm for automatic TVC, respectively, Fig. 37.1

No of block	Function of the block	Contents of the block
1	Input database of the DME	Import the data for building indicator diagram, moment; dynamic coefficients for FTV, ETV; PTV
2	Calculate free torsional vibrations	Defining $\omega_{0j}, \alpha_{ij}; j = 1-2; i = 1-n$
3	Calculate coefficients of the equivalent dynamic model in the main—axes method (MAM), Eq. (37.5)	Calculating equivalent coefficients of the inertial moments, torsional stiffness, damping in accordance with main axes
4	Import the firing coefficient vector	Input vector: $\mathbf{Cf} = [\mathbf{Cf}(1) \dots \mathbf{Cf}(z)]$
5	Calculate indicated pressure, moments and their processing in FFT	Calculate: ID1, IM1 and $IM_i (i = 1-z)$, MPr; MR, MTT –Indicated pressures and moments of first, other cylinder, of the propeller and their FFT processing
6	Calculate equivalent moments in the MAM in FFT form with different harmonics in complex numeric or in amplitude and phase features: ZR, ZTT, see Eq. (37.7)	Calculating equivalent harmonic components of the moments in main-axes model (MAM) for the 3 axes: y_0, y_1, y_2 (see Eq. (37.4))
7	Solve MAM (37.5) by combinations of methods: main—axes method; superposition; harmonic balance in the complex numeric	Solving MAM, eq. () to define y_0, y_1, y_2 and φ_k following the Eq. (37.5)
8	Export the results of the TVC in the experiment regime \mathbf{Cf} and state of the DME	– Drawing the $\tau(\lambda)$, PTP((λ) ; – Exporting in the table the resonance TV in the revolution interval $\lambda \in [0.4, 1.2]$

is appeared as absolute rigid body. In practice, there are important and meaningful in the counting with the y_0 and the first two axes (y_1 and y_2) of the ω_{01} and ω_{02} .

37.2.2 Probated Object for TV Monitoring on Marine MPP

There are TV calculations of the MPP on the marine cargo vessel with 34000 DWT, called MV.HR.34000 DWT in the probation aspect to clarify above mentioned points. The manufactory data for TVC are inputted and the results of the TV calculation using the SSMTVs shall be compared with the calculated results by the Hudong Heavy Machinery Co. Ltd. [3].

Table 37.3 Dynamic parameters for TVC of the MV.HR.34000 DWT [3]

No	Inertial mass item	J	$e = 1/C$	b_{in}	b_{out}	D/d_{in}
		kg . m ²	nrad/Nm	%	%	mm
1	33 tuning wheel	7000	0.001	0.0	0.5	1000.0/0.0
2	38 Flange	121	1.322	0.0	0.0	560/85.0
3	1 cylinder	3256	1.639	1.00	0.85	560/85.0
4	2 cylinder	3256	1.617	1.00	0.85	560/85.0
5	3 cylinder	3256	1.673	1.00	0.85	560/85.0
6	4 cylinder	3256	1.625	1.00	0.85	560/85.0
7	5 cylinder	3256	1.550	1.00	0.85	560/85.0
8	6 cylinder	3256	1.103	0	0.85	560/85.0
9	27 camdriver +thrust	882	0.001	0	0.85	560/85.0
10	28 moment compens	316	0.687	0	0.85	560/85.0
11	32 turning wheel	3095	39.710	0	0.50	375/0.0
12	43 flange	221.90	18.780	0	0.0	440/0.0
13	73 main propeller	21,725			5.50	

The input data of the dynamic model for TVC is given in Table 37.3.
ME MAN-BW: 6S46MC-C 7860 KW @ 129 RPM

Engine load	kW	RPM (MCR)
	7860	129

Fire order: 1-5-3-4-2-6

Oscillating mass: 2246 kg

Permitted torsional pressure of the crankshaft: $[\tau] = 40 \text{ MN/mm}^2$

Propeller Wartsila Propulsion Drumen. The Netherlands

Number of blade	4
Diameter (m)	5.6
Inertial moment in air	16,799 kg . m ²
Inertial moment in water	21,631 kg . m ²

Addition database of the DME 6S46 MCC-7 using for calculating the indicator diagram of cylinder (ID) and indicated (gas combustion) moment is given by information of the engine manufacturer [13] and by other technical documents of the shipyard (PhaRung, Vietnam) [11].

37.3 Results and Discussion

37.3.1 Calculated Results of the Free Torsional Vibrations of the MV.HR.34000 DWT

The results receiving by authors on the base using the SSTVs (see Fig. 37.2) and by Hudong Heavy Machine Co. Ltd prove exactness of the SSTVs is similar and showing in Table 37.4 for their comparison. The free frequencies ω_{01} , ω_{02} , and α_{i1} of the two database are equal ($\delta\% = 0$). The forms α_{i2} are small different ($<6.75\%$), and the differences could be belong in the calculation errors.

37.3.2 Results of the Monitoring TV on the MV.HR.34000 DWT Using SSTVs

The excited TVs and calculated torsional pressure of the intermediate shaft are shown in Figs. 37.3, 37.4 and 37.5.

Figures 37.3, 37.4 and 37.5 show the calculated torsional pressure curves via n (rpm) of the main propulsion plant on the MV.HR.34000 DWT, and also the red curve, that presents the permitted torsional pressure $[\tau_1](\lambda)$. Figure 37.3 shows results when $Cf = [1\ 1\ 1\ 1\ 1]$ —normal working regime. Figure 37.4—when $Cf = [0\ 1\ 1\ 1\ 1]$ —first cylinder is misfired. Figure 37.5—when $Cf = [1\ 0\ 1\ 1\ 0\ 1]$ —second and fifth cylinders are misfired together. In the figures, we could estimate the main resonance when $k = 6$ with $n_{01} = 337$ rpm and others minor resonances with $n \approx 85$, $n \approx 112$, $n \approx 120$, $n \approx 144$. There are the interesting resonances in the minor

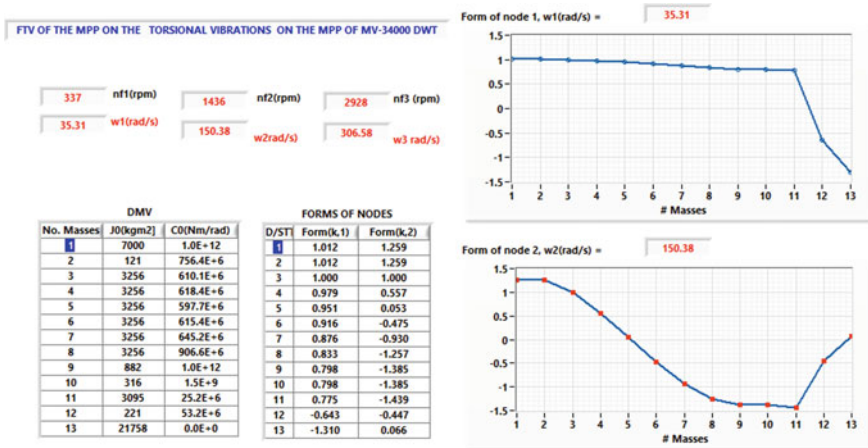


Fig. 37.2 Results of calculated FTV of MV.HR.34000 DWT

Table 37.4 Compare results of FTV calculating on the base of SSTVs and by Hudong [3]

No	Comparison item	ω_{01} (rad/s); n_{01} (rpm)			ω_{02} (rad/s); n_{02} (rpm)		
		SSTVs	HR [3]	$\delta\%$	SSTVs	HR [3]	$\delta\%$
1	Free frequency	35.308	35.307	0	150.38	150.38	0
2	Free revolutions	337.17	337.16	0	1436	1436	0
3	$\alpha_{1,j}$	1.0119	1.012	-0.01	1.2708	1.259	0.94
Form curves $\alpha_{i,j}$	$\alpha_{2,j}$	1.0119	0.012	-0.01	1.2705	1.259	0.91
	$\alpha_{3,j}$	1.0000	1.000	0.00	1.0000	1.000	0.00
	$\alpha_{4,j}$	0.97863	0.979	-0.04	0.54391	0.557	-2.35
	$\alpha_{5,j}$	0.95111	0.951	0.01	0.055185	0.053	4.12
	$\alpha_{6,j}$	0.91619	0.916	0.02	-0.50696	-0.475	6.73
	$\alpha_{7,j}$	0.87623	0.876	0.03	-0.96707	-0.930	3.99
	$\alpha_{8,j}$	0.83260	0.833	-0.05	-1.2956	-1.257	3.07
	$\alpha_{9,j}$	0.79782	0.798	-0.02	-1.4241	-1.385	2.82
	$\alpha_{10,j}$	0.79780	0.798	-0.03	-1.4242	-1.385	2.83
	$\alpha_{11,j}$	0.77532	0.775	0.04	-1.4777	-1.439	2.69
	$\alpha_{12,j}$	-0.64280	-0.643	-0.03	-0.46589	-0.447	4.23
	$\alpha_{13,j}$	-1.3101	-1.310	0.01	0.05639	0.066	0.59

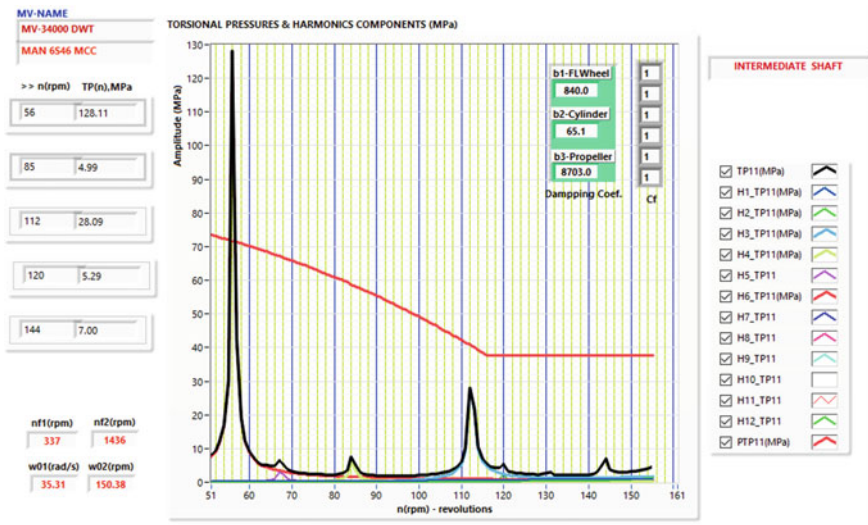


Fig. 37.3 Results of calculated FTV of MV.HR.34000 T, in normal state of MDE

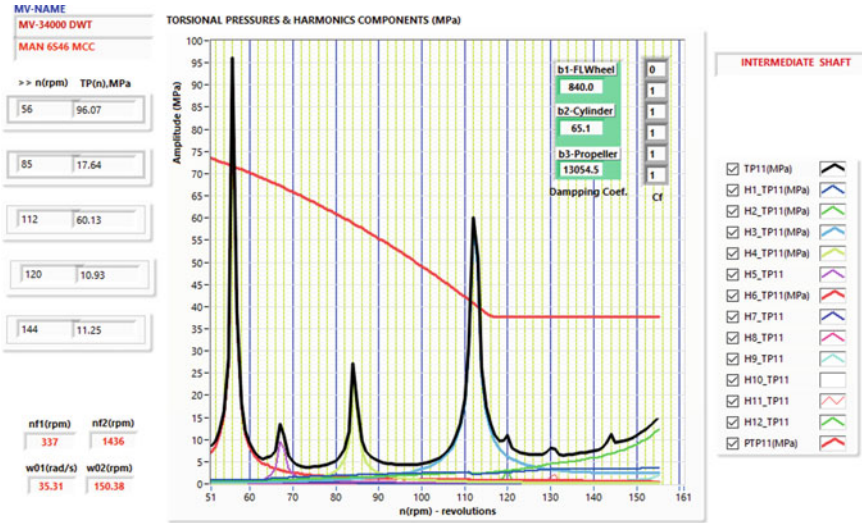


Fig. 37.4 Results of calculated FTV of MV.HR.34000 T, in Misfire.Case1.1

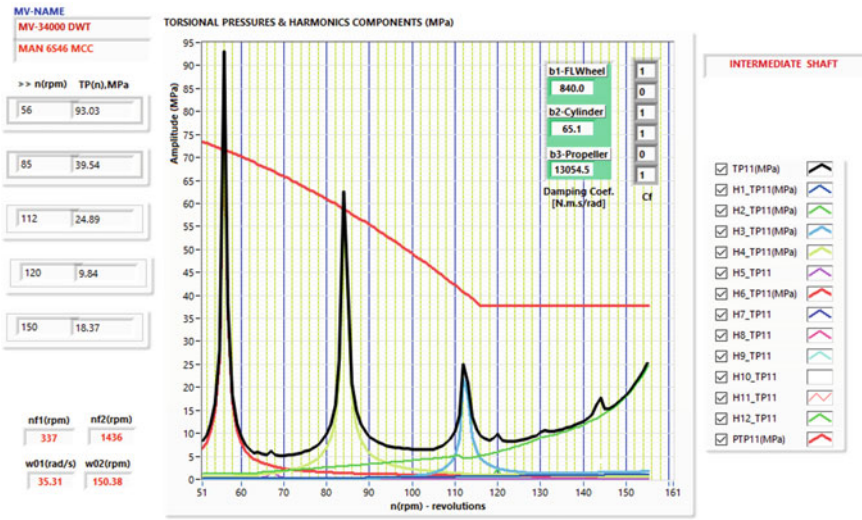


Fig. 37.5 Results of calculated FTV of MV.HR.34000 T, in Misfire.Case4.2a5 state

situation: (a) Misfire.Case1.1, in that is misfire of combustion chamber of once cylinder (cylinder number 1), at the second resonances $n \approx 112$ (see Fig. 37.3), and (b) Misfire.Case2.2a5 (see Fig. 37.5) at $n \approx 85$ rpm, comparing with other normal state regime of the MDE.

In Table 37.5, there are clearly shown the dangerous main resonance with frequency ω_{01} ($n \approx 56$ rpm; $k = 6$) in the all of the Normal/Misfire.Case1(2), and dangerous minor resonances with frequencies (ω_{01} and ω_{02}) at $n \approx 85$ and $n \approx 112$ rpm in the Misfire.Case1 or Misfire.Case2.

In Table 37.5, we remark the values with red color, that means the calculated values $\tau(\lambda)$ are bigger than the permitted $[\tau_1(\lambda)]$. In addition, for intermediate shaft [1], at the λ -speed the calculated $\tau(\lambda)$ are smaller than $[\tau_2(\lambda)] = 1.7 [\tau_1(\lambda)]$, we could pass the speed quickly through this revolution $n = \lambda \cdot n_{MCR}$, rpm. In the probated calculation, the resonance $n_{res} = 56$ rpm, the barred speed range $[n^*_{1.1}, n^*_{1.2}]$ is defined by [1]:

$$n^*_{1.1} = \frac{16}{18 - n_{res}/n_{MCR}} \leq n \leq \frac{18 - n_{res}/n_{MCR}}{16} = n^*_{1.2}$$

$$[n^*_{1.1}, n^*_{1.2}] = [51.0, 61.4]$$

In Misfire.Case1, we could monitor the TVs and suddenly decrease speed under the $n^*_{2.1} = 16/(18 - 112/129) = 104.6$ rpm and increase speed over $n^*_{2.2} = 119.9$ rpm, since $\tau(\lambda) < 1.7 [\tau_1(\lambda)] \approx 1.8 \cdot 40.1 = 78$ MPa.

In some conditions of the Misfire.Case2, we could be monitor the very dangerous TVs and have not suddenly pass though the $[n^*_{2.1}, n^*_{2.2}] = [104.6, 119.9]$ rpm, since $\tau(\lambda) \gg 78$ MPa.

Table 37.5 Calculated results of ETVs in resonances and near resonances

Exp N ^o	Regime	τ , MPa; n-rpm			Exp N ^o	Regime	τ , MPa; n-rpm		
		n= 56	85	112			n=56	85	112
	$[\tau_1]$, MPa	73.2	59.1	40.1		$[\tau_1]$, MPa	73.2	59.1	40.1
1.	Normal	101.7	4.9	22.6	12.	[011110]	94.3	27.3	30.9
2.	[011111]	96.1	17.6	60.1	13.	[100111]	92.1	23.3	103.3
3.	[101111]	97.1	22.6	58.7	14.	[101011]	92.1	20.6	24.2
4.	[110111]	96.8	19.6	56.9	15.	[101101]	93.3	39.5	24.9
5.	[111011]	97.7	17.4	47.7	16.	[101110]	92.8	21.3	25.9
6.	[111101]	97.6	33.8	46.1	17.	[110011]	92.1	16.2	24.8
7.	[111110]	91.9	17.2	45.5	18.	[110101]	92.2	21.4	23.4
8.	[001111]	91.4	19.3	106.0	19.	[110110]	93.2	34.9	28.1
9.	[010111]	91.5	29.3	104.4	20.	[111001]	92.7	19.9	88.6
10.	[011011]	91.5	35.4	29.7	21.	[111010]	92.8	15.7	87.2
11.	[011101]	91.3	18.8	12.4	22.	[111100]	93.5	19.9	85.6

Note Damping coefficients of damper, cylinders, and propeller (Nms/rad) =[840 85 13055]

37.4 Conclusion

The shaft—line of the MPP on marine cargo ships with high power, 2-MDE-driven propeller normally has dangerous torsional vibrations in the restricted range $[n_{\text{res}} - \Delta n_{\text{res}}, n_{\text{res}} + \Delta n_{\text{res}}]$, n_{res} —resonance revolution, in which the torsional pressures $\tau(\lambda)$ are exceeded the permitted ones $[\tau_1(\lambda)]$ and permit to pass quickly through if $\tau(\lambda)$ are smaller than permitted values $[\tau_2(\lambda)]$ (for intermediate, propeller shafts: $[\tau_2(\lambda)] = 1.7 [\tau_1(\lambda)]$). The theoretic (calculation) torsional vibrations have to be carried out in the normal state (Normal, in which all of the cylinders are fire normal) and in Misfire.Case1 (one of the cylinders is misfired) in accordance with the rules for classification and construction of the sea-going ship (such as, RMR Edit 14). The results of the probated TMTVs on the MPP of the MV.HR.34000 DWWT show the necessities to calculate torsional vibrations not only in the Normal and Misfire.Case1 states (regimes) of the MDE, but also in the addition Misfire.Case2 states, in which two of cylinders are misfired together. The results of the demonstrated TMTVs prove the prediction TMTVs in the design and manufactory stages of the marine ships to achieve recommendations of the technical exploitation of the MPP in every stage of MDE, especially in the abnormal sates, such as Misfire.Case1 and Misfire.Case2.

Acknowledgements We, the authors would thank to Vietnam Maritime University and the Management Board headed by Prof. L. C. Nho of the National Independent Science—Technology Project in Viet Nam (with ID: DTDL.CN-14/15), since permitting us to use the Simulation Software for TVC on the MV.HR.34000 DWT for realizing proposed points of the paper.

This work was supported by the Domestic Master/Ph.D. Scholarship Program of Vingroup Innovation Foundation.

References

1. Russian Maritime Register of Shipping: Edit 2014: Rules for Classification and Construction of Sea-going Ships. Saint Petechuarg, Russian (2014)
2. Luu, D.D.: Torsional Vibrations on the main propulsion plan using diesel engine driven propeller of the modern marine vessel. Publisher “Maritime”, Hai Phong (2019)
3. Hudong heavy machinery Co. Ltd: Torsional Vibration Calculation Report DE 6S46MC–C7860 kW @ 129 r/min 34,000 DWT. PhaRung Shipyard. DNV Approved 2007
4. MAN B&W: Torsional Vibration Calculation. BachDang Shipyard T209/HT30. (For the main propulsion on M/V Vinashinsky 15.000 DWWT). Vibration Analysis. Hai Phong (2005)
5. Luu, D.D.: Dynamics and diagnostics of marine diesel engine by vibration technique. Publisher “Transport”, Ha Noi (2009)
6. Jones, N.B., Li, Y.-H.: A review of condition monitoring and fault diagnosis for diesel engines. *Tribotest J.* 6, 267–291 (2000). ISSN 1354-4063
7. Li, Z., et al.: Intelligent fault diagnosis method for marine diesel engines using instantaneous angular speed. *J. Mech. Sci. Technol.* **26**(8), 2413–2423 (2012)
8. DNV GL Maritime Advisory: Torsional Vibration Calculation Roll–Royce AB. Report No. 2014-0429, Rev. 1. Date 2014-07-03 (for the main propulsion on Vinashin Saigon Shipmarine H/N BA 27, on the M/V BinhAn Valiant) (2014)
9. Minchev, N.D.: Dynamics of marine machines. Publisher “Army”, Sophia (1983)

10. Daniel, P.G., et al.: Torsional system dynamics of low speed diesel engines based on instantaneous torque: application to engine diagnosis. *J. Mech. Syst. Sig. Process.* **116**, 858–878 (2019)
11. Nho, L.C., Luu, D.D., et al.: Researching, building simulation of main propulsion plant and main switch-board on the marine cargo ship. National Independent Project on Science and Technology with ID. DTDL.CN-14/15 carried out in Vietnam Maritime University, Hai Phong (2015–2019)
12. Luu, D.D., Nguyen, Q.V.: Theoretical and experimental integration for working process simulation on marine diesel engine. In: Fujita, H., Cong, N.D., Pi, V.N., Long, B.T., Puta, H.H.: International Conference, ICERA 2018. Lecture Notes in Networks and Systems 63. *Advances in Engineering Research and Application*. pp.580–588. Springer Nature Switzerland AG 2019
13. MAN B&W: 46S MCC7. Project guide Camshaft Controlled Two-Stroke Engines, 4th edn (2009)

Chapter 38

Analysing Different Full Adder Based on 45 nm Technology



Ankit Kumar, Shyam Akashe, and Seelam VSV Prabhu Deva Kumar

Abstract The current scenario of research in electronics based on how to achieve high efficiency, low-power consumption, and most importantly how to reduce a given circuitry system to make it compact. Full adder is an important element in designing any high-performance arithmetic circuit that is why it is an integral part of the processor and controller. This paper presents an analytic comparison of three different full adder circuits. The conventional 28T full adder circuit with 20T and 18T full adder circuit is compared. These three circuits are designed in Cadence Virtuoso, and then their power consumption, delay, and noise are calculated and compared with each other.

38.1 Introduction

Since the beginning of an era of silicon-based electronic technology, there is always huge efforts which were made to improve the performance of the devices whether it is to reduce the number of transistor and size of the chip or to make system energy efficient as much as possible. Talking about VLSI technology, the explosive growth of this technology is tempted to make a device portable which strives us for smaller silicon area, higher speeds, less power consumption electronics circuits. Similar efforts are made in full adder circuits also where different types of 1-bit full adder circuits are implemented with the help of numbers of transistors. By varying the numbers of transistors, full adder circuits' performance is increased or decreased according to our requirement and what the circuitry demands. Recalling the basics

A. Kumar (✉) · S. Akashe
ITM University, Gwalior, India
e-mail: ankitajay17@gmail.com

S. Akashe
e-mail: shyam.akashe@itmuniversity.ac.in

S. V. P. D. Kumar
Pusan National University, Pusan, South Korea
e-mail: vasavisai9999@gmail.com

© The Editor(s) (if applicable) and The Author(s), under exclusive license to Springer Nature Singapore Pte Ltd. 2021

Y.-D. Zhang et al. (eds.), *Smart Trends in Computing and Communications: Proceedings of SmartCom 2020*, Smart Innovation, Systems and Technologies 182,
https://doi.org/10.1007/978-981-15-5224-3_38

of the full adder, then it is the circuit that performs the arithmetic addition and is extensively used in VLSI technology. Below is the symbol diagram of a 1-bit full adder.

The full adder is having three ports and two ports of input and outputs, respectively, as shown in Fig. 38.1. While half adder is based on two inputs, irrespective of that full adder are of three inputs and whenever there are two 1's as input, then the carry output activates. In the full adder equation, we can see that the output we get from the SUM is similar to the 3-input EXOR output. Hence, SUM is nothing but a 3-input EXOR gate. The truth table of a 1-bit full adder is given in Fig. 38.2.

The equation for SUM and CARRY is stated below.

$$\text{SUM} = A(\text{XOR})B(\text{XOR})C \tag{38.1}$$

$$\text{CARRY} = C \text{IN}(A + B) + AB \tag{38.2}$$

The logic gate level of a full adder is shown in Fig. 38.3.

Fig. 38.1 Block diagram of a 1-bit full adder

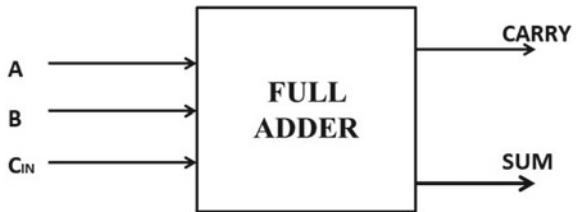


Fig. 38.2 Truth table of a 1-bit full adder

INPUT			OUTPUT	
A	B	C	SUM	CARRY
0	0	0	0	0
0	0	1	1	0
0	1	0	1	0
0	1	1	0	1
1	0	0	1	0
1	0	1	0	1
1	1	0	0	1
1	1	1	1	1

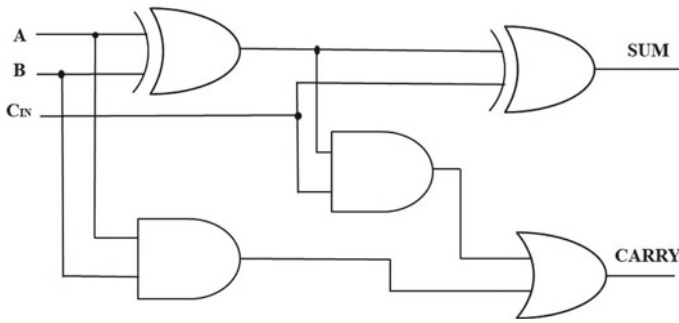


Fig. 38.3 1-bit full adder using the logic gates

The full adder is important in any device, so it is very necessary to increase the performance at very first as the overall performance of the device depends on a full adder. The idea behind this paper is to calculate the power, delay, noise of each full adder in one place, and at last compare these parameters in tabular form so that it is easy for the designer to make choices among these which one is more suitable to meet the designer's perspective.

The whole paper is divided into different sections where research elaborations, findings of 28T, 20T, and 18T are shown, respectively, and at last, the conclusion is made.

38.2 Analysis of Full Adder Circuits

38.2.1 28T Full Adder Circuit

This full adder circuit consists of 28 transistors and is based on static CMOS structure with having PMOS and NMOS transistor and generates carry through a static gate which gives better output and better driving capabilities [1]. The advantage of this circuit is that it has low operating power and high noise margin; at the same time, it has good layout regularity and easily implemented and widely used in low power circuit design [2, 3]. Since due to the presence of the high number of transistors, it takes more area and has more delay which results in high power in the output stage; hence, this circuit is slow [4, 5]. This circuit is shown in Fig. 38.4.

38.2.2 20T Full Adder Circuit

This full adder circuit consists of 20 transistors and is implemented using transmission gate logic having consists of the EXOR gate which is implemented using TG

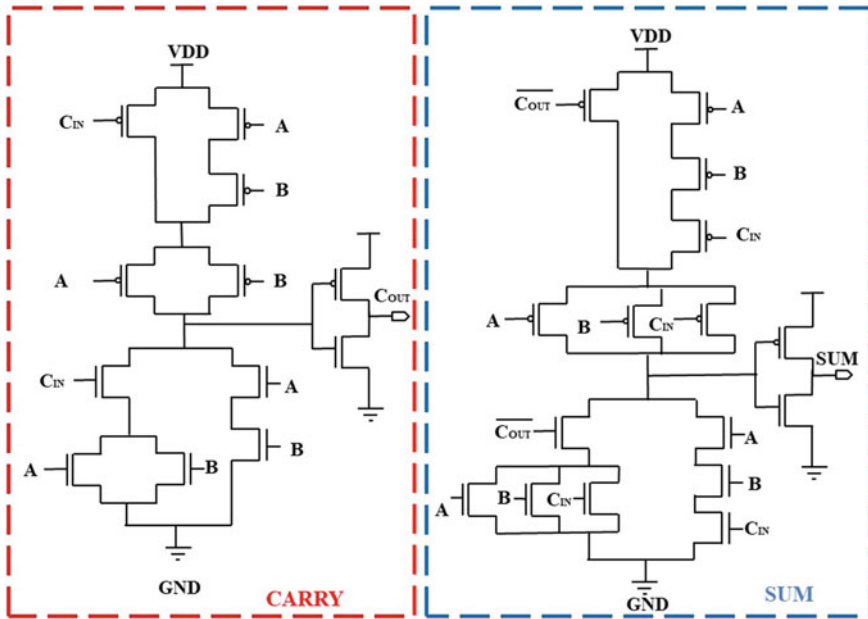


Fig. 38.4 28T full adder using static CMOS

logic. It gives us an advantage of less area consumption compare to that of above 28T full adder. The transmission gate (TG) logic came into existence to overcome the problem which is persisting into pass transistor logic (PTL). Though both TG and PTL logics are almost same with having difference is that TG uses both NMOS and PMOS transistor pair in parallel and both works together simultaneously where PMOS provides strong 1, but at the same times, it provides poor 0 and NMOS provides strong 0 but having poor 1 while PTL uses either of NMOS and PMOS transistor [6]. The advantage of using TG logic is that there is no direct signal connection to the power supply VDD or GND. The advantage of using this circuit is that it has full swing output, so it gives a better speed than that of 28T full adder [7]. Talking to its disadvantages, then it fails to perform good enough in large arithmetic circuits [2]. The 20T full adder circuit using transmission gate logic is shown in Fig. 38.5.

38.2.3 18T Full Adder Circuit

This full adder circuit is having 18 transistors and can be implemented using eliminating all PMOS transistor, i.e. all PMOS transistor is substituted by one PMOS having a gate which is grounded both in carry and sum circuit as shown in Fig. 38.6. That is why this logic is termed as pseudo-NMOS logic. This circuit always remains in 'ON' because PMOS is not driven by the signal. It gives us the advantage of less

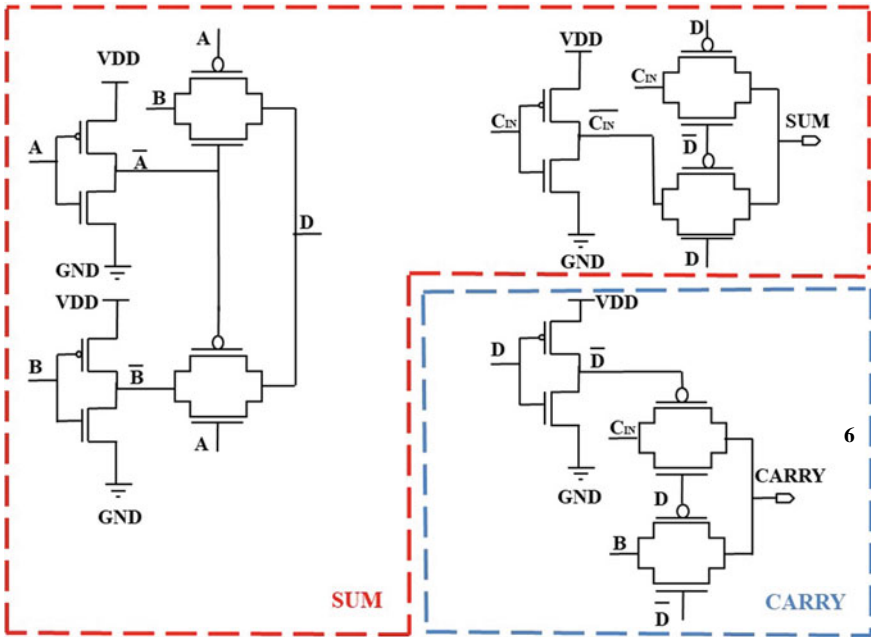


Fig. 38.5 20T full adder using transmission gate

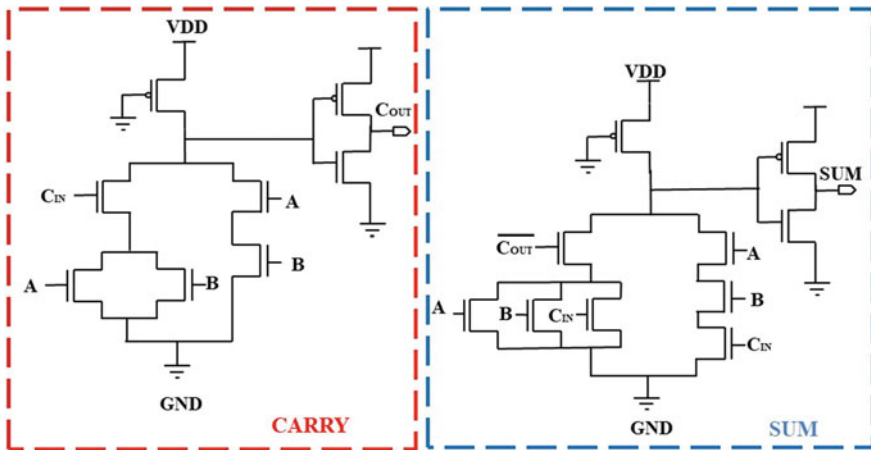


Fig. 38.6 18T full adder using pseudo-NMOS

Table 38.1 Comparison between the designed full adder circuit

S. No.	Parameter	28T	20T	18T
1	Technology (nm)	45	45	45
2	Logic used	Static CMOS	Transmission gate	Pseudo-NMOS
3	Average power (W)	2.536E-3	209.0E-3	4.465E-3
4	Carry noise (V ²)	1.523e-10	1.086e-8	1.536e-10
5	Sum noise (V ²)	1.770e-10	2.266e-10	1.536e-10
6	Carry delay (s)	-16.56E-9	13.03E-9	-11.49E-9
7	Sum delay (s)	-373.3E-12	13.07E-9	-21.36E-9

area, high speed, less delay; but at the same time, it is shown that it has the reduction in output swing, high power consumption and has more noise susceptibility than that of conventional 28T full adder [2]. The circuit of 18T full adder using pseudo-NMOS logic is shown in Fig. 38.6.

38.3 Result

All the above three mention full adder circuits, i.e. 28T, 20T, 18T, were simulated in Cadence Virtuoso Environment using 45 nm technology. The comparison between these three circuits on the basis of average power, carry noise, sum noise, carry delay, sum delay has been made and mention in tabular form in Table 38.1.

38.4 Conclusion

It is clearly shown in Table 38.1 that in terms of power consumption 28T is better followed by 18T and 20T and in terms of both carry and sum delay 28T are better to use again followed by 18T and 20T. Noise is less in 18T. So, in terms of less transistor count and delay, then 18T pseudo-NMOS full adder has the upper hand, and for less power consumption, then 28T is useful for designer perspective. Further, we can improve these 1-bit full adders using addition of resistor, capacitors, etc., and by varying the transistor count, the optimum desired parameters can be achievable for the designer. Researches are going on, and different logic techniques are implementing to obtain desirable results from the full adder circuits.

References

1. Rana, S., Mehra, R.: Optimized CMOS design of full adder using 45 nm technology. *Int. J. Comput. Appl.* (0975–8887) **142**(13) 2016
2. Manisha, A.: Comparative study of full adder using static CMOS logic style. *IJRET: Int. J. Res. Eng. Technol.* eISSN: 2319-1163|ISSN: 2321-7308
3. Tiwari, N., Sharma, R., Parihar, R.: Implementation of area and energy efficient Full adder cell. In: *IEEE International Conference on Recent Advances and Innovations in Engineering (ICRAIE-2014)*, Jaipur, India, 09–11 May 2014
4. Kumar, R., Roy, S., Bhunia, C.T.: Study of threshold gate and CMOS logic style based full adders circuits. In: *IEEE Sponsored 3rd International Conference on Electronics and Communication Systems (ICECS 2016)*, ISSN NO: 2395-0730
5. Nigam, A., Singh, R.: Comparative analysis of 28T full adder with 14T full adder using 180 nm. *Int J Engg Sci Adv Res* **2**(1), 27–32 (2016)
6. Manjunath, K.M., Lateef, A., Haroon, P.S., Pagi, A., Ulaganathan, J.: Analysis of various full-adder circuits in cadence. In: *International Conference on Emerging Research in Electronics, Computer Science and Technology* (2015)
7. Z. Yang, J. Han, F. Lombardi: Transmission gate-based approximate adders for inexact computing. In: *Proceedings of the 2015 IEEE/ACM International Symposium on Nanoscale Architectures (NANOARCH'15)*, Boston, MA, USA, 08–10 July 2015

Chapter 39

Design of RF Energy Harvesting Circuit at 900 MHz for Low-Powered DC Applications



Anoop Chiluveru, Shyam Akashe, and Shailendra Singh Ojha

Abstract This report describes the design of RF energy harvesting circuit using the 900 MHz microstrip patch antenna and the HSMS-285B Schottky diode rectifier. The aim of this circuit is to transform the radio frequency signals in the GSM frequency band to direct current (DC) voltage. This research also provides a guideline for the design of the 900 MHz microstrip patch antenna used in the circuit mentioned below. The rectifier design is based on the doubler circuit of Villard voltage developed at 900 MHz. Three-stage voltage doubling is modelled and simulated in this paper. The proposed antenna harvests the RF power and transforms it into DC voltage ranging up to 7.5 V that can be used in low-power DC applications. This paper cited a variety of parameters of antenna such as gain, radiation pattern and return loss of the envisaged antenna. Advanced Design System (ADS) and CST Microwave Studio were used to design and simulate the following circuit.

39.1 Introduction

Solar and motion energy harvesting are not uncommon methods to power a system. But what about RF energy harvesting? Here is a run-down of RF to DC technology [1]. Electronic devices are further isolating themselves from everyday life, and, of course, they all need electricity to continue to work in some way. Currently, daylight is probably the most popular source of power that can be turned into DC voltage [2].

Not as widespread, but the process of harvesting energy from RF/microwave signals such as radio/television broadcasting stations, wireless equipment and mobile base stations is rapidly growing in popularity. By harvesting energy in this way,

A. Chiluveru (✉) · S. Akashe · S. S. Ojha
ITM University, Gwalior, Madhya Pradesh 475001, India
e-mail: chiluveru.anoop@gmail.com

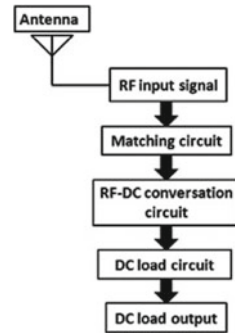
S. Akashe
e-mail: shyam.akashe@itmuni.ac.in

S. S. Ojha
e-mail: ssojha20@gmail.com

© The Editor(s) (if applicable) and The Author(s), under exclusive license to Springer Nature Singapore Pte Ltd. 2021

Y.-D. Zhang et al. (eds.), *Smart Trends in Computing and Communications: Proceedings of SmartCom 2020*, Smart Innovation, Systems and Technologies 182,
https://doi.org/10.1007/978-981-15-5224-3_39

Fig. 39.1 Schematic view of RF energy harvesting system



batteries can be replaced in low-power applications such as Internet of things (IOT) sensors and RFID tags [3]. This research focuses on transmitting energy (i.e. voltages and currents) from electromagnetic field to the electrical domain. The antenna–rectifier configuration impedance alternative is addressed as it plays a crucial role in optimizing harvester sensitivity and efficiency of power conversion [4].

This research provides a process to design microstrip patch antenna as well as an efficient rectifier circuit to convert the antenna’s RF energy into usable DC voltages. The combination of these two, i.e. the antenna and rectifier, is called a rectenna. Here, the concept of Villard voltage multiplication is being used to convert the radio frequency signals into usable DC supply voltages using the HSMS 285B Schottky diodes.

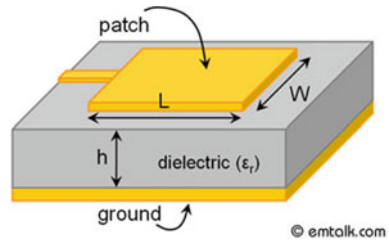
Figure 39.1 shows the energy harvesting process principle. It is made up of antenna circuits, network matching, RF-DC conversion rectifier and loading. Using the appropriate circuit antenna, the RF input signal is processed. The equivalent circuit is used in the rectifier circuit to lower the reflected energy from the source.

39.2 Design Parameters of Patch Antenna

A simplistic microstrip patch antenna comprises of a metallic patch and ground between which is a dielectric medium called the substrate [4]. Here, we used the FR-4 lossy dielectric material for the substrate. The layout of a microstrip patch antenna is clearly schemed in Fig. 39.2.

where L = length; W = width; h = thickness of the dielectric substrate and ϵ_r = dielectric constant.

Fig. 39.2 Layout of the rectangular patch antenna



39.3 Designing Methods and Procedure

In this study, the method of transmission line was used to design the rectangular microstrip patch antenna. There are few parameters to be taken into account for an antenna to work at specific frequency like the length, width of the rectangular patch, the height of the substrate and also the dielectric material, constant [5]. Here, we used the FR-4 material as a substrate because it is known for its strong electrical and mechanical isolating properties in both dry and milder climates. The primary approach in the fabrication process is to quantify the length of the microstrip patch (W) and the size can be small enough to prevent the excitation of the transverse resonance mode; the width dimension of the microstrip is calculated using the following formula as given in Eq. 39.1,

$$W = \frac{c}{2f_o \sqrt{\frac{(\epsilon_r + 1)}{2}}} \tag{39.1}$$

where c = speed of light, f_o = operating frequency, ϵ_r = dielectric constant.

So, the second step in the design would be to pick the ideal dielectric constant value. Since the lower dielectric constant value gives a wider impedance range [5], here we used a dielectric constant value of 4.3; however, antenna would be of greater component size with higher dielectric constants.

The effective dielectric constant value can be derived from Eq. 39.2,

$$E_{\text{eff}} = \frac{\epsilon_r + 1}{2} + \frac{\epsilon_r - 1}{2} \left(\frac{1}{\sqrt{1 + \frac{2h}{w}}} \right) \tag{39.2}$$

where h = height of the microstrip patch and w = width of the microstrip patch.

Moving to the substrate thickness, the denser substrate provides better performance and greater bandwidth. Where the sparser substrates result in smaller component sizes, minimize coupling with lower efficiency and relatively smaller bandwidths [6]. The effective patch length can be determined from the following Eq. 39.3,

$$L = \frac{c}{2f_r \sqrt{\epsilon_r}} = \frac{\lambda}{2} \tag{39.3}$$

Table 39.1 Summary of calculated results for antenna

Parameters	Module
Material of the substrate	FR-4
Dielectric constant	4.3
Thickness of substrate (mm)	1.6
Dimensions of substrate (mm)	100 × 120
Dimensions of patch (mm)	77 × 98

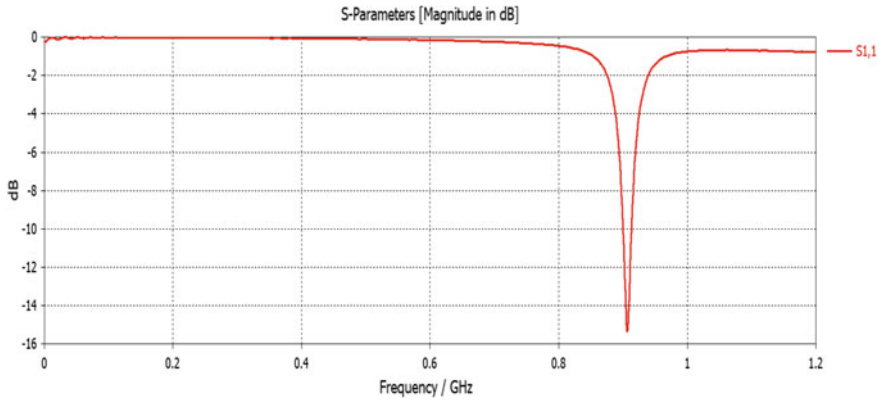


Fig. 39.3 S-parameter (s11) result at 900 MHz

The length extension of the patch can be ascertained from the following Eq. 39.4,

$$\Delta L = 0.412h \frac{(E_{\text{eff}} + 0.3)\left(\frac{w}{h} + 0.264\right)}{(E_{\text{eff}} - 0.258)\left(\frac{w}{h} + 0.8\right)} \tag{39.4}$$

where h = height of the patch and w = width of the patch

The above steps were used for antenna design at 900 MHz, and the parameters are shown in Table 39.1 and Figs. 39.3, 39.4.

39.4 Rectifier Design

Using the Villard voltage multiplication circuit, this study testifies to the rectifier design at three-stage rectification. A voltage multiplier is a specialized rectifier circuit that generates an output which is, for example, an integer of the AC peak input, i.e. 2, 3, or 4 times the AC peak input. Such voltages will be decreased by any load in a realistic circuit [7].

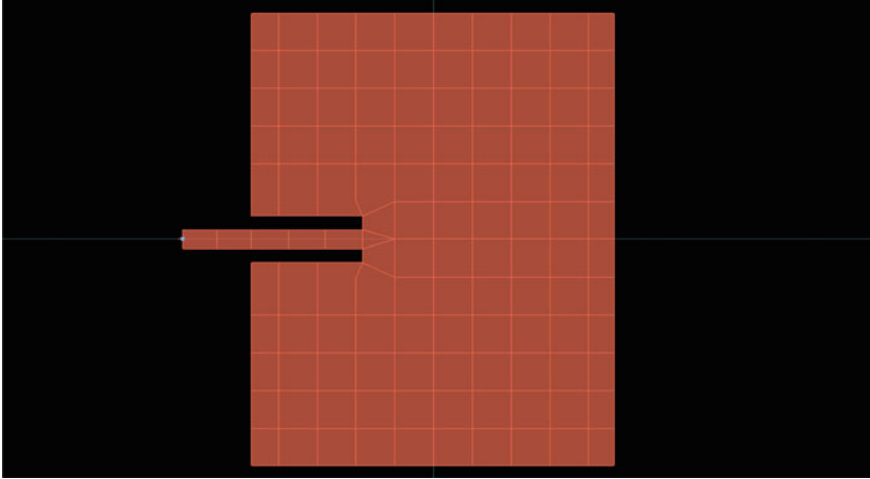


Fig. 39.4 Design of microstrip patch antenna

39.4.1 Three-Stage Voltage Multiplier Circuit

The development of the three-stage voltage multiplier was carried out using six HSMS-285B diodes and six 100 picofarad condensers. HSMS-285B is a low-frequency RF detector diode which can detect frequencies of up to 1.5 GHz. This circuit has two half cycles, namely positive and negative half cycles at each stage.

The combination of a pair of diodes and capacitors represents a single-stage rectification. Here, three of such rectification stages are used to get high output voltages. The incoming RF signal is rectified in the input loop's positive half phase, followed by the negative half cycle. Through the first half, the voltage is retained in the input capacitor and shifted during the second half to the output capacitor [8] (Fig. 39.5).

The below circuit simulation was performed using the Advanced Design System (ADS), and the results of the simulation are plotted in Fig. 39.6. The plot below shows that the output voltage is thrice the input voltage. The AC line showed the input signal in the time domain, and the DC line showed the rectifier circuit's output DC voltage, while the port P1 represents the equivalent antenna that was designed above.

From the ADS harmonic balance simulation, it can be found that the three-stage output is 3.074 V at 0 dBm.

The output DC voltage can be further improved by adding an equivalent matching circuit between the RF input and the rectifier circuit to match the RF signal impedance with the artificial circuit [9]. The matching circuit ensures that the reflected energy is minimal and also improves the rectifier performance and maximizes the power transfer between the RF source and the rectifier (Figs. 39.7 and 39.8).

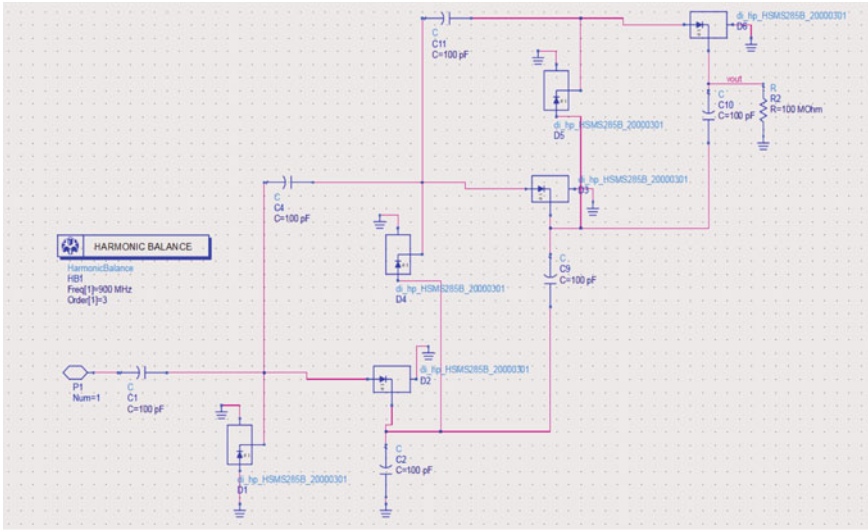


Fig. 39.5 Design of three-stage voltage multiplier circuit using ADS (2019)

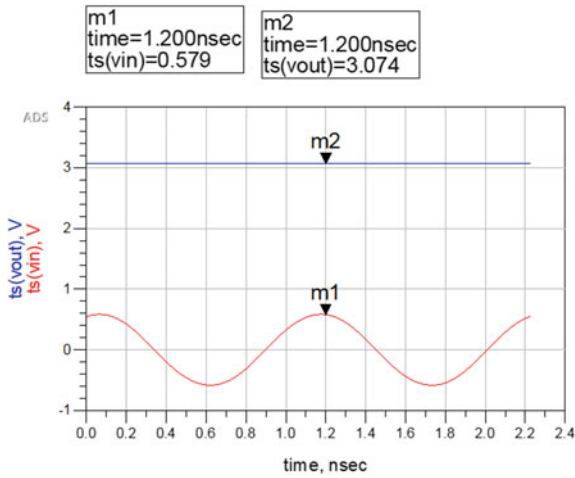


Fig. 39.6 Simulation result of three-stage voltage multiplier

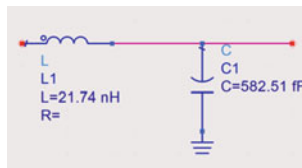


Fig. 39.7 Impedance matching network

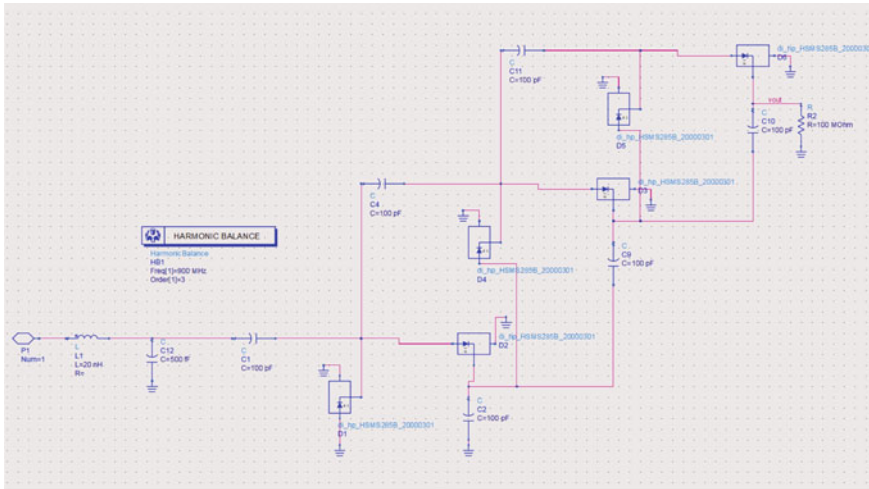
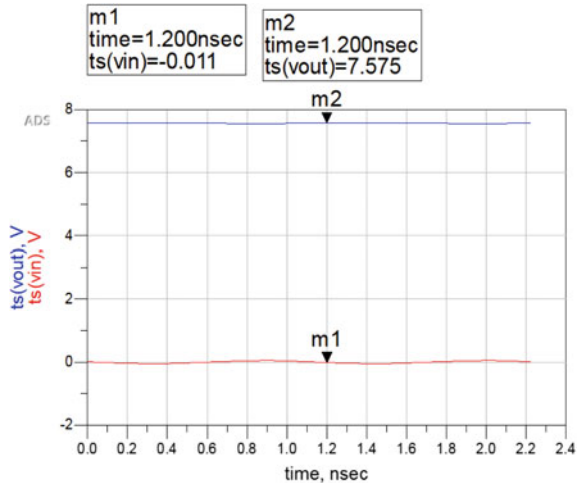


Fig. 39.8 Design of three-stage voltage multiplier with matching circuit using ADS (2019)

The design of the above circuit is the same as that of the circuit in Fig. 39.5 except that a matching circuit which is a combination of inductor and capacitor is added between the RF source and rectifier circuit to match their impedances and reduce the loss of energy due to reflection. This makes sure that maximum energy is transferred between the source and rectifier circuit (Fig. 39.9).

Fig. 39.9 Simulation result of three-stage voltage multiplier with matching circuit

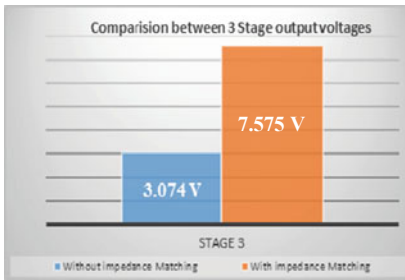


39.5 Results and Discussion

The RF energy harvesting circuit has been developed and tested successfully using the Advanced Design System software. The 900 MHz frequency antenna works perfectly with a return loss of -15.386 dBi as predicted by the software. The results would enable this antenna to be used in the RF energy harvesting circuit. The far-field directivity polar graphs are shown in Fig. 39.10.

The following graphs illustrate the far-field directivity of the suggested microstrip patch antenna when ϕ is 90° and 0° . The graphs indicate that the antenna has a good directivity pattern and can be used in this application.

From the ADS harmonic equilibrium simulation, it can be found that the three-stage output is 3.074 V at 0 dBm and the peak is 7.575 V after adding matching circuit. This is similar to a ripple-superimposed direct current signal. Because of this distinctive feature, successive stages in the circuit will increase the output voltage compared to the first stage [10]. Thus, the more the stages are added, the more the output voltage is generated, regardless of the input. The table below compares the output voltages in each stage [11].



Matching circuit	Stage 3 (V)
Before adding it	3.074
After adding it	7.575

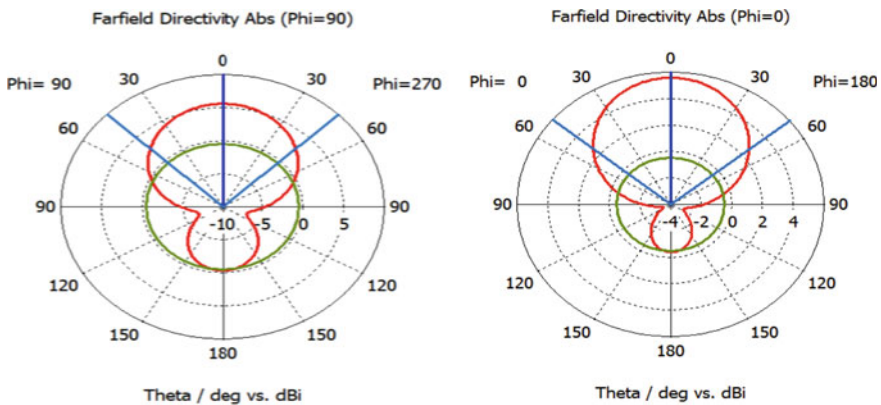


Fig. 39.10 Far-field directivity of the antenna designed at 900 MHz using CST Microwave Studio

The output voltage has been increasing with the voltage multiplier stages. Though the output voltage was only over 3 V in the beginning, it gradually increased to over 7.5 V by the end of the third stage.

39.6 Conclusion

This study provides instructions for developing an RF energy harvesting circuit using the rectangular microstrip patch antenna and a voltage multiplier circuit. The RF power source in the rectifier circuit design is simply replaced by the antenna designed to achieve the desired results. Every stage in the rectifier model has increased output voltage designed with/without matching circuit. The future applications of proposed circuit are mentioned below.

39.6.1 Future Applications

Energy harvesting from radio frequency (RF) holds a promising future for producing a limited amount of electrical energy to operate partial circuits in wireless electronic devices. In wireless sensor networks, rising power consumption has become a major challenge. Energy consumption in wireless sensor networks is a critical factor affecting system cost and lifetime. Energy harvesting technology penetrates several popular fields such as Internet of things, body area networks and fifth-generation networks, offering viable solutions for wide-scale, reliable, minimal-price environmental monitoring and wireless transfer of information [12].

Health care of Animals. A significant but difficult problem is how to track the mental status of a significant number of animals at the zoo or farm. A cost-effective solution is provided by the multi-tier radio frequency-EHWC network. The bio-sensors which are powered by RF energy harvesting are injected into an animal's body (collar, ear or leg) to monitor the health status of large number of animals at zoo.

Wearable Devices. For health and physical activity tracking, portable devices including the fitness tracker and the smart wristband have become quite popular lately. The high consumption of energy ends up making the current portable electronic devices heavily dependent on batteries of high capacity. The wearable device's energy consumption will be highly diminished so that they can be driven by renewable sources of energy (RF). *Wireless Power Harvesting Network (IOT/WSN).* In recent years, WSNs have gained widespread prominence alongside the advancement of micro-electro-mechanical systems (MEMS) technology. WSN sensor nodes are low-powered machines, so reducing energy usage and WPH application to replenish power storage components to find efficient WSN control solutions like RF power harvesting.

References

1. Hughes, M.: Wireless RF energy harvesting: RF to DC conversion and look at power cast device, from allaboutcircuits.com
2. Gabay, J.: DigiKey articles, RF energy harvesting: batteries not included (2015)
3. Brown, J.: Harvest energy from RF sources, mwrf (2019)
4. Afridi, M.A.: Microstrip Patch Antenna. Science Singpost Publishings Inc. (2015)
5. Ali, E.M., Yahaya, N.Z., Perumal, N., Zakariya, M.A.: Design of microstrip patch antenna at 900 MHz for charging mobile applications. *J. Eng. Appl. Sci.* **12**(4), 988–993 (2017)
6. Balanis, C.A.: *Antenna Theory: Analysis & Design*. John Wiley & Son's, New Jersey, USA (2016)
7. Ali, E.M., Yahaya, N.Z., Perumal, N., Zakariya, M.A.: Design of RF to DC rectifier at GSM band for energy harvesting applications. *A. J. Eng. Sic. Soc.* **10**, 15–22 (2014)
8. Hasan, N., Giri, S.K.: Design of low power RF to DC generator for energy harvesting application. *Int. J. Appl. Sci. Eng. Res.* **1**, 562–568 (2012)
9. HSMS-2850.: Surface Mount Zero Bias Schottky Detector diodes
10. Akter, B.H.N., Kabir, H., Bhuiyan, A.H.: Design and performance analysis of 10 stage voltage doublers RF energy harvesting circuit for wireless sensor network. *J. Commun. Eng. Netw.* **2**(2), 84–91 (2014)
11. Vera, G.A.: Efficient rectenna design for ambient microwave energy recycling
12. Tran, L.-G., Cha, H.-K., Park, W.-T.: RF power harvesting: a review on designing methodologies and applications. *Micro Nano Syst. Lett.* (2017)

Chapter 40

Noise Voltage: A New Dependability Concern in Low-Power FinFET-Based Priority Encoder at 45 nm Technology



Vishwas Mishra, Abhishek Kumar, Shobhit Tyagi, Divya Mishra, and Shyam Akashe

Abstract The first design goal is to design a low-power device that meets the system requirements. Leakage power is a careful parameter when designing low-power devices because it plays a major role in increasing the total power consumption of the device. In IC designing, the major concern we have to take is packaging (density) and lower leakage parameters in that denser medium, but still the reliability issues occur in the circuitry. When we are talking about priority encoder in the IC, then at that time we have to take these issues seriously; out of that, noise is the major issue which affects due to variation of temperature, low supply voltage, and variable threshold voltage. This paper focuses on the calculation and analysis of noise of CMOS-based and FinFET-based priority encoder circuit. Minimum noise was found to be lowest at 0.7 V in case of FinFET-based priority encoder.

40.1 Introduction

The MOSFET after the 90 nm technology requires enhancements of the parameters because scaling down affects the device and its functioning, and channel length modulation and short-channel effect come into sight. The most cited limits are tunneling of carriers through thin gate oxide in MOSFET and finite sub-threshold slope [1].

V. Mishra (✉) · A. Kumar · S. Tyagi · D. Mishra
Swami Vivekanand Subharti University, Meerut, India
e-mail: vishwasmishra88@gmail.com

A. Kumar
e-mail: abhishekec02@gmail.com

S. Tyagi
e-mail: shobhityagi.1857@gmail.com

D. Mishra
e-mail: mishradivya1311@gmail.com

S. Akashe
ITM University, Gwalior, India
e-mail: shyam.akashe@itmuniversity.ac.in

© The Editor(s) (if applicable) and The Author(s), under exclusive license to Springer Nature Singapore Pte Ltd. 2021

Y.-D. Zhang et al. (eds.), *Smart Trends in Computing and Communications: Proceedings of SmartCom 2020*, Smart Innovation, Systems and Technologies 182,
https://doi.org/10.1007/978-981-15-5224-3_40

This limitation led toward suspicious expectation of end of technology in semiconductor industry. For this asserted manners, continue scale down and pushing technology toward lower supply voltage, shorter channel length, thinner substrate film thickness, and steps toward nanotechnology [2]. The vital method that examines the lowest dimensions in technology eventually led toward the submicron era by keeping length below 1 μm channel length. But, the barrier of scaling is not below 0.35 μm due to sub-threshold region [3]. The imperative task in this cohort of IC designing is to increase power dissipation in the circuit which reduces the battery life as well as power; it also affects the reliability of the circuit due to interconnect aging process and accelerated device [4]. Designing a low-power circuitry without affecting the functioning of integrated circuits (ICs) has become necessary for semiconductor industry. SOI has the skills that are widely accepted for use in conventional high recital logic and for low power application in 45 nm technologies. The issues that are affected on SOI devices partially or fully by the floating-body as well as parasitic characteristics effects variation in threshold (V_{th}) due to hysteresis are major anxiety in designing of circuit/design are mitigating by the new technique and design development [5]. In VLSI, hypothetically SOI can be manufactured on 22 nm, but right now practically the channel length is 45 nm technology on which SOI is working [6]. In CMOS below 90 nm technology, the field-effect transistor (FET) will remain the vital design element of choice for the high-speed logic designer. The evolution of new device must be in such a way that it can fulfill the some aimed, i.e., increasing mobility, reduced short-channel effect, and variable threshold voltage [7]. All these effects can be controlled by multi-gate FET. The temporary stay toward scaling offers by double-gate (DG) MOSFET.

40.2 Factors That Are Different in MOSFET and Double-Gate MOSFET

40.2.1 Channel Length

We cannot find out the channel length formula directly; for that, we needed the equation of channel current which is as follows:

$$I_{DS} = \mu_n C_{\text{ox}} \frac{W}{L_{\text{eff}}} (V_{\text{GS}} - V_{\text{T}}) V_{\text{DS}} \quad (40.1)$$

where I_{DS} = channel current, μ_n = permittivity of oxide, C_{ox} = oxide capacitance, W = width of channel, V_{GS} = gate-to-source voltage, V_{T} = threshold voltage, V_{DS} = drain-to-source voltage, and L_{eff} = channel length is as follows:

$$L_{\text{eff}} = L_m - \Delta L \quad (40.2)$$

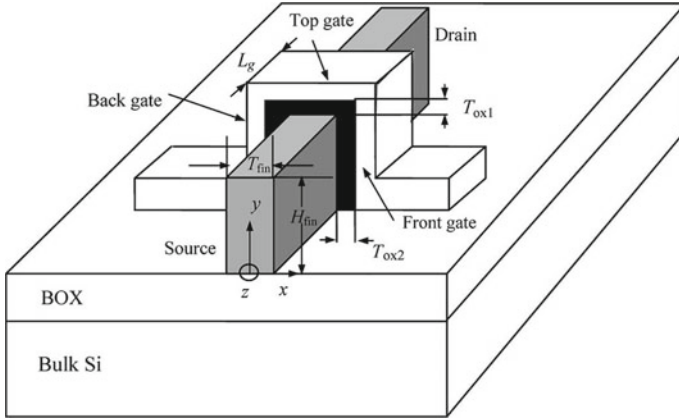


Fig. 40.1 Cross-sectional view of FinFET

$$m = (L_{m2} - L_{m1})(L_{m1} - \Delta L) \tag{40.3}$$

where m denotes slope of channel length.

Channel length in double-gate MOSFET is as follows:

$$\lambda = \sqrt{\frac{\epsilon_{si}}{2\epsilon_{ox}} t_{si} t_{ox}} \tag{40.4}$$

where λ helps to measure short-channel length (Fig. 40.1).

$$L_g = n\lambda \tag{40.5}$$

$$\frac{L_g}{n} = \lambda = \sqrt{\frac{\epsilon_{si}}{2\epsilon_{ox}} \left(1 + \frac{\epsilon_{ox}}{4\epsilon_{si}} \frac{t_{si}}{t_{ox}} \right) t_{si} t_{ox}} \tag{40.6}$$

40.2.2 Channel Width

It shows the width of that layer of the channel between the drain and source, and we can find out the formula of that using the same equation of channel current, and we get the channel width of MOSFET which is as follows:

$$k = (W_{m1} - W_{m2}) / (W_{m2} - \Delta W) \tag{40.7}$$

In double-gate MOSFET, there is $FinW_{\text{eff}}$ not a channel width, and this is as follows:

$$FinW_{\text{eff}} = Fin_{\text{WIDTH}} + 4 \frac{\epsilon_{\text{si}}}{\epsilon_{\text{ox}}} t_{\text{ox}} \tag{40.8}$$

40.3 New Reliability Concern: Noise Voltage

Noise can limit the minimum value of signal level in which circuits can work properly. It also affects the power, speed, and synchronization. Noise is a random value that gets affected by many ways in the circuit either by human interference, fluctuation in supply voltage, input variable toggling, low power mode, and short-channel effect. We cannot remove the noise voltage [8], but we can reduce its effect in low power mode on the data by changing either the technology or the working device (Figs. 40.2 and 40.3).

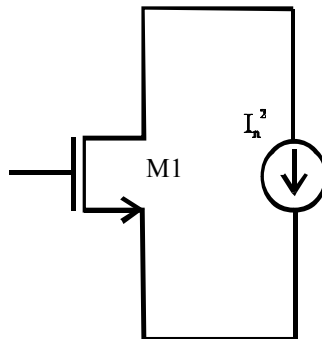


Fig. 40.2 MOSFET noise circuit diagram

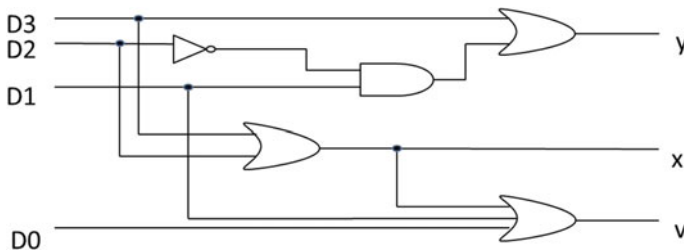


Fig. 40.3 Priority encoder

40.3.1 Thermal Noise

The arbitrary movement of electron in devices fluctuates the voltage measured across the output terminal even if the total current is zero [9].

$$S_v(f) = 4KTR \quad (40.9)$$

40.3.2 Flicker Noise

The interference mismatch between gate oxide and substrate (silicon/germanium) in MOSFET includes flicker noise.

$$\bar{V}_n^2 = \frac{K}{C_{ox}WL} \cdot \frac{1}{f} \quad (40.10)$$

40.3.3 Shot Noise

This occurs in misalignment of electron near the junction and occurs at high electric field [10].

$$\bar{V}_n^2 = 4KT \frac{2}{3} g_m \quad (40.11)$$

40.4 Priority Encoder

The method of providing output is similar to a simple encoder with one advantage of selecting operations with the priority function. With this feature of the priority function, the highest priority input is provided first whenever there is a need to select from multiple outputs. The highest priority is given to the highest index number of the input.

SG FinFETs are constructed by shorting two P-type MOSFETs and two N-type MOSFETs to form P-type and N-type FinFETs, respectively. Priority encoder is implemented using a rhythm masters tool. Simulate the output using a cadence spectrum simulator. The gates of two PMOS or NMOS transistors are connected together to form a FinFET-like structure.

Table 40.2 Integrated noise of CMOS-based and FinFET-based priority encoder

Supply voltage	Output port	Integrated noise (V^2/Hz)	
		CMOS	FinFET
0.7 V	V	$1.05532e^{-10}$	$5.7792e^{-11}$
	X	$1.05532e^{-10}$	$5.7792e^{-11}$
	Y	$1.44134e^{-10}$	$7.20816e^{-11}$

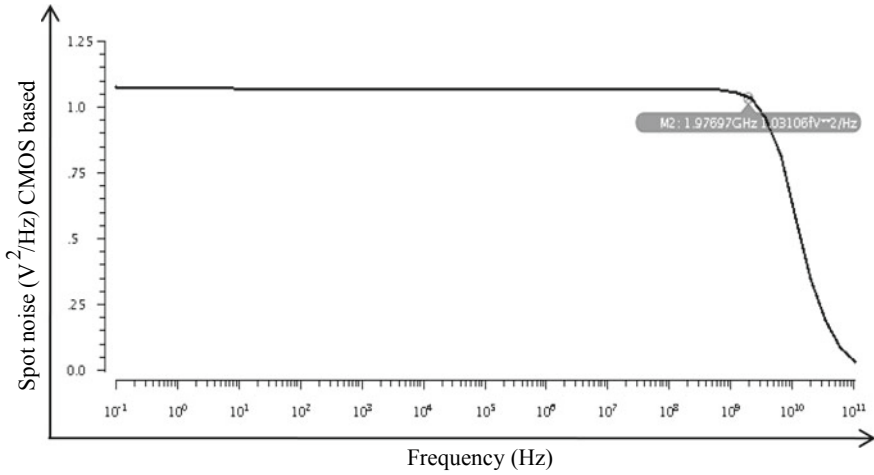


Fig. 40.5 Spot noise of CMOS-based priority encoder

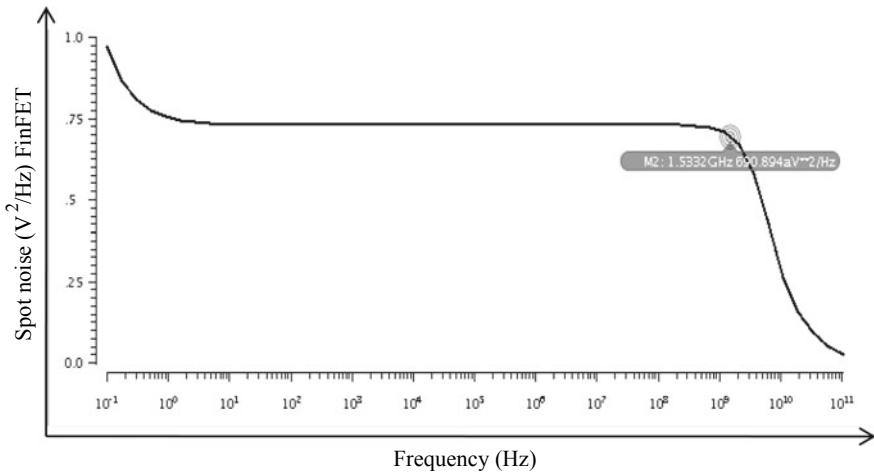


Fig. 40.6 Spot noise of FinFET-based priority encoder

40.6 Conclusion

In this paper, average noise voltage is obtained by designing and analyzing over FinFET-based priority encoder and conventional priority encoder at 45 nm technology. FinFET has variable threshold voltage, and working on that, V_{well} shows the fixed minimum value onto which priority encoder works properly. A repeated layout pattern has come into priority encoder which accounts the testing of reliability issue. Priority encoder in this simulation shows variation in susceptibility to noise voltage compared to the conventional and FinFET-based devices. At 45 nm technology, FinFET-based priority encoder cell gives the minimum noise value at 0.7 V.

References

1. Bernstein, K.: Design and CAD challenges in sub-90 nm CMOS technologies. In: Proceeding International Conference Computer Aided Design, pp. 129–136 (2003)
2. Bohr, M.T.: Nanotechnology goals and challenges for electronic applications. *IEEE Trans. Nanotechnol.* 1(1), 56–62 (2002)
3. Roy, K., Prasad, S.C.: *Low Power CMOS VLSI Circuit Design*. Wiley India Publication (2011)
4. Akashe, S., Shrivies, J., Tiwari, N., Sharma, R.: A novel high speed and power efficient half adder design using MTCMOS technique in 45 nanometer regime. In: Proceeding IEEE International Conference on Advanced Communication Control and Computing Technologies (ICACCCT), Ramanathapuram (2012)
5. Ko, H.-J., Hsiao, S.-F.: Design and application of faithfully rounded and truncated multipliers with combined deletion, reduction, truncation and rounding. *IEEE Trans. Circuits Syst. II Exp. Briefs* 58(5), 304–308 (2011)
6. Powell, M.D., Yang, S.H., Falsafi, B., et al.: Gated—VDD. A circuit technique to reduce leakage in cache memories. In: Proceedings of International Symposium on Low Power Electronics and Design (2000)
7. Agarwal, A., Li, H., Roy, K.: DRG cache: a data retention gated-ground cache for low power. In: Proceedings of the 34th Design Automation Conference (2002)
8. Manorama, S.K., Akashe, S.: Design of a FinFET based inverter using MTCMOS and SVL leakage reduction technique. In: Proceeding IEEE Conference on Engineering and Systems (SCES), Allahabad (2013)
9. Mishra, P., Jha, N.K.: Low-power FinFET circuit synthesis using surface orientation optimization. In: Proceeding Design Automation and Test in Europe, pp. 311–314 (2010)
10. Pushpa Raikwal, V., Katiyal, N.S.: Low power with improved noise margin for domino CMOS nand gate. *Int. J. Comp. Eng. Res.* 2(2), 520–525 (2012)

Chapter 41

Assessment of Suitability of Metaheuristics and Machine Learning for Task Scheduling Process: A Review of Aptness in Heavy Task Environments



Shantanu Anandrao Lohi and Nandita Tiwari

Abstract Considering the advanced nature of computational abilities, task scheduling is a measure of success in any multiprocessing environment performing many different tasks in real-time and effective scheduling process and so on. Cost-effective resource scheduling or CERS algorithm has been a crucial algorithm for many cloud deployments over the years. This algorithm is computationally simple, has minimum overheads, and is based on keeping the cloud utilization to the most optimum level. We analyzed that keeping effective task response time is one of the main drawbacks of the CERS algorithm. In this paper, we propose new machine learning-based optimization algorithm that utilizes the concept as proposed by CERS but in process improves it further using an amalgamation of pre-learning and continuous adaptation techniques in order to reduce the mean response time for a given set of tasks. The proposed algorithm will further be compared with the standard CERS implementation, and the results will be evaluated in terms of resource cost and mean response time.

41.1 Introduction

Scheduling and allocation of resources is one of the most important factors which decide the efficiency of task execution in a multiprocessing environment like cloud structures and so on. Generally, algorithms which aim to perform optimum resource allocation take into consideration the following system parameters:

- The number of jobs/tasks to be executed
- The number of virtual machines (VMs) available for task execution

S. A. Lohi (✉) · N. Tiwari
Department of Computer Science and Engineering, RKDF Institute of Science and Technology,
Sarvepalli RadhaKrishnan University, Bhopal, MP, India
e-mail: shantanulohi.kits@gmail.com

N. Tiwari
e-mail: nandita_pandit@gmail.com

© The Editor(s) (if applicable) and The Author(s), under exclusive license to Springer Nature Singapore Pte Ltd. 2021

Y.-D. Zhang et al. (eds.), *Smart Trends in Computing and Communications: Proceedings of SmartCom 2020*, Smart Innovation, Systems and Technologies 182,
https://doi.org/10.1007/978-981-15-5224-3_41

- Processing parameters like bandwidth, memory, and millions of instructions executed per second (MIPS) for the VMs
- Task parameters like task size, memory needed for task execution, task deadlines, and mutual exclusiveness.

All these parameters when taken into consideration for resource allocation generate a very complex computational algorithm, which aims at maximizing the cloud's efficiency and minimizing the task queue per unit time. These algorithms follow the given architectural steps in order to allocate resources: Initialize the task parameters, and create a task queue so that the overall task requirements are evaluated.

1. Evaluate the VMs processing parameters, and generate a per unit time processing queue
2. Apply mathematical algorithms to run the task queue on the processing queue; in most cases, the task queue is larger than the processing queue; thus, the algorithm takes this into consideration and executes the remaining task queue in the next processing cycle
3. For any new task, repeat steps 1 and 3
4. For any changes to the VMs, repeat steps 2 and 3
5. Model the system for any unexpected events and contingencies.

Using these steps, a multiprocessing system is generally modeled, and tasks are scheduled. In the above steps, modeling of Step 3 is of utmost importance, and all resource planning is done in this step. In our research, we would be applying bio-inspired techniques to optimize Step 3, and add deadline awareness to the system. In addition to this, we will be exploring the effect of using cloud containers in place of simple VMs, and evaluate its performance in comparison with the non-container counterpart. Previous work related to resource planning generally does not take into consideration all these issues, and thus, our work should achieve better cloud performance in comparison with existing algorithms like dCloud [1], differential evolution (DE) [2], and improved DE [2] models.

The next section of this document describes various algorithms proposed by other researchers for resource allocation, wherein we compare the nuances of these algorithms, followed by a statistical analysis between them. Finally, we propose our two-stage machine learning-based task scheduling algorithm with some finer observations which are made specifically to resource planning, and how to further enhance the security level of this work with the help of more complicated computational structures, which are not in the scope of our work.

41.2 Existing System

Due to the emerging trends of small to medium enterprises shifting onto the cloud, there is a need for high-speed task scheduling algorithms to be evolved. Researchers around the world have been proposing various techniques for task scheduling, in

order to optimize the resource utilization, and thereby optimize the QoS of the system. In the work presented by Arghavan Keivani, Farzad Ghayoor, and Jules-Raymond Tapamo in [2], they have reviewed simple heuristic scheduling algorithms like min-min scheduling algorithm, max-min scheduling algorithm, minimum completion time scheduling algorithm, cloud-dynamic level scheduling algorithm, market-oriented scheduling policies, and round-robin scheduling algorithm. They have also reviewed evolutionary algorithms like bees life algorithm, particle swarm optimization algorithm, simple genetic algorithm, parallel genetic algorithm, generalized genetic algorithm, ant colony optimization, ant algorithm, genetic simulated annealing algorithm, priority-based job scheduling algorithm, and the Berger model. With the help of this extensive comparison, they have concluded that the min-min, market-oriented scheduling, round-robin, and min-max algorithms are the simplest, but create large queuing delays for larger tasks, while algorithms like cloud DLS are most reliable in terms of task execution. Furthermore, they have observed that swarm intelligence techniques and genetic algorithms reduce the run time, but usually do not consider the computational cost on the multiprocessing environment such as a cloud environment for executing the given workload. They also suggest that all these algorithms can be efficiently implemented in either Java or GridSim environments.

41.2.1 Noteworthy Contributions

Looking at models from a computational end point is one thing, but in the work done in [3], researchers have designed a protocol which uses trust-based agents for service composition in mobile environments where cloud computing is used. They claim to have achieved high success ratios of service matching and better user satisfaction, using the trust-based methods. The parameters which they have suggested are largely manual and are based on human emotion, and thus, their research work might not be applicable to all kinds of cloud computing environments. The experimentation in [3] outperforms the experimentation in [1] and compares more than eight algorithms of task scheduling. Shantanu Lohi et al. [4] discuss utilization of metaheuristics and efficient nature of the cuckoo search algorithm over firefly algorithm. They put forth their points through experiments of assembly-line task scheduling process. Genetic algorithms are also used for improving the energy efficiency in data centers, like the algorithm mentioned in [3], which utilizes the scalability of GA in order to improve not only the efficiency of the task scheduling algorithm, but also the overall energy efficiency of the network under test. This algorithm is acronymically known to be HIGA or harmony-inspired genetic algorithm, where the main objective of the algorithm is to schedule the tasks, followed by some of the secondary objectives to reduce energy consumption.

41.3 Proposed Methodology

In the pre-execution phase, the system performs static allocation of tasks to VMs w.r.t. the VMs capacity, and therefore, it should be run only once for the entire allocation process.

Initialize machine learning parameters

Number of solutions is represented as N_s

Number of learning iterations is represented as N_i

Learning rate is represented as LR

Number of execution units is represented as N

Capacity of each execution unit is represented as $C_1, C_2, C_3, \dots, C_N$

Minimum number of execution units for each solution as N_{min}

Maximum number of execution units for each solution as N_{max}

Pre-step:

Mark all solutions which are needed to be changed in the current round

Step I:

Go to each iteration from 1 to N_i

Go to each solution from 1 to N_s

If the solution is needed to be changed, then

Find a random number between $(N_{min}$ to $N_{max}) = N_{sol}$

Select random N_{sol} numbered execution units from the total list of execution units

Execute the task on the selected execution units and find the learning factor (lf)

$$lf = \text{Total task to be scheduled} / \text{Capacity of unit} \quad (41.1)$$

in the given equation,

$$\text{Total task to be scheduled} = \text{No. of tasks} \times \text{time taken by each task} \quad (41.2)$$

$$\begin{aligned} \text{Capacity of execution unit} &= \text{Tasks executed per unit time} \\ &\times \text{No. of task engines} \end{aligned} \quad (41.3)$$

Step II:

Find the mean learning factor (MLf) as

$$MLf = \sum lf_i / NS \quad (41.4)$$

Find learning factor threshold (THlf) as

$$THlf = Mlf \times LR \quad (41.5)$$

Table 41.1 Proposed methodology

Number of selected units	Selected unit indices	Unit to task mapping	Learning factor
--------------------------	-----------------------	----------------------	-----------------

Step III:

– if $lf_i > THlf$

Solution is needed to be changed in next round

– else

Solution can be kept as it is for next round

Step IV:

Mark the solutions which are needed to be changed, and pass them to Step I, and repeat it for N_r rounds

Step V:

Select the solution with minimum learning factor or maximum efficiency with respect to total task.

Create a machine learning lookup table, which contains the following entries:

The execution phase

- Once the pre-execution phase is gone, the system is performing task execution; the value of learning factor is evaluated after successful completion of ‘ k ’ execution cycles.
- In this case, ‘ k ’ is the algorithm’s complexity factor and can be in the range of $[1 - N]$, where N is the max number of execution cycles needed for all the tasks to be completed.
- Once the value of learning factor (LF) is evaluated, it is compared with Table 41.1.
- If the value of LF is higher than any entry, then the table is revisited, and the execution unit to task mapping is changed accordingly.
- The current value of LF is updated in the table, and the process is repeated.

All tasks are executed using this algorithm, and due to its simplicity of execution, the time needed for evaluation of execution unit to task mapping is minimum; thereby, the response time of the algorithm is minimized. This allows the system to have maximum speed, with better QoS than the existing non-machine learning-based systems. We evaluated the performance of the proposed algorithm and compared it with an existing CERS algorithm. The results for the same are described in the next section.

41.4 Result Analysis

After designing the given algorithm and executing it on various workloads, we evaluated the following parameters,

- Machine effort is the number of execution cycles that some or all the machines have to run for completing all the tasks
- Delay for executing the algorithm is the time needed for the system to compute the execution unit to task mapping
- Response time is the time needed by the system to complete all the tasks.

We utilized the University of Luxemburg Gaia Cluster log and the KIT ForHLR II log. Both the workloads were taken from the Parallel Workloads Archive which is a standard repository of workloads submitted by various recognized laboratories working in task scheduling. More information can be obtained from the website (<https://www.cse.huji.ac.il/labs/parallel/workload/>). This contains logs from around 40 different organizations. We selected the ones from the University of Luxemburg Gaia Cluster (ULGC) log and the KIT ForHLR II (KFH) log due to their task exclusive nature and variation in different kinds of task sets. Each of the experiments was performed using the following configurations as showcased in Table 41.1.

In this work, Table 41.2 showcases the machine effort results obtained for both the datasets on the given execution unit configuration.

Table 41.2 Comparison between machine efforts for the proposed algorithm

Number of tasks	Dataset	Machine effort (CERS)	Machine effort (proposed technique)
1000	ULGC	25	18
1000	KFH	31	22
5000	ULGC	125	90
5000	KFH	155	110
10,000	ULGC	250	180
10,000	KFH	310	220
20,000	ULGC	500	360
20,000	KFH	620	440
40,000	ULGC	1000	720
40,000	KFH	1240	880
50,000	ULGC	1250	900
50,000	KFH	1550	1100
60,000	ULGC	1500	1080
80,000	ULGC	2480	1760
90,000	ULGC	2250	1620
100,000	ULGC	3100	2200

41.5 Conclusion

From the results, we can conclude that the machine learning would be more suitable alternative for task scheduling process than metaheuristics. Our proposed machine learning-based task scheduling algorithm performs 30% better than the existing CERS algorithm in terms of overall machine effort. This advantage is evident due to the extensive pre-execution phase, wherein most of the mapping processes and calculations are predominantly done. This work can be further improved by evaluating the performance for mutually dependent tasks. More research is needed to evaluate and expand the belief in machine learning-based task scheduling. We are striving hard to carry out more experimentation in furthering our proposed methodology by considering world standard datasets and archives.

References

1. Xin-She Yang, F.: Nature-Inspired Metaheuristic Algorithms. Luniver Press, London (2008)
2. Xin-She Yang, F.: Firefly algorithms for multimodal optimization. Stochastic algorithms: foundations and applications. In: SAGA, Lecture Notes in Computer Science, pp. 169–178 (2009)
3. Yang, D., Liu, Z., Zhou, J.: Chaos optimization algorithms based on chaotic maps with different probability distribution and search speed for global optimization. *Commun. Nonlinear Sci. Numer. Simul.* **19**(4), 1229–1246 (2014)
4. Lohi, S.A., Jaiswal, A.A., Gorewar, H.V., Snehal, L.: Analytical assessment of nature-inspired metaheuristic algorithms to elucidate assembly line task scheduling problem. *Advances in Intelligent Systems and Computing*, vol. 933, pp. 217–228. Springer, Singapore (2019)
5. Mayer, R., Mayer, C., Laich, L.: The TensorFlow partitioning and scheduling problem: it's the critical path! In: *Proceedings of the 1st Workshop on Distributed Infrastructures for Deep Learning*, pp. 1–6. ACM (2017)
6. Iztok Fister, F., Iztok Fister, S. Jr., Xin-She Yang, T., Janez Brest, F.: A comprehensive review of firefly algorithms. In: *Swarm and Evolutionary Computation* (2013)
7. Xin-She Yang, F.: Nature-Inspired Metaheuristic Algorithms, 2nd edn. Luniver Press (2010)

Chapter 42

A Review on Indian UID-Based Automated Electoral Roll Generation Mechanism Shunning Duplication and Redundancy



Harish Vasantrao Gorewar and Nandita Tiwari

Abstract The purpose of this paper is to prepare an electoral roll by ensuring non-duplication and maintaining the truthfulness of voter details as well as providing a economical resolution to the government. This ensured great convenience to the voters while casting votes. The scheme is strictly designed to safeguard that all appropriate voters have a universal identification number—their country’s UID (e.g., Aadhaar number in India) is allowed to cast their respective votes. The electorates, who have registered many times in the different constituencies, will be removed, and correct constituency registration will be kept in the final electoral roll during the election period. Further, to ensure authentication of eligible voters, cast their vote with the help of any biometric identification and confine them to vote again during the actual voting process.

42.1 Introduction

Elections in India were still held and based on the electoral rolls of the Constituent Assembly and related constituencies. “Electoral roll” is a list of persons with the needed personal details, who are qualified to cast their vote in a particular Constituent Assembly and who are enrolled to vote. Elections were started on the basis of electoral rolls containing the names and descriptions of local people in India for the first time under the Indian Council Act, 1909 (Morley Minto Reform). After the independence of the India in 1947, to fulfill the ambitions and expectations of the people of India, the Constituent Assembly decided that under the Constitution of India, the parliament and State Assemblies should be elected based on the of universal adult suffrage [1].

H. V. Gorewar (✉) · N. Tiwari
Department of Computer Science and Engineering, RKDF Institute of Science and Technology,
Sarvepalli RadhaKrishnan University, Bhopal, MP, India
e-mail: harish.gorewar80@gmail.com

N. Tiwari
e-mail: nandita_pandit@gmail.com

© The Editor(s) (if applicable) and The Author(s), under exclusive license
to Springer Nature Singapore Pte Ltd. 2021

Y.-D. Zhang et al. (eds.), *Smart Trends in Computing and Communications: Proceedings of SmartCom 2020*, Smart Innovation, Systems and Technologies 182,
https://doi.org/10.1007/978-981-15-5224-3_42

As maximum portion of the preparation of the electoral roll is manual in nature, it is prone to errors. Being a citizen of India, we have witnessed many elections conducted in past and have following flaws:

1. Duplication and redundancy in electoral rolls.
2. Also, there are various challenges faced like verification and authentication of the voter, as again this kind of process is carried out manually.
3. Real-time updates are not guaranteed by persons doing it and are not feasible even.
4. Total Indian population with metadata is difficult to address and handle.
5. ASD (Absent—Shift—Dead) list handled and maintained with the help of BLO.

This paper proposed an automated system to overcome from the manual errors while preparing electoral rolls. It is proposed with the one basic need that all the voter's UID (Aadhaar Card Number) is attached with the voter ID (Electoral Photo Identity Card Number—EPIC).

42.2 Existing System

42.2.1 *Review of the Existing System*

Following are the few related work carried out by the researchers and experts:

- (a) Generation and alteration of electoral rolls—Demonstration of the People Act (1950)
 - (1) Generation and modification of electoral roll in the recommended fashion with reference to the due date and will impose instantly upon its absolute declaration in accordance with the guidelines constructed in this Act [2].
 - (2) The supposed “Electoral Roll”:
 - (a) Election Commission shall be instructed for explanations to be documented in writing, be modified in the recommended style with reference to the due date:
 - (i) prior to each common election to the House of the People or to the Parliamentary Assembly of a State; and
 - (ii) prior to each bye-election to fill the spontaneous positions in a seat allotted to the constituency and
can be modified any time in the approved means with reference to the due date if such modification has been absorbed by the Election Commission:

It should be considered that if the electoral roll is not modified as abovementioned, the rationality or continued operation of the supposed electoral list will not be affected.

- (3) Nevertheless contained everything in Sect. (2), at any time, the Election Commission may, for explanations to be logged, instruct a special modification of the electoral roll for part of a constituency or any constituency would look right:
- It should be considered that, subject to the other requirements of this Act, the electoral roll for the constituency, as active at the time of the issue of any such instructions, shall be considered as active till the achievement of the special modification so instructed [3].
- (b) Since a couple of decades, the Government had been assessing various possibilities for an identity scheme, so the concept of national identity scheme is not very new for India [4]. According to the policy overview document published by (UIDAI 2010d, p. 1), “the very first time effort was taken by the Government of India in 1993, try to give a clear identity to the citizens, by issuing a photo ID to the Election Commission and then in 2003, when the Multipurpose National Identity Card (MNIC) was approved. In January 2009, as an attached office to the Planning Commission the Unique Identification Authority of India (UIDAI) was established [5, 6]. The aim of UIDAI is to provide a unique identification number (UID) to all Indian citizens that is (a) vigorous enough to eliminate replica and fake individualities, and (b) can be “certified and authenticated in an easy, economical way” [7].
- (c) In the general election process, we know that Booth Level Officer (BLO) takes updated information of the voters by cross checking the existing list and conveys it to the district election authorities.

42.2.2 *Noteworthy Contributions*

1. Elections have been conducted with the help of ballot papers for many years in India, but this method was very costly, slow, misty and environment unfriendly. So, Election Commission of India decided to switch to EVM. Electronic voting machine (EVM) used instead of ballot paper, which saves the time of counting and result declaration. The electronic voting machine (EVM) was first used in the Kerala’s “Parur Assembly” polls in 1982.

Maximum 2,000 votes can be recorded in EVMs used in India. Election Commission’s Technical Expert Committee (TEC) has been designed these EVMs in association with two PSUs, Bharat Electronics Limited, Bangalore and Electronic Corporation of India Limited, Hyderabad.

A good property of these EVMs is that electricity is not required in their operation because they already have a battery backup system. Therefore, with the help of these machines, elections can be conducted in those areas which do not have electricity.

Composed with NOTA, the M2 EVMs can furnish to an extreme of 64 candidates. There is establishment for 16 candidates in a balloting unit. More balloting

units can be joined together up to a maximum of 64 candidates by connecting four balloting units if the total number of candidates exceeds than 16.

2. To assuring to the voter that the vote was cast to the correct candidate, new method of providing feedback to voters using a ballot less was introduced called voting system verifiable paper record (VPR) or voter verifiable paper audit trail (VVPAT). To detect possible election fraud or failure, to allow voters to verify that their vote was cast correctly and to afford a means to audit the stored electronic results, a voting machine was designed called VVPAT is intended as an independent verification system. It consists of the name of the candidate (for whom vote has been cast) and icon of the party/individual candidate.
3. In this paper, we have given the introductory details of EVP program. Objective of voter ID EVP scheme is to give facility to update voter ID details using NVSP EVP and add family member. Election Commission of India (ECI) launched its mega Electoral Verification Program (EVP) on September 1, 2019, all over India. EVP Voter ID correction and verification through “Electoral Verification Program (EVP) 2019”— this mega launch took place in all the state and Union Territories of India. The program aimed to update and validate electoral details through public gathering.

42.3 Proposed Methodology

This system would generate an electoral roll automatically by incorporating and replacing the manual work carried out previously, in the following manner.

As depicted, it includes all the government and semigovernment as well as the non-government bodies who are giving different services to the public will be considered as a part of this system. A central Repository will keep all the data of the voters. All the relevant information (general personal information required to identify a person) of the voter is stored and is linked with the UID known as Aadhaar in India, as shown in the following Fig. 42.1.

Information required for the electoral roll can be generated by using maximum part of the existing government and non-government public utility and service provider systems. In India, large amount was spent for general elections, in which electoral roll preparation is one of the major activities handled by the election commission. A staggering Rs. 55,000–60,000 crore was spent in the Lok Sabha elections, 2019, according to a study by the Center for Media Studies (CMS). Using this system, election commission can be able to save more money with less efforts as it is a cost-effective kind of system.

As per the proposed system, the following steps should be carried out:

- (a) New registration done in the similar way as done nowadays by attaching the UID number with the voter ID number.
- (b) Existing voter list can be filter out by the concept of the data science and nature-inspired metaheuristic algorithms [8].

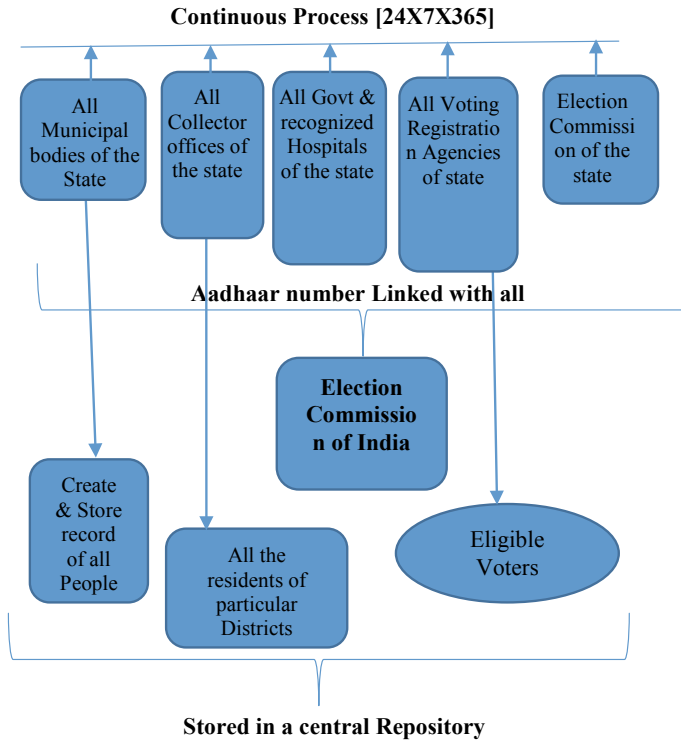


Fig. 42.1 Proposed methodology

- (c) Deep learning would be used during the voting process for the authentication and verification process.
- (d) Use of handheld device for the authentication and verification by the BLO.

As shown in Fig. 42.2, the use of the administrative structure of India becomes mandatory and necessary to carried out above listed process.

Every component of the system will store the data of the person by automatically ensuring that there is no previous data is available for the same entity as all the personal information of the voter is linked with the UID.

Authentication can be done at various level by simply using the UID details through the biometric process.

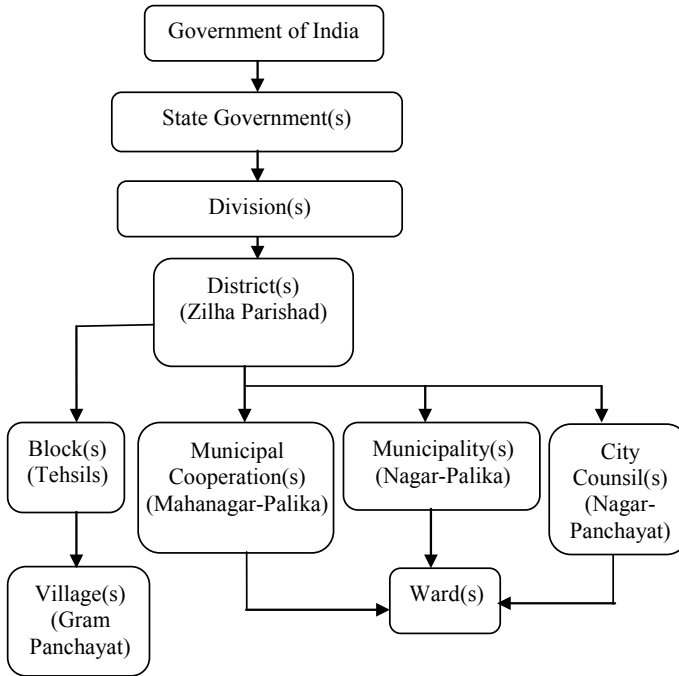


Fig. 42.2 Administrative structure of India

42.4 Conclusion

This paper proposed an automated system to overcome from the manual errors while preparing electoral rolls. It is expected that it will produce the following kind of outcomes:

- (a) It will generate the updated electoral roll automatically whenever required.
- (b) It will give the correct number of the voters actually available in the assembly constituency/parliament.
- (c) At the end of voting on Election Day, election commission will be in position to give the correct voting percentage done at a particular constituency.
- (d) Authentication and verification can be done automatically and more accurately and efficiently.
- (e) Providing a cost-effective solution to the government.
- (f) Ensuring non-duplication and preserve the integrity of the voter details.
- (g) Provide great convenience to voters while casting their votes.

References

1. Jain, A.K., Nandakumar, Karthik, Ross, Arun: 50 years of biometric research: accomplishments, challenges, and opportunities. *Pattern Recogn. Lett. Elsevier* **79**, 80–105 (2016)
2. Election Commission of India: The representation of the people act (1950)
3. Election Commission of India: Manual on code of conduct (2019)
4. Dass, R.: Unique identification for Indians: a divine dream or a miscalculated heroism. *Indian Institute of Management Ahmedabad, W.P. No. 2011-03-04* (2011)
5. Dass, R., Pal, S.: Challenges of identity management—a context in rural India. In: Weerasinghe, D. (ed.) *Information Security and Digital Forensics*, vol. 41, pp. 172–183. Springer, Berlin, Heidelberg, London, UK (2010)
6. UIDAI (n.d.): UID and PDS System: Unique Identification Authority of India, Planning Commission, Government of India
7. Gold, S.: Preventing electoral fraud using biometrics. *Biometric Technol. Today Elsevier J.* (2012)
8. Lohi, S.A., Gorewar, H.V., et.al.: Analytical assessment of nature-inspired metaheuristic algorithms to elucidate assembly line task scheduling problem. In: Tuba, M., Akashe, S., Joshi, A. (eds.), *Information and Communication Technology for Sustainable Development. Advances in Intelligent Systems and Computing*, vol. 933. Springer, Singapore (2019)

Chapter 43

A Review of Deep Learning Techniques for Identification and Diagnosis of Plant Leaf Disease



Ravindra Namdeorao Joglekar and Nandita Tiwari

Abstract This paper focuses on review of deep learning techniques on plant leaf disease detection and its diagnosis. As we know agricultural farming plays a crucial role in world economy but the sad part is, it is adversely affected by damage due to diseases to plants all around the world. It is observed, plants are one of important source of energy for human being as well as other animals, and hence it is prime to save not only plant but their leaves too. It is then important to identify infected leaves which are affected by disease; this will be great help for farmers to protect it from sowing till process of harvesting which can reflect in reduction in economic loss. But manual work in this regard will be absolute burden on labour hence Automatic identification of diseases and it's diagnose will be add-on tool for agricultural yield and it will also help to maximize the production of crop. In this paper, comparative analysis between the performances of distinguish deep learning approaches for identification and diagnosis of various diseases on plant leaves with the help of different patterns of plant leaf images is discussed. In many experiments and evaluations, process of segmentation, feature extractions and classification methods are being done for quick diagnosis on selected plant leaf diseases. Here, we are trying to help farmers to identify and diagnose the disease on banana leaves by using deep convolutional neural network which can be treated at early stage.

43.1 Introduction

India is largest country in banana production as per the report of United Nations (FAO) which is about 28-30 million tons per year, major production is in southern part of India and they export to other states of the country as well. In global market

R. N. Joglekar (✉) · N. Tiwari
Department of Computer Science and Engineering, RKDF Institute of Science and Technology,
Sarvapalli RadhaKrishnan University, Bhopal, MP, India
e-mail: ravindra.joglekar79@gmail.com

N. Tiwari
e-mail: nandita_pandit@yahoo.com

© The Editor(s) (if applicable) and The Author(s), under exclusive license
to Springer Nature Singapore Pte Ltd. 2021

Y.-D. Zhang et al. (eds.), *Smart Trends in Computing and Communications: Proceedings of SmartCom 2020*, Smart Innovation, Systems and Technologies 182,
https://doi.org/10.1007/978-981-15-5224-3_43

Ecuador, China and Philippines are ranked after India, about 11% of the total global area under banana belongs to India and its contribution at world level is about 23% in pool of banana production. As we know, banana is declared a decisive fruit crop probably in hot and humid area of northern part of Country. In India, states like Tamil Nadu (TN), Gujarat, Andhra Pradesh, Karnataka and Maharashtra have maximum stake of banana production which is cultivated under the area of 830.5 thousand hectare, this result around production of 29,779.91 thousand tons. In many ways banana plant and other flora and fauna affect environment hence if these are infected with diseases then it will be difficult to address environmental issue so it should be treated on time [1]. There are available methods for disease identification on plant leaves like traditional method which help to identify problem with naked eyes by overlooking the crops, but it involves huge manpower and the results are not that accurate on other side it is time consuming and tedious for larger field area, it is not only expensive affair but need regular and continuous monitoring by team of experts. Hence, to overcome such problems various researchers across the globe are working on inventing new systems with the help of Deep learning (DL) techniques which gives better insight to farmers in detection of crop diseases. DL is a reliable prediction technique which can use for detecting the bacterial, fungal and viral diseases on different plant leaves. However, prediction of diseases by using leaf image feature extraction and using various classification algorithms in DCNN architecture with training and testing dataset, it will give more accurate results with minimum man power for the same [2].

43.2 Literature Review

Ramesh et al. [3] proposed diseases classification using Random Forest to identify the healthy and diseased images and collectively trained the healthy and diseased images under the same. Author also proposed implementation in various phases like creation of dataset of healthy and diseased images, then training to the classifier and classification later. For feature extraction of leaves images, author used Histogram of an Oriented Gradient (HOG).

Ferentinos [4] Convolutional neural network (CNN) models were proposed to detect diseases on plant leaves, in which researcher took sample of images of healthy and diseased leaves then applied various deep learning methods. Open database with 87848 images for training the models which has leaves of 25 different plants in a set of distinct 58 classes under diseased and healthy plants. In this process 99.53% accuracy was achieved.

Goncharov et al. [5] Deep Siamese Convolutional Network was developed to solve the problem of small databases of plant leaves images, for implementation researcher collected images of special leaves of the grape plant in four different sets. And accuracy more than 90% achieved in detection of diseases like Black rot, Esca and Chlorosis. In addition to this, researcher also gave comparative results of different models on diseased plants.

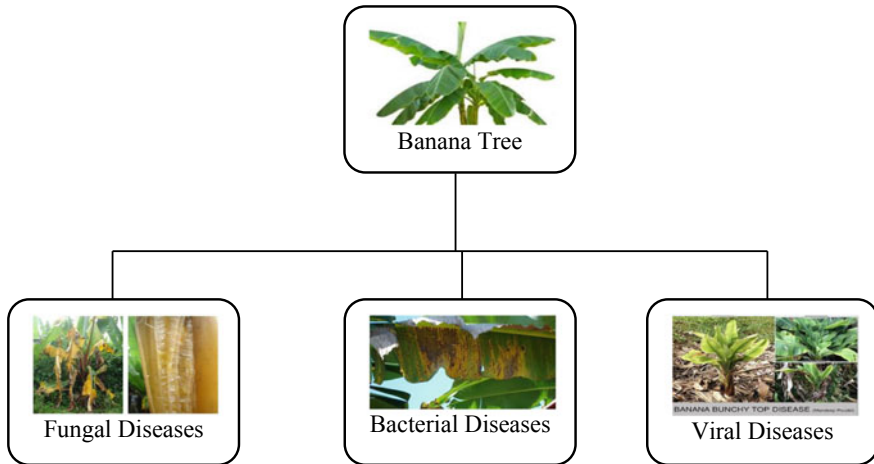


Fig. 43.1 Classification of plant leaf disease

Pantazi et al. [6] collected a special database of the vine leaves and applied LBP algorithm with image segmentation and accuracy level crossed by 92% in identification of powdery mildew diseases on the vine leaves. They also provided recognition capability comparison of different health conditions tested on sample leaves for variety of crops.

Figure 43.1 illustrates work of Pujari J. D., Yakkundimath R., and Byadgi A. S., proposed SVM for disease detection on various vegetable, cereal, commercial crops respectively and along with SVM they applied Artificial Neural Network (ANN), Probabilistic Neural Network (PNN) which classifies the fungal, viral and bacterial diseases on various vegetables crop [2].

Waghmare et al. [7] proposed Multiclass Support Vector Machine as classification algorithm on grapes leaves and he identified the disease like Black rot, Downey mildew on grapes leaves with reported accuracy of 96.6% but accuracy can be increase only by increasing the number of testing and training dataset samples of plant leaves.

Fuentes et al. [8] developed Convolutional Neural Network (CNN) models for the detection of nine variety of different tomato leaves diseases with satisfactory performance and proposed related pesticides for classified disease.

Brahimi et al. [9] proposed Convolutional Neural Network (CNN) to classify tomato leaves diseases based on available dataset. In this study, researcher extracted dataset of about 14,828 tomato leaves images from public dataset PlantVillage and after applying classification it is divided into nine classes of diseases. For developing a classifier, researcher used standard architectures AlexNet and GoogLeNet and it was trained, then they showed a better accuracy of the CNN models trained with fine-tuning as compare to models *trained* from scratch. The fine-tuning of GoogLeNet improved its accuracy from 97.71 to 99.18% and for AlexNet; the fine-tuning surprisingly increased its accuracy from 97.35 to 98.66%. In this work, authors gave

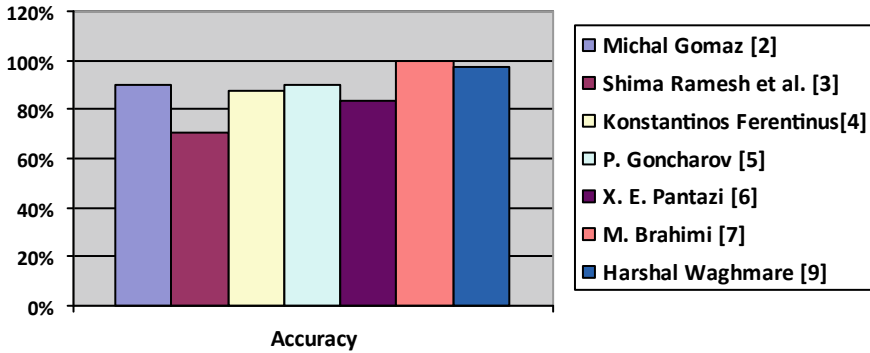


Fig. 43.2 A graphical comparative study of accuracy to detect the leaf disease

accuracy comparison of SVM with CNN and shallow models with Random Forest. Finally, they propose the occlusion experiment to visualize and then locate the plant leaves disease areas and its symptoms which can help users to provide better information on the same.

Figure 43.2 demonstrates the Graphs of comparative study for plant leaves disease detection by using different algorithm on known diseases.

43.3 Classification of Algorithm

In this section, we have given information about various machine learning algorithms used for classification of diseases in plant leaves. Its accuracy varies and entirely depends on how much plant leaves data samples taken. As per available literature, there are two classes of classification algorithm such as supervised and unsupervised classification algorithms. Figure 43.3 illustrates the various types of classification algorithms for plant leaf disease detection. The proposed classification algorithm in this research is Deep Convolution Neural Network which is a class of Deep Feed-Forward Artificial Neural Network and it consists of input, with multiple hidden layers followed by, convolutional layers, pooling layers, fully connected layers, normalization layers and output layer. Pooling reduces the mobility of features maps by condensing the production of small regions of neurons into a single output. Therefore, it reduces the ambiguity of disease identification of given sample dataset. [2].

43.4 Proposed Work

Figure 43.4 represents the proposed work based on deep convolutional neural networks (DCNNs) its breakthrough success in leaf feature extraction and classification with computer vision applications. In this paper we propose the identification of

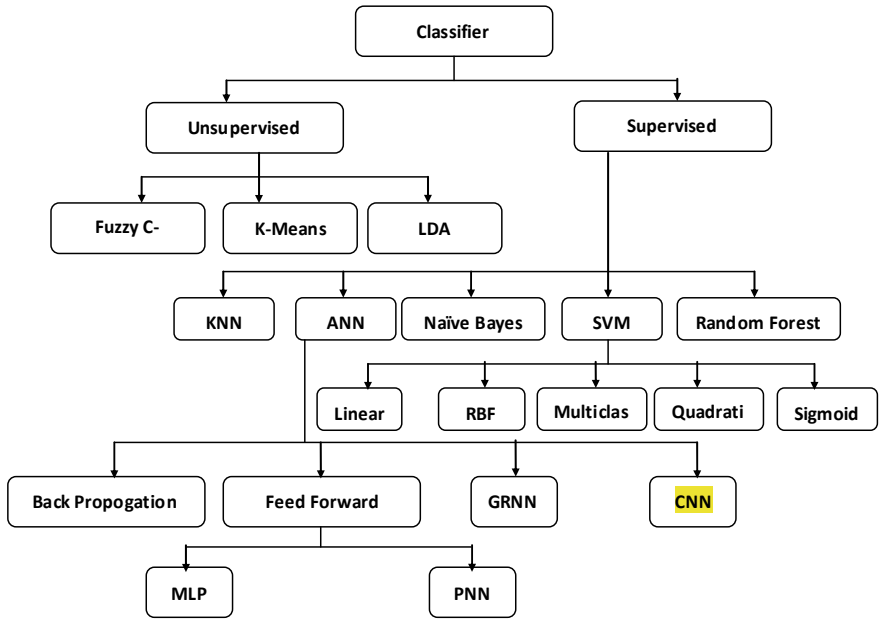


Fig. 43.3 Classification of algorithm

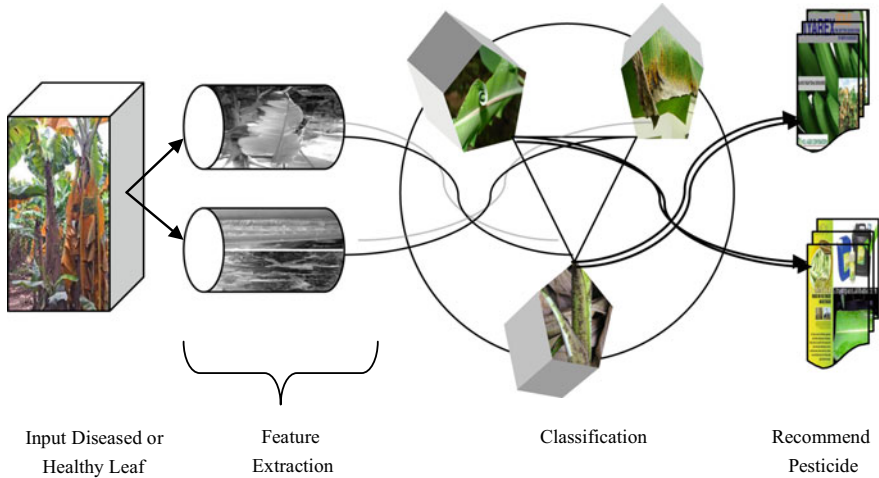


Fig. 43.4 DCNN architecture—detection of leaf disease and recommend pesticide

banana diseases such as *Fusarium oxysporum*, yellow sigatoka, *Erwinia carotovora*, *Pentalonia nigronervosa*. During the training of each DCNN, we try to train the system with live images of leaves and testing with available dataset images. We have also used the cross-entropy of loss function for all the DCNN architectures, and try to fix the number of iteration, by choosing the minimum size of matrix is of 256×256 , and also set the learning rate very small and reduce it exponentially in consequent stages [10]. Although freeing users from the troublesome we try to use handcrafted feature extraction by providing a unique and uniform feature extraction classification framework which come under DCNN architecture for various plant diseases. We also propose the genetic Deep Convolutional Neural Network, an autonomous learning algorithm for additional classification to minimize loss on the available data for some specific image classification problem. The main goal for subsequent research is to develop web application which can detect banana plant leaf diseases and it will provide automatic plant disease diagnosis with visual inspection to users.

43.5 Conclusion

This paper reviews and summarizes the various techniques used to detect diseases on plant leaves due to bacteria, fungi, and viral plant leaves [2]. The deep convolution neural network (DCNN) techniques help in automatic diseases detection of plant leaves and provide the suggestion after training the system which works on captured image or dataset image similar to captured diseased leaves. Deep convolution neural networks is more accurate even with less number of image dataset as Compared to other machine learning techniques like logistic regression, Support Vector Machine (SVM), linear discriminant analysis (LDA) and Gaussian Naïve Bayes. Research shows DCNN algorithm techniques identify plant leaf diseases by classifying them and suggests pesticides to recover from diseases at early stage of plant life. Work will carry out to investigate the use of computer vision for classifying banana leaf diseases.

References

1. Akhtar, A., Khanum, A., Khan, S.A., Shaukat, A.: Automated plant disease analysis (APDA): performance comparison of machine learning techniques. In: 2013 11th International Conference on Frontiers of Information Technology
2. Sherly Pushpa Annabel, L., Annapooranai, T., Deepalakshmi, P.: Machine learning for plant leaf disease detection and classification—a review. In: International Conference on Communication and Signal Processing, 4–6 Apr 2019, India
3. Ramesh, S., Hebbar, R., Niveditha, M., Pooja, R., Prasad Bhat, N., Shashank, N., Vinod, P.V.: Plant disease detection using machine learning. In: 2018 International Conference on Design Innovations for 3Cs Compute Communicate Control
4. Ferentinos, K.P.: Deep learning models for plant disease detection and diagnosis. *Comput. Electron. Agric.* **145**, 311–318 (2018)

5. Goncharov, P. Ososkov, G., Nechaevskiy, A., Uzhinskiy, A., Nestsiaenia, I.: Disease detection on the plant leaves by deep learning. In: Kryzhanovsky, B., et al. (eds.), *Neuroinformatics 2018*, SCI 799, pp. 151–159 (2019)
6. Pantazi, X.E., Moshou, D., Tamouridou, A.A.: Automated leaf disease detection in different crop species through image features analysis and one class classifiers. *Comput. Electron. Agric.* **156**, 96–104 (2019)
7. Waghmare, F., Kokare, R., Dandawate, Y.: Detection and classification of diseases of grape plant using opposite colour local binary pattern feature and machine learning for automated decision support system. In: 3rd International Conference on Signal Processing and Integrated Networks (SPIN) (2016)
8. Fuentes, A., Yoon, S., Kim, S.C., Park, D.S.: A robust deep-learning-based detector for real-time tomato plant diseases and pest recognition. *Sensors* **17**, 2022 (2017)
9. Brahim, M., Arsenovic, M., Laraba, S., Sladojevic, S., Boukhalfa, K., Moussaoui, A.: Deep learning for plant diseases: detection and saliency map visualization. In: 2nd International Conference on Health Sciences and Medical Technologies, Tlemcen, Algeria, 10–12 Oct 2017
10. Ma, B., Li, X., Xia, Y., Zhang, Y.: Autonomous deep learning: a genetic DCNN designer for image classification. *Neurocomputing* (2019)

Chapter 44

Analysis and Prediction of Student Data Using Data Science: A Review



Sandeep S. Ganorkar, Nandita Tiwari, and Varsha Namdeo

Abstract Development of algorithm and inferring the data is now the integral part of the data science, used for analyzing and predicting the result of the large form of database using data mining techniques. Clustering and visualization are the key process for cleaning the improper data set and using algorithm, useful parameters from the available students' data can be identified. The present paper reviews the work done by various researchers on analysis and prediction of students' data for identifying important attributes.

44.1 Introduction

The data science refers to the analysis and prediction of data collected from database of college. Student's educational result and performance are affected by many factors like personal, social, and lack of knowledge about the technology and many more [1].

The aim of every administrative authority is to introduce relevant methodologies to find the strength and weaknesses of performing students so as to award academic grades. But it is getting difficult to manage because of large form of databases. To solve this problem, data science and methodology applied for mining techniques are used for finding students educational work. The best alternative to accomplish the performance of student is to analyze factors affecting it. For various data sets like decision tree, k-nearest neighbor, regression, etc., data mining method is implemented on many important attributes like association rules, clustering, classifications,

S. S. Ganorkar (✉) · N. Tiwari · V. Namdeo
Department of Computer Science and Engineering, RKDF Institute of Science and Technology,
Sarvepalli RadhaKrishnan University, Bhopal, MP, India
e-mail: sandeep.ganorkar@gmail.com

N. Tiwari
e-mail: nandita_pandit@gmail.com

V. Namdeo
e-mail: varsha_namdeo@yahoo.com

© The Editor(s) (if applicable) and The Author(s), under exclusive license
to Springer Nature Singapore Pte Ltd. 2021

Y.-D. Zhang et al. (eds.), *Smart Trends in Computing and Communications: Proceedings of SmartCom 2020*, Smart Innovation, Systems and Technologies 182,

https://doi.org/10.1007/978-981-15-5224-3_44

and outlier detection [2]. These attributes help the authority to understand the pattern of students' academic performance.

44.2 Literature Survey

Patel in his paper [3] "Student Performance Analysis Using Data Mining Technique" implemented data mining techniques for standard procedure for analyzing student's performance in the given data set, which helps in obtaining the relevant information for further use. It involves applying various algorithms to the data for student estimation and performance.

Mohd Sharifuddin Ahmad in his paper [4] "Analyzing Students Records to Identify Patterns of Students' Performance" used data mining methods to know the parameters that are essential in understanding the academic performance of the students, which is important for taking out further inferences.

Abu Tair in his research [2] "Mining Educational Data to Improve Students' Performance: A Case Study" has applied data mining tools to enhance the credentials of the undergraduating students, obtaining low academic grades.

Pal in his paper [5] "Challenges in Data Science: A Comprehensive Study on Application and Future Trends" applied process in data mining to analyze the random data to extract useful information for enhancing the performance of slow learners.

Yassein [1] in his research article "Predicting Student Academic Performance in KSA using Data Mining Techniques" has applied data mining techniques for classifying and sorting the data into proper form for analysis. In this classification and reduction, features are used for reducing error rate.

Kabakchieva in his paper [6] "Predicting Student Performance using Data Mining Methods for Classification" worked on high potential data mining process to the university students, data, which helped in understanding the performance parameters and further improvement therein.

44.3 Proposed Methodology

44.3.1 Data Mining Techniques

Data mining is a technique applied for extracting useful information from a large database. Prime data mining methodologies, which have been executed, are association, classification, clustering, prediction, and decision tree [1]. The main technique is described which is used in the analysis of student's performance.

In the initial stage, an appropriate methodology that governs the work must be adopted as Fig. 44.1 shows.

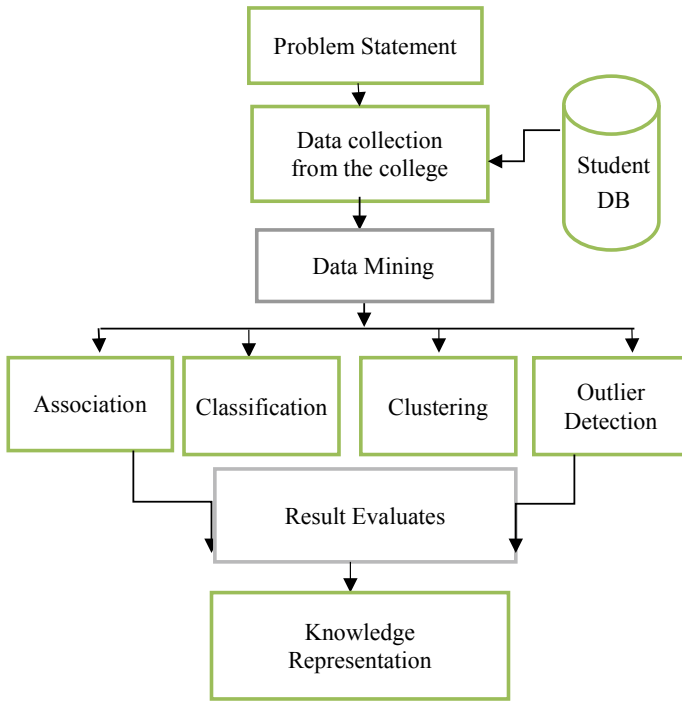


Fig. 44.1 Data mining work flow

The research problem, which is related to the data of an institution, is identified. After collection of the data, relevant data mining methods mentioned in the flowchart are used to obtain the results that give effective prediction of the students’ performance [5].

A. Classification

Data mining process is a classification technique wherein, various optimization methods like LPP, neural network, etc., are used to classify the entire data in distinct groups by learning and ordering the data. [1].

B. Clustering

Quality cluster is obtained through clustering the different sets of data using k-means algorithm [2].

C. Association Rules

Data mining rules which are most perfect find something new relationships among in the given data set as in connection with association method, FP-Growth algorithm is applied to the data set. [1].

Table 44.1 Student's data set description

Attribute	Description
Student ID	The student ID
Student name	The name of the student
Gender	The gender of the student; male or female
Date of birth	The date of birth for the student
Place of birth	The place of birth for the student
Speciality	The speciality of the student
Enrolment_year	The year of enrolment in the college
Graduation_year	The year of graduation from the college
City	The city for the student
Location	The location in the city
Address	The address of the student
Telephone	The telephone number for the student
Matriculation	GPA for the student in the matriculation
Secondary school_type	The type of the matriculation adabi or lime
Matriculation_obtained_place	The place of obtained matriculation in Palestine or other countries
Matriculation_year	The obtained year of the matriculation
College_GPA	GPA for the student in the college
Grade	The grade for the student; excellent, very good, or average

D. Outlier Detection

Outlier detection detects the data points, which are different from the others. Two distinct outlier's detection methods are present for discovering the outlier [2].

Table 44.1 shows the attributes from the students' data set and its description

44.4 Proposed Research Model

Serially the procedure is adopted for implementation model:

- Step 1: Gather the students' data (demographic and behavioral knowledge, academic credits, etc.) from the college.
- Step 2: After collecting the data set, preprocessing, and filtering the data.
- Step 3: Demonstrate data mining process (classification, clustering, and association rules) on students' data set.
- Step 4: After classifying the data, show the same in the graphical form and give the students count.
- Step 5: Perform the data science on the student data set for analyzing their performance from the generated knowledge.

Step 6: After analyzing the performance, predicting the strength and weakness in the performance by finding the most customized model from knowledge [3].

44.5 Objective of Research Model

- It is used for finding the factors affecting student’s academic performance as shown in Fig. 44.2.
- In addition, the projection is done for finding the student’s weakness and strength in their field.
- It helps to decide who is doing do best can be pushed to achieve them an excellent level in every field of college.
- On the contrary, students who are low-grade performers could be assisted to gain better achievement in their academics.
- This study is a separate part or progress is to ensure the quality of the students in their performance in a conclusive side [3].

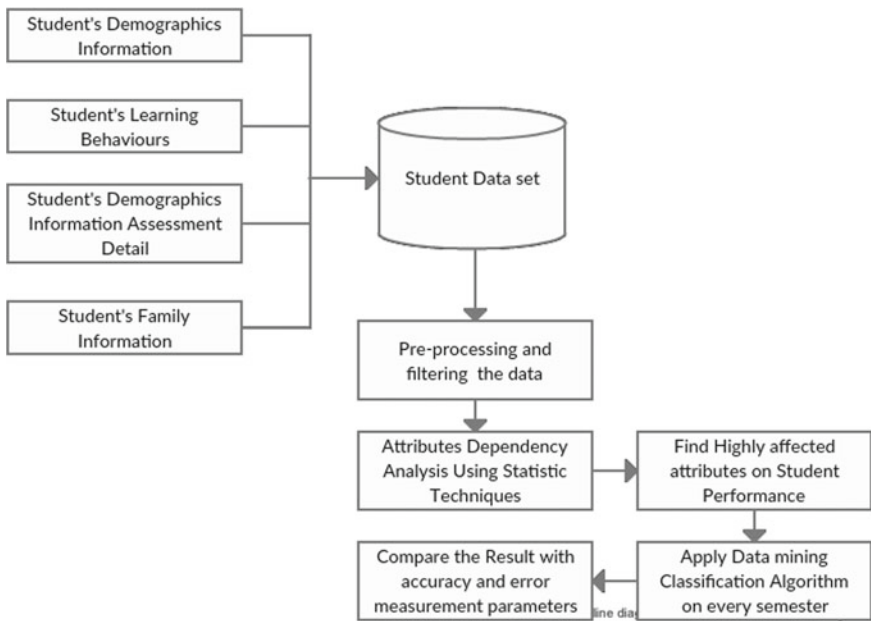


Fig. 44.2 Research model

44.6 Conclusion

From the literature reviewed, it is concluded that

1. The data mining system of working can be applied for the analysis and prediction of students' academic performance
2. To identify the important attributes from the large database
3. To identify the strength and weaknesses of the performing students and appropriate actions to be taken.

References

1. Ali, N., Yassei, R., Gaffer, M.H., Mohomad, S.B.: Predicting student academic performance in KSA using data mining technique. *J. Inf. Technol. Softw. Eng.* **7**, 5 (2017). <https://doi.org/10.4172/2165-7866.1000213>
2. Abuteir, M.M., El-Halees, A.M.: Mining educational data to improve students' performance: a case study. *Int. J. Inf. Commun. Technol. Res.* **2**(2) (2012)
3. Patel, B., Gondaliya C.: Student performance analysis using data mining technique. *IJCSMC* **6**(5), 64–71 (2017)
4. Hoe, A.C.K., Ahmad, M.S., Hooi, T.C., Shanmugam, M., Gunasekaran, S.S., Che Cob, Z., Ramasamy, A.: Analyzing Students Records to Identify Patterns of Students' Performance
5. Pal, P., Mukherjee, T., Nath, A.: Challenges in data science: a comprehensive study on application and future trends
6. Kabakchieva, D.: Predicting student performance by using data mining methods for classification. *Cybern. Inf. Technol.* **13**(1)

Chapter 45

Efficient Target Detection and Classification of SAR Images Using Z-Buffer Convolutional Neural Networks



P. Vasuki, A. Shakin Banu, S. Mohamed Mansoor Roomi, and G. Maragatham

Abstract Target detection and classification for military, geographical, and other scientific research areas are the demanding requirement. This paper aims to detect the targets effectively as well as enhances the quality of detected image before classification by deep learning techniques. A Z-buffer convolutional neural network (Z-BCNN) model consisting of two phases is more suitable for target detection, and classification of SAR image is proposed in this paper. In the first phase, the region of interest (ROI) is extracted from the background of the SAR image by means of cavity detection algorithm and elliptical Fourier descriptors are computed to describe the characteristics of target outline, whereas in the second phase, the noise present in the detected SAR image is reduced by using wavelet transform-based brute force thresholding algorithm with directional smoothing. Afterward the detection of hidden targets, classification of military vehicles from SAR images is done by using Z-buffer convolutional neural network. The proposed methodology gives significant results in terms of classification accuracy compared with the other existing algorithms.

45.1 Introduction

A synthetic aperture radar (SAR) image is a system of dynamic imaging sensors, with its all-weather, all-time capabilities, etc., and finds its application in civil and military areas. It is necessary to find out the presence of a target in a SAR image and consequently categorize the kind of the target [1–2].

P. Vasuki (✉)

Sethu Institute of Technology, Virudhunagar, Tamil Nadu, India
e-mail: vasakime@gmail.com

A. Shakin Banu

K.L.N. College of Information Technology, Sivagangai, Tamil Nadu, India

S. Mohamed Mansoor Roomi

Thiagarajar College of Engineering, Madurai, Tamil Nadu, India

G. Maragatham

UCE – Dindigul, Anna University, Silvarpatti, Tamil Nadu, India

© The Editor(s) (if applicable) and The Author(s), under exclusive license to Springer Nature Singapore Pte Ltd. 2021

Y.-D. Zhang et al. (eds.), *Smart Trends in Computing and Communications: Proceedings of SmartCom 2020*, Smart Innovation, Systems and Technologies 182,

https://doi.org/10.1007/978-981-15-5224-3_45

Target detection in automatic target recognition is performed in order to detect and locate the presence of region of interest (targets) in the SAR image. The most frequently used method for SAR image target detection is the constant false alarm rate (CFAR) [3] that detects the presence of targets by finding difference in statistical model between the target and the background. The performance of the CFAR detection algorithm is good for simple scenes consisting of single target in homogeneous background. However, the detection accuracy of the CFAR method of target detection is low for complex scenes consisting of multiple targets, and also, there are more false alarms. Yang et al. [4] proposed the rotation and scale invariant Hu moments for extracting the features. He also proposed principal component analysis (PCA) and independent component analysis (ICA). Even though PCA gives good results, it is complex to compute the eigen decomposition values of the covariance matrix. Similarly, the ICA does not give much better results compared to PCA. To overcome the above-said drawbacks, we propose a segmentation stage to isolate the target region from the background of the SAR image by using cavity detection algorithm followed by computation of target outline descriptors called elliptical Fourier descriptors (EFDs) for addressing target detection of SAR images which describe any closed contour. EFD not only describes effectively the target region contours, they were also more economic in denoting the representation of contour outlines than any other descriptors.

SAR image despeckling algorithms are divided into two: spatial domain filters and frequency domain methods. The existing spatial domain filters available for speckle reduction in SAR images are mean, median, Lee, Kaun, Kalman, Frost and maximum a posteriori filters, etc. Even though these spatial domain filters are better in terms of speckle suppression, they loss significant details. Hence, we go for frequency domain methods. In frequency domain methods, wavelet-based despeckling algorithms [5–6] are proposed by some researchers since it provides multi-resolution decomposition for analysis of image. In recent years, wavelet-based thresholding methods are adopted for despeckling process such as wavelet-based soft or hard threshold [7, 8], wavelet-based Bayesshrink, Visushrink, sureshrink, oracle thresh, etc. These thresholding algorithms suffer from some drawbacks. This paper proposes a wavelet transform-based brute force Thresholding along with directional smoothing performs better speckle reduction as well as protecting the edges than other existing thresholding techniques.

The deep learning algorithms have proved to give accurate results in target classification of SAR images due to their automatic feature extraction capability. Xing et al. proposed classification algorithms such as support vector machine [9] and sparse representation [10]. Lin et al. proposed dictionary learning [11] to perform classification. Vasuki et al. proposed neural network-based classification algorithms for SAR images [11, 12] Although these classifiers provide better performance, the features are to be designed carefully while there are large number of targets present in the image. To overcome the above-mentioned drawback, the deep learning-based methods are divided into three: the deep belief network (DBN) [12], the auto encoder (AE) [13], and the convolutional neural network (CNN) [14]. In DBN and AE, optimization is carried out by unsupervised training and supervised tuning of the parameters.

But for CNN, the features are trained by the forward pass and backpropagation. Similarly for AE and DBN, the spatial information is certainly vanished but CNN can protect the spatial information since the input given here is 2D. Also there is a need to detect the hidden targets from the SAR Images. Hence in this paper, a CNN-based SAR image target classification algorithm called Z-buffer CNN has been proposed for detecting the hidden targets and classifying the military vehicle targets from SAR images effectively.

The organization of this paper includes proposed methodology, experimentation, and conclusion.

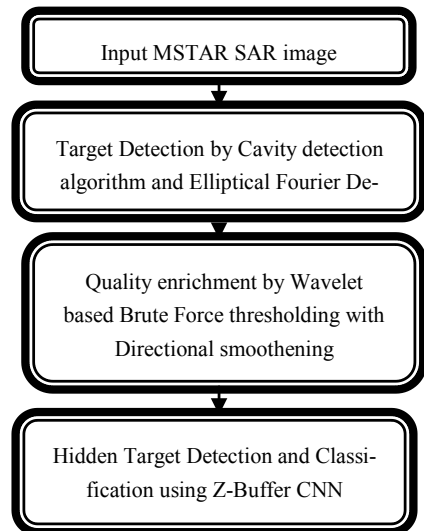
45.2 Proposed Methodology

The pipeline of Z-buffer conventional neural network (Z-BCNN) is shown in Fig. 45.1.

The proposed target detection and classification algorithm consist of two phases: **In first phase** of *Target Detection*,

- From the input SAR image, the interested targets are segmented from the background by using the cavity detection algorithm. Then after that the fine sharp region boundaries of the target pixels are obtained by using the elliptical Fourier descriptor segmentation method.

Fig. 45.1 Pipeline of the proposed methodology



In second phase of Target *Classification*,

- The output of the first phase is investigated for strong and varying speckle noise. The quality of the output of the target detection phase has been enhanced through wavelet-based brute force thresholding with directional smoothening method, and then the despeckled image can be again examined for any other hidden objects after that classification of target military vehicles from SAR images is done by using the Z-buffer CNN.

45.2.1 Target Detection by Cavity Detection Algorithm

The cavity detection algorithm used for segmenting the region of interest (ROI) from the background mainly consists of the three steps: computing horizontal and vertical Gauss blur, computing edges, detecting the roots.

45.2.2 Elliptical Fourier Descriptors for Target Outline Description

In automatic target recognition, there is a need for describing the contours of target outlines and elliptical Fourier descriptors (EFD) are used for obtaining the fine sharp region boundaries of original targets which are very helpful to detect and locate the target effectively in the SAR images. The elliptical Fourier descriptors are parametric representation fit into the harmonically related ellipse.

45.2.3 Quality Enrichment Using Wavelet-Based Brute Force Thresholding and Directional Smoothing

The output image obtained from the target detection stage is checked for the presence of speckle noise by decomposing into wavelet sub-bands and applying thresholding. The directional smoothing filter is then applied to obtain details of the image [15, 16].

45.2.4 Hidden Target Detection and Classification Using Z-Buffer Convolutional Neural Network

Normally, SAR images consists of non-transparent or invisible objects and targets, and it is not possible to see those targets which are hidden behind the objects by eye,

and hence, there is a need to detect those hidden targets from the background. The Z-buffer method is a hidden target detection method to check the Z-depth of each surface to identify the hidden surface.

The convolutional neural network (CNN) is a one of the deep learning methods used for image analysis tasks such as denoising in the images, object detection, image classification, and shape recognition. The various layers in the conventional convolutional neural network are convolutional, rectification linear unit, pooling, and fully connected layers.

45.3 Experimentation

In order to quantify the proposed algorithm, performance measures such as classification accuracy, precision, recall, and F-measure were computed.

We adopt a SAR image containing multiple military targets for experimentation.

45.4 Performance Analysis

Tables 45.1, 45.2, 45.3, 45.4, 45.5, 45.6 and Figs. 45.2, 45.3, 45.4 show that the classification accuracy, precision, recall, and F-measure (%) of proposed methodology is high compared with the existing methodology of despeckling and classification coupled CNN (DCC-CNN).

Table 45.1 Training and testing sets of ten class MSTAR dataset

Military vehicle image	No. of. training images (depression angle 17°)	No. of. testing images (depression angle 15°)
BMP2	233	195
BRDM2	298	274
BTR60	256	195
D7	299	274
T72	232	196
ZIL131	299	274
ZSU234	299	274
Total images	2747	2425

Table 45.2 Confusion matrix table of the proposed method

	BMP2	BRDM2	BTR60	D7	T62	T72	2S1	ZIL131	ZSU23 4	Accuracy (%)
BMP2	190	1	0	1	0	1	0	1	1	97.4
BRDM2	0	273	0	0	0	1	0	0	0	99.6
BTR70	0	0	256	0	0	2	0	0	0	99.2
D7	0	0	0	273	0	0	0	0	1	99.6
T62	0	0	0	0	271	0	1	1	0	99.3
T72	0	0	0	0	0	196	0	0	0	100
2S1	0	0	1	0	0	0	272	0	1	99.6
ZIL131	0	0	0	0	0	0	0	273	1	99.6
ZSU23 4	0	0	1	0	0	1	0	0	273	99.2

Table 45.3 Comparison of classification accuracy (%)

Parameter value	DCC-CNNs [5]	Z-Buffer CNN (proposed)	PCA and ICA [17]	Deep CNN [18]
10	80.5	92.5	91.4	92.1
20	80.2	93.2	92	93
30	86.1	99.3	97.5	97.8
40	92.3	97.3	96.1	96
50	91.9	97.4	96.6	96.5
60	69.3	98.2	97.1	98
70	88.6	100	99	99.2
80	85.7	95.7	94	93.9
90	82.4	92.4	91.9	92
100	90.8	99.0	98	98.3
Average	93.4	96.5	95.3	95.6

Table 45.4 Comparison of recall (%)

Parameter value	DCC-CNNs [5]	Z-buffer CNN (proposed)	PCA and ICA [17]	Deep CNN [18]
10	92.3	96.72	94.2	92.1
20	95.6	97.85	96.5	95
30	95.6	97.85	95	96
40	95.6	97.85	91	92.9
50	95.6	97.85	91	92.9
60	95.6	97.85	91	92.9
70	95.6	97.85	91	92.9
80	95.6	97.85	91	92.9
90	95.6	97.85	91	92.9
100	95.6	97.85	91	92.9
Average	95.2	97.7	92.2	93.34

45.5 Conclusion

This paper proposes an algorithm for detection of hidden targets and classification of targets from SAR images using Z-Z-buffer conventional neural network (BCNN). Here the cavity detection algorithm was first applied on the input SAR image to separate the ROIs from the background, whereas the elliptical Fourier descriptors are applied to retain the discriminatory information and to obtain closed contours of the extracted target region. Then the quality of the SAR image is enhanced by using wavelet-based brute force thresholding with directional smoothing. After that the hidden target detection and the classification of SAR images are performed using

Table 45.5 Comparison of precision (%)

Parameter value	DCC-CNNs [5]	Z-buffer CNN (proposed)	PCA and ICA [17]	Deep CNN [18]
10	90.8	92.36	91.0	92
20	91.32	92.84	91.2	92.1
30	91.74	93.65	92	92.5
40	92.05	93.77	92.4	92.7
50	92.48	94	93.2	92.9
60	92.76	94.25	93.5	93.2
70	93	94.68	93.7	93.4
80	93.47	94.97	93.9	93.6
90	93.59	95.02	94.3	93.9
100	93.99	95.49	94.7	94
Average	92.5	94.1	92.9	93

Table 45.6 Comparison of F-measure (%)

Parameter value	DCC-CNNs [5]	Z-buffer CNN (proposed)	PCA and ICA [17]	Deep CNN [18]
10	81.25	85.9	84.3	82
20	85.32	87.9	84.69	83.1
30	90	91	85.02	83.9
40	91.26	92	85.64	84.2
50	91.74	92.8	85.99	85.5
60	92.68	93.1	86.12	86.7
70	92.84	93.8	86.56	87.7
80	93.15	94	87.09	88.1
90	93.40	94.5	87.28	89
100	93.54	94.5	87.48	90
Average	90.5	91.9	86	86

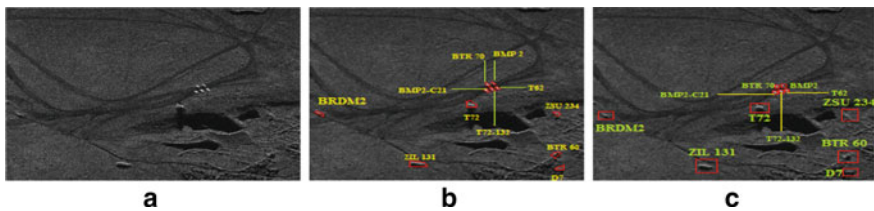


Fig. 45.2 Target detection output. **a** Large scene SAR image. **b** Extracting ROIs using cavity detection algorithm. **c** Extracting target outlines using EFDs

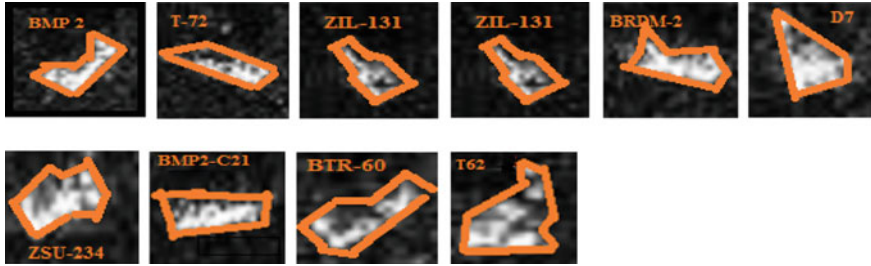


Fig. 45.3 Target detection outputs of various MSTAR dataset SAR images

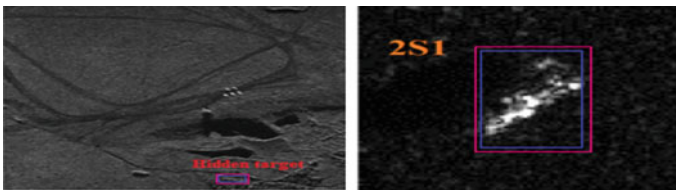


Fig. 45.4 Hidden target detection using Z-buffer technique

the Z-BCNN. The proposed methodology yields a classification accuracy of 99.3% which is high compared to the existing methodology. If more number of training images are taken for experimentation, execution time will be more. It would be more interesting to consider training networks like ResNet, VGGNet, and GoogleNet for automatic target classification algorithms.

References

1. Xing, X., Ji, K., Zou, H., Chen, W., Sun, J.: Ship classification in TerraSAR images with feature space based sparse representation. *IEEE Geosci. Remote Sens. Lett.* **10**, 1562–1566 (2013)
2. Yang, Y., Qiu, Y., Lu, C. (n.d.). Automatic target classification—experiments on the MSTAR SAR Images. In: Sixth International Conference on Software Engineering, Artificial Intelligence, Networking and Parallel/Distributed Computing and First ACIS International Workshop on Self-Assembling Wireless Networks (SNPD/SAWN '05). <https://doi.org/10.1109/snpd-sawn.2005.25>
3. Gao, G., Liu, L., Zhao, L., Shi, G., Kuang, G.: An adaptive and fast CFAR algorithm based on automatic censoring for target detection in high-resolution SAR images. *IEEE Trans. Geosci. Remote Sens.* **47**(6), 1685–1697 (2009)
4. Yang, Y., Qiu, Y., Lu, C.: Automatic Target Classification Experiments on the MSTAR SAR Images. *SNPD/SAWN'05*, pp. 2–7 (2005)
5. Vasuki, P., Mohamed Mansoor Roomi, S.: Automatic noise identification in images using moments and neural network. In: International IEEE Conference on Machine Vision and Image Processing, PSGTECH, Coimbatore (2012)
6. Vasuki, P., Mohamed Mansoor Roomi, S.: Particle swarm optimization-based despeckling and decluttering of wavelet packet transformed synthetic aperture radar images. *J. Appl. Remote*

- Sens. **7** (2013)
7. Guo, H., Odegard, J.E., Lang, R.A. Gopinath, Selesnick, I., Burrus, C.S.: Speckle reduction via wavelet shrinkage with application to SAR based ATD/R. In: Technical Report CML TR94-02, CML, Rice University, Houston (1994)
 8. Zhang, X.P.: Thresholding neural network for adaptive noise reduction. *IEEE Trans. Neural Netw.* **12**(3), 567–584 (2001)
 9. Chen, G., Liu, X.: Wavelet-based despeckling SAR images using neighbouring wavelet coefficients. In: Proceedings of IEEE (2005)
 10. Huang, Z., Pan, Z., Lei, B.: Transfer learning with deep convolutional neural network for SAR target classification with limited labeled, Data Received: 7 July 2017; Accepted: 28 August 2017; Published: 31 August 2017
 11. Perumal, V.: Automatic target classification of manmade objects in synthetic aperture radar images using Gabor wavelet and neural network. *J. Appl. Remote Sens.* **7**, 073592-1 (2013). <https://doi.org/10.1117/1.JRS.7.073592>
 12. Vasuki, P.: Automatic target classification in SAR images by multilayer back propagation neural network. *Res. J. Appl. Sci. Eng. Technol.* 2040-7467, vol. 4, pp. 5510–5514 (2012)
 13. Hou, B., Kou, H., Jiao, L.: Classification of polarimetric SAR images using multilayer autoencoders and superpixels. *IEEE J. Sel. Top. Appl. Earth Obs. and Remote Sens.* **9**(7), 3072–3081 (2016). 10.1109/JSTARS.2016.2553104
 14. He, S., Lau, R., Liu, W., Huang, Z., Yang, Q.: SuperCNN: a uperpixelwise convolutional neural network for salient object detection. *Int. J. Comput. Vision* **115**(3), 330–344 (2015). <https://doi.org/10.1007/s11263015-0822-0>
 15. Donoho, D.L., Johnstone, I.M.: Adapting to unknown smoothness via wavelet shrinkage. *J. Am. Stat. Assoc.* **90**(432), 1200–1224 (1995)
 16. Chang, S.G., Yu, B., Vetterli, M.: Adaptive wavelet thresholding for image denoising and compression. *IEEE Trans. Images Process.* **9**(9), 1532–1546 (2000)
 17. Yang, Y., Qiu, Y., Lu, C.: Automatic target classification—experiments on the MSTAR SAR images. In: Sixth International Conference on Software Engineering, Artificial Intelligence, Networking and Parallel/Distributed Computing and First ACIS International Workshop on Self-Assembling Wireless Networks (SNPD/SAWN'05) (n.d.). <https://doi.org/10.1109/snpd-sawn.2005.25>
 18. Huang, Z., Pan, Z., Lei, B.: Transfer learning with deep convolutional neural network for SAR target classification with limited labeled Data Received: 7 July 2017; Accepted: 28 August 2017; Published: 31 August 2017
 19. Vasuki, P., Mohamed Mansoor Roomi, S.: Noise variance estimation in SAR images using wavelets and filter selection. In: International IEEE Conference on Computing Communication and Networking Technologies, ICCCNT '2013, Vivekananda College of Engineering for Women, Tiruchengode (2013)
 20. Lang, H., Wu, S., Xu, Y.: Ship classification in SAR image improved by AIS knowledge transfer. *IEEE Geosci. Remote Sens. Lett.* **15**, 439–443 (2018)

Chapter 46

Context-Aware Deep Convolutional Neural Network Application for Fire and Smoke Detection in Virtual Environment for Surveillance Video Analysis



Akm Ashiquzzaman, Sung Min Oh, Dongsu Lee, Jihoon Lee, and Jinsul Kim

Abstract Detecting fire and smoke in video footage is crucial that is surveillance analysis. In a disastrous situation or after the accident occurred, it is vital to pinpoint the origin and gathers proper context. However, processing the data this kind of video is often labor-intensive and needs human assistance and moderation. In this research, we have proposed a trained neural network that van detects the fire and smoke from the images and combined this model to the context-aware video analysis. The module first detects the context-based images or the important images from the video frame with time sources which later processed by the deep convolutional neural network for assisting and detecting fire and smoke. We also implemented this model in the virtual environment for quick deployment and universal using ability. The deep convolutional neural network was trained with state-of-the-art normalizing method for maximum accuracy (99%). As a result, this novel analytic application can be a unique and state-of-the-art tool for surveillance video analysis.

A. Ashiquzzaman · S. Min Oh · D. Lee · J. Lee · J. Kim (✉)
School of Electronics and Computer Engineering, Chonnam National University,
Gwangju, South Korea
e-mail: jsworld@jnu.ac.kr

A. Ashiquzzaman
e-mail: zamanashiq3@gmail.com

S. Min Oh
e-mail: osm5252kr@gmail.com

D. Lee
e-mail: ready1819@gmail.com

J. Lee
e-mail: suda43@gmail.com

© The Editor(s) (if applicable) and The Author(s), under exclusive license
to Springer Nature Singapore Pte Ltd. 2021

Y.-D. Zhang et al. (eds.), *Smart Trends in Computing and Communications: Proceedings of SmartCom 2020*, Smart Innovation, Systems and Technologies 182,
https://doi.org/10.1007/978-981-15-5224-3_46

46.1 Introduction

Fire and smoke damages are one of the leading disasters in modern human civilization. As society and technologies are getting complex with wider ranges of application, the risk of fire and smoke damages is increasing with them. Especially, modern factories and automated homes often control machines and fire and smoke detection in real time are an absolute necessity for these environments. The early detection of fire and smoke can seriously reduce the damage and help the industries to automate the whole process with the more safer standards. According to the report by the Center of Fire Statistics (CTIF), Europe, in the twenty-first century had the reported 2–2.5 million fire incidents with 20,000–30,000 approximate death with double the injury [4]. This indicates the importance of fire and smoke detection and incident pinpoint for smart detection. The modern transportation system is also very prone to fire and smoke damage. In the Republic of Korea, 5595 cases 12.75% from a fire causing the entire facilities to burn down or caused partial damages [14].

In addition to advancing computer vision and image processing, video-based fire detection is essentially a surprisingly common innovation with noteworthy benefits over conventional methods, such as rapid response and a wide area of identification. Smoke is the indicator for fire forecasting, and identification of smoke offers earlier fire extinguishers than a prediction of flames. But the main shortcomings of the traditional methods are there are fairly manual feature extractors or filter-based system that heavily relies on handcrafted feature selection. With the rise of video surveillance and generation to complete scene-aware algorithms, the fire and smoke detection is a very prominent field for this type of application as there are not advanced content detection algorithms.

In this study, one of our achievements is that we proposed a deep learning convolutional neural network (DCNN) for fire and smoke identification. To the best of our knowledge, the earlier literature does not quite produce a standard dataset and evaluation protocol which makes it hard to compare different methods for identifying fire and smoke. We gathered the series of fires from some prior literature and our own dataset and made a video to image framing algorithm for deep learning to understand and classify. We expect this benchmark can facilitate future researches in this area. We also experimented with the neural network pruning to make an effective neural network that can solve the problem of high computation load in the neural networks in the remote server situation. Context-aware and threshold-based video footage analysis to extract images will help the DCNN to process less important frames over important frames and make faster result outcome. The rest of the paper is progressing as follows. Section 46.2 discusses the previous work and shortcomings. Section 46.3 discusses the proposed method, and Sect. 46.4 presents the analysis of our experiments and the results. Section 46.5 discusses the future work and application thus end to the conclusion.

46.2 Related Works

Even though there was much research especially focused on fire and smoke detection from images and videos, the majority of the research lacks real-life application feasibility. Most of the modern data and image processing research also do not focus on CNN-based applications. The traditional method applies various filters and kernel-based feature selection such as histogram of gradient (HOG)[1] filter of Gabor filter. These systems are very easy to implement but prone to human bias selection and skewed accuracy for manual feature selection. This leads to a custom solution for detection that often renders impractical into real-life dynamic situations [9].

The main use case of the open and closed environment fire and smoke detection is early detection. Most of the common cases for building such a system rely heavily on the process of selecting these smoke and another fire precursor in the feature extraction with traditional feature extraction algorithms and the detect it with machine learning or statistical method to classify or predict. The research conducted by Gubbi et al. [8] detects the smoke in videos with wavelets and SVM. This process is effective but the accuracy of this model is high on very specific datasets, and detailed validation on the generalized dataset was not conducted.

According to the research conducted by Appana et al. [2], a video-based smoke detection scheme for smoke flow pattern detection and the analysis of the smoke spatial-temporal energy analysis were done to make an alarm system. This type of system heavily relies on Gabor filters to detect the smoke in the present video image frame flow [13]. However, the Gabor filter is prone to fail in environmental background noise and extreme background change. Scarcity of images or real samples of videos is also the main problem of these traditional models. As these models learning is not generalized, these models usually perform very crude to practically unreliable in real-life deployment as monitoring systems.

Tao et al. [16] proposed a deep convolutional neural network for smoke detection, and the process has a very high accuracy for detecting some videos. However, the scope of fire was not included in the detection and the system is not applicable in fire and smoke both detection in real life. Zhang et al. [17] proposed a DCNN for detecting forest fire based on similar DCNN algorithms, and their later research has a significant improvement for forest fire detection with faster R-CNN detection. But this research was done with synthetic smoke images which often varies in real-life situations. The main research was also condensed in specific fire detection in forest scenario which is the majority of the outside environment with satellite images.

All of the related research gave a great pathway for modern DCNN for environmental neural fire and smoke detection based on the video and images. Rise of a present-day closed-circuit camera and live feed-based surveillance camera usually records a long video. Most of these systems are very stable with context, and the frame by frame analysis usually renders wastage of computation. In this research, the context-aware and threshold-based image extraction from the video were mainly researched to pinpoint fire and smoke incidents in the videos. Integration of context-aware of threshold base image frame extractor from video with smoke and fire detec-

tion will help offload computation overhead. This will eventually make the DCNN faster and feasible to deploy in the video footage analysis and real-time monitoring faster and lightweight applications. Our research was focus based on this principle to develop a model that will detect context-aware images from the video and detect fire or smoke within the image to classify.

Neural network pruning is a term used for removing the least activated neuron on a neural network in each data flow, and based on some ranking of these nodes, the least activated neural network nodes were cut off and the DCNN then trained into achieving same or more accuracy with lightweight post pruned self. The idea was first proposed by Lecunn [10]. There is a practical application with neural network pruned in cloud computing as the pruned neural network in a compact and less computation need for achieving for the same or more accurate classification [3]. In the next Sect. 46.3, we have proposed the DCNN architecture for classifying fire and smoke in images in both real-time and past footage analysis. We also have introduced a new training methodology with network pruning to make compact fast DCNN.

46.3 Proposed Method

In this section, we will discuss our proposed method for context-aware DCNN and the architecture of the given DCNN with the data augmentation-based training strategy and neural network pruning.

In the 1960s, Hubel and Wiesel found that the visual cortex of cat and monkey comprises neurons that respond independently to small areas of the visual field [11]. Convolutional neural network's main idea is emerged from the principle of doing input matrix convolution to manipulate edge features for understanding and recognizing the network. Lecunn et al. [12] first used convolutional neural networks successfully with a backpropagation algorithm to optimize and gradient update. The new neural network paradigm prevailed in 2012 and opened the door for using CNN in various applications for image classification. A deep feed artificial neural network models are being developed by CNN, which now represents a crucial tool for the processing of visual images.

Convolution processing generates high value for a given position if there is a convolution function in that region; otherwise, a low value is generated. More precisely, we take the element-wise multiplication of each kernel cell value and the corresponding image pixel value overlapping the kernel cell at a given position of the convolution matrix and then take the sum of it. The precise value is then calculated as follows.

$$h_{i,j} = \sum_{k=1}^m \sum_{l=1}^m w_{k,l} * x_{i+k-1,j+l-1} \quad (46.1)$$

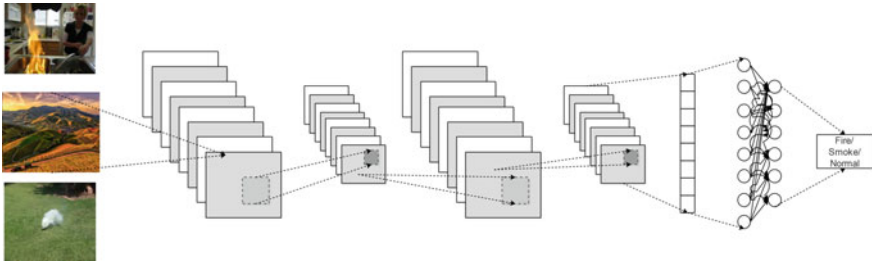


Fig. 46.1 Proposed CNN for fire and smoke detection

Here the convolutional output h with w kernel with (m, m) dimension that works on the input matrix x .

The layer of pools (or so-called sub-samples) is invariant CNN with regard to the output of the convergence. There are two various practically used pooling mechanisms (max pooling and average pooling). For contrast with normal pooling, pooling also referred as to peak pooling. More specifically, the pooling process emits the full input value in a certain location within the kernel. So mathematically,

$$p_{i,j} = \max(x_{i+k-1,j+l-1}) \tag{46.2}$$

as the polling operation reduces the size between convolution and reduced convolution operation and makes shift the features into the centre eventually.

In our CNN model, there are eight convolutional layers and ELU [6] is used as the activation function. The image size $(224, 224, 3)$ is the input to layer 1 which is convoluted by the kernel of 3×3 size and of 64 combinations, and after dropping 25% layer, 2 begins with the size of 224×224 and of 64 combinations. Now, the convolution layers were varied, and thus so until we got 10 convolutional layers. Now this will be flattened into a one-dimensional array. Thus, feature extraction procedure is completed. The classification consists of a 1 input layer, two hidden layers and one output layer. The input layer consists of 256 neurons which are fully connected to the hidden layer 1 (contains 256 neurons). After 50% dropping [15], this will be forwarded to the output layer (contains 3 neurons) through hidden layer 2 (contains 128 neurons) with the same procedure and dropping percentage. From the output layer, we calculate the output using the softmax function. The proposed DCNN simplified is shown in Fig. 46.1.

SceneDetect is an algorithm that analyses a video looking for scene changes or cuts. The output time codes can then be used with another tool to split the video into individual clips. But the main application in the context-aware algorithm in this setting is to extract the important scene cut of the images rather than processing every frame of the videos. This will take a long time, and eventually, the size of the neural network will be slow. Figure 46.2 shows the neural network context-aware module part that processes the video based on a threshold change to detect the change of context. So the proposed neural network only processes the time-stamped image

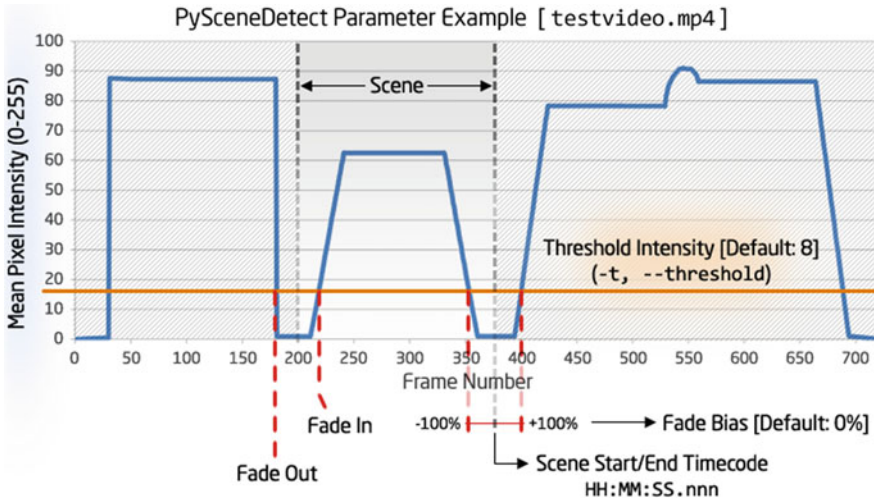


Fig. 46.2 Context-aware/threshold scene detection algorithm

frame of the context-aware video analysis output to get the final result. Hu et al. [10] proposed to explore sparsity inactivation for network pruning. Exponential linear unit (ReLU) [6] activation function imposes sparsity during inference, and the average percentage of positive activation at the output can determine the importance of the neuron. L1 normalization is useful to estimate the saliency of feature maps in a given layer. This idea can be used to make the order of ranking of filters in each layer. So the trained neural network is then pruned to make compact size with the same accuracy to make proper results with less computation overhead.

46.4 Experiments and Results

These models were developed in Keras [5] and Tensorflow, a python focused torch framework for deep learning simulations, at the Python-based open-source repository. The Nvidia CUDA Library was used to speed up the training cycle with the aid of dual Nvidia Geforce 2080-Ti GPU instance, which has a total of 64 Gb DDR4 RAM on a device with Intel i7 8 core CPU. There is 8 GB VRAM in the above GPU. Throughout Hadoop file systems (HDFS), all of the trained weights are preserved for security purposes. The neural network was educated to unsure correct generalization using the data increase model (Fig. 46.3).

The dataset that was used for both training and testing the DCNN was collected from [7]. The dataset contains 8 fire videos, 6 smoke videos and 13 normal video to distinguishes between natural phenomena to reduce false positive. The dataset video was then read with proper codes and then processed with OpenCV to make

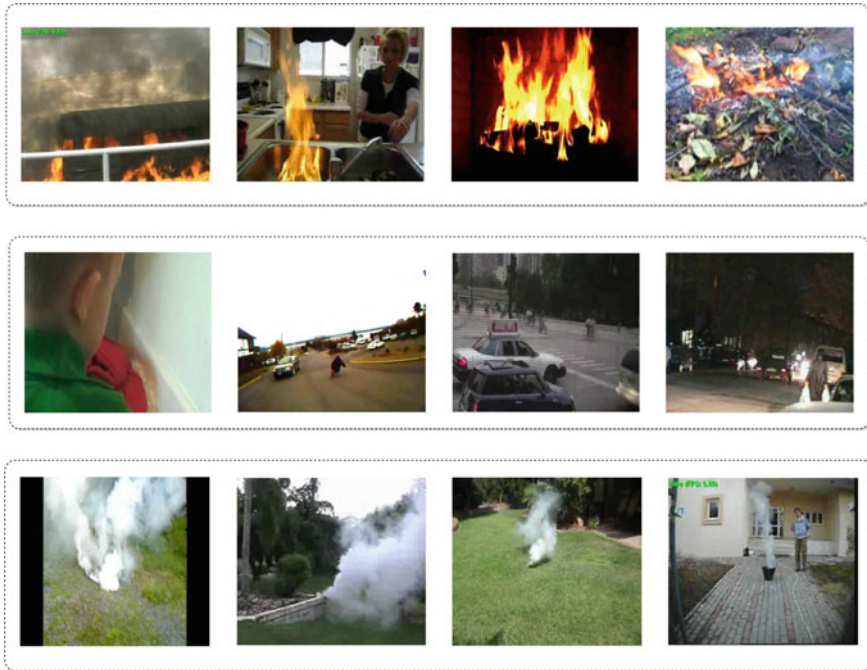


Fig. 46.3 Dataset examples for fire, smoke and normal scenario

frame form with videos. This rendered into an image dataset that is fed into the neural network. The training process is also heavily augmented with programmed random rotation on both horizontal and vertical axes with shifting and zoom in and out in a random fashion to unsure maximum general learning. The best training of the DCNN was achieved in the 100 epoch, and then it gets into 92% accurate. Later the node pruning was done to reduce the network size. Only the convolutional layered was pruned in this experiment. The idea of neural network pruning is data independent. This implies to the fact all of the datasets, regardless of the variation factor can be adapted to the DNN pruning methodology. For this study, the DNN study was experimented in various handwritten digit datasets to verify its utility. Before the original DCNN had 7, 962, 467 parameters. After 7, 569, 857 parameters were pruned based on the L1 normalization-based filter ranking. The pruned and new saved model has the final 392,610 parameters pruned. This is the ratio of. 1.05% compression. This model will later perform 89% accurately to the training dataset and the context-aware system also had the 50 computation reduction rate. This means that the original frame check of the neural network gets reduced by 50% in any given video as the context-aware takes only the half-frame to classify as fire or smoke.

46.5 Conclusion

Convolutional neural networks nowadays make a huge impact on fire and smoke detection systems. Although the fire and smoke detection with image processing is not a new process, implementing the deep convolutional neural network is the latest technology regarding detecting fire and smokes. There is some work that produced DCNN is very highly accurate. In this research, we have proposed a new type of DCNN that is combined with content-aware technology. The content-aware technology greatly reduces computational load and thus makes this model every fast and lightweight to run. Moreover, we have combined a pruning technology that will reduce the parameter of the neural network within border terms and make a mode compact DCNN, that is, suitable for lightweight cloud computing and IoT-based applications.

Acknowledgements The Institute for Knowledge & Communications Technology Promotion (IITP), which was controlled by the Minister of Science and ICT (MSIT), Korea, under the funding scheme of ITRC(IITP)(IITP-2020-2016-0-00314). The work was also sponsored by the Korea National Research Foundation's (NRF) provided basic research system (MEST) (Grant No. NRF 2017R1D1A1B03034429), which is a system provided by the Ministry of Education, Science and Technology.

References

1. Ahmed, E., Shakhnarovich, G., Maji, S.: Knowing a good hog filter when you see it: efficient selection of filters for detection. In: European Conference on Computer Vision, pp. 80–94. Springer, Berlin (2014)
2. Appana, D.K., Islam, R., Khan, S.A., Kim, J.M.: A video-based smoke detection using smoke flow pattern and spatial-temporal energy analyses for alarm systems. *Inform. Sci.* **418**, 91–101 (2017)
3. Ashiquzzaman, A., Van Ma, L., Kim, S., Lee, D., Um, T.W., Kim, J.: Compacting deep neural networks for light weight iot & scada based applications with node pruning. In: 2019 International Conference on Artificial Intelligence in Information and Communication (ICAIIIC), pp. 082–085. IEEE (2019)
4. Brushlinsky, N., Ahrens, M., Sokolov, S., Wagner, P.: World fire statistics. Center of fire statistics. 2006 Report (10) (2016)
5. Chollet, F.: keras. <https://github.com/fchollet/keras> (2015)
6. Clevert, D.A., Unterthiner, T., Hochreiter, S.: Fast and accurate deep network learning by exponential linear units (elus). arXiv preprint [arXiv:1511.07289](https://arxiv.org/abs/1511.07289) (2015)
7. Foggia, P., Saggese, A., Vento, M.: Real-time fire detection for video surveillance applications using a combination of experts based on color, shape and motion. *IEEE Trans. Circ. Syst. Video Technol.* (2015)
8. Gubbi, J., Marusic, S., Palaniswami, M.: Smoke detection in video using wavelets and support vector machines. *Fire Saf. J.* **44**(8), 1110–1115 (2009)
9. Hall, M.A.: Correlation-based feature selection for machine learning (1999)
10. Hu, H., Peng, R., Tai, Y., Tang, C., Trimming, N.: A data-driven neuron pruning approach towards efficient deep architectures. arxiv preprint. [arXiv preprint arXiv:1607.03250](https://arxiv.org/abs/1607.03250) (2016)

11. Jung, R., Kornhuber, H., Da Fonseca, J.S.: Multisensory convergence on cortical neurons neuronal effects of visual, acoustic and vestibular stimuli in the superior convolutions of the cat's cortex. *Progr. Brain Res.* **1**, 207–240 (1963)
12. LeCun, Y., Bengio, Y., et al.: Convolutional networks for images, speech, and time series. In: *The Handbook of Brain Theory and Neural Networks*, vol. 3361(10) (1995)
13. Mehrotra, R., Namuduri, K.R., Ranganathan, N.: Gabor filter-based edge detection. *Pattern Recogn.* **25**(12), 1479–1494 (1992)
14. Song, J.Y., Sa, S.H., Nam, J.W., Cho, Y.J., Kim, J.P., Park, N.K.: Analysis on vehicle fires caused by damage of diesel particulate filter (DPF). *Fire Sci. Eng.* **26**(4), 70–76 (2012)
15. Srivastava, N., Hinton, G.E., Krizhevsky, A., Sutskever, I., Salakhutdinov, R.: Dropout: a simple way to prevent neural networks from overfitting. *J. Mach. Learn. Res.* **15**(1), 1929–1958 (2014)
16. Tao, C., Zhang, J., Wang, P.: Smoke detection based on deep convolutional neural networks. In: *2016 International conference on industrial informatics-computing technology, intelligent technology, industrial information integration (ICIICII)*. pp. 150–153. IEEE (2016)
17. Zhang, Q., Xu, J., Xu, L., Guo, H.: Deep convolutional neural networks for forest fire detection. In: *2016 International Forum on Management, Education and Information Technology Application*. Atlantis Press, Paris (2016)

Chapter 47

Design and Development of Efficient Cost-Saving Algorithms for Guiding Customer Purchasing Patterns in Modern Consumerism Scenario Using Feed Forward Back Propagation Neural Networks



Sonia Maria D'Souza and K. Satyanarayan Reddy

Abstract This research deals with the development of a new architecture. The system deals with self-scanning and self-checkout of the products. Here, we have made an effort to take the system which is a very handy through app. It uses neural networks, fuzzy logic, and genetic algorithms. The database is maintained in the local server, and both mobile and the local host are connected to the same network. As a result, the user can use all the features of this system and send and receive the data which is required by the user. This framework takes care of taxations such as GST. The concept involves designing and implementation of cost-saving algorithms by using feed forward back propagation neural networks for guiding customer purchasing, retrieval, and faster method of accessibility with respect to different patterns.

47.1 Introduction

Most of the Indian metropolitan cities have IT industries, and millions of people have settled down from different places due to availability of various job opportunities, family, education, and for many other reasons; where ever they stay, shopping has become routine. An app that helps these people to easy shopping is the e-commerce app or the Web sites. But these have few limitations as it takes more time for delivery and sometimes out of stock, No assurance of the product and many more. And when people go to shopping malls, they enjoy shopping but get frustrated in the billing counter due to long queues. This work suggests “queue-less shopping cart with self-checkout” (Qless) system. This research deals with the development of a new

S. M. D'Souza (✉) · K. S. Reddy
Cambridge Institute of Technology, Bangalore, India
e-mail: soniapradeepkumar@gmail.com

K. S. Reddy
e-mail: satyanarayan.reddy@gmail.com

© The Editor(s) (if applicable) and The Author(s), under exclusive license to Springer Nature Singapore Pte Ltd. 2021

Y.-D. Zhang et al. (eds.), *Smart Trends in Computing and Communications: Proceedings of SmartCom 2020*, Smart Innovation, Systems and Technologies 182,

https://doi.org/10.1007/978-981-15-5224-3_47

architecture. The system deals with self-scanning and self-checkout. The user needs to go through series of steps to use the major features of the system as authentication, i.e., the username as unique name and a password. Before the user undergoes the process of authentication, he/she can register to the system and then login. This system is a very handy app based system guiding people about the routes to the mall and due consideration on ensured budget. Here, all the data is stored in the cloud server, and based on the input given by the user, the data is fetched from it and displayed to the user by using efficient algorithms like neural networks (FFBP-NN) [1]. The database is maintained in the local server, and both mobile and the local host are connected to the same network. As a result, the user can use all the features of this system and send and receive the data which is required by the user. Since to keep up the nearby server portable that the client utilizes, it must be conveyed at first, and afterward, the client can use whatever number as could reasonably be expected. This framework can likewise think about GST.

47.2 Literature Review

Preparing frame mind that is roused by the way natural glossal, for instance, the thinker, forms ammunition. The key component of this frame of mind is the tale makeup of the data governance arrangement. It is made out of extensive exceptionally between associated groom constituent (neurons) working as one to apparatus precise concern. ANNs are similar to individuals. An ANN is configured for a specific pertinence, for illustration, draft acceptance or statistics classification, down a literacy operation [2]. Literacy in natural frame of mind incorporates changes in accordance with the translation hookup that escapes route between the neurons. Neural systems, with their exceptional stowage to get significance from confounded or fickle acquired facts, can be exploited to remove designs and recognize patterns that are too whimsical to ever be seen by either mob or other apparatus methods. A capable neural system can be thought of as a savant in the stratum of data it has been given to dissect. During the learning procedure, frame mind collection is required. Ideal models of administered learning incorporate blunder adjustment learning, fortification enlightenment, and stochastic enlightenment. A significant mistake assembly is, for example, the derogate of omission betwixt ideal and sort out constituent. Bespeak is to poll a lot loads which limit overestimate [2]. Interpret in particular technique, which is rudimentary to many intellect ideal models, least mean square (LMS) assembly. Solo learning uses farthest instructor to be contingent on just quarter data. Moreover, implied patterned-relationship, patterned-makes data showed to the framework and distinguishes their new total properties. Ideal models of solo learning are Hebbian enlightenment.

47.3 Propound Practice

47.3.1 Statics Battering Innovation

The Discrete Cosine Transform (DCT)

The discrete cosine change backing brake down picture partway is contrasting significance, and it changes flag. Blisteringly prominent utilization of DCT picture pressure as it shapes the reason for worldwide cut and dried misfortune picture pressure calculation is known as JPEG [3, 4]. In only a couple of coactive, the greater part of depicted data about the picture potent. Extricated DCT coefficients can utilize acknowledgment undertakings, for example, activity acknowledgment. DCT regularly disposes of high-recurrence coefficients, changes the recurrence ones, and diminishes the information volume without giving up an excessive amount of picture aspect.

A 2D-DCT of a $M \times N$ network characterized pursues [4]:

$$F(u) = \left(\frac{2}{N}\right)^{\frac{1}{2}} \sum_{i=0}^{N-1} \Lambda(i) \cdot \cos\left[\frac{\pi \cdot u}{2 \cdot N}(2i + 1)\right] f(i)$$

furthermore, relating converse 1D DCT change straightforward $F - 1(u)$, i.e.,

$$\Lambda(i) = \begin{cases} \frac{1}{\sqrt{2}} & \text{for } \xi = 0 \\ 1 & \text{otherwise} \end{cases}$$

Universal parity 2D-DCT

$$F(u, v) = \left(\frac{2}{N}\right)^{\frac{1}{2}} \left(\frac{2}{M}\right)^{\frac{1}{2}} \sum_{i=0}^{N-1} \sum_{j=0}^{M-1} \Lambda(i) \cdot \Lambda(j) \cdot \cos\left[\frac{\pi \cdot u}{2 \cdot N}(2i + 1)\right] \cos\left[\frac{\pi \cdot v}{2 \cdot M}(2j + 1)\right] \cdot f(i, j)$$

Harmonize inverse 2D-DCT revamping unsophisticated $F - 1(u, v)$, i.e.,

$$\Lambda(\xi) = \begin{cases} \frac{1}{\sqrt{2}} & \text{for } \xi = 0 \\ 1 & \text{otherwise} \end{cases}$$

Fundamental activity of DCT following:

- Absorption picture N by M . $f(i, j)$ is the force constituent in push i and segment j ;
- $F(u, v)$ coactive push k_1 and section k_2 form 2D-DCT matrix.
- Blisteringly pictures, a great part of the sign vitality lies at low frequencies.

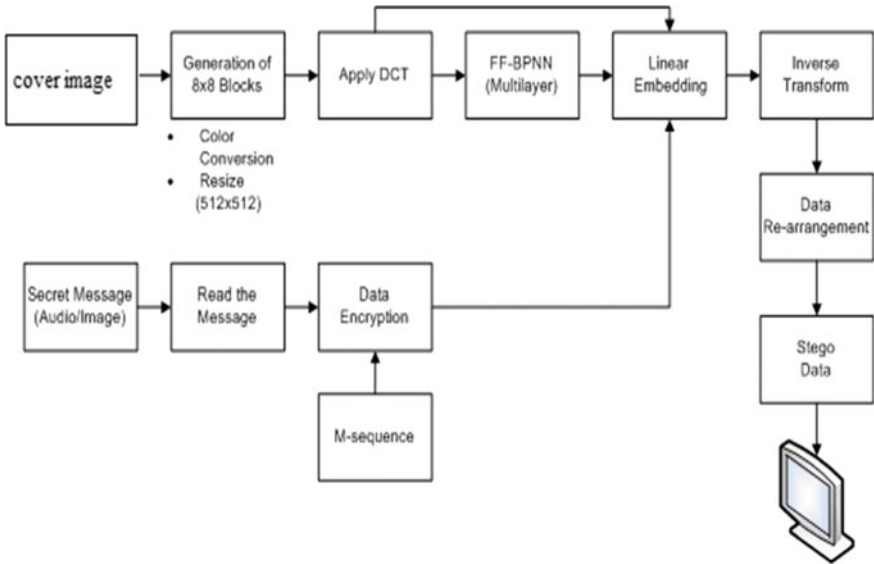


Fig. 47.1 Enterprise environment

- Condensing wised up since the lower right qualities speak to formidable gradient, and are regularly abrupt disregarded minutest noticeable bending.
- The DCT input is 8 by 8 cluster of numerals. Eight-piece constituent have levels from 0 to 255 (Fig. 47.1).
- Thereupon, 8 bit DCT would be

$$\Lambda(\xi) = \begin{cases} \frac{1}{\sqrt{2}} & \text{for } \xi = 0 \\ 1 & \text{otherwise} \end{cases}$$

47.4 Implementations and Measures

MATLAB stage picked to build up calculation. MATLAB structure covered infinite athenaeum and proficient ingredient of neural system and engraving preparing valuable in examining the codes. Designers may utilize other programming language too. Ammunitions, installing twisting and inserting rate can utilize plans for assessing the presentation of the information concealing plans.

47.4.1 Mean Squared Error and PSNR

Burdened blunder in thick of spread picture and the stego-picture (implanting mutilation) can be utilized as measures to survey overall detectable quality of the inserted information. Indistinctness exploits fallible certifiable drawn repetition, which is hard to measure.

47.4.2 Correlation

Connect a standout among other known strategies that assess the level of illiberality mid capacities. This estimate can be utilized to decide the degree that first picture and the committal to writing near one another, significantly in the wake of inserting information restrain, recognition of the nearness of the concealed information depends on the utilization of cross-connection work of two pictures X and Y defined as [5, 6].

47.4.3 DCT Algorithm

The discrete cosine change (DCT) backing recognizes the picture differing significance, and it changes flag or picture from the territorial space recurrence area. Greatest utilization of DCT picture pressure shapes reason for worldwide grade misfortune picture pressure calculation which is known as JPEG [6, 7]. In only a couple of coefficients, the greater part of the optic data is picture dense. Separated DCT coactive has utilized acknowledgment errands, for example, activity acknowledgment. Activity of pictures and sound has high connection and excess data which causes computational weight as far as handling pace and memory use. DCT regularly disposes of high-recurrence coactive and changes the truncated recurrence, which diminishes information magnitude without giving up an excess of picture caliber. For situation, a discrete cosine change (DCT) is utilized, change 8×8 pixel squares picture to 64 DCT coactive. This method is utilized for documents put away in the JPEG picture design. The change of a solitary DCT coactive influences every one of the 64 picture pixel squares. Therefore, the flatten of the constituent adjustment basically is inconceivable for recognition.

$$y(k) = w(k) \sum_{n=1}^N x(n) \cdot \cos\left[\frac{\pi}{2N}(2n-1)(k-1)\right], \quad k = 1, 2, \dots, N$$

where

$$w(k) = \begin{cases} \frac{1}{\sqrt{N}}, & k = 1 \\ \sqrt{\frac{2}{N}}, & 2 \leq k \leq N, \end{cases}$$

N is the dimension of x . In the event that x is a framework, DCT changes segments. The arrangement is recorded $n = 1$ and $k = 1$ rather than typical $n = 0$ and $k = 0$. $y = \text{dct}(x, n)$ cushions changing. The DCT firmly identified with the discrete Fourier change. To reproduce an arrangement precisely from just a couple DCT coactive [8, 9].

47.4.4 Inverse DCT

Opposite discrete cosine change remakes grouping discrete cosine change (DCT) coactive. The IDCT work is opposite to the DCT work [10–12].

47.5 Result Analysis

We train a lot of pictures which is haphazardly taken from examining codes, QR codes and bar codes. These pictures have different memory sizes. Picture utilizes the attributes got from 2D-DCT coefficients alongside FFBP-NN. Figure 47.2 shows Mean Square Error Performance versus number of iterations to train the system and Fig. 47.3 shows the training state of the system and clarity of pixel is recovered in different iterations.

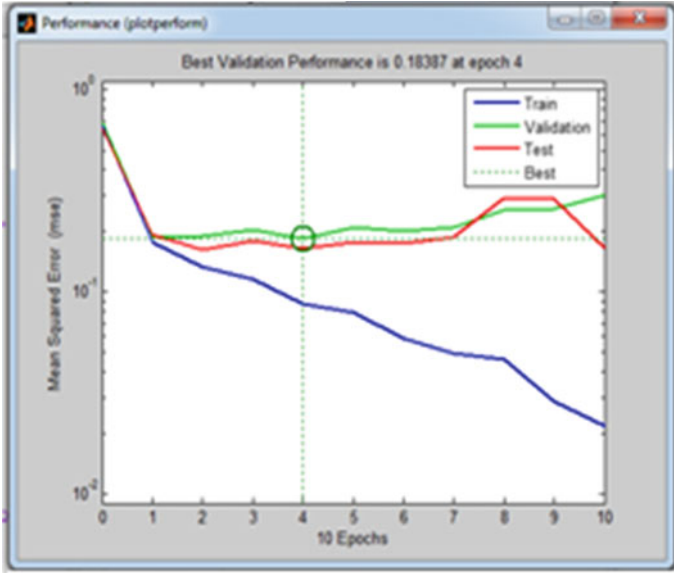


Fig. 47.2 Performance graph MSE versus epochs

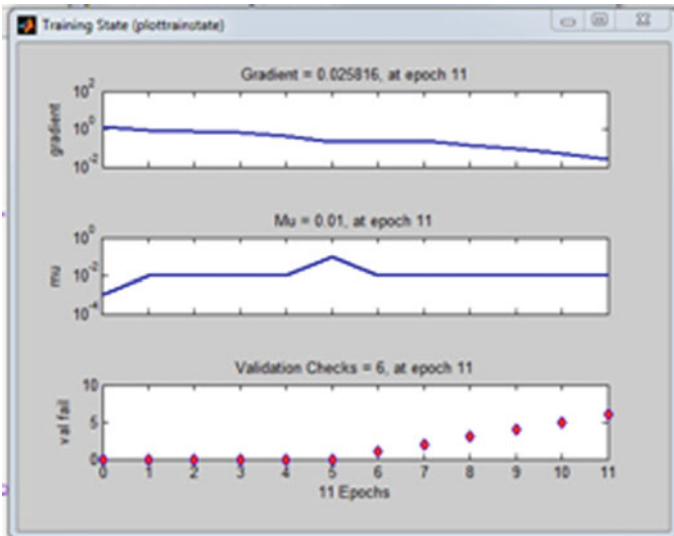


Fig. 47.3 Training state graphs

47.6 Conclusion

FFBP-NN is put together on delineation from one datum for around 1000 epoch, and the mind of frame achieved 94.20% for quickest technique draw up schedule. The 2D-DCT and FFBP-NN are the benevolence plan nearby the usage conceal and deciphering some portion enigma proof. Inclination very well actualized slave frame of mind. Application can be upgraded underpins HDF, RAS picture position. As a shopkeeper or the owner he/she will update of what product is sold more, which kind of people purchase what kind of commodities, which is highest sold product or item in particular month, on which days the products are sold more, which company item are in demand, which products are in demand (e.g., stationary, clothing, footwear, electronics, etc.), he/she can plan to replenish stocks efficiently. This queue-less system motivates to work on minimal amount with respect to GST and as well as budget planning which will helpful to the customers.

References

1. Isaac, B., Santhi, V.: A study on digital image and video water marking schemes using neural network. *Int. J. Emerg. Tech. Adv. Eng.* **12**, 1 (2012)
2. Chang, C.C., Lin, I.C.: Robust image watermarking systems using neural network. *Ser. Innov. Intell.* **7**, 402–404 (2004)
3. Al-Momen, S.M.A., George, L.E.: Image hiding using magnitude modulation on the DCT coefficients. *J. Appl. Compute. Sci. Math.* **8**, 9 (2010)
4. Priyadarshini, R., Dash, N., Swarnkar, T., Misra, R.: *Functional Analysis of Artificial Neural Network for Dataset Classification*. August (2010)
5. Usha, B.A., Srinath, N.K., Cauvery, N.K.: Data embedding technique in image steganography using neural network (IJARCCE). *Int. J. Adv. Res. Comput. Commun. Eng.* **2**, 2177–2180 (2013)
6. Rouhania, S., Ravasan, A.Z.: *An Artificial Neural Network Approach*. Scientia Iranica E October (2012)
7. Lin, C.C., Shi, P.F.: High capacity data hiding scheme for DCT-based images. *J. Inf. Hid. Mult. Sign. Proc.* **1**(3) (July, 2010). ISSN 2073-4212
8. Chen, P.Y., Lin, H.J.: A DWT based approach for image steganography. *Int. J. Appl. Sci. Eng.* **275**, 275–290 (2006)
9. Gallegos-Funes, F.J., Carvajal-Gamez, B.E., Lopez-Bonilla, J.L., Ponomaryov, V.I.: Steganographic method based on wavelets and center weighted median filter. In: *International Kharkov Symposium on Physics and Engineering of Microwaves. Millimeter and Submillimeter Waves (MSMW)*. pp. 1–3. (2010)
10. Chakraborty, P., Sarkar, B.: Statistical steganalysis scheme of using block DCT. *Int. J. Comput. Sci. Inf. Tech.* **5**, 3 (2014)
11. Rastogi, A., Kapoor, A., Srivastava, A.: Steganography using wavelet and neural networks. *The International Society for Optical Engineering*, vol. 5916. *Mathematical Methods in Pattern and Image Analysis*. October (2006)
12. Bergman, C., Davidson, J.: *An Artificial Neural Network for Wavelet Steganalysis*. October (2006)

Chapter 48

Mild Cognitive Impairment and Technology for Older Adults: A Review



Nita Rosa Damayanti and Nazlena Mohamad Ali

Abstract When life expectancy increases, so does the number of parents. This increase raises challenges related to the cognitive abilities of adults who experience mild cognitive impairment in emotional change. There are various ways to reduce or help emotional changes in older adults mild cognitive impairment (MCI) including by using technology. To help older adults who experience unstable emotions in mild cognitive impairment, future long-term research needs to be conducted. Technology can be accepted by older adults if the technology developed is easy to play. Innovative technology in daily activities is the key to successful health care, especially for older adults, technology providers, and healthcare providers. Games are a good idea to help older adults, especially in helping mild cognitive impairment. This paper literature reviews on game technology that can help older adults mild cognitive impairment include cognitive and emotional changes.

48.1 Introduction

The increase in the number of older adults every year is big. In 2020, the number of older adults is predicted to be the same as the number of children under five. Eleven percent of 6.9 billion people in the world are older adults [1]. The 2016 World Health Statistics data, the population aged 60 years and over, amounted to 24,754,500 people (9.34%) of the total population. According to the Population Division, Department of Economic and Social Affairs, the number of elderly population in the world (>60 years) is estimated to reach nearly 668 million people in 2005 and projected to be 2 billion in 2050 [2]. Older adults have problems with various declines in health status, especially cognitive function and thus, declining health in older people will

N. R. Damayanti (✉)
Universitas Bina Darma, Palembang, Indonesia
e-mail: nita_rosa@binadarma.ac.id

N. M. Ali
Institute of Visual Informatics (IVI), Universiti Kebangsaan Malaysia, Bangi, Malaysia
e-mail: nazlena.ali@ukm.edu.my

© The Editor(s) (if applicable) and The Author(s), under exclusive license to Springer Nature Singapore Pte Ltd. 2021

Y.-D. Zhang et al. (eds.), *Smart Trends in Computing and Communications: Proceedings of SmartCom 2020*, Smart Innovation, Systems and Technologies 182,
https://doi.org/10.1007/978-981-15-5224-3_48

affect their quality of life and emotions. This group of older adults is categorized as older adults through a process called the aging process. Furthermore, older adults with mild cognitive impairment (MCI) are at high risk of developing dementia. If there is no prevention of mild cognitive impairment, it is feared that the memory will suffer. MCI is usually experienced in people aged 60 years and over. Mild cognitive impairment (MCI) is a common condition in older adults but this disorder can be overcome by brain training [3]. Then MCI is characterized by a decrease in memory, attention and can develop into dementia by 10–15% per year. Therefore, it is very important to protect older adults who experience MCI from developing into dementia. It should be noted that MCI patients experience emotional changes from 35 to 85% [4]. Most common in older adults with mild cognitive impairment are depression, anxiety, irritability, indifference, among some people who may even have difficulty controlling emotional changes associated with daily activities [5]. In fact, more concern about the inability to control emotions among older adults with mild cognitive impairment can cause them to have Alzheimer's disease [6]. Thus, Nashiro et al. [7] argues that positive emotions are a combination of high levels of satisfaction and emotions. Technology with new innovations can help older adults in their old lives [8]. It is interesting to note that many therapeutic media can be used for older adults who experience MCI. One of them is in the form of a game. Apparently, this tends to be effective, as in puzzle games, chess, reading, drawing, and playing musical instruments as a therapeutic medium [9].

48.2 Method

Literature review is done with technology on the Internet using the US National Medical Library (PubMed[®]), Web of Science (ISI[®]), and Scopus[®] database. His initial search was analyzed and yielded 646 references by database search that obtained 11 references in a total of 657 articles at the start. After identifying then the researchers deleted the duplicate documents so that the total article became 285 left. Then 285 will be filtered to see the feasibility of the article. Articles that did not meet the criteria based on titles or abstracts were deleted so that the total articles became 76. From 76 articles, a full-text analysis was performed and after reading each article, then all articles were analyzed, and 25 additional articles were excluded because they did not match the title and abstract. The article produced a total of 51 full texts which were included in the final review [10] (Fig. 48.1).

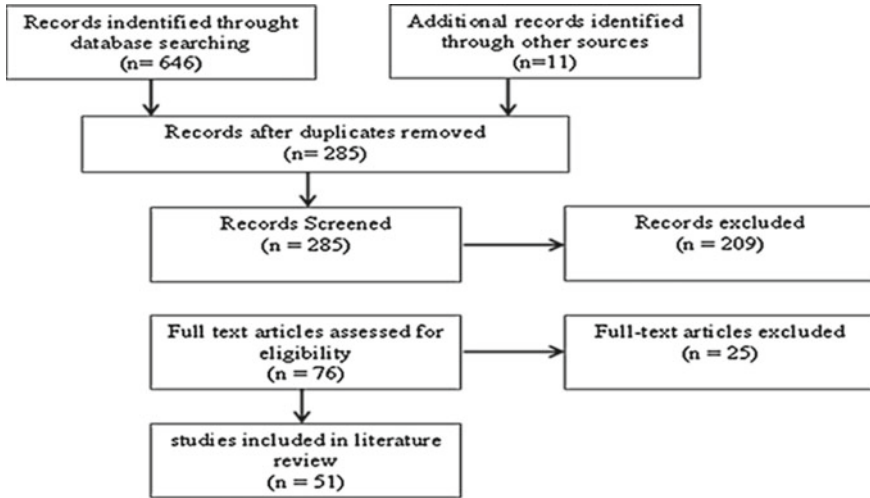


Fig. 48.1 Filtering articles

48.3 Games Technology for Older Adults that Experience MCI in Emotion Change

The main process in technology for the older adults who experience MCI is the gaming training technology. Adoption of technology involves many factors and it is significant. The literature review suggests the main actors in the context: the older adults, technology, games, and therapy MCI in the importance of caring for the health of the older adults [11] (Table 48.1).

Table 48.1 List of journal

Name of article	Number of article located (n = 51)
Aging and mental health	8
Aging and society	6
Gerontologist	6
Healthcare analysis	8
Journal of technology and older adults	8
Journal games technology for health	8
Journal older adults	7

48.3.1 *Emotion and Therapy MCI*

MCI patients experienced an emotional change of 35–85% and the most common symptoms of older adults with mild cognitive impairment are depression, anxiety, irritability, indifference, and may even have difficulty controlling emotional changes associated with daily activities. In fact, more worrying about the inability to control emotions among older adults with mild cognitive impairment could lead them to have Alzheimer's disease [12]. Reference [13] argues that positive emotions are a combination of high levels of satisfaction and emotions. Fun or enjoyable emotional experiences are considered positive emotions. Positive emotions help one to cope with stress because positive emotions help one to think more objectively [14]. According to a recent study [15], older people are found to be more likely to exhibit less stable and uncontrolled emotions. Anger is caused by negative thoughts inherent in something. The thought continues so much that the individual cannot control himself. On the other hand, stable emotions can help an individual to develop or build social competence, thus overcoming the pressures they face. In addition, [16] said that older people have conflicts such as family conflict, citing social support due to the death of a person near death, isolation, lack of confidence, and skepticism that affect cognitive function and can cause emotion. Stable emotional capacity can motivate oneself to control self, regulate mood, and maintain mood so that stress does not impair thinking ability. To overcome the burden or stress experienced, positive changes in emotions, especially among older adults are very important. In addressing the cognitive functioning of cognitive change in older adults experiencing MCI is to enhance the training of cognitive function in order to influence positive emotions. Currently, therapies are known to help seniors with mild concussions [17]. Therapy is defined by the treatment of rehabilitation in patients who have had any illness or experience any inconvenience. Therapeutic methods can help older adults problems and inability to achieve cognitive, emotional, and social development [18]. various therapies: Therapy Music then [19] stated that music therapy can influence mood, and that emotion can influence individual emotional development, Therapy CBT The next most commonly used therapies for emotion is Cognitive Behavior Therapy or CBT [20], Therapy Art [21] also stated that Art Therapy is an oral and written expression of experiences and feelings through the art media, Therapy [22] say Laughter therapy is a humor that is a cultural heritage and can play a part in the process of psychotherapy, Therapy Spiritual In addition, the spiritual therapy approach adopted by the United States Psychiatric Association (APA, 1992) is known as the "biopsico-socio-spiritual" approach. Sabrina [23], and Therapy Group Further [24] states that the brief therapy group is short-term therapy (typically 10–20 sessions).

48.3.2 *Emotion Theory and MMSE*

Emotional theory of two factors Schacter and Singer [25] is recognized as a stimulus-oriented theory, i.e., if stimulation is excited, then it is called pleasure and a dangerous stimulus is called fear. Psychologists see this theory in accordance with cognitive theory. For example, when someone faces an emotionally arousing event, he will generally experience neutral and unclear physiological disorders. In theory, what applies then depends on whether he feels angry and how he feels if he is unsure about the emotions he feels, he might look for an answer to a situation that might help him understand what he feels. Then Lazarus' cognitive theory. Based on cognitive assessments, we decide whether there are positive, negative, or neutral states. Positive or negative judgments trigger physiological stimuli and emotional feelings. Emotions, cognition, and commitments are closely related emotions that arise rather than ongoing relationships or transactions that are influenced by nature [26]. MMSE is a measuring tool for knowing older adults who experience mild cognitive impairment. Mini-Mental State Examination (MMSE) is one of the most widely used screening tests in clinical trials and in general practice to detect cognitive improvement in older adults [27].

48.3.3 *Technology and Games*

Older adults have the picture of being a major social challenge and access to technology is one of the important strategies in future healthcare services [28]. Technology may have high progress to support one's work performance, which means helping the actual implementation of work. Technology needs are expected to later have an impact on the quality of life, which can be defined as: individuals' perceptions of their lives in life in daily activities and systems their lives in relation to goals and expectations [29]. Older adults are slower to adopt new technology than younger adults, but will do so if technology seems to have value, for example, in maintaining their quality of life [30]. To make technology more friendly to adults, it is important to understand the strengths and weaknesses that adults feel when using it, technology in playing is a modern area because of the current technological sophistication, many games can help older adults such as kitchen and cooking, smart uber, cards, and so on. Certainly, the benefits of a digital game can change the lives of older adults [31]. There are several technological devices used for older adults who experience MCI such as [1] Tablets. Types of portable computers that have touch screens are increasingly increasing and are in demand by older adults. Then, computer technology can provide cognitive and intellectually challenging activities because Internet-based services may have special benefits for parents [32], and virtual reality is a technology that is in demand by older adults; considering this technology is like the real world [33]. Table 48.2 can be seen how the role of technology and games can help MCI.

Table 48.2 Technology games for MCI (older adults)

Technology/platform and games	Health games category	Game description
Computer [35] neurofeed-back	Attention and memory	Improve cognitive performance
Computer [36] video dance	Physical	Dance video games can help in improving cognitive and motor functions
Computer [37] card	Memory	Can help further improve and make their memory strong
Computer [38] kitchen and cooking	Memory	This game trains the memory of the brain
Computer [39] Wii sport	Physical	A sport games which is actually a collection of sport: tennis, baseball for physical exercise
iPad [40] show game	Motivation and confidence	Cognitive performance has very specific tests and interactions and improves memory
iPad [41] egocentric image	Memory	Egocentric image can help with memory focus
iPad [42] lumosity	Processing episodic speed, attention, and memory	improve memory, attention, flexibility, speed of processing, and problem solving
Tablet [43] Smartkuber	Motivation	Engaging and motivating gaming experience to elderly players
DMS48 [44] object picture	Memory	Improve memory

48.4 Conclusion

This review of the study revealed important findings. First, an interesting point for game technology for parents who experience MCI is that many games developed for the purpose of helping older adults MCI [34]. Our work presents a broader view of game technology for older adults who experience MCI and the relative study of their efficacy. The main point flowing through our literature review is that the game in older adults who experience mild cognitive impairment has an effect on parents with cognitive and emotional disorders. To determine whether the effect is long-lasting and/or can be transferred to daily activities is a matter of further scientific investigation. During this literature review, we analyzed applied therapies, technology, and games. As a result of this interaction, we develop “EmoGame” game technology for older adults who experience MCI in emotional change, which will be presented in a future publication.

Acknowledgements The work was supported by Universiti Kebangsaan Malaysia Research Grant (GUP-2019-066) and Universitas Bina Darma.

References

1. Apperley, T.: Genre and game studies: towards a critical approach to videogame genres. *Simul. Gam. Int. J. Theor. Pract. Res.* **37**(1), 6–23 (2006)
2. WHO: International statistical classification of diseases and related health problems 10th revision (ICD-10). F00: Dementia in Alzheimer Disease (2016). Available from <http://apps.who.int/classifications/icd10/browse/2016/en#/F00>. Accessed 15 May 2017
3. Preeyam, K. et al.: The impact of memory change on daily life in normal aging and mild cognitive impairment (2015). <https://doi.org/10.1093/geront/gnv030>
4. Petersen, R.C., Roberts, R.O., Knopman, D.S., et al.: Mild cognitive impairment: ten years later. *Arch. Neurol.* **66**(12), 1447–1455 (2009)
5. Bennett, D.A., Wilson, R.S., Boyle, P.A., Buchman, A.S., Schneider, J.A.: Relation of neuropathology to cognition in persons without cognitive impairment. *Ann. Neurol.* **72**(4), 599–609 (2012)
6. Gross, J.J.: *Handbook of emotion regulation*. Guilford Press, New York (2007)
7. Nashiro, K., Sakaki, M., Mather, M.: Age differences in brain activity during emotion processing: reflections of age-related decline or increased emotion regulation? *Gerontology* **58**, 156–163 (2012)
8. Ann: Technology use to improve everyday occupations in older persons with mild dementia or mild cognitive impairment: a scoping review (2018). <https://doi.org/10.1177/0308022618771533>
9. Vaportzis, E., Clausen, M.G., Gow, A.J.: Older adults perceptions of technology and barriers to interacting with tablet computers: a focus group study (2017). <https://doi.org/10.3389/fpsyg.2017.01687>
10. Pluye, P., Garcia Bengoechea, E., Granikov, V., Kaur, N., Tang, D.L.: A world of possibilities in mixed methods: review of the combinations of strategies used to integrate the phases, results, and qualitative and quantitative data. *Int. J. Mult. Res. Appr.* **10**(1), 41–56 (2018)
11. Hagošková, M., Dzvonič, O., Olekszyová, Z.: Comparison of two cognitive training programs with effects on functional activities and quality of life. *Res. Gerontol. Nurs.* **10**, 172–180 (2017)
12. Charles, S.T., Piazza, J.R.: Age din affective well being: context matters. *Soc. Personal. Psychol. Compass.* **3**, 711–724 (2009)
13. Lantrip, C., Isquith, P.K., Koven, N.S., Welsh, K., Roth, R.M.: Executive function and emotion regulation strategy use in adolescents. *Appl. Neuropsychol. Child.* **5**, 50–55 (2016)
14. McClintock, S.M., Husain, M.M., Greer, T.L., Cullum, C.M.: Association between depression severity and neurocognitive function in major depressive disorder: a review and synthesis. *Neuropsychology* **24**, 9–34 (2010)
15. Mosby's. *Medical Dictionary*, 8th edn (2009). <http://medicaldictionary.thefreedictionary.com/Alternativemedical>
16. McIntyre, R.S., Cha, D.S., Soczynska, J.K., Woldeyohannes, H.O., Gallagher, L.A., et al.: Cognitive deficits and functional outcomes in major depressive disorder: determinants, substrates, and treatment interventions. *Depress. Anxiety* **30**, 515–527 (2013)
17. Orgeta, V.: Psychological treatments for depression and anxiety in dementia and mild cognitive impairment (2014). <https://doi.org/10.1002/14651858.cd009125>
18. Snowdon, J., Almeida, O.: The diagnosis and treatment of unipolar depression in late life. In: Lavretsky, H., Sajatovic, M., Charles, F.R.I.I.I. (eds.) *Late-life mood disorders*, pp. 79–103. Oxford University Press, United States (2013)

19. Gallego, G.: Music therapy and Alzheimer's disease: cognitive, psychological, and behavioural effects Alzheimer (2017). <https://doi.org/10.1016/j.nrleng.2015.12.001>
20. Kashimura, M., Nomura, T., Ishiwata, A., Kitamura, S., Tateno, A.: Improving mood with cognitive behavioral therapy in a woman with mild cognitive impairment-a case report (2019). https://doi.org/10.1272/jnms.jnms.2019_86-603
21. Chancellora, B.: Art therapy for Alzheimer's disease and other dementias (2013). <https://doi.org/10.3233/jad-131295>
22. Ghodsbin, F., Ahmadi, Z.S., Sharif, F.: The effects of laughter therapy on general health of elderly people referring to Jahandidegan community center in Shiraz, Iran: a randomized controlled trial. *IJCBNM* **3**(1), 31–38 (2015)
23. Sabrina: Association of spiritual well-being, social support, self-esteem, subjective well-being, optimism and hope scores with mild cognitive impairment and mild dementia (2018). <https://doi.org/10.3389/fpsyg.2018.00371>
24. Agronin, M. (2009). Group therapy in older adults. Doi: 10.1007/s11920-009-0005-1
25. Schachter, S.: The interaction of cognitive and physiological determinants of emotional state. In: Berkowitz, L. (ed.) *Advances in experimental social psychology*, vol. 1. Academic Press, New York (1962)
26. Lazarus, R.S., Launier, R.: Stress-related transactions between person and environment. In: Pervin, L.A., Lewis, M. (eds.) *Perspectives in interactional psychology*, pp. 287–327. New York, Plenum (1978)
27. Folstein, M.F., Folstein, S.E., McHugh, P.R.: A practical method for grading the cognitive state of patients for the clinician. *Mini-Mental State* **12**, 189 (1975). [https://doi.org/10.1016/0022-3956\(75\)90026-6](https://doi.org/10.1016/0022-3956(75)90026-6)
28. Ball, K., Berch, D.B., Helmers, K.F., Jobe, J.B., Leveck, M.D., Marsiske, M.: Effects of cognitive training interventions with older adults: a randomized controlled trial. *JAMA* **288**(18), 2271–2281 (2002)
29. Heller, R., Jorge, J., Guedj, R.: Ec/nsf workshop on universal accessibility of ubiquitous computing: providing for the elderly event report. In: *Proceedings of the 2001 EC/NSF workshop on Universal accessibility of ubiquitous computing: providing for the elderly*. pp. 1–10. WUAUC '01, ACM (2001)
30. Khosravi, Pouria, Rezvani, Azadeh, Wiewiora, Anna: The impact of technology on older adults' social isolation. *Comput. Human Behav.* **63**, 594 (2016). <https://doi.org/10.1016/j.chb.2016.05.092>
31. Mattke, S., Klautzer L., Mengistu T., Garnett J., Hu J., Wu, H.: Health and well-being in the home: a global analysis of needs, expectations, and priorities for home health care technology. Rand Corporation (2010). Available at http://www.rand.org/pubs/occasional_papers/OP323.html. Accessed 17 March 2011
32. Alvseike, H., Brønnick, K.: Feasibility of the iPad as a hub for smart house technology in the elderly; effects of cognition, self-efficacy, and technology experience. *J. Multidiscip. Healthc.* **5**, 299–306 (2012). <https://doi.org/10.2147/JMDH.S35344>
33. Syed-Abdul, S., Malwade, S., Nursetyo, A.A., Sood, M., Bhatia, M., Barsasella, D., Liu, M.F., Chang, C.C., Srinivasan, K., Raja, M., Li, Y.C.J.: Virtual reality among the elderly: a usefulness and acceptance study from Taiwan (2019). <https://doi.org/10.1186/s12877-019-1218-8>
34. Al Mahmud, A., Slikboer, R., Stargatt, J., Bhar, S.: Computer-based cognitive interventions for mild cognitive impairment and dementia in older adults: protocol for a systematic review of published studies and meta-analysis. *System. Rev.* **8**, 1 (2019). <https://doi.org/10.1186/s13643-019-1146-x>
35. Baranowski, T., Maddison, R., Maloney, A., Medina, E., Simons, M.: Building a better mouse-trap (Exergame) to increase youth physical activity. *Games Health J* **3**(2), 72–78 (2014). <https://doi.org/10.1089/g4h.2014.0018>
36. Azman, N.: Effect of dance video game training on elderly's cognitive function. *Sci. Tech.* (2017). https://www.jstage.jst.go.jp/article/jsmbe/55Annual/Proc/55Annual_526/_pdf-char/ja

37. Gielis, K., Brito, F., Tournoy, J., Abeele, V.V.: Can card games be used to assess mild cognitive impairment? A study of Klondike solitaire and cognitive functions (2017). <https://doi.org/10.1145/3130859.3131328>
38. Manera, V.: 'Kitchen and cooking,' a serious game for mild cognitive impairment and Alzheimer's disease: a pilot study. *J. Aging Neuro Sci.* (2015). <https://doi.org/10.3389/fnagi.2015.00024>
39. Weybright, E.H.: Effects of an interactive video game (Nintendo Wii) on older women with mild cognitive impairment. *Therap. Recreat. J.* (2010). <https://www.researchgate.net/publication/260284248>
40. Savulich, G.: Cognitive training using a novel memory game on an iPad in patients with amnesic mild cognitive impairment (aMCI). *Int. J. Neuropsychopharm.* (2017). <https://doi.org/10.1093/ijnp/pyx040>
41. Legouverneur, G., Pino, M., Boulay, M., Rigaud, A.S.: Wii sports, a usability study with MCI and Alzheimer's patients (2011). <https://doi.org/10.1016/j.jalz.2011.05.2398>
42. Lageman, S., Cash, T., Mickens, M.: A-50 feasibility and initial results of a randomized-controlled computer-based cognitive training trial in individuals with Parkinson's disease. *Arch. Clin. Neuropsychol.* **29**(6), 521–522 (2014)
43. Boletsis, C. et al.: Smartkuber: a serious game for cognitive health screening of elderly players (2016). <https://doi.org/10.1089/g4h.2015.0107>
44. Didic, M., Felician, O., Barbeau, E.J., Mancini, J., Latger-Florence, C., Tramon, E., Ceccaldi, M.: Impaired visual recognition memory predicts Alzheimer's disease in amnesic mild cognitive impairment (2013). <https://doi.org/10.1159/000347203>
45. Diener, L., Larsen, R.: The contributions of positive and negative affect to emotional well-being. *Diakses pada 1 Januari 2019. Daripada ISSN 1849-0395 (Electronic); 1332-0742 (Print) (2006)*
46. Eshkoo, S.A., Hamid, T.A., Mun, C.Y., Ng, C.K.: Mild cognitive impairment and its management in older people. *Clin. Interv. Aging* **10**, 687 (2015)
47. Jirayucharoensak, S. et al.: A game-based neurofeedback training system to enhance cognitive performance in healthy elderly subjects and in patients with amnesic mild cognitive impairment (2019). <https://doi.org/10.2147/cia.s189047>

Chapter 49

Identify Education Quality Based on Islamic Senior High School Data in *Kompetisi Sains Madrasah* Using Fuzzy C-Means Clustering



Dian Candra Rini Novitasari , Abdullah Faqih , Noor Wahyudi , Nurissaidah Ulinnuha , Zakiyatul Ulya , Ali Mustofa , Ahmad Fauzi , Ahmad Hanif Asyhar , Kusaeri , Dwi Rolliawati , and Ahmad Yusuf 

Abstract The education system in a country certainly has goals to be achieved. Many attempts were made to achieve the success of an education system that was created. This case causes competition between educational institutions and between students. The results of the competition can also represent schools that need special attention to improving learning systems. The learning system in Indonesia needs evaluation because of educational quality not perfectly. In this research, the fuzzy c-means (FCM) method is used to cluster the quality of existing *Kompetisi Sains Madrasah* (KSM) participant data to find schools that have good quality education. Next, a cluster evaluation is performed to determine the success of the cluster using silhouettes. Based on 4 trials, that are 3 clusters, 4 clusters, 5 clusters, and 6 clusters, the best results are on 3 clusters with the best silhouette value of 0.6499 with a standard deviation value of 0.2419. In the identification process, the results obtained that SMA has the best education quality in KSM.

49.1 Introduction

Education is one of the conditions for the country's development. The education system in a country has a goal to be achieved [1]. Many attempts were made to achieve the success of the education system. This causes a lot of competition between educational institutions and students [2]. Competition in education usually occurs in a competent competition. Competence is the ability or skill to execute anything without considering competitors, but only knowledge and abilities [2]. Verhoeff,

D. C. R. Novitasari (✉) · N. Wahyudi · N. Ulinnuha · Z. Ulya · A. Mustofa · A. Fauzi · A. H. Asyhar · Kusaeri · D. Rolliawati · A. Yusuf
UIN Sunan Ampel Surabaya, Ahmad Yani 117, Surabaya, Indonesia
e-mail: diancrini@uinsby.ac.id

A. Faqih
Kementerian Agama RI, Lapangan Banteng 3-4, Jakarta, Indonesia

© The Editor(s) (if applicable) and The Author(s), under exclusive license to Springer Nature Singapore Pte Ltd. 2021

487

Y.-D. Zhang et al. (eds.), *Smart Trends in Computing and Communications: Proceedings of SmartCom 2020*, Smart Innovation, Systems and Technologies 182,
https://doi.org/10.1007/978-981-15-5224-3_49

Lawrence, Fulu, and others suggested that competition in education has excellent benefits because it can increase student motivation and learning, even weaker students can survive by participating in the competition [3].

Indonesia is a developing country that has challenges in competition between nations in the global era to improve the quality and productivity of educated people [4]. One of the efforts made by the Ministry of Religious Affairs is the holding of Kompetisi Sains Madrasah (KSM). KSM is a madrasah science competition that was held in Indonesia. Initially, this competition was intended for students of Madrasah Ibtidaiyah (Islamic Elementary School), Madrasah Tsanawiyah (Islamic Junior High School), and Madrasah Aliyah (Islamic Senior High School). However, since 2016, the KSM has expanded its reach to elementary, junior high school, and senior high school students. KSM competition is held at the district/city provincial and national levels [5].

The competition scores show the results of learning and the ability of students to the learning system that has been applied. Roberta et al., in their research, also stated that the results of a competition held could evaluate the quality of the education system in a country [6]. The results of the competition can also represent schools that need special attention to improving learning systems [7]. The technique to find out schools that need quality improvement can use the clustering method [8]. Clustering is a method for grouping data in multidimensional data based on the similarity of data characteristics [9]. The success rate of the clustering process is at the center of the cluster. The more precise cluster center in representing data differences can provide better clustering results [10].

Elock Emvula Shikalepo has researched clustering on the quality of education in rural Namibian schools. The clustering method used is the Five Cluster Center Principals (CCPs) that have a good result [11]. Lotfi Nadji and Brahim Er-Raha have also studied the clustering method in education. The method used for clustering is the Within-cluster Sum of Square (WSS) method. The study successfully conducted a cluster based on student quality at IBN-ZOHR University. In that research, recommend the fuzzy c-means (FCM) method for clustering to determine the quality of each student. Based on the suggestion of the research, this study will use the FCM method to carry out the clustering process in identifying the quality of education in Indonesia [12].

FCM is a technique for clustering data where at each point that is located in the cluster is determined by the membership value [13–15]. Govindasamy and Velmurugan also researched student performance in a class by comparing several clustering methods such as k-means, k-medoids, and FCM. The results of this research on each method using purity as a cluster evaluation are 0.375, 0.374, and 0.624, and the best results in the research are using the FCM method [16]. Results using FCM obtain good purity values. Based on these results, this research uses the FCM method to cluster the quality of existing KSM participants to find schools that have good quality education.

49.2 Fuzzy C-Means (FCM) Clustering

Fuzzy c-means (FCM) is a method of clustering data whose membership value determines the existence of each data point in a cluster [15]. The centroid is used to determine the cluster of data. In the initial condition, the cluster center is not accurate and needs to be repaired repeatedly until an accurate centroid is obtained based on the membership value [17, 18]. The output of the FCM is the membership value of each data point and the row of the centroid [19].

Clusters in FCM have a stage that is almost the same as fuzzy logic with the initial stage to determine the value of the membership function of a data [20]. Initial membership value (μ_{ik}) of the FCM is defined in a random manner to determine and update the membership value (μ_{ik}) using Eq. (1).

$$\mu_{ik} = \frac{\left[\sum_{j=1}^m (X_{ij} - V_{kj})^2 \right]^{\frac{-1}{w-1}}}{\sum_{k=1}^c \left[\sum_{j=1}^m (X_{ij} - V_{kj})^2 \right]^{\frac{-1}{w-1}}} \tag{49.1}$$

where X_{ij} is the initial data for the clustering, and V_{kj} is the centroid in FCM. Variable i is the number of the data and c is the number of clusters. Variable w is the weight of the data whose default value is 2 [13]. Centroid in FCM can be calculated using Eq. (2).

$$V_{kj} = \frac{\sum_{i=1}^n ((\mu_{ik})^w * X_{ij})}{\sum_{i=1}^n (\mu_{ik})^w} \tag{49.2}$$

The FCM method will continue to iterate until it meets two conditions, namely the iteration (t) and the objective function (P_t). The condition for FCM to cease based on the objective function is $P_{t-1} - P_t < \text{error} (\epsilon)$ [15]. The objective functions used in the FCM method can be seen in Eq. (3).

$$P_t = \sum_{i=1}^n \sum_{k=1}^c \left(\left[\sum_{j=1}^m (X_{ij} - V_{kj})^2 \right] (\mu_{ik})^w \right) \tag{49.3}$$

49.2.1 FCM Algorithm

The steps to determine clusters using the FCM method [21]:

1. Input the data to be clustered, such as a matrix of size $n \times m$ where the number of data samples (n), attributes per data (m) and i th sample data with $i = 1, 2, \dots, n$ and j -attribute with $j = 1, 2, \dots, m$ (X_{ij}).

2. Determine the number of clusters = c , weight = w , maximum iteration = $MaxIter$, error = ϵ , initial objective function ($P_0 = 0$), and initial iteration ($t = 1$).
3. Generating initial membership degrees with random numbers (μ_{ik}) with $i = 1, 2, \dots, n$ and $k = 1, 2, \dots, c$; as an initial partition matrix element (U). Calculate the number of columns from the matrix using Eq. (4).

$$Q_i = \sum_{k=1}^c \mu_{ik} \tag{49.4}$$

with $j = 1, 2, \dots, n$. calculate the random matrix can be seen in Eq. (5).

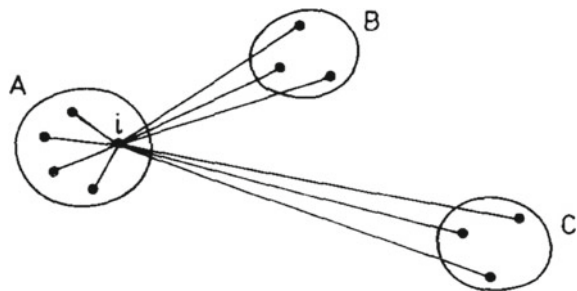
$$\mu_{ik} = \frac{\mu_{ik}}{Q_i} \tag{49.5}$$

4. Calculate the center of the cluster using Eq. (2).
5. Calculate the objective function using Eq. (3).
6. Calculate changes in the value of membership values using Eq. (1).
7. The FCM process stops on this condition:
 - a. $P_{t-1} - P_t < \text{error} (\epsilon)$
 - b. $MaxIter$ limit reached
8. Define a cluster of data using Euclidean distance.

49.3 Silhouette Evaluation

The silhouette evaluation was proposed by Rousseeuw in 1987 [22]. The method is often used to measure the quality of a cluster. An illustration of the silhouette evaluation can be seen in Fig. 49.1.

Fig. 49.1 Silhouette evaluation illustration [23]



In Fig. 49.1 can be seen in the data x_i located in Clusters A. Regions B and C are clusters other than A. In the silhouette evaluation, there is also a_i which is the average length of data x_i with data A and b_i is the minimum of average line length between data x_i and data from each other clusters [24]. Based on the illustration in Fig. 49.1, we get the silhouette value of the x_i data [22].

49.4 Result and Discussion

This study uses KSM data in 2019 with a total of 11,457 data with the distribution of data in 6 subjects which is biology, physics, chemistry, mathematics, geography, and economics with the amount of data for each study such as 1116, 1105, 1106, 1125, 1120, and 1117. The data contains the score of the correct answer, the score of the wrong answer, and the score of the wrong answer. Based on these parameters, clustering can occur regarding the quality of education in each school. The score data used is KSM participants consisting of several provinces with each province, and it can be used as a sample of the quality of high school education in every school in the regions in Indonesia. Samples of the distribution of data used can be seen in Fig. 49.2.

In Fig. 49.2, the green lines indicate data with a score of questions that were answered incorrectly. The blue color indicates the score data of the questions that were answered correctly, and the data in orange are the score data of the blank answer. The data will be clustered, including using 3 clusters, 4 clusters, 5 clusters, and 6 clusters. Then, the results of clustering were evaluated using silhouettes. The results used to measure the evaluation of clustering are the value of the silhouette (Si) and also the distribution of data on the silhouette using standard deviation (Std). Table 49.2 shows the results of the clustering process with 4 experiments.

Table 49.1 shows that the highest silhouette values limit to 1 are found in clustering with 3 clusters. The high silhouette value with a low standard deviation represents good clustering results with small data simulations. Figure 49.3 shows the results of the silhouette of each subject area with 3 clusters. The results of silhouette values are more than 0.50 which indicates good structure category according to the Kaufman table. The next process is determining the label of a cluster. The technique that can

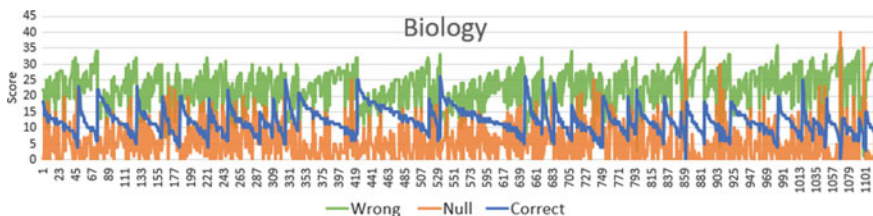


Fig. 49.2 Sample data on KSM scores

Table 49.1 Results of clustering using the FCM method

Subject	3 Clusters		4 Clusters		5 Clusters		6 Clusters	
	Si	Std	Si	Std	Si	Std	Si	Std
Mathematics	0.6499	0.2419	0.5783	0.2497	0.5910	0.2427	0.5642	0.2585
Chemistry	0.6195	0.2667	0.5266	0.2658	0.5385	0.2699	0.5364	0.2847
Geography	0.5220	0.2962	0.5265	0.3099	0.4933	0.3144	0.5049	0.3054
Physics	0.5941	0.2648	0.5539	0.2571	0.5542	0.2654	0.5764	0.2812
Economy	0.5773	0.3253	0.4937	0.3091	0.5161	0.3273	0.5361	0.3196
Biology	0.5663	0.2659	0.5406	0.2671	0.5285	0.2807	0.5143	0.2994

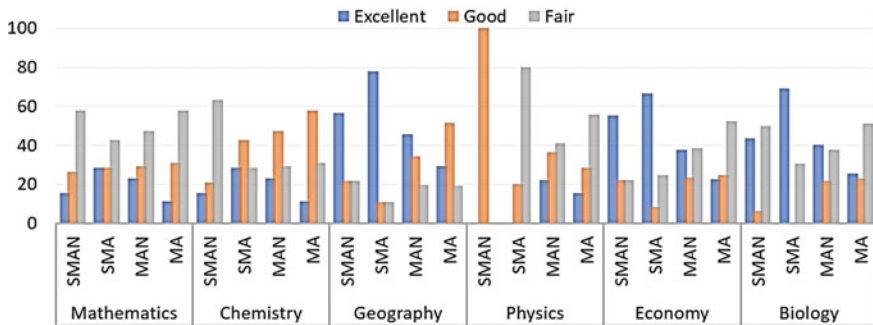


Fig. 49.3 Education quality identification results for each school

be used is to identify data through a cluster center to identify education quality, based on the results obtained by using 3 clusters in Table 49.2.

Table 49.2 carried out the process of defining labels, namely excellent, good, and fair. Labeling is obtained by identifying the cluster center and analyzing the data. The analysis is carried out to determine cluster 1 included in the label excellent, good, or fair. After the labeling process has been completed, next is to identify the distribution of schools in Indonesia to be identified in each subject based on State Senior High School (SMAN), Private Senior High School (SMA), Private Islamic Senior High School (MA), or State Islamic Senior High Schools (MAN) who are superior in terms of quality of education and schools can know the level of success in teaching and educating their students. The results of each Senior High School included in each cluster that has been labeled can be seen in Table 49.3. The table contains the number of SMAN, SMA, MA, and MAN in each existing cluster.

Table 49.3 shows the distribution of education quality data in each high school based on subject areas, specifically mathematics (math), physics (phy), biology (bio), chemistry (chem), geographic (geo), and economy (eco). The results of identifying the quality of each school in Indonesia can be seen in Fig. 49.3.

In Fig. 49.3, it can be seen that in mathematics almost all schools are weak in this subject. In mathematics, the school categorized best in high school with a percentage

Table 49.2 Centroid of clustering result

Subject	Cluster	Data			Label
		Wrong	Null	Correct	
Mathematics	Cluster 1	14.7775	5.7261	4.4964	Good
	Cluster 2	19.3779	0.4471	5.1751	Fair
	Cluster 3	7.8210	14.780	3.0010	Excellent
Chemistry	Cluster 1	22.5352	0.7791	6.6857	Fair
	Cluster 2	16.4525	7.3475	6.2001	Good
	Cluster 3	9.0388	16.7895	4.1717	Excellent
Geography	Cluster 1	15.7173	14.0193	10.2634	Good
	Cluster 2	19.3867	4.5296	16.0837	Fair
	Cluster 3	26.5779	1.3441	12.0780	Excellent
Physics	Cluster 1	13.8807	5.6817	5.4376	Good
	Cluster 2	8.2458	12.5996	4.1546	Excellent
	Cluster 3	18.6352	0.5096	5.8552	Fair
Economy	Cluster 1	19.9990	0.8497	9.1513	Fair
	Cluster 2	12.0580	2.7344	15.2077	Excellent
	Cluster 3	12.1813	8.8399	8.9789	Good
Biology	Cluster 1	27.5889	1.5281	10.8830	Fair
	Cluster 2	15.9453	14.0424	10.0124	Good
	Cluster 3	19.4739	5.3286	15.1975	Excellent

Table 49.3 Senior high school distribution for each cluster

High school	Cluster	Subject					
		Math	Phy	Bio	Chem	Geo	Eco
SMAN	Excellent	3	0	7	3	13	10
	Good	5	10	1	4	5	4
	Fair	11	0	8	12	5	4
SMA	Excellent	2	0	9	2	7	8
	Good	2	1	0	2	1	1
	Fair	3	4	4	3	1	3
MAN	Excellent	76	98	207	81	241	179
	Good	96	161	112	161	182	109
	Fair	156	180	195	198	104	180
MA	Excellent	87	101	145	77	164	140
	Good	239	187	132	215	289	153
	Fair	445	363	292	348	108	324

of students at 30% who have high-quality education. In chemistry, almost all schools are at a good level, but at SMAN, some students are dominantly weak toward this subject and the percentage of students who are not experts in chemistry is around 65%. In geography, SMA is the most upper-quality school with a smart student percentage of around 78%. SMA has sufficient quality because almost all students cannot achieve good quality, while SMAN achieves the best quality acquisition in physics with all students having good quality. In economics and biology, it has a percentage that is almost the same as the best quality achieved by SMAN and SMA. Based on the results that have been shown, it can be concluded that SMA is a school that has good quality among other schools. In the comparison of results between SMAN and SMA, the best results are obtained in SMA except in physics. In the comparison of results between MA and MAN, the best results are obtained on MAN. Based on this description, the school that needs evaluation and treatment regarding educational development is the MA.

49.5 Conclusion

This research was conducted to find out education quality that has been applied in several schools in Indonesia. This research is based on KSM 2019 scores using clustering methods with several experiments. The best results are clustering into 3 clusters. Evaluation of cluster performance uses silhouette (si) and standard deviation (std) on each subject data distribution, where math has a value of $si = 0.6499$; $std = 0.2419$, chemistry has a value of $si = 0.6195$; $std = 0.2667$, geography has a value of $si = 0.5220$; $std = 0.2962$, physics has a value of $si = 0.5941$; $std = 0.2648$, economics has a value of $si = 0.5774$; $std = 0.3253$, and biology has a value of $si = 0.5663$; $std = 0.2559$. The results obtained are high schools which are schools with good quality among other schools. In the comparison of results between SMAN and SMA, the best results are obtained in SMA except in physics. In the comparison of results between MA and MAN, the best results are obtained on MAN. Based on this description, the school that needs evaluation and treatment regarding educational development is the MA.

References

1. Sujarwo, S.: Pendidikan Di Indonesia Memprihatinkan. *WUNY UNY*. **15**(1) (2013)
2. Nelson, R., Dawson, P.: Competition, education and assessment: connecting history with recent scholarship. *Assess. Eval. High. Educ.* **42**(2), 304–315 (2017)
3. Cantador, I., Conde, J.M.: Effects of competition in education: a case study in an e-learning environment (2010)
4. Munirah, M.: Sistem Pendidikan di Indonesia: antara keinginan dan realita. *AULADUNA J. Pendidik. Dasar Islam*. **2**(2), 233–245 (2015)
5. Kementerian Agama, R.I.: Petunjuk Teknis Kompetensi Sains Madrasah (KSM) Tahun (2016)

6. Biondi, R.L., Vasconcellos, L., de Menezes-Filho, N.A.: Evaluating the impact of participation in the Brazilian Public School Mathematical Olympiad on math scores in students' standardized tests. *J. LACEA Econ.* (2012)
7. Idrus, M.: Mutu pendidikan dan pemerataan pendidikan di daerah. *Psikopedagogia J. Bimbingan dan Konseling*. **1** (2012)
8. Park, Y., Yu, J.H., Jo, I.-H.: Clustering blended learning courses by online behavior data: A case study in a Korean higher education institute. *Internet High. Educ.* **29**, 1–11 (2016)
9. Omran, M.G.H., Engelbrecht, A.P., Salman, A.: An overview of clustering methods. *Intell. Data Anal.* **11**(6), 583–605 (2007)
10. Santra, A.K., Christy, C.J.: Genetic algorithm and confusion matrix for document clustering. *Int. J. Comput. Sci.* [Internet]. **9**(1), 322–328 (2012). Available from <http://ijcsi.org/papers/IJCSI-9-1-2-322-328.pdf>
11. Shikalepo, E.E.: School cluster system for quality education in rural namibian schools. *Afr. Educ. Res. J.* **6**(2), 48–57 (2018)
12. Najdi, L., Er-raha, B.: Use of unsupervised clustering to characterize graduate students profiles based on educational outcomes. *Int. J. Comput. Tech.* **3**(2) (2016)
13. Chuang, K.-S., Tzeng, H.-L., Chen, S., Wu, J., Chen, T.-J.: Fuzzy c-means clustering with spatial information for image segmentation. *Comput. Med. Imaging Graph.* **30**(1), 9–15 (2006)
14. Hathaway, R.J., Bezdek, J.C.: Fuzzy c-means clustering of incomplete data. *IEEE Trans. Syst. Man, Cybern. Part B.* **31**(5), 735–744 (2001)
15. Bezdek, J.C., Ehrlich, R., Full, W.: FCM: The fuzzy c-means clustering algorithm. *Comput. Geosci.* **10**(2–3), 191–203 (1984)
16. Dutt, A., Aghabozrgi, S., Ismail, M.A.B., Mahrooian, H.: Clustering algorithms applied in educational data mining. *Int. J. Inf. Electron. Eng.* **5**(2), 112 (2015)
17. Zhou, K., Yang, S.: Exploring the uniform effect of FCM clustering: a data distribution perspective. *Knowledge-Based Syst.* [Internet] **96**, 76–83 (2016). Available from <http://dx.doi.org/10.1016/j.knsys.2016.01.001>
18. Novitasari, D.C.R.: Klasifikasi Sinyal EEG Menggunakan metode fuzzy C-means clustering (FCM) dan adaptive neighborhood modified Backpropagation (ANMBP). *J. Mat. MANTIK.*, pp. 31–36 (2015)
19. Kalavathi, P., Dhavapandiammal, A.: Segmentation of Lung Tumor in CT Scan Images using FA-FCM Algorithms. *Res. Gate* **18**(5), 74–79 (2016)
20. Zhao, Q., Li, X., Li, Y.: X Zhao (2017) A fuzzy clustering image segmentation algorithm based on hidden Markov random field models and Voronoi tessellation. *Patt. Recogn. Lett.* **85**, 49–55 (2017)
21. Swindiarito, V.T.P., Sarno, R., Novitasari, D.C.R.: Integration of fuzzy C-means clustering and TOPSIS (FCM-TOPSIS) with silhouette analysis or multi criteria parameter data. In: 2018 International Seminar on Application for Technology of Information and Communication, IEEE, pp. 463–468 (2018)
22. Rousseeuw, P.J.: Silhouettes: a graphical aid to the interpretation and validation of cluster analysis. *J. Comput. Appl. Math.* **20**, 53–65 (1987)
23. Dolfe, R., Matinzadeh, K.: Investigating skin cancer with unsupervised learning (2019)
24. Aranganayagi, S., Thangavel, K.: Clustering categorical data using silhouette coefficient as a relocating measure. In: International Conference on Computational Intelligence and Multimedia Applications (ICCIMA 2007), IEEE, pp. 13–17 (2007)

Chapter 50

Obstacle Avoidance with Sensors Using Soft Computing Techniques



Amit Yadav, Garima Jain, Divya Mishra, and Dharvendra P. Yadav

Abstract Robotics design is an exciting design for engineer, researcher, and interdisciplinary field of study. The purpose of this robot is to introduce the fundamentals of robotics and control of smart robot. It should also be useful for engineer and industrial persons. In this research paper, we compare micro-controller-based program and virtual instrumentation program control. So, we implement the virtual instrument control program for this robot to make decisions like vision, task planning, and obstacle avoidance. An autonomous robot, capable of performing different tasks for a human who is physically disabled, has been designed and developed. To avoid accident with unpredicted obstacles, the autonomous robot uses ultrasonic sensor and finds range for recognition and mapping. The obstacle avoidance approach used for this system is described. Since this approach depends deeply on the concert of the ultrasonic sensors, these sensors and the consequence of their restrictions on the obstacle avoidance algorithm and techniques are discussed in detail.

50.1 Introduction

The intelligent moving machine may keep away so many difficulties, move wisely, and reach to the goal securely, precisely in such a least cost and least time. The idea of fluffy rationale has been presented by Zadeh [1], which is broadly utilized in

A. Yadav
Dayalbagh Educational Institute, Agra, UP 282005, India
e-mail: amitphd2@gmail.com

G. Jain (✉) · D. Mishra
Swami Vivekanand Subharti University, Meerut, UP 250005, India
e-mail: jaingarima2011@gmail.com

D. Mishra
e-mail: mishradivya1311@gmail.com

D. P. Yadav
ISTRAC, ISRO, Bengaluru, Karnataka 560013, India
e-mail: Dharvendra.yadav@istrac.org

© The Editor(s) (if applicable) and The Author(s), under exclusive license to Springer Nature Singapore Pte Ltd. 2021

Y.-D. Zhang et al. (eds.), *Smart Trends in Computing and Communications: Proceedings of SmartCom 2020*, Smart Innovation, Systems and Technologies 182,
https://doi.org/10.1007/978-981-15-5224-3_50

many designing applications, for example, versatile mechanical autonomy, picture handling, and so on. Priorly, many moving machines were created utilizing various strategies for a continuous way discoverer framework. Human–intelligent moving machine has become a significant point in the field of robots network. A progressed keen moving machine must incorporate abilities to identify human’s quality in their region and decipher their movement for a functioning communication; the machine should likewise have the option to follow the static and dynamic deterrent in its way. The people and moving machines exist together to intently connect and play out a specific measure of work. Insight and example acknowledgment innovations have gained ground in mechanical technology [2], PC designing [3, 4], well-being-related issues [5], and regular sciences [6]. This examination work is isolated into two sections. The initial segment manages the increment of safe intelligent moving machine (SIMM), which keeps up a specific relative positional connection between the human and moving machine [7]. The canny machine can function as a right hand for people in different circumstances. Communicating with nature and indoor circumstance includes taking in and adjustment from evolving condition [8]. The intelligent machine can fill in as a right hand for people in different circumstances.

50.1.1 Steps for Design and Development of Intelligent Machine

Figure 50.1 depicts the flowchart of intelligent vehicle. The intelligent moving machine is safe running motor which takes action according to the situations.

Figure 50.2 design a block diagram panel for giving the commands to our automatic vehicle. In this section, our receiver antenna gets the information from the DAQ card and start doing task. The vehicle moves forward, backward, left, and right, and also avoids obstacle in his path. The UV sensor is used to detect the objects and gives commands to control motor and speed of front wheels to take turns of automatic vehicle. The speed of automatic vehicle is 10 km/h. It takes turn very fast in motion.

The commands will be forward, backward, left, and right. The command will be transmitted through the DAQ card to the receiver station. Figure 50.3 depicts the functional block which is shown below.

50.1.2 Proposed Work

On the basis of historical evidences microcontroller, embedded systems, and appropriate communication systems work to let us understand the engineering and define the understanding of different difficulty detection and their verified solutions. The state-of-art is that both microcontroller and moving machine took advance steps in developing intelligent moving vehicle. This work focuses on the basic proposal and

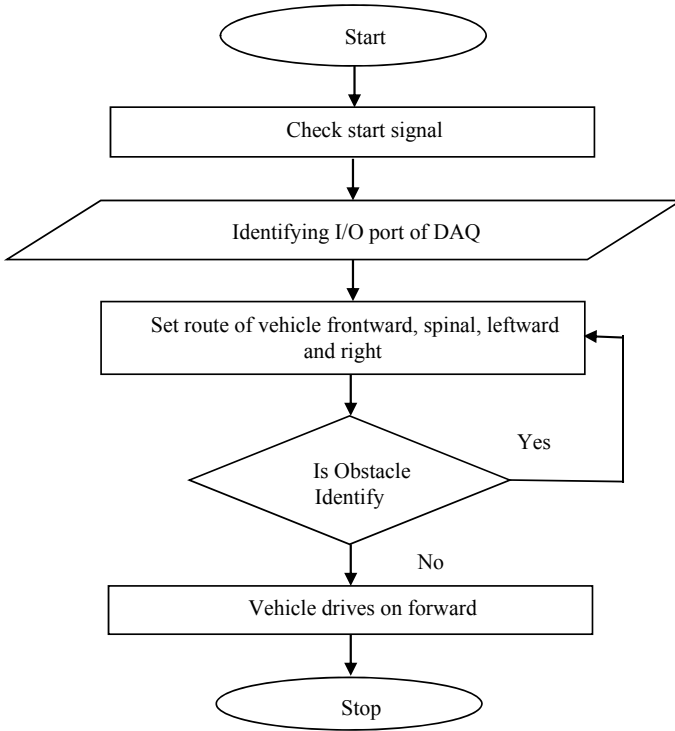


Fig. 50.1 Flowchart of intelligent vehicle

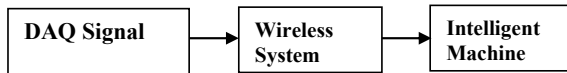


Fig. 50.2 Block diagram of intelligent machine



Fig. 50.3 Block diagram of tran-receive system

advances of safe intelligent moving vehicle which has the capability to avoid obstacle in real time. These obstacles may be known or unknown, static or dynamic.

50.2 Related Work

The most straight-forward approaches are for obstacle detection and depth estimation, and there can be found different methods associated with motion control of the independent moving robot.

50.2.1 Background

Arvind et al. [9] have suggested that obstacle location and shirking during route of a self-ruling vehicle is one of the difficult issues. Investigating the earth utilizing administered learning procedures has demonstrated to be a costly procedure because of the preparation of various deterrents for various situations. Their paper concentrated on reinforcement learning (RL) systems is utilized to comprehend the dubious condition dependent on sensor data to settle on the choice.

Diep et al. [10] proposed the procedure to present a strategy for swarm robot to get the moving objective and to keep away from numerous powerful deterrents in the obscure condition. In their work, the reenactment results are additionally exhibited to show that the snag shirking and getting objective undertaking that can be arrived at utilizing this technique, in which the robot is considered as a progression of water spilling out of high to low.

Swapna Rekha et al., [11] proposed the soft computing which manages advancement of surmised models in discovering answers for certifiable issues, and it is considered as one of the rising zones of research in all fields of designing and sciences. In their paper, a thorough diagnostic point of view of delicate figuring procedures and their application in apply autonomy have been outlined. Additionally, their paper reveals insight into different issues and difficulties of the examined research zone to show the predominance of delicate processing strategies in the advancement of different applications in mechanical technology.

Reddy et al. [12] as indicated by author the interest for autos ascends for everybody, and there has been a ceaseless increment in the quantity of vehicle robberies. Their paper additionally introduces another programmed motor locking framework which distinguishes the liquor content on the driver, and the start framework consequently kills if the liquor substance of the driver is more than the edge level. Their paper displays another instrument for expanding the security for autos by utilizing unique mark-based biometric security framework.

Levkovits-Scherer. et al. [13] in this paper propose a vision-based study on monocular infrastructure that uses a MobileNet SSD CNN for deterrent discovery and crash shirking in GPS-denied open air situations. Item discovery and arrangement are computationally serious undertakings, and the handling is taken out away load up on a ground control station that gets accessible symbolism and information of the UAV during the self-governing flight.

Adarsh et al. [14] in their paper introduced the exhibition correlation of ultrasonic and infrared estimation methods crosswise over hindrances of various sorts of materials. As per the research, vehicle model is coordinated with the sensors, moving with consistent speed toward various sorts of snags for catching the separation parameter.

Mohanty and Parhi [15] present the benefits of neural system and fluffy surmising framework. Their paper centers on the use of a versatile neuro-fuzzy induction framework (ANFIS) to way age and snag shirking of a self-ruling portable robot in an obscure static and dynamic condition.

Pandey et al. [16] in their paper exhibited the recreation of way arranging system for a self-sufficient versatile robot. The figure shows recreation of the versatile robot with four obstructions. At that point, it needs to design a way toward wanted objective. The route arrangement of a portable robot needs to distinguish every single potential impediment so as to look for an impact freeway.

50.3 Objective of Paper

The primary objective of this research is to work and develop a real-time obstacle avoidance machine to complete the defined job that involves distributed functionalities. In this context, the core research objectives of the thesis are given by:

1. To design and develop the machine in laboratory.
2. To design and develop an obstacle avoidance algorithm for moving machine.
3. To implement a research in laboratory for a defined and a required framework which is required for vehicle and the obstacle avoidance structure.

50.3.1 Methodology

The graphical idea in like manner defines non-programming specialists to accumulate programs by moving virtual depictions of laboratory gear with which they are starting at now common. The Lab VIEW programming condition, with at one point included different models and the documentation, makes it simple to make little applications. This is a favorable position on one side, yet there is also a particular risk of barely caring about the skill required for considerate mindset of programming. For complex estimations or colossal scale code, it is huge that the product engineer has a wide data on the extraordinary Lab VIEW language structure and the topology of its memory the officials. Also, it is possible to make appropriated applications, which pass on by a server plot and are thusly less difficult to execute as a result of the characteristically parallel nature of code.

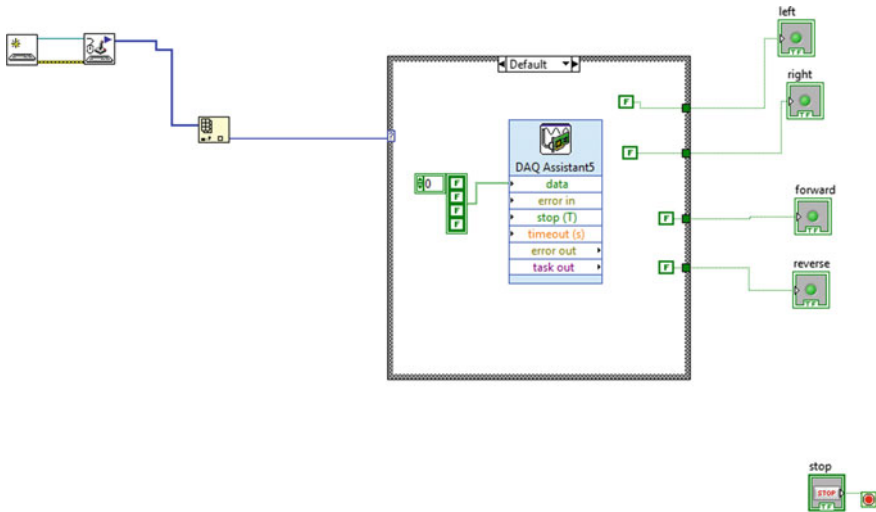


Fig. 50.4 Block diagram panel

50.3.2 Block Diagram Panel for IMM

The Lab VIEW is a graphical-based approach, so we start from the block diagram panel. In Fig. 50.4, we design a code programming for our moving machine which generates the signal in true/false conditions. If the condition is true, then our machine will move forward, and if the condition is false, our machine will stop. In this panel, the control output depends on five outcomes which are known as no action, forward, backward, left, and right. These signals generate output which we can see at the front panel and from here we can send the signals to the DAQ card. The front panel result of Lab VIEW code is shown in Fig. 50.5. This work is totally radio frequency based in this experimental setup no use of any type of chords. In programming code, four keys have been used which gives the signal for moving to the machine. This machine can be changing its position according to the path. So, it is called safe intelligent moving machine (SIMM). The most exceptional Lab VIEW development outlines offer the possibility of building and organizing different applications.

50.4 Results

Intelligent moving machine has been developed which is moving forward, backward, left, and right. This is a smooth running machine which is controlled by software-based controlling technique. This is a machine which is highly convenient intelligent machine for all the facts and figures of engineering purpose which will work more efficiently in existent time engineering conditions. This moving machine is absolutely



Fig. 50.5 Front panel result of Lab VIEW code

in controlled with a defined control station maintained at different steps. The result we visualize in moving machine additionally adequately maintains a strategic distance from the hindrances coming in its way detecting them through the sensor reaction. It changes its movement very fast. When we provide a signal, it changes its directions in 0.3 s. The trajectory angle with obstacle is 45° when machine is moving forward and sudden change in its phase.

50.5 Conclusions

The intelligent moving machine developed in this work is smooth running and gives fast response against all type of situations. This examination work accomplishing research center manual was intended for a course in mechanical autonomy at the higher level understudies. The developed automatic intelligent machine also senses and avoids the obstacles in its path. So, the moving machine is very useful in industrial and airport as a load vehicle. These Lab View programming ventures serve both as a persuasive and as a support system for structure and advancement of smart robots. In this research, we try to focus at miniaturized scale controller-based program and virtual instrumentation program control. So, we actualize the virtual instrument control program for this robot.



Fig. 50.6 Intelligent moving machine

50.6 Experimental Setup of Intelligent Moving Machine

Figure 50.6 depicts the experimental setup of intelligent moving machine which is used for industrial and defense application performing a task transforming load one place to another place. Another application we can use in defense is autonomous drone on border security purpose.

References

1. Zadeh, L.A.: The concept of a linguistic variable and its application to approximate reasoning-I. *ELSEVIER Inf. Sci.* **8**(3), 199–249 (1975)
2. Zhan, Y., Kuroda, T.: Wearable sensor-based human activity recognition from environmental background sounds. *J. Ambient Intell. Hum. Comput.* **5**, 77–89 (2014)
3. Jalal, A.: Security architecture for third generation (3G) using GMHS cellular network. *Proc. Int. Conf. Emerg. Tech. Islamabad, Pakistan* **12–13**, 74–79 (2008)
4. Shire, A.N., Khanapurkar, M.M., Mundewadikar, R.S.: Plain ceramic tiles surface defect detection using image processing. *Proc. Int. Conf. Emerg. Trends Eng. Tech. Port Louis, Mauritius* **18–20**, 215–220 (2012)
5. Shang, L., Yang, Q., Wang, J., Li, S., Lei, W.: Detection of rail surface defects based on CNN image recognition and classification. *Proc. Int. Conf. Adv. Commun. Tech. Chuncheon-si, Korea* **11–14**, 45–51 (2018)
6. Jalal, A., Kim, S.: Advanced performance achievement using multi-algorithmic approach of video transcoder for low bitrate wireless communication. *ICGST Int. J. Graph. Vis. Image Process.* **5**, 27–32 (2004)

7. Alonso-Mora, J., Breitenmoser, B., Rufli, R., Beardsley, P., Siegwart, R.: Optimal reciprocal collision avoidance for multiple non-holonomic robots. *J. Distrib. Auton. Robot. Syst.* 203–216 (June 2013)
8. Kim, S.J., Choi, W.K., Jeon, H.T.: Intelligent machine control with personal digital assistants using Fuzzy logic and Neural network. *Knowl. Based Intell. Inf. Eng. Syst.* **3215**, 589–595 (2004)
9. Arvind, C.S., Senthilnath, J.: Autonomous vehicle for obstacle detection and avoidance using reinforcement learning soft computing for problem solving, pp. 55–66. Springer, Singapore (2020)
10. Diep, Q.B., Zelinka, I., Senkerik, R.: An algorithm for swarm robot to avoid multiple dynamic obstacles and to catch the moving target. In: *International Conference on Artificial Intelligence and Soft Computing*. Springer, Cham (2019)
11. Swapna Rekha, H. et al.: Soft computing in robotics: a decade perspective, pp. 59–78 (2019)
12. Reddy C.R.S. et al.: Advanced protection for automobiles using MSP430. *Soft Computing and Signal Processing*. Springer, Singapore, pp. 665–672 (2019)
13. Levkovits-Scherer, D.S., Cruz-Vega, I., José, M.C.: Real-time monocular vision-based UAV obstacle detection and collision avoidance in GPS-denied outdoor environments using CNN MobileNet-SSD. In: *Mexican International Conference on Artificial Intelligence*. Springer, Cham (2019)
14. Adarsh et al.: Performance comparison of infrared and ultrasonic sensors for obstacles of different materials in vehicle/robot navigation applications. In: *IOP Conference Series: Materials Science and Engineering*, vol. 149, No. 1. IOP Publishing (2016)
15. Mohanty, P.K., Parhi, D.R.: Path generation and obstacle avoidance of an autonomous mobile robot using intelligent hybrid controller. *International Conference on Swarm, Evolutionary, and Memetic Computing*. Springer, Berlin, Heidelberg (2012)
16. Pandey, A., et al.: Path planning navigation of mobile robot with obstacles avoidance using fuzzy logic controller. In: *2014 IEEE 8th International Conference on Intelligent Systems and Control (ISCO)*. IEEE (2014)

Author Index

A

Aberathne, Iroshan, 125
Ahmed, Rehib Uddin, 355
Akashe, Shyam, 393, 401, 411
Ali, Nazlena Mohamad, 477
Anand, V., 69
Anil Kumar, Tipparti, 49
Anjaneyulu, Lokam, 49
Anton, Anton, 291
Ara, Jasmine, 331
Arnita, 259
Asfaqur Rahman, Md., 135
Ashiquzzaman, Akm, 459
Asyhar, Ahmad Hanif, 211, 221, 281, 487

B

Bab-Hadiashar, Alireza, 113
Bandhopadhyay, Ayan Kumar, 241
Bhattacharjee, Disha, 269
Bhattacharjee, Payal, 1
Bhor, Harsh Namdev, 339

C

Chiluveru, Anoop, 401

D

Damayanti, Nita Rosa, 477
Das, Utpal Chandra, 147
Dey, Anup, 201, 269
Diah Nugraheni Setyowati, R. R., 249, 259
D'Souza, Sonia Maria, 469

E

Eriksson, Niklas, 39

F

Fagerstrøm, Asle, 39
Faqih, Abdullah, 487
Fauzi, Ahmad, 211, 221, 281, 487
Febrianti, Fitria, 259
Feng, Li, 95
Foady, Ahmad Zoebad, 259

G

Ganguly, Amrita, 331
Ganorkar, Sandeep S., 443
Gao, Biying, 25
Gautham, K., 101
Gorewar, Harish Vasantrao, 427
Gostar, Amirali K., 113
Goswami, Bijoy, 201, 269
Gupta, Anshu, 345
Gupta, Manisha, 311

H

Hadianti, Sri, 231
Hafiyusholeh, Moh., 259
Hanh, Cao Duc, 379
Haque, Munima, 147
Haque, Shahina, 147
Hasna Hena, Most., 135, 183
Hastuti, Nanik Puji, 221
Helal Sheikh, Md., 183
Heryadi, Yaya, 301
Hoseinnezhad, Reza, 113

© The Editor(s) (if applicable) and The Author(s), under exclusive license to Springer Nature Singapore Pte Ltd. 2021

Y.-D. Zhang et al. (eds.), *Smart Trends in Computing and Communications: Proceedings of SmartCom 2020*, Smart Innovation, Systems and Technologies 182,

<https://doi.org/10.1007/978-981-15-5224-3>

I

Indriyati, Ratna, 281
 Ishtiaq, Nida, 113

J

Jain, Garima, 497
 Jana, Abir, 201, 269
 Jogekar, Ravindra Namdeorao, 435

K

Kalla, Mukesh, 339
 Karuppiyah, Anupama, 319
 Kim, Jinsul, 459
 Kissaka, Mussa M., 83
 Koley, Chaitali, 241
 Kumar, Abhishek, 411
 Kumar, Amit, 345
 Kumar, Ankit, 393
 Kumar, Arun, 69
 Kumar, Deepak, 365
 Kumar, Seelam VSV Prabhu Deva, 393
 Kumar, S. S., 57
 Kumar, Suresh, 211
 Kumari, Komal, 201, 269
 Kusaeri, 211, 221, 281, 487

L

Lakkhanawannakun, Phoemporn, 159
 Lee, Dongsu, 459
 Lee, Jihoon, 459
 Leela Velusamy, R., 101
 Li, Danyang, 25
 Li, Xinlai, 25
 Lohi, Shantanu Anandrao, 419
 Loktongbam, Paikhomba, 241
 Lukas, 301
 Luu, Do Duc, 379

M

Mahbubur Rahman, Md., 135
 Maheshwari, Raghav, 319
 Maragatham, G., 449
 Marouf, Ahmed Al, 183
 Maryunah, 281
 Merlina, Nita, 231
 Min Oh, Sung, 459
 Mishra, Divya, 411, 497
 Mishra, Vishwas, 411
 Mohamed Mansoor Roomi, S., 449
 Mustofa, Ali, 211, 221, 281, 487

Mvungi, Nerey H., 83
 Mwifunyi, Rukia J., 83

N

Namdeo, Varsha, 443
 Nampromma, Jatupol, 159
 Nandi, Poushali, 201
 Nariswari, Rinda, 259
 Noersasongko, Edi, 231
 Novitasari, Dian Candra Rini, 211, 221, 249,
 259, 281, 487
 Nurtantio, Pulung, 231

O

Ojha, Shailendra Singh, 401

P

Pal, Debashish, 241
 Panicker, Sabita, 113
 Paul, Bijan, 331
 Pradeep, Arun, 57
 Pramanik, Ankita, 345
 Pramulya, Rahmat, 249
 Puspitasari, Wahyu Tri, 249

Q

Qiu, Liwen, 95
 Quamruzzaman, M., 147

R

Raghavendra, G. S., 69
 Ramachandran, Anita, 319
 Ramya, M. M., 1
 Rathnayake, Udara, 125
 Ravi, Akshay, 101
 Reddy, K. Satyanarayan, 469
 Riana, Dwiza, 231
 Richard, 301
 Rohayani, Hetty, 249
 Rolliawati, Dwi, 211, 221, 281, 487
 Rozi, Muhammad Fahrur, 249
 Rustad, Supriadi, 291

S

Saha, Prabir, 355, 365
 Santi, Dwi Rukma, 249
 Sarkar, Subir Kumar, 201, 269
 Setiawan, Fajar, 259

Shahriar Nawal Shoumik, Md., 135
Shakin Banu, A., 449
Shamim Reza, Md., 183
Shankar Lingam, M., 69
Sharma, Akhilesh Kumar, 17
Shidik, Guruh Fajar, 291
Shrivastav, Devesh K., 17
Sigurdsson, Valdimar, 39
Soeleman, M. A., 231
Sreeja, K. A., 57
Sripranav, S., 101
Sudhakara, A. M., 69
Syukur, Abdul, 291

T

Taj, Malaika Afra, 319
Tangtrakul, Ekaphong, 159
Tiwari, Nandita, 419, 427, 435, 443
Tiwari, Vivekanand, 193
Trisetyarso, Agung, 301
Tsujioka, Keiko, 171
Tyagi, Shobhit, 411

U

Ulinuha, Nurissaidah, 211, 221, 281, 487

Ulya, Zakiyatul, 211, 221, 281, 487
Umar, A., 211

V

Vasuki, P., 449

W

Wahyudi, Noor, 211, 221, 281, 487
Walgampaya, Chamila, 125
Widjajanto, Ary, 249
Wulandari, Putri, 259

Y

Yadav, Amit, 497
Yadav, Dharvendra P., 497
Yadav, Dinesh, 193
Yao, Shumin, 95
Yusuf, Ahmad, 211, 221, 281, 487

Z

Zhang, Lianbo, 95
Zhao, Jing, 95
Zhao, Qinglin, 95